The *App*^{NLGF} Mouse Model of Amyloid Pathology: Characterisation of Cognitive Function and Neuronal Activity

Ffion Ann Boxall

A thesis submitted for the degree of Doctor of Philosophy

Cardiff University

April 2025

Thesis Summary

Transgenic mouse models overexpressing Amyloid Precursor Protein (APP) have been widely used to model the amyloid-beta (Aβ) pathology of Alzheimer's Disease (AD), but the overexpression of other APP fragments may result in artificial phenotypes (Sasaguri et al., 2022). *The App^{NLGF}* mouse, a newer knock-in model that expresses humanised mutant APP at endogenous levels, avoids such artefacts (Saito et al., 2014). However, relatively little is known about how this more restricted expression of mutant APP influences cognition and neural activity. This thesis therefore aimed to characterise memory function (including episodic-like and spatial working memory), and anxiety-like behaviour in *App^{NLGF}* mice across a range of ages, while also examining neural activity using *in vivo* two-photon Calcium (Ca^{2+}) imaging and immediate early gene (*c-fos*) expression.

Behavioural deficits in *App^{NLGF}* mice were mild and predominantly emerged in the oldest age group (22-23 months). At this age, *App^{NLGF}* mice exhibited intact object novelty memory but were impaired in the object location and object-in-place spatial memory tasks. *App^{NLGFs}* also exhibited impaired performance in the spontaneous alternation spatial working memory task at 22-23 months. Moreover, *App^{NLGFs}* exhibited increased thigmotaxis in the open field at 22-23 months, consistent with anxiety-like behaviour. In contrast, consistent disinhibitory or anxiolytic-like behaviour in the elevated plus maze was observed from as early as 4 months of age. Subtle changes in neuronal activity were also observed: at 22-23 months, *App^{NLGFs}* exhibited reduced stimulus-evoked Ca^{2+} transients in the retrosplenial cortex (RSC), a region involved in navigation and episodic memory that exhibits early Aβ pathology (Alexander et al., 2023; Buckner et al., 2005; Klunk et al., 2004). While *c-fos* expression in the RSC remained preserved at 14-16 months, reduced basal levels were observed in the hippocampus, a region critical for spatial and episodic memory that also exhibits early Aβ pathology (Rao et al., 2022).

Together, these findings suggest that *App^{NLGF}* mice exhibit mostly mild, age-dependent cognitive impairments and reduced neuronal activity. The modest phenotype likely reflects the absence of overexpression-related artefacts and may suggest a subtle effect of amyloid on synaptic dysfunction. Whilst these findings support the relevance of *App^{NLGFs}* to early or preclinical AD, the subtlety of its phenotype may limit its utility for evaluating the efficacy of therapeutic interventions.

Table of Contents

Figures

Abbreviations

Abbreviation	Definition
ΔF	*Change in fluorescence*
Aβ	*Amyloid beta*
ACh	*Acetylcholine*
AChI	*Acetylcholinesterase inhibitor*
AD	*Alzheimer's Disease*
AICD	*Amyloid precursor protein intracellular domain*
AMPAR	*Alpha-amino-3-hydroxy-5-methyl-4-isoxazolepropionic acid receptor*
ANOVA	*Analysis of variance*
APOE	*Apolipoprotein E*
APP	*Amyloid precursor protein*
APPs	*Soluble N terminal APP fragment*
ARIA	*Amyloid related imaging abnormality*
ATP	*Adenosine triphosphate*
AUC	*Area under the curve*
BACE1	*Beta-APP-cleaving enzyme-1*
BBB	*Blood-brain barrier*
Ca^{2+}	*Calcium ion*
CaM	*Calmodulin*
CaMKII	*Ca^{2+}/CaM-dependent protein kinase II*
CaN	*Calcineurin*
CI	*Confidence interval*
CNS	*Central nervous system*
CREB	*Cyclic adenosine monophosphate response element-binding protein*
CSF	*Cerebrospinal fluid*
CTF	*C terminal fragment*
DAB	*3, 3'-diaminobenzidine*
DR	*Discrimination ratio*
DSM-5	*Diagnostic and Statistical Manual of Mental Disorders (5th Edition)*
EC	*Entorhinal cortex*
ELISA	*Enzyme-linked immunosorbent assay*
EPM	*Elevated plus maze*
ER	*Endoplasmic reticulum*
ETC	*Electron transport chain*
FAD	*Familial Alzheimer's disease*
FDA	*Food and Drug Administration*
FDG-PET	*Fluorodeoxyglucose positron emission topography*
fMRI	*Functional magnetic resonance imaging*
GABA	*Gamma-aminobutyric acid*
GFP	*Green fluorescent protein*
HPC	*Hippocampus*
IEG	*Immediate early gene*
IHC	*Immunohistochemistry*

IL	*Interleukin*
IMS	*Industrial methylated spirit*
IP_3R	*Inositol 1,4,5-trisphosphate receptor*
IR	*Infra-red*
IZR	*Inner zone ratio*
K^+	*Potassium ion*
KI	*Knock-in*
LOAD	*Late onset AD*
LTD	*Long-term depression*
LTP	*Long-term potentiation*
MCI	*Mild cognitive impairment*
MCU	*Mitochondrial Ca^{2+} uniporter*
MMSE	*Mini-Mental State Examination*
mPFC	*Medial prefrontal cortex*
mPTP	*Mitochondrial permeability transition pore*
MRI	*Magnetic resonance imaging*
MWM	*Morris water maze*
Na^+	*Sodium ion*
NCX	*Na^+/Ca^{2+} exchanger*
NFT	*Neurofibrillary tangle*
NGS	*Normal goat serum*
NICE	*National Institute for Health and Care Excellence*
NMDAR	*N-methyl-D-aspartate receptor*
NPS	*Neuropsychiatric symptom*
OAR	*Open arm ratio*
OF	*Open field*
OiP	*Object-in-place*
OL	*Object location*
ON	*Object novelty*
PBS	*Phosphate buffered saline*
PET	*Positron emission topography*
PFA	*Paraformaldehyde*
PFC	*Prefrontal cortex*
PMCA	*Plasma membrane ATPase*
PRh	*Perirhinal cortex*
PrP^c	*Cellular prion protein*
PSEN (1/2)	*Presenilin 1 or 2*
RAM	*Radial arm maze*
ROI	*Region of interest*
ROS	*Reactive oxygen species*
RSC	*Retrosplenial cortex*
RyR	*Ryanodine receptor*
SE	*Standard error*
SEM	*Standard error of the mean*
SOCC	*Store operated calcium channel*
SSRI	*Selective serotonin reuptake inhibitor*
TNF-α	*Tumour necrosis factor alpha*
TO	*Temporal order*

TREM2	*Triggering Receptor Expressed on Myeloid Cells 2*
VBA	*Visual Basic for Applications*
VDAC	*Voltage dependent anion channel*
VGCC	*Voltage gated Ca^{2+} channel*

Contributions

- Ms Fangli Chen performed the cranial window surgery for two-photon Ca^{2+} imaging and helped with data acquisition.
- Dr Adam Ranson and Dr Rosie Craddock developed MATLAB codes to perform two-photon Ca^{2+} imaging, including the codes to present visual stimuli to the animal, to record timestamped fluorescent data, and to convert raw images from experiment files into TIFFs for downstream analysis.
- Dr Rosie Craddock developed the MATLAB code to convert timestamped fluorescent data from imaging experiments into Excel spreadsheets for the purpose of this thesis

Acknowledgements

As I come to the end of writing this thesis, there are so many people I wish to thank who have helped me reach this point. I'll keep this brief as my writing capacity feels truly maxed out (!), but please know how deeply grateful I am to all of the incredible people in my life.

Firstly, I am immensely thankful to the Alzheimer's Society for generously funding this PhD. The work you do is extraordinary and is a cause that's very close to my heart. Whilst this thesis is just a small piece of a much larger puzzle, I am proud to have contributed in some way. I hold onto hope that one day, no one will have to endure the effects of Alzheimer's Disease.

To my supervisors, Professors Mark Good and Frank Sengpiel, thank you for your kindness, encouragement, and unwavering support through every unpredictable twist and turn of this PhD. After each of our many discussions, I've left with a huge sense of relief, enhanced self-confidence, and a renewed motivation to carry on the work that I love. Beyond your remarkable expertise, this speaks volumes about your strengths as mentors, and for that I am truly grateful. Thank you also to Professor Dominic Dwyer, who often felt like my unofficial third supervisor. I am incredibly grateful for your support and guidance throughout this PhD.

From Frank's lab, I want to thank Fangli, Beth, and Rosie – three incredibly skilled women who were instrumental in helping me obtain the calcium imaging data in this thesis. This part of my PhD pushed me far out of my comfort zone, and with the added challenge of major, unpredictable technical issues, it was no easy feat. Each of you went above and beyond to support me with these experiments, and I am deeply grateful for that.

From the BNL, I want to say a special thank you to Katie, who generously shared her time and taught me many practical skills in behavioural testing throughout my PhD, all while juggling the demands of her own. Thank you for being a wonderful friend and a constant source of support and knowledge. I'm especially grateful for the many *very* senior mice I inherited from you at the start of my PhD. They were clearly very well cared for and gave me such a rare and valuable opportunity to study the *App*^{NLGF} model at such an advanced age. On the topic of mice, thank you to the Taylor group for kindly providing the mice that enabled me to establish my own colonies of *App*^{NLGFs} for the younger cohorts. I'm also deeply grateful to everyone in the wider BNL community, including Moira, for her practical support and great chats,

to Eman, for her expert guidance with the c-Fos staining, to the wonderful cleaning staff who always made me smile (and made the lab a little less lonely at 7am!), and to the animal technicians, whose training and ongoing advice made this work possible.

To my family – thank you. Mum, for always reiterating the importance of education to me, as “it’s the only thing no one can take away from you”, and Dad, for supporting me through everything. I credit you both for my drive to achieve the most I possibly can, and I hope you’ll be proud.

I also wish to say a special thank you to my “mother-in-law” Deb, a lady with an incredibly kind heart who has supported me like I’m her own daughter. Thank you, Deb, for always being there. Thank you for looking after Anna whilst I worked - I was able to fully concentrate on writing because I knew she was safe with you. I knew this because it’s clear how deep your love is for her, and what a wonderful thing it is to see my daughter growing up surrounded by such warmth and affection. And thank you Deb (circa 29 years ago), for giving birth to Luke, the most amazing person I know. Thank you, Luke, for being a wonderful partner and the most incredible Dad to our babies. If there’s one person I should thank for getting me through these five years, it’s you. I honestly couldn’t have done it without your love and support so thank you, sincerely.

And lastly, to my babies. To Louis, my feline child, for keeping me company through the countless hours I have spent at my desk writing this thesis. Your purring at my feet truly soothed the soul. And to my daughter Anna, to whom this thesis is dedicated, thank you for coming into this world and giving me the motivation to carry on, all whilst bringing so much joy to our family. Some may have assumed that I wouldn’t finish this PhD after I became pregnant, and yes, it’s been harder than it would have been otherwise, but at no other point in my life have I felt as strongly determined as I do now that I am a mother. So, thank you Anna. I hope I have shown you to pursue your passions and never give up. If, one day, you become a mother, I hope the working world is kinder to you. But know that, regardless, you can rely on me for anything. I love you endlessly.

For Anna

Chapter 1: General Introduction

1.1 Chapter Overview

This General Introduction chapter provides an overview of the background supporting the use of the *App*^{NLGF} model in Alzheimer's Disease (AD) research. It begins with a general introduction to AD, outlining the prevalence, pathogenesis, and progression of the disease. The alternative enzymatic processing of Amyloid Precursor Protein (APP) will be described, alongside discussion of the role of APP in physiology, the accumulation of amyloid beta (Aβ) according to the Amyloid Cascade Hypothesis, and how such pathology impacts neuronal function. As the *App*^{NLGF} model is based on Aβ pathology, this introduction will focus primarily on Aβ, while briefly acknowledging limitations of the Amyloid Cascade Hypothesis and the involvement of other pathological features such as tau hyperphosphorylation, neuronal loss, and immune dysfunction. This chapter will also outline the physiological role of calcium (Ca^{2+}) in neuronal function and how its intricate signalling processes become disrupted in AD, providing a foundation for later discussion in the thesis. Current and emerging therapeutic strategies for AD, including recent anti-amyloid therapies, will be briefly introduced. Finally, the chapter will then review the historical use of mouse models in AD research, beginning with 1st generation transgenic models and progressing to 2nd generation knock-in models, including the *App*^{NLGF} model. The pathological and behavioural profiles of transgenic and *App*^{NLGF} models will be discussed, highlighting the limitations of transgenic approaches that led to the development of 2nd generation models.

1.2 Alzheimer's Disease

1.2.1 Introduction to Alzheimer's Disease

AD was first described by Alois Alzheimer in 1906 (Alzheimer et al., 1995; Ryan et al., 2015). Alzheimer examined the brain of Auguste Deter, a 51-year-old woman who died after experiencing rapid loss of memory, disorientation, and delusions. In his paper titled *An Unusual Illness of the Cerebral Cortex* (translated from German), Alzheimer described severe loss of cortical neurons along with substances that we now recognise as neurofibrillary tangles (NFTs) and amyloid-β (Aβ) plaques (Alzheimer et al., 1995; Ryan et al., 2015). The term 'Alzheimer's Disease' was coined four years later in Emil Kraepelin's 1910 'Handbook of Psychiatry', where it was declared as a specific clinical disease entity (Ryan et al., 2015).

Today it is universally accepted that AD is a progressive neurological disorder that causes a variety of debilitating symptoms including memory loss, disorientation, and agitation (Avila & Perry, 2021). AD is broadly categorised into sporadic AD (SAD) and familial AD (FAD) (Ulaganathan & Pitchaimani, 2023). SAD, also referred to as late onset AD (LOAD), accounts for around 95% of AD cases and is typically

diagnosed after the age of 65 (Dorszewska et al., 2016). FAD, which accounts for the remaining 5% of AD cases, typically presents with symptoms before the age of 60 (Bekris et al., 2010).

1.2.2 Prevalence of Alzheimer's Disease

Over the last three decades, the prevalence of AD and other dementias has increased by around 160% (Li et al., 2022). Interestingly, AD prevalence is significantly higher among elderly women compared to elderly men, which may be explained by the longer lifespan of females compared to males, as well as biological and sociocultural differences between the sexes (Lopez-Lee et al., 2024; Mielke, 2018; Rahman et al., 2019; Rajan et al., 2021; Rosende-Roca et al., 2021). While women are disproportionately affected, the overall number of people living with AD is rising rapidly; in 2021, the number of people over the age of 65 with AD was 6.3 million, but this number is expected to reach 7.2 million by 2025 and 13.8 million by 2060 (Rajan et al., 2021). The rapid rise in AD cases can be attributed, at least in part, to exponential population growth and increased life expectancy (Li et al., 2020). Additionally, many people born during the post-World War II "baby boom" have now reached the age of 65 or older, placing the largest population cohort in the age rage at greatest risk of AD (Dhana et al., 2022; Guerreiro & Bras, 2015). However, the increasing prevalence of lifestyle and environmental risk factors, such as obesity and air pollution, may also be contributing to the growing incidence of AD (Flores-Cordero et al., 2022; Killin et al., 2016).

AD imposes profound burdens on patients, caregivers, and the economy (Tahami Monfared et al., 2022). For patients, the progressive cognitive decline leads to the loss of independence, diminished income, institutionalisation, and a severely compromised quality of life (Castro et al., 2010). Caregivers, who are often unpaid family members, bear the emotional toll of witnessing this decline while often facing financial stress, especially if institutionalisation is required (Lindeza et al., 2020; Manzini & do Vale, 2020; Tahami Monfared et al., 2022). Furthermore, AD places a heavy economic strain on the healthcare and social care systems, with the total annual cost of dementia in the UK estimated to be around £34.7 billion (Edwards et al., 2024). The rising prevalence of AD, along with the severity of its consequences to the individual and society and the limited available treatment options, highlights the urgent need for the development of effective therapies. This can only be achieved by gaining a deeper understanding of the mechanisms of AD through comprehensive animal model research.

1.2.3 Symptoms, Diagnosis, and Staging of Alzheimer's Disease

For both SAD and FAD, the gold standard of diagnosis is the pathological identification of key features in post-mortem brain tissue, including neuronal loss and the presence of Aβ plaques and NFTs (Avila & Perry, 2021), the cardinal hallmarks described more than a century ago by Alzheimer and Fisher (Alzheimer et al., 1995; Goedert, 2009). However, in life, a probable AD diagnosis can be made via a combination of approaches. These include evaluating a patient's medical history alongside reports of behavioural and cognitive changes from family members, and cognitive assessments such as the Mini-Mental State Examination (MMSE) to assess memory, orientation, language, and visuospatial skills, such as the ability to draw a complex polygon (Barthélemy et al., 2024; Bomasang-Layno & Bronsther, 2021; Bouwman et al., 2022; Folstein et al., 1975). Structural imaging such as magnetic resonance imaging (MRI) and computed tomography (CT) scans may be performed to help confirm a diagnosis by ruling out other conditions such as tumours or strokes, and by detecting brain atrophy (Chouliaras & O'Brien, 2023). Furthermore, positron emission topography (PET) scans can be used to detect key biomarkers of AD such as Aβ plaques and NFTs, as well as to detect glucose hypometabolism associated with the condition (Jack et al., 2018). However, although PET scans are increasingly utilised to support a clinical AD diagnosis, they are not yet routinely available on the NHS (Ou et al., 2019). Furthermore, lumbar punctures may be offered to measure cerebrospinal fluid (CSF) levels of Aβ and tau proteins (Bouwman et al., 2022). However, growing research efforts are aimed at developing less invasive diagnostic methods, including blood-based biomarkers (Bouwman et al., 2022; Jack et al., 2018).

The Diagnostic and Statistical Manual of Mental Disorders (5th Edition; DSM-5) serves as a useful framework for understanding and classifying neurocognitive disorders such as AD. According to the DSM-5, a diagnosis of AD requires evidence of impairment in learning and memory, along with deficits in at least one other cognitive domain such as executive function, language, perceptual-motor, complex attention, and social cognition (American Psychiatric Association, 2022). These impairments must interfere with the activities of daily living (American Psychiatric Association, 2022). Due to its progressive nature, AD symptoms range in extent and severity, depending on the stage. Several staging systems have been developed to categorise the progression of the disease, each with slight variations in the definition of stages, but generally encompassing the presence of pathological hallmarks, cognitive deficits, and behavioural abnormalities (Dubois et al., 2010; Jack et al., 2018; Porsteinsson et al., 2021; Sabbagh et al., 2019). For example, the National Institute on Aging and Alzheimer's Association (NIA-AA) created diagnostic guidelines for two symptomatic stages of AD; mild cognitive impairment (MCI) and dementia (Albert et al., 2011; McKhann et al., 2011). It was later recommended that a third stage should be created to categorise individuals without overt symptoms,

known as preclinical AD (Sperling et al., 2011). Preclinical AD is generally defined as the early asymptomatic stage in which individuals are cognitively unimpaired but show evidence of AD brain lesions such as Aβ plaques, NFTs, and atrophy upon postmortem examination (Dubois et al., 2010; Dubois et al., 2016). Preclinical AD can last up to 20 years before eventually progressing to MCI (also known as prodromal AD) (Mark & Brehmer, 2022). Around 20-30% of patients will progress from preclinical AD to MCI (Cho et al., 2021; Vermunt et al., 2019). MCI is defined as cognitive decline that is greater than expected for the individual's age but does not dramatically interfere with day-to-day life (Gauthier et al., 2006). Whilst usually still relatively independent, patients with MCI may present with memory and language impairments, such as struggling to find the correct word in a conversation (Porsteinsson et al., 2021). Patients may also become disorientated in familiar surroundings and struggle to complete familiar tasks (Porsteinsson et al., 2021).

Approximately 30-70% of MCI patients will develop AD with dementia within four years (Cho et al., 2021; Roberts et al., 2018; Ye et al., 2018). AD with dementia is subdivided into progressively mild, moderate, and severe stages (Jack et al., 2018). As AD progresses from mild to severe, patients experience increasingly severe cognitive deficits (Jahn, 2013). Episodic memory deficits are an early hallmark, with patients often being unable to recall a list of words (Tromp et al., 2015). They may also experience mild problems with working memory and executive functions such as planning, problem solving, and following multi-step instructions (Jahn, 2013; Laczó et al., 2018; Perry & Hodges, 1999). In the moderate stage, memory systems further deteriorate, with patients commonly experiencing time distortion and forgetting specific personal events (El Haj & Kapogiannis, 2016). Visuospatial deficits may become apparent, with patients experiencing difficulties recognising familiar surroundings and perceiving spatial relationships between landmarks, often resulting in them becoming lost in familiar places (Laczó et al., 2018). Speech and language difficulties may also be observed, and impairment in executive function becomes more pronounced, resulting in requiring assistance with daily activities (Klimova et al., 2015). At the severe stage of AD, cognitive decline may become so profound that patients no longer recognise their loved ones, speech may be completely lost, and they become fully reliant on caregivers for all aspects of daily living (Klimova et al., 2015; Werheid & Clare, 2007). As cognitive functions deteriorate, patients may develop dysphagia, which often results in severe weight loss near the end of life (Kalia, 2003). Dysphagia increases the risk of food or liquids entering the lungs, resulting in aspiration pneumonia, the leading cause of death in AD (Kalia, 2003; Manabe et al., 2015).

In addition to the cognitive deterioration of AD, there are also psychiatric and behavioural changes, often referred to as neuropsychiatric symptoms (NPS) (Chen et al., 2021a; Lyketsos et al., 2011; Lyketsos et al., 2002). As AD progresses, NPS become more pronounced, and their presence is associated with faster cognitive decline and earlier mortality (Chen et al., 2021a; Peters et al., 2015). In the mild

stage of AD, individuals may experience poor mental health characterised by depression and anxiety (Pless et al., 2023). If the patient is aware of their own decline in cognitive function, anxiety may be particularly heightened (Baillon et al., 2019; Farina et al., 2023). The patient may exhibit subtle apathy, appearing to have little motivation for activities they previously enjoyed, a symptom that is often mistaken for depression (Pless et al., 2023). The patient may exhibit rapid mood changes from depression to a state of mania, and appear irritable or frustrated (Koenig et al., 2016). In the moderate stage of AD, the patient may also become restless, agitated, and may exhibit impulsivity such inappropriate language or lack of social conduct (Migliaccio et al., 2020). The patient may also experience hallucinations, which often cause severe distress to individuals and caregivers (El Haj et al., 2017; Kaufer et al., 1998; Rocca et al., 2010). In severe AD, patient may also become physically and verbally aggressive towards others (Pless et al., 2023).

1.3 Pathological Features of Alzheimer's Disease

1.3.1 Amyloid Beta

In 1984, biochemists Glenner and Wong isolated Aβ from meningovascular deposits in patients with AD (Glenner & Wong, 1984). Now known to be neuritic plaques, Aβ was identified as the main constituent of these extracellular deposits (Cras et al., 1991). Subsequently, the *APP* gene was sequenced, confirming that Aβ is by-product of the processing of the APP molecule (Kang et al., 1987). The *APP* gene was later mapped to chromosome 21 (Tanzi et al., 1987). Genetic analysis of a family with AD (confirmed at most-mortem) revealed point mutations of the *APP* gene (Goate et al., 1991).

APP is widely produced in the brain, including in neurons, blood cells, and astrocytes (Hampel et al., 2021; Lee et al., 2008). The APP molecule spans the plasma membrane; the Aβ-coding domain is partially embedded in the membrane, the first 12-14 residues lie within the transmembrane domain, and the following residues protrude outside the membrane (Kang et al., 1987). APP is enzymatically processed via two main pathways; the α-secretase (non-amyloidogenic) and the β-secretase (amyloidogenic) pathways (Fig. 1.1) (Hampel et al., 2021). In the non-amyloidogenic pathway, α-secretase cleaves APP at a residue within the Aβ-coding domain, releasing a large, soluble N terminal APP fragment (APPsα) (Ling et al., 2023; Zhang et al., 2011). The remainder of the APP molecule, the C-terminal fragment (CTF-α), is cleaved by the γ-secretase enzyme, composed of presenilin-1 and presenilin-2 protein subunits, releasing a short peptide (p3) (Kepp et al., 2023; Ray et al., 2020). The APP intracellular domain (AICD) is subsequently released into the cytoplasm of the cell (Ng et al., 2024). In the amyloidogenic pathway, β-secretase (or β-APP-cleaving enzyme-1, BACE1) cleaves APP at a residue in the ectodomain upstream of the Aβ, again releasing a large soluble APP fragment (APPsβ) (Hampel et al.,

2021). Subsequently, γ-secretase cleaves the remaining C terminal fragment (CTF-β) at the cell membrane, the terminus of the Aβ region, often at residues 40 or 42, producing fragments of Aβ ($Aβ_{40}$ or $Aβ_{42}$) that are released into the extracellular domain, while the remaining AICD is internalised (Hampel et al., 2021). During physiological APP processing, AICD is transported to the nucleus where it serves as a transcription factor, influencing the expression of genes relating to cell cycle activation, apoptotic pathways, neurotransmission, and synaptic plasticity (Ng et al., 2024). However, evidence suggests that elevated AICD levels in AD are associated with the upregulation of pro-apoptotic genes, Ca^{2+} dysregulation, tau hyperphosphorylation, and neuroinflammation, all of which contribute to neurodegeneration (Ghosal et al., 2009; Ng et al., 2024).

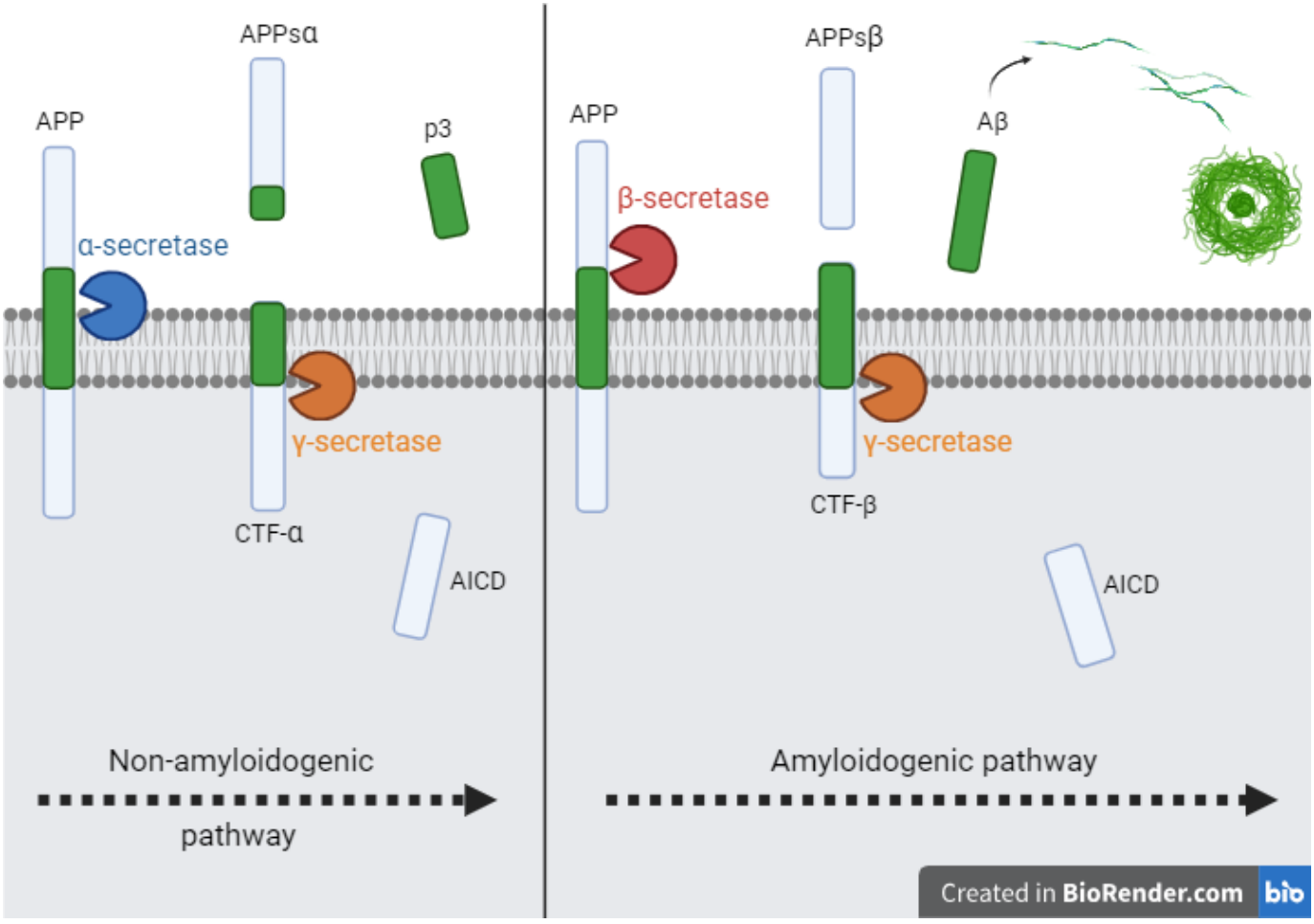

Figure 1.1: Non-amyloidogenic and Amyloidogenic Processing of Amyloid Precursor Protein. Amyloid Precursor Protein (APP) is enzymatically processed via two main pathways: the non-amyloidogenic pathway and the amyloidogenic pathway. In the non-amyloidogenic pathway, APP undergoes sequential cleavage by α-secretase and γ-secretase, which results in the creation of various fragments including APPsα, p3, and AICD (Zhang et al., 2011). In the amyloidogenic pathway, APP is first cleaved by β-secretase, releasing APPsβ, before undergoing γ-secretase processing. γ-secretase cleaves the remaining C terminal fragments at various sites, commonly at residues 40 or 42, resulting in the intracellular release of AICD and extracellular release of Aβ fragments, which undergo aggregation into oligomers, fibrils, and plaques (Hampel et al., 2021). Image created in https://BioRender.com.

The physiological function of APP and Aβ have been debated, with some theories suggesting that they may be neuroprotective at low levels (Masliah et al., 1992; Morley et al., 2019; Soucek et al., 2003). One identified physiological role of Aβ is its neurotrophic effect on immature hippocampal neurons *in vitro* (Yankner et al., 1990). It was later reported that immunodepletion of Aβ or inhibition of β and γ secretases reduced cultured neuronal cell viability, which was rescued by the addition of physiological concentrations of $Aβ_{40}$ (Plant et al., 2003). Highlighting the physiological role of APP and Aβ *in vivo*, APP and BACE1 knockout mice showed impaired hippocampal long-term potentiation (LTP; a synaptic model of memory) and cognitive deficits (Dawson et al., 1999; Laird et al., 2005; Seabrook et al., 1999; Wang et al., 2008). Moreover, intracerebral infusions of physiologically relevant concentrations of monomeric and oligomeric Aβ have been shown to enhance LTP and improve spatial memory performance in rodents (Puzzo et al., 2008; Wu et al., 1995).

In AD, Aβ abnormally aggregates in the brain, primarily in the cortex and hippocampus (HPC) but also within the cerebrovasculature (Chen et al., 2017; Viswanathan & Greenberg, 2011). The Aβ monomers generated from the proteolytic breakdown of APP associate into dimers and trimers, intermediate aggregate states (Hampel et al., 2021). These small α-helical structures can aggregate to form much larger oligomers that are susceptible to spreading throughout the brain (Hampel et al., 2021). Aβ further aggregates within the brain as insoluble protofibrils and fibrils (Walsh et al., 1997). $Aβ_{42}$ is less soluble than $Aβ_{40}$ and thus more likely to form further aggregates (Chen et al., 2017; Snyder et al., 1994; Wang et al., 1999). Protofibril and fibril structures are organised into β-sheets with a stable core (Chen et al., 2017; Hashimoto et al., 2020) and subsequently assemble into plaques that form the characteristic histological lesions first noted by Alzheimer in 1906 (Alzheimer et al., 1995; Lu et al., 2013; Walsh et al., 1997). These extracellular Aβ aggregates have been shown to cause interference in neuronal networks, disrupting memory encoding communications (Mokhtar et al., 2013; Shankar et al., 2008).

Amyloid in its aggregated plaque formation is detectable using *in vivo* PET imaging, but soluble amyloid species evades detection as they do not bind to amyloid PET ligands (Chapleau et al., 2022). Due to the challenges in distinguishing the direct consequences of soluble amyloid from plaques in AD models, research has largely focused on plaques as the primary pathogenic form of Aβ. However, recent studies have increasingly suggested that soluble amyloid is more neurotoxic and plays a crucial role in driving early AD pathogenesis (Tolar et al., 2021; Viola & Klein, 2015). For example, in cell culture, soluble Aβ have been shown to induce synaptic degeneration via NMDAR dysfunction, promote Ca^{2+} dysregulation, tau hyperphosphorylation, and induce neuronal death (Bode et al., 2017; De Felice et al., 2007; Jin et al., 2011; Joshi et al., 2023; Lambert et al., 1998; Ono et al., 2009; Shankar et al., 2007). Furthermore, *in vivo* infusion of oligomeric Aβ has been shown to trigger a range of pathological events including neuroinflammation, synaptic

plasticity dysfunction, and behavioural impairments (Forloni & Balducci, 2018; Lourenco et al., 2013; Reed et al., 2011; Townsend et al., 2006). These key pathological events in AD will be described below under The Amyloid Cascade Hypothesis, with further detail regarding Ca^{2+}-mediated toxicity and synaptic dysfunction reserved for Chapter 4 of this thesis.

1.3.2 The Amyloid Cascade Hypothesis

1.3.2.1 AD Risk Factors and Initiating Events

The Amyloid Cascade Hypothesis was first described in the early 1990s by Hardy and Higgins (Hardy & Higgins, 1992). It was hypothesised that the deposition of Aβ peptides in the brain initiates a series of pathological events including immune dysregulation, NFT accumulation, vascular damage, and neuronal loss, that eventually result in the cognitive dysfunction observed in AD (Fig 1.2) (Hardy & Higgins, 1992; Zhang et al., 2023b). The cause of aberrant accumulation of Aβ is still not fully understood, however it is posited that it involves an imbalance between the production and clearance of Aβ from the brain, resulting in its accumulation and aggregation (Hampel et al., 2021). In FAD, Aβ accumulation is genetically driven, with genetic sequencing studies identifying mutations in the *APP, Presenilin 1 (PSEN1), and Presenilin 2 (PSEN2)* genes in families with a history of FAD (Dorszewska et al., 2016; Levy-Lahad et al., 1995; Rogaev et al., 1995; Sherrington et al., 1995). These mutations are believed to disrupt the normal cleavage of APP, resulting in excessive Aβ production, particularly the more aggregation prone $Aβ_{42}$ peptide (Borchelt et al., 1997; Duff et al., 1996; Hampel et al., 2021; Li et al., 2016; Scheuner et al., 1996). In SAD, Aβ accumulation is believed to be due to the failure of proteostasis networks, cellular mechanisms that maintain the balance of synthesis, folding, and degradation of proteins, resulting in insufficient clearance and thus aggregation of Aβ (Hampel et al., 2021; Mawuenyega et al., 2010). SAD is not strictly a genetic condition, with age being one of the primary risk factors; however, age alone is not sufficient to cause AD (Nelson et al., 2011). SAD involves a complex interplay between age and several environmental factors, including diabetes, obesity, smoking, hypertension, and lack of cognitive engagement (Baumgart et al., 2015). However, genetic predisposition likely plays a role in SAD, with family history of the disease being another significant risk factor (Fratiglioni et al., 1993; Green et al., 2002; Lautenschlager et al., 1996). Several studies including genome wide association studies have identified the Apolipoprotein E (APOE) ε4 allele, a variant of the *APOE* gene involved in Aβ clearance, is the most significant genetic risk factor for SAD (Allwright et al., 2023; Corder et al., 1993; Farrer et al., 1997; Neuner et al., 2020; Rebeck et al., 1993). The presence of this allele significantly accelerates AD progression, reducing the average age of onset by around 10 years (Corder et al., 1993; Hunsberger et al., 2019).

1.3.2.2 Altered Ionic Homeostasis and the Calcium Hypothesis of AD

According to the Amyloid Cascade Hypothesis, Aβ disrupts the balance of key ions, including calcium (Ca^{2+}) (Wang et al., 2025). Ca^{2+} is a second messenger molecule that is essential for neuronal functions such as neurotransmitter release, synaptic plasticity, and apoptosis (Berridge et al., 2000). These functions depend on tightly regulated spatiotemporal fluctuations of Ca^{2+} concentrations, achieved through mechanisms involving the endoplasmic reticulum (ER), plasma membrane channels and transporters, and mitochondria (Cascella & Cecchi, 2021). The Calcium Hypothesis of AD, which will be discussed in greater depth in Chapter 4 of this thesis, proposes that dysregulation of physiological intracellular Ca^{2+} signalling plays a pivotal role in the development and progression of the disease (Joshi et al., 2023). In AD, intracellular Ca^{2+} signalling is disrupted through multiple mechanisms, including by the presence of Aβ (Joshi et al., 2023). Oligomeric Aβ promotes excessive Ca^{2+} influx into neurons through N-methyl-D-aspartate receptors (NMDARs), voltage-gated channels (VGCCs), and possibly through the formation of membrane pores (Tong et al., 2018). This leads to the release of Ca^{2+} from internal stores of the neuron, including the ER, further exacerbating the Ca^{2+} load of the cell (Ferreiro et al., 2004; Supnet et al., 2006). Aβ also impairs glutamate reuptake following synaptic transmission, resulting in NMDAR overactivity and neuronal excitotoxicity (Koffie et al., 2011; Li & Selkoe, 2020). Aβ-induced remodelling of Ca^{2+} signalling pathways impairs mitochondrial function, triggering oxidative stress, stimulating neuroinflammation, leading to neuronal death (Garcia-Casas et al., 2023; Joshi et al., 2023). A wealth of *in vivo* infusion and *in vitro* neuronal culture studies has shown that soluble amyloid species isolated from AD brains (at pathological levels) impair hippocampal LTP, a process essential for synaptic strengthening and memory formation, while promoting LTD, which weakens synaptic connections — effects attributed to overactivation of NMDARs (Gulisano et al., 2018; Li et al., 2009; Li et al., 2011; Li et al., 2018; Li & Selkoe, 2020; Puzzo et al., 2008; Shankar et al., 2007; Shankar et al., 2008; Walsh et al., 2002). These mechanisms not only directly contribute to cognitive decline, but also exacerbate both Aβ and tau pathologies, creating a vicious cycle of neurodegeneration (Wang et al., 2017).

1.3.2.3 Immune Dysregulation

In AD patients and many animal models of AD, Aβ accumulation leads to the chronic overactivation of the brain's immune system, commonly recognised as a hallmark of AD alongside Aβ plaques and NFTs (Kinney et al., 2018). Some of the most compelling evidence linking neuroinflammation and AD is from mutations in Triggering Receptor Expressed on Myeloid Cells 2 (TREM2) and Complement Receptor Type 1 (CR1) genes involved in immune regulation, which are associated with an increased risk of SAD (Guerreiro et al., 2013; Jonsson et al., 2013; Zhu et al., 2015).

In the healthy brain environment, microglia, the resident immune cells, activate in response to threats such as injury or disease (Kinney et al., 2018). Microglia also play a crucial neuroprotective role by clearing proteins and cellular debris, including Aβ, through phagocytosis (Galloway et al., 2019). Microglia migrate to plaques, and during Aβ clearance, release a number of pro-inflammatory cytokines such as tumour necrosis factor alpha (TNF-α), interleukins such as IL-1β and IL-6, complement component 1q, and reactive oxygen species (ROS) (Wang et al., 2015). Prolonged microglial activation in AD driven by persistent Aβ deposition results in increased production of pro-inflammatory cytokines and ROS, which disrupt synaptic function and stimulate neuronal apoptosis, contributing to neurodegeneration (Ji et al., 2019; Wang et al., 2015). Additionally, sustained microglial activation diminishes their ability to bind, engulf, and degrade Aβ, thereby exacerbating its accumulation (Krabbe et al., 2013; Michelucci et al., 2009). Aβ accumulation also activates astrocytes, which are crucial for maintaining homeostasis in the central nervous system (CNS) (Verkhratsky & Nedergaard, 2018). Sustained astrocyte activation impairs their homeostatic function, resulting inefficient glutamate clearance and excitotoxicity, blood-brain barrier (BBB) breakdown, and neuronal damage due to impaired neurotrophic support (Rodríguez-Giraldo et al., 2022). Astrocyte overactivation also results in sustained neuroinflammation through the release of pro-inflammatory cytokines (Rodríguez-Giraldo et al., 2022). Furthermore, persistent release of pro-inflammatory cytokines through chronically activated microglia and astrocytes stimulates the amyloidogenic processing of APP through activating β-secretase and γ-secretase, resulting in further Aβ deposition (Liao et al., 2004; Zhao et al., 2011).

In addition to the cytotoxic positive feedback associated with Aβ, the inflammatory response observed in AD has been proposed as a potential link between Aβ and NFT development (Garwood et al., 2011; Kitazawa et al., 2004). Evidence supporting this includes the administration of lipopolysaccharide, a known inducer of neuroinflammation, significantly increased tau hyperphosphorylation in 3xTg-AD mice, a transgenic model containing mutant *APP*, *PSEN1*, and *Microtubule Associated Protein Tau (MAPT)* genes (Kitazawa et al., 2005). Similarly, the application of Aβ oligomers to a hippocampal culture significantly increased tau phosphorylation (Ma et al., 2009).

1.3.2.4 Neurofibrillary Tangle Development

Tau is a soluble microtubule-associated protein, encoded by the *MAPT* gene, that is essential for maintaining the stability of microtubules; key cytoskeletal structures that support cell differentiation and growth (Barbier et al., 2019). Tau is dynamically regulated by a number of post-translational modifications, including phosphorylation and dephosphorylation, carried out by kinases and phosphatases, respectively (Parra Bravo et al., 2024). In neurodegenerative diseases such as frontotemporal dementia and AD, tau becomes hyperphosphorylated (Grundke-Iqbal et al., 1986;

Parra Bravo et al., 2024). In AD, the Amyloid Cascade Hypothesis postulates that Aβ, through its disruption of ionic homeostasis (Fig. 1.2), triggers changes in kinase and phosphatase activity, including hyperactivation of kinases such as glycogen synthase kinase-3β and cyclin-dependent kinase 5, and reduced activity of phosphatase such as protein phosphatase 2A, resulting in hyperphosphorylated tau (Reddy, 2013; Wang et al., 2020). Hyperphosphorylated tau has a reduced affinity for binding microtubules, thus it detaches (Sengupta et al., 1998). Hyperphosphorylation of tau also disrupts its normal structure, causing it to misfold (Mroczko et al., 2019). Misfolded tau proteins clump together into oligomers, that aggregate into paired helical filaments and eventually NFTs, insoluble filamentous tangles (Grundke-Iqbal et al., 1986; Parra Bravo et al., 2024; Perl, 2010). In the AD, these filaments accumulate intracellularly, particularly within neuronal cell bodies and dystrophic neurites (Braak et al., 1986). NFTs contribute to neurodegeneration by destabilising microtubules, which disrupts axonal transport of key molecules such as neurotransmitters and cellular nutrients, hindering neuronal communication and triggering cell death (Alonso et al., 1994; Li et al., 2007). NFTs also trigger a cascade of neuroinflammation through microglia overactivation and induce neurotoxicity, resulting in neuronal dysfunction and cell death (Chen & Yu, 2023; Parra Bravo et al., 2024).

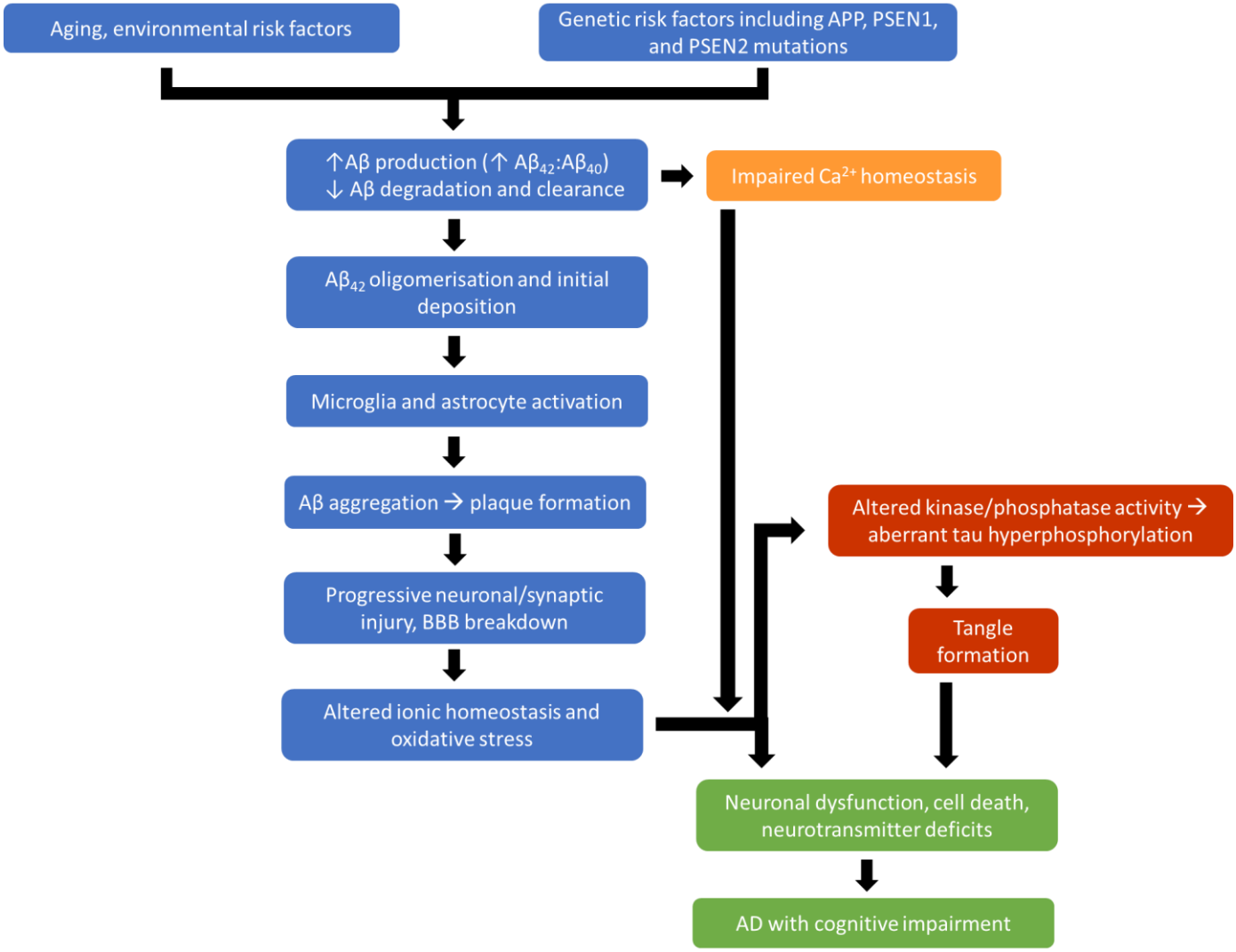

Figure 1.2: The Amyloid Cascade Hypothesis of Alzheimer's Disease; as recently reviewed in Zhang et al., 2023b.

1.3.2.5 Supporting Evidence and Counterarguments for the Amyloid Cascade Hypothesis

Since identified by Alzheimer in 1906, Aβ plaques have consistently been observed in post-mortem analysis of brain tissue from AD patients, indicating the role of Aβ as a key pathological feature of AD (Alzheimer et al., 1995; Hong et al., 2023). Since then, multiple lines of evidence have suggested that this characteristic accumulation of Aβ usually occurs many years before the onset of clinical symptoms, preceding NFT development and synaptic loss (Hampel et al., 2021). As described earlier, the Amyloid Hypothesis of AD suggests that the accumulation of Aβ in the brain is the initiating event in the pathogenesis of AD, leading to a cascade of pathological events including tau hyperphosphorylation, neuronal loss, and cognitive decline (Dubois et al., 2014). Arguably, the most compelling argument for this hypothesis stems from the fact that FAD mutations, most of which result in increased amyloid aggregation, are associated with early onset AD (Hatami et al., 2017; Ricciarelli & Fedele, 2017). Most FAD mutations are in close proximity to secretase sites and thus affect the processing of APP (van der Kant & Goldstein, 2015). For example, FAD mutations in *APP*, *PSEN1*, and *PSEN2* alter the proteolytic cleavage of APP, increasing the production of self-aggregating $A\beta_{42}$ species (Borchelt et al., 1997; Chen et al., 2014; De Jonghe et al., 2001; Suzuki et al., 1994). Furthermore, as discussed earlier, the most significant genetic risk factor for developing SAD is the presence of the APOE ε4 variant, which is associated with impaired Aβ clearance and increased aggregation (Allwright et al., 2023). Conversely, the rare A673T *APP* variant that reduces Aβ production appears to protect against AD development (Baranello et al., 2015). Further genetic evidence supporting the central role of amyloid in AD comes from individuals with Down's syndrome, who possess an extra copy of chromosome 21 (which also carries the *APP* gene), leading to increased amyloid production and early-onset dementia (Leverenz & Raskind, 1998; McCarron et al., 2014; Wiseman et al., 2015).

However, there are several streams of evidence that are inconsistent with the idea of amyloid as the root cause of AD. Arguably the strongest counterargument for the central role of amyloid in AD is the fact that Aβ plaque burden does not consistently correlate to neuronal loss or the severity of cognitive decline (Aizenstein et al., 2008). In fact, individuals with substantial Aβ burden do not always present with cognitive symptoms of AD (Klunk, 2009; Villemagne et al., 2011). According to the Amyloid Cascade theory, these individuals should have dementia, but they do not, suggesting that amyloid accumulation may be a feature of healthy aging. The duration for which Aβ can persist in the brain with without causing cognitive decline is unknown, however it is believed to be in the magnitude of years (Villemagne et al., 2013). Naturally, this raises a question about the extent of the contribution of Aβ to the pathogenesis of AD. It could be argued that if it is possible to possess Aβ plaques without exhibiting dementia, then amyloid is insufficient to cause AD. However, a large body of evidence suggests that soluble Aβ species, rather than insoluble plaques, is more neurotoxic and correlates better with the severity of

cognitive deficits (Bao et al., 2012; Tolar et al., 2021). This may explain why some people with substantial plaque load are cognitively normal, with studies suggesting that their oligomeric Aβ levels are low in comparison to plaque load (Esparza et al., 2013).

Nevertheless, NFTs and neuronal loss appear to exhibit a stronger correlation with cognitive decline than amyloid plaque volume (Giannakopoulos et al., 2003). As such, there has been a lot of debate around the relative importance of amyloid and tau in the pathogenesis of AD. According to the Amyloid Cascade Hypothesis, NFTs are a downstream consequence of amyloid deposition (Kepp et al., 2023). A common analogy for the relationship between the two pathologies describes Aβ as the trigger that initiates the pathology, while tau acts as the bullet that inflicts the damage (Bloom, 2014). Supporting this, studies show that neurons deficient in tau are resistant to Aβ-induced toxicity, suggesting that amyloid is the initiating factor but tau is required for its toxic effect (Rapoport et al., 2002). Furthermore, reducing the number of tau alleles in the transgenic hAPPxTau and APP/PS1xTau mouse models protects against memory deficits and Aβ-driven neurotoxicity, emphasizing the critical role of tau in mediating neurodegeneration initiated by Aβ (Leroy et al., 2012; Roberson et al., 2007). However, other studies have shown that tau pathology precedes amyloid deposition (Braak et al., 2011; Price et al., 1991; Schönheit et al., 2004). Furthermore, there is evidence that tau can induce neurodegeneration independently of Aβ. For example, intracerebral injection of a viral vector to express an isoform of Tau in the HPC of C57BL6/J mice induced cortical and hippocampal cell death even in the absence of Aβ (Jaworski et al., 2009). This finding directly challenges the notion that tau pathology is merely a downstream consequence of amyloid aggregation, instead suggesting that tau may have a more primary role in disease progression.

A further challenge to the Amyloid Cascade Hypothesis is that transgenic mice exhibiting Aβ overexpression as the sole disease model do not sufficiently mirror every aspect of AD. For example, whilst transgenic modes overexpressing mutant *APP* and/or *PSEN1* capture some of the pathological and behavioural features of AD, such as plaques, neuroinflammation, alterations in synaptic plasticity, and memory impairment, there is no widespread neuron loss, and any neurodegeneration by these models appears mild and rescuable (Wirths & Zampar, 2020; Zhong et al., 2024). Even refined 2nd generation mouse models with endogenously expressed *APP* show early and substantial Aβ deposits but exhibit only modest behavioural deficits and no overt neurodegeneration, suggesting that high levels of Aβ alone do not trigger neurodegeneration *in vivo* (Sasaguri et al., 2022). Furthermore, NFTs do not naturally emerge in amyloid-based mouse models without specific genetic modifications to express tau proteins. This contradicts the idea that tau is a downstream consequence of amyloid accumulation.

The failure of mouse models to fully replicate AD pathology highlights the gaps in the understanding of genetic factors and the complex mechanisms underlying the pathogenesis of AD. For example, while most FAD mutations are known to result in increased Aβ deposition in the brain, this alone does not confirm Aβ as the primary driver of AD and it does not prove that Aβ triggers other AD pathologies (Herrup, 2015). This limitation suggests that mouse models based solely on FAD mutations do not accurately capture AD pathogenesis. Several pharmacological approaches aimed at reducing Aβ levels using antibody-based therapies have successfully decreased amyloid burden and improved cognitive deficits in mouse models of Aβ pathology, prompting the launch of many clinical trials targeting Aβ as a potential treatment for AD (Yadollahikhales & Rojas, 2023; Zhang et al., 2023b). However, many clinical trials targeting amyloid have failed, with few achieving Food and Drug Administration (FDA) approval. As will be discussed in section 1.4 of this chapter, anti-amyloid drugs that were granted FDA approval show only modest clinical benefit. This suggests that research may have been over reliant on amyloid as the central cause of AD, overlooking other potential causative factors. The complex aetiology of AD likely involves multiple mechanisms, including inflammation, tau pathology, and synaptic and biochemical alterations, which cannot be fully encompassed by a single theory. For example, the early onset of AD in individuals with Down's syndrome may not be solely due to the extra copy of the *APP* gene on chromosome 21, as this chromosome contains over 200 other genes, including those required for Ca^{2+} binding and ion channel formation (Kepp et al., 2023). Therefore, while this doesn't necessarily disprove the involvement of Aβ in AD, it suggests that there may be several contributing factors to AD pathogenesis, such as Ca^{2+} dysregulation, that should be directly addressed, as will be discussed later in this thesis. Therefore, it is very possible that a unique combination of genetic and environmental risk factors initiates an equally unique cocktail of biochemical alterations in the human brain. With this idea, there may be a common path to AD but multiple ways of accessing this path, with amyloid being a frequent but not necessarily essential path.

Despite its limitations, the Amyloid Cascade Hypothesis remains a central framework in the current understanding of AD pathogenesis, as it does appear to be linked to several other hallmarks of the disease. However, there is a pressing need to better understand how Aβ influences cognition and other biochemical changes, such as Ca^{2+} dysregulation, in more advanced and accurate mouse models of amyloid pathology, as will be discussed later in this chapter.

1.3.3 Anatomical and Functional Changes

As discussed in the previous section, the key pathological hallmarks of AD, including Aβ plaques, NFTs, and neuroinflammation, contribute to cellular neurotoxicity

(Hampel et al., 2021). On a broader scale, these factors have a substantial impact on the brain and its function.

Throughout the progression of AD, plaques and NFTs follow distinct patterns of deposition in the brain. Imaging studies evidence that Aβ initially accumulates in brain regions with high metabolic activity, such as the association cortex, then spreads across the neocortex and continues to the allocortex, including the HPC and entorhinal cortex (EC), before depositing in other subcortical regions such as the basal ganglia, midbrain, and eventually the cerebellum (Hampel et al., 2021; Thal et al., 2002; Ávila-Villanueva et al., 2022). NFT deposition follows a different pattern, originating in the transentorhinal region, before progressing to the EC, HPC, and neocortex (Braak & Braak, 1991; Parra Bravo et al., 2024; Ávila-Villanueva et al., 2022). NFTs spread in a prion-like manner by imparting their misfolded state onto soluble tau molecules, transmitting across synapses, and propagating the spread (Mroczko et al., 2019; Parra Bravo et al., 2024).

As described earlier, pathological events in AD, including Aβ and NFT accumulation, Ca^{2+} dysregulation, and chronic neuroinflammation, contribute to neurodegeneration in AD (Hampel et al., 2021; Parra Bravo et al., 2024). This occurs through synaptic degeneration, neuronal loss, and axonal damage due to myelin breakdown, progressively disrupting large scale brain network connectivity and communication (Goel et al., 2022; Huang et al., 2024). This progressive neuronal injury contributes to the decline of cognitive function in AD (Goel et al., 2022; Griffiths & Grant, 2023). Eventually, synaptic loss progresses to cerebral atrophy, which appears to follow a similar pattern of progression to tau progression (Whitwell, 2010). These key structural abnormalities correlate to functional impairments in AD. For example, hippocampal volume loss correlates with severity of episodic memory impairments in MCI and AD (McDonald et al., 2012; Sarazin et al., 2010). Furthermore, early atrophy of the amygdala and EC are linked to anxiety in AD (Mah et al., 2015; Poulin et al., 2011).

Neuronal loss in AD is closely linked to glucose hypometabolism, as detected by fluorodeoxyglucose (FDG)-PET, an *in vivo* marker of synaptic activity (Chen et al., 2021b; Strom et al., 2022). For example, medial temporal lobe atrophy is related to hypometabolism of the RSC, one of the first areas to show metabolic changes in AD, indicating reduced synaptic activity and neurodegeneration (Buckner et al., 2005; Drzezga et al., 2011; Minoshima et al., 1997; Nestor et al., 2003; Strom et al., 2022; Terstege et al., 2024). Neurotransmitter systems are also altered in AD. For example, the loss of cholinergic neurons, decline in choline acetylase, and subsequent reduction of acetylcholine (ACh) synthesis and release, is linked to deficits in learning and memory (Yang et al., 2023). Furthermore, as eluded to earlier, excessive activation of NMDARs by enhanced glutamate release result in increased levels of glutamate in the synapse, further enhancing Ca^{2+} entry and

contributing to neuronal death and cognitive decline (Liu et al., 2019). Moreover, degeneration of dopaminergic and serotonergic neurons leads to the reduced levels of dopamine and serotonin, respectively, affecting mood and motivation (Vakalopoulos, 2017; Yamamoto & Hirano, 1985; Yang et al., 2023). Overall, these key anatomical and functional changes contribute to the cognitive deficits and neuropsychiatric dysfunction observed in AD.

1.4 Current and Developing Treatments for Alzheimer's Disease

Currently, treatments for AD focus on symptom management. For example, acetylcholinesterase inhibitors (AChIs) such as donepezil (Aricept™), rivastigmine (Exelon™), and galantamine (Razadyne®) are used for mild to moderate AD (Yiannopoulou & Papageorgiou, 2020). These drugs work by preventing the breakdown of ACh, thus restoring synaptic communication and memory processes (Singh et al., 2024). Memantine (Namenda®) is an NMDAR antagonist used for moderate to severe AD and is thought to preserve neuronal function by selectively blocking excessive glutamate activity, restoring Ca^{2+} homeostasis and reducing excitotoxicity (Plosker, 2015). Patients with moderate to severe AD may also be offered a combination of memantine and donepezil (Yiannopoulou & Papageorgiou, 2020).

Drugs to manage NPS are often prescribed alongside drugs to improve cognitive symptoms. For example, selective serotonin reuptake inhibitors (SSRIs) such as sertraline are commonly prescribed for anxiety and/or depression in AD (Scuteri et al., 2021). SSRIs work by inhibiting the reuptake of serotonin into presynaptic neurons, thereby increasing its availability in synapses and enhancing its signalling, which supports mood regulation (Hillhouse & Porter, 2015). Furthermore, short-term anxiolytic drugs such as benzodiazepines (e.g. lorazepam) may be prescribed, and act by rapidly enhancing the inhibitory effects of gamma-aminobutyric acid (GABA) on GABA-A receptors, reducing neural hyperactivity and producing an anxiolytic effect (Insel et al., 1984; Mendez, 2021). However, these are prescribed conservatively as they may increase the risk of confusion, poor gait, and falls in AD patients (Osman et al., 2022). In cases where anxiety is associated with agitation, physical aggression, or psychosis, an atypical antipsychotic medication such as risperidone may be prescribed, however, it carries an FDA black-box warning due to the increased risk of stroke and mortality with its use in AD (Mendez, 2021; Scuteri et al., 2021).

While these treatments may help alleviate symptoms and improve the quality of life for some patients, they address downstream effects rather than the root pathological causes, and thus they do not slow cognitive decline. Consequently, there is a need

for new disease modifying therapies to prevent, slow, or reverse AD pathology. Recently, several therapies have been developed to address the root cause of AD pathogenesis, particularly by targeting Aβ accumulation, however there has been very limited clinical success.

Recently, marketed as disease modifying therapies, aducanumab (Aduhelm®) and lecanemab (Leqembi®) have received accelerated FDA approval (Vaz et al., 2022; Vitek et al., 2023), and donanemab (Kisunla™) has gained traditional FDA approval for AD treatment (Mintun et al., 2021). These anti-amyloid antibodies promote plaque clearance by binding aggregated amyloid, triggering microglial phagocytosis, direct amyloid hydrolysis, and promoting Aβ efflux via a peripheral sink mechanism (Loeffler, 2023; Singh et al., 2024; Taguchi et al., 2008). Lecanemab and donanemab are now licenced by the Medicines and Healthcare Products Regulatory Agency (MHRA) in the UK as a treatment for early-stage AD, with aducanumab currently under review. However, the National Institute for Health and Care Excellence (NICE) have not recommended any of these drugs for use in the NHS due to concerns over cost-effectiveness, limited clinical benefit, and safety risks. Crucially, the major side effect associated with these antibodies is the development of amyloid-related imaging abnormalities (ARIAs), which present as cerebral oedemas or microhaemorrhages and can lead to serious complications, potentially overshadowing any clinical benefit of the treatment (Honig et al., 2024; Salloway et al., 2022).

Driven by the limitations of current therapies, new strategies are emerging. Remternetug, a next-generation anti-amyloid treatment developed as a successor to donanemab, targets pyroglutamated Aβ (a highly stable neurotoxic variant) and is currently in Phase III clinical trials. Additionally, small molecule therapies, such as buntanetap, are being explored for their BBB penetration and oral/intranasal availability (Wu et al., 2023). Buntanetap blocks *APP* mRNA translation to prevent, rather than clear, amyloid accumulation (Fang et al., 2023). However, whether these new approaches will offer greater clinical benefit or reduce side effects like ARIAs remains uncertain.

1.5 Modelling Alzheimer's Disease

1.5.1 1st Generation Models

The hope of identifying new disease modifying drugs for AD relies on the development of robust animal models to provide a reliable basis for preclinical testing. Since 1995, efforts have largely focused on developing transgenic mouse models of AD through overexpression of well characterised genetic mutations

associated with FAD. Transgenic models of AD typically exhibit modest to severe behavioural deficits that often emerge before detectible plaque deposition, with spatial working memory impairments generally preceding simple object recognition deficits (Zhong et al., 2024).

One of the earliest of these first generation models is the PDAPP model (Games et al., 1995). This model expresses human *APP* carrying the Indiana (V717F) FAD mutation, with expression levels approximately 10-fold higher than endogenous murine *App* (Games et al., 1995). Consequently, PDAPP mice develop amyloid plaques from around 6-9 months of age (Games et al., 1995). This model also exhibits evidence of enhanced astrocyte and microglia activation, early changes in tau phosphorylation, and decreased synaptic density, but no overt neuron loss (Games et al., 1995; Masliah et al., 2001). The PDAPP model exhibits functional impairments across a broad array of cognitive tasks, including deficits in spatial working memory assessed by the Radial Arm Maze (RAM) task at 3-4 months, and impaired object recognition memory from 6 months of age (Dodart et al., 1999). Another widely used transgenic model is the Tg2576, which expresses the Swedish *APP* FAD mutation (KM670/671NL) (Hsiao et al., 1996). This mutation is located at the BACE1 cleavage domain of the *APP* gene, enhancing *APP* cleavage by β-secretase and resulting in increased Aβ production, particularly the $A\beta_{42}$ variant (Hsiao et al., 1996). Tg2576 mice develop plaques at around 11-13 months and increased microglial density and size associated with plaques (Frautschy et al., 1998; Hsiao et al., 1996). Tg2576 animals also show earlier impairments prior to plaque formation such as dendritic spine loss at 4.5 months and LTP impairments at 5 months, but no evidence of NFTs or neuron loss (Irizarry et al., 1997; Jacobsen et al., 2006; Lanz et al., 2003). Tg2576 mice develop deficits in spatial learning and working memory at around 9-14 months of age (Deacon et al., 2008; Hsiao et al., 1996; Kawarabayashi et al., 2001), with visuospatial deficits in object recognition tasks appearing at around 14 months (Hale & Good, 2005).

Double and triple transgenic models of AD were developed in an attempt to better capture the complex pathologies of AD, as well as to accelerate the onset of pathology and cognitive deficits. The APP/PS1 model contains both the Swedish mutant *APP* and a human *PSEN1* gene containing the L166P mutation (Radde et al., 2006). The APP/PS1 model develops plaques and activated microglia from as early as 6 weeks of age, with dendritic spine loss occurring around 4 weeks after plaque development (Bittner et al., 2012; Radde et al., 2006). There is also evidence of impaired hippocampal LTP at 8 months and modest neuron loss at 17 months (Gengler et al., 2010; Rupp et al., 2011). APP/PS1 mice also show phosphorylated tau in neuritic processes, but no mature NFTs (Radde et al., 2006). Cognitive impairments include spatial learning and memory in the Morris Water Maze (MWM) task at 7 months and novel object recognition at 15 months of age (Radde et al., 2006; Webster et al., 2013).

The 5xFAD is a triple transgenic model that harbours three *APP* mutations (Swedish (K670N/M671L), Florida (I716V), and London (V717I)) and two *PSEN1* mutations (M146L and L286V) (Oakley et al., 2006). This model exhibits plaque deposition and gliosis from around 2 months of age (Oakley et al., 2006). There is also evidence of LTP deterioration from 4 months of age, and cortical neuron loss from around 6 months of age (Eimer & Vassar, 2013; Oakley et al., 2006). The 5xFAD model exhibits impaired alternation in the Y-maze spontaneous alternation task from 4 months of age, impaired spatial memory in the MWM task at 6 months, with object recognition deficits occurring around the same age (Oakley et al., 2006; Pádua et al., 2024; Xiao et al., 2015). Importantly, however, NFTs do not develop in this model (Oakley et al., 2006). The 3xTg-AD triple transgenic model was developed to capture both amyloid and tau pathology by expressing the MAPT P301L mutation in addition to the Swedish *APP* and M146V *PSEN1* mutation (Oddo et al., 2003). These animals exhibit reduced LTP by 4 months, plaque deposition from 6 months, and increased microglia and astrocyte immunoreactivity from 7 months (Caruso et al., 2013; Javonillo et al., 2021; Oddo et al., 2003). Spatial learning and memory deficits in the MWM arise at around 4-6 months (Belfiore et al., 2019; Billings et al., 2005). Tau pathology occurs at around 12 months, with extensive hyperphosphorylated tau detected in the CA1, however, no neuron loss was observed (Oddo et al., 2003; Zhong et al., 2024). Since the 3xTg-AD model, several tau-specific models such as the PS19 and Tg4510 have been generated to isolate tau driven pathologies. These mice exhibit early NFT formation, as well as rapid neuronal loss, and an age dependent decline in spatial memory (Zhong et al., 2024). However, as will be discussed in the General Discussion chapter, the accuracy of modelling human tau pathology in rodents is questionable due to differences in splicing of the *MAPT* gene and aggregation of tau filaments (Corsi et al., 2022; Hernández et al., 2019).

Overall, transgenic models of AD have been valuable for investigating the mechanisms and consequences of Aβ accumulation, however, there are several key criticisms regarding their suitability and accuracy. The primary critiques centre on the overexpression of the relevant transgenes and the method used to drive their overexpression. Transgenic models are often created by the insertion of a genetic construct containing the gene(s) of interest into a mouse embryo or embryonic stem cells. A DNA plasmid vector, a circular piece of extrachromosomal DNA, is often used to carry the selected genes and integrate them randomly into the host DNA. The plasmid constructs contain an artificial promotor, commonly the Thy1 promotor, that drives aberrant overexpression of the transgene in the host. For example, in the Tg2576 model, *APP* harbouring the Swedish mutation is randomly inserted into the mouse genome using a hamster prion cosmid vector, resulting in *APP* expression at levels that are far beyond that observed in AD (Hsiao et al., 1996). There are several issues with this method of developing animal models. For instance, random integration of genetic constructs has been shown to destruct large portions of the host's genetic loci (Gamache et al., 2019). Moreover, expression of the mutant *APP* may not necessarily be specific to axons, as it has been shown to mislocalise to soma and dendrites (Sasaguri et al., 2022). Furthermore, overexpression of *APP* in

transgenic models results in an overexpression of the non-amyloid fragments produced from the processing of APP, and the effects of which remain unclear. For example, in the Tg2576 model, the Swedish mutation increases the production and accumulation of CTF-β, generated from the cleavage of APP by β-secretase, and AICD, generated from γ-secretase cleavage (Sasaguri et al., 2022). CTF-β have been shown to induce neurotoxicity, leading to synaptic loss and memory impairments *in vivo* (Kametani & Haga, 2015; Kaur et al., 2017; Kwart et al., 2019; Lauritzen et al., 2012; Oster-Granite et al., 1996; Sasaguri et al., 2022). Additionally, AICDs have demonstrated neurotoxic effects *in vivo*, while also transactivating neprilysin gene promoters, which play a crucial role in driving Aβ-degradation (Kim et al., 2003; Ohkawara et al., 2011; Pardossi-Piquard et al., 2005). Aberrant *APP* overexpression is also linked to ER stress, and calpain activation resulting in generation of p25, a contributor to tau phosphorylation and neuronal apoptosis (Hashimoto et al., 2018; Lee et al., 2000).

Whilst aberrant transgene overexpression is convenient for studying Aβ as it leads to substantial plaque deposition and early cognitive impairments, the consequences of its effects remain poorly understood, and likely introduce behavioural confounds that standard control strains (e.g. C57BL6/J animals) cannot account for. It could therefore be argued that the behavioural effects of *APP* overexpression may not actually reflect the consequences of Aβ accumulation. For example, transgenic models often exhibit early behavioural changes that precede plaque deposition, suggesting that these changes may be due to the accumulation of non-amyloid products of APP processing (Zhong et al., 2024).

1.5.2 2nd Generation Models

Overall, aberrant *APP* overexpression and its associated artefacts present a problem as i) it is not clear to what extent Aβ is responsible for any behavioural changes in the presence of additional cellular artefacts and ii) it does not accurately mimic the brain environment of an AD patient and so does not present a reliable basis for drug development. This key limitation may offer an insight into why drug treatments tested using these models often fail in clinical trials.

A 2nd generation of mouse models were developed to overcome the shortcomings of transgenic models by achieving Aβ pathology without *APP* overexpression (Saito et al., 2014). Saito and colleagues from the RIKEN Brain Science Institute, Japan, generated three strains of mice using a knock-in (KI) strategy to insert mutant *APP* into the mouse genome. These models are the App^{NL}, App^{NLF}, and App^{NLGF} mice, collectively referred to as APP-KI mice (Saito et al., 2014; Zhong et al., 2024). To generate these lines, the C57BL6/J *App* sequence on chromosome 16 was isolated and humanised by substituting three amino acid residues (G676R, F681Y, and

H684R) (Saito et al., 2014; Sasaguri et al., 2017). Subsequently, a series of FAD mutations were introduced to the *App* sequence. For the App^{NL} model, the Swedish 'NL' (KM670/671NL) mutation was incorporated to exon 16, which resides at the β-secretase cleavage site and elevates the total amount of $Aβ_{40}$ and $Aβ_{42}$ (Citron et al., 1992; Mullan et al., 1992). In addition to the Swedish mutation, the App^{NLF} model was generated by also incorporating the Beyreuther/Iberian 'F' (I716F) mutation, which is located on exon 17 and increases the ratio of $Aβ_{42}$:$Aβ_{40}$ (Lichtenthaler et al., 1999; Saito et al., 2014). To create the triple mutant App^{NLGF} model, the Arctic 'G' (E693G) mutation was also incorporated into exon 17, which promotes aggressive aggregation of Aβ into protofibrils (Fig. 1.3) (Nilsberth et al., 2001; Ono, 2018; Saito et al., 2014). This KI technique results in mutant *App* that is under control of the endogenous mouse promotor, resulting in *App* that is selectively expressed in axons at a level that is not significantly different to that of C57BL6/J littermates (Saito et al., 2014; Sasaguri et al., 2022).

As a result of the Swedish and Beyreuther/Iberian *APP* mutations, the App^{NLF} model exhibits high overall Aβ production, with an increased ratio of $Aβ_{42}$:$Aβ_{40}$, and plaque deposition occurring at around 6 months in the cortex and HPC (Saito et al., 2014). There is also evidence of neuroinflammation in this model, occurring concurrently with plaque formation, as indicated by inflammatory markers for microgliosis (Iba1) and astrocytosis (GFAP) detected in the vicinity of plaques (Saito et al., 2014). Furthermore, the App^{NLF} model also exhibits some evidence of synaptic loss, with a reduced synaptophysin (pre-synaptic marker) and PSD-95 (post-synaptic marker) observed around plaques from 9 months of age, suggesting a loss of both pre and post synaptic terminals (Saito et al., 2014). App^{NLF} animals also exhibit impairments in Y-maze spontaneous alternation task at 18 months (Saito et al., 2014).

The App^{NLGF} model, which is the focus of this thesis, develops Aβ pathology approximately three times faster than the App^{NLF} model, with plaques starting to develop at 2 months and reaching saturation by 7 months of age (Saito et al., 2014). Notably, unlike App^{NLF} mice, App^{NLGFs} exhibit amyloid deposition in wider subcortical regions in addition to the HPC (Saito et al., 2014). App^{NLGFs} also exhibit enhanced microgliosis and astrocytosis, along with synaptic degeneration detectable in the vicinity of plaques (Mehla et al., 2019; Saito et al., 2014). A recent study demonstrated that App^{NLGF} animals exhibit high levels of both oligomeric Aβ and plaques, with astrocytic and microglial activation being more strongly associated with oligomers than plaques (Tang et al., 2024). Additionally, they demonstrated an age-dependent decline in neuronal and synaptic density markers (Tang et al., 2024). App^{NLGF} mice also exhibit mitochondiral dysfunction characterised by ROS overproduction, reduced adenosine triphosphate (ATP) production, and altered mitochondiral morphology by 7 months (Wang et al., 2022). Alongside biochemical alterations, App^{NLGF} mice display several behavioural impairments, which will be explored in greater detail in Chapter 3 of this thesis. Notably, Saito et al. originally reported impairments in Y-maze spontaneous alternation task at 6 months of age

(Saito et al., 2014). Finally, as will be discussed below, the *App*^{NL} model is considered a negative control for the *App*^{NL} and *App*^{NLGF} models, as it does not develop plaques but accounts for the potential effects of genetic manipulation (Saito et al., 2014).

Despite the key benefit of substantial amyloid deposition without the issues associated with *APP* overexpression, there are several drawbacks to the *APP*-KI models. However, the most salient drawback of *APP*-KI models is that despite showing evidence of synaptic loss, they do not exhibit widespread neuron loss or NFTs, key hallmarks of AD (Avila & Perry, 2021; Saito et al., 2014). This may explain why, as will be discussed with reference to the *App*^{NLGF} model in the General Discussion, they exhibit a lack of severe phenotypes. As a result, it is argued that the APP-KI models should be considered models of pre-clinical AD, as they do not replicate pathologies generally associated with late-stage disease (Saito et al., 2014; Sasaguri et al., 2017). Furthermore, it is unknown whether these mutations interact and if so, what the functional effect of this is. Another vital limitation of the *App*^{NLF} and *App*^{NLGF} models is that, as with many transgenic models, they contain multiple FAD mutations. FAD cases account for under 5% of all AD cases (Bekris et al., 2010), raising questions about the relevance of these models to the broader AD population. This concern is further compounded by the fact that the combination of FAD mutations in the *App*^{NLF} and *App*^{NLGF} models do not occur naturally in AD, so it may be argued that they are not representative of the disease.

Additional critiques for the *APP*-KI models arise from the products of mutant *APP* they harbour. For example, the Swedish mutation in all three APP-KI models results in the increased production of CTF-β compared to C57BL6/J littermates (Saito et al., 2014). However, levels of CTF-β do not reach those observed in transgenic models overexpressing *APP* with the Swedish mutation (Saito et al., 2014). Additionally, there is a concurrent decrease in CTF-α levels compared to C57BL6/Js, resulting in the total CTF levels remaining comparable to C57BL6/Js (Saito et al., 2014). Moreover, it was demonstrated that in the *App*^{NL} model, which carries only the Swedish *APP* mutation, elevated CTF-β did not have an observable effect on pathology or cognitive function (Masuda et al., 2016; Saito et al., 2014). However, this model is often used as a negative control for the *App*^{NLF} and *App*^{NLGF} lines to account for potential effects arising from changes in *App* processing due to the Swedish mutation (Masuda et al., 2016; Saito et al., 2014).

A further limitation, specific to the *App*^{NLGF} model, is the inclusion of the Arctic mutation. This mutation renders Aβ highly prone to aggregation and resistant to proteolytic degradation, rendering the model unsuitable for testing of amyloid clearing immunotherapies, despite being regarded as a preclinical model (Nilsberth et al., 2001; Sasaguri et al., 2022; Tsubuki et al., 2003). This limitation, along with other key limitations of the *App*^{NLGF} model, will be discussed in greater depth in the

General Discussion chapter of this thesis. Despite these limitations, the *App*^{NLGF} and related models may still provide valuable insights into the effects of amyloid on cognitive processes and other aspects of AD pathology.

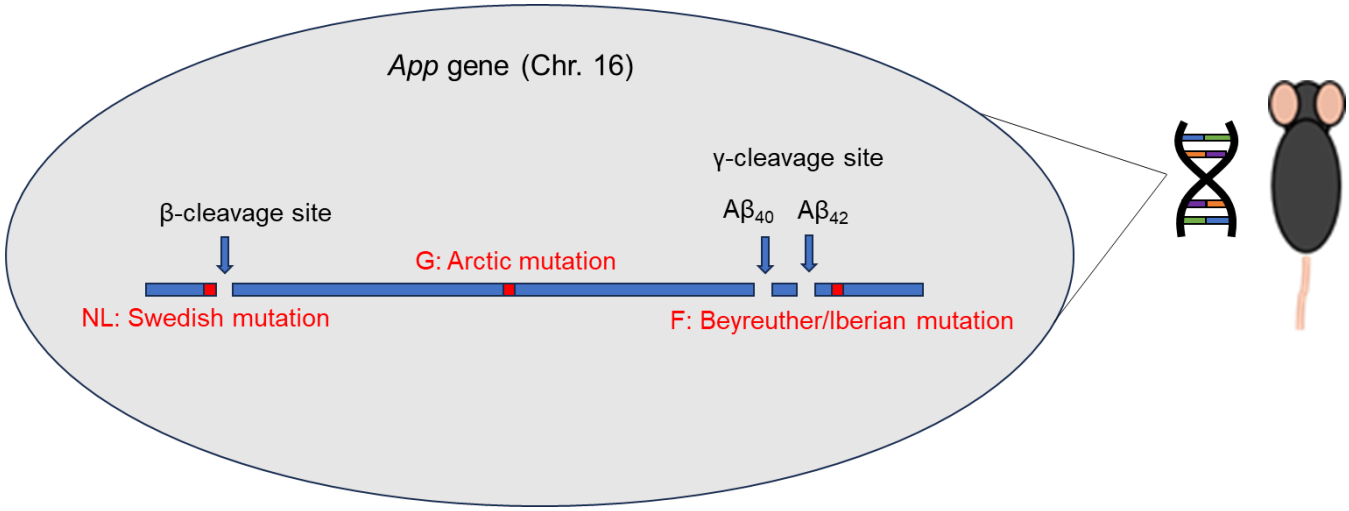

Figure 1.3: The App^{NLGF} Mouse Model of Amyloid Pathology. Diagram depicting the arrangement of mutations in the *App*^{NLGF} *App* gene on Chromosome 16, highlighting their positions relative to the β- and γ- cleavage sites. The alternative γ-secretase cleavage sites are shown, where cleavage at 40 amino acids generates Aβ$_{40}$, while cleavage at 42 amino acids results in the Aβ$_{42}$ fragment (Saito et al., 2014; Sasaguri et al., 2022).

1.6 Thesis Aims and Hypotheses

The *App*^{NLGF} mouse is a relatively new model amyloid pathology that circumvents the issue of overexpression related artefacts that are associated with transgenic amyloid models. Given the paucity of disease-modifying therapies for AD, especially in the context of multiple failed or only modestly effective anti-amyloid treatments, it is crucial that a reliable model is developed and thoroughly characterised. However, relatively little is known about the cognitive phenotype of the *App*^{NLGF} model in comparison to transgenic models. The aim of this thesis was therefore to investigate the progression of deficits in memory and affective behaviour in the *App*^{NLGF} mouse model. Memory performance, a central issue in AD, was assessed with a battery of tests including the Object Novelty (ON), Object-in-Place (OiP), Object Location (OL), and spontaneous alternation tasks, employed to interrogate several aspects of memory including novelty recognition, spatial memory, and spatial working memory. A less well understood aspect of AD, and consequently a less well characterised

phenotype in AD mouse models, is anxiety-like behaviour. Chapter 3 of this thesis therefore aimed to address this gap by assessing anxiety-like behaviours in the *App*^{NLGF} mouse model using the Open Field (OF) and Elevated Plus Maze (EPM) tests. To provide a comprehensive characterisation of the *App*^{NLGF} model and to track potential behavioural changes with age, multiple age groups were assessed across most behavioural tasks. Given the prominence of the Amyloid Cascade theory, it was hypothesised that *App*^{NLGF} mice would exhibit progressive memory deficits and heightened anxiety-like behaviour, consistent with the progressive amyloid deposition observed in this model (Saito et al., 2014). However, it was anticipated that deficits would appear less severe than transgenic models due to the lack of overexpression-related artefacts (Saito et al., 2014; Sasaguri et al., 2022).

Beyond behavioural alterations, characterising changes in neuronal activity in the *App*^{NLGF} model is essential to determine whether synaptic dysfunction may underlie these potential changes. Chapter 4 of this thesis therefore aimed to characterise neuronal activation in the *App*^{NLGF} model using two experimental approaches: *in vivo* two-photon Ca^{2+} imaging and *c-fos* expression analysis. The primary objective of the two-photon imaging experiment was to capture Ca^{2+} dynamics in the retrosplenial cortex (RSC), a region implicated in early AD pathology (Buckner et al., 2005; Klunk et al., 2004; Terstege et al., 2024), of awake *App*^{NLGFs} and C57BL6/J mice at 22-23 months of age. To enable detailed comparisons of RSC Ca^{2+} dynamics at baseline levels and during visual stimulation, a novel analysis protocol was developed, which is outlined in this chapter. Given the pivotal role of Ca^{2+} signalling in neuronal activity and its dysfunction in AD, studying *in vivo* Ca^{2+} dynamics in the *App*^{NLGF} offers valuable insights into potential amyloid-mediated deficits in synaptic function and neuronal excitability. Based on the Calcium Hypothesis of AD, which associates Aβ pathology with neuronal Ca^{2+} overload (Cascella & Cecchi, 2021), it was hypothesised that *App*^{NLGFs} at 22-23 months, with theoretically maximal plaque burden, would exhibit significantly elevated RSC Ca^{2+} levels compared to C57BL6/J controls. Such an increase may suggest Aβ-related disruptions in Ca^{2+} signalling pathways and reflect functional changes of the RSC that contributes to cognitive decline, potentially correlating with pronounced behavioural deficits at this age.

Following unexpected failure of the two-photon imaging equipment, the aim of the c-Fos experiment was to provide an additional insight into neuronal activity of the *App*^{NLGF} model at mid-age (14-16 months). This experiment focused on the RSC to parallel the intended Ca^{2+} imaging experiment, while also examining the HPC as another critical region implicated in AD pathogenesis (Rao et al., 2022). Given that *c-fos* is closely associated with neuronal activity in conditions of learning (Minatohara et al., 2015), it was hypothesised that following exposure to a novel object set, mid-aged *App*^{NLGF} mice would exhibit altered patterns of *c-fos* expression, reflecting compromised neuronal activity and suggesting underlying synaptic deficits that contribute to cognitive impairments.

Overall, this thesis aimed to provide a comprehensive behavioural characterisation of the *App*^{NLGF} model of amyloid pathology, alongside a detailed analysis of baseline and experience-induced neuronal activity. By establishing these key features, this thesis provides valuable insights into phenotype of the *App*^{NLGF} model, inferring the impact of amyloid on these critical functions. These findings inform the future application of this model and may contribute to the development of therapeutic strategies for AD.

Chapter 2: General Methods

2.1 Chapter Overview

For ease of reference, methodologies that are used in both experimental chapters in this thesis are outlined in this General Methods chapter. This includes details of animal husbandry, behavioural assessments and apparatus, and statistical approaches. Although the majority of behavioural assessments were used exclusively in Chapter 3, the c-Fos experiment in Chapter 4 also contained an object recognition protocol, so all behavioural methodologies are presented in this General Methods chapter for completeness. Moreover, the procedures for brain tissue collection and immunohistochemistry (IHC) are described here, as they were utilised for the representative amyloid stain described in Chapter 3 and the c-Fos stain in Chapter 4. Specific experimental designs and corresponding analyses are described in detail within the relevant chapters.

2.2 Breeding and Maintenance of the *App^{NLGF}* Colony

2.2.1 Husbandry

In accordance with Home Office guidelines, all animals were kept in holding rooms with a 12-hour light/dark cycle (all experiments conducted in the light period, 08:00 – 20:00) and of stable temperature (21±2°C) and humidity (60±10%). All mice, with the exception of surgical animals, were housed in standard cages (41 x 15 x 13cm). Surgically prepared animals were kept in larger cages (41 x 24 x 13cm) to allow more room for movement and thus reduce the risk of injury to the surgical site. Mice were given *ad libitum* access to water and standard chow. All mice were provided with environmental enrichment, such as cardboard tubes and chewsticks. Males and females were housed separately, and wherever possible, in groups of up to five. Occasional single housing was necessary in specific cases, such as when a retired sire was not reintroduced to group housing to prevent fighting, and when there was only one of a particular sex in a litter and they were weaned to a separate cage to prevent sibling mating.

All experiments were conducted in accordance with the Animals in Scientific Procedures Act (1986) and reviewed by Cardiff University's Animal Welfare Ethical Review Body.

2.2.2 Animal Breeding and Acquisition

The 22–23-month-old *App^{NLGF}* and C57BL6/J groups (Table 2.1) were bred-in house and obtained from stock animals bred by K Sedgwick (Cardiff University). These animals were maintained until the suitable age and monitored closely for signs of weight loss and health deterioration as per conditions of the Home Office licence.

To establish the 4-6-, 8-10-, 12-14- and 14–16-month-old groups (Table 2.1), homozygous breeding pairs of *App*^{NLGF} mice, derived from the RIKEN Institute colony (Japan), were obtained from the Taylor group at Cardiff University. With permission from T Saido, colonies were produced from pairing these animals. Two pairs of male and female C57BL6/Js were purchased from Charles River, UK, and bred alongside the *App*^{NLGF} pairs to provide controls reared in-house. To maintain *App*^{NLGF} and C57BL6/J colonies, progeny from the first original breeding pair were crossed with progeny from the second original breeding pair. Back-crossing of the *App*^{NLGF} colony was not required as the number of generations did not exceed 3 (Sasaguri et al., 2022). Pups were weaned at approximately 21 days, or when deemed appropriate by the Named Animal Care and Welfare Officer. Ear notches were taken at this stage for identification purposes. Due to the homozygous crosses, no genotyping was performed. Animals were maintained until the appropriate age for experiment and weighed weekly once they had reached 6 months of age.

Animals transferred from separate University facilities or obtained from Charles River were all acclimatised to the holding room for one week before breeding or experiments commenced.

Table 2.1: Experimental Animal Cohorts. The age (in months) and distribution of male and female *App*^{NLGF} and age-matched C57BL6/Js for each cohort used in Open Field (OF), Object Location (OL), Spontaneous Alternation (SA), Elevated Plus Maze (EPM), Object Novelty (ON), Object-in-Place (OiP), c-Fos, and two-photon calcium (Ca^{2+}) imaging experiments.

Cohort age (months)	C57BL6/J		*App*^{NLGF}		Experiment
	Males	Females	Males	Females	
4-6	7	5	5	7	OF, OL, SA, EPM
8-10	6	6	6	6	OF, OL, SA, EPM
12-14	6	6	4	8	SA, EPM
14-16	10	10	10	10	OF, c-Fos
22-23 (cohort I)	10	3	3	11	OF, ON, OiP, OL, SA, EPM
22-23 (cohort II)	7	1	3	6	Two-photon Ca^{2+} imaging

2.3 Behavioural Testing

2.3.1 Apparatus

OF, ON, OiP and OL experiments were conducted in a square arena elevated 50cm from the floor (Fig. 2.1a). The arena comprised of a square sheet of MDF (60 x 60cm) with clear Perspex walls (40cm tall). The walls of the arena were internally covered with white opaque film to around 60% of the wall height, ensuring that the

mouse did not see reflections of itself in the plastic walls whilst allowing view of extra-maze cues. The floor of the arena was painted in non-toxic grey paint and covered lightly with standard husbandry bedding, providing a familiar environment to allow for natural behaviour, as previously described (Vogel-Ciernia & Wood, 2014). Between each animal, the bedding was changed and the arena thoroughly cleaned with 70% Industrial Methylated Spirit (IMS) to mitigate the use of olfactory cues.

Spontaneous alternation testing was performed in a T-maze, consisting of three arms meeting at a single junction, elevated 50cm from the floor (Fig. 2.1b). The maze comprised of a MDF floor painted in grey non-toxic paint and clear Perspex walls. Each arm of the maze was 25 x 10 x 25cm. EPM testing was performed in a cross shaped maze, elevated 75cm from the ground floor (Fig. 2.1c). Two opposite arms of the maze had opaque black walls, 15cm high ('closed' arms). The remaining two opposite arms had clear 2cm walls ('open' arms). Each arm was 40cm long and 7cm wide. For the spontaneous alternation and EPM experiments, the mazes were also thoroughly cleaned with 70% IMS between animals.

The OF, ON, OiP, OL, and c-Fos experiments were performed in the same room and the spontaneous alternation and EPM experiments were conducted in a different room. Each room was equipped with distinctive extra-maze cues, including various A4 prints on the walls featuring stripes and spots of differing size and colour contrasts. All experiments were recorded on a USB camera (ELP Webcam 1080P, Amazon.com), positioned near a ceiling light directly above the arena. Video clips were then uploaded to analysis software EthoVision XT13 (Noldus, UK).

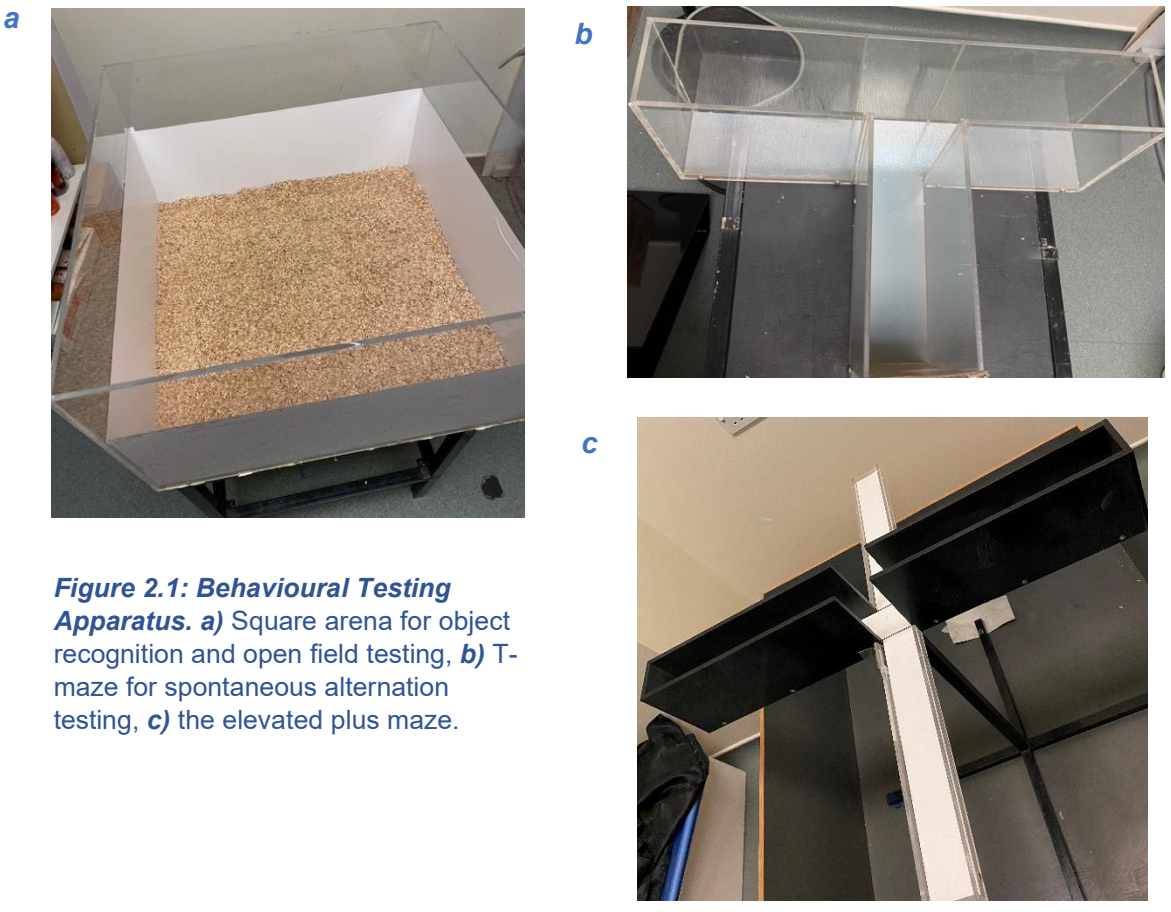

Figure 2.1: Behavioural Testing Apparatus. a) Square arena for object recognition and open field testing, ***b)*** T-maze for spontaneous alternation testing, ***c)*** the elevated plus maze.

2.3.2 Objects

Objects were selected as previously validated stimuli from the Good laboratory. Objects consisted of a range of different materials such as glass, wood, and plastic, and were tall and heavy to avoid the animal climbing on and/or tipping the object during the experiment. For example, full cosmetic bottles, glasses, and ornaments were used (Fig. 2.2). Objects were modified to exhibit visually stimulating characteristics such as stripes and spots with dark and light contrasting colours. Objects were placed approximately 15cm away from the walls of the arena and approximately 25cm apart. A variety of object sets and novel object locations were used and counterbalanced to ensure that the animals were not exposed to the same set of objects in more than one test, and that novel locations were not predictable.

Figure 2.2: Example of Objects Used for Object Recognition Testing. Chosen objects were tall, heavy, and had distinctive visual features such as spots or stripes.

2.3.3 Procedure and Analysis

2.3.3.1 Open Field and Object Recognition Habituation

For ON, OiP, and OL testing, mice received 3 days of habituation to the arena. Day 1 consisted of 10 minutes of OF testing. OF testing was also utilised as habituation for the c-Fos experiment described in Chapter 4.

During the OF test, the mouse was positioned in the centre of an empty square arena and allowed to freely explore for 10 minutes. Each OF test was recorded via overhead camera and videos were uploaded to EthoVision XT13. The time spent in the inner zone (central 30 x 30cm) and outer zone (remaining outer perimeter of the arena, Fig. 2.3) was calculated. An inner zone ratio (IZR) was then calculated, using the below formula:

$$IZR = time\ in\ inner\ zone\ (s) \div total\ time\ in\ arena\ (s)$$

a

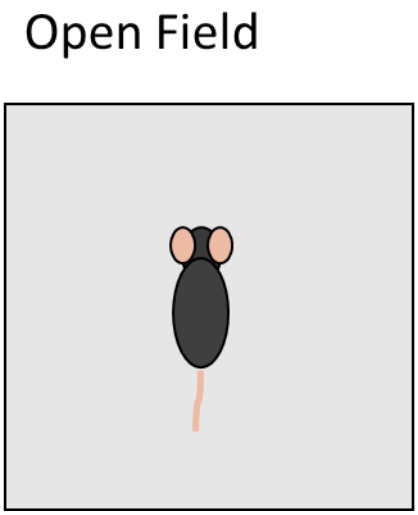

Figure 2.3: The Open Field Arena. a) The animal was placed in the centre of an empty square arena and allowed to freely explore for 10 minutes. ***b)*** Inner and outer zones were defined using EthoVision XT13 for analysis.

b

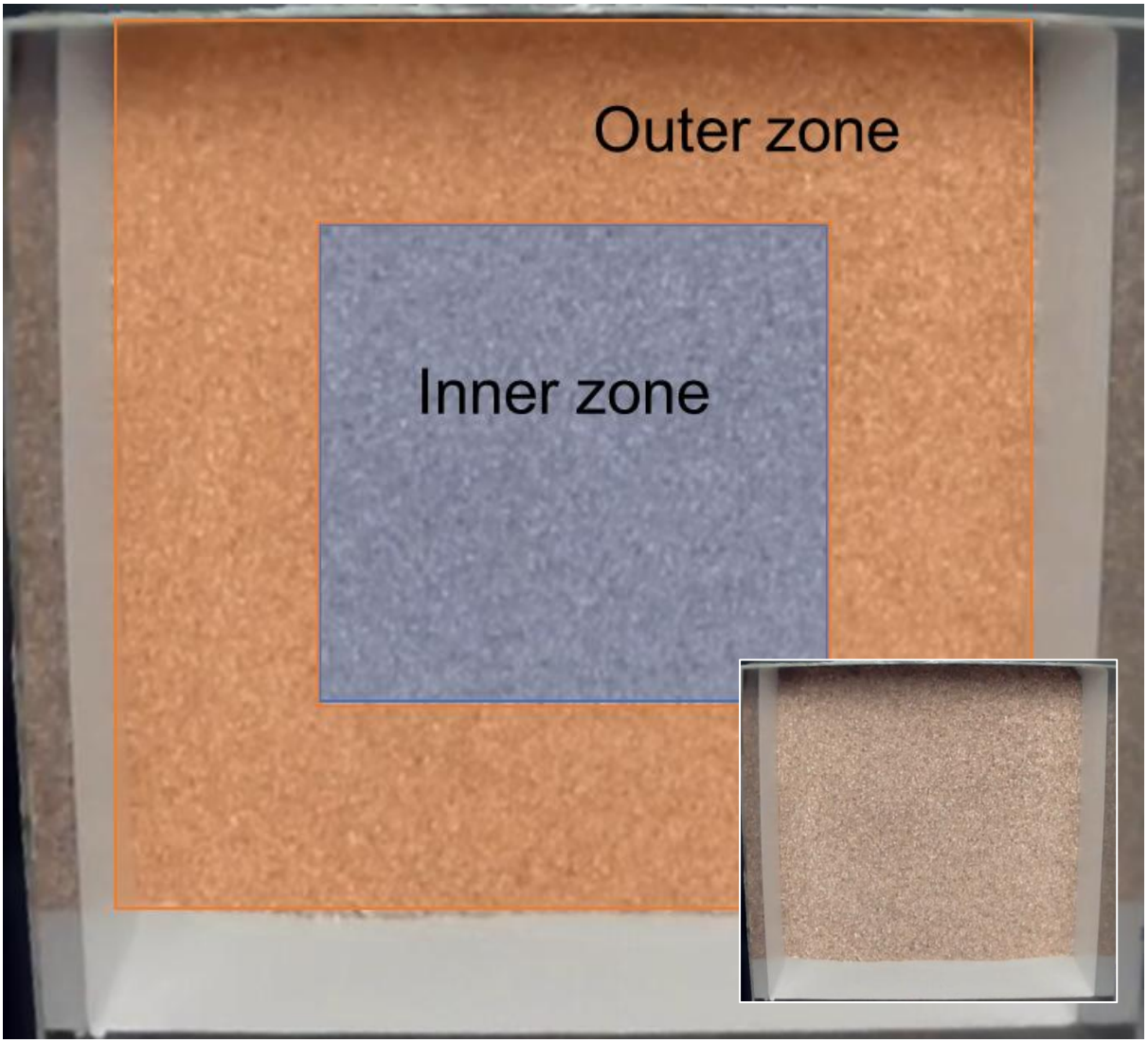

Habituation for object recognition testing followed a protocol previously published by the Good laboratory (Evans et al., 2019). As described above, day 1 of habituation for object recognition tests consisted of OF testing. On days 2 and 3 of habituation, animals were exposed to an array of objects in the OF arena. Objects were used as part of the habituation protocol to minimise the likelihood that object interaction during test trials was driven by the novelty of the presence of objects in the arena, rather than by the specific manipulation of object novelty or the location of objects. The number of objects used during habituation reflected the complexity of object arrays used for the relevant test. For example, for ON and OiP testing, which were conducted on the same test days in a counterbalanced order, the animals were exposed to sets of four objects on day 2 and 3 of habituation. For OL testing, which was conducted separately, animals were exposed to two objects on these habituation days. For each object recognition test, day 2 of habituation consisted of 3 x 5-minute trials with random objects and day 3 consisted of 3 x 5-minute trials of new objects. No objects used for habituation were re-used for experiments.

2.3.3.2 Object Interaction

For ON, OiP and OL, object exploration was defined as previously described (Ennaceur & Delacour, 1988; Evans et al., 2020). Exploration events occurred when the animal's head was facing the object, within approximately 2cm, and showing active investigation (such as sniffing). This did not include instances when the mouse was near or in contact with the object but facing away from it. To avoid errors with automated tracking (i.e., counting an animal as interacting with an object when it was within 2cm but not actively investigating the object), object interaction for all object recognition tests was manually scored using EthoVision XT13. To minimise potential experimenter bias, manual scoring was performed blind to both the animal genotype and the identity/location of the novel object. For instance, all animals were assigned an identification code, and the gentoype of each animal was only decoded after manual scoring was completed. Additionally, object sets and locations were counterbalanced, with objects serving as both "novel" and "familiar" across the experiments conducted, and all available object positions in the arena used for novel object locations where relevant. This design ensured that novel objects or locations could not be inferred by the experimenter during manual scoring.

With the manually scored object exploration times, the Discrimination Ratio (DR) was calculated as follows:

$$DR = time\ exploring\ novel\ object\ (s) \div time\ exploring\ all\ objects\ (s)$$

Regardless of the number of objects in the array, the ratio of novel to previously explored objects was always 1:1, ensuring a 50% chance level for analysis. Therefore, mean DRs significantly greater than 0.5 indicated preferential exploration of novel objects.

2.3.3.3 Object Novelty Testing

For ON testing, four random objects were placed in each corner of the arena (Fig. 2.4). Animals were placed in the centre of the arena using a cardboard tube. The animal was then allowed to explore the arena for 10 minutes before it was returned to its home cage for a further 10 minutes. This was repeated twice so the animal had three sample trials, in accordance to the protocol previously used in the Good laboratory (Evans et al., 2019). 10 minutes after the final sample trial, two of the objects were replaced with two previously unseen 'novel' objects, and the animal was returned to the arena and allowed to explore for a further 10 minutes. Object exploration time was manually scored and a DR was calculated, as described above.

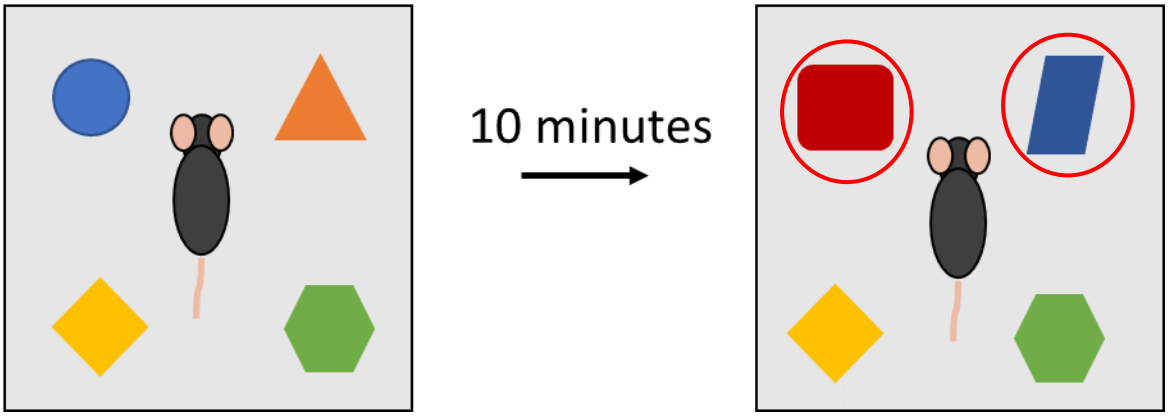

Figure 2.4: Schematic Diagrams of the Object Novelty Test. The left diagram depicts the sample trial of objects. The animal explored this array of objects three times, with a 10-minute rest in its home cage between each trial. Following the final 10-minute delay, two of the objects were replaced by novel objects (circled in red) and the animal was returned to the arena for a further 10 minutes, as shown in the diagram on the right.

2.3.3.4 Object-in-Place Testing

OiP testing used a new set of four objects in each corner of the arena (Fig. 2.5). The animals received the same 3 x 10-minute sample trials as described above, however after the final 10-minute delay, two objects were switched diagonally, and thus in novel spatial locations. The animal was returned to the arena for a further 10 minutes. Object exploration time was manually scored, and the DR was subsequently calculated.

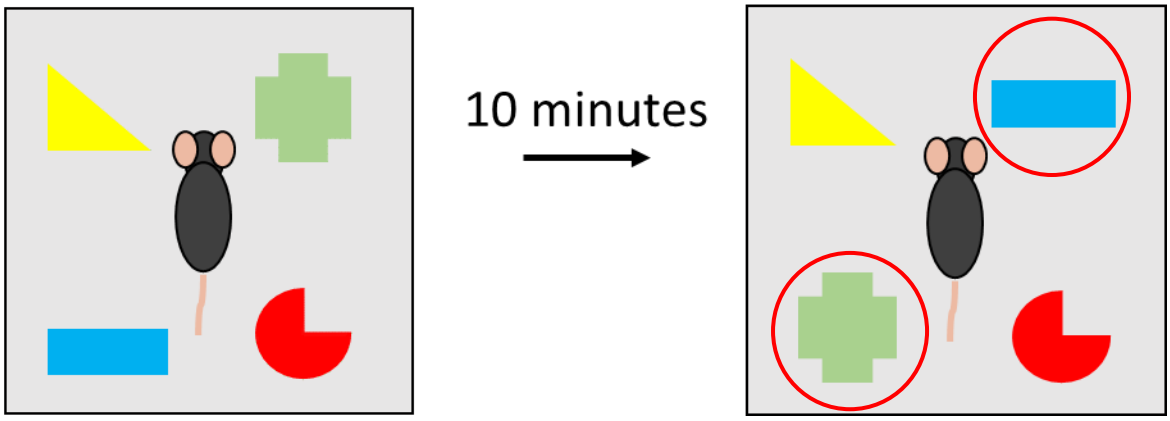

Figure 2.5: Schematic Diagrams of the Object-in-Place Test. The left diagram depicts the sample trial of objects. The animal explored this array of objects three times, with a 10-minute rest in its home cage between each trial. Following the final 10-minute delay, two diagonally positioned objects were switched (circled in red) and the animal was returned to the arena for a further 10 minutes, as shown in the diagram on the right.

2.3.3.5 Object Location Testing

OL testing used a two-object array as shown in Fig. 2.6. The animal received 3 x 10-minute sample trials with two objects in adjacent corners of the arena. After the final 10-minute delay, one of the objects was moved to a location previously unoccupied and the animal was allowed to explore for a further 10 minutes. Object exploration time was manually scored and a DR was calculated.

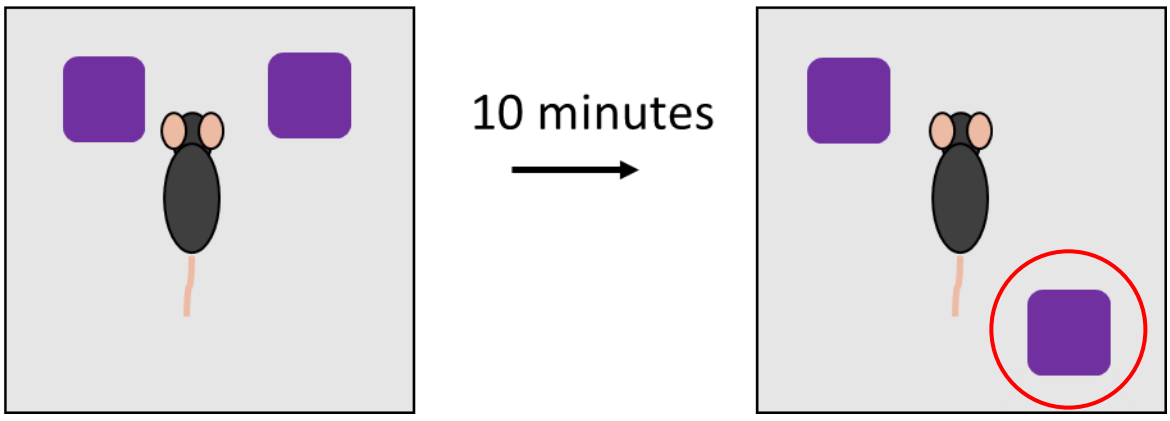

Figure 2.6: Schematic Diagrams of the Object Location Test. The left diagram depicts the sample trial of objects. The animal explored this array of objects three times, with a 10-minute rest in its home cage between each trial. Following the final 10-minute delay, one of the objects was moved to a previously unoccupied location (circled in red) and the animal was returned to the arena for a further 10 minutes, as shown in the diagram on the right.

2.3.3.6 T-Maze Spontaneous Alternation

For spontaneous alternation testing, animals were placed in the central arm of the T-maze (arm C, Fig. 2.7), facing the central junction, and allowed to freely explore the maze for 10 minutes. The animal was then returned to its home cage.

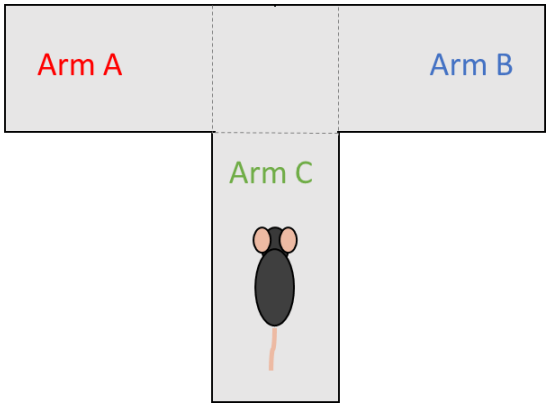

Figure 2.7: Schematic Diagram of the T-Maze Spontaneous Alternation Test. The animal was placed in the central arm of a T-maze and allowed to freely explore for 10 minutes. The sequence of entry into each arm was then manually scored. The dashed lines represent the boundaries used to classify arm entries, and do not indicate physical barriers.

The number of alternations during the spontaneous alternation task was manually scored. To do this, each arm of the T-maze was figuratively labelled (Fig. 2.7). The experimenter, blind to the animal genotype, recorded the sequence of arm entries and the total number of arm entries made throughout the experiment. An arm entry was defined as the animal moving all four paws past the threshold of the arm junction. The number of alternations was subsequently calculated as follows:

$$\%\,\boldsymbol{alternation} = \left(\boldsymbol{number\ of\ alternations} \div \left(\boldsymbol{total\ number\ of\ arm\ entries} - \mathbf{2}\right)\right) \times \mathbf{100}$$

An alternation was defined as three consecutive entries into different arms (Miedel et al., 2017). In the below reproduced example (not actual data), each bracket indicates where an alternation has occurred.

ABCBCABCBACAABBABCACAAB

To account for the three-arm structure of the T-maze, a chance level of 22% rather than 50% was used for spontaneous alternation analysis (Holcomb et al., 1999; Wolf et al., 2016). Percentage alternation significantly greater than 22% indicated a preference to explore less recently visited arms of the maze.

2.3.3.7 Elevated Plus Maze

For EPM testing, animals were placed in the central zone of a cross shaped maze with two ‘open’ and two ‘closed’ arms, elevated from the ground. The animal then explored the maze for 10 minutes. The number of entries and the total time spent in each arm were automatically detected using manually defined zones in EthoVision XT13 (Fig. 2.8).

a

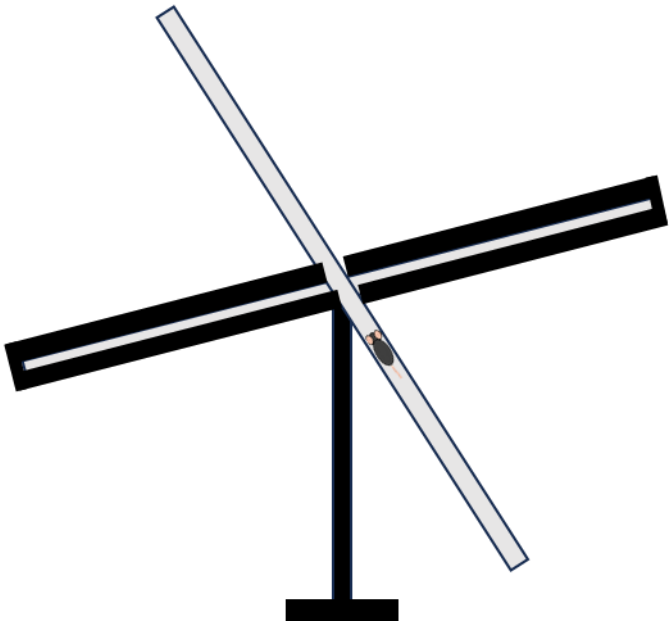

b

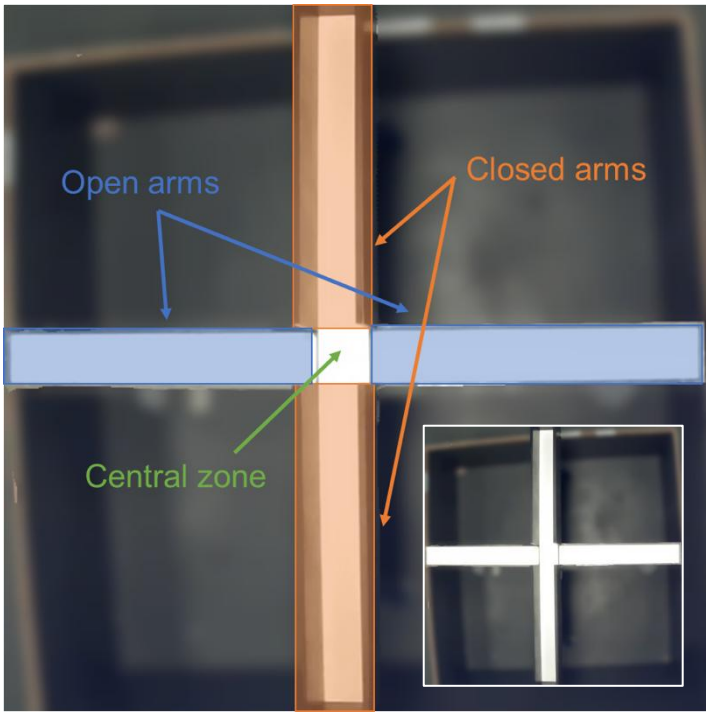

Figure 2.8: The Elevated Plus Maze. a) The animal was placed in the central zone and allowed to freely explore for 10 minutes. ***b)*** EthoVision XT13 was used to define the open and closed arms of the maze for analysis.

An open arm ratio (OAR) was then calculated using the below equation:

$$\boldsymbol{OAR = time\ in\ open\ arms\ (s)\ \div\ total\ time\ in\ maze\ (s)}$$

Head dipping and stretching behaviours were manually scored for all EPM experiments using EthoVision XT13. Head dipping was defined as the lowering of the mouse's head over the edge of an open arm, and is considered as an anxious exploration of the environment (Carola et al., 2002; Fernandes & File, 1996; Rodgers & Cole, 1993; Walf & Frye, 2007; Wall & Messier, 2000). Stretching, also described as stretch attend posture, was defined as the animal stretching its head and front legs into an open arm, with its hind legs remaining in a closed arm or within the central zone of the arena (Carola et al., 2002). This action has been associated with risk assessment behaviour and may reflect enhanced anxiety-like state (Fernandes & File, 1996; Rodgers & Cole, 1993; Walf & Frye, 2007; Wall & Messier, 2000).

2.3.3.8 Distance Travelled

For all behavioural tests in this thesis, the total distance travelled was recorded using the automated animal tracking feature in EthoVision XT13. This measure of locomotor activity was included to determine whether any differences in behaviour (e.g., object exploration during object recognition tasks or percentage alternation during the spontaneous alternation task) may be confounded by differences in total path length.

2.4 Statistical Analysis

All statistical analysis was performed using SPSS and all graphs presented in this thesis were created using GraphPad Prism. The statistical results of interest are displayed on data graphs using asterisks (* = $p < 0.05$, ** = $p < 0.01$, *** = $p < 0.001$, **** = $p < 0.0001$) or ns to denote a non-significant effect.

Prior to analysis, all data was checked for the assumptions of parametric testing using SPSS. Normality was assessed using the Shapiro-Wilk test; a p value of > 0.05 indicated a normal distribution and p value of < 0.05 indicated a non-normal distribution. To test the homogeneity of variance in each dataset, Levene's test was performed; a p value of > 0.5 indicated equal variance within the dataset, whereas a p value of < 0.05 indicated unequal variance.

For data that met the above assumptions, parametric testing was performed. This included unpaired T-tests, one-sample t-tests, two-way analysis of variance (ANOVA), three-way ANOVA, or two-way mixed ANOVA, where appropriate. Where datasets exhibited unequal variance or non-normal distribution, data was transformed by $\log_{10}$ or square root transformation. To determine which transformation was required, the distribution of the data was visually inspected using the histograms produced during SPSS analysis. Generally, $\log_{10}$ transformation was performed for severely skewed data, whereas square root transformation was performed on moderately skewed data. For data that still did not exhibit normal distribution or equal variance after transformation, alternative non-parametric tests were performed. For example, in place of an unpaired T-test, a Mann-Whitney U test was performed for non-normally distributed data and a Welch's T-test was performed for data that exhibited unequal variance. Where a non-parametric alternative to a two-way mixed ANOVA was required, a Friedman test followed by Mann-Whitney U tests were performed and the alpha was adjusted by Bonferroni correction to control for increased risk of type I error.

Following a significant interaction in an ANOVA ($p < 0.05$), simple main effects analyses were conducted to assess the specific effect of one independent variable at different levels of another. Bonferroni adjustments were applied to control for the increased risk of type I error from multiple comparisons. If an interaction was not significant, but a main effect (e.g., age), was significant, Bonferroni *post hoc* testing was performed to establish the specific points at which significant differences occurred.

2.5 Transcardial Perfusion and Brain Tissue Preparation

Mice were anaesthetised with approximately 0.05ml of sodium pentobarbital (Euthetal or Dolethal) by intraperitoneal injection and placed in a cage with bedding and a cardboard tube. Once mice showed lack of movement, they were checked for the presence of pedal reflexes by firmly grasping the paws with metal forceps. Once there was a clear absence of pedal reflex, the mouse was dissected to expose the heart by making a transverse incision across the thorax-abdomen boundary, then cutting through the diaphragm and ribcage. An incision was made into the right atrium and a needle was positioned into the left ventricle, parallel to the midline of the heart. Cold phosphate buffered saline (PBS) was flushed through the circulatory system to remove the blood using a Watson Marlow SCIQ 323 peristaltic pump. Once the fluid ran clear, 4% paraformaldehyde (PFA) was pumped through the body until the tail curled and the body became stiffened. Following transcardial perfusion, whole brains were removed from the animal and placed in 4% PFA for 24hrs. The brains were then moved to a 30% sucrose solution where they remained until they had sunk to the bottom of the container. Subsequently, the brains were embedded in

OCT embedding medium and sliced coronally to approximately 30µM using a Leica Jung SM1400 freezing microtome at approximately -40°C. The slices were stored in cryoprotectant solution in 25-well plates at -20°C until ready for IHC.

2.6 Immunohistochemistry

To detect the presence of c-Fos or amyloid proteins, IHC was performed. Brain tissue was harvested and prepared for IHC as described in the General Methods chapter of this thesis. The brain slices containing the brain region of interest (ROI) were placed in net-bottomed pots and inserted into a large 6-well plate, to enable submersion of the brain slices in relevant solutions. Plates containing brain slices were put on a rocking shaker at slow speed (1.5-2) for each wash or incubation for even coating of the slices.

Following removal from cryoprotectant, 0.1M PBS was added to the 6-well plates and the slices were washed six times for 10 minutes each, by removal of old solution and replacement with fresh solution each time. The slices were then treated with a quench solution (10% methanol, 10% hydrogen peroxide, and 80% dH_2O) for 5 minutes. The slices were then washed with PBS-T (PBS with 0.2% Triton-X-100) four times for 10 minutes each. A blocking solution of 1% normal goat serum (NGS) in PBS-T was then added and the slices incubated for 1 hour. Without washing, the slices were transferred to the primary antibody solution. For the representative amyloid stain, Amyloid-β D54D2 rabbit monoclonal antibody (Cell Signalling Technology), designed to detect several isoforms of Aβ, was diluted 1:500 in 1% NGS in PBS-T. As this primary antibody was used in a pilot study aimed at confirming Aβ deposition and validating the staining protocol, only App^{NLGF} brains were stained, and not those from C57BL/6J controls. Consequently, the specificity of the Amyloid-β D54D2 antibody is not directly demonstrated in this thesis. However, its specificity has been well established in previous studies, including one that reported a progressive increase in plaque staining with age in both App^{NLGF} and APP/PS1 mice, with no detectable staining in age-matched C57BL6/J controls (Manocha et al., 2019).

For the c-Fos experiment, the primary antibody used was the c-Fos 9F6 rabbit monoclonal antibody (Cell Signalling Technology), diluted 1:2500 in 1% NGS in PBS-T. The slides were agitated for 10 minutes then stored at 4°C for 72hrs. Following a series of four washes with PBS-T, the slides were incubated with the secondary antibody (goat anti-rabbit from Abcam ABC kit) for 2 hours at room temperature. The slices were washed and incubated with streptavidin peroxidase for 1 hour at room temperature then washed with PBS-T a further four times. The slices were then incubated twice for 10 minutes with fresh tris buffer (pH 7.4), rinsing with dH_2O between each wash. A 3, 3'-diaminobenzidine (DAB) solution (DAB Substrate

Kit, Vector labs) was then made up per the manufacturer's instructions. The slices were incubated with the DAB solution until they turned light brown, then the reaction was stopped by washing them with cold PBS. The slices were stored in PBS at 4°C for 24hrs.

The slices were then mounted onto microscope slides subbed with gelatine and left to air dry at room temperature for 24hrs. The slices were then dehydrated by submersion into increasing concentrations of IMS (70% → 95% → 100% I → 100% II → 100% III) for two minutes in each solution. The slides were then cleared in xylene three times, for 10 minutes each. The slides were left to air dry at room temperature for approximately 30 minutes before adding DPX mounting medium to adhere the coverslips. The prepared slides were subsequently stored at 4°C until imaging. Imaging was performed using a Leica DMRB brightfield microscope equipped with an Olympus DP73 camera.

Chapter 3: Behavioural Characterisation of the *App*^{NLGF} Mouse Model

3.1 Chapter Overview

AD is characterised by progressive memory deterioration along with NPS such as anxiety (Chen et al., 2021a; Kamatham et al., 2024). While transgenic mouse models of amyloid pathology have provided valuable insight into the role of amyloid in the cognitive and psychological alterations of AD, it remains unclear to what extent behavioural phenotypes in these models are influenced by biochemical artefacts associated with transgene overexpression. As a result, transgenic models are often criticised for their limited capacity to reflect AD with suitable accuracy, a shortcoming that may contribute to the limited success of amyloid-targeting therapies in clinical trials. This chapter therefore aimed to characterise the cognitive and anxiety-like phenotype of the *App*^{NLGF} model, which expresses humanised mutant *App* at endogenous levels, thereby avoiding artefacts associated with transgenic overexpression (Sasaguri et al., 2022). Behavioural characterisation of the *App*^{NLGF} model is limited, particularly at advanced ages; therefore, memory and anxiety processes were assessed across multiple age groups, including young (4-6 months), mid aged (8-16 months), and old animals aged up to 23 months. To evaluate different domains of memory in the *App*^{NLGF} model, ON, OiP, OL, and spontaneous alternation tests were conducted. Notably, *App*^{NLGF} animals displayed intact novelty recognition in the ON task at 22-23 months. However, spatial memory impairments were observed in the OL test, and associative spatial memory deficits were detected during the OiP task at the same age. Furthermore, while spontaneous alternation performance was preserved at earlier ages, *App*^{NLGFs} exhibited significant deficits at 22-23 months.

Anxiety-like behaviour was assessed using the OF and EPM tests. In the OF test, *App*^{NLGF} mice exhibited anxiogenic-like behaviour at 22-23 months, preferring to remain in the perimeter of the testing arena. In contrast, in the EPM task, *App*^{NLGFs} consistently demonstrated seemingly anxiolytic behaviour across all ages tested, showing a strong preference for the open arms relative to controls. Additionally, they displayed significantly more head-dip risk assessment behaviours, but fewer stretch-attend postures compared to C57BL/6J mice, suggesting complex alterations in risk assessment.

3.2 Introduction

3.2.1 Behavioural Assessment of Memory

Memory is a complex cognitive function that involves the encoding, storage, and retrieval of information (Tromp et al., 2015). The long-term memory system is divided into implicit (non-declarative) memory, involving experience-based memories retrieved without conscious awareness, and explicit (declarative) memory, which involves the conscious recall of information (Squire, 1987). Declarative memory is subdivided into semantic memory, relating to facts and knowledge, and episodic memory, relating to specific events (Bouyeure & Noulhiane, 2020). In humans, the term “episodic memory” refers to the conscious recollection of an experience with relation to what happened, when it happened, and where it happened (Bouyeure & Noulhiane, 2020). A decline in this form of memory is widely reported as an early clinical symptom of AD (Bäckman et al., 2004; Dubois et al., 2007; Ringman, 2005; Schwindt & Black, 2009). In rodents, the term “episodic-like memory” is often used to describe behaviours that resemble human episodic memory. However, the term is controversial as rodents cannot consciously or verbally recall a past event as humans can. Nevertheless, experimental paradigms have been developed to model certain aspects of episodic memory, providing a means to study the relevant memory systems in rodents. Utilising the innate tendency of rodents to explore novelty in their environment, Ennaceur and Delacour described object recognition protocols that involve manipulations of an array of objects to stimulate novelty-driven behaviour (Ennaceur & Delacour, 1988). Specifically, tasks such as the ON, OL, OiP, and Temporal Order (TO) are commonly used object recognition protocols that assess separate and combined aspects of episodic-like memory in rodents. Typically, recognition testing begins with a series of sample trials, during which the animal is exposed to a set of objects in an otherwise empty arena for each trial. Between and following the sample trials, the animal is returned to its homecage for a defined period. The time in which the animal spends in its home cage following the final sample trial may be adjusted to manipulate retention time, and typically ranges from 5 minutes to 24 hours depending on the retention being tested. Following the final delay period, the objects are manipulated, and the animal is returned to the arena. In the ON test, a subset of the objects from the sample phase are replaced with entirely new objects that the animal has not previously encountered. In the OL task, one object is moved to a previously unoccupied location in the arena. In the OiP task, two objects are diagonally swapped. In the TO task, one object from the second, more recent sample trial and one object from the first, less recent sample trial are placed in the arena.

Due to the innate preference of rodents to explore novel or less recently explored objects, functioning episodic-like memory drives them to spend relatively more time exploring the novel object in the ON task, the repositioned object in the OL task, the switched object in the OiP task, and the less recently encountered object in the TO

task (Ennaceur & Delacour, 1988). Preferential exploration of the novel object(s) in the ON task reflects intact recognition memory, indicating that the animal can distinguish between familiar and novel stimuli (Ennaceur & Delacour, 1988). Impaired novelty detection is inferred by a lack of significant preference for the novel object(s) (Ennaceur & Delacour, 1988). Reflecting this, patients with early AD often exhibit difficulties discriminating similar but distinct objects or performing tasks that require fine perceptual discrimination of objects (Bastin & Delhaye, 2023; Frick et al., 2023). Rodent lesion studies have demonstrated that the perirhinal cortex (PRh) plays a critical role in encoding and retaining object-specific information, making it essential for novelty detection during ON testing (Bussey et al., 1999; Mumby & Pinel, 1994; Norman & Eacott, 2004; Warburton & Brown, 2015). The PRh is affected in early stages of AD progression (Braak & Braak, 1991, 1997).

Building upon simple novelty discrimination, the OL and OiP tasks both assess spatial memory, but tap into distinct cognitive processes. The OL task evaluates the ability to recall the location of objects within an environment, focusing exclusively on spatial memory (Ennaceur et al., 1996; Vogel-Ciernia & Wood, 2014). The OiP task, however, assesses associative memory by evaluating the ability to integrate information about a specific object within its spatial context, requiring both spatial memory and novelty recognition (Barker et al., 2007; Barker & Warburton, 2011). Rodents with impaired spatial or associative memory systems will fail to show significant preference for exploring the relocated objects in the OL and OiP spatial tasks, respectively (Barker et al., 2007; Barker & Warburton, 2011). In AD, such impairments commonly manifest as functional deficits such as spatial disorientation and difficulties recalling the sequence of recent events (Tromp et al., 2015). Lesion studies have demonstrated that the OL task is highly dependent upon the intact HPC for spatial encoding, whereas the OiP task is dependent upon the functional interaction between the medial prefrontal cortex (mPFC)-HPC-PRh network, collectively supporting a complex integration between novelty and spatial encoding (Barker & Warburton, 2011; Warburton & Brown, 2015). The TO task, which assesses the ability to discriminate less recently presented objects from those presented more recently, also depends on functional communications of the mPFC-HPC-PRh circuit (Barker et al., 2007; Barker & Warburton, 2011; Fortin et al., 2002; Mitchell & Laiacona, 1998). In AD, the HPC is particularly sensitive to Aβ plaques, NFTs, and neuron loss (Giannakopoulos et al., 2003; Jack et al., 2013; Mormino et al., 2009). Furthermore, lesion studies have also implicated the RSC, also a prominent site of AD pathology, in “what-where” and “what-when” episodic-like memory (Braak & Braak, 1991; Powell et al., 2017; Todd & Bucci, 2015; Vann & Aggleton, 2002; Vann et al., 2009). The broader roles of the RSC will be discussed in more detail in Chapter 4 of this thesis, however, in relation to episodic memory, the RSC is believed to integrate sensory stimuli, orientations, spatial locations, and sequences of events, enabling the creation of coherent episodic memories while supporting error correction processes (Alexander et al., 2023).

Mouse models of AD display inconsistent deficits in episodic-like memory. For example, Tg2576 mice typically display intact ON and TO memory but impaired OiP memory from 13-16 months (Evans et al., 2020; Evans et al., 2019; Good & Hale, 2007; Good, Hale, et al., 2007; Hale & Good, 2005; Hsiao et al., 1996). Similarly, PDAPP mice retain ON memory but show OiP deficits from 14-16 months (Evans et al., 2019). Contrastingly, 5xFAD and APP/PS1 mice exhibit ON and OL deficits (Joyashiki et al., 2011; Webster et al., 2013; Zhang et al., 2023a). In *App*^{NLGF} mice, several studies have reported ON deficits that generally appear around 9-12 months (Auta et al., 2022; Degawa et al., 2021; Locci et al., 2021; Mehla et al., 2019). One study suggests that deficits appear at 6 months (Pauls et al., 2021), however this is contrasted by other studies that show intact novel object recognition at this age (Mehla et al., 2019; Whyte et al., 2018). Interestingly, however, one study suggests it is intact at both 6-9 and 12-14 months (Fig. 3.1) (Broadbelt et al., 2022). Whilst there is limited object recognition data in *App*^{NLGF} mice, Broadbelt et al., (2022) also show that OL memory is intact at 6-9 and 12-14 months (Fig. 3.1). However, a combined "what-where-when" test and different object paired associative learning (dPAL) task suggest temporal and contextual spatial memory deficits appear in *App*^{NLGFs} from 3-4 months of age (Saifullah et al., 2020; Tan et al., 2023).

A further memory system that is sensitive to AD pathology is working memory (Baddeley et al., 1986; Baddeley et al., 1991; Becker, 1988). While episodic memory is responsible for the long-term storage and retrieval of memories surrounding life events, working memory involves short-term memory (Chai et al., 2018). Working memory is a cognitive system that allows the brain to temporarily hold and manipulate restricted amounts of information to make decisions and guide behaviour (Chai et al., 2018). Baddeley and Hitch's model defines several components of human working memory: i) the central executive which controls attention, and guides the phonological loop and visuospatial sketchpad, ii) the phonological loop, which processes auditory information, iii) the visuospatial sketchpad, which processes visual and spatial information and iv) the episodic buffer, which integrates information across the systems and links information to long-term memory (Baddeley, 2000; Baddeley & Hitch, 1974; Chai et al., 2018). In humans, spatial working memory is crucial to navigate a new route in an unfamiliar environment, for example (Chai et al., 2018). According to the Baddeley and Hitch model, the visuospatial sketchpad allows for the visualisation street layouts, including the relative position of landmarks and the path to the destination, the phonological loop is utilised if given verbal directions, the central executive directs attention and coordinates navigational decisions, and the episodic buffer integrates the various forms of information and combines it with prior knowledge such as similar routes or familiar landmarks to support navigation (Baddeley, 2000; Baddeley & Hitch, 1974; Chai et al., 2018). Whilst Baddeley and Hitch's model provides a theoretical framework for understanding different components of working memory, later work by Olton, particularly through the use of the RAM, highlights how rodents manage and manipulate spatial information in single trials using working memory (Olton et al., 1978). The complexity of spatial working memory in rodents differs to that of humans

as rodent working memory does not involve language or complex reasoning (Stopford et al., 2012). However, similarly to humans, it is argued that rodents use spatial working memory to remember locations and form a ‘cognitive map’ of their surroundings that is continuously updated and used to guide exploratory behaviour (Wang et al., 2020). The cognitive map enables rodents to employ distinct navigational strategies. For example, in a process called allocentric navigation, rodents encode the locations of landmarks in their surroundings relative to another, allowing the animal to understand the layout of its environment independent of its current position (Wang et al., 2020). In egocentric navigation, the rodent assesses the position of landmarks in relation to its own body, enabling it to navigate through its environment based on its position within that environment (Wang et al., 2020). A further navigational strategy called path integration is also utilised in spatial working memory as it allows updating of the current position in the environment relative to its position of origin (Kozhevnikov & Puri, 2023). In the wild, functional spatial working memory is necessary for survival as it allows rodents to adapt their behaviour to different spatial contexts, allowing them to efficiently explore their surroundings to gather resources and avoid predation (Ma et al., 2023).

In summary, spatial working memory is experimentally measured by the ability of rodents to remember spatial information over a short period of time, which is typically assessed by observing their navigation behaviour in various maze tasks. For example, in the spontaneous alternation task, the animal is positioned in a Y or T shaped maze and allowed to freely explore for a short period of time (typically 5 or 10 minutes). With intact spatial working memory, rodents navigate the maze in a pattern that avoids entering recently visited arms and favours entering the least recently visited arm, reflecting the innate preference of rodents to efficiently explore their surroundings (Deacon & Rawlins, 2006). In contrast to object recognition testing, the information that guides rodent exploration in the spontaneous alternation task is gathered and utilised within the task and is not recalled from previous sample trials, enabling the animal to continuously update memory to make adaptive decisions based on its surroundings (Collett & Graham, 2004). In the spontaneous alternation test, significantly higher alternation compared to the chance entry of maze arms is typically considered indicative of functional spatial working memory (Lalonde, 2002). However, the selection of the least recently visited arm during the spontaneous alternation task may not necessarily solely reflect the animals’ memory of which arm they had previously entered. For example, behaviour during the spontaneous alternation task may reflect motivation, attention, the potential effects of self-generated olfactory cues, and responsiveness to different levels of brightness in the maze, complicating the interpretation of spontaneous alternation as a measure of spatial memory alone (Hughes, 2004). Therefore, while spontaneous alternation may provide an insight into spatial working memory in rodents, there may be alternative cognitive and behavioural influences. Other tests, such as the RAM and MWM are also frequently used and may be combined to provide a more holistic assessment spatial working memory in rodents. The RAM apparatus consists of eight arms around a central platform, typically each containing a food reward (Olton et al.,

1978). In contrast to the spontaneous alternation task, the RAM relies on training the rodent to efficiently navigate the maze to collect all rewards and avoid re-visiting arms which no longer contain any rewards (Penley et al., 2013). Therefore, a rodent with impaired spatial working memory will show lower accuracy in the RAM test compared to a rodent with intact spatial working memory (Olton et al., 1978). The MWM is a large body of water with a platform submerged just below the surface. The aversive nature of water drives the rodent to find the platform in an attempt to escape the maze. During the training phase, the animal is placed in the water at different locations and must rely on spatial information to find the hidden platform. During the test trial, the platform is removed and the time the animal spends in the former location of the platform is recorded as a measure of spatial working memory. With impaired spatial working memory, the rodent will typically show longer latency to the target zone and decreased time in the target zone compared to an unimpaired rodent (Morris, 1984).

The function of several brain regions is critical for processing and retaining information during spatial working memory tasks. For example, place cells in the HPC help form the cognitive map by firing when the animal occupies specific locations (O'Keefe, 1976). This process supports the encoding, maintenance, and updating of spatial information during navigation tasks (Moser et al., 2015; O'Keefe, 1976). MRI-based studies in AD patients have implicated the HPC along with the medial temporal lobe in the episodic buffer component of working memory (Berlingeri et al., 2008; Twick & Levy, 2021). Rodent lesion studies reinforce the importance of the HPC in spatial working memory tasks as damage to this region impairs performance in MWM, RAM, and T/Y-maze tasks (Bannerman et al., 1999; Dillon et al., 2008; Dudchenko et al., 2000). Furthermore, the closely linked EC plays a pivotal role in spatial working memory, consequently, lesions or inactivation of the EC also commonly result in spatial working memory deficits (Coutureau & Di Scala, 2009). The EC particularly contributes to spatial working memory through its grid, boarder, and head direction cells (Moser et al., 2015). Grid cells are specialised neurons that fire in a hexagonal grid-like pattern, creating an internal coordinate system that contributes to path integration (Sanders et al., 2015). Border cells fire when the animal approaches an environmental boundary, working to anchor the spatial map to stable features in the environment (Solstad et al., 2008). Head direction cells, which will be discussed in greater detail with reference to the RSC in Chapter 4, fire in response to the animal's head direction, providing directional information during navigation (Weiss & Derdikman, 2018). The RSC has also been implicated in spatial working memory, particularly in integrating allocentric and egocentric frames of reference, enabling the flexible transition between these strategies (Vann et al., 2009). This process is also supported by head direction cells and contributes to path integration and adaptive navigation (Aggleton et al., 2021; Alexander & Nitz, 2015; Stacho & Manahan-Vaughan, 2022; Vann et al., 2009; Weiss & Derdikman, 2018). RSC lesion and inactivation studies reveal deficits in MWM, RAM, and T-maze tests which require the use of spatial landmarks for orientation (Alexander et al., 2023; Keene & Bucci, 2009; Nelson et al., 2015; Vann & Aggleton, 2004). It is suggested

that the RSC integrates spatial cues and sensory stimuli to form a mental representation of its location in an environment, which is continuously updated with movement during spatial working memory tasks, allowing adjustment of navigation based on environmental feedback (Alexander et al., 2023). However, there has been ongoing debate about whether the role of the RSC in spatial working memory is essential or auxiliary, given its functional overlap with the highly interconnected HPC region (Mitchell et al., 2018). It has been suggested that the HPC and anterior thalamic nuclei may compensate for loss of RSC function during spatial working memory tasks (Nelson et al., 2015).

Lesion and inactivation studies also evidence the role of the PFC in spatial working memory tasks (Dunnett et al., 1999; Funahashi, 2013; Sawaguchi & Iba, 2001; Yang et al., 2014). Specifically, neuroimaging studies suggest the PFC contributes to spatial working memory by integrating spatial information with sensory and motor inputs to direct behaviour during a task (Funahashi, 2013). Electrophysiological studies have demonstrated firing of the PFC during spatial working memory tasks that persists during the delay period between tasks, suggesting a role in maintaining spatial representations independently of immediate sensory input (Lim & Goldman, 2013; Wang, 1999; Yu et al., 2024). Furthermore, the PFC plays a pivotal role in executive control during spatial working memory tasks, a function closely linked to Baddeley's central executive component (Funahashi, 2017). It achieves this by suppressing irrelevant details to prioritise relevant information, facilitating adaptive decision making and goal-directed navigation (Barbas & Zikopoulos, 2007).

Working memory, including spatial working memory, is frequently impaired in AD, with deficits usually beginning in MCI and serving as early indicators of progression to AD (Kirova et al., 2015). These deficits, alongside episodic memory impairments discussed earlier, are reflected by pathological alterations in key areas such as the HPC, EC, PFC, and RSC, which commonly exhibit plaques, NFTs, reduced functional connectivity, atrophy, and/or hypometabolism (Berlingeri et al., 2008; Berron et al., 2021; Braak & Braak, 1991; Strom et al., 2022). These impairments commonly manifest in the inability of patients to temporarily hold and manipulate information in order to follow multi-step instructions, or getting lost in familiar and unfamiliar environments (Perry & Hodges, 1999; Vlček & Laczó, 2014). Specifically, functional MRI (fMRI) studies reveal that even in the early stages of AD, patients exhibit deficits in the ability to use path integration, and both allocentric and egocentric navigational strategies during spatial navigation tests (Mokrisova et al., 2016; Vlček & Laczó, 2014). Transgenic mouse models of AD also show early impairments in spatial working memory, which often emerge prior to deficits in associative learning, reference memory, and recognition memory (Webster et al., 2014). For example, the Tg2576 model exhibits impaired alternation from 9-10 months of age (Hale & Good, 2005; Hsiao et al., 1996). Furthermore, the PDAPP model exhibits RAM and MWM deficits from 3-4 months of age (Chen et al., 2000; Dodart et al., 1999; Hartman et al., 2005). However, in the less characterised

App^{NLGF} model, three studies suggest there is a deficit that emerges around 10-12 months (Auta et al., 2022; Degawa et al., 2021; Locci et al., 2021). Contrastingly, initial findings by Saito and colleagues demonstrated alternation deficits at 6 months of age (Fig. 3.1) (Saito et al., 2014). Other studies have reported intact spontaneous alternation at 6-9 and 12-14 months (Broadbelt et al., 2022; Whyte et al., 2018). *App*^{NLGF} performance in the MWM test appear equally varied, with some studies reporting increased escape latency from 6-12 months (Locci et al., 2021; Mehla et al., 2019; Wang et al., 2022), and other studies reporting no deficit during this age range (Latif-Hernandez et al., 2019; Saifullah et al., 2020; Whyte et al., 2018) (Fig. 3.1). This suggests that any spatial working memory deficit in the *App*^{NLGF} model may be subtle or not robust enough to replicate in different laboratory settings.

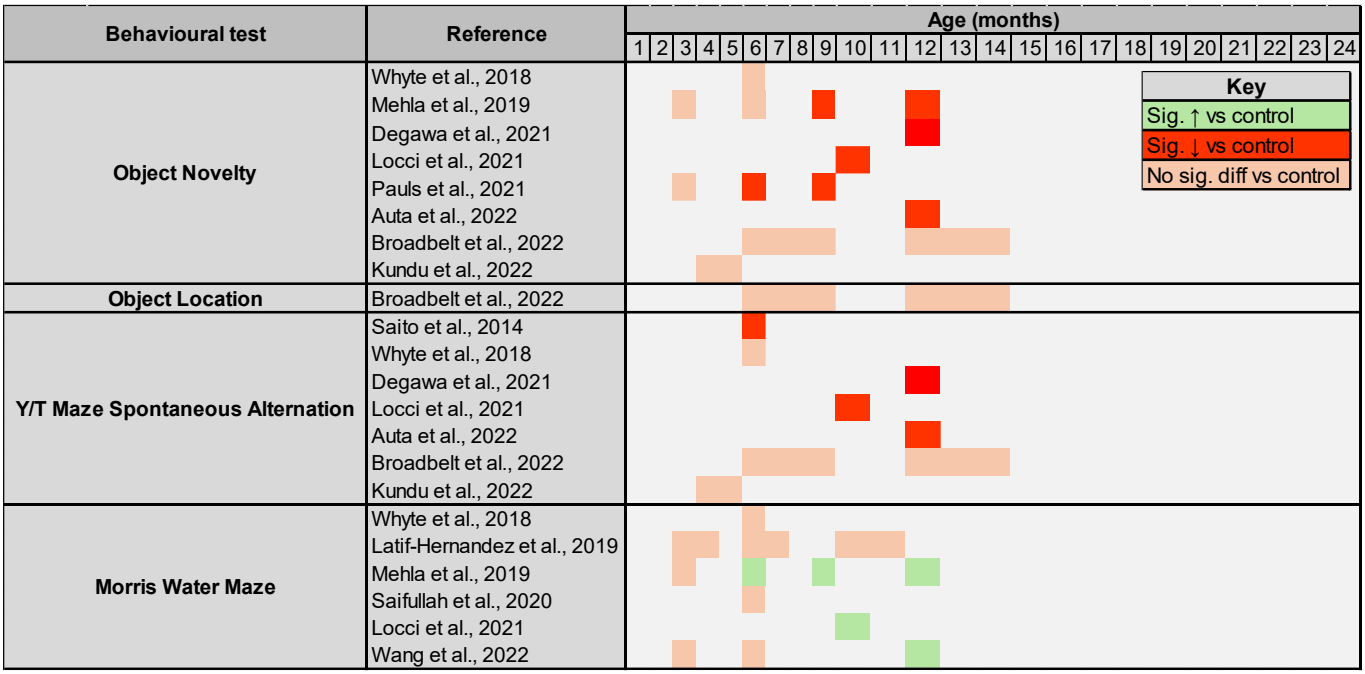

Figure 3.1: Timeline of Cognitive Deficits in the App^{NLGF} Mouse Model. The behavioural phenotype of the *App*^{NLGF} model in a range of cognitive tasks including the Object Novelty (ON), Object Location (OL), Y or T-maze spontaneous alternation, and Morris Water Maze (MWM). The colour code indicates a significant increase (green) or decrease (red) from the control line ($p < 0.05$) or no significant difference from the control line (orange) ($p > 0.05$). The control lines used are *App*^{NL} or C57BL6/J. For the ON and OL test, the measure used is discrimination ratio/index or percentage of time interacting with novel object(s). For the spontaneous alternation test, the measure is percentage spontaneous alternation. For MWM, the measure is escape latency.

3.2.2 Behavioural Assessment of Anxiety

Other than the cognitive changes above, AD is also characterised by NPS (Pless et al., 2023). In his original 1906 paper, Alzheimer described Auguste Deter as exhibiting emotional disturbances and paranoia (Alzheimer et al., 1995; Maurer et al., 1997). Today, it is well established that common NPS in AD include depression, anxiety, aggression, agitation, apathy, and disinhibition, which are highly comorbid and mutually reinforcing (Goodwin et al., 2023). It is estimated that up to 97% of AD patients experience NPS at some stage of their illness, substantially impacting the patients' quality of life, increasing the practical, emotional, and financial burden on families and caregivers and accelerating the need for institutionalisation (Lyketsos et al., 2011; Mendez, 2021; Steinberg et al., 2008). NPS symptoms frequently emerge in the early stages of cognitive decline and are often regarded as prognostic and diagnostic indicators for progression from MCI to AD (Diniz et al., 2013; Edwards et al., 2009; Leoutsakos et al., 2015). Furthermore, NPS in AD are linked to increased morbidity and mortality, with the severity of NPS corelated with the extent of cognitive decline (Clement et al., 2020). Despite this, clinical research and pharmaceutical development of NPS drugs remains scarce (Pless et al., 2023).

Much of the current literature surrounding NPS in AD focuses on depression and apathy, the two most prevalent symptoms (Lyketsos et al., 2011). However, anxiety is less well understood. Anxiety is the third most common NPS in AD, with up to 71% of patients suffering from this symptom (Ferretti et al., 2001; Mendez, 2021; Teri et al., 1999). In AD, anxiety often manifests as excessive worry and is linked to avoidance behaviours, irritability, and agitation, and is often accompanied with sleep disturbances (Baillon et al., 2019; Farina et al., 2023). Anxiety symptoms can appear from early stages of the disease process and worsen throughout disease progression, with symptoms often preceding or presenting alongside memory loss during MCI (Donovan et al., 2018; Gallagher et al., 2011; Geda et al., 2008; Li & Li, 2018; Lyketsos et al., 2011; Mendez, 2021; Pietrzak et al., 2015). There is also evidence that anxiety can preclude AD and promote progression of prodromal AD and MCI to clinical AD (Li & Li, 2018; Mah et al., 2015; Mendez, 2021). Furthermore, individuals who suffer from anxiety are at a significantly greater risk of developing AD in their lifetimes, suggesting a complex and bidirectional relationship between NPS and cognitive decline (Petkus et al., 2016). Reflecting this, current medications aimed to treat cognitive symptoms of AD, such as memantine or AChIs, occasionally worsen or stimulate anxiety in AD patients (Mendez, 2021). Similarly, many current pharmacological agents prescribed for NPS, such as SSRIs and short-term anxiolytic drugs such as benzodiazepines, often fail to alleviate symptoms, pose substantial side effects and risks, or even worsen cognitive decline (Koenig et al., 2016; Mendez, 2021; Tampi et al., 2016). Treatment of anxiety in AD therefore typically involves non-pharmacological interventions such as reducing known triggers, maintaining a calm environment and steady routine, therapeutic activities such as art

and music, along with conservative prescription of mediation (Cohen-Mansfield, 2001; Mendez, 2021).

Anxiety behaviours in humans and rodents are regulated by key brain areas, including the amygdala, HPC, and PFC, which play crucial roles in processing fear, stress, and anxiety responses, and are modulated by anxiolytic drugs such as SSRIs and benzodiazepines (Bannerman et al., 2004; Cao et al., 2018; Dale et al., 2016; Davis et al., 1994; Griessner et al., 2021; Hillhouse & Porter, 2015; Insel et al., 1984; Kenwood et al., 2022; Shin & Liberzon, 2010; Tassone et al., 2024). As discussed earlier in this thesis in relation to memory, the HPC and PFC are prominent sites of AD pathology including amyloid plaques, tau tangles, and atrophy (Rao et al., 2022). The amygdala is also a site of early AD pathology, with the severity of atrophy in this area reported as comparable to that of the HPC in early disease stages (Braak & Braak, 1991; Poulin et al., 2011; Stouffer et al., 2024). Similarly, anxiety is linked to atrophy and hypometabolism of key areas such as the EC, and the presence of NFTs (Hashimoto et al., 2006; Johansson et al., 2020; Mah et al., 2015; Ramakers et al., 2013). However, despite evidence that other AD pathologies play a role in anxiety in AD, several PET studies combined with MMSEs highlight the role of amyloid in anxiety by evidencing that elevated neuronal amyloid is associated with increased anxiety and predicts faster cognitive decline (Donovan et al., 2018; Johansson et al., 2020; Pietrzak et al., 2015; Pietrzak et al., 2014). Furthermore, in patients with MCI, anxiety is also associated with abnormal CSF levels of $A\beta_{42}$ (Ramakers et al., 2013).

Whilst there are some variations depending on the source, anxiety is broadly defined in human psychology as a negative emotional state marked by excessive worry, tension, and hypervigilance, often accompanied by physiological responses such as elevated heart rate and blood pressure (American Psychiatric Association, 2013; Kwak et al., 2017; Pentkowski et al., 2021). The psychological state of anxiety is thought to be a pathological secondary response to another emotion such as fear, to another unidentified stressor, or as an anticipatory response to a perceived forthcoming threat, often interfering with daily life (McTeague & Lang, 2012). An important issue in anxiety research is whether this complex emotional response can be translated to rodent research without anthropomorphising the behaviour of these animals. Interestingly, however, there are several key similarities between humans and rodents that allow researchers to draw meaningful similarities between anxiety states in both species. For example, the neuroanatomy, connectivity, and function of the amygdala, a key brain structure involved in anxiety processing, is largely conserved between primates and rodents (Belzung & Philippot, 2007). Furthermore, physiological changes that occur with human anxiety, such as altered cardiovascular and respiratory output, are also present in rodents (Lang et al., 2000). Behaviourally, an anxiety-like state in rodents is expressed as defensive actions, including risk assessment behaviours such as freezing or avoidance of potentially dangerous areas, paralleling rumination and hypervigilance observed in human anxiety

(Blanchard et al., 2011). It is argued that this is a primitive state in rodents that is triggered by potential, perceived, and/or ambiguous threats to survival or wellbeing, facilitating the “fight or flight” response (Belzung & Philippot, 2007). In humans, however, whilst the primitive function of anxiety to detect and respond to danger is likely still retained to some degree, it is more of a complex psychological state that is shaped by higher cognitive processes such as self-awareness and abstract thinking (Hohoff, 2009). In both humans and rodents, some degree of anxiety is considered normal, however, elevated, persistent, and disproportionate anxiety responses are indicative of a pathological state, as commonly observed in AD and mouse models of AD (Mendez, 2021; Robinson et al., 2013). Therefore, whilst the complex emotional anxiety response seen in humans may not be fully replicated in animal models, it is possible to draw parallels between the two species.

Historically, dementia research has primarily focused on characterising and manipulating the cognitive phenotypes of various animal models, with comparatively less attention given to NPS such as anxiety in AD. However, various behavioural tests have been developed to assess anxiety-like behaviour in rodents. Examples of experiments commonly used to probe this behaviour in rodents include social interaction tasks, which assess how anxiety modulates social behaviour, and the marble burying task, which evaluates repetitive behaviours associated with anxiety or stress (Lezak et al., 2017; Pentkowski et al., 2021). Other tests rely on the aversive nature of the environment, incorporating mild stressors such as white light, novel surroundings, and perceived vulnerability to predation (Crawley & Goodwin, 1980). For example, the light/dark box test assesses anxiety-like behaviour based on the approach-avoidance conflict of entering aversive (light) zone of a divided box, with anxiolytic compounds such as benzodiazepines increasing the time or entries into the light zone (Bourin & Hascoët, 2003; Crawley, 1981). Variations of this concept include the OF and EPM tasks, which will be the focus of this thesis. As described in more detail in the General Methods section of this thesis, the OF test consists of a square arena in which the animal freely ambulates for 10 minutes. During video footage analysis, inner and outer zones of the arena are retrospectively defined and the time the animal spends in each zone is quantified. The outer zone of the OF arena is a darker, more sheltered environment in which rodents innately explore more than the brighter, more exposed inner zone of the arena (La-Vu et al., 2020). However, significantly reduced exploration of the inner zone compared to control animals is indicative of an anxiogenic phenotype in rodents (Prut & Belzung, 2003). This behaviour coincides with thigmotactic behaviour, i.e., a preference to explore the outer zone of the arena and avoid the centre, remaining close to the walls where there is greater perceived shelter. Conversely, increased exploration of the centre of the arena indicates anxiolytic behaviour (Prut & Belzung, 2003). Pharmacological studies have validated the use of the OF test as a measure of anxiety-like behaviour in rodents, demonstrating that anxiolytic drugs such as diazepam and buspirone increase the time rodents spend exploring the centre of an OF arena (Griebel & Holmes, 2013; Prut & Belzung, 2003).

The concept of the EPM test is similar to that of the OF task. In the EPM task, the animal freely explores a maze consisting of two arms with high dark walls (the closed arms), and two arms with very short Perspex walls (the open arms). The animal can freely choose between entering the more sheltered and thus perceived safer closed arms, or the brighter, more exposed open arms. Rodents tend to prefer the closed arms of the maze as they offer perceived protection from potential predation (Dawson & Tricklebank, 1995). However, it is suggested that the EPM task creates an approach avoidant conflict between their innate motivation to explore novel environments and the aversive nature of the open arms, which is considered a mild anxiogenic stimulus due to their innate fear of heights (Lister, 1990; Pellow et al., 1985; Treit et al., 1993). Similarly to the OF test, increased exploration of the closed arms relative to control animals is cited as indicative of anxiety-like behaviour (Pellow et al., 1985). On the contrary, increased exploration of the open arms of the EPM has been reported as anxiolytic behaviour (Pellow et al., 1985). Pharmacological studies have evidenced that treatment of rodents with anxiolytic drugs such as diazepam increase the number of open arm entries and the time spent in the open arms of the EPM, indicating reduced anxiety (Handley & Mithani, 1984; Lister, 1987; Pellow et al., 1985). Conversely, anxiogenic drugs such as picrotoxin reduce these measures, suggesting heightened anxiety (Handley & Mithani, 1984; Lister, 1987; Pellow et al., 1985). In addition to arm preference, the accuracy of the EPM in detecting anxiety-like behaviour can be enhanced by incorporating ethological analyses of behaviours such as head dips and stretch attend postures, which have also been pharmacologically validated as measures of anxiety related behaviour (Carobrez & Bertoglio, 2005; Cole & Rodgers, 1994; Rodgers, Perrault, Sanger, et al., 1997; Rodgers et al., 1994). A stretch attend posture is defined as a stationary position in which the rodent uses its hindlegs to stretch its body into an open arm, while the hindlegs remain in the closed arm (i.e., orientated towards an anxious stimulus) (Cole & Rodgers, 1994; Rodgers, 1999; Rodgers, Perrault, Sanger, et al., 1997; Setem et al., 1999). Head dipping is defined as the downward movement of the rodents' head over the edge of the open arm of the EPM, towards the floor of the room (File & Wardill, 1975; Rodgers, Perrault, Sanger, et al., 1997; Setem et al., 1999). Head dipping and stretch attends are generally regarded as risk assessment behaviours that indicate increased anxiety (Walf & Frye, 2007).

The OF and EPM tests were selected for this thesis as they provide a non-invasive behavioural assessment that minimises stress to the animal as they do not require forced aversion or deprivation, allowing the focus to be on natural avoidance behaviours. Importantly, chronic stress can exacerbate amyloid production (Justice, 2018), so minimising experimental stress is particularly important in the context of AD research. Furthermore, OF and EPM tests allow for easy measurement of locomotion and exploratory behaviour. Locomotion, such as the total distance travelled during testing, is an important factor to consider during NPS assessments in rodents as it helps determine whether any differences in anxiety-like behaviour

could be explained by differences that may affect movement, such as lethargy or physical impairments that may not be obvious to the experimenter.

The manifestation of anxiety-like behaviour in mouse models of AD, as assessed through OF and EPM testing, is complex. Studies report inconsistent and seemingly contradictory phenotypes, both within individual models and across different models. For example, in the Tg2576 model, some studies show increased exploration of open arms in the EPM test from 7 months, indicating decreased anxiety-like behaviour, but this appears to be somewhat confounded by hyperactivity (Gil-Bea et al., 2007; Lalonde, 2002; Lalonde et al., 2003). However, other studies have evidenced that this model spends more time head-dipping but less time in the stretch attend posture compared to C57BL6/Js (Ognibene et al., 2005). Other studies have noted increased anxiety-like behaviour during the OF test in the PDAPP transgenic model (Beauquis et al., 2014). In the APP/PS1 model, however, there appears to be no significant difference in behaviour during the OF and EPM tasks at ages ranging from 7-24 months (Arendash et al., 2001; Webster et al., 2013). Similarly, there is a lack of consensus regarding the OF phenotype of the *App*^{NLGF} model in the scientific literature. On the one hand, several studies report no significant difference in the time spent in the central zone between *App*^{NLGFs} and C57BL6/Js at ages ranging from 6 to 10 months (Fig. 3.2) (Broadbelt et al., 2022; Kundu et al., 2022; Locci et al., 2021; Maezono et al., 2020; Whyte et al., 2018). However, one study has reported a significant increase in time spent in the central zone at 6 months, suggesting anxiolytic behaviour at this age, however this was not replicated in 10-month-old animals in this study (Latif-Hernandez et al., 2019). A recent study has also observed an increase in exploration of the centre zone in *App*^{NLGFs} at 12 months (Wang et al., 2022). Conversely, other studies have reported decreased exploration of the OF central zone in *App*^{NLGFs} at 8 and 10 months, indicative of anxiogenic behaviour (Locci et al., 2021; Pervolaraki et al., 2019). Similarly, two studies reported reduced duration in the light compartment of the light-dark box at 10 and 12 months, further supporting the presence of heightened anxiety-like behaviour in the *App*^{NLGF} model (Auta et al., 2022; Locci et al., 2021).

The phenotype of *App*^{NLGFs} during EPM testing, however, is more consistent in the literature. Several studies have shown that *App*^{NLGFs} exhibit a preference for the open arms of the EPM, and sometimes even an aversion to the closed arms, at ages ranging from 3 to 18 months of age (Fig. 3.2) (Degawa et al., 2021; Latif-Hernandez et al., 2019; Pervolaraki et al., 2019; Sakakibara et al., 2018). The discrepancy between anxiolytic and anxiogenic behaviour has been described as behavioural disinhibition possibly caused by impairments in the PFC, affecting decision making, which may be reflective of disinhibitory behaviour in AD patients such as impulsivity and inappropriate social conduct (Chung & Cummings, 2000; Migliaccio et al., 2020; Pervolaraki et al., 2019).

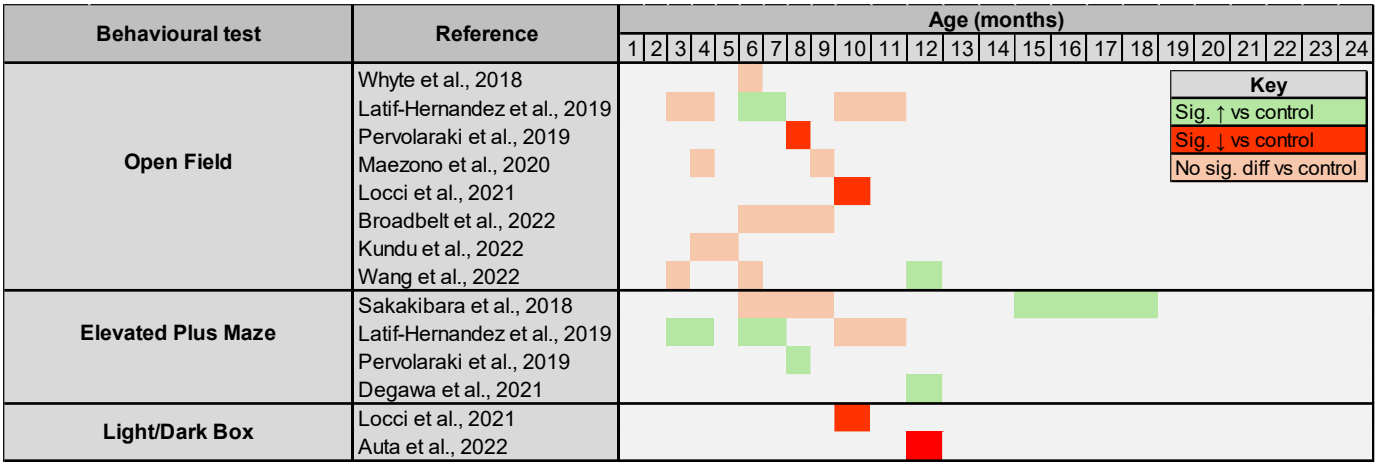

Figure 3.2: Timeline of Affective Alterations in the App^{NLGF} Mouse Model. The behavioural phenotype of the *App^{NLGF}* model in a range of affective tests including the Open Field (OF), Elevated Plus Maze (EPM), and Light/Dark Box (LDB). The colour code indicates a significant increase (green) or decrease (red) from the control line ($p < 0.05$) or no significant difference from the control line (orange) ($p > 0.05$). The control lines used are *App^{NL}* or C57BL6/J. For the OF test, the measure used is time spent in the inner zone or inner zone ratio. For EPM, the measure is time in the open arms or number of open arm crossings. For LDB, the measure is time spent in the light compartment.

3.3 Methods

3.3.1 Introduction

The Methods section of this chapter will summarise the methodologies that were used in behavioural testing, including assessment of memory and anxiety-like behaviour. As behavioural testing was also carried out for Chapter 4 of this thesis, detailed experimental procedures for behavioural testing are reserved for the General Methods chapter of this thesis.

3.3.2 Subjects

Animals were obtained, bred, and maintained as described in the General Methods chapter of this thesis. The total number of animals included in each experimental cohort is detailed in Table 2.1 in the General Methods chapter, and will be presented in the figure legends for each graph in this chapter.

Briefly, *App^{NLGF}* and C57BL6/J control animals of a range of ages underwent behavioural testing. The groups indicate different groups of animals and do not imply

that the same group of animals were tested multiple times throughout their lives. Most groups underwent multiple different behavioural tests within the timespan indicated by the age bracket, but no behavioural test was performed more than once on the same group. OiP and ON testing was performed on 22–23-month-old animals only. OL testing was performed on 4-6-, 8-10-, and 22–23-month animals. OF was performed on 4-6-, 8-10-, 14-16-, and 22–23-month animals. Spontaneous alternation and EPM testing were performed on 4-6-, 8-10-, 12-14-, and 22–23-month animals.

For all experiments, a mixture of male and female animals was used. Where possible, an approximately equal number of male and female animals were selected for each experiment.

3.3.3 Behavioural Assessment

ON, OL, OiP, SA, and EPM tests were performed as described in the General Methods section of this thesis. The experimental procedures, readouts, and analysis of each test is explained in more detail within the General Methods chapter. Each behavioural test was scored using EthoVision XT13, as described in the General Methods chapter.

Memory assessment consisted of object recognition and spontaneous alternation testing. Object recognition testing included ON, OiP, and OL tests, each selected to interrogate a different aspect of recognition memory. Prior to object recognition testing, all animals underwent a series of three habituation days. The first day consisted of one session, conducted in an empty arena, which was utilised to assess anxiety-like behaviour through OF testing. Subsequent habituation days consisted of repeated exposure to relevant arrays of objects within the arena, as described in the General Methods chapter. On the test day, the animals received three 10-minute sample trials in which they were exposed to a further set of objects in the arena. Each sample and test trial were 10 minutes in duration, and between each trial the animal was returned to its homecage. For ON testing, one object from the arena from was replaced by an object that had not been previously encountered, and the animal was returned to the arena. During the OL test, one of two identical objects was moved to a previously unoccupied location within the arena. OiP testing combined assessments of spatial and novelty recognition by swapping two diagonally positioned objects in the arena. To evaluate the animals' preference for exploring the novel object(s) versus the familiar or unmoved object(s) in each object recognition test, object exploration was manually scored, and a Discrimination Ratio (DR) was calculated, as outlined in the General Methods chapter. Spatial working memory was assessed using spontaneous alternation testing, during which the animal freely explored a T-maze for 10 minutes. Its entry into each arm was

recorded, and the percentage of arm alternations was calculated, as described in the General Methods chapter.

To assess anxiety-like behaviour, OF and EPM testing was conducted. The OF test consisted of an empty square arena in which the animal freely explored for 10 minutes. OF analysis was performed by tracking animal exploration around the arena using EthoVision XT13. The time spent by the animal exploring the centre of the arena was determined, followed by the calculation of the Inner Zone Ratio (IZR) to evaluate the animals' tendency to enter the central part of the arena, as described in the General Methods chapter. For EPM testing, each animal freely explored the maze for 10 minutes. Anxiety-like behaviour was assessed by automatically determining the time each animal spends in the open and closed arms using EthoVision XT13, and an OAR was subsequently calculated, as described in the General Methods chapter. Additional measures included the number of entries into the open and closed arms, as well as manually scored risk-assessment behaviours such as head dipping and stretch attend postures.

For each behavioural test analysed with EthoVision XT13, the total distance moved by the animal was calculated and has been presented alongside the behavioural data in this chapter.

3.3.4 Statistical Analysis

To compare object recognition and spontaneous alternation data to a theoretical chance level (0.5 for object recognition tests or 22% for spontaneous alternation), one-sample T-tests were performed. To compare the means of two independent groups in a parametric dataset, unpaired two-tailed T-tests were performed, or the non-parametric alternative was used when necessary, as outlined in the General Methods chapter. To analyse the effects of two independent variables on one dependent variable, two-way ANOVAs were performed. Similarly, to analyse the effects of three independent variables on one dependent variable, a three-way ANOVA was performed. As also described in the General Methods chapter, simple main effects analysis was performed when significant interactions were detected. Bonferroni adjustment was applied to the simple main effects analysis to control for the increased rate of type I error from multiple comparisons. Where there was a significant main effect of age, but a non-significant interaction, Bonferroni *post hoc* testing was used to perform pairwise comparisons between age groups whilst controlling for increased type I error rate.

3.4 Results

3.4.1 Representative Image of *App*^{NLGF} Cortical Amyloid Deposition at 23 Months of Age

Although time constraints prevented a full quantitative analysis of amyloid deposition across relevant brain regions and age groups, a pilot IHC stain was performed on brain tissue from the 22–23-month *App*^{NLGF} animals used for behavioural testing. Consistent with previous findings (e.g., Saito et al., 2014), substantial amyloid accumulation was observed in the frontal cortex (Fig. 3.3), confirming the presence of pathology in the oldest cohort assessed behaviourally. This corresponds to the same age group examined for Ca^{2+} imaging in Chapter 4 of this thesis.

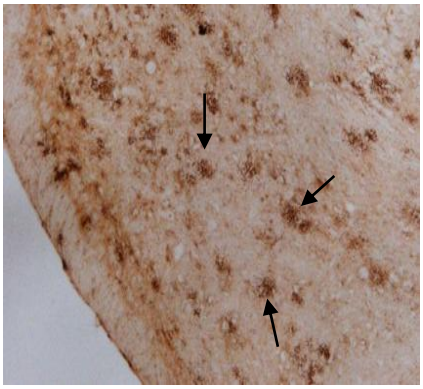

Figure 3.3: Representative Image of Amyloid-β Plaques in the App^{NLGF} Frontal Cortex. Image of cortical region from 22–23-month-old *App*^{NLGF} mouse. Plaques shown by black arrows. Immunohistochemistry was performed as described in the General Methods chapter of this thesis, using Amyloid-β D54D2 antibody (1:500 dilution) obtained from Cell Signalling Technology.

3.4.2 Object Novelty Memory at 23 Months of Age

3.4.2.1 Object Contact Times

ON testing was conducted on animals at 22–23 months of age to evaluate their ability to detect object novelty in advanced age. For the ON task, 12 C57BL6/Js and 11 *App*^{NLGFs} were used. Mice were exposed to four different objects for three 10-minute sample trials. Following a 10-minute delay, two objects were replaced for novel objects.

The mean total time the animals spent interacting with the novel and familiar objects during the test phase were manually scored using EthoVision XT13. This data was not normally distributed (Shapiro-Wilk test $p < 0.05$) and showed unequal variance

(Levene's test $p < 0.05$), so a square root transformation was applied prior to analysis.

A two-way ANOVA was then performed to assess any significant difference in contact times between C57BL6/J and *App*^{NLGF} animals. The test revealed a significant main effect of genotype ($F(1,42) = 4.377$, $p = 0.043$, $\eta p^2 = 0.094$), and object type ($F(1,42) = 117.639$, $p < 0.001$, $\eta p^2 = 0.737$). The genotype*object type interaction was also significant ($F(1,42) = 4.321$, $p = 0.044$, $\eta p^2 = 0.093$). Pairwise comparisons indicated significant differences in contact times between novel and familiar objects for both C57BL6/J and *App*^{NLGF} mice. C57BL6/J animals spent significantly longer interacting with novel objects compared to familiar objects (Mean Difference = 2.211, SE = 0.349, $p < 0.001$, 95% CI:[1.507, 2.914], Fig. 3.4). Similarly, for *App*^{NLGF} animals, the duration of contact with the novel objects was significantly higher than that with familiar objects (Mean Difference = 3.259, SE = 0.364, $p < 0.001$, 95% CI:[2.524, 3.994], Fig. 3.4). Further pairwise comparisons were conducted to explore the effect of genotype on contact time with familiar and novel objects. There was no significant difference in contact time with the familiar objects between C57BL6/J and *App*^{NLGF} animals (Mean Difference = -0.003, SE = 0.357, $p = 0.993$, 95% CI:[-0.723, 0.716] Fig. 3.4). However, *App*^{NLGF} animals exhibited significantly higher novel object contact times compared to C57BL6/J animals (Mean Difference = 1.052, SE = 0.357, $p = 0.005$, 95% CI:[0.332, 1.771], Fig. 3.4).

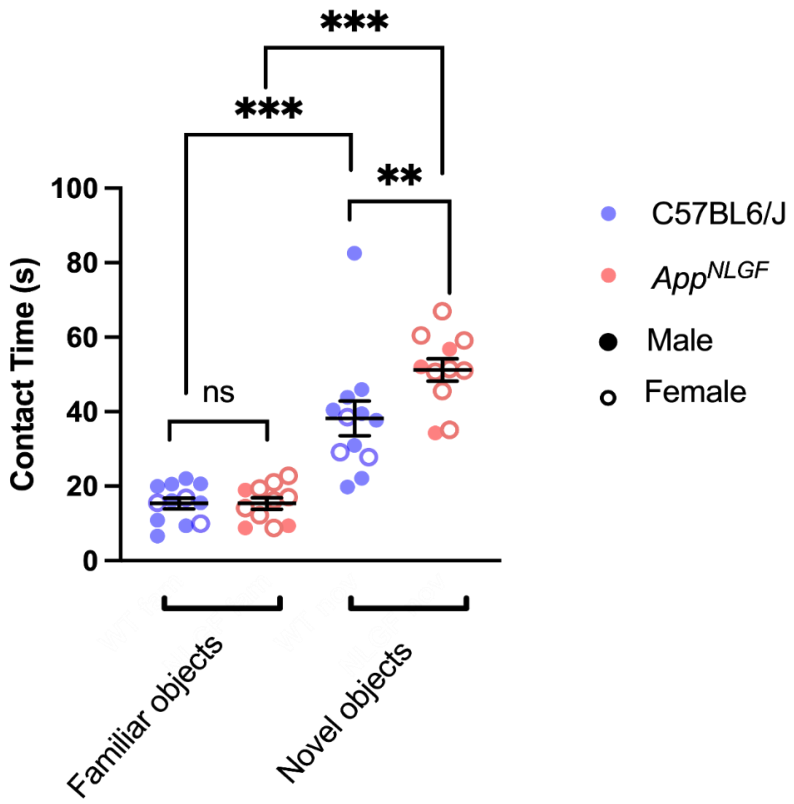

Figure 3.4: Object Contact Times During the Object Novelty Test. The mean interaction times (in seconds) with the novel and familiar objects during object novelty testing, conducted after a 10-minute delay, in animals aged 22–23 months. Raw (untransformed) data shown, with black bars representing the mean +/- standard error of the mean. The results of simple main effects analysis from two-way ANOVA are shown (ns = non-significant, ** = $p < 0.01$, *** = $p < 0.001$). The key indicates animal genotype and sex. C57BL6/J n = 12, *App*^{NLGF} n = 11.

3.4.2.2 Discrimination Ratios

To account for individual differences in interaction time, total object contact times during ON testing were converted into DRs, calculated as the time spent exploring the novel object divided by the total time spent exploring all objects. Additionally, to determine the potential presence of a novelty preference in the initial half of the test, which may have diminished towards the end, EthoVision XT13 was used to separately calculate object exploration times in the first (0–5-minutes, first test phase) and second (5.01-10-minutes, second test phase) halves of the test, which were subsequently converted into separate DRs. No violations of normality (Shapiro-Wilk test $p > 0.05$) or homogeneity of variance (Levene's test $p > 0.05$) were observed.

To establish whether the mice preferentially explored the novel objects, and that novel object interaction was not purely due to chance, one sample T-tests were performed versus a chance probability of 0.5. If the animal spent significantly more time exploring the novel object, the DR would be significantly above chance, indicating that the innate preference for novelty is intact (Ennaceur & Delacour, 1988). One sample T-tests revealed that both C57BL6/Js and *App*^{NLGFs} discriminated the novel objects significantly above chance for the entire trial (C57BL6/J*:* $t(11) = 5.628$, $p = 0.0002$, *App*^{NLGF}: $t(10) = 12.680$, $p < 0.0001$, Fig. 3.5). One sample T-tests also revealed that both genotypes discriminated the novel objects significantly versus chance, for both the first (C57BL6/J: $t(11) = 5.334$, $p = 0.0002$, *App*^{NLGF}: $t(10) = 14.290$, $p < 0.0001$ Fig. 3.5) and second (C57BL6/J: $t(11) = 4.174$, $p = 0.0016$, *App*^{NLGF}: $t(10) = 6.043$, $p = 0.0001$ Fig. 3.5) phases of the test.

An unpaired T-test was performed to compare the mean DRs between C57BL6/J and *App*^{NLGF} mice throughout the entire ON test. The analysis revealed no significant difference in DR between the genotypes ($t(21) = 1.845$, $p = 0.0792$, Fig. 3.5). To examine the effect of genotype and test phase (0–5-minute vs 5.01-10 minute) on DRs, a two-way ANOVA was conducted. The ANOVA revealed no significant main effect of genotype on DR ($F(1,42) = 2.439$, $p = 0.133$, $\eta p^2 = 0.053$), indicating no significant difference in DRs between C57BL6/J and *App*^{NLGF} mice. There was also no significant main effect of test phase on DRs ($F(1,42) = 0.701$, $p = 0.407$, $\eta p^2 = 0.016$), suggesting that the DRs did not significantly differ between the first and second halves of the test. Furthermore, the interaction between genotype and test half was not significant ($F(1,42) = 0.075$, $p = 0.786$, $\eta p^2 = 0.002$), indicating that any effect of genotype on the DR did not change as a function of test duration.

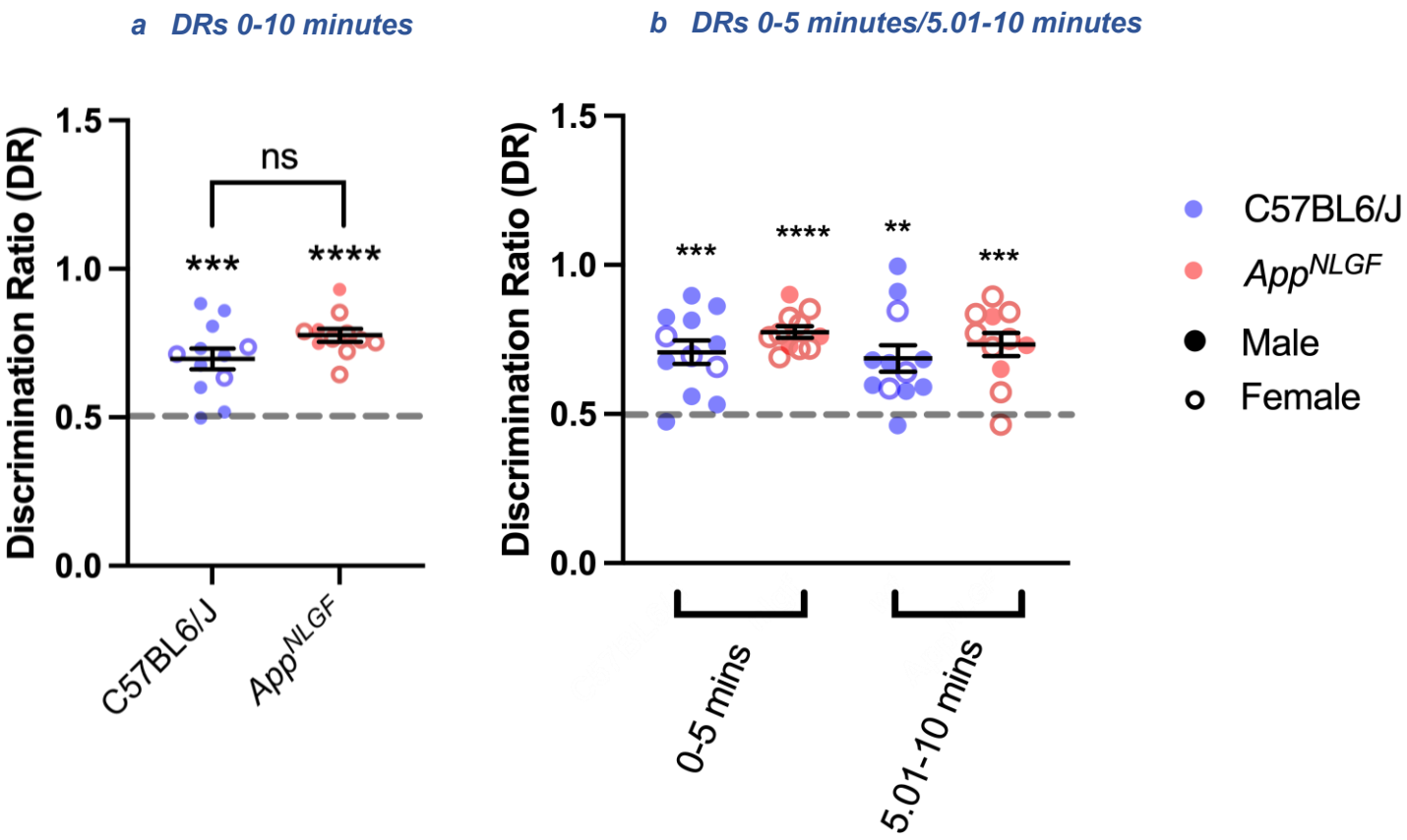

Figure 3.5: Discrimination Ratios During the Object Novelty Test. The mean Discrimination Ratios (DRs) during Object Novelty testing, conducted after a 10-minute delay, in animals aged 22–23 months. Black bars represent mean +/- standard error of the mean. Grey dashed line indicates chance (0.5). Asterisks indicate results of one sample T-test (** = $p < 0.01$, *** = $p < 0.001$, **** = $p < 0.0001$). ***a)*** DRs calculated for the entire 10-minute test. Bracket indicates results of unpaired T-test (ns = non-significant). ***b)*** Separate DRs calculated for the first and second phases of the test. Non-significant interactions in two-way ANOVA not shown. The key indicates animal genotype and sex. C57BL6/J n = 12, *App*^{NLGF} n = 11.

3.4.2.3 Distance Travelled

To determine whether any differences in object interaction could be accounted for by differences in general locomotor activity, the mean total distance travelled was automatically tracked using EthoVision XT13. This data was normally distributed (Shapiro-Wilk test $p > 0.05$) but exhibited unequal variance (Levene's test $p < 0.05$). As transformation did not resolve the unequal variance, a Welch's T-test was performed to compare the mean distance travelled during ON testing between both genotypes. This test revealed no significant difference in the distance travelled between C57BL6/Js and *App*^{NLGFs} during the entire testing period ($t(10.57) = 0.639$, $p = 0.536$, Fig. 3.6).

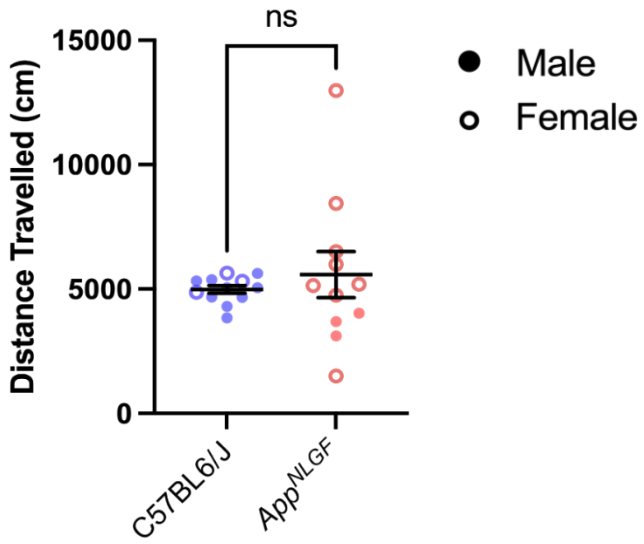

Figure 3.6: Distance Travelled During the Object Novelty Test. The mean distance travelled during the Object Novelty task (in centimetres), in animals aged 22-23 months. Black bars represent mean +/- standard error of the mean. Results of Welch's T-test shown (ns = non-significant). The key indicates animal sex. C57BL6/J n = 12, *App*^{NLGF} n = 11.

3.4.3 Object-in-Place Memory at 23 Months of Age

3.4.3.1 Object Contact Times

OiP testing was carried out to evaluate the animals' ability to detect object-place associations at this advanced age. This test was performed on the same animals as ON, and the order of the tests were counterbalanced (i.e., approximately half of the cohort received ON testing first, and half received OiP testing first). During OiP

testing, the animals were exposed to three 10-minute sample trials with four different objects. Following a final 10-minute delay, two objects were switched diagonally. To investigate spatial novelty preference, the total time the animals spent interacting with each object was manually scored using EthoVision XT13. This data exhibited normal distribution (Shapiro-Wilk test $p > 0.05$) and equal variance (Levene's test $p > 0.05$).

A two-way ANOVA was performed to examine the effect of genotype on object contact times during the OiP test phase. The main effect of genotype was not significant ($F(1, 42) = 0.208$, $p = 0.651$, $\eta p^2 = 0.005$), indicating that there was no significant difference in object contact times between C57BL6/J and *App*^{NLGF} animals. Similarly, the main effect of object type was not significant ($F(1, 42) = 0.069$, $p = 0.795$, $\eta p^2 = 0.002$), suggesting there was no significant difference in contact times between novel and familiar objects during OiP testing. Furthermore, the interaction between genotype and object type was also non-significant ($F(1, 42) = 0.616$, $p = 0.437$, $\eta p^2 = 0.014$), suggesting that the effect of object type on contact time did not significantly differ between genotypes (Fig. 3.7).

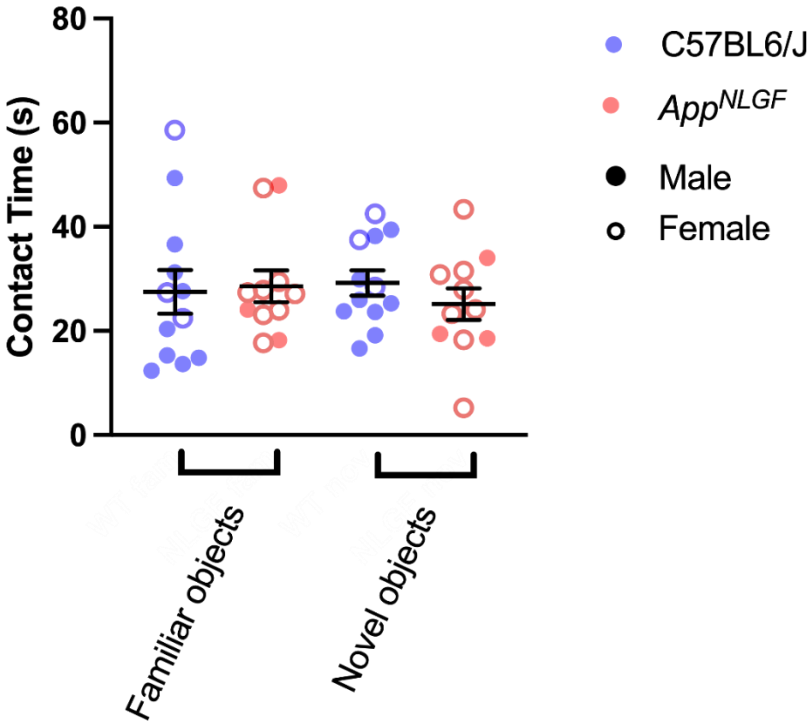

Figure 3.7: Object Contact Times During the Object-in-Place Test. The mean interaction times (in seconds) with the novel and familiar objects during Object-in-Place testing, conducted after a 10-minute delay, in animals aged 22–23 months. Black bars represent mean +/- standard error of the mean. The key indicates animal genotype and sex. C57BL6/J n = 12, *App*^{NLGF} n = 11.

3.4.3.2 Discrimination Ratios

As with the ON test, DRs were calculated for the entire test, as well as separately for the first and second phases. All data exhibited normal distribution (Shapiro-Wilk test $p > 0.05$) and equal variance (Levene's test $p > 0.05$).

One sample T-tests were performed on DRs to determine whether novel object exploration significantly differed to chance (0.5). If the animal spent significantly more time investigating the novel object locations versus the probability of chance, the DR would be significantly higher than 0.5, suggesting intact object-place associative memory (Barker et al., 2007). The results of one sample T-tests showed that for the entire test, neither C57BL6/Js or *App*^{NLGFs} were able to discriminate the switched objects from the objects that had remained in the same position (C57BL6/J: $t(11) = 1.026$, $p = 0.327$, *App*^{NLGF}: $t(10) = 1.332$, $p = 0.212$, Fig. 3.8). During the first 5 minutes of the trial, both C57BL6/J and *App*^{NLGF} animals were unable to discriminate the switched objects from the ones in the same position (C57BL6/J: $t(11) = 1.264$, $p = 0.233$, *App*^{NLGF}: $t(10) = 0.832$, $p = 0.425$, Fig. 3.8). Similarly, neither genotypes could discriminate the switched objects in the final half of the trial (C57BL6/J: $t(11) = 0.462$, $p = 0.653$, *App*^{NLGF}: $t(10) = 1.111$, $p = 0.292$, Fig. 3.8).

An unpaired T-test showed no significant difference in DRs between C57BL6/J and *App*^{NLGF} animals for the entire OiP task ($t(21) = 1.655$, $p = 0.113$, Fig. 3.8). To examine whether genotype and test phase influenced DRs, a two-way ANOVA was performed on the DRs calculated separately for the first and second halves of the test. The main effect of genotype was not statistically significant ($F(1, 42) = 3.017$, $p = 0.090$, $\eta p^2 = 0.067$), suggesting no overall significant difference in DRs between C57BL6/J and *App*^{NLGF} mice. The main effect of test phase was not significant ($F(1, 42) = 0.263$, $p = 0.611$, $\eta p^2 = 0.006$), suggesting that DRs did not significantly differ between the two halves of the test. The interaction effect between genotype and test phase was also not significant ($F(1, 42) = 0.001$, $p = 0.976$, $\eta p^2 = 0.000$), indicating that any effect of the test phase on DRs did not significantly differ between C57BL6/J and *App*^{NLGF} animals during OiP testing.

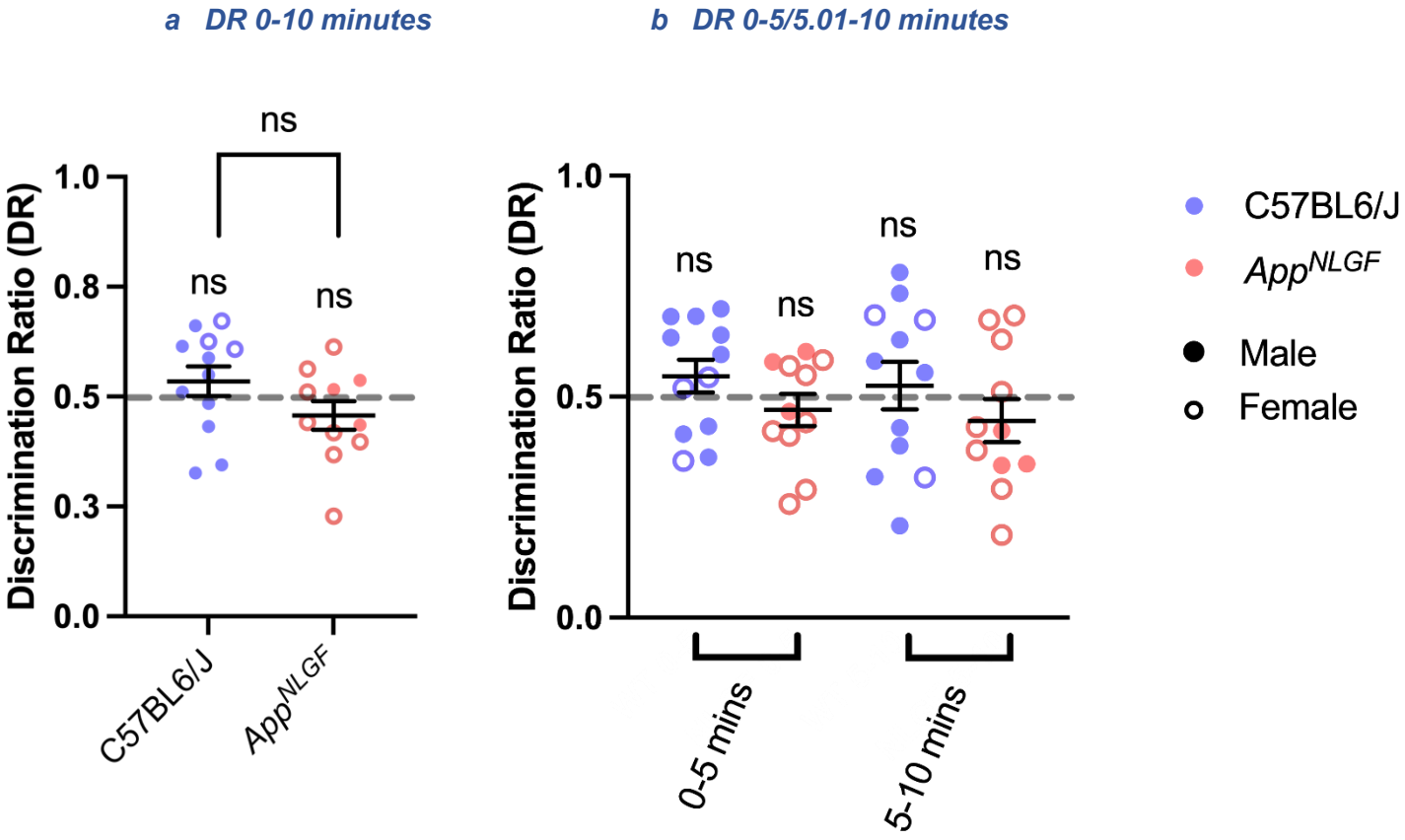

Figure 3.8: Discrimination Ratios During the Object-in-Place Test. The mean Discrimination Ratios (DRs) during Object-in-Place testing, conducted after a 10-minute delay, in animals aged 22–23 months. Black bars represent mean +/- standard error of the mean. Grey dashed line indicates chance (0.5). Non-significant (ns) results of one sample T-test denoted above data points. ***a)*** DRs calculated for the entire 10-minute test. Bracket indicates results of unpaired T-test. ***(b)*** Separate DRs calculated for the first and second phases of the test. The key indicates animal genotype and sex. C57BL6/J n = 12, *App*^{NLGF} n = 11.

3.4.3.3 Distance Travelled

As with ON testing, the mean total distance travelled during OiP testing was determined using EthoVision XT13 tracking software. This data exhibited equal variance (Levene's test $p > 0.05$) but did not show normal distribution (Shapiro-Wilk test $p < 0.05$). As transformation did not resolve this, a Mann-Whitney U test was performed to compare the mean distance travelled between C57BL6/J and *App*^{NLGF} animals. The test revealed no significant differences between C57BL6/Js and *App*^{NLGFs} during OiP testing ($U = 38$, $z = -1.73$, $p = 0.0908$, Fig. 3.9).

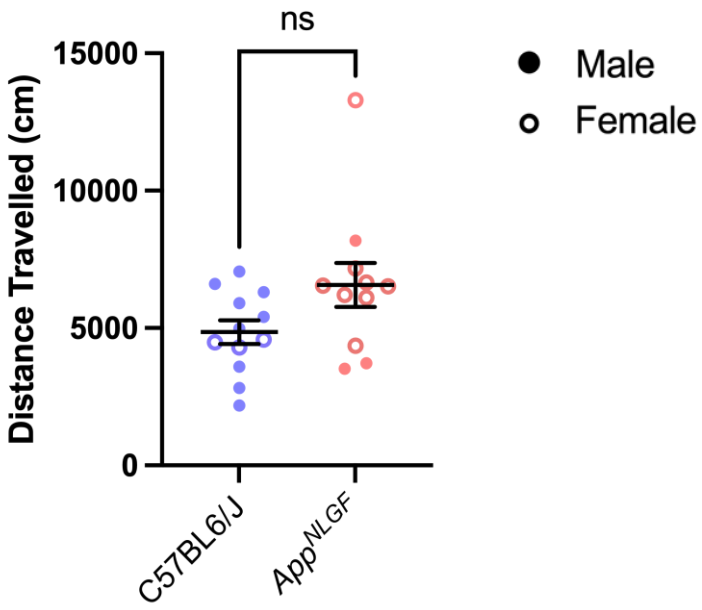

Figure 3.9: Distance Travelled During the Object-in-Place Test. The mean distance travelled during the Object-in-Place task, following a 10-minute delay, in animals aged 22-23 months. Black bars represent mean +/- standard error of the mean. Results of Mann-Whitney U test shown (ns = non-significant). The key indicates animal sex. C57BL6/J n = 12, *App*^{NLGF} n = 11.

3.4.4 Object Location Memory at 5, 9, and 23 Months of Age

3.4.4.1 Object Contact Times

Since neither C57BL6/J or *App*^{NLGF} animals were able to discriminate novel objects in the OiP task, the OL task was utilised as a simpler, more overt hippocampal-dependent spatial task in these 22–23-month-old animals (Barker & Warburton, 2011). To detect the emergence of any deficits in OL testing, separate cohorts aged 4-6 and 8-10 months also underwent OL testing, with 12 animals in each group. As with ON and OiP testing, the animals underwent three 10-minute sample trials, but with two identical objects positioned in the arena. Ten minutes following the final sample trial, one of the objects was moved to a previously unoccupied location within the arena. The total time the animals spent interacting with each object during the OL task was manually scored using EthoVision XT13. This data exhibited unequal variance (Levene's test $p < 0.05$), and some groups were not normally distributed (Shapiro-Wilk test $p < 0.05$), so a $\log_{10}$ transformation was performed to remedy this.

To examine the differences in contact times between C57BL6/J and *App*^{NLGF} animals, a three-way ANOVA was performed. The main effect of object type (the repositioned 'novel' vs unmoved 'familiar' object) was significant ($F(1, 130) = 20.477$, $p < 0.001$, $\eta p^2 = 0.136$). Age also had a significant main effect ($F(2, 130) = 10.811$, $p < 0.001$, $\eta p^2 = 0.143$). However, the main effect of genotype was not significant ($F(1,130) = 1.960$, $p = 0.164$, $\eta p^2 = 0.015$). The interaction between genotype and object type was non-significant ($F(1, 130) = 3.248$, $p = 0.074$, $\eta p^2 = 0.024$). The interaction between genotype and age was also not significant ($F(2,130) = 1.477$, $p = 0.232$, $\eta p^2 = 0.022$). Likewise, the interaction between object type and age was not significant ($F(2,130) = 0.803$, $p = 0.450$, $\eta p^2 = 0.012$). The three-way interaction between object type, age, and genotype was also non-significant ($F(2,130) = 0.177$, $p = 0.838$, $\eta p^2 = 0.003$). Bonferroni *post hoc* tests revealed significant differences in contact times between 22–23-month animals and 4-6 month animals (Mean Difference = 0.212, SE = 0.047, $p < 0.001$, 95% CI:[0.0974, 0.327], Fig. 3.10), and between 22-23 month and 8-10 month animals (Mean Difference = 0.1577, SE = 0.047, $p = 0.004$, 95% CI:[0.0409, 0.2705], Fig. 3.10).

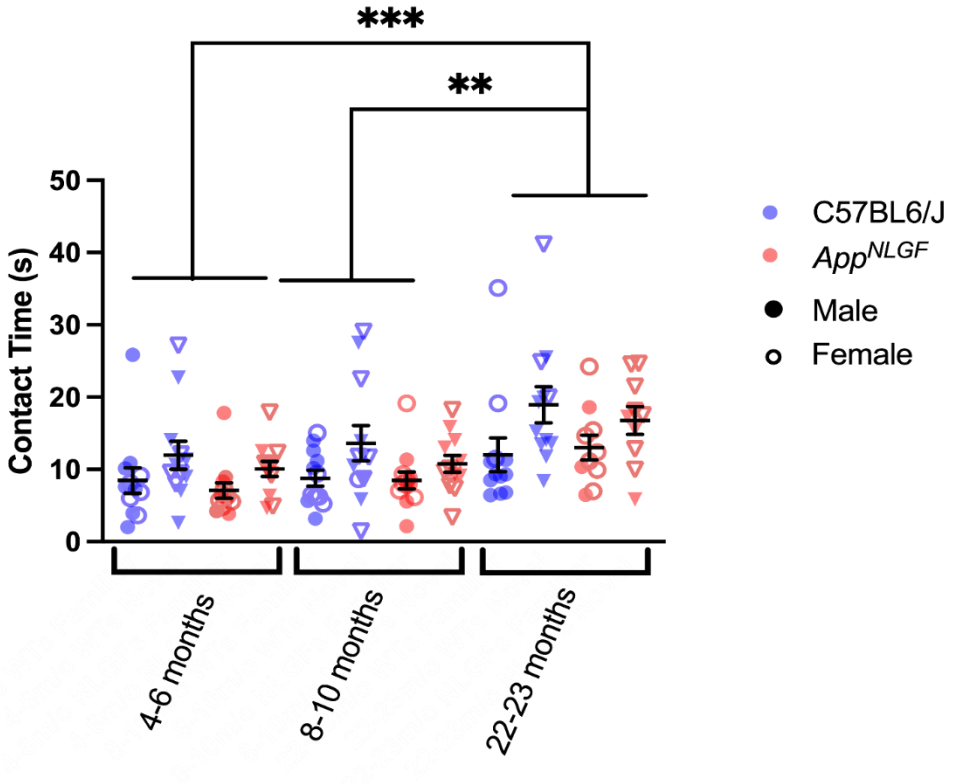

Figure 3.10: Object Contact Times During the Object Location Test. The mean interaction times (in seconds) with the novel and familiar objects during Object Location testing, conducted after a 10-minute delay, in animals aged 4-6, 8-10, and 22-23 months. The raw (untransformed) data is presented with the black bars representing the mean +/- standard error of the mean. Results of Bonferroni *post hoc* tests from two-way ANOVA are shown (** = $p < 0.01$, *** = $p < 0.001$). The key indicates genotype and sex. Object position is denoted by symbol shape, where circular symbols indicate the object in the familiar position and triangular symbols indicate the object in the novel position. C57BL6/J: 4-6m/o n = 12, 8-10m/o n = 12, 22-23m/o n = 12. *App*^{NLGF} 4-6m/o n = 12, 8-10m/o n = 12, 22-23m/o n = 11.

3.4.4.2 Discrimination Ratios

DRs for the entire OL test were calculated using the object contact data, as described earlier in this thesis. All data exhibited normal distribution (Shapiro-Wilk test $p > 0.05$) and equal variance (Levene's test $p > 0.05$).

One sample T-tests were performed to determine whether animals spent significantly more time interacting with novel objects versus the probability of chance (0.5). The tests revealed that, for the 4–6-month animals, both C57BL6/Js and *App*^{NLGFs} preferentially explored the object that had moved, significantly above chance (C57BL6/J: $t(11) = 4.320$, $p = 0.0014$, *App*^{NLGF}: $t(11) = 2.215$, $p = 0.0488$, Fig. 3.11). In the 8–10-month-old group, C57BL6/Js still preferentially explored the moved object ($t(11) = 2.382$, $p = 0.0364$, Fig. 3.11), however, at this age *App*^{NLGFs} could not significantly discriminate the moved object vs the object in the same position ($t(11) = 1.491$, $p = 0.164$, Fig. 3.11). At 22-23 months, C57BL6/Js were still able to discriminate the moved objects ($t(11) = 4.305$, $p = 0.0012$, Fig. 3.11), but *App*^{NLGFs} still could not ($t(10) = 0.6022$, $p = 0.561$, Fig. 3.11). A two-way ANOVA was performed to compare the DRs of both genotypes at all ages. The ANOVA revealed a significant main effect of genotype ($F(1, 65) = 4.915$, $p = 0.030$, $\eta p^2 = 0.070$). The main effect of age, however, was not significant ($F(2, 65) = 1.031$, $p = 0.362$, $\eta p^2 = 0.031$). The interaction between genotype and age was not significant ($F(2, 65) = 0.218$, $p = 0.804$, $\eta p^2 = 0.007$).

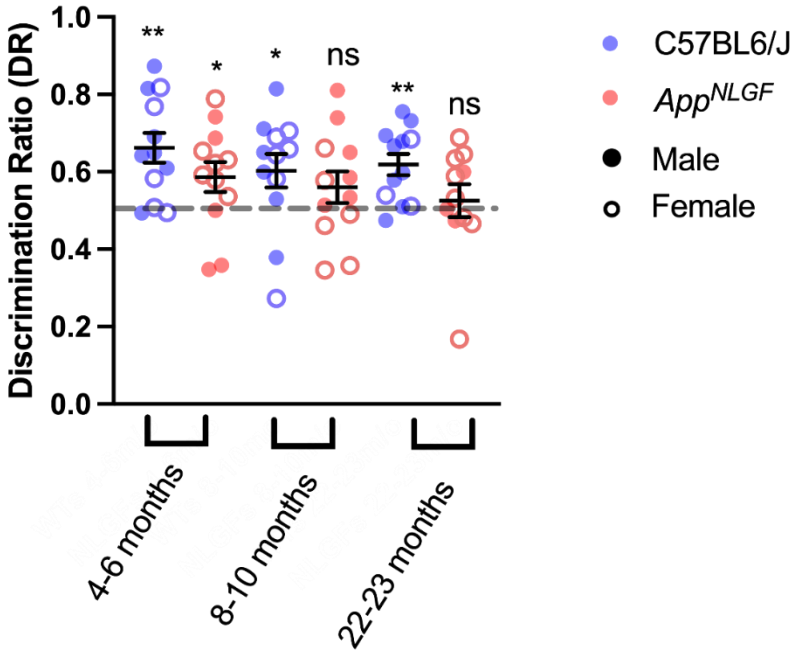

Figure 3.11: Discrimination Ratios During the Object Location Test. The mean Discrimination Ratios (DRs) during Object Location testing, conducted after a 10-minute delay in animals aged 4-6, 8-10, and 22-23 months. Black bars represent mean +/- standard error of the mean. Grey dashed line indicates chance (0.5). Results of one sample T-test denoted above data points (ns = non-significant, * = $p < 0.05$, ** = $p < 0.01$). The key indicates animal genotype and sex. C57BL6/J: 4-6m/o n = 12, 8-10m/o n = 12, 22-23m/o n = 12. *App*^{NLGF} 4-6m/o n = 12, 8-10m/o n = 12, 22-23m/o n = 11.

3.4.4.3 Distance Travelled

EthoVision XT13 tracking software was also utilised to automatically record the distance travelled for all animals during OL testing. This data had equal variance (Levene's test $p > 0.05$) but was not normally distributed (Shapiro-Wilk test $p < 0.05$), so it underwent square root transformation.

A two-way ANOVA was performed to determine the effect of age and genotype on the distance moved during OL testing. The analysis revealed a significant main effect of age ($F(2, 65) = 6.640$, $p = 0.002$, $\eta p^2 = 0.10$). The main effect of genotype, however, was not significant ($F(1, 65) = 0.001$, $p = 0.980$, $\eta p^2 = 0.000$). The interaction between genotype and age was also not significant ($F(2, 65) = 2.028$, $p = 0.140$, $\eta p^2 = 0.059$). Bonferroni *post hoc* test revealed significant differences in distance travelled between 22-23 month and 4–6-month animals (Mean Difference = -11.579, SE = 4.604, $p = 0.043$, 95% CI:[-22.893, -0.265], Fig. 3.12), and between 22-23 month and 8-10 month animals (Mean Difference = -16.655, SE = 4.604, $p = 0.002$, 95% CI:[-27.699, -5.341], Fig. 3.12).

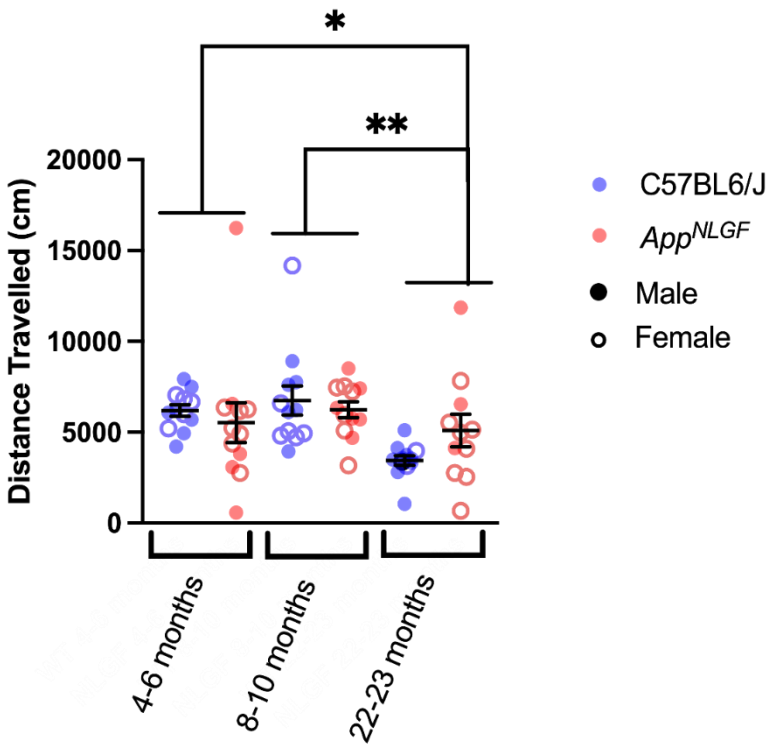

Figure 3.12: Distance Travelled During the Object Location Test. The mean distance travelled during the Object Location task, following a 10-minute delay, in animals aged 4-6, 8-10, and 22-23 months. Raw (untransformed) data shown with black bars representing the mean +/- standard error of the mean. Results of Bonferroni *post hoc* tests from two-way ANOVA are shown (* = $p < 0.05$, ** = $p < 0.01$). The key indicates animal genotype and sex. C57BL6/J: 4-6m/o n = 12, 8-10m/o n = 12, 22-23m/o n = 12. *App*^{NLGF} 4-6m/o n = 12, 8-10m/o n = 12, 22-23m/o n = 11.

3.4.5 T-maze Spontaneous Alternation at 5, 9, 13 and 23 Months of Age

3.4.5.1 Alternation

The 4-6-, 8-10-, and 22–23-month-old groups from object recognition testing, along with an additional 1 C57BL6/J and 3 *App*^{NLGF} mice added to the 22–23-month-old group to improve statistical reliability, underwent the T-maze spontaneous alternation task. Additionally, a 12–14-month-old group (consisting of 12 C57BL6/J and 12 *App*^{NLGF} mice) was included to provide an intermediate age point. During the test, the mice were positioned in the central arm of a T-maze and allowed to freely explore for 10 minutes. The entries into each arm were scored and percentage alternation calculated (percentage alternation = number of alternations/total number of arm entries (-2)). The data exhibited normal distribution (Shapiro-Wilk test $p > 0.05$) and equal variance (Levene's test $p > 0.05$).

To establish whether mice preferentially entered arms of the maze that were least recently visited, versus the chance of entering a random arm, one sample T-tests were performed. Percentage alternation significantly above chance (22%) suggests intact spatial alternation, consistent with functional spatial working memory (Holcomb et al., 1999; Wolf et al., 2016). One sample T-tests revealed that, at all ages tested, C57BL6/Js consistently chose alternative arms when navigating the maze (4-6 months: $t(11) = 20.10$, $p < 0.0001$, 8-10 months: $t(11) = 27.53$, $p < 0.0001$, 12-14 months: $t(11) = 12.89$, $p < 0.0001$, 22-23 months: $t(12) = 11.88$, $p < 0.0001$, Fig. 3.13). Similarly, *App*^{NLGFs} showed above chance alternation at all ages: (4-6 months: $t(11) = 31.66$, $p < 0.0001$, 8-10 months: $t(11) = 12.44$, $p < 0.0001$, 12-14 months: $t(11) = 12.24$, $p < 0.0001$, 22-23 months: $t(13) = 8.652$, $p < 0.0001$, Fig. 3.13).

To examine the effects of age, genotype, and the interaction of the two factors on percentage alternation, a two-way ANOVA was performed. The main effect of age was significant ($F(3, 90) = 3.912$, $p = 0.011$, $\eta p^2 = 0.115$). The main effect of genotype was also significant ($F(1, 90) = 7.086$, $p = 0.009$, $\eta p^2 = 0.073$). Furthermore, the interaction between age and genotype was significant ($F(3, 90) = 3.677$, $p = 0.015$, $\eta p^2 = 0.109$). To investigate the nature of this interaction, simple main effects analysis was performed. At 4-6 months, there was no significant difference between performance of C57BL6/J and *App*^{NLGF} animals (Mean Difference = -0.810, SE = 2.617, $p = 0.758$, 95% CI:[-6.009, 4.389], Fig. 3.13). Similarly, at 12-14 months there was also no significant difference between percentage alternation between both genotypes (Mean Difference = -0.251, SE = 2.617, $p = 0.924$, 95% CI:[-5.450, 4.948], Fig. 3.13). At 8-10 months, there was a significant drop in performance in *App*^{NLGF} animals compared to C57BL6/Js (Mean Difference = -5.308, SE = 2.617, $p = 0.045$, 95% CI:[-10.507, -0.110]), Fig. 3.13). At 22-23 months, *App*^{NLGFs} animals exhibited a significant reduction in percentage alternation

compared to their C57BL6/J counterparts (Mean Difference = -9.549, SE = 2.514, p < 0.001, 95% CI:[-14.543, -4.554], Fig. 3.13).

Within-genotype simple main effects revealed no significant effect of age in C57BL6/J mice ($F(3, 90) = 1.65$, $p = 0.183$, $\eta p^2 = .052$). However, a significant effect of age was found in *App*^{NLGF} mice ($F(3, 90) = 5.94$, $p < 0.001$, $\eta p^2 = 0.165$), indicating that alternation performance varied across the different age groups. Pairwise comparisons revealed a significant difference in 22–23-month-old *App*^{NLGFs} compared to each younger group: (4–6-month-old: Mean Difference = −10.044, SE = 2.566, p < 0.001, 95% CI:[-16.966, -3.121], 8–10-month-old: Mean Difference = −7.776, SE = 2.566, p = 0.019, 95% CI:[-14.698, -0.853],12–14-month-old *App*^{NLGFs} (Mean Difference = -7.644, SE = 2.566, p = 0.022, 95% CI:[-14.567, -0.722]). Every other pairwise comparison was non-significant (p > 0.05).

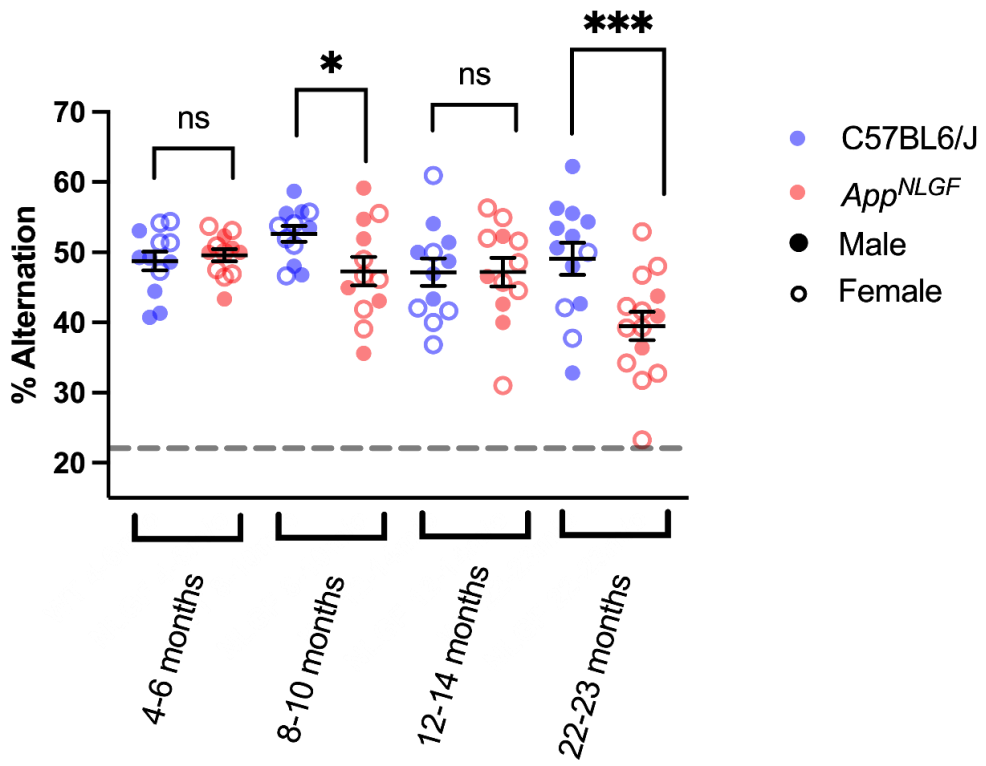

Figure 3.13: Percentage Alternation During the Spontaneous Alternation Test. The mean percentage of alternation during the spontaneous alternation test, in animals aged 4-6, 8-10, 12-14, and 22-23 months. Black bars represent the mean +/- standard error of the mean. Grey dashed line indicates chance (22%). Results of simple main effects analysis from two-way ANOVA are shown (ns = non-significant, * = p < 0.05, *** = p < 0.001). The key indicates animal genotype and sex. C57BL6/J: 4-6m/o n = 12, 8-10m/o n = 12, 12-14m/o n = 12, 22-23m/o n = 13. *App*^{NLGF} 4-6m/o n = 12, 8-10m/o n = 12, 12-14m/o n= 12, 22-23m/o n = 14.

3.4.5.2 Arm Entries

To assess whether changes in alternation performance could be attributed to differences in exploration, the number of arm entries during the spontaneous alternation task was recorded. This data was non-normally distributed but showed equal variance, so a square root transformation was applied prior to analysis. A two-way ANOVA revealed a significant main effect of genotype ($F(1, 91) = 4.60$, $p = 0.035$, $\eta p^2 = 0.048$). There was also a significant main effect of age ($F(3, 91) = 3.84$, $p = 0.012$, $\eta p^2 = 0.112$). However, the genotype × age interaction was not significant ($F(3, 91) = 1.08$, $p = 0.360$, $\eta p^2 = 0.034$). Post hoc Bonferroni comparisons showed that 22–23-month-old mice made fewer arm visits than 4–6-month-old mice (Mean Difference = - 0.72, SE = 0.266, p = 0.050, 95% CI:[-1.435, -0.001], Fig. 3.14).

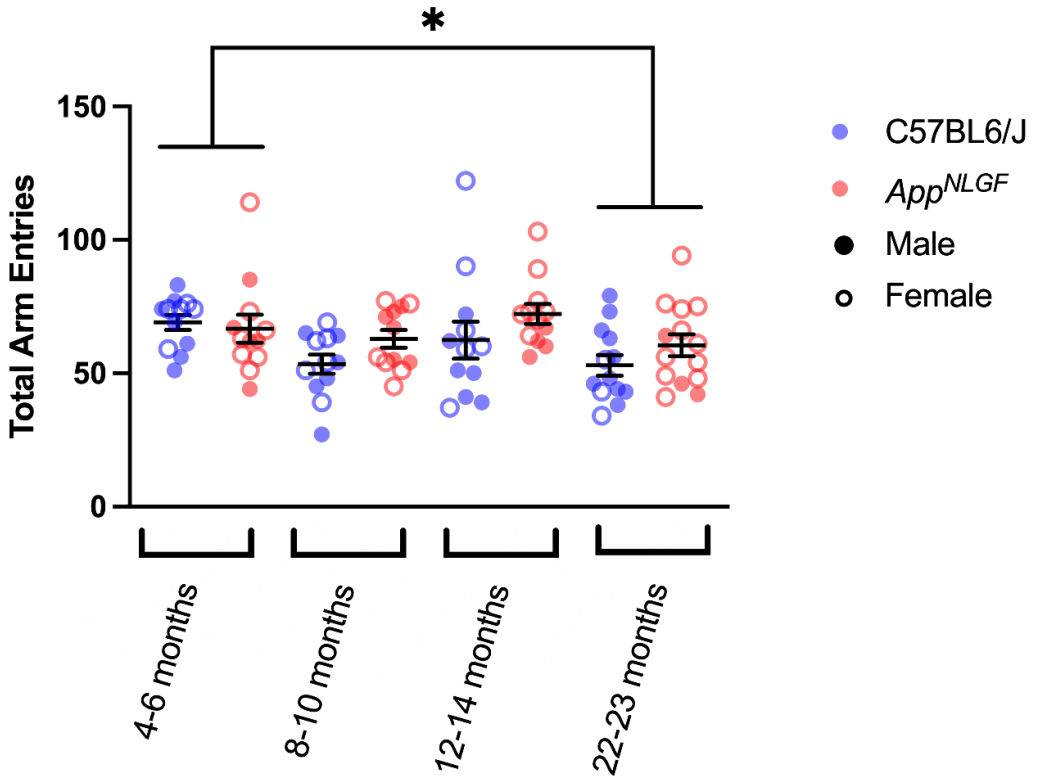

Figure 3.14: Total Arm Entries During the Spontaneous Alternation Test. The total number of arm entries of a T maze during the spontaneous alternation test, in animals aged 4-6, 8-10, 12-14, and 22-23 months. Black bars represent the mean +/- standard error of the mean. Results of Bonferroni post-hoc test shown (* = $p < 0.05$). The key indicates animal genotype and sex. C57BL6/J: 4-6m/o n = 12, 8-10m/o n = 12, 12-14m/o n = 12, 22-23m/o n = 13. *App*^{NLGF} 4-6m/o n = 12, 8-10m/o n = 12, 12-14m/o n= 12, 22-23m/o n = 14.

3.4.5.3 Distance Travelled

As with object recognition testing, EthoVision XT13 automatically measured the total distance travelled by animals during spontaneous alternation testing. This data had unequal variance (Levene's test $p < 0.05$) and some groups were not normally distributed (Shapiro-Wilk test $p < 0.05$), so a $\log_{10}$ transformation was performed to remedy this prior to analysis.

A two-way ANOVA was performed to assess the effects of age, genotype, and the interaction of the two factors on distance moved during spontaneous alternation testing. The analysis revealed that the main effect of genotype was not significant ($F(1,90) = 0.612$, $p = 0.436$, $\eta p^2 = 0.007$). However, the main effect of age was significant ($F(3,90) = 26.145$, $p < 0.001$, $\eta p^2 = 0.466$). The interaction between genotype and age was also significant ($F(3, 90) = 5.020$, $p = 0.003$, $\eta p^2 = 0.143$), indicating that the effect of genotype on the distance moved varied across different age groups. Simple main effects analysis revealed that, at 4-6, 8-10, and 12-14 months, there were no significant differences in distance moved between C57BL6/J and *App*^{NLGF} animals (4-6 months: Mean Difference = 0.020, SE = 0.062, $p = 0.751$, 95% CI:[-0.103, 0.142], 8-10 months: Mean Difference = -0.024, SE = 0.062, $p = 0.700$, 95% CI:[-0.146, 0.099], 12-14 months: Mean Difference = -0.110, SE = 0.062, $p = 0.079$, 95% CI:[-0.232, 0.013], Fig. 3.15). However, at 22-23 months, C57BL6/J animals travelled significantly further versus *App*^{NLGF} animals (Mean Difference = 0.209, SE = 0.059, $p < 0.001$, 95% CI:[0.092, 0.327], Fig. 3.15).

Within-genotype simple main effects revealed a significant effect of age on C57BL6/J mice ($F(3, 90) = 6.97$, $p < 0.001$, $\eta p^2 = 0.189$). Pairwise comparisons revealed that the youngest C57BL6/J group (4-6 months old) travelled significantly further than the oldest C57BL6/J group (22–23-month-old) (Mean Difference = 0.268, SE = 0.061, $p < 0.001$, 95% CI:[0.105, 0.432]). Within-genotype simple main effects also revealed a significant effect of age on *App*^{NLGF} mice, ($F(3, 90) = 24.19$, $p < 0.001$, $\eta p^2 = 0.446$). Pairwise comparisons revealed that 22-23-month-old *App*^{NLGFs} travelled significantly less distance than each younger *App*^{NLGF} group (4-6 months: Mean Difference = -0.458, SE = 0.061, $p < 0.001$, 95% CI:[-0.621, -0.295], 8–10-months: Mean Difference = -0.378, SE = 0.061, $p < 0.001$, 95% CI:[-0.541, -0.215]), 12–14-months: Mean Difference = -0.398, SE = 0.061, $p < 0.001$, 95% CI:[-0.562, -0.235]). No other comparisons were significant within the C57BL6/J or *App*^{NLGF} groups.

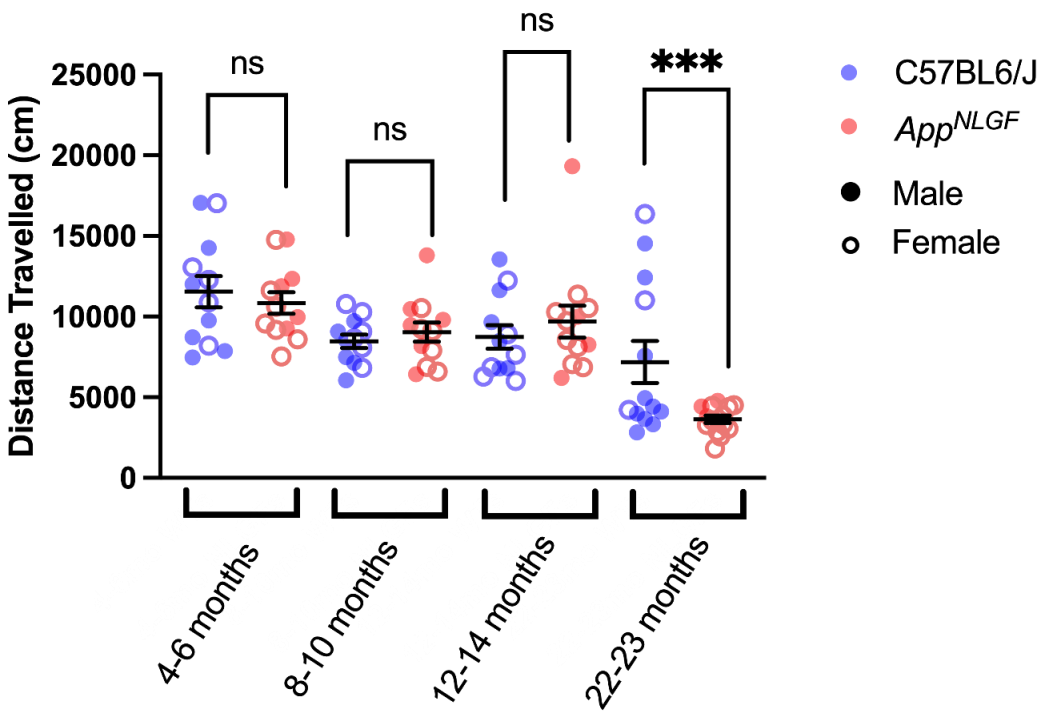

Figure 3.15: Distance Travelled During the Spontaneous Alternation Test. The mean distance travelled during the spontaneous alternation test, in animals aged 4-6, 8-10, 12-14, and 22-23 months. Raw (untransformed) data presented with black bars representing the mean +/- the standard error of the mean. Results of simple main effects analysis from two-way ANOVA are shown (ns = non-significant, *** = $p < 0.001$). The key depicts genotype and sex. C57BL6/J: 4-6m/o n = 12, 8-10m/o n = 12, 12-14m/o n = 12, 22-23m/o n = 13. *App*^{NLGF} 4-6m/o n = 12, 8-10m/o n = 12, 12-14m/o n= 12, 22-23m/o n = 14.

3.4.6 Open Field at 5, 9, 15 and 23 Months of Age

3.4.6.1 Inner Zone Ratio

OF testing was conducted on the 4-6-, 8-10-, and 22–23-month-old groups as part of the habituation protocol for object recognition testing. An additional 14–16-month-old group also underwent OF testing as part of the habituation protocol from the c-Fos experiment presented in Chapter 4 of this thesis. Each group consisted of 12 C57BL6/Js and 12 *App*^{NLGFs}. For the 22–23-month group that received more than one OF habituation session (as they experienced ON, OiP, and OL testing), the animals' first exposure to the OF was used for analysis.

For each OF test, the mouse was placed in the centre of a square arena (see Fig. 2.1a in the General Methods chapter) and allowed to freely explore for 10 minutes whilst recorded from above. EthoVision XT13 was then used to determine the time the animal spent exploring the central zone of the arena, versus the perimeter (Fig. 2.3). An inner zone ratio (IZR) was then calculated (time spent in the inner zone of arena/total time in the arena (s)). Exposure to an empty arena provides a valuable method to examine anxiety-related behaviour, as significantly lower IZR is indicative of an anxiogenic phenotype that overrides their natural exploratory behaviour (Prut & Belzung, 2003; Seibenhener & Wooten, 2015). This dataset was not normally distributed (Shapiro-Wilk test $p < 0.05$) and had unequal variance (Levene's test $p < 0.05$), so it was transformed by $\log_{10}$ transformation, which rendered the data suitable for parametric analysis.

To examine the effect of genotype and age on IZR, a two-way ANOVA was conducted. The ANOVA revealed a significant main effect of genotype ($F(1, 88) = 4.247$, $p = 0.042$, $\eta p^2 = 0.046$), and a significant main effect of age ($F(3, 88) = 4.980$, $p = 0.003$, $\eta p^2 = 0.145$). The interaction between genotype and age was also significant ($F(3, 88) = 3.685$, $p = 0.015$, $\eta p^2 = 0.112$). To explore this interaction, simple main effects analysis was performed. At 4-6, 8-10, and 14-16 months, there were no significant differences in IZR between C57BL6/Js and *App*^{NLGFs} (4-6 months: Mean Difference = 0.079, SE = 0.061, p = 0.200, 95% CI:[-0.043, 0.201], 8-10 months: Mean Difference = 0.055, SE = 0.061, p = 0.372, 95% CI:[-0.067, 0.177], 14-16 months: Mean Difference = -0.084, SE = 0.061, p = 0.173, 95% CI:[-0.206, 0.038], Fig. 3.16). However, at 22-23 months, *App*^{NLGFs} displayed significantly lower IZR than C57BL6/Js (Mean Difference = -0.203, SE = 0.061, p = 0.001, 95% CI:[-0.324, -0.081], Fig. 3.16).

Within-genotype simple main effects revealed a non-significant effect of age on C57BL6/J mice ($F(3, 88) = 2.39$, $p = 0.074$, $\eta p^2 = 0.075$). However, there was a significant effect of age on *App*^{NLGF} mice ($F(3, 88) = 6.27$, $p < 0.001$, $\eta p^2 = 0.176$). Pairwise comparisons revealed that 14–16-month *App*^{NLGFs} had significantly higher IZR than 8–10-month *App*^{NLGFs} (Mean Difference = 0.195, SE = 0.061, p = 0.012, 95% CI: [0.030, 0.361]), 22–23-month *App*^{NLGFs} (Mean Difference = 0.211, SE = 0.061, p = 0.005, 95% CI: [0.046, 0.376]) and 4–6-month-olds (Mean Difference = 0.236, SE = 0.061, p = 0.001, 95% CI: [0.071, 0.401]). No other significant comparisons were detected.

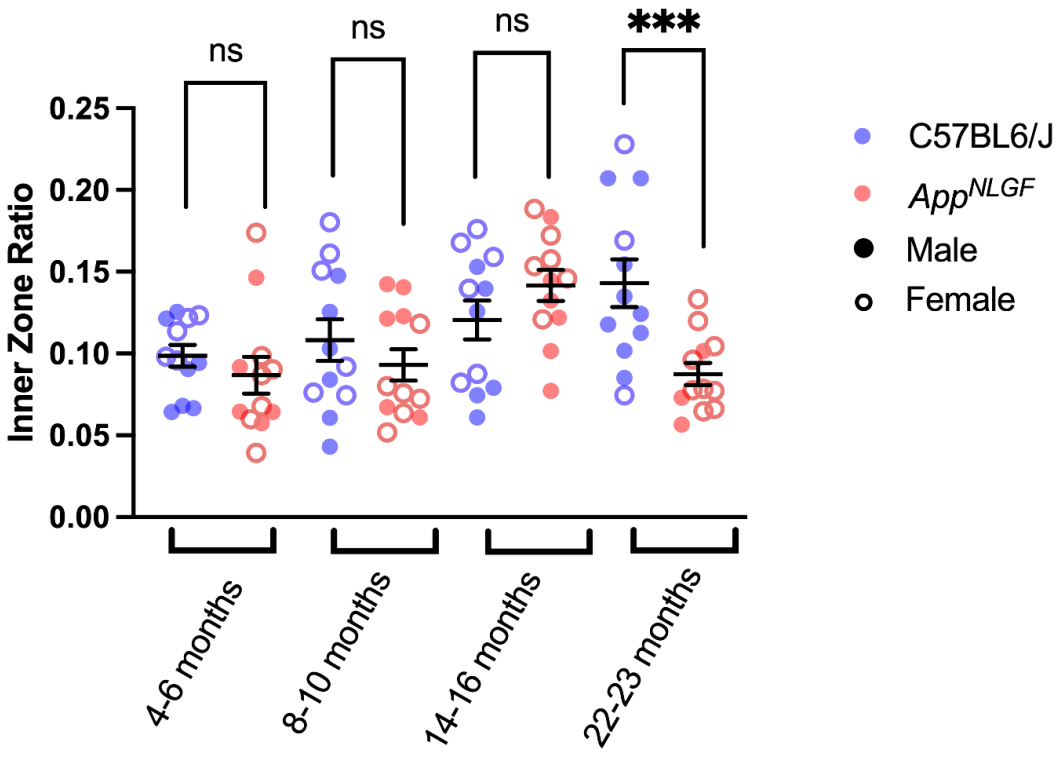

Figure 3.16: Inner Zone Ratios During the Open Field Test. The mean Inner Zone Ratios during the Open Field task, in animals aged 4-6, 8-10, 14-16, and 22-23 months. The raw (untransformed) data is presented with black bars representing the mean +/- the standard error of the mean (SEM). Results of simple main effects analysis from two-way ANOVA are shown (ns = non-significant, *** = $p < 0.001$). The key indicates genotype and sex. Each age group consisted of 12 C57BL6/Js and 12 *App*^{NLGFs}.

3.4.6.2 Distance Travelled

As with object recognition testing, the distance travelled by each animal during OF testing was recorded using EthoVision XT13, to determine whether any differences in IZR could be accounted for by differences in locomotion. This data exhibited equal variance (Levene's test $p > 0.05$) but was not normally distributed (Shapiro-Wilk test $p < 0.05$), so $\log_{10}$ transformation was applied prior to statistical analysis.

To determine the effect of age and genotype on distance travelled, a two-way ANOVA was then performed. The test revealed no significant main effect of genotype ($F(1, 88) = 1.484$, $p = 0.226$, $\eta p^2 = 0.017$), however there was a significant main effect of age ($F(3, 88) = 10.988$, $p < 0.001$, $\eta p^2 = 0.273$). The interaction between genotype and age was not significant ($F(3, 88) = 1.806$, $p = 0.152$, $\eta p^2 = 0.058$). Bonferroni *post hoc* tests showed significant differences between 22-23

month animals and all three younger groups (4-6 month: (Mean Difference = -0.115, SE = 0.0347, p = 0.008, 95% CI:[-0.2083, -0.0212], 8-10 month: (Mean Difference = -0.132, SE = 0.0347, p = 0.002, 95% CI:[-0.225, -0.0384]), 14-16 month: (Mean Difference = -0.195, SE = 0.0347, p < 0.001, 95% CI:[-0.288, -0.101], Fig. 3.17).

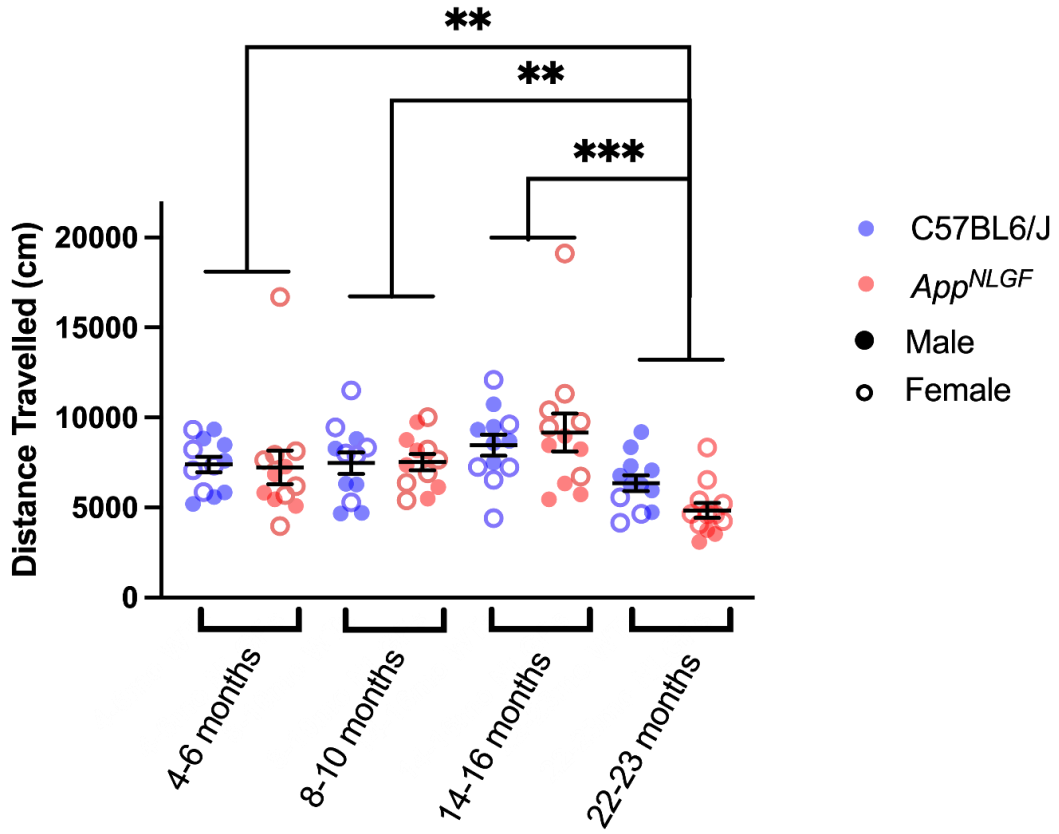

Figure 3.17: Distance Travelled During the Open Field Test. The mean distance travelled during the Open Field test, in animals aged 4-6, 8-10, 14-16, and 22-23 months. Raw (untransformed) data presented with black bars representing the mean +/- the standard error of the mean. Results of Bonferroni *post hoc* tests from two-way ANOVA are shown (** = p < 0.01, *** = p < 0.001). The key indicates genotype and sex. Each age group consisted of 12 C57BL6/Js and 12 *App*^{NLGFs}.

3.4.7 Elevated Plus Maze at 5, 9, 13, and 23 Months of Age

3.4.7.1 Open Arm Duration

EPM testing was carried out on the 4-6-, 8-10-, and 22-23-month-old animals that underwent object recognition and spontaneous alternation testing, as well as the 12-14 month group that also underwent spontaneous alternation testing. The 4-6, 8-10, and 12-14 month groups each consisted of 12 C57BL6/J and 12 *App*^{NLGF} mice, while the 22-23 month group included 13 C57BL6/J and 14 *App*^{NLGF} mice. For each group, EPM testing was conducted at least two weeks after other behavioral tests. During the EPM test, the animal was positioned in the central zone of a plus shaped maze, elevated from the ground (see Fig. 2.1c in General Methods). Each animal was allowed to freely explore the arena for 10 minutes whilst recorded from an overhead camera. EthoVision XT13 was used to determine the duration each animal spent in the open arms of the maze. This data exhibited normal distribution (Shapiro-Wilk test $p > 0.05$) and equal variance (Levene's test $p > 0.05$).

A two-way ANOVA was performed to examine the effect of genotype and age on open arm time. This revealed a significant main effect of genotype ($F(1, 91) = 162.989$, $p < 0.001$, $\eta p^2 = 0.642$), and age ($F(3, 91) = 12.168$, $p < 0.001$, $\eta p^2 = 0.286$), and the genotype*age interaction was also significant ($F(3, 91) = 7.148$, $p < 0.001$, $\eta p^2 = 0.191$). Simple main effects analysis was performed to examine this interaction. Pairwise comparisons revealed that, for each age group tested, *App*^{NLGF} mice spent significantly more time in the open arms of the maze compared to age-matched C57BL6/Js (4-6 months: Mean Difference = 81.227, SE = 18.760, $p < 0.001$, 95% CI:[43.962, 118.493], 8-10 months: Mean Difference = 107.581, SE = 18.760, $p < 0.001$, 95% CI:[70.316, 144.847], 12-14 months: Mean Difference = 191.166, SE = 18.760, $p < 0.001$, 95% CI:[153.901, 228.431], 22-23 months: Mean Difference = 92.416, SE = 17.700, $p < 0.001$, 95% CI:[57.258, 127.574], Fig. 3.18).

Within-genotype simple main effects revealed a significant effect of age on C57BL6/J mice ($F(3, 91) = 6.354$, $p < 0.001$, $\eta p^2 = 0.173$). Pairwise comparisons revealed that 8-10-month-old C57BL6/Js spent significantly longer in the open arms compared to every other group (4-6 months: (Mean Difference = 62.12, SE = 18.76, $p = 0.008$, 95% CI:[11.522, 112.721], 12-14 months (Mean Difference = 77.06, SE = 18.76, $p < 0.001$, 95% CI:[26.455, 127.655], 22-23 months: (Mean Difference = 50.637, SE = 18.34, $p = 0.043$, 95% CI:[1.020, 100.254]). Within-genotype simple main effects also revealed a significant effect of age on *App*^{NLGF} mice ($F(3, 91) = 13.025$, $p < 0.001$, $\eta p^2 = 0.300$). Pairwise comparisons revealed that the 8-10- and 12-14-month groups spent significantly longer in the open arms compared to the 4-6 month group (8-10 months: Mean Difference = 88.48, SE = 18.76, $p < 0.001$, 95% CI:[37.876, 139.075], 12-14 months: (Mean Difference = 95.005, SE = 18.76, $p < 0.001$, 95% CI:[44.405, 145.605]). Both 4-6- and 8–10-month-old *App*^{NLGFs} also spent

significantly longer in the open arms compared to the 22–23-month group (4-6 months: Mean Difference = 65.802, SE = 18.08, p = 0.003, 95% CI:[-17.043, 114.561], 8-10 months: Mean Difference = 72.33, SE = 18.08, p < 0.001, 95% CI:[23.57, 121.090]). No other significant comparisons were observed.

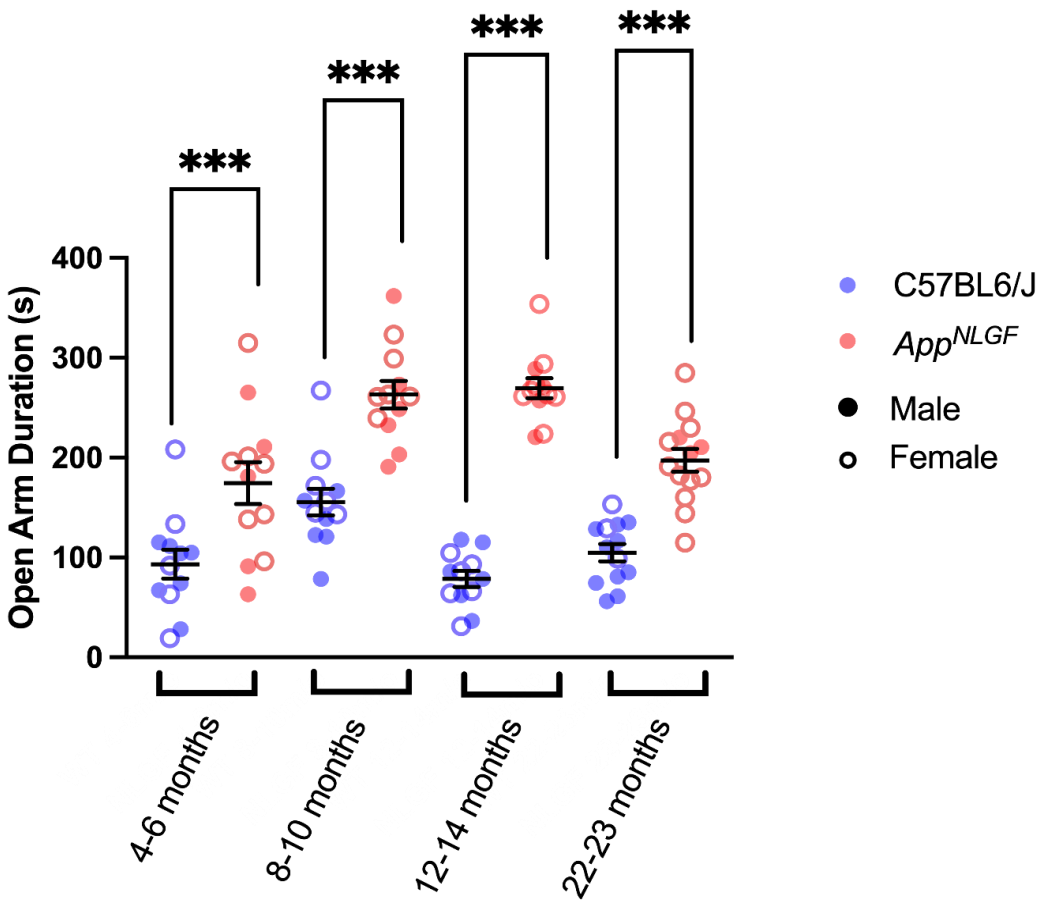

Figure 3.18: Open Arm Duration During the Elevated Plus Maze Test. The mean duration spent in the open arms of the Elevated Plus Maze (in seconds), in animals aged 4-6, 8-10, 12-14, and 22-23 months. Black bars represent the mean +/- the standard error of the mean (SEM). The results of simple main effects analysis from two-way ANOVA are shown (*** = p < 0.001). The key indicates animal genotype and sex. C57BL6/Js: 4-6m/o n = 12, 8-10m/o n = 12, 12-14m/o n = 12, 22-23m/o n = 13. *App*^{NLGFs}: 4-6m/o n = 12, 8-10m/o n = 12, 12-14m/o n = 12, 22-23m/o n = 14.

3.4.7.2 Closed Arm Duration

EthoVision XT13 was also used to determine the duration each animal spent in the closed arms of the EPM. This data also exhibited normal distribution (Shapiro-Wilk test p > 0.05) and equal variance (Levene's test p > 0.05).

A two-way ANOVA was performed to examine the effect of genotype and age on the mean total time spent in the closed arms. This analysis also revealed significant main effects of genotype ($F(1, 91) = 111.965$, $p < 0.001$, $\eta p^2 = 0.552$), age ($F(3, 91) = 8.865$, $p < 0.001$, $\eta p^2 = 0.226$), and a significant interaction between the two factors ($F(3, 91) = 5.950$, $p < 0.001$, $\eta p^2 = 0.164$). Simple main effects analysis revealed that, at all ages tested, *App*^{NLGFs} spent significantly less time in the closed arm compared to age matched C57BL6/Js (4-6 months: Mean Difference = -91.070, SE = 19.726, $p < 0.001$, 95% CI:[-130.253, -51.887], 8-10 months: Mean Difference = -64.952, SE = 19.726, $p = 0.001$, 95% CI:[-104.135, -25.768], 12-14 months: Mean Difference = -172.962, SE = 19.726, $p < 0.001$, 95% CI:[-212.145, -133.779], 22-23 months: Mean Difference = -82.697, SE = 18.611, $p < 0.001$, 95% CI:[-119.665, -45.730], Fig. 3.19).

Within-genotype simple main effects revealed a significant effect of age on C57BL6/J mice ($F(3, 91) = 9.812$, $p < 0.001$, $\eta p^2 = 0.244$). Pairwise comparisons revealed that 8-10-month-old C57BL6/Js spent significantly less time in the closed arms compared to each other C57BL6/J group tested (4-6 months: Mean Difference = -76.871, SE = 19.726, $p = 0.001$, 95% CI:[-130.075, -23.667], 12-14 months: Mean Difference = -102.353, SE = 19.726, $p < 0.001$, 95% CI:[-155.557, -49.149], 22-23 months: Mean Difference = -67.562, SE = 19.343, $p = 0.004$, 95% CI:[-119.733, -15.391]). Similarly, within-genotype simple main effects revealed a significant effect of age on *App*^{NLGF} mice ($F(3, 91) = 5.048$, $p = 0.003$, $\eta p^2 = 0.143$). Pairwise comparisons revealed that the 12-14 month *App*^{NLGF} group spent significantly less time in the closed arms compared to the 4-6 month and 22-23 month *App*^{NLGF} groups (4-6 months: Mean Difference = -56.410, SE = 19.726, $p = 0.032$, 95% CI:[-109.614, -3.206], 22-23 months: Mean Difference = -55.474, SE = 19.008, $p = 0.027$, 95% CI:[-106.742, -4.205]). All other pairwise comparisons within each genotype were non-significant ($p > 0.05$).

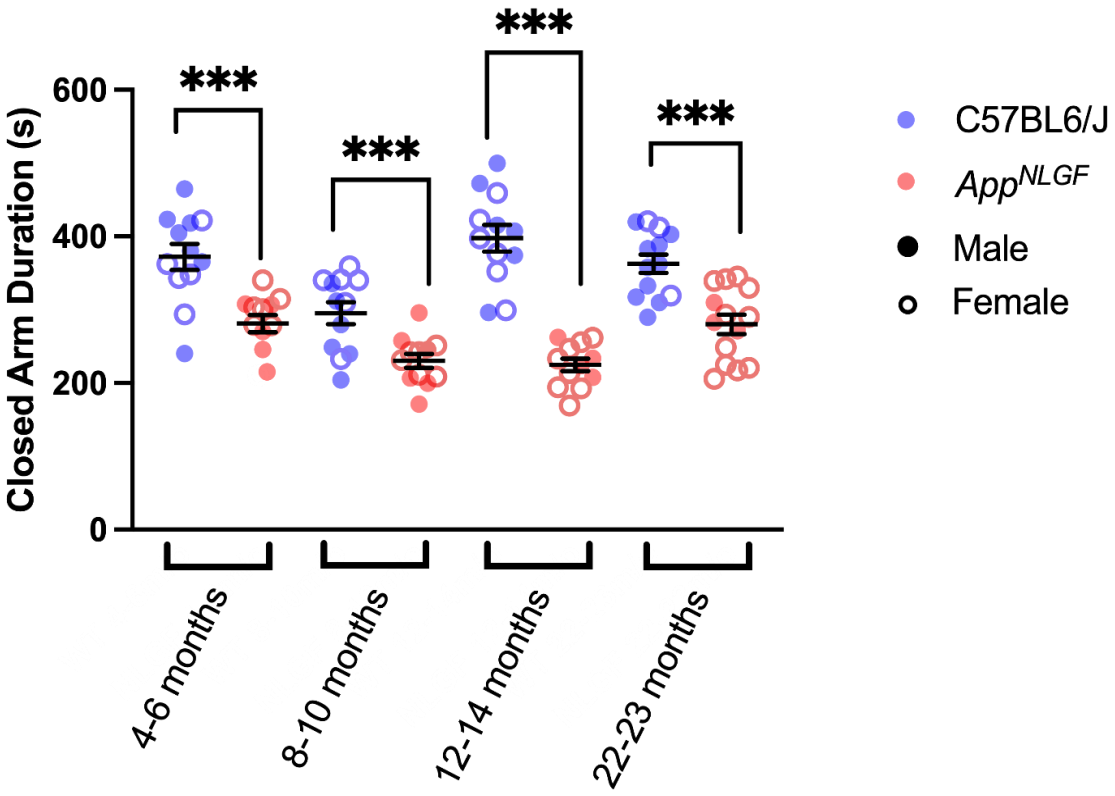

Figure 3.19: Closed Arm Duration During the Elevated Plus Maze Test. The mean duration spent in the closed arms of the Elevated Plus Maze (in seconds), in animals aged 4-6, 8-10, 12-14, and 22-23 months. Black bars represent the mean +/- the standard error of the mean (SEM). The results of simple main effects analysis from two-way ANOVA are shown (*** = $p < 0.001$). The key indicates animal genotype and sex. C57BL6/Js: 4-6m/o n = 12, 8-10m/o n = 12, 12-14m/o n = 12, 22-23m/o n = 13. *App*^{NLGFs}: 4-6m/o n = 12, 8-10m/o n = 12, 12-14m/o n = 12, 22-23m/o n = 14.

3.4.7.3 Open Arm Ratio

An Open Arm Ratio (OAR) for each animal was then calculated by divding the total time spent in open arm by the total time in the maze. Increased OAR is generally described as an anxiolytic or disinhibitory phenotype (Chung & Cummings, 2000; Lister, 1987; Pentkowski et al., 2021). OAR data exhibited normal distribution (Shapiro-Wilk test $p > 0.05$) and equal variance (Levene's test $p > 0.05$).

To examine the effect of genotype and age on OAR, a two-way ANOVA was performed. This test showed significant main effects of genotype ($F(1, 91) = 162.683$, $p < 0.001$, $\eta p^2 = 0.641$) and age ($F(3, 91) = 12.172$, $p < 0.001$, $\eta p^2 = 0.286$). The interaction between genotype and age was also significant ($F(3, 91) = 7.113$, $p < 0.001$, $\eta p^2 = 0.190$). To examine this interaction, simple main effects analysis was performed. Pairwise comparisons showed that, at 4-6 months, *App*^{NLGF} mice

exhibited significantly higher OAR compared to C57BL6/J controls (Mean Difference = 0.136, SE = 0.031, $p < 0.001$, 95% CI:[0.074, 0.198], Fig. 3.20). Similarly, *App*^{NLGF} mice at 8-10 months had a significantly higher OAR than C57BL6/J mice (Mean Difference = 0.179, SE = 0.031, $p < 0.001$, 95% CI:[0.117, 0.241], Fig. 3.20). At 12-14 months, *App*^{NLGF} mice also exhibited significantly higher OAR than C57BL6/Js (Mean Difference = 0.319, SE = 0.031, $p < 0.001$, 95% CI:[0.256, 0.381], Fig. 3.20). At the maximum age tested, 22-23 months, *App*^{NLGFs} again showed significantly higher OAR compared to C57BL6/Js (Mean Difference = 0.154, SE = 0.030, $p < 0.001$, 95% CI:[0.095, 0.213], Fig. 3.20).

Within-genotype simple main effects revealed a significant effect of age on C57BL6/J mice ($F(3, 91) = 6.352$, $p < 0.001$, $\eta p^2 = 0.173$). Pairwise comparisons revealed that 8-10-month-old C57BL6/Js exhibited significantly higher OAR than every other C57BL6/J group (4-6 months: Mean Difference = 0.104, SE = 0.031, $p = 0.008$, 95% CI:[0.020, 0.188], 12-14 months: Mean Difference = 0.128, SE = 0.031, $p < 0.001$, 95% CI:[0.044, 0.213], 22-23 months: Mean Difference = 0.084, SE = 0.031, $p = 0.043$, 95% CI:[0.002, 0.167]). Similarly, within-genotype simple main effects revealed a significant effect of age on *App*^{NLGF} mice ($F(3, 91) = 12.996$, $p < 0.001$, $\eta p^2 = 0.300$). Pairwise comparisons revealed that 8-10 month and 12-14-month-old *App*^{NLGFs} exhibited significantly higher OAR than the 4-6 month *App*^{NLGF} group (8-10 months: Mean Difference = 0.148, SE = 0.031, $p < 0.001$, 95% CI:[0.063, 0.232], 12-14 months: Mean Difference = 0.158, SE = 0.031, $p < 0.001$, 95% CI:[0.074, 0.243]). The 8-10 and 12-14 month groups also exhibited significantly higher OAR than the 22-23 month group (8-10 months: Mean Difference = 0.110, SE = 0.030, $p = 0.003$, 95% CI:[0.028, 0.191], 12-14 months: Mean Difference = 0.121, SE = 0.030, $p < 0.001$, 95% CI:[0.039, 0.202]). No other significant comparisons were observed.

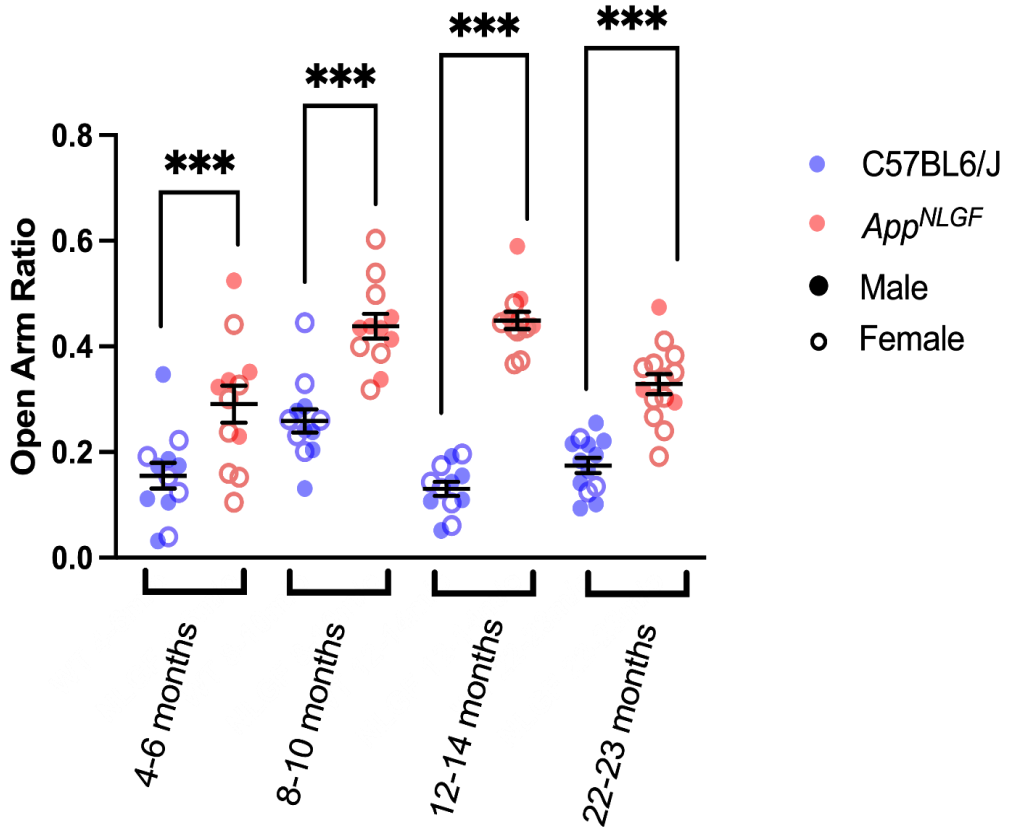

Figure 3.20: Open Arm Ratios During the Elevated Plus Maze Test. The mean Open Arm Ratios during the Elevated Plus Maze test, in animals aged 4-6, 8-10, 12-14, and 22-23 months. Black bars represent the mean +/- the standard error of the mean. The results of simple main effects analysis from two-way ANOVA are shown (*** = $p < 0.001$). The key indicates genotype and sex. C57BL6/Js: 4-6m/o n = 12, 8-10m/o n = 12, 12-14m/o n = 12, 22-23m/o n = 13. *App*^{NLGFs}: 4-6m/o n = 12, 8-10m/o n = 12, 12-14m/o n = 12, 22-23m/o n = 14.

3.4.7.4 Open Arm Entries

The number of times the animal entered the open arm during EPM testing was also recorded as an additional measure of anxiety-like behaviour. This data exhibited normal distribution (Shapiro-Wilk test $p > 0.05$) and equal variance (Levene's test $p > 0.05$).

A two-way ANOVA was performed to examine the effect of age and genotype on the number of open arm entries during EPM testing. The test revealed non-significant main effects of age ($F(3, 91) = 2.152$, $p = 0.099$, $\eta p^2 = 0.066$), and a significant main effect of genotype ($F(1, 91) = 94.021$, $p < 0.001$, $\eta p^2 = 0.508$). The age*genotype interaction was also significant ($F(3, 91) = 2.959$, $p = 0.036$, $\eta p^2 = 0.089$). Simple main effects analysis showed that, at every age tested, *App*^{NLGFs} displayed significantly more open arm entries during EPM testing compared to C57BL6/Js (4-6

months: Mean Difference = 7.750, SE = 1.8801, p < 0.001, 95% CI:[4.015, 11.485], 8-10 months: Mean Difference = 8.083, SE = 1.8801, p < 0.001, 95% CI:[4.348, 11.818], 12-14 months: Mean Difference = 13.667, SE = 1.880, p < 0.001, 95% CI:[9.932, 17.402], 22-23 months: Mean Difference = 6.463, SE = 1.7741, p < 0.001, 95% CI:[2.938, 0.985], Fig. 3.21).

Although the two-way ANOVA did not reveal a significant main effect of age across both genotypes, the significant interaction suggests that the effect of age on open arm visits differed between genotypes. Within-genotype simple main effects revealed no significant effect of age on C57BL6/J mice ($F(3, 91) = 1.600$, $p = 0.195$, $\eta p^2 = 0.050$). However, there was a significant effect of age on *App*^{NLGF} mice ($F(3, 91) = 3.549$, $p = 0.018$, $\eta p^2 = 0.105$). Pairwise comparisons revealed that mice at 12-14 months entered the open arms significantly more times than 22–23-month *App*^{NLGF} animals (Mean Difference = 5.083, SE = 1.812, p = 0.006, 95% CI:[1.484, 8.683]). No other significant comparisons were observed.

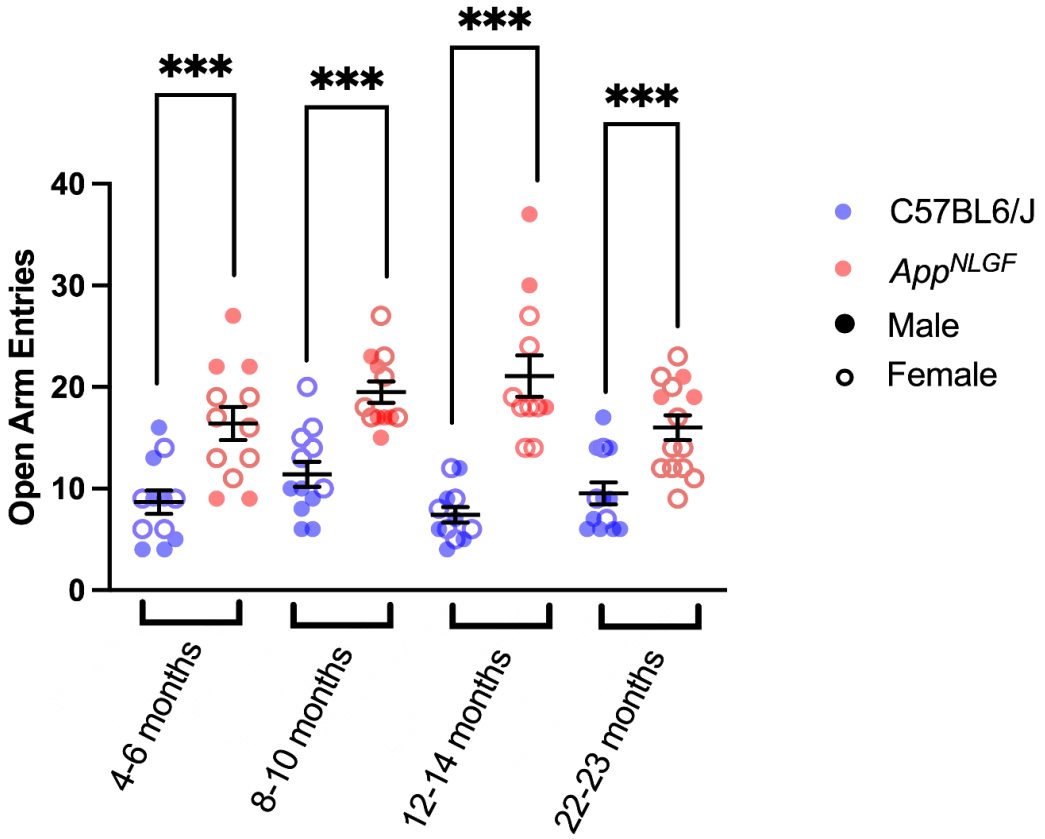

Figure 3.21: Open Arm Entries During the Elevated Plus Maze Test. The mean number of entries into the open arms during the Elevated Plus Maze test, in animals aged 4-6, 8-10, 12-14, and 22-23 months. Black bars represent the mean +/- the standard error of the mean. The results of simple main effects analysis from two-way ANOVA are shown (*** = p < 0.001). The key indicates genotype and sex. C57BL6/Js: 4-6m/o n = 12, 8-10m/o n = 12, 12-14m/o n = 12, 22-23m/o n = 13. *App*^{NLGFs}: 4-6m/o n = 12, 8-10m/o n = 12, 12-14m/o n = 12, 22-23m/o n = 14.

3.4.7.5 Closed Arm Entries

The number of times the animal entered the closed arm during EPM testing was also recorded. This data also exhibited normal distribution (Shapiro-Wilk test $p > 0.05$) and equal variance (Levene's test $p > 0.05$).

A two-way ANOVA was performed to determine the effect of genotype and age on the number of closed arm visits during EPM testing. This analysis revealed significant main effects of genotype ($F(1, 91) = 4.433$, $p = 0.038$, $\eta p^2 = 0.046$). The main effect of age was also significant ($F(3, 91) = 4.210$, $p = 0.08$, $\eta p^2 = 0.122$). However, the interaction between the two factors was not significant ($F(3, 91) = 0.437$, $p = 0.727$, $\eta p^2 = 0.014$). Bonferroni *post hoc* testing revealed a significant difference between the number of closed arm visits of animals at 4-6 months versus 12-14 months (Mean Difference = 4.667, SE = 1.615, $p = 0.029$, 95% CI:[0.310, 9.024], Fig. 3.22).

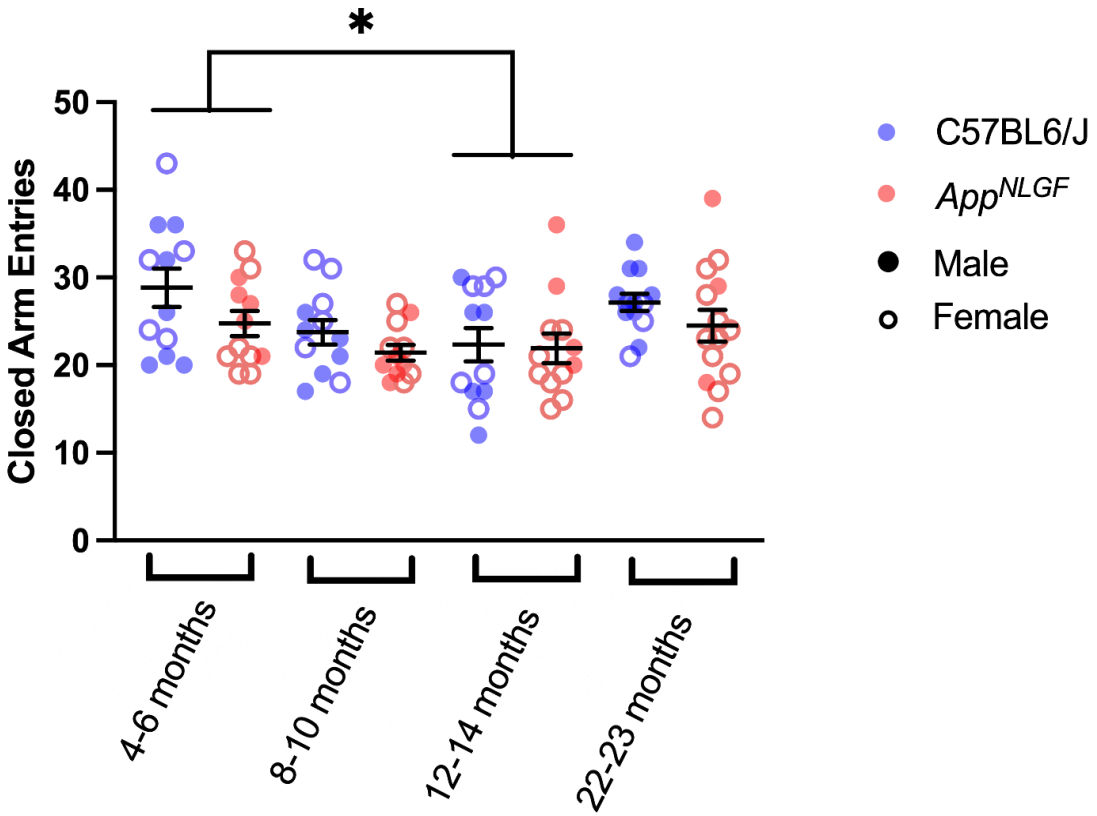

Figure 3.22: Closed Arm Entries During the Elevated Plus Maze Test. The mean number of entries into the closed arms during the Elevated Plus Maze test, in animals aged 4-6, 8-10, 12-14, and 22-23 months. Black bars represent the mean +/- the standard error of the mean. Significant result of Bonferroni *post hoc* tests from two-way ANOVA is shown (* = $p < 0.05$). The key indicates genotype and sex. C57BL6/Js: 4-6m/o n = 12, 8-10m/o n = 12, 12-14m/o n = 12, 22-23m/o n = 13. *App*^{NLGFs}: 4-6m/o n = 12, 8-10m/o n = 12, 12-14m/o n = 12, 22-23m/o n = 14.

3.4.7.6 Head Dipping

For each EPM test, the time the animal spent head dipping was manually scored using EthoVision XT13. A 'head dip' was defined as the animal lowering its head from an open arm of the maze, whilst its paws remained within the arm. Increased duration of head dipping indicates increased risk assessment suggestive of anxiogenic behaviour (File & Wardill, 1975; Rodgers, Perrault, Sanger, et al., 1997; Setem et al., 1999; Walf & Frye, 2007). This data was not normally distributed (Shapiro-Wilk test $p < 0.05$) and had unequal variances (Levene's test $p < 0.05$). Therefore, it underwent square root transformation prior to statistical analysis.

A two-way ANOVA was performed to assess the effect of genotype and age on the time spent head dipping during EPM testing. The main effect of genotype was significant ($F(1, 91) = 25.600$, $p < 0.001$, $\eta p^2 = 0.220$). The main effect of age was also significant ($F(3, 91) = 10.354$, $p < 0.001$, $\eta p^2 = 0.254$). However, the interaction between age and genotype was not significant ($F(3, 91) = 2.382$, $p = 0.075$, $\eta p^2 = 0.073$). Bonferroni *post hoc* tests revealed significant differences in head dipping between 4-6- and 12-14-month animals (Mean Difference = 1.0065, SE = 0.351, $p = 0.031$, 95% CI:[0.0598, 1.953], Fig. 3.23), and between 8-10- and 12-14-month animals (Mean Difference = 1.634, SE = 0.351, $p < 0.001$, 95% CI:[0.687, 2.5802], Fig. 3.23). There were also significant differences between 4-6- and 22-23-month animals (Mean Difference = 0.946, SE = 0.341, $p = 0.040$, 95% CI:[0.0260, 1.8661], Fig.3.23), and 8-10- and 22-23-month animals (Mean Difference = 1.573, SE = 0.341, $p < 0.001$, 95% CI:[0.6529, 2.4930], Fig. 3.23).

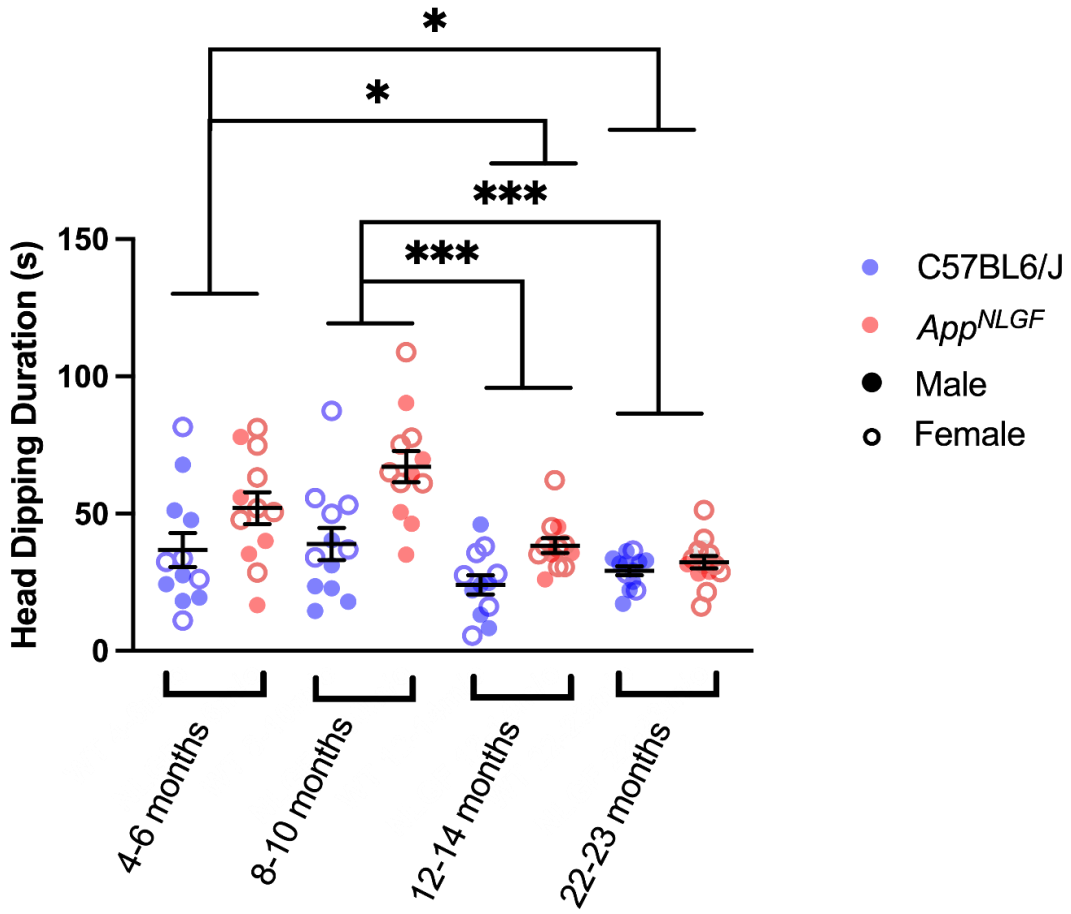

Figure 3.23: Head Dipping During the Elevated Plus Maze Test. The mean duration spent head dipping during the Elevated Plus Maze test, in animals aged 4-6, 8-10, 12-14, and 22-23 months. Raw (untransformed) data presented with black bars representing the mean +/- the standard error of the mean. Results of Bonferroni *post hoc* tests from two-way ANOVA are shown (* = $p < 0.05$, *** = $p < 0.001$). The key indicates genotype and sex. C57BL6/Js: 4-6m/o n = 12, 8-10m/o n = 12, 12-14m/o n = 12, 22-23m/o n = 13. *App*^{NLGFs}: 4-6m/o n = 12, 8-10m/o n = 12, 12-14m/o n = 12, 22-23m/o n = 14.

3.4.7.7 Stretch Attend Postures

In addition to head dips, the time the animal spent in the stretch attend posture (i.e., stretching into an open arm, with its hind legs remaining in a closed arm or within the central junction of the maze) was also manually scored using EthoVision XT13. As with head dipping, increased duration of stretching into open arms is cited as an anxiogenic behavioural phenotype (Cole & Rodgers, 1994; Rodgers, 1999; Rodgers, Perrault, Sanger, et al., 1997; Setem et al., 1999; Walf & Frye, 2007). This data exhibited equal variance (Levene's test $p > 0.05$), but it was not normally distributed (Shapiro-Wilk test $p < 0.05$). It therefore underwent $\log_{10}$ transformation prior to analysis.

A two-way ANOVA was performed to analyse the effect of age and genotype on the stretch attend duration during EPM testing. The test revealed significant main effects of age ($F(3, 91) = 10.233$, $p < 0.001$, $\eta p^2 = 0.252$), and genotype ($F(1, 91) = 17.971$, $p < 0.001$, $\eta p^2 = 0.165$). The age*genotype interaction, however, was not significant ($F(3, 91) = 1.212$, $p = 0.310$, $\eta p^2 = 0.038$). Bonferroni *post hoc* tests revealed significant differences between 4-6 and 12-14 months (Mean Difference = 0.193, SE = 0.054, p = 0.003, 95% CI:[0.0473, 0.3386], Fig. 3.24). There was also a significant difference between 4-6 and 22-23 (Mean Difference = 0.282, SE = 0.525, p < 0.001, 95% CI:[0.1402, 0.4234], Fig. 3.24), and between 8-10- and 22-23-month animals (Mean Difference = 0.1806, SE = 0.525, p = 0.005, 95% CI:[0.0390, 0.3222], Fig. 3.24).

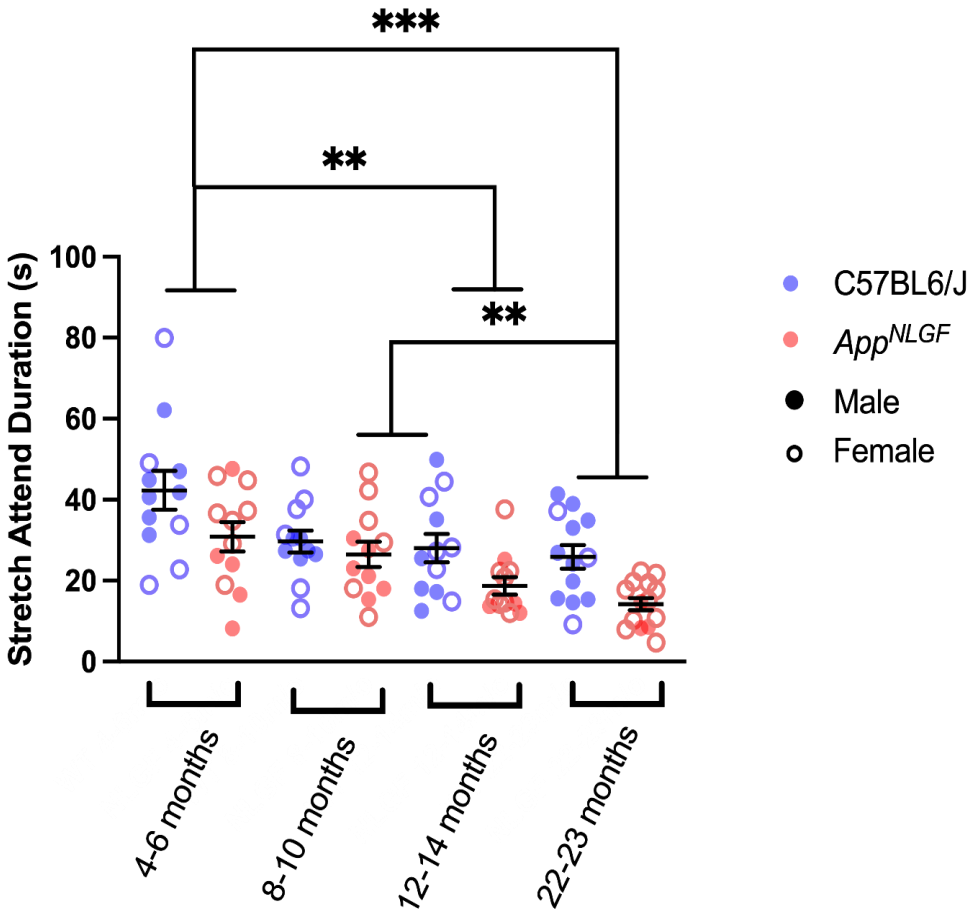

Figure 3.24: Stretching During the Elevated Plus Maze Test. The mean duration spent in the stretch attend posture during the Elevated Plus Maze test, in animals aged 4-6, 8-10, 12-14, and 22-23 months. Raw (untransformed) data presented with black bars representing the mean +/- the standard error of the mean. Results of Bonferroni *post hoc* tests from two-way ANOVA are shown (** = p < 0.01, *** = p <0.001). The key indicates genotype and sex. C57BL6/Js: 4-6m/o n = 12, 8-10m/o n = 12, 12-14m/o n = 12, 22-23m/o n = 13 App^{NLGFs}: 4-6m/o n = 12, 8-10m/o n = 12, 12-14m/o n = 12, 22-23m/o n = 14.

3.4.7.8 Distance Travelled

During the EPM test, the total distance travelled by each animal was automatically recorded using EthoVision XT13. This dataset exhibited unequal variance (Levene's test $p < 0.05$) and was not normally distributed (Shapiro-Wilk test $p < 0.05$), so it underwent square root transformation prior to statistical analysis.

A two-way ANOVA was performed to investigate the effect of genotype and age on the distance travelled during EPM testing. The main effect of genotype was not significant ($F(1, 91) = 0.17$, $p = 0.896$, $\eta p^2 = 0.000$), but the main effect of age was significant ($F(3, 91) = 2.888$, $p = 0.040$, $\eta p^2 = 0.087$). The genotype*age interaction was also significant ($F(3, 91) = 3.327$, $p = 0.023$, $\eta p^2 = 0.099$). To investigate this significant interaction, simple main effects analysis was performed. The analysis revealed that at 4-6, 8-10, and 22-23 months, there was no significant difference in the distance travelled between C57BL6/J and *App*^{NLGF} animals (4-6 months: Mean Difference = 4.461, SE = 3.984, $p = 0.266$, 95% CI:[-3.453, 12.375], 8-10 months: Mean Difference = -3.611, SE = 3.984, $p = 0.367$, 95% CI:[-11.525, 4.303], 22-23 months: Mean Difference = 6.745, SE = 3.759, $p = 0.076$, 95% CI:[-0.722, 14.211], Fig. 3.25). However, at 12-14 months, *App*^{NLGF} animals travelled significantly further than C57BL6/J animals (Mean Difference = 8.625, SE = 3.984, $p = 0.033$, 95% CI:[0.711, 16.538], Fig. 3.25).

Within-genotype simple main effects revealed a non-significant effect of age on C57BL6/J mice ($F(3, 91) = 1.828$, $p = 0.148$, $\eta p^2 = 0.057$). However, there was a significant effect of age on *App*^{NLGF} mice ($F(3, 91) = 4.491$, $p = 0.006$, $\eta p^2 = 0.129$). Pairwise comparisons revealed that the 8-10- and 12–14-month-old *App*^{NLGFs} travelled significantly further than 22–23-month *App*^{NLGFs} during EPM testing (8-10 months: Mean Difference = 12.499, SE = 3.839, $p = 0.010$, 95% CI:[-2.144, 22.854], 12-14 months: Mean Difference = 11.541, SE = 3.839, $p = 0.021$, 95% CI:[1.186, 21.896]). No other significant comparisons were observed.

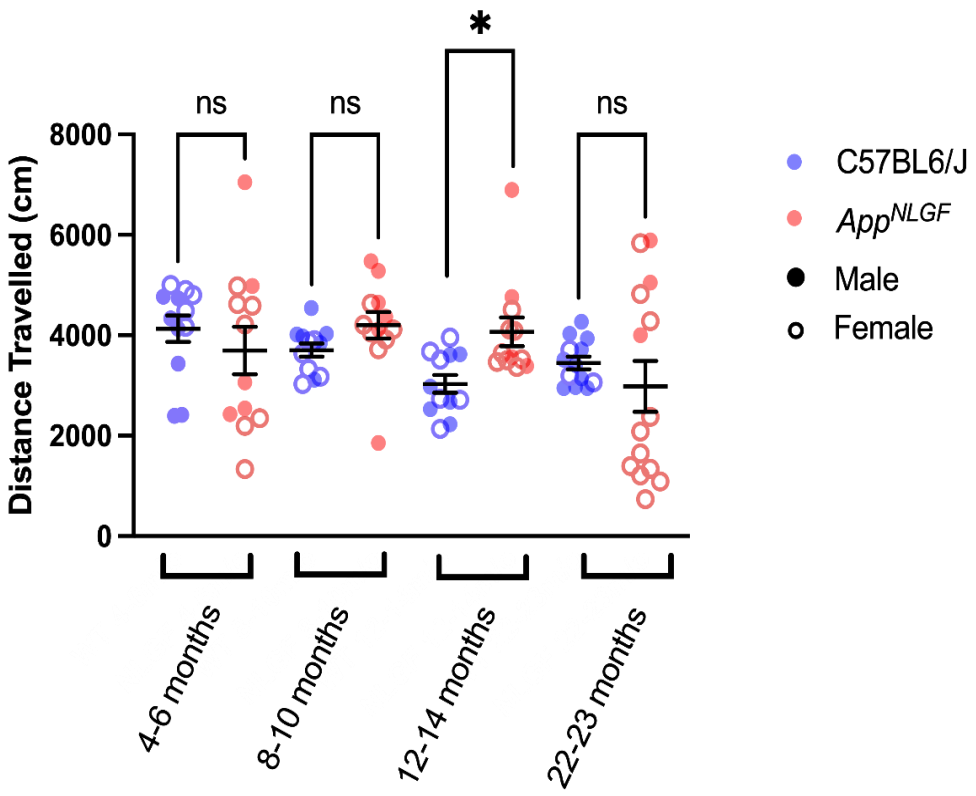

Figure 3.25: Distance Travelled During the Elevated Plus Maze Test. The mean distance travelled during the Elevated Plus Maze test, in animals aged 4-6, 8-10, 12-14, and 22-23 months. Raw (untransformed) data presented with black bars representing the mean +/- the standard error of the mean. Results of simple main effects analysis from two-way ANOVA are shown (ns = non-significant, * = $p < 0.05$). The key indicates genotype and sex. C57BL6/Js: 4-6m/o n = 12, 8-10m/o n = 12, 12-14m/o n = 12, 22-23m/o n = 13. *App*^{NLGFs}: 4-6m/o n = 12, 8-10m/o n = 12, 12-14m/o n = 12, 22-23m/o n = 14.

3.5 Discussion

3.5.1 Assessment of Memory

3.5.1.1 Overview

The experiments in this chapter aimed to provide a comprehensive assessment of memory processes and anxiety-like behaviour in *App*^{NLGF} and C57BL6/J mice across a developmental age range. Memory testing began with a series of object recognition tests, consisting of the Object Novelty (ON), Object-in-Place (OiP), and Object Location (OL) tasks. Together, these tests examined the "what" and "where", and associative aspects of object recognition memory, providing insights into the impact of age and presumed progressive Aβ deposition on the medial temporal lobe and cortical regions of the brain that are critical for object memory (Barker & Warburton, 2011). In addition to recognition memory, the spontaneous alternation test was also carried out to assess spatial working memory, a process also strongly dependent on hippocampal integrity (Deacon & Rawlins, 2006).

3.5.1.2 Object Novelty

Object recognition experiments begun with testing the most maximally aged animals available (22-23 months). These animals underwent ON and OiP tests in a counterbalanced order. When examining object interaction times during ON testing, both C57BL6/J and *App*^{NLGFs} had a greater tendency to explore the novel objects compared to the familiar objects. Unexpectedly, *App*^{NLGFs} showed significantly greater contact with the novel object compared to C57BL6/Js. This could not be accounted for by any overt locomotive differences between the genotypes as there was no significant difference in the distance travelled between both genotypes during ON testing. Therefore, it may be hypothesised that the increased exploration of the novel objects by *App*^{NLGF} mice could be explained by mutant APP-induced enhanced curiosity or novelty-seeking behaviour.

Whilst the contact time data provides an initial overview of exploratory behaviour during the ON test, Discrimination Ratios (DRs) provide a measure of the relative preference for the novel object whilst controlling for overall exploration levels. Analysis of DRs revealed that both C57BL6/J and *App*^{NLGF} demonstrated a significant preference for the novel objects, spending significantly more time exploring them than would be expected by chance. Discrimination remained significant even after applying the Bonferroni-adjusted threshold (adjusted $\alpha = 0.025$). These findings indicate that both C57BL6/Js and *App*^{NLGFs} were able to successfully discriminate the novel from the familiar objects. Importantly, there was

no significant difference in discrimination performance between the two genotypes, indicating that novelty recognition memory was preserved in the *App*^{NLGF} mice. To assess whether there were any temporal changes in object discrimination that may be explained by habituation or fatigue effects, overall DR data was divided into separate DRs for the first and second halves of the test. Analysis of the split data revealed that the DRs remained consistent across both genotypes throughout the test, indicating that there was no significant decline in performance over time. Furthermore, discrimination relative to chance remained significant for each genotype during both halves of the test, even after applying the Bonferroni-adjusted threshold (adjusted $\alpha = 0.0125$), indicating consistent novelty recognition throughout the session.

Overall, data from the ON experiment indicates that in aged *App*^{NLGF} mice, encoding of object information and reaction to novelty is intact. Lesion studies, notably work by Barker and Warburton, have implicated a network involving the PRh, HPC, and PFC in tasks probing various aspects of object recognition memory (Barker et al., 2007; Barker & Warburton, 2011; Warburton & Brown, 2015). Studies have suggested a specific role of the PRh in the visual detection of novel objects from recently observed stimuli in the ON task (Aggleton et al., 2010; Barker & Warburton, 2011; Brown & Aggleton, 2001; Bussey et al., 1999; Ennaceur et al., 1996; Mumby & Pinel, 1994; Norman & Eacott, 2004). Whilst the results from this thesis do not directly confirm the integrity of the PRh in the *App*^{NLGF} model, the findings suggest that this region of the network, to the scope of the ON test, remains functionally intact, despite reported Aβ deposition in the *App*^{NLGF} PRh (Mehla et al., 2022). This initial finding is important as it demonstrates that vision and novelty-induced exploratory activity likely remain intact in these animals, even at the extremely advanced age of 22-23 months. Since the ON task assesses object recognition without requiring spatial memory, intact performance in the task allows the dissociation of potential deficits in spatial-based memory tasks, i.e., any potential deficits discovered during the OiP task can be attributed to deficits in integrating object identity with spatial information, rather than a failure to encode the object identity.

In object recognition tests, the delay period is important as it determines whether short or long-term memory processes are engaged, which may be affected differently in the *App*^{NLGF} model. Both short and long-term object familiarity memory in the ON test requires intact AMPAR activity in the PRh (Winters & Bussey, 2005). When retention delays exceed 1 hour, blocking NMDARs in the PRh, mPFC and HPC has produced deficits in ON memory (Baker & Kim, 2002; Barker et al., 2006; Warburton et al., 2013; Winters & Bussey, 2005). However, it has been reported that some deficits observed after long retention intervals could reflect alterations in the animal's drug state affecting retrieval or expression of memory rather than actual encoding of long-term memory (Chan et al., 2019). Moreover, inactivation studies have indicated a role of the anterior RSC and its interaction with the PRh, mPFC, medial EC, and anteromedial thalamic nuclei in the long-term consolidation of novel

object recognition memory (de Landeta et al., 2020; de Landeta et al., 2021). In contrast, short-term familiarity discrimination appears dependent on kainite receptors, another class of ionotropic glutamate receptors, as well as muscarinic and nicotinic receptors in the PRh (Barker et al., 2006; Tinsley et al., 2011). In this thesis, 10-minute delay periods were used for all object recognition tasks, likely engaging short-term memory processes. While *App*^{NLGFs} at 22-23 months exhibited intact ON memory after a 10-minute delay, this approach potentially limited sensitivity to subtle memory deficits which may have reflected Aβ-mediated synaptic disruption in wider circuits including the HPC and RSC. Thus, increasing the delay period could have provided a more sensitive assay for detecting amyloid-related synaptic disruptions in the *App*^{NLGF} model. However, the existing literature regarding *App*^{NLGF} ON performance is highly variable and doesn't necessarily point towards a delay-dependent effect. For example, Whyte et al., (2018), Broadbelt et al., (2022), and Kundu et al., (2022) report intact ON memory with a 24-hour delay in *App*^{NLGFs} from 6 months of age. In contrast, Mehla et al., (2019), Degawa et al., (2021), and Pauls et al., (2021) report impairments with this retention delay in *App*^{NLGFs} ranging from 6 to 12 months old. Additionally, two other studies have reported ON deficits in *App*^{NLGFs} at 10 or 12 months after a 1hr retention delay (Auta et al., 2022; Locci et al., 2021). Likewise, some studies have reported intact novel object recognition following delay periods ranging from 2 minutes to 24 hours in the PDAPP and Tg2576 models tested up to 16 months (Evans et al., 2019; Good & Hale, 2007; Hale & Good, 2005). Contrastingly, however, other studies have observed ON deficits in the 5xFAD and APP/PS1 transgenic AD models with delays of 30 minutes to 1 hour (Joyashiki et al., 2011; Webster et al., 2013). These inconsistencies suggest that factors beyond delay duration, such as strain differences, experimental variability, habituation, and stress may impact ON performance.

Habituation, where present, varies drastically among the studies of *App*^{NLGF} ON performance. For example, Izumi et al., (2018) and Degawa et al., (2021) do not mention any habituation prior to ON testing. Auta et al., (2022) and Pauls et al., (2021) describe habituation as one previous exposure to the OF arena for 10 and 5 minutes, respectively. Habituation in the Locci et al., (2021) study consists of three 10-minute OF exposures, whereas the Broadbelt et al., (2022) and Mehla et al., (2019) studies use six 5-minute OF exposures. The experiment for this thesis consisted of three consecutive habituation days consisting of one 10-minute OF exposure on day 1 and three x 5-minute exposures to different arrays of objects in the OF arena on days 2 and 3. Importantly, the studies mentioned above do not include objects in the habituation protocols. It could be argued that extended exposure to the testing arena and the presence of objects during habituation in this thesis may have diminished neophobic behaviours, which may have otherwise confounded novelty recognition. A further inconsistency between ON experiments across different studies is the sample phase. The above studies use one 10-minute trial period of the familiar objects before introduction of the novel object during the test phase. For the experiment in this thesis, the animals received three sample trials prior to the test trial. The ability to discriminate the novel object(s) during the test trial

is known to be sensitive to exploration time during sampling (Antunes & Biala, 2012; Ennaceur & Delacour, 1988). Thus, the ability of animals to discriminate in the experiment of this thesis may reflect the overall increased available time or the repeated opportunities to encode familiar objects during the sampling, compared to other studies with single sample phases.

Overall, it could be concluded that *App*^{NLGFs} exhibit intact encoding and short-term retention of novelty information at 22-23 months. However, in the context of inconsistent phenotypes reported in the literature, future work should manipulate the delay period to explore whether this is retained for longer periods of time. Nevertheless, this is a novel phenotype that, at the time of writing, has not previously been presented in *App*^{NLGF} animals, or any AD model of such an advanced age. Younger cohorts were not assessed during this task, so tracking potential age-related changes in ON performance was not possible. However, given that intact ON processes were observed in *App*^{NLGFs} at 22-23 months, it can reasonably be inferred that these processes are also intact in younger *App*^{NLGFs}.

3.5.1.3 Object-in-Place

OiP testing was also conducted in 22–23-month-old *App*^{NLGFs} and C57BL6/Js to evaluate associative recognition memory, specifically their ability to integrate object identity with spatial location. The OiP task is reliant on the functional interaction between the mPFC-HPC-PRh circuit, as shown by bilateral lesion studies (Barker & Warburton, 2011). Furthermore, electrophysiological and lesion studies have evidenced EC involvement in OiP-like association tasks but not in OL and ON tasks (Tsao et al., 2013; Wilson et al., 2013). Lesion studies have also implicated the RSC in discriminating the switched objects during the OiP task, suggesting a potential role of the RSC in integrating information from distal and local cues during this task (Vann & Aggleton, 2002).

Analysis of object contact times revealed no significant differences in exploration of novel or switched objects between both genotypes. Furthermore, analysis of DRs indicated that neither *App*^{NLGFs} or C57BL6/J controls were able to significantly discriminate the switched objects from the stationary objects during the OiP task. Unexpectedly, no significant difference in DRs between the two genotypes was observed, despite the C57BL6/J group exhibiting a numerically higher mean DR. Splitting the DR data into first and second halves also revealed no significant differences in performance throughout the test, suggesting that neither genotype exhibited an initial novelty preference that diminished with increased exposure to the objects. There was also no significant difference in the distance travelled between *App*^{NLGF} and C57BL6/J animals, despite the *App*^{NLGF} group possessing an outlier, indicating that the similar levels of object exploration between genotypes was not confounded by differences in locomotion.

Given that the ON task demonstrated that the PRh is likely functionally intact in both C57BL6/J and *App*^{NLGFs} at 22-23 months, deficits in the OiP task suggest there may be involvement of a wider network including the mPFC, HPC, EC, and RSC (Barker & Warburton, 2011; Good, Barnes, et al., 2007; Tsao et al., 2013; Vann & Aggleton, 2002; Warburton & Brown, 2015; Wilson et al., 2013). NMDA receptors in the HPC have been shown to be essential for OiP associative memory, but not for ON detection (Barker & Warburton, 2015). Moreover, in addition to activity in the PRh required for ON memory, AMPARs in the mPFC are essential for encoding and retrieval of OIP memory (Barker & Warburton, 2008). Furthermore, the role of concurrent glutamate transmission in the HPC and cortical regions appears to be delay-dependent, with different network contributions required for short and long-term memory (Barker & Warburton, 2015). For example, crossed unilateral infusion studies suggest that short-term OiP memory depends on NMDAR activity in the HPC-mPFC, as well as kainite receptor activity in the PRh (Barker & Warburton, 2008, 2015). Long-term OIP memory (> 1 hour retention delays), however, is also dependent on NMDAR activity in the HPC-PRh regions (Barker & Warburton, 2015), and RSC (McElroy et al., 2024). Early and widespread amyloid deposition evidenced in key regions such as the PFC, HPC, and PRh in the *App*^{NLGF} model may indeed underlie potential alterations in NMDAR activity and related signalling required for OiP memory (Latif-Hernandez et al., 2020; Latif-Hernandez et al., 2019; Liu et al., 2019; Mehla et al., 2019; Saito et al., 2014; Tang et al., 2024). Furthermore, there is evidence of increased prefrontal-hippocampal connectivity prior to plaque deposition, indicating an early compensatory response to the neurotoxic effects of soluble Aβ species in these critical regions involved in associative memory (Latif-Hernandez et al., 2019).

Given the 10-minute retention delay used in this thesis, the task primarily engaged short-term memory mechanisms, suggesting a dysfunction within specific short-term memory networks. However, given the unexpected failure of C57BL6/J animals to discriminate the switched object in the OiP task, it cannot be concluded that the deficits observed in the *App*^{NLGF} model are entirely driven by Aβ-related pathology. At 22-23 months, this task was evidently too difficult for even C57BL6/J animals, despite the relatively short retention delay. It could therefore be argued that these associative spatial deficits may largely reflect natural age-related decline, which is evident even in C57BL6/Js at such an advanced age, mirroring episodic memory impairments observed in elderly individuals without AD (Dubois et al., 2007). A key limitation of this study therefore is that no younger animals were tested, so there is no indication to when these deficits emerge in both genotypes. At younger ages, it is possible that C57BL6/J animals may still retain the ability to discriminate the switched objects, whereas at the same age *App*^{NLGFs} may exhibit impairments, likely reflecting Aβ-mediated disruptions in the neural substrates of spatial processing (Barker & Warburton, 2011). Therefore, future work should test *App*^{NLGFs} at a wide range of ages to better assess the trajectory of cognitive decline and provide an opportunity for pharmacological intervention at earlier ages. To date, no other

studies have specifically examined OiP memory in *App*^{NLGF} mice, rendering it difficult to pinpoint when these deficits may emerge. However, transgenic models such as the PDAPP and Tg2576 generally exhibit impairments in OiP performance from around 14 months of age, despite intact familiarity recognition in the ON task, suggesting that impairments in the *App*^{NLGFs} may emerge later (Evans et al., 2019; Good & Hale, 2007; Hale & Good, 2005).

3.5.1.4 Object Location

As neither C57BL6/Js or *App*^{NLGFs} could discriminate the switched objects in the OiP task, the OL task was carried out. This task was simpler for the animals as it did not incorporate memory for individual object-place associations; the OL task used a set of identical objects in different locations within the arena, one of which was moved to a novel location during the test trial. The task is also sensitive to hippocampal lesions, hippocampal NMDAR function, and aging (Assini et al., 2009; Barker & Warburton, 2011, 2015; Hunsaker et al., 2007; Mumby et al., 2002; Wimmer et al., 2012; Yamada et al., 2017). There is also some evidence that object-location association requires intact RSC function (Ennaceur et al., 1997; Parron & Save, 2004; Sheppard et al., 2024).

In this thesis, separate cohorts of animals aged 4-6, 8-10, and 22-23 months underwent OL testing. Analysis of object contact times revealed that the object type influenced contact times, with animals spending significantly more time exploring the repositioned object compared with the object that remained stationary. Age also had a significant impact on object exploration, with 22–23-month-old animals spending more time interacting with the objects compared to both younger groups. Genotype did not significantly alter object contact time, indicating that the overall levels of object interaction was comparable between C57BL6/Js and *App*^{NLGFs}. Analysis of locomotor activity during OL testing indicated that aging influenced locomotion regardless of genotype, with 22–23-month-old animals travelling a shorter total distance compared to both younger groups. This suggests that the increase in object contact times may be due to decreased mobility or reduced exploratory behaviour with age, leading to longer periods of interaction with the objects.

Analysis of DRs revealed that, in contrast to the object contact time data, genotype, but not age, significantly affected DRs during OL testing. Therefore, while overall exploration times were comparable between genotypes and increased with age, *App*^{NLGFs} were specifically impaired in their ability to preferentially explore the repositioned object. At all ages tested, C57BL6/J animals consistently demonstrated significant preference for the object in the novel location, whereas *App*^{NLGFs} displayed a noticeable decline in discrimination with age. Specifically, *App*^{NLGFs} only showed significant preference for the novel location at the youngest age tested, with the two older groups performing similarly to chance, indicating a gradual loss of

discrimination with age. To account for the increased risk of type I error associated with conducting multiple one-sample T-tests, especially in this context where deficits appear subtle and age-related changes are not clear cut, a Bonferroni correction was applied (adjusted α = 0.008). With this more conservative threshold, 4–6-month-old C57BL6/Js retained significant discrimination, while *App*^{NLGFs} at this age did not. At 8-10 months, neither group showed significant discrimination, with the C57BL6/J group falling below the adjusted threshold. However, at 22-23 months, while *App*^{NLGFs} did not significantly discriminate the repositioned object, C57BL6/J discrimination survived correction. Given that OL discrimination in *App*^{NLGF} mice failed to survive Bonferroni correction at all ages, whereas C57BL6/Js retained significance at 4-6 and 22-23 months, this strengthens the evidence of a spatial deficit in *App*^{NLGF} mice. While C57BL6/J performance at 8-10 months dropped below the adjusted threshold, the recovery at 22-23 months implies that this decline does not necessarily reflect a memory deficit in these animals. Importantly, some of the age-related reduction in discrimination observed in *App*^{NLGFs} may be associated with the decrease in total distance travelled with age. However, as this decline in locomotion occurred across both genotypes, the selective drop in DRs in *App*^{NLGF} groups likely reflects a genuine impairment in spatial memory rather than a general reduction in activity.

As noted earlier, there was no overall effect of genotype on object contact times, further indicating that inherent differences in exploratory behaviour during the OL test likely did not account for the impaired ability for *App*^{NLGFs} to discriminate the repositioned object. Nevertheless, a key limitation of the OR experiments presented in this thesis is that sample phase data were not analysed. Without confirmation that animals engaged with all objects during the sample phases, and that there were no group differences in sample phase exploration, it is difficult to interpret any observed impairments. For instance, it is possible that the apparent deficits observed in the *App*^{NLGF} group during the OL task reflect differences in initial object engagement rather than genuine impairments in spatial memory. Similarly, in the OiP task, it is unclear whether poor performance across both groups reflected a lack of engagement at sample phase. However, no overall genotype differences were observed in object contact times during both the OL and OiP tests, and *App*^{NLGFs} actually showed greater engagement with the novel object in the ON test phase, indicating that they did not exhibit a pattern of reduced engagement. Consistent with this, previous studies have reported comparable contact times across both sample and test phases in C57BL6/Js and *App*^{NLGFs} (Broadbelt et al., 2022; Degawa et al., 2021). Nevertheless, future studies should analyse sample-phase data to confirm that recognition memory impairments are not confounded by initial differences in object engagement.

The deficit in OL memory observed here appears to contrast with a recent study showing intact OL discrimination in *App*^{NLGF} mice at 6-9 and 12-14 months of age (Broadbelt et al., 2022). Moreover, 16-month-old Tg2576 mice also showed intact OL

discrimination following a 2 minute delay (Good & Hale, 2007). This is an intriguing contrast, especially considering the delay used in the Broadbelt paper was 6 hours, and the experiment in this thesis used a 10-minute retention delay, suggesting that incorporating a longer delay interval does not necessarily reveal a more pronounced spatial deficit in *App*^{NLGF} mice. Therefore, it may be suggested that the deficit observed here could be confounded by non-memory related factors, such as reduced motivation or boredom during the task, which may also explain why C57BL6/J performance appears to drop at 8-10 months. Mice displayed relatively low object interaction times during the OL task compared to the ON and OiP tasks, which may have contributed to lower discrimination. It is possible that the mice were over-habituated to the environment, or that the objects selected for the OL experiment were not sufficiently stimulating. It is argued that sufficient object interaction is required to engage the HPC in object-based memory tasks (Cohen & Stackman, 2015). Consequently, the lower contact times during the OL task in this thesis may suggest that the results are not fully reflective of the integrity of the *App*^{NLGF} HPC. However, these results may still point to a hippocampal deficit in these animals, consistent with previous studies reporting substantial amyloid deposition in the HPC from around 4 months of age (Latif-Hernandez et al., 2019; Mehla et al., 2019; Saito et al., 2014; Tang et al., 2024). Additionally, these results may also reflect the impact of amyloid deposition in the RSC, as previously reported in the *App*^{NLGF} model at 12 months (Mehla et al., 2022). These deficits likely, at least in part, also contribute to the observed OiP memory impairment (Barker & Warburton, 2011; Vann & Aggleton, 2002).

The overall spatial deficit observed here is unexpectedly mild. It has been suggested that traditional experimental paradigms may not be sensitive enough to detect deficits in models of early AD, which the *App*^{NLGF} model is said to reflect (Saifullah et al., 2020; Saito et al., 2014). To address this, a recent study developed an integrated "what-where-when" paradigm to assess the ability to recall the specific locations of an inanimate object or a female mouse within a divided arena at specific times of the day (Tan et al., 2023). Over two consecutive training days, the mice encountered a novel object in the morning and a female mouse in the evening, within the same chamber of the arena. The following day, the mice were placed in an empty arena and exploration time and scent-marking analysis was used to test the ability to associate the object and female mouse with their prior location in the morning and evening. At 3-4 months, prior to reported overt plaque formation in this study, *App*^{NLGF} mice failed to show an overall preference for exploring the target zone associated with the object and female mouse, compared to the consistently empty zone, indicating a deficit in "what-where" episodic-like memory (Tan et al., 2023). However, the same animals exhibited significantly more scent marking of the target zone during the evening compared to the day, which suggests the memory of when the female mouse was encountered, i.e. "what-when" memory, was intact (Tan et al., 2023). These findings suggest that tasks requiring greater cognitive demand and flexibility may reveal subtle deficits in the *App*^{NLGF} model, potentially reflecting

preclinical AD, in which patients may show occasional memory lapses before more pronounced cognitive decline becomes evident (Rabin et al., 2017).

3.5.1.5 Spontaneous Alternation

Spatial working memory is an important day-to-day process that is affected in AD (Lester et al., 2017). The spontaneous alternation task is widely used to evaluate spatial working memory in rodents as it assesses their ability to retain and use spatial information over a short period of time to guide navigation of a T or Y-maze (Kim et al., 2023). This task relies on the innate preference of rodents to explore less recently visited arms of the maze, providing an insight into their ability to update and utilise spatial memory to alternate efficiently through different arms of the maze (Deacon & Rawlins, 2006). As opposed to tasks such as the RAM and MWM, the spontaneous alternation test does not require training, excessive handling, or reinforcement, thereby minimizing the risk of inducing fear or stress that could confound behaviour (Kim et al., 2023).

For this thesis, spontaneous alternation testing was performed on separate cohorts of *App*^{NLGFs} and C57BL6/J controls aged 4-6, 8-10, 12-14, and 22-23 months. At all ages tested, both C57BL6/J and *App*^{NLGF} animals exhibited significantly higher spontaneous alternation versus chance (22%), all surviving Bonferroni adjustment (adjusted $\alpha = 0.00625$). At 4-6 and 12-14 months, there were no significant differences in alternation patterns between the two genotypes. However, at 8-10 and 22-23 months, *App*^{NLGF} animals showed significantly reduced spontaneous alternation compared to C57BL6/J animals. At 8-10 months, the difference was modest ($p = 0.045$). However, at 22-23 months, there was stronger evidence of a significant impairment in *App*^{NLGF} mice ($p < 0.001$). These data indicate that, at all ages tested, both C57BL6/J and *App*^{NLGF} animals demonstrated a significant preference for less recently visited arms during spontaneous alternation testing. However, at 8–10 and especially at 22–23 months, *App*^{NLGF} performance was significantly reduced relative to controls, suggesting progressive deficits in spatial working memory with advancing age. For C57BL6/J animals, percentage alternation during the spontaneous alternation task appears stable across all ages tested. However, 22–23-month-old *App*^{NLGFs} exhibited significantly reduced alternation compared to every younger *App*^{NLGF} group tested. This suggests that *App*^{NLGFs} exhibited an age-dependent decline in the ability to retain and utilise spatial information in the spontaneous alternation task, which may indicate progressive deterioration of spatial working memory processes, potentially driven by advancing amyloid pathology and associated network dysfunction. Specifically, impairments in the spontaneous alternation may reflect Aβ-mediated disruptions in hippocampal function HPC and associated NMDAR signalling, aligning with the deficits observed in the hippocampal-dependent OL task (Lalonde, 2002; Walker & Gold, 1992; Zhou, 2015). Moreover, impaired alternation may be attributed to neurodegenerative

changes in wider networks supporting spatial working memory, including the PFC and EC (Coutureau & Di Scala, 2009; Dunnett et al., 1999; Lalonde, 2002).

In addition to alternation performance, the number of arm entries was analysed to assess exploratory activity during the task. Across ages, *App*^{NLGFs} made significantly more arm visits than C57BL/6Js. While this effect was modest ($p = 0.035$), it appears in contrast to previous studies reporting no genotype differences in males (Degawa et al., 2021) and reduced arm entries in female, but not male, *App*^{NLGFs} (Kundu et al., 2022). These discrepancies likely reflect methodological and cohort differences. For example, Degawa et al., (2021) tested 12-month-old males in a 7-minute Y-maze, while Kundu et al., (2022) examined 4–5-month-old animals in a 5-minute Y-maze and observed effects only in females (Degawa et al., 2021; Kundu et al., 2022). In contrast, the present study used a T-maze, included mixed-sex cohorts, and assessed animals across a broader age range (4–23 months) with longer 10-minute trials, all of which may have influenced exploratory activity. Such differences in maze type, trial duration, sex, and age range may account for the contrasting findings in exploratory behaviour during the task.

The overall difference in arm entries observed in this thesis complicates interpretation of alternation scores, since the number and timing of arm entries influence percentage alternation (Jaffard et al., 1981). Typically, a higher number of arm entries would be expected to reflect hyperactivity (Miedel et al., 2017). However, at 22–23 months, *App*^{NLGFs} travelled significantly less distance than C57BL/6Js while still making more arm entries overall. This pattern suggests that *App*^{NLGFs} engaged in shorter, more fragmented arm visits, whereas C57BL6/Js displayed more sustained exploration across arms. Importantly, in the continuous-trial design used in this thesis, the interval between arm choices could not be controlled, and longer delays are known to reduce alternation (d'Isa et al., 2021; Dudchenko, 2001). Nonetheless, the finding that *App*^{NLGFs} alternated significantly less than C57BL6/Js at 22–23 months, despite making more arm entries, supports the interpretation that their deficit reflects a genuine impairment in spatial working memory rather than reduced exploratory drive. Specifically, the higher number of arm entries in *App*^{NLGFs} suggests that they did not generally experience prolonged inter-choice delays that could have artificially depressed alternation scores. That said, age-related reductions in activity were evident across genotypes: animals at 22-23 months made fewer arm entries and travelled less than mice at 4-6 months. For C57BL6/J mice, distance travelled declined between the youngest and oldest groups, while 22–23-month-old *App*^{NLGFs} travelled significantly less than all younger *App*^{NLGF} groups and age-matched controls. Therefore, reduced activity in older *App*^{NLGFs} may have contributed to the lower alternation performance, meaning the deficit cannot be attributed solely to impaired spatial working memory. Future studies could address the methodological complication of variable exploratory activity and inter-choice timing by equating the number of arm entries and controlling delays between choices. This could be achieved by restricting the task to a fixed number of trials and by implementing

controlled inter-trial intervals, such as in a forced alternation design. This approach would help disentangle memory performance from differences is locomotion and exploratory strategy, providing a clearer and more direct assessment of spatial working memory.

The locomotive deficit observed in 22–23-month-old *App*^{NLGFs} is unlikely to be explained by hippocampal neurodegeneration. Rather, lesions of the CA1 in C57BL6/J animals have been shown to induce hyperactivity in the spontaneous alternation task rather than the observed hypoactivity in this experiment (Dillon et al., 2008). The exaggerated hypoactivity in *App*^{NLGFs} with age could potentially be attributed to increased hesitancy during the task, reflecting PFC deficits that affect decision-making (Lalonde, 2002). Alternatively, hypoactivity may be attributed to heightened anxiety-like behaviour or neophobia in *App*^{NLGFs} at 22-23 months, which may indicate deficits in other brain regions that regulate anxiety and stress responses, such as the amygdala (Hohoff, 2009; Lalonde, 2002). Indeed, alternation rates are known to decline in mice subjected to mild stress beforehand (Bats et al., 2001), suggesting that reduced spontaneous alternation in 22–23-month-old mice may be in part driven by increased levels of stress or anxiety.

Despite some differences in locomotor activity or anxiety that may add a level of confound to the comparison between genotypes, there was a clear difference in alternation at the oldest age tested. The alternation impairment reported here is consistent with previous observations in Tg2576 mice, but in the transgenic model it manifested at an earlier age (9-14 months) (Deacon et al., 2008; Hsiao et al., 1996). The earlier onset of spontaneous alternation deficits in this transgenic model could be attributed to its more aggressive amyloid production and/or the overexpression of toxic biproducts of APP processing, governed by the nature of its transgenic expression of mutant *APP* (Sasaguri et al., 2022). In *App*^{NLGF} mice, intact alternation has been reported in animals of 4-6, 6-9 and 12-14 months (Broadbelt et al., 2022; Kundu et al., 2022; Whyte et al., 2018). Although these studies did not include animals older than 14 months, they appear to align with the results of this thesis that show predominantly intact alternation in the *App*^{NLGFs} model until the age of 22 months. Contrastingly, however, Saito et al., (2014) originally reported spontaneous alternation deficits in *App*^{NLGF} mice as young as 6 months. Moreover, further studies have shown deficits from 10-12 months (Auta et al., 2022; Degawa et al., 2021; Locci et al., 2021). It has also been reported that alternation in the *App*^{NLF} model, with one fewer mutation than the *App*^{NLGF} model, is intact at 9-12 months but deficient at 18 months (Izumi et al., 2018; Saito et al., 2014). This observation is intriguing, as behavioural deficits would typically be expected to emerge at a later age in this model compared to *App*^{NLGF} animals due to the absence of the Arctic mutation, which accelerates amyloid pathology (Saito et al., 2014). Similar to object recognition testing, variations in the observed timeline of deficits during spontaneous alternation testing may be at least partially explained by methodological differences between research groups, such as the different durations of the test which may

influence the animals' ability to sustain engagement during the task, differences in handling which may impact the animals' stress levels, and differences in sample sizes which may affect statistical power to detect subtle deficits in alternation.

Overall, this data contributes to the characterisation of the spatial working memory of *App*^{NLGF} animals. Despite the potential confounds of locomotive differences, it demonstrates a possible Aβ-mediated deficit in the short-term spatial memory of *App*^{NLGFs}. Arguably, the most interesting finding from this experiment is that overt deficits do not appear until the extremely advanced age of 22-23 months. Whilst some other research groups have discovered spontaneous alternation deficits at younger ages, the variation of phenotype, along with the advanced age of deficit onset shown in this thesis, indicates a more subtle phenotype of spatial working memory deficit compared other models of AD. Along with the results from OL and OiP testing, these data indicate that the extent of spatial impairments in this model is mild. However, as previously noted, it has been suggested that spontaneous alternation should not be used as a solitary measure of memory, as it may also reflect changes in motivation, attention, and sensory behaviour (Hughes, 2004). For instance, reduced motivation or impaired attention could reduce alternation independent of memory function, while sensory deficits may hinder the animals' ability to distinguish between maze arms, confounding interpretation of memory performance (Hughes, 2004). Indeed, attention deficits have been reported in the *App*^{NLGF} model before, reflected by increased response latencies and a high number of missed trials during a serial reaction time task in which mice were trained to detect and respond to a yellow LED light stimuli within a limited time window (Masuda et al., 2016). Therefore, further research is required to determine whether any detectable spatial working memory deficits are translatable to other tasks with more complex requirements, such as the MWM and RAM tasks. To date, no studies have assessed RAM performance in *App*^{NLGF} mice and data on MWM performance is extremely variable. For example, three studies report intact escape latencies in *App*^{NLGFs} at various age points between 3 and 12 months (Latif-Hernandez et al., 2019; Saifullah et al., 2020; Whyte et al., 2018), whereas others have observed increased escape latencies at multiple points within the same age range (Locci et al., 2021; Mehla et al., 2019; Wang et al., 2022). This variability highlights the need for further research to clarify the progression and severity of spatial working memory deficits in *App*^{NLGF} mice.

The subtlety of behavioural deficits observed in the *App*^{NLGF} model, both in this thesis and the wider scientific literature, suggests that cognitive decline in these mice may be relatively mild or emerge mostly in later disease progression. However, a recent study found that, despite showing no impairments in long- or short-term memory in the SA, OL, and ON tasks, *App*^{NLGF} mice exhibited a specific impairment in novelty-promoted memory, assessed by behavioural tagging and capture (BTC) at 6-9 months (Broadbelt et al., 2022). BTC is a mechanism by which novelty introduced shortly before or after a learning event promotes memory persistence

(Moncada et al., 2015). Strong stimulation during the exposure to novelty is believed to induce the production of plasticity-related proteins (PRPs), which are captured by synaptic tags induced by weak stimulation during the learning event, inducing lasting changes in plasticity (Frey & Morris, 1997; Moncada et al., 2015; Moncada & Viola, 2007). This novelty-promoted memory is sensitive to age-dependent decline (Gros et al., 2022; Gros & Wang, 2018). In the study by Broadbelt et al., (2022), BTC was assessed using appetitive delayed matching-to-place (ADMP) task, in which rodents encoded the specific locations of hidden food rewards and were tested on their ability to recall the locations after a delay of 6 hours. In this task, rodents were exposed to an arena containing two novel objects between the encoding and retrieval trials. While C57BL6/J mice showed improved memory performance following novelty exposure, evidence by increased correct digging, *App*^{NLGF} mice did not benefit from novelty exposure and performed significantly worse than C57BL6/J mice during the retrieval trial (Broadbelt et al., 2022). This deficit occurred despite both genotypes exhibiting comparable learning during the encoding trial, as indicated by the number of digging errors and latency to find the rewards (Broadbelt et al., 2022). These findings suggest that, although *App*^{NLGFs} may maintain the ability to form strong memories, as demonstrated by intact object-based memory performance in this paper, they struggle to stabilise weak memories with novelty. This impairment may reflect early Aβ-mediated disruptions in PRP synthesis and synaptic plasticity in the *App*^{NLGF} model, which may impair consolidation of weak memories before overt memory deficits become detectable in standard behavioural tests, such as those used in this thesis. Specifically, the ADMP and object recognition tasks have been shown to engage neuronal populations in the CA1 and CA3 regions of the HPC, areas known to exhibit disrupted glutamatergic transmission in the *App*^{NLGF} mouse (Benitez et al., 2021; Gros et al., 2022). Therefore, these regions may represent key sites of early Aβ mediated dysfunction in the model.

In line with this, although overt behavioural deficits are limited in the *App*^{NLGF} model, there is evidence of early and progressive circuit-level dysfunction. For example, a recent *in vivo* electrophysiological study reported mildly disrupted spatial coding of the medial EC in 3–5-month-old *App*^{NLGFs}, including a reduction in the number of grid cells and disrupted spatial tuning whilst foraging in an OF arena (Jun et al., 2020). Remapping, the process by which neurons change their firing patterns in response to environmental changes, was also impaired in this group during navigation of different running tracks (Fyhn et al., 2007; Jun et al., 2020; Muller & Kubie, 1987). Notably, at this age, CA1 place cell activity was intact during foraging, and spatial memory during a foot shock context discrimination task was also unimpaired (Jun et al., 2020). However, by 7-13 months of age, spatial tuning and remapping in the medial EC was severely impaired, and the population of grid cells were severely diminished (Jun et al., 2020). This was accompanied by a reduction in the number of active place cells in the CA1, less pronounced firing peaks, and severely diminished remapping (Jun et al., 2020). Moreover, fast gamma oscillatory coupling between the medial EC and CA1 was reduced, indicating disrupted communication needed for encoding spatial information (Griffiths & Jensen, 2023; Jun et al., 2020). Slow

gamma signalling between the CA3 and CA1, however, remained relatively intact, suggesting that memory retrieval mechanisms may be preserved for longer than encoding (Griffiths & Jensen, 2023; Jun et al., 2020). Behaviourally, mice at this age were unable to discriminate the context associated with the aversive stimulus (Jun et al., 2020). These findings suggest a progressive degeneration of the neural substrates underlying spatial memory, beginning in the EC and extending to the HPC with age. Notably, a reduction in the number of active CA1 place cells have also been reported in *App*^{NLGFs} using chronic Ca^{2+} imaging (Takamura et al., 2021), reinforcing evidence of neural dysfunction in this model. However, these alterations appear to contrast with broader behavioural data, including findings from this thesis and the Broadbelt et al., (2022) study, which report intact spatial memory or mild deficits that emerge later in life. This apparent discrepancy may reflect the presence of compensatory mechanisms that maintain cognitive function despite the emerging circuit abnormalities, thereby delaying or masking the emergence of overt and consistent behavioural impairments.

Overall, as hypothesised, *App*^{NLGF} mice exhibited a subtle pattern of memory impairments, indicating that while basic novelty recognition remained intact, memory processes reliant on spatial and associative networks became compromised, particularly by 22–23 months. However, the onset of pronounced impairments in spatial working memory appeared later than anticipated. Further research is necessary to pinpoint the precise timing of associative memory decline, to further probe spatial working memory function, and to clarify the relationship between progressive amyloid deposition and the emergence of cognitive deficits in the *App*^{NLGF} model.

3.5.2 Assessment of Anxiety-Like Behaviours

3.5.2.1 Overview

Anxiety is an important and often overlooked NPS symptom of AD (Mendez, 2021). PET imaging studies have evidenced a correlation between amyloid accumulation and anxiety in AD, suggesting that amyloid may contribute to anxiety symptoms in AD (Donovan et al., 2018; Johansson et al., 2020; Pietrzak et al., 2015; Pietrzak et al., 2014). Relatively little is known about how anxiety-like phenotypes manifest in mouse models of AD, particularly in the context of aging. The aim of these experiments was therefore to assess the effect of aging on anxiety-like behaviour in the *App*^{NLGF} model. The OF and EPM tests, two widely used behavioural assays, were conducted in *App*^{NLGF} mice and age-matched C57BL6/J controls to evaluate anxiety-like behaviour across a range of different ages.

3.5.2.2 Open Field

OF testing was performed on *App*^{NLGFs} and age-matched C57BL6/J animals at 4-6, 8-10, 14-16, and 22-23 months old. During OF testing, the animal was allowed to freely explore a square arena for 10 minutes, and the proportion of time spent in the centre relative to the total time in the arena was calculated as the inner zone ratio (IZR). At 22-23 months, *App*^{NLGFs} exhibited significantly lower IZR than C57BL6/J controls, an effect not observed at younger ages. This suggests the emergence of an anxiogenic phenotype in the *App*^{NLGF} model at this advanced age, characterised by increased avoidance of the central, more exposed zone of the OF arena (Prut & Belzung, 2003). In the C57BL6/J group, IZR was stable throughout all ages tested. However, *App*^{NLGFs} exhibited a peak in IZR at 14-16 months that was significantly higher than *App*^{NLGFs} all other age groups, despite not reaching significant difference to C57BL6/Js at this age. This indicates that the anxiety phenotype within the *App*^{NLGF} model is changeable with time and not directly linear with age. Analysis of locomotor activity indicated that age influenced the distance travelled during the OF test, regardless of genotype. In the oldest age group (22-23 months), mice travelled significantly less distance than each of the younger groups during OF testing. The age-dependent locomotive deficit observed in this thesis has been reported before in C57BL6/J mice throughout their lifespan (Dean et al., 1981; Shoji et al., 2016), suggesting a natural decline in exploratory behaviour with age. Such decline may have contributed to the reduced outer zone exploration observed in *App*^{NLGF} mice. Importantly, diminished locomotion with age could confound interpretation of performance during object recognition tasks, as reduced arena exploration with age could lower overall object interaction and thus reduce the likelihood of novelty preference. As discusses earlier, reduced locomotor activity with age was similarly observed in the OL task. However, the OiP task was only conducted in the 22–23-month group, preventing direct comparisons across ages. Therefore, potential age-related locomotor impairments at 22-23 months may be considered a confounding factor when interpreting the OiP results, particularly given that both C57BL6/J and *App*^{NLGF} animals failed to discriminate the switched objects.

The scientific literature regarding *App*^{NLGF} performance during OF testing is mixed. Recent studies reported no significant difference in the distance travelled and time in the outer or central zones for *App*^{NLGFs} aged 4-9 months compared to C57BL6/Js (Broadbelt et al., 2022; Kundu et al., 2022; Maezono et al., 2020). A similar study also demonstrated no significant difference in the percentage of time spent in the central zone of an OF arena at 6 months, despite *App*^{NLGFs} at this age showing reduced speed and increased grooming behaviour (Whyte et al., 2018). Consistent with the findings from Whyte et al., (2018), Maezono et al., (2020), Kundu et al., (2022), and Broadbelt et al., (2022), the OF data in this thesis shows no significant differences in anxiety-like behaviour between C57BL6/J and *App*^{NLGFs} at young age points. However, these studies did not perform this experiment on animals older than 9 months. Notably, no significant differences in OF exploration have been reported in the APP/PS1 transgenic model even at 24 months, suggesting that amyloid related

anxiety-like behaviour may only emerge at much later stages of disease progression (Webster et al., 2013). In contrast, however, an anxiolytic phenotype was reported in the *App*^{NLGF} model at 6 months, with *App*^{NLGFs} spending more time in the centre of the arena compared to *App*^{NL} controls, but no significant difference in the distance travelled (Latif-Hernandez et al., 2019). This behaviour, however, was not replicated in older age groups in this study, suggesting that this is not a stable phenotype. Nevertheless, a separate study reported increased duration in central zone in 12-month-old *App*^{NLGFs} compared to C57BL6/J controls (Wang et al., 2022). On the other hand, an anxiogenic phenotype was reported in the *App*^{NLGF} model at 8 months of age, with *App*^{NLGFs} spending significantly less time in the centre zone of the OF arena compared to C57BL6/J controls, despite also exhibiting no difference in the distance travelled during the experiment (Pervolaraki et al., 2019). However, this study included the theoretical presence of a "middle zone", which may confound results when comparing to experiments that did not include this zone. Nevertheless, this anxiogenic phenotype during the OF test has also been reported in separate studies with *App*^{NLGFs} at 10 months and PDAPP model at 5 months (Beauquis et al., 2014; Locci et al., 2021). Given the vast discrepancy in OF phenotypes in *App*^{NLGF} animals, particularly the opposing reports of anxiogenic and anxiolytic behaviour in the *App*^{NLGF} model, it could be argued that the effect of age-related pathology on anxiety-like behaviour is not a stable effect across laboratories, but rather dependent on a range of factors. The mixed findings could be explained by differences in laboratory practices, handling, or data analysis. For example, the differing definitions of the dimensions of the inner zone, the presence of a middle zone, and the use of time rather than the ratio of time spent in the inner zone could have substantial impact on data and thus difficulties comparing between findings from different laboratories.

Overall, findings from this thesis indicate an anxiogenic phenotype in *App*^{NLGF} mice that does not appear until the advanced age of 22-23 months. This data perhaps adds more weight to the studies that have found no significant difference in anxiogenic behaviour in younger *App*^{NLGF} mice. However, the discrepancies between studies could suggest that the phenotype is not robust in this model of AD, or that the phenotype is so subtle that it is sensitive to even minor variations to laboratory practice.

3.5.2.3 Elevated Plus Maze

EPM testing was also employed as a behavioural tool to assess anxiety-like behaviours in *App*^{NLGF} mice. EPM testing was performed on animals at 4-6, 8-10, 12-14, and 22-23 months, at least two weeks following OF testing. During the test, the animals were allowed to freely explore the EPM for 10 minutes and the total duration each animal spent in the open and closed arms was recorded. Across all age groups, *App*^{NLGF} mice consistently spent significantly more time in the open arms of the maze compared to age-matched C57BL6/Js, with the largest mean difference

observed between the 12–14-month-old groups. Within genotype comparisons revealed that age also affected open arm duration, with age-related changes following distinct patterns in C57BL6/J and *App*^{NLGF} animals. In C57BL6/J mice, open arm duration peaked at 8-10 months, while in *App*^{NLGFs} this peak extended between 4-6 and 12-14 months before declining at 22-23 months. Analysis of the total time exploring the closed arms of the maze revealed an inverse pattern of behaviour relative to the open arm analysis. At each age tested, *App*^{NLGF} animals spent significantly less time in the closed arms of the EPM compared with C57BL6/J animals, with the largest mean difference also appearing at 12-14 months. Within genotype comparisons revealed age-related changes in closed arm duration that mirrored changes observed in open arm duration. In C57BL6/J mice, closed arm duration was at its lowest at 8-10 months, whereas in *App*^{NLGF} mice the lowest closed arm duration was observed at 12-14 months. The ratio of time spent in the open arms relative to the duration of the test (open arm ratio, OAR) revealed that *App*^{NLGF} mice consistently spent a greater proportion of time in the open arms compared to C57BL6/J controls. The higher OAR in *App*^{NLGF} mice was significant across all ages, with the largest mean difference observed between C57BL6/Js and *App*^{NLGFs} at 12-14 months. Age-related fluctuations in OAR within each genotype reflected changes observed in open arm duration; C57BL6/J mice exhibited a peak in OAR at 8-10 months, while *App*^{NLGFs} showed a peak between 8-10 and 12-14 months.

To examine the patterns of locomotor activity during the EPM test, the number of entries into the open and closed arms of the maze were analysed. At each age tested, *App*^{NLGF} mice entered the open arms of the maze significantly more times than C57BL6/J animals, with the greatest mean difference also appearing at 12-14 months. While overall the preference for entering the open arm of the EPM did not significantly change as a function of age, the pattern differed between genotypes: C57BL6/J mice showed stable open arm entries across age groups, whereas *App*^{NLGFs} exhibited a significant reduction between 12-14 and 22-23 months. Analysis of closed arm entries revealed that age and genotype had independent effects on the propensity to enter the closed arms. *App*^{NLGF} mice overall made fewer entries into the closed arms compared to C57BL6/J mice. However, regardless of genotype, 4–6-month mice entered the closed arms more frequently than 12–14-month mice. Analysis of movement patterns during EPM testing revealed that the distance travelled by C57BL6/J animals was stable throughout all ages tested, whereas *App*^{NLGFs} exhibited a peak between 8-10 and 12-14 months. At 12-14 months, *App*^{NLGFs} travelled significantly further than age-matched C57BL6/Js. This suggests that there was an age-related hyperactivity during the EPM test that was elicited by the aversive nature of the maze.

In summary, the findings of this thesis demonstrate that *App*^{NLGF} mice consistently visited the open arms more often and spent a greater proportion of their total exploration time there compared to C57BL6/J controls. Conversely, *App*^{NLGFs} entered

the closed arms of the EPM on fewer occasions than C57BL6/Js, and when they did enter, they did not remain in those enclosed spaces for as long as C57BL6/Js. These findings suggest that *App*^{NLGF} mice exhibited a reduced avoidance of the open arms of the EPM test, which is commonly cited as indicative of lower levels of anxiety (Pellow et al., 1985; Pentkowski et al., 2021). This seemingly anxiolytic behaviour was most pronounced in *App*^{NLGFs} at 12-14 months, as reflected by the largest mean differences in open arm duration, closed arm duration, open arm entries, and OAR at this age. However, this peak coincides with the age at which *App*^{NLGFs} travelled significantly further than C57BL6/Js, suggesting that increased open arm exploration may have been influenced by hyperactivity in the *App*^{NLGF} model. However, the lack of genotype-related differences in distance travelled at other ages indicates that increased open arm exploration is not entirely accounted for by heightened activity in the *App*^{NLGF} model.

The findings of this thesis are generally consistent with the existing literature on *App*^{NLGF} performance in the EPM task. For example, Pervolaraki et al., (2019) also observed both a significant increase in open arm duration and a decrease in closed arm duration in 8-month-old *App*^{NLGFs}. A separate study also observed an increase in open arm exploration in *App*^{NLGFs} at 12 months, although closed arm exploration was not included for analysis (Degawa et al., 2021). Furthermore, Latif-Hernandez et al., (2019) quantified entries into open and closed arms during EPM testing using infra-red (IR) beams. At 3 months of age, *App*^{NLGFs} exhibited a significant increase in open arm crossings, however, there was no significant difference in closed arm crossings (Latif-Hernandez et al., 2019). At 6 months, *App*^{NLGFs} exhibited significantly more open arm crossings and fewer closed arm crossings (Latif-Hernandez et al., 2019). However, at 10 months, the *App*^{NLGFs} in this study exhibited no significant difference in open arm crossings despite significant decrease in closed arm crossings (Latif-Hernandez et al., 2019). The Latif-Hernandez study, despite some age-related inconsistencies, indicates that *App*^{NLGFs} generally entered the open arms more and the closed arms less than control animals, aligning with the findings of this thesis. However, Latif-Hernandez et al., (2019) incorporated a 1-minute habituation period prior to recording, which was not implemented for the experiment in this thesis. Therefore, prior exposure to the maze may have influenced novelty-driven exploration, potentially reducing initial exploratory behaviour in the EPM test and contributing to the inconsistent pattern of increased open arm and decreased closed arm crossings. Moreover, direct comparisons with this thesis are complicated by the differences in control groups, as Latif Hernandez et al., used *App*^{NL} mice, which, despite also lacking Aβ plaques, may exhibit distinct behavioural differences from C57BL6/Js due to potential effects of the Swedish mutation and subsequently elevated CTF-β levels (Saito et al., 2014).

A study by Sakakibara et al., (2018) also investigated open arm entries and the duration of open arm exploration in *App*^{NLGF} mice during the EPM task. However, this study employed a two-phase version of the task rather than the single-phase design

utilised in the above studies and in this thesis. This study reported that 6–9-month-old *App*^{NLGFs} spent significantly more time in the open arms of the maze compared to *App*^{NL} controls, but not when compared to C57BL6/J controls, in the first trial (Sakakibara et al., 2018). However, they did not observe a significant increase in open arm entries in this cohort (Sakakibara et al., 2018). During the second trial, 6-9 month *App*^{NLGFs} spent significantly longer in the open arms compared to both control groups and exhibited significantly more open arm entries compared to C57BL6/Js but not *App*^{NLs} (Sakakibara et al., 2018). At 15-18 months old, *App*^{NLGFs} exhibited significantly increased open arm duration and visits compared to *App*^{NLs} but not C57BL6/Js during the first trial (Sakakibara et al., 2018). In the second trial, however, there was an increase in open arm duration and open arm visits that was significant against both control groups (Sakakibara et al., 2018). These findings indicate an age-dependent anxiolytic-like behaviour in the *App*^{NLGFs} model, which aligns with the findings presented in this thesis. However, the variability in significant differences in open arm exploration may be attributed to differences in baseline anxiety-like behaviour among control groups. Notably, *App*^{NLs} exhibited reduced open arm exploration at 15-18 months, suggesting variations in behaviour with age that may influence the relative differences between groups (Sakakibara et al., 2018). Moreover, variations in observed behaviour may be explained by the test/retest protocol used in the Sakakibara experiment. Studies using the test/retest EPM protocol have shown that anxiolytic drugs increase open arm exploration in naïve rodents, but not in rodents who have already explored the EPM in a previous test (Bertoglio & Carobrez, 2002; Cruz-Morales et al., 2002; File, 1993; File et al., 1993; Lister, 1987). This could be explained by locomotor habituation leading to reduced exploration of the maze rather than specific changes in anxiety (Dawson et al., 1994). Alternatively, it could reflect an experimentally induced sensitisation to anxiety or fear due to memory of the aversive nature of the open arms, reducing the effect of anxiolytic drugs (Bertoglio & Carobrez, 2002; Treit et al., 1993).

Naturally, however, the abolished response to anxiolytic drugs during EPM retest calls into question the true nature of the specific behavioural processes being assessed. It has been suggested that the response to the EPM shifts from unconditioned fear/anxiety during initial exposure, to learnt avoidance of the open arms in subsequent trials, which anxiolytic drugs may not counteract effectively (Bertoglio & Carobrez, 2003; Carobrez & Bertoglio, 2005; File & Zangrossi, 1993). This suggests that any seemingly anxiogenic response to the EPM during retest is not necessarily fear related, but may be a lack of incentive or motivation to enter the open arms of the maze once they have already realised the lack of food and shelter. Therefore, if avoidance of open arms during EPM testing is not necessarily an anxiogenic response, it could be questioned whether the preference of *App*^{NLGFs} for open arms is truly an anxiolytic response. It could be argued that the behaviour of *App*^{NLGFs} during the EPM task could initially be explained by reduced anxiety or indeed reduced neophobia, but with increased exposure to the maze the response could reflect an increased motivation to explore potentially dangerous areas of the maze that is uninhibited by normal self-protective mechanisms. This disinhibitory

shift could reflect impaired decision making process or heightened exploratory tendencies (Gil-Bea et al., 2007). Therefore, the age-dependent variations observed in the Sakakibara experiment, particularly the stronger anxiolytic-like response to the second trial at 15-18 months, suggests that *App*^{NLGFs} exhibit progressive disinhibition. This aligns with the idea that repeated testing can shift the nature of the aversive response from unconditioned fear to learned avoidance, influencing how different genotypes respond to the EPM. In the single trial used in this thesis, *App*^{NLGFs} consistently entered the open arms significantly more times than C57BL6/Js, suggesting not only a preference for exploring these zones, but also a heightened motivation to repeatedly enter them, supporting a disinhibitory phenotype. However, future work should develop on the work in this thesis by performing a test/retest EPM protocol on *App*^{NLGFs} at a broad range of ages, which could provide a deeper insight into the specific effects of aging on the underlying psychological processes influencing their behaviour during this task.

The dichotomy between the seemingly early anxiolytic phenotype observed in the EPM test and the late-emerging anxiogenic phenotype in the OF test is an intriguing, though not an entirely novel finding. This phenomenon has also been reported in Tg2576 mice, who exhibited increased thigmotaxis during OF testing yet a heightened preference for open arms in the EPM (Lalonde et al., 2003). A similar pattern has also been observed in *App*^{NLGFs} at 8 months of age (Pervolaraki et al., 2019). The fact that this behavioural profile is present in both transgenic and *App*^{NLGFs} suggests it is unlikely to be a result of overexpression-related artefacts, but more likely reflects the impact of amyloid or other related pathologies such as neuroinflammation. Supporting this, mouse models of traumatic brain injury also exhibit increased open arm exploration in the EPM along with reactive gliosis (Logsdon et al., 2017; Mannix et al., 2014; Mouzon et al., 2018). Notably, both *App*^{NLGFs} and Tg2576 mice also exhibit neuroinflammation such as reactive gliosis (Benzing et al., 1999; Saito et al., 2014), suggesting that neuroinflammatory processes may contribute to the anxiolytic-like behaviour in the EPM test.

The opposing behaviours during OF and EPM testing reinforces the idea of increased open arm exploration reflecting a disinhibitory phenotype rather than a true anxiolytic response. This behaviour has previously been attributed to disruptions in the mechanisms underlying decision making, suggesting that *App*^{NLGFs} fail to inhibit the decision to enter the open, more dangerous arm of the maze during EPM testing (Gil-Bea et al., 2007; Migliaccio et al., 2020; Pervolaraki et al., 2019). Consistent with this idea, *App*^{NLGF} mice have previously demonstrated alterations in glutamatergic gene expression and NMDA-dependent gamma oscillations in the PFC, an area associated with risk assessment and decision making, potentially explaining why *App*^{NLGF} animals decide to enter the open arms of the EPM more than C57BL6/Js (Dias et al., 1996; Pervolaraki et al., 2019). Biochemical changes to the PFC may reflect degeneration observed in early AD pathology (Jobson et al., 2021). These alterations, however, were absent in the amygdala, an area of the

brain involved in the mediation of fear and anxiety (Davis et al., 1994; Pervolaraki et al., 2019). The lack of such changes in the amygdala supports the hypothesis that the changes observed in these animals during EPM testing are not truly anxiolytic, but a more complex behaviour such as disinhibition. However, it has been argued that seemingly anxiolytic behaviour should co-occur with hyperactivity to conclude the behaviour of disinhibition (Gil-Bea et al., 2007). This has previously been observed in the Tg2576 model, who showed preference for the open arms alongside hyperactivity during the EPM task (Gil-Bea et al., 2007; Lalonde, 2002; Lalonde et al., 2003; Ognibene et al., 2005). In this thesis, overall levels of activity were largely comparable between *App*^{NLGF} and C57BL6/J animals, with the exception of a significant increase in the mean distance travelled by *App*^{NLGFs} at 12-14 months compared to C57BL6/Js. Previous studies using the EPM test have also not reported substantial hyperactivity in *App*^{NLGF} animals (Latif-Hernandez et al., 2019; Pervolaraki et al., 2019; Sakakibara et al., 2018). Therefore, it could be suggested that *App*^{NLGF} animals exhibit reduced anxiety with some disinhibitory tendencies. Other distinct or complementary explanations may include heightened curiosity or increased novelty-seeking behaviour, as suggested during the ON test in this thesis, where *App*^{NLGFs} spent significantly more time exploring the novel object compared to C57BL6/Js.

Additionally, the increased open arm exploration observed during EPM testing may reflect diminished perception of threat or impaired ability to appropriately respond to threat. Previous studies have reported deficits in trace and contextual fear conditioning in *App*^{NLGF} mice, indicative of altered fear learning and memory processes (Maezono et al., 2020; Mehla et al., 2022; Mehla et al., 2019). These tasks rely heavily on hippocampal-dependent learning and memory, as well as contributions from the amygdala and PFC (Sharma et al., 2018; Tovote et al., 2015). It has been hypothesised that these neural networks control fear and anxiety-like responses by constraining such behaviours to contexts or cues that are predictive of aversive events (Bannerman et al., 2004; Mehla et al., 2022). Indeed, cytotoxic lesions of the ventral HPC have produced anxiolytic-like behaviour in rats across unconditioned tests of anxiety, including both the standard and modified versions of the EPM test (Bertagna et al., 2021; Kjelstrup et al., 2002; McHugh et al., 2004). Therefore, although the EPM doesn't involve an explicitly learned aversive association, the increased open arm exploration in *App*^{NLGFs} may reflect a failure of these systems to appropriately regulate avoidance of the aversive (open) arms, which may typically prevent frequent re-entry into these arms in normal mice. According to Gray and McNaughton's model, the HPC detects conflicts between competing goals, such as the drive to explore open arms versus the fear of open spaces (Fowles, 2024; Gray, 1982). It triggers the Behavioural Inhibition System, a network including the septo-hippocampal system and amygdala, to temporarily suppress behaviour and heighten attention to environmental stimuli in order to resolve the conflict (Good & Bannerman, 2025; Gray, 1982). Thus, hippocampal dysfunction, as suggested by increased open arm exploration in *App*^{NLGFs}, may reflect impaired response to the conflicting environment and reduced behavioural

inhibition under anxiety-provoking conditions. This interpretation is consistent with the subtle deficits observed in hippocampal-dependent OL and spontaneous alternation tasks in this thesis, suggesting that a broad hippocampal deficit that at least partially underlies both cognitive and affective phenotypes observed in this model.

In AD patients, disinhibition often manifests as impulsive or socially unacceptable behaviour (Gil-Bea et al., 2007; Migliaccio et al., 2020; Rochat et al., 2013). Likewise, the behaviour of *App*^{NLGFs} during EPM testing may reflect increased impulsivity. Masuda et al., (2016) reported increased impulsivity in *App*^{NLGF} mice, evidenced by an increased number of premature responses during a serial reaction time task in which mice were trained to withhold nose-pokes into reward ports during a delay period before responding to a stimulus to receive a reward (Masuda et al., 2016). This suggests that deficits in inhibitory control in the *App*^{NLGF} model may extend beyond increased open arm exploration observed in the EPM test. Supporting this, *App*^{NLGF} mice exhibit alterations in dopaminergic, serotonergic, and noradrenergic systems, dysfunctions of which have previously been linked to impulsivity in both humans and animals (Dalley & Roiser, 2012; Economidou et al., 2012). For example, *App*^{NLGF} animals at 10 months exhibited a reduction in dopamine and serotonin in the CA1 region of the HPC compared to C57BL6/J controls at the same age (Wang et al., 2018). Levels of these hormones were increased by administration of SAK3, a T-type Ca^{2+} channel enhancer, suggesting a role of Ca^{2+} dysregulation underlying these alterations (Wang et al., 2018). Furthermore, *App*^{NLGF} mice exhibited reduced cholinergic and noradrenergic neurons from 6 and 9 months, respectively (Mehla et al., 2019). Strikingly, a mouse model in which serotonergic dysfunction was induced via localised inflammation to the raphe nucleus also demonstrated increased open arm exploration in an EPM test (Howerton et al., 2014). This suggests that in the *App*^{NLGF} model, amyloid may be disrupting neuromodulatory pathways, potentially impairing threat detection and resulting in heightened impulsivity or disinhibitory-like behaviour during the EPM test.

In this thesis, additional measures of anxiety-like behaviour were assessed during the EPM test through the analysis of ethological behaviours, including the extending of the head and neck over the edge of the open arms (“head dipping”) and the stretch attend posture (“stretching”). Including these behaviours in the analysis of behaviour during the EPM task provides a more nuanced assessment of anxiety-like behaviour, reflecting decision-making and risk-assessment behaviours that are less affected by potential confounds of activity differences than measurements of open and closed arm preference (Tucker & McCabe, 2021). Stretching and head dipping have been described as risk assessment behaviours that are commonly associated with enhanced anxiety during the EPM test (Cole & Rodgers, 1994; File & Wardill, 1975; Rodgers, 1999; Rodgers, Perrault, & Sanger, 1997; Setem et al., 1999; Walf & Frye, 2007). During EPM testing, *App*^{NLGFs} spent significantly more time head dipping but significantly less time in the stretch attend posture compared to

C57BL6/J animals. Both behaviours were similarly affected by age in both C57BL6/J and *App*^{NLGF} animals, with time spent in each position decreasing as the animals aged. Interestingly, Tg2576 animals also exhibited an increase in head dipping but decrease in stretch attend postures at 7-12 months compared to C57BL6/J controls (Ognibene et al., 2005). Given that these behaviours are considered indicators of risk assessment, the contrasting pattern of increased head dipping alongside decreased stretch attend postures is particularly intriguing. It could therefore be argued that these ethological behaviours capture distinct aspects of risk-assessment that do not directly correlate with increased anxiety. For example, head dipping over the open arms of the EPM may reflect exploratory curiosity whereas stretch attend postures may be linked to caution and hesitation during exploration of the EPM (Fernández Espejo, 1997; Hoshino et al., 2004). Based on this distinction, *App*^{NLGF} mice appeared to be more curious than C57BL6/J mice, further suggesting an increased propensity for novelty, and less cautious than C57BL6/J mice, suggesting they were less inhibited by potential threats. However, the observed increase in head dipping behaviour in *App*^{NLGF} animals may be partially confounded by the increase in duration spent in the open arms of the maze, naturally enabling more opportunity to engage in head dipping over these open arms. Nevertheless, this pattern may still support a disinhibitory phenotype, as greater open arm exploration itself may also suggest a diminished ability to assess and appropriately respond to risk.

It may be argued that further experiments are required to better understand anxiety-like behaviour in the *App*^{NLGF} model. The use of the OF and EPM tests have been contested as unequivocal tests of anxiety due to their several pitfalls (Ennaceur & Chazot, 2016). Importantly, the OF and EPM tests were validated as tests of anxiety based on observations that treatment with benzodiazepines increased exploration of the central zone or open arms of the maze (Griebel & Holmes, 2013; Handley & Mithani, 1984; Lister, 1987; Pellow et al., 1985; Prut & Belzung, 2003). However, Ennaceur and Chazot argue that this validation is flawed since it assumes that behavioural changes induced by these drugs directly reflect reduced anxiety, but they also have broader effects such as sedation, fear reduction, and memory impairments, which can influence behaviour independent of anxiety (Ennaceur & Chazot, 2016). Additionally, there is no direct evidence supporting the theory that these tests present a conflict between the motivation to explore and the drive to avoid perceived danger. Ennaceur and Chazot argue that these tests over-rely on the natural preference of enclosed spaces, which does not necessarily indicate an anxious state, but may just reflect the secure nature of these areas as preferable to risk taking (Ennaceur & Chazot, 2016). In contrast, situations in which escape is not possible may be more likely to induce a true anxiety-like response (Zvolensky et al., 2000). Therefore, as an alternative or complementary approach, the 3D maze was suggested (Ennaceur & Chazot, 2016). This maze is a modification of the RAM, with 8 open arms connected to a central platform by upward angled bridges (Mostafa et al., 2002). The bridges limit visibility, offering a more ambiguous escape context. In this test, a reduction in anxiety is indicated by an increase in bridge entries (Ennaceur & Chazot, 2016). Therefore, performing this test in the *App*^{NLGF} mouse

model may help clarify the true extent of anxiety-like behaviour independent of the animals' natural preference for enclosed spaces, and determine whether the disinhibitory-like behaviour observed in the EPM test persists in a scenario where shelter and escape options are less predictable.

To summarise, whilst the EPM results suggest early and consistent anxiolytic behaviour, potentially reflecting disinhibitory tendencies, findings from OF testing indicate that anxiety is likely present in the model, as hypothesised, but emerges only at a very advanced age. This contrasts with the behaviour commonly observed in AD patients, who often suffer with anxiety during MCI or early stages of AD, whereas disinhibitory tendencies emerge in later stages of the disease (Lanctôt et al., 2017). This challenges the validity of the *App*^{NLGF} model in accurately reflecting AD processes; could the early symptom of anxiety in AD result from pathological mechanisms that the *App*^{NLGF} model does not exhibit, such as neuron loss and tau accumulation? This key limitation of the *App*^{NLGF} model will be explored in the General Discussion of this thesis. Supporting this notion, transgenic mice expressing mutant tau genes (e.g., rTg4510 and TAU58/2 mice) exhibit similar behavioural patterns, with seemingly early anxiolytic behaviour in the EPM task but anxiogenic behaviour in the OF task (Cook et al., 2014; Przybyla et al., 2016). Data from these animals, which exhibit tau accumulation but do not develop Aβ plaques, suggest that the similar behavioural patterns observed in *App*^{NLGF} animals may not be Aβ-dependent or an exclusive effect of Aβ-pathology. This could explain why the anxiolytic-like behaviour observed during the EPM test in this thesis does not worsen significantly with age, despite theoretical progressive Aβ deposition. Similarly, the subtlety of deficits observed in the OL test and the late onset of spontaneous alternation deficits suggest that amyloid accumulation alone in insufficient to drive widespread behavioural impairments. Cortical amyloid deposition was confirmed in the 22–23-month-old *App*^{NLGFs} in this study (Fig. 3.3), and previous reports have shown that such deposition begins at around 2 months and becomes saturated by 7 months (Saito et al., 2014). Therefore, the delayed onset of behavioural changes in the *App*^{NLGF} model may instead reflect downstream factors such as neuroinflammation, synaptic dysfunction, and network alterations that emerge with age.

Chapter 4: Neuronal Activity in the *App*^{NLGF} Mouse Model

4.1 Chapter Overview

The term 'neuronal activity' describes chemical and electrical changes in the brain that allow neurons to communicate and respond to stimuli. Neuronal Ca^{2+} and c-Fos are two integral components of neuronal activation that are commonly disrupted in AD and mouse models of AD (Babaei et al., 2025; Corbett et al., 2017; Joshi et al., 2023; Lu et al., 1998). This chapter will therefore exist as two subchapters to address each measure of neuronal activity in the *App*^{NLGF} mouse model.

Firstly, this chapter will explore the role of Ca^{2+} in physiological neuronal function and examine its dysregulation in AD, as outlined by the Calcium Hypothesis of AD. This hypothesis was first postulated by Khachaturian and colleagues in the 1980s, after experiments from the Landfield group evidenced prolonged Ca^{2+} currents in hippocampal slices from aged rats (Khachaturian, 1987, 1989; Landfield, 1987; Landfield & Pitler, 1984). Since then, disruption of neuronal Ca^{2+} homeostasis has been evidenced in normal aging and, to a more severe extent, in AD patients (Bezprozvanny, 2009; Toescu & Verkhratsky, 2007). Over the recent decades, accumulating evidence has linked Ca^{2+} dyshomeostasis with AD pathogenesis, with increased emphasis placed upon the theory as an enhancement of the Amyloid Cascade Hypothesis (Joshi et al., 2023). However, very little is known about neuronal Ca^{2+} function in 2nd generation AD models such as the *App*^{NLGF} model, particularly in extrahippocampal regions such as the retrosplenial cortex (RSC). Experiment 1 of this chapter therefore assessed the role of the RSC in normal brain function and its disruption in AD. It details the process of *in vivo* two-photon imaging with Ca^{2+} indicators to capture Ca^{2+} dynamics in the RSC of awake *App*^{NLGF} mice. Additionally, it presents a novel data analysis protocol to examine resting and stimulus-induced Ca^{2+} activity in this model. This experiment focused on the 22–23-month-old *App*^{NLGF} group, as the strongest behavioural phenotype manifested at this age (Chapter 3). Therefore, if Aβ disrupts neuronal Ca^{2+} signalling, alterations in neuronal Ca^{2+} dynamics in this experiment were expected in this experiment. Indeed, *App*^{NLGF} animals at 22-23 months exhibited significantly reduced Ca^{2+} levels and altered Ca^{2+} peaks in response to visual stimuli, despite exhibiting marginally increased resting Ca^{2+} levels compared to age-matched C57BL6/J controls.

Unfortunately, due to an unexpected failure of the two-photon imaging equipment, subsequent younger groups of animals were not tested. Therefore, to provide an alternative indirect assessment of Ca^{2+}-related signalling, experience-induced *c-fos* expression was assessed in mid-aged *App*^{NLGFs}. *c-fos* is an immediate early gene (IEG) that is widely used as a marker of neuronal activity linked to synaptic plasticity and learning (Lara Aparicio et al., 2022). Expression of *c-fos* is stimulated by increases in intracellular Ca^{2+} concentration ($[Ca^{2+}]_i$) during action potentials (Lara Aparicio et al., 2022; Minatohara et al., 2015). *c-fos* expression is irregular in rodent models of AD, with both increased and reduced expression observed (Chin et al.,

2005; España et al., 2010; L'Esperance et al., 2024; Palop et al., 2005; Palop et al., 2003; Poirier et al., 2011; Tan et al., 2023). The variability appears to be linked to levels of amyloid peptides present rather than the extent of plaque deposition (Palop et al., 2005; Palop et al., 2003). A recent study has evidenced increased c-Fos levels in the pre-plaque *App*^{NLGF} CA1 following a test of episodic-like memory (Tan et al., 2023). However, there remains very limited data regarding the integrity of *c-fos* expression in the *App*^{NLGF} model. Experiment 2 of this chapter therefore assessed *c-fos* expression in the *App*^{NLGF} model at 14-16 months, with focus on the RSC and CA1. The results here indicated no significant changes in baseline and experience-induced *c-fos* expression in the RSC of *App*^{NLGF} mice compared to C57BL6/J controls. However, a reduction in overall *c-fos* expression in the HPC was observed, indicating region-specific alterations in neuronal activity patterns in the *App*^{NLGF} model.

4.2 Experiment 1: Calcium Imaging of the Retrosplenial Cortex

4.2.1 Introduction

4.2.1.1 The Role of Calcium in Neuronal Physiology

Ca^{2+} is a ubiquitous second messenger molecule and its signalling is involved in a range of physiological pathways throughout the body, including cell proliferation, differentiation, survival, and apoptosis (Berridge et al., 2000). In the brain, Ca^{2+} fluctuations control neurotransmitter release, synaptic plasticity, gene expression, and other key neuronal functions (Berridge, 1998; Cascella & Cecchi, 2021; Lynch & Seubert, 1989; Mattson et al., 2000).

At resting state, intracellular calcium concentration ($[Ca^{2+}]_i$) is maintained at approximately 100nM, whereas the extracellular space has a substantially higher concentration at around 1-2mM (Cascella & Cecchi, 2021). Upon neuronal stimulation, $[Ca^{2+}]_i$ can increase to around 1-3μM (Cascella & Cecchi, 2021). To facilitate this change in concentration, Ca^{2+} crosses the plasma membrane through a range of Ca^{2+} channels, receptors, pumps, and transporters such as VGCCs, store operated Ca^{2+} channels (SOCCs), NMDARs, α-amino-3-hydroxy-5-methyl-4-isoxazolepropionic acid receptors (AMPARs), transient receptor potential canonical (TRPC), Na^{+}/Ca^{2+} exchangers (NCX), and plasma membrane ATPases (PMCA) (Joshi et al., 2023). To aid cellular equilibrium, Ca^{2+} can be sequestered by and released from internal stores such as the ER via inositol 1,4,5-trisphosphate receptors (IP_3Rs) or ryanodine receptors (RyRs) (Santulli et al., 2017). Fine intracellular Ca^{2+} homeostasis is also aided by sensors and buffers that detect and stabilise changes in $[Ca^{2+}]_i$, along with NCX and PMCA, to restore physiological

levels of Ca^{2+} (Schwaller, 2010). In the cell, Ca^{2+} employs several downstream protein targets such as transcription factors, kinases, and phosphatases to carry out key cellular functions (Brini et al., 2014; Cascella & Cecchi, 2021; Pchitskaya et al., 2018).

Mitochondria are also essential for maintaining cellular Ca^{2+} homeostasis by regulating uptake and release mechanisms (Joshi et al., 2023). Following cell stimulation, excess intracellular Ca^{2+} is taken up by the mitochondria, primarily through voltage dependent anion channels (VDAC) or mitochondrial Ca^{2+} uniporters (MCU) (Gincel et al., 2001; Kirichok et al., 2004). Uptake of Ca^{2+} into the mitochondrial matrix stimulates mitochondrial dehydrogenases to enhance hydrogen extrusion, stimulating ATP production (Hajnóczky et al., 2006). However, with increased Ca^{2+} uptake, mitochondria initiate programmed cell death through opening of the mitochondrial permeability transition pore (mPTP) (Basso et al., 2005; Zoeteweij et al., 1992). This results in the release of pro-apoptotic factors such as cytochrome c from the mitochondrial intermembrane space to the cytoplasm, triggering apoptosome formation, caspase activation, and eventually cell death (Tait & Green, 2013). Physiologically, controlled cell death is essential for the generation of functional neuronal circuitry during development, and throughout life it is critical for removing damaged, infected, or old cells (Buss et al., 2006).

4.2.1.1.1 Calcium and Synaptic Plasticity

In the brain, Ca^{2+} signalling underpins the frameworks of LTP and LTD (Bliss & Collingridge, 1993). LTP and LTD are two major forms of synaptic plasticity that facilitate memory storage and formation (Bliss et al., 2014). The phenomena of LTP and LTD have been extensively studied in CA1 area of the HPC but are also applied elsewhere in the brain. LTP and LTD are mediated by Ca^{2+} signalling through glutamate-gated NMDARs and AMPARs, and both processes can occur in the same synapse in response to different patterns and strengths of NMDAR and AMPAR activation (Arias-Cavieres et al., 2018; Citri & Malenka, 2008; Del Prete et al., 2014; Hunt & Castillo, 2012; Joshi et al., 2023; Malenka, 1994). NMDARs are formed by an assembly of variable subunits (GluN1, GluN2A-D, GluN3A-B) and are permeable to sodium (Na^+), potassium (K^+), and Ca^{2+} (Hansen et al., 2018). AMPARs are comprised of different combinations of subunits (GluA1, GluA2, GluA3, and GluA4), and only AMPARs lacking the GluA2 subunit are permeable to Ca^{2+} ions (Henley & Wilkinson, 2013; Lee, 2006; Lüscher & Malenka, 2012).

LTP and LTD are initiated by Ca^{2+} pulses with specific location, duration, and amplitudes for each function (Yang et al., 1999). Depending on the quantitative characteristic of Ca^{2+} signals, AMPARs are either inserted or removed from the synaptic membrane, triggering either LTP, or LTD, respectively (Bliss et al., 2014). LTP is typically initiated by high-frequency stimulation that triggers the release of

neurotransmitters, such as glutamate, into the synaptic cleft (Bliss & Collingridge, 1993). Subsequently, glutamate binds to and opens AMPARs, through which Na^+ enters the neuron, triggering depolarisation of the postsynaptic membrane (Lüscher & Malenka, 2012). Under resting conditions, NMDARs are blocked by Mg^{2+}, however, following sufficient membrane depolarisation, the Mg^{2+} is removed from NMDAR channels, allowing Ca^{2+} entry into the cell (Park et al., 2014). Intracellular Ca^{2+} binds Ca^{2+} sensor calmodulin (CaM), which then activates Ca^{2+}/CaM-dependent protein kinase II (CaMKII) by disrupting the association between the catalytic and inhibitory subunits (Lisman et al., 2002; Lisman et al., 2012). Activation of CaMKII promotes the trafficking and insertion of AMPARs into the synaptic membrane, leading to strengthening of synaptic transmission by promoting the post-synaptic response to glutamate (Citri & Malenka, 2008; Hidalgo & Arias-Cavieres, 2016; Joshi et al., 2023; Lüscher & Malenka, 2012). In contrast, LTD is typically induced by low-frequency synaptic stimulation, leading to prolonged moderate intracellular Ca^{2+} elevation in the postsynaptic neuron (Yang et al., 1999). This moderate Ca^{2+} influx leads to the preferential activation of phosphatases such as calcineurin (CaN), which has a higher affinity for Ca^{2+} than the Ca^{2+}/CaMKII complex (Joshi et al., 2023; Lee, 2006; Lüscher & Malenka, 2012). CaN activation promotes the dephosphorylation and endocytosis of membrane bound AMPARs, resulting in a reduced postsynaptic response to glutamate and thus a reduced ability respond to glutamate release (Citri & Malenka, 2008; Hidalgo & Arias-Cavieres, 2016; Lee, 2006; Lisman et al., 2012; Lüscher & Malenka, 2012).

Over time, LTP and LTD can induce structural changes in synaptic connections (Ramiro-Cortés et al., 2014). For instance, increased AMPAR expression strengthens dendritic spines and reinforces certain synaptic connections, which is key in the encoding and storage of memories (Matsuzaki et al., 2004; Park, 2018). AMPAR internalisation in LTD, however, causes the shrinkage of dendritic spines, which can lead to long-lasting reductions in the integrity of neuronal circuits (Hanley, 2008; Pikor et al., 2024; Shinoda et al., 2010). Physiologically, LTD weakens redundant synaptic connections to support the flexible remodelling of memory circuits (Chidambaram et al., 2019; Wiegert & Oertner, 2013). Therefore, a homeostatic balance between LTP and LTD is required to support healthy memory systems (Bliss et al., 2014).

4.2.1.2 The Calcium Hypothesis of Alzheimer's Disease

The Calcium Hypothesis of AD proposes that Aβ-induced Ca^{2+} dyshomeostasis disrupts neuronal function via a series of mechanisms that will be discussed below (Fig. 4.1) (Joshi et al., 2023). Supporting this theory, experiments conducted in cultured neurons evidenced that oligomeric Aβ directly causes Ca^{2+} mediated toxicity (Demuro et al., 2005). Furthermore, multiple lines of evidence suggest that the progressive accumulation of Aβ in AD similarly leads to toxic Ca^{2+} overload (Berridge, 2010; Bezprozvanny & Mattson, 2008; Kuchibhotla et al., 2008; Sanz-

Blasco et al., 2008; Shirwany et al., 2007). Data from *in vitro* models and mouse models of AD have evidenced that Aβ-induced chronic Ca^{2+} elevation in AD favours LTD-promoting pathways, enhancing LTD and reducing LTP (Koffie et al., 2011; Li et al., 2011; Liebscher et al., 2014; Shankar et al., 2008). There is limited data regarding synaptic plasticity processes in the *App*^{NLGF} mouse model, however, it appears to exhibit LTP impairment in the HPC at 6-8 months old (Latif-Hernandez et al., 2020; Moriguchi et al., 2018), and at 3-4 months old in the PFC (Latif-Hernandez et al., 2020). Although disruption of LTP and LTD has not been directly proven in AD patients, studies in transgenic AD models suggest that impairment of synaptic function is an early event in hippocampal-dependent memory disruption, preceding plaque formation and neuronal cell death (Ferreira & Klein, 2011; Ferreira et al., 2015; Koffie et al., 2011; Selkoe, 2002; Tanzi, 2005). Therefore, it is hypothesised that enhancement of LTD results in the excessive weakening of synaptic connections, which gradually disrupts neural connections involved in forming and retaining memories, compromising the structural integrity of the brain and contributing to cognitive decline (Pozueta et al., 2013).

As discussed above, dysregulation of synaptic plasticity processes in AD appears to be mediated by neuronal Ca^{2+} overload. This can occur through i) enhancing Ca^{2+} influx from the extracellular space and ii) stimulation of Ca^{2+} release from internal stores (Berridge, 2010; Laurén et al., 2009). One possible mechanism through which Aβ enhances Ca^{2+} influx is through Aβ itself forming Ca^{2+} permeable pores in the plasma membrane, allowing extracellular Ca^{2+} to flood into the cell (Arispe et al., 2007; Arispe et al., 1993). Interestingly, oligomeric forms of Aβ share structural and functional homology with pore-forming bacterial toxin proteins alpha-haemolysin and perforin, corroborating the idea of Aβ as a likely plasma membrane channel through which Ca^{2+} passes (Yoshiike et al., 2007). Moreover, there is a linear correlation between the amount of oligomeric Aβ species bound to the neuronal cell membrane and the rate of Ca^{2+} influx, further suggesting a direct role of Aβ in neuronal Ca^{2+} overload (Evangelisti et al., 2016). Additionally, there is evidence that following progressive Aβ accumulation in early AD pathogenesis, Aβ oligomers directly bind and modulate NMDARs, facilitating cellular Ca^{2+} entry (De Felice et al., 2007; Ferreira et al., 2012; Hardingham & Bading, 2010; Parameshwaran et al., 2008; Texidó et al., 2011; Zhang et al., 2016). It is also posited that Aβ oligomers enhance cellular Ca^{2+} entry by interacting with Ca^{2+} impermeable AMPARs, rendering them permeable to Ca^{2+} and resulting in cytotoxic Ca^{2+} overload (Zhao et al., 2010). Aβ oligomers can also block physiological glutamate reuptake following synaptic transmission, resulting in excessive glutamate accumulation, overactivation of other localised NMDARs and AMPARs, and subsequent neuronal hyperactivity (Alberdi et al., 2010; Busche et al., 2012; Busche et al., 2008; Harkany et al., 2000; Joshi et al., 2023; Koffie et al., 2011; Li et al., 2011; Mattson et al., 1992; Parameshwaran et al., 2008; Wang et al., 2017; Zott et al., 2019). In an excitotoxic cycle, NMDAR overactivation stimulates amyloidogenic *APP* processing by inhibiting α-secretase and enhancing β-secretase activity (Lesné et al., 2005). Enhanced $[Ca^{2+}]_i$ also induces the phosphorylation of APP and tau, triggering further plaque and tangle

formation and subsequent neurodegeneration observed in AD (Berridge, 2010; Itkin et al., 2011; Pierrot et al., 2004; Pierrot et al., 2006; Querfurth & Selkoe, 1994).

A further mechanism through which Ca^{2+} enters the cell during AD pathogenesis may be via cellular prion proteins (PrP^c) (Joshi et al., 2023). PrP^c are receptors anchored to the outer surface of the cell, with high affinity for oligomeric Aβ (Purro et al., 2018). It is argued that, upon PrP^c binding of Aβ, a Fyn-mediated signalling cascade disrupts Ca^{2+} channels such as NMDARs, altering membrane permeability and eliciting Ca^{2+} influx (Um et al., 2012; Zhang et al., 2019). However, evidence for the role of PrP^c in AD pathogenesis remains controversial. Intracerebroventricular administration of an antibody that binds the putative Aβ binding site on PrP^c prevents LTP inhibition in Wistar rats administered with soluble Aβ extracted from AD brains (Barry et al., 2011). Conversely, hippocampal slices from $PrP^{c-/-}$ mice show LTP depression following treatment with Aβ precursor APPct100 (Balducci et al., 2010; Kessels et al., 2010), suggesting PrP^c may not be necessary to facilitate Ca^{2+} entry or that Ca^{2+} entry alone is not necessary or sufficient to induce LTP depression.

In addition to enhanced neuronal Ca^{2+} influx, there is also evidence that Aβ oligomers trigger Ca^{2+} release from internal stores by interacting with IP_3Rs and RyRs on the ER (Ferreiro et al., 2004; Supnet et al., 2006). Furthermore, AICD, the bi-product of amyloidogenic APP processing, is transcriptionally active and alters the expression of RyRs and Ca^{2+} buffer calbindin, enhancing Ca^{2+} release from the ER and dampening Ca^{2+} sequestering pathways (Leissring et al., 2002; Smith et al., 2005; Stutzmann et al., 2006). As mentioned with reference to cellular physiology, enhanced mitochondrial Ca^{2+} uptake triggers mPTP mediated cell death (Joshi et al., 2023). In conditions of Ca^{2+} overload associated with Aβ, excessive Ca^{2+} influx into the mitochondria occurs both directly via the MCU and through Aβ -mediated ER-mitochondria coupling, facilitating direct Ca^{2+} transfer (Calvo-Rodriguez et al., 2019; Garcia-Casas et al., 2023). This results in aberrant mPTP opening, triggering mitochondrial swelling (Joshi et al., 2023). This structural change of the mitochondria compromises the integrity of the inner mitochondrial membrane and reduces the efficiency of the associated electron transport chain (ETC), responsible for ATP synthesis (Berridge, 2010; Spät et al., 2008; Wang et al., 2017). Furthermore, Aβ can directly bind complexes of the ETC, further disrupting ATP formation (Spuch et al., 2012). Disruption of ATP synthesis mechanisms enhances the production of ROS, such as hydrogen peroxide and hydroxyl radicals, as byproducts of cellular metabolism (Joshi et al., 2023). Under physiological conditions, cellular antioxidant systems neutralise ROS, however, excessive ROS formation overwhelm these defences, leading to a state of oxidative stress in which DNA, proteins, and lipids are damaged (Cheignon et al., 2018). ROS formation during Aβ oligomerisation can also depolarise the cell membrane and activate VGCCs, providing an additional route of entry for Ca^{2+} into the cytoplasm (Bezprozvanny & Mattson, 2008; Mark et al., 1997; Nimmrich et al., 2008; Ueda et al., 1997). Overall, Ca^{2+}-mediated mitochondrial dysfunction results in a feedback loop that further worsens mitochondrial function,

exacerbates oxidative stress, and triggers an inflammatory response (Yu & Luo, 2024). ER and mitochondrial stress induced by cellular Ca^{2+} overload can induce cell death pathways. For example, Ca^{2+} imbalance of the ER can lead to the misfolding of proteins, triggering the unfolded protein response, which activates pro-apoptotic pathways (Ajoolabady et al., 2022). Furthermore, disruption of ATP production in the mitochondria can lead to the release of pro-apoptotic factors such as cytochrome c, which activates the caspase cascade and stimulates apoptosis (Joshi et al., 2023; Pacher & Hajnóczky, 2001). Excessive caspase activation and apoptosome formation depletes the cell of ATP, triggering necrotic cell death (Nicotera et al., 1998). Moreover, conditions of enhanced $[Ca^{2+}]_i$ can also lead to the activation of Ca^{2+}-dependent proteases which can inhibit transmembrane proteins such as PMCA, leading to structural degradation of the cell and subsequent necrosis (Bano & Ankarcrona, 2018). Excessive apoptosis and necrosis have been observed in AD, underpinning the progressive neurodegeneration and characteristic cognitive decline of the disease (Goel et al., 2022).

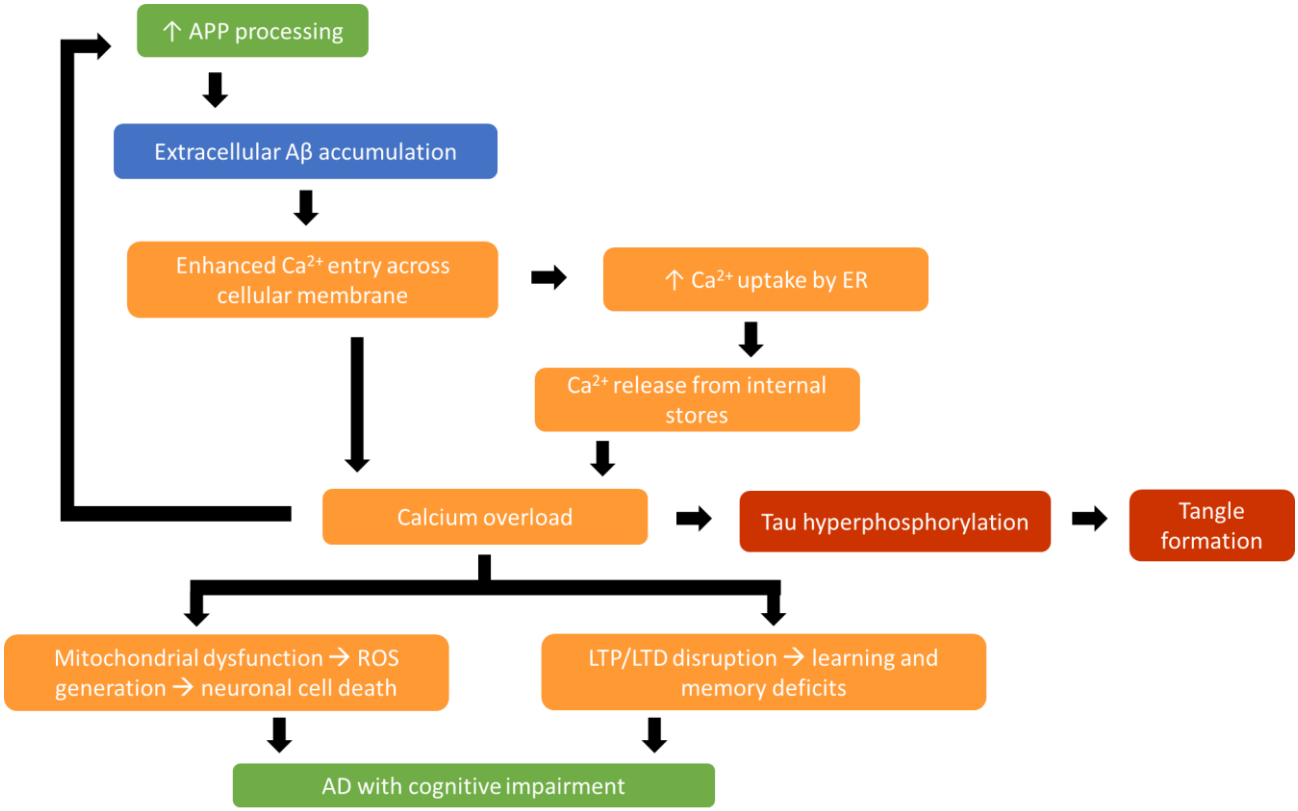

Figure 4.1: The Calcium Hypothesis of Alzheimer's Disease. Key pathological processes involved in the Calcium Hypothesis of Alzheimer's Disease, as recently reviewed in Joshi et al., (2023).

Together with the disruption of synaptic plasticity discussed earlier, the Ca^{2+} hypothesis of AD argues that neuronal Ca^{2+} remodelling leads to AD and cognitive impairment (Joshi et al., 2023). This hypothesis may explain why AD is a progressive disease; the gradual deposition of Aβ disrupts memory processes and eventually leads to cell death. This can also explain why memory loss symptoms often appear before any evidence of cell death and could highlight a potential pharmacological target to slow or stop the progression of AD.

The positive feedback mechanism between Ca^{2+} and Aβ presents the key question of which process is the first to be dysregulated and thus which should be preferentially targeted. Several lines of evidence from FAD mutations points towards Ca^{2+} as a proximal cause of AD. A paper from over 20 years ago shows that individuals possessing *PSEN* mutations with FAD history show perturbation in IP_3-mediated Ca^{2+} responses prior to clinical presentation of AD (Etcheberrigaray et al., 1998), suggesting that Ca^{2+} dysregulation could occur before Aβ and tau aggregation. Moreover, animal and cell studies of FAD mutations in *PSEN1* and *PSEN2* show enhanced Ca^{2+} release from the ER via suggested interaction of presenilins with IP_3Rs (Cai et al., 2006; Cheung et al., 2010; Green et al., 2008; Mattson, 2010). *PSEN1* and *PSEN2* mutations may also enhance expression and recruitment of RyRs, increasing RyR-mediated Ca^{2+} release from the ER (Chan et

al., 2000; Del Prete et al., 2014; Paula-Lima et al., 2011; Stutzmann et al., 2006). Interestingly, presenilins themselves can function as ER 'leak' channels; cation-permeable channels in the lipid bilayer of the ER responsible for facilitating passive Ca^{2+} movement from the ER (Joshi et al., 2023; Tu et al., 2006). Many *PSEN* mutations present in FAD impair the function of this leak channel, leading to ER Ca^{2+} accumulation (Bezprozvanny & Mattson, 2008; Tu et al., 2006). Therefore, it could be argued that Ca^{2+} dysregulation may be the proximal cause of AD and as such should be explored further and targeted by new experimental drugs.

4.2.1.2.1 Neuronal Calcium Imaging of Mouse Models of AD

The effects of mutant *APP* on neuronal Ca^{2+} dynamics in mouse models of AD remain relatively unexplored. In particular, very little is known about neuronal Ca^{2+} dynamics of 2nd generation models such as the App^{NLGF} model, as most research to date has concentrated on transgenic models of AD, leaving a gap in understanding how Ca^{2+} signalling pathways are influenced in newer models without overexpression-related artefacts.

A study by Busche et al., (2008) performed *in vivo* two-photon imaging on 6-10-month-old APP23xPS45 mice, a transgenic model that overexpress both *APP* and mutant *PSEN1* under the control of Thy-1 promoter. By simultaneously loading Ca^{2+} indicator Oregon Green 488 BAPTA-1 AM (OGB-1) and fluorescent Aβ label thioflavin S, an overall decrease in neuronal activity in 29% cortical neurons of layer 2/3 was observed, however, an increase in the frequency of Ca^{2+} transients exclusively in neurons within 60µm of plaque borders was also present (Busche et al., 2008). In the same year, Kuchibhotla et al., (2008) assessed cortical Ca^{2+} dynamics in 5–6-month-old Tg2576 and APP/PS1 mice using multiphoton imaging, a related technique to two-photon imaging. With application of the genetically encoded Ca^{2+} indicator yellow cameleon 3.6 (YC3.6), hyperactive neurons in close proximity to Aβ plaques in both models were observed, corroborating previous findings (Kuchibhotla et al., 2008). However, resting Ca^{2+} levels in young Tg2576 and APP/PS1 mice (with no cortical plaques) were unaffected compared to age-matched non-transgenic controls (Kuchibhotla et al., 2008). Localised Ca^{2+} hyperactivity in the APP/PS1 model was later reproduced in a 2021 two-photon study, which showed aberrantly high GCaMP6s expression within 40µm of Aβ plaques in the frontal cortices of 4-5-month-old animals (Korzhova et al., 2021). Kuchibhotla et al., (2014) also assessed the effect of NFT pathology on Ca^{2+} activity in the visual cortex. Two-photon Ca^{2+} imaging with YC3.6 Ca^{2+} indicator was performed on 9-month-old rTg4510 mice, a transgenic model that overexpresses a human mutant form of tau (P301L) and shows NFT pathology by around 7 months old. Interestingly, no significant differences in the resting Ca^{2+} profile in the visual cortices of rTg4510 and control mice were observed (Kuchibhotla et al., 2014).

A subsequent study by Busche et al., (2012) performed two-photon imaging of the HPC of 6–7-month-old APP23xPS45 mice. Interestingly, when assessing the transients per minute of hippocampal neurons, an increase in hyperactive neurons in animals that exhibited soluble Aβ species (but no plaques) was observed (Busche et al., 2012). Oral treatment with γ-secretase inhibitor LY-411575 reduced soluble Aβ levels and rescued neuronal hyperactivity, suggesting that soluble Aβ species rather than plaques may underlie the local hyperactivity impairment observed in these studies (Busche et al., 2012). Supporting this, direct hippocampal application of soluble Aβ species in C57BL6/J mice by micropipette increased neuronal hyperactivity versus vehicle controls (Busche et al., 2012). A later two-photon Ca^{2+} imaging study used 3-month-old APPswe/PS1dE9 mice expressing GCaMP6s under the Thy-1 promoter in a treadmill running experiment. When stationary, the mice showed significantly reduced Ca^{2+} activity in the motor cortex compared to non-AD transgenic littermate controls (Bai et al., 2017). However, when running, the duration and amplitude of neuronal Ca^{2+} transients in APPswe/PS1dE9 mice was significantly increased compared to control animals (Bai et al., 2017). APPswe/PS1dE9 mice at 3 months do not exhibit plaque formation (Garcia-Alloza et al., 2006), suggesting a role of pre-aggregated Aβ in neuronal Ca^{2+} dysregulation and corroborating the results from Busche et al. Testing this theory, a further study observed aberrant Ca^{2+} transients while running in C57BL6/J mice injected with soluble $Aβ_{42}$ (Bai et al., 2017).

Research is increasingly utilising 2nd generation AD models in transgenic crosses for two-photon Ca^{2+} imaging studies. Recently, *App*^{NLGF} mice were crossed with Thy1-G-CaMP7-T2A-DsRed2 (WT-G-CaMP7) animals to make the *App*^{NLGF} /Thy1-G-CaMP7-T2A-DsRed2$^{+/-}$ (AD-G-CaMP7) mouse, a genetic cross that facilitates neuronal expression of fluorescent Ca^{2+} indicator GCaMP7. Chronic two-photon Ca^{2+} imaging was performed on head fixed AD-G-CaMP7 animals positioned on a treadmill. Imaging sessions began at 4 months of age and continued over a period of 9 months. Using a virtual reality behavioural paradigm, the animals were trained to run only during certain locations in the virtual reality. Analysis of Ca^{2+} transients in the CA1 region revealed an overall decrease in active neurons in AD-G-CaMP7 mice compared to WT-G-CaMP7 mice (Takamura et al., 2021). Interestingly, however, in corroboration with the above studies in transgenic mice, an increased number of hyperactive neurons were observed near Aβ aggregates in AD-G-CaMP7 mice with increasing age (Takamura et al., 2021). A similar two-photon imaging study also showed that Aβ load is associated with increased neuronal Ca^{2+} hyperactivity in cortical regions of *App*^{NLGF} mice expressing GCaMP6s under *Thy-1* (Doostdar et al., 2021). Also supporting the findings of Takamura et al., (2021), a similar study showed that 12-month-old *App*^{NLGF}×*Thy1*-GCaMP6s$^{+/-}$ (A-TG) mice exhibited a lower average neuronal Ca^{2+} amplitude of firing in the CA1 compared to control animals, and this effect was more pronounced when the mice were running (Inayat et al., 2023). Interestingly, however, A-TG mice exhibited a larger number of Ca^{2+} transients per minute compared to control mice (Inayat et al., 2023).

Overall, current research of the HPC and various cortical regions indicates that Aβ induces local neuronal Ca^{2+}-induced hyperactivity in both transgenic animals and App^{NLGF} animals harbouring transgenic Ca^{2+} indicators. Given the question of how accurately the transgenic brain environment mimics the AD state, it is important to observe how neuronal Ca^{2+} is affected in the App^{NLGF} model with no transgenic expression. As described above, there are some suggestions that despite the evidence of localised neuronal hyperactivity, overall Ca^{2+} activity in the App^{NLGF} brain is reduced compared to control animals (Inayat et al., 2023). However, so far this has only been indicated in the CA1 region of the HPC, therefore research is required to test this result in other areas of the brain that play key roles in AD, such as the RSC.

4.2.1.3 The Retrosplenial Cortex

4.2.1.3.1 Anatomy and Functions of the Retrosplenial Cortex

The RSC comprises of cortical regions 29 and 30, as defined by Brodmann over 100 years ago (Brodmann, 1909). In humans and non-human primates, the RSC is a central structure that wraps around the splenium of the corpus callosum and forms part of the posterior cingulate cortex, along with areas 23 and 31 (Mitchell et al., 2018; Vann et al., 2009). Rodents lack areas 23 and 31, and their RSC is positioned towards the surface of the brain, occupying a proportionally larger area compared to primates (Fig. 4.2) (Bermudez-Contreras et al., 2020; Martins et al., 2014; Milczarek & Vann, 2020). Brodmann areas 29 and 30 are commonly described as the granular and dysgranular RSC, respectively (Aggleton et al., 2021). The granular RSC is located ventrally relative to the dysgranular RSC, and has a dense layer IV containing granular cells (van Groen & Wyss, 1990; Vogt & Peters, 1981; Wyss & Van Groen, 1992). The dysgranular RSC is positioned dorsally relative to the granular RSC, and exhibits a wider but sparser layer IV (Sugar et al., 2011; van Groen & Wyss, 1992a; Vogt & Peters, 1981; Wyss & Van Groen, 1992).

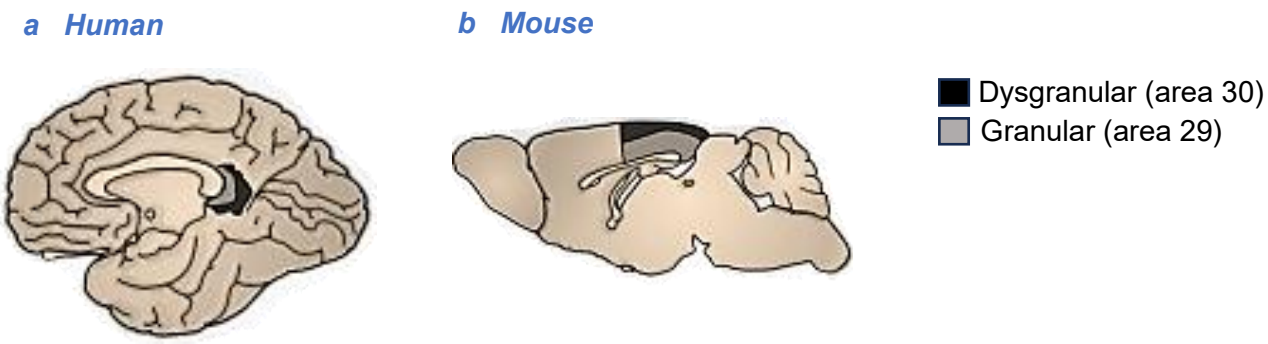

Figure 4.2: The Retrosplenial Cortex. Location of the dysgranular and granular retrosplenial cortex within the ***a)*** human brain and ***b)*** rodent brain. Image adapted from Milczarek and Vann (2020).

The granular and dysgranular RSC have distinct connectivity patterns that are largely conserved among humans and rodents (Vann et al., 2009). The granular RSC is strongly linked to the HPC and its associated network (Aggleton et al., 2021). For example, it receives predominantly unidirectional input from the CA1 and forms reciprocal links with the subiculum, presubiculum, postsubiculum, EC, and anterior thalamic nuclei (Aggleton et al., 2012; Aggleton et al., 2021; Sugar et al., 2011; Vann et al., 2009). The dysgranular RSC receives sparser hippocampal input and is more strongly connected with visual areas 17 and 18b, with most interactions concentrated in its caudal region (van Groen & Wyss, 1990, 1992a; Van Groen & Wyss, 2003; Vogt & Miller, 1983). The granular and dysgranular RSC are also connected through intrinsic reciprocal connections (Sugar et al., 2011). Although the precise role of the RSC is yet to be fully understood, its anatomical connections along with evidence from imaging, lesion, and IEG studies have indicated the RSC as a site of integration of spatial memory and sensory information (Alexander et al., 2023).

In humans, fMRI studies revealed that activity in the RSC is modulated by a range of tasks involving scene processing and spatial navigation, episodic memory, and autobiographical memory retrieval (Awad et al., 2007; Epstein, 2008; Epstein et al., 2007; Ferris et al., 2024; Maguire, 2001a, 2001b; Svoboda et al., 2006). The functions of the RSC appear anatomically heterogeneous, with scene processing and navigation primarily associated with the caudal RSC and episodic memory linked to the rostral RSC (Chrastil, 2018). Patients with damage to the RSC have exhibited varying degrees of amnesia, including reduced memory for episodic details from stories, deficits in autobiographical memory, difficulties in recalling the positional relationships between familiar landmarks and failure to navigate effectively through familiar environments (Epstein, 2008; Maguire, 2001b; Takahashi et al., 1997; Vann et al., 2009).

Along with regions such as the anterior thalamus, postsubiculum, EC, and HPC, the RSC is part of a neural network known as the Head Direction System (Weiss & Derdikman, 2018). A subset of neurons in the RSC fire maximally when the head is orientated in a specific direction (Chen, Lin, Green, et al., 1994; Cho & Sharp, 2001; Jacob et al., 2017). These cells use visual cues such as external landmarks to provide an external anchoring reference, with both human neuroimaging and rodent electrophysiological studies suggesting that they are most responsive to stable landmarks rather than those that can shift position (Auger et al., 2012; Lozano et al., 2017). This system is therefore believed to function as a neural compass by encoding the direction of the animal's head in relative to its environment, contributing to the egocentric frame of reference (Butler et al., 2017; Taube, 2007). However, the directional tuning of these cells in area 30 can be maintained in darkness, indicating an internal representation of direction (Butler et al., 2017; Dudchenko et al., 2019; Jacob et al., 2017). Furthermore, a subset of cells in the RSC, including head direction cells, are modulated by running speed and angular head velocity (Chen, Lin, Barnes, et al., 1994; Cho & Sharp, 2001; Keshavarzi et al., 2022; Lozano et al.,

2017). This suggests that the RSC contributes to the continuous updating of representations of self-position using self-movement cues, a process known as path integration, a critical process in navigation (Etienne & Jeffery, 2004). The RSC also appears to contribute to context discrimination, allowing the animal to distinguish between novel and familiar environments (Walsh et al., 2022). Electrophysiological recordings showed that exposure to environmental novelty elicits a significant increase in the rate, amplitude, and duration of β-frequency oscillations in the RSC (Walsh et al., 2022). This increased strength of β-frequency oscillations was associated with transient increases in neuronal spiking and θ–α/β cross-frequency coupling, suggesting that the RSC may both encode novel spatial information and coordinate this signal with wider neural networks supporting spatial memory and contextual representation (Walsh et al., 2022).

Lesions of the RSC reveal deficits in spatial navigation tasks that are most apparent when intra- and extra-maze cues are placed in conflict. For example, RSC lesioned rats show minimal deficits in standard T-maze forced alternation tasks, where they are trained to choose the opposite arm to the arm visited in a previous sample trial (Aggleton et al., 1995; Neave et al., 1994; Pothuizen et al., 2008). However, when the maze is rotated, their performance is significantly impaired (Nelson et al., 2015). Similarly, rotating the RAM also produces significant impairments in performance in RSC lesioned rats (Pothuizen et al., 2008; Vann & Aggleton, 2004; Vann et al., 2003). Furthermore, lesion or inactivation of the RSC results in deficits in RAM navigation, foraging tasks, and T-maze alternation in the dark, where visual cues are removed and path integration is required (Cooper et al., 2001; Cooper & Mizumori, 1999; Elduayen & Save, 2014; Pothuizen et al., 2008). Rodents have various navigational strategies available when they are solving a maze (e.g. alternation with use of extra-maze landmarks, intra-maze cues, heading direction, and patterns of movement (Futter & Aggleton, 2006)), but when the spatial relationship between the maze and the extra-maze landmarks change (e.g., maze rotation), or when a cue-type is removed (e.g., removing visual cues by performing the task in the dark), RSC lesioned rodents struggle to adapt. This supports the theory that the RSC plays a critical role in transitioning egocentric (self-centred) with allocentric (world-centred) frames of reference, to achieve efficient navigation through different strategies (Chen, Lin, Green, et al., 1994; Miller et al., 2014; Vann et al., 2009).

Specific roles of the granular and dysgranular RSC have emerged from lesion and IEG studies. For example, dysgranular RSC lesions impair the use of allocentric cues, as shown by deficits in RAM performance following maze rotation (Vann & Aggleton, 2005). Moreover, lesions of the granular RSC produce deficits in RAM performance in both light and dark conditions that are comparable to complete RSC lesions (Pothuizen et al., 2010). Furthermore, expression of IEGs *c-fos* and *zif268* increases in the granular RSC during a RAM task in both light and dark conditions, whereas their expression in the dysgranular RSC only increased in the light (Pothuizen et al., 2009). Collectively, these findings suggest that the RSC plays a

greater role using internal cues for navigation, whereas the dysgranular RSC is primarily processes visual cues to guide behaviour, reflecting its connectivity to the visual cortex (Aggleton et al., 2021).

Beyond its role in navigation, the RSC has also been implicated in mnemonic processing, including the encoding and retrieval of episodic memories (Alexander et al., 2023). For example, highlighting its role in processing the spatial properties of the environment, lesions of the rodent RSC generally impair performance in spatial-related tasks that test episodic-like memory such as the OiP (Vann & Aggleton, 2002) and OL tasks (Ennaceur et al., 1997; Parron & Save, 2004), however, one recent study showed intact OL performance following RSC lesions (Hayashi et al., 2020), but the lack of observed difference may speak to the extent and method of lesions used. There is also evidence that RSC lesions impair object recency discrimination in the TO task (Hayashi et al., 2020; Powell et al., 2017). However, lesions of the RSC generally spare object identity memory in the ON task (Ennaceur et al., 1997; Hayashi et al., 2020; Parron & Save, 2004; Vann & Aggleton, 2002). Consistent with the findings from traditional object recognition task, a recent touchscreen based dPAL study showed that lesions of the granular RSC impaired the retrieval of previously learned and the learning of new object-location associations (Sheppard et al., 2024). However, when tested with single-modality tasks assessing either spatial working memory or visual discrimination, no impairments were observed (Sheppard et al., 2024), suggesting that the granular RSC is specifically involved in integrating object and spatial information. Contrastingly, a recent study has implicated the anterior RSC in long-term consolidation and retrieval of object identity information, as selective temporary inactivation of this area shortly after the sample phase of the ON task (consolidation) or before the test phase (retrieval), but not before the sample phase (acquisition), impaired novel object recognition in the test phase (de Landeta et al., 2020).

Overall, anatomical, lesion, and activation studies support the role of the RSC as an integrative hub, receiving sensory, spatial, and mnemonic information, and linking internal representations with external environmental cues to support navigation, memory, and cognitive flexibility (Alexander et al., 2023). However, its role isn't limited to spatial memory, with lesions of the RSC associated with reduced freezing during contextual fear conditioning and trace fear conditioning tasks and decreased locomotion in the central zone of an OF, suggesting the RSC also plays a role in fear learning and anxiety-related behaviour (Keene & Bucci, 2009; Kwapis et al., 2014; Kwapis et al., 2015; Lukoyanov & Lukoyanova, 2006; Pan et al., 2022).

4.2.1.3.2 Retrosplenial Cortex Dysfunction in Alzheimer's Disease and Mouse Models of Alzheimer's Disease

Dysfunction of the RSC has been observed in normal age-related memory impairment and AD (Trask & Fournier, 2022). The RSC of patients with early AD exhibits Aβ accumulation, with plaques typically first emerging across the cortex, including the posterior cingulate cortex (Buckner et al., 2005; Klunk et al., 2004). Furthermore, several volumetric MRI studies have shown significant atrophy of these areas in the early stages of AD, with some indications that the volume of this region is a predictor for the conversion of MCI to AD (Choo et al., 2010; Chételat et al., 2005; Frisoni et al., 2009; Pengas et al., 2010; Scahill et al., 2002; Tan et al., 2013). Moreover, PET and fMRI studies have consistently shown acute glucose hypometabolism in the RSC of patients with MCI and early AD, which appears to precede atrophy (Buckner et al., 2005; Drzezga et al., 2011; Minoshima et al., 1997; Mosconi et al., 2006; Nestor et al., 2003; Terstege et al., 2024). The temporal relationship between amyloid deposition and metabolic changes is not fully understood. However, there is evidence that amyloid pathology precedes hypometabolism, with the latter following a similar pattern of regional expansion but with a delay (Förster et al., 2012). Furthermore, resting state fMRI studies have shown altered functional connectivity of the posterior cingulate cortex in AD, with evidence suggesting it is initially increased in MCI and early stages of AD but decreases with AD development (Bai et al., 2009; Gili et al., 2011; Shah et al., 2022; Zhang et al., 2010). Interestingly, children with FAD mutations exhibit increased functional connectivity of the posterior cingulate cortex with medial temporal regions before cognitive symptoms are evident (Quiroz et al., 2015).

In mouse models of AD, substantial Aβ deposition in the RSC has been observed by several studies. For example, in the 5XFAD model of AD, Aβ deposition is apparent at 4 months, with the RSC being the most affected brain region by plaque (Kim et al., 2020; Tsui et al., 2022). In the PDAPP mouse model, amyloid accumulation is detectable in the RSC at around 6 months (Reilly et al., 2003), and at around 5 months in the Tg2576 model (Poirier et al., 2011). Interestingly, metabolic changes of the RSC have also been observed in the Tg2576 mouse model, where increased cytochrome oxidase activity is present before any evidence of plaque formation (Poirier et al., 2011). Contrary to human studies, this is indicative of hypermetabolism in the RSC. The Tg2576 mouse model, however, appears to lack any RSC atrophy (Poirier et al., 2011; Ribé et al., 2005). In J20 mice, a transgenic model that overexpresses human APP carrying FAD mutations, amyloid deposition in the RSC was detected at 7 months and was accompanied by exaggerated β-frequency oscillations in the dysgranular RSC in response to both novel and familiar environments, compared to C57BL6/J controls (Walsh et al., 2022). Additionally, the J20 model exhibited a loss of coupling between β-bursts and RSC spiking activity, indicating a disruption in the neural encoding of environmental novelty within the RSC and impairment in the formation of neuronal ensembles required for contextual memory (Walsh et al., 2022). Such disruptions may underlie the spatial learning and

memory impairments previously reported in the J20 model, as demonstrated in tasks such as the MWM and RAM which depend on the accurate encoding and retrieval of contextual and spatial information (Cheng et al., 2007; Wright et al., 2013).

Very little is known about the integrity of the RSC in 2nd generation mouse models of AD including the *App*^{NLGF} model. Amyloid deposition in the RSC has been reported in *App*^{NLGF} mice at 12 months (Mehla et al., 2022), however, it is likely to emerge earlier, though this has yet to be demonstrated. *App*^{NLF} mice, which harbour the Swedish and Beyreuther/Iberian mutation without the additional Arctic mutation (Saito et al., 2014), exhibit increased functional connectivity in the cingulate cortex prior to amyloid accumulation, as was observed in human AD (Shah et al., 2022). Interestingly, these mice also exhibited increased Ca^{2+} activity in cingulate neurons alongside a concurrent decrease in astrocyte Ca^{2+} activity (Shah et al., 2022). Recovery of astrocyte Ca^{2+} activity using designer receptors exclusively activated by designer drugs (DREADDs) mitigated neuronal hyperactivity and normalised cingulate connectivity, suggesting a role of early immune changes driving functional alterations in the RSC (Shah et al., 2022). Increased cortical and hippocampal functional connectivity has also been reported in *App*^{NLGF} mice prior to plaque formation, suggesting that potential changes in RSC Ca^{2+} activity may be similarly linked to functional connectivity alterations driven by astrocyte dysfunction (Latif-Hernandez et al., 2019).

4.2.2 Methods

4.2.2.1 Introduction

The Methods section of this chapter will introduce and describe the entire process of two-photon Ca^{2+} imaging, including the cranial window surgery, the presentation of visual stimuli, fluorescence data acquisition, the data analysis pipeline, and statistical analysis. For details of the data analysis codes designed for this thesis, please refer to Appendices 1, 2, and 3.

4.2.2.2 Two-Photon Calcium Imaging

For many years, electrophysiological studies have been the gold standard for recording neuronal activity. However, its invasive nature and limited capacity for the number of cell recordings is a major limitation. Subsequently, imaging of Ca^{2+} transients as an indication of neuronal activity is a popular alternative. Two-photon imaging is a widely used technique to record neuronal Ca^{2+} activity in the intact rodent brain. Ca^{2+} imaging is based on the principle that intracellular Ca^{2+} levels rise upon firing of neuronal action potentials, so it is therefore used to indirectly assesses

neuronal activity. This concept has been proven in studies that perform simultaneous electrophysiological recordings during Ca^{2+} imaging in single neurons, showing a correlation of electrical firing and Ca^{2+} transients (Wei et al., 2020).

Fluorescent molecules are utilised to visualise Ca^{2+} pulses as they bind free Ca^{2+} ions during an action potential, causing a change in fluorescent intensity (Grienberger et al., 2022). The introduction of fluorescent molecules *in vivo* can be achieved through injection via micropipette into the ROI. Commonly used fluorescent indicators include chemical indicators such as Fluo-4 (Gee et al., 2000). Although chemical indicators offer the advantage of high Ca^{2+} sensitivity, they are transient and are degraded over time so are not suitable for long-term experiments. To overcome this issue, genetically encoded Ca^{2+} indicators such as GCaMP are commonly preferred in two-photon imaging experiments. GCaMP is an adapted version of the fluorophore green fluorescent protein (GFP) that also contains the Ca^{2+} sensor CaM and the peptide M13 from myosin light chain kinase (Nakai et al., 2001). Upon the binding of Ca^{2+} to CaM, GCaMP undergoes a conformational change that enhances fluorescent intensity of the cell (Grienberger et al., 2022). To improve the stability of the molecule and quality of the fluorescent signal, GCaMP has undergone several redevelopments as denoted by a number, with CGaMP1 being the original proof-of-concept molecule and GCaMP8 is the most recent version (Zhang et al., 2023c). GCaMP6 is commonly used in two-photon Ca^{2+} imaging, and is available in the fast (GCaMP6F), slow (GCaMP6S), or medium (GCaMP6M) response versions that are suitable for various speeds of Ca^{2+} transients. Whilst the kinetics of GCaMP may be slightly slower than chemical indicators, it remains in the brain for several weeks and thus is often the molecule of choice for laboratories interested in learning and memory (Grienberger et al., 2022). It also offers high spatial and temporal resolution of Ca^{2+} signals, so it can detect *in vivo* Ca^{2+} transients with high accuracy (Grienberger et al., 2022; Zhang et al., 2023c). CGaMP is often packaged in viral vectors that facilitate its integration into the rodent genome, thus allowing for long-term expression without the need for repeated injections. To visualise changes in fluorescent intensity within the intact rodent brain, it is typically necessary to create a cranial window by removing a portion of the skull and securing a glass disk in its place. This approach provides a clear optical pathway to the underlying structures to facilitate high resolution imaging of cellular activity (Grienberger et al., 2022).

Performing two-photon imaging requires a complex set-up comprising of highly specialised equipment (Fig. 4.3). The basic layout of a two-photon microscope includes a power modulation system such as a Pockels cell, a beam scanning system, a laser as the source of excitation light, one or more photomultiplier tubes (PMTs) to detect the generated fluorescence, and an objective that is aligned with the cranial window of the animal. During two-photon imaging, the laser beam emits high intensities of pulsed light. Subsequently, two photons of IR light are simultaneously absorbed by the fluorophore in the tissue, such as GCaMP. This

causes excitation of the fluorophore, which subsequently emits fluorescence at a higher energy level (in the visible light range). In two-photon imaging, the laser is focused though a high numerical aperture objective lens, therefore the two photons are present in a small, localised area, so only the focal point of the laser is excited (Grienberger et al., 2022). This allows high resolution of deep tissues within the brain, up to approximately 500-800µm, with minimal photodamage of the tissue (Wilt et al., 2009). In contrast, conventional fluorescent microscopy uses one high-energy photon in the ultra violet or visible light range, which does not penetrate tissue as deeply as IR wavelengths, and excites fluorophores above and below the focal plane (Wilt et al., 2009). The Pockels cell of the two-photon set-up allows precise adjustment of excitation by modulating the intensity of the laser and thus limiting damage to the underlying tissue. The beam scanning system moves the laser beam across both the X and Y axes within the ROI, progressively building a complete image of the entire region over the course of the imaging session. PMTs are used to amplify the signal produced by the fluorophore, which is then digitised to form an image. The image and associated data are subsequently processed and analysed to quantify changes in fluorescence during the experiment.

As the two-photon setup is minimally invasive to the animal and there is lower risk of tissue photodamage, it is often performed in awake animals. For such set-ups, animals are often fixed to the microscope rig via a headpiece and positioned upon a treadmill to allow naturalistic movement whilst minimising imaging artefacts from motion. Assessing neuronal activity in awake animals, versus anaesthetised, offers the benefit of capturing physiological neuronal activity that may be perturbed by the effects of anaesthetic drugs (Berg-Johnsen & Langmoen, 1992). In two-photon Ca^{2+} imaging experiments with awake animals, visual, cognitive, or motor stimuli may be presented to the animal to engage different areas of the brain. This allows real-time recording of Ca^{2+} transients in response to the presented stimuli. For the RSC, visual stimuli such as drifting gratings (alternating light and dark moving bars) or changing patterns can be presented on LCD computer screens to engage activity (Murakami et al., 2015). This is based upon studies showing that the RSC is activated by rectilinear shapes in the visual field as it is particularly sensitive to geometric structures (Henderson et al., 2008; Nasr et al., 2014; Wolbers et al., 2011). Furthermore, the RSC has been shown to modulate its activity based on specific angles of stimuli in the visual field, i.e., it is selectively responsive to preferred orientations of gratings (Powell et al., 2020). Therefore, to study the response of RSC to gratings of varying orientations, the Sengpiel laboratory has developed an *in vivo* two-photon Ca^{2+} imaging protocol in which awake head-fixed mice are positioned on a treadmill and presented with a series of visual stimuli. In advance of imaging, the animals are prepared with a craniotomy, allowing infusion of GCaMP6F into the RSC and insertion of a cranial window. In this thesis, a specifically designed protocol looping periods of dark screen followed by visual stimuli of different orientations was designed to study the baseline levels and stimulus-induced Ca^{2+} dynamics in the App^{NLGF} mouse model.

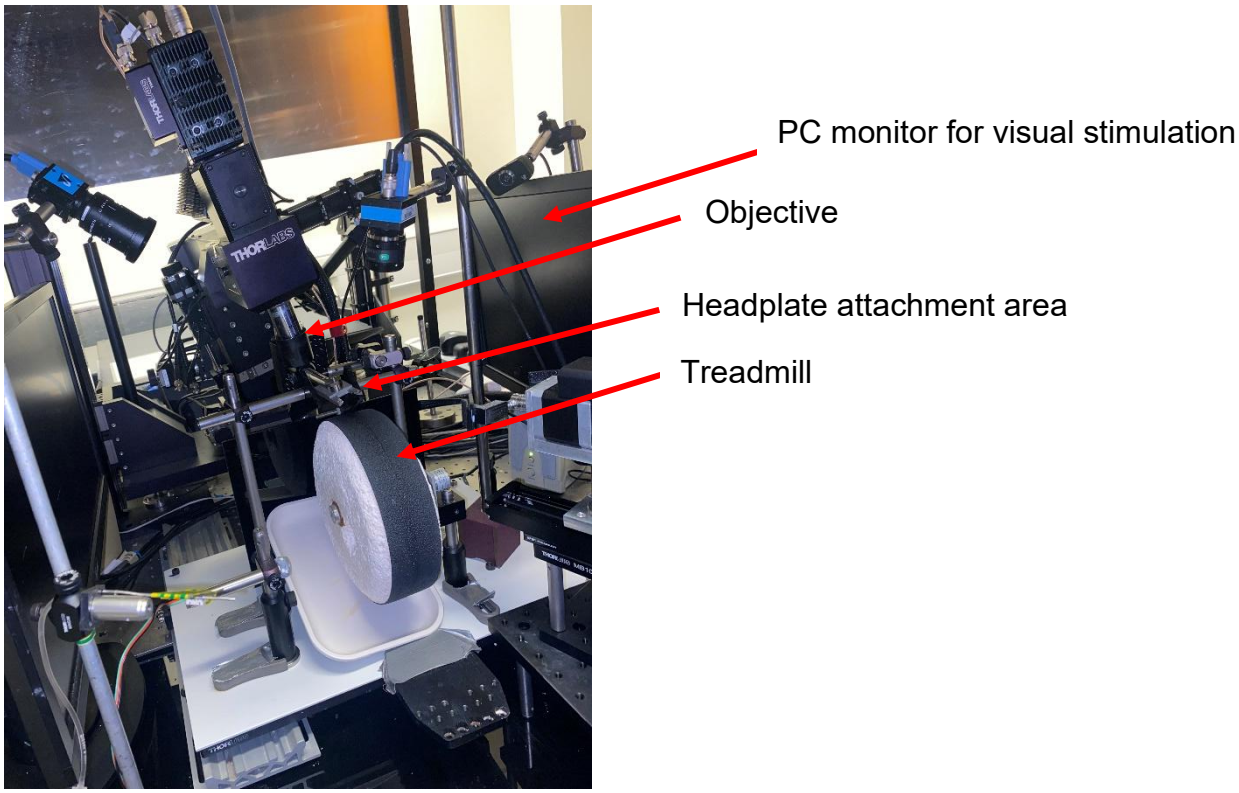

Figure 4.3: Two-photon Microscope Set-up. Image depicting some of the key components of the two-photon imaging set-up in the Sengpiel laboratory, including the treadmill on which the animal is positioned, the rig on which the animal's head is secured, the microscope objective, and the PC monitor positioned to the left of the animal.

4.2.2.2.1 Surgical Preparation

Animals were anaesthetised using 5% isoflurane in oxygen and a surgical plane of anaesthesia was maintained at approximately 2% isoflurane throughout surgery. The animal was secured to a stereotaxic head frame and administered with anti-inflammatory drugs Rimadyl (5mg/kg, subcutaneous) and Baytril (0.15mg/kg, intramuscular). Fur from the surgical zone was removed using scissors and hair removal cream (Nair). Local anaesthetic (2% lidocaine) was then injected into the scalp and the site was then cleaned with iodine solution. Using surgical scissors, a portion of the scalp and periosteum was removed, exposing the skull. Using a biopsy tool and a surgical drill, a 3mm craniotomy was formed approximately 2.5mm caudal to bregma, positioned over the right hemisphere but incorporating the central sinus for landmarking (Fig. 4.4a & 4.4c). A viral construct driving GCaMP6F expression was then injected into the caudal dysgranular RSC. A custom-made head plate (Fig. 4.4b & 4.4c) with a glass window was then positioned over the craniotomy and secured to the skull with surgical glue and dental cement. All surgical procedures were carried out under aseptic conditions.

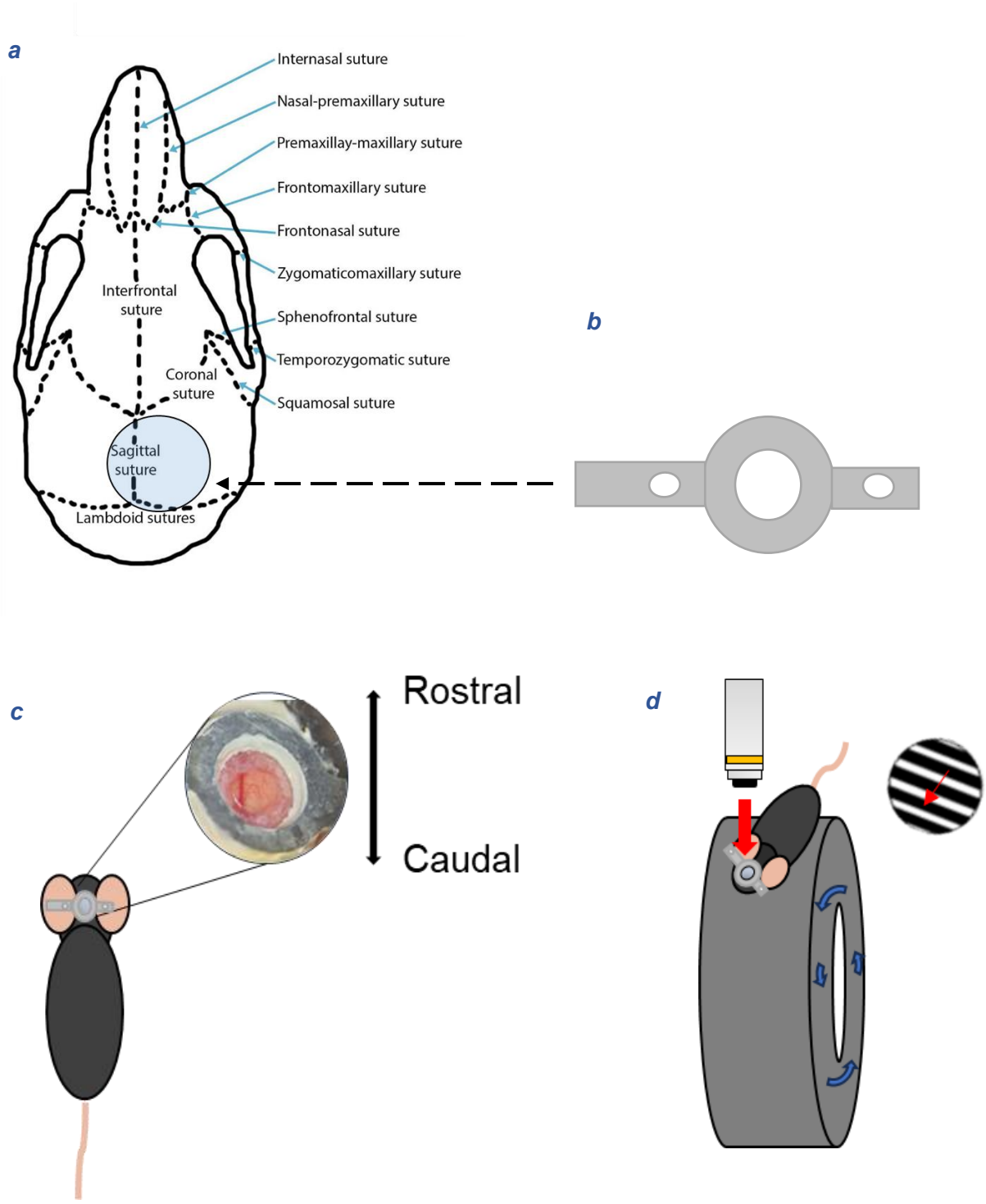

Figure 4.4: Surgical Preparation and Imaging. a) The approximate craniotomy position, adapted from (White et al., 2021). ***b)*** Diagram of head plate to be positioned over craniotomy. ***c)*** The imaging region of interest; the caudal dysgranular RSC. ***d)*** *in-vivo* imaging set-up, showing the animal positioned on treadmill under the microscope objective with the presentation of visual stimuli.

4.2.2.2.2 Imaging Apparatus and Visual Stimuli

Imaging was performed using a two-photon resonant scanning microscope (Thorlabs, BScope) with a 16 x 0.8NA objective (Nikon). GcaMP6F was excited at 920nm using a Ti:sapphire laser (Coherent, Chameleon) with power set at approximately -100mW. Visual stimuli were presented to the animal on two LCD screens (26 x 47cm), positioned at right angles to another, to the front and left side of the animal and 20cm away from the eye.

Based on previous work showing that the RSC is responsive to visual stimuli of large drifting gratings at low spatial and temporal frequency, a visual stimuli protocol was designed using MATLAB psychophysics toolbox (Murakami et al., 2015; Powell et al., 2020). The stimuli consisted of circular drifting gratings of 40° diameter at a spatial frequency of 0.08 and temporal frequency of 1Hz, at 100% contrast. 24 trials were presented to the animal and were repeated 10 times in a random order. The trials consisted of an equal mix of stimuli positions and orientations: positions were y = 10 and either x = 80 or x = 20 and orientations were 0, 45, 90, or 225° (referred to as stimulus orientations 1-4) (Fig. 4.5). Each trial consisted of 2 seconds of stimulus followed by a 6 second intertrial interval, where the screen was black, allowing baseline Ca^{2+} measurements for normalisation of stimulus induced Ca^{2+} levels.

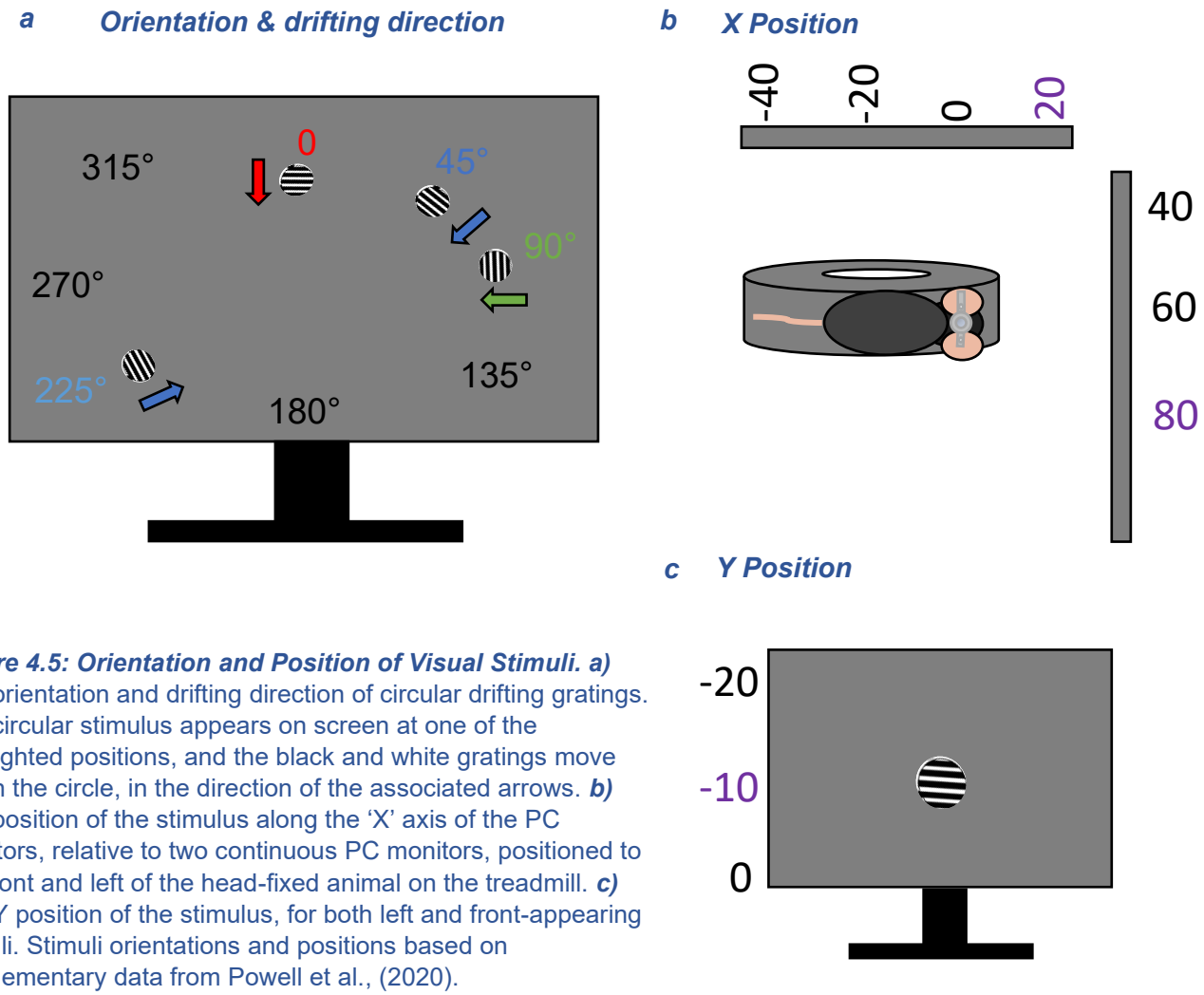

Figure 4.5: Orientation and Position of Visual Stimuli. a) The orientation and drifting direction of circular drifting gratings. The circular stimulus appears on screen at one of the highlighted positions, and the black and white gratings move within the circle, in the direction of the associated arrows. ***b)*** The position of the stimulus along the 'X' axis of the PC monitors, relative to two continuous PC monitors, positioned to the front and left of the head-fixed animal on the treadmill. ***c)*** The Y position of the stimulus, for both left and front-appearing stimuli. Stimuli orientations and positions based on supplementary data from Powell et al., (2020).

4.2.2.2.3 Habituation and Imaging

For all experiments, the animal was positioned on a cylindrical treadmill and head fixed to the microscope apparatus via a screw through their headplates, allowing the head to stay in position whilst the animal was free to run (Fig. 4.4d & 4.5b). Attachment of the animals' headplate to the microscope apparatus was carried out to lessen movement of the head and thus improve image quality. The option of movement on the treadmill was designed as an attempt to reduce the stress and anxiety for the animal and to reduce likelihood of the headplate detaching from the head whilst screwed in place. A plastic cone was positioned on top of the headplate, screwed in place, and filled with water, before the water immersion objective was lowered in place. Prior to imaging, all animals were habituated to the apparatus until they tolerated the procedure and did not attempt to escape the head fixed position. Typically, this required two half-day sessions, where the animal was gradually familiarised with the equipment then repeatedly fixed onto the head stage for brief periods (< 5 minutes), followed by regular rests in its home cage. Adequate habituation resulted in very minimal running on the treadmill during imaging. Throughout habituation and imaging, the animal was monitored with a camera, and imaging was ceased if the animal exhibited any signs of distress such as grimace, vocalisation, or excessive movement. Typically, each animal received one imaging session which lasted approximately 30 minutes.

4.2.2.3 Data Acquisition and Processing

Using the central sinus of the brain as a landmark, the caudal dysgranular RSC was located and imaged at approximately 200-300μm depth. Once the ROI was located, the microscope was set to x2 zoom and a MATLAB code from the Sengpiel laboratory (written by Dr A Ranson) was entered to trigger stimulus presentation and fluorescence signal acquisition (Fig. 4.7, step 1).

After data acquisition, a series of MATLAB codes from the Sengpiel laboratory (written by Dr A Ranson and Dr R Craddock) were employed to process fluorescent data from each experiment. Firstly, stimulus metadata was rewritten into a useable format and annotated with information such as the stimulus type, timeline data, and wheel movement data (Fig. 4.7, step 2a). Responses of neurons in the RSC are highly modulated by locomotion, regardless of the presence of visual stimuli (Powell et al., 2020), so the code binned data into 'still' and 'moving' categories, and only the data from the 'still' category was processed, to confirm that any responses present were a result of the visual stimuli rather than locomotion. Following this, the mean image frame from each experiment was registered to Suite2P and ROIs, defined as cell bodies or neurons, were automatically detected then manually verified (Pachitariu et al., 2017) (Fig. 4.6 & 4.7, step 2b). For each experiment, approximately 50-100 ROIs (referred to as cells) were analysed.

a *b*

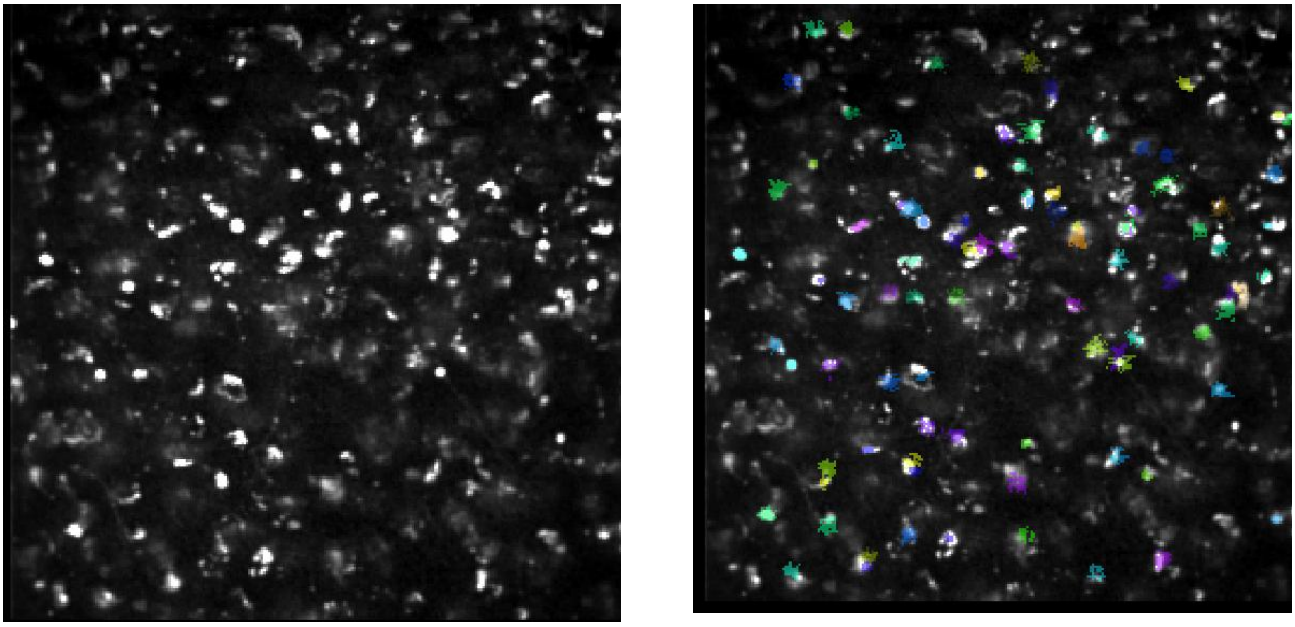

Figure 4.6: Regions of Interest in the Retrosplenial Cortex. a) Representative image depicting the mean image frame of the caudal dysgranular retrosplenial cortex from two-photon calcium imaging. ***b)*** Neurons in focus were automatically detected by Suite2P, as shown by the highlighted regions (Pachitariu et al., 2017). The automatically detected neurons were then manually verified.

Following semi-automatic anatomical detection of cells in the RSC, a further series of MATLAB codes from the Sengpiel laboratory (Dr A Ranson and Dr R Craddock) were employed to retrieve the fluorescent data from each frame per cell, collate it into one dataset, calculate a mean change in fluorescence (ΔF) across all 10 repeats of each trial, and organised it into an Excel spreadsheet consisting of the timeline and average ΔF at each timepoint for each 24 trials per cell (Fig. 4.7, steps 2c-2e). For each cell per animal, the code automatically generated a corresponding graph showing the average ΔF of each trial for the entire baseline and stimulus period. These graphs were used to manually exclude any traces that may have been misidentified as cells during image registration on Suite2P. For example, if the graph was completely flat and did not show even subtle Ca^{2+} fluctuations, this was indicative of an imaging artefact (e.g. loose dental cement) rather than a cell, so it was excluded from further analysis.

To analyse the Excel spreadsheets containing ΔF values at each timestamp for all 24 trials, a series of Visual Basic for Applications (VBA) codes were generated for this thesis using XLTools package in Excel. As there were a vast number of Excel spreadsheets to analyse (1 spreadsheet per cell, 50-100 cells per animal, and 17 animals in total) the VBA codes were structured as loop macros, i.e., programmes of instruction that use a loop structure to repeat calculations through a series of multiple

.xls files. The initial loop macro (Appendix 1) was designed to calculate the mean raw ΔF of the entire 2s of baseline immediately prior to stimulus onset (Fig. 4.7, step 3). The mean ΔF of the entire baseline period refers to an average of the 2s of baseline across all 24 trials per cell. As repeats of stimuli were presented to the animal on a loop (i.e. 6s of dark/baseline → 2s of stimulus → 6s of dark/baseline of next trial, etc.), the 2s of baseline immediately prior to stimulus onset was chosen for analysis (i.e. the latter part of the baseline), to reduce the chances of residual Ca^{2+} signal from the previous stimulus confounding baseline data (Craddock et al., 2023). After the VBA code had looped through every cell for each animal, a total mean baseline ΔF for each animal was calculated. The mean raw ΔF for each animal was then inputted into SPSS and the difference in mean baseline ΔF between C57BL6/J and *App*^{NLGF} animals was analysed. For baseline ΔF analysis, the raw data was compared between C57BL6/J and *App*^{NLGF} animals because stimulus data was normalised by the mean baseline ΔF (discussed below), so normalisation of the baseline would not allow for accurate comparison between the two genotypes. As discussed below, normalising data has key benefits, but for the purpose of investigating broad overall differences in baseline Ca^{2+}, rather than specific stimulus-induced Ca^{2+} fluctuations, it was decided that raw data analysis was preferable.

For analysis of overall stimulus response, a further VBA loop macro was created (Fig. 4.7, step 4a). Overall stimulus response refers to the mean ΔF of the total 2s of stimulus across all 24 trials during the experiment. The VBA code was created to calculate an average ΔF at each timestamp, across all 24 trials, and normalise it by dividing it by the total mean ΔF of the 2s of baseline immediately prior to stimulus onset (Appendix 2). Normalisation was performed on stimulus-response data as it sets the baseline to 1, so it is easy to interpret fold changes from baseline Ca^{2+} levels. Furthermore, it also reduces variability between different cells in an experiment, and different experiments (i.e., different animals), by minimising the impact of different levels of fluorescent dye loading, dye uptake, cell size, and other factors that may lead to inherent fluorescent variability between cells. This ensures consistency and ensures any changes in fluorescent response is due to experimental parameters rather than inherent cell differences. The mean timestamp data collected from step 4a was collated in a new dataset for each animal, and an average ΔF at each timestamp per animal was calculated (Fig. 4.7, step 5a). A mean ΔF (+/- SEM) for each genotype was subsequently calculated. This data was used to produce a graph to visualise the average response at each second of stimulus for C57BL6/J and *App*^{NLGF} animals. To obtain a mean overall stimulus ΔF for each animal, from the mean timestamp dataset described above, a total mean ΔF for the entire stimulus period for each animal was calculated (Fig. 4.7, step 5b). This data was inputted into SPSS to compare the mean overall stimulus-induced ΔF between C57BL6/J and *App*^{NLGF} animals.

As the stimuli presented to the animal during the experiment consisted of different stimuli orientations on the LCD screen, the VBA code from step 4a was amended to

calculate an average normalised ΔF at each stimulus timepoint for each individual orientation (Fig. 4.7, step 4b). As the Excel spreadsheets generated in step 2e contained 1 row of ΔF values per stimulus trial, and although the trials were presented in a random order to the animal, the outputted spreadsheet was arranged in the original order of the stimulus design, it was known which row corresponded to which trial. Therefore, a VBA loop macro was designed to take an average ΔF at each stimulus timepoint for all trials presenting orientations 1, 2, 3, and 4 separately (Appendix 3). For example, if rows 1-4 represented trials that presented stimulus orientation 1 to the animal, the ΔF at each stimulus timepoint across these 4 trials was averaged. For each orientation, the average ΔF at each timestamp was normalised by the total 2s of baseline ΔF immediately prior to stimulus, but only from the relevant trials, rather than an average across all 24 trials. As described for the overall stimulus data, the mean ΔF at each timestamp across all cells was averaged, then an average for each genotype at each orientation was calculated to visualise the average timeline of response to each orientation of stimuli (Fig. 4.7, step 5a). The mean overall response to each stimulus orientation for the entire stimulus period was then calculated per animal, as described above (Fig. 4.7, step 5b).

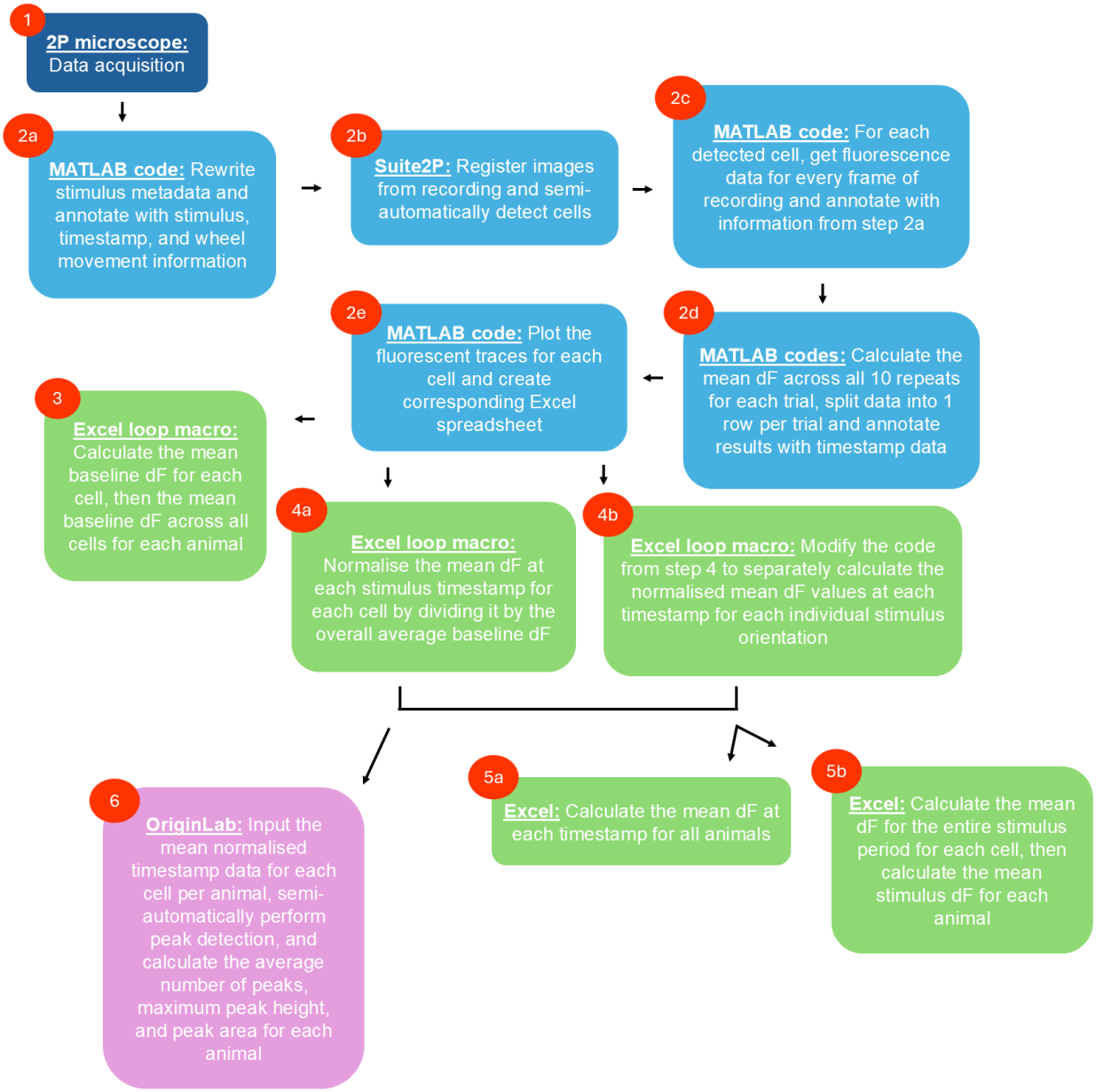

Figure 4.7: Overview of the Calcium Imaging Data Analysis Pipeline. The blue sections (steps 1-2e) indicate methods of analysis from the Sengpiel laboratory. The green sections (parts 3-5b) indicate custom-made codes designed for this thesis. The pink section (step 6) indicates use of OriginLab technology for this thesis.

In addition to the levels of Ca^{2+} fluorescence, the properties of Ca^{2+} peaks during visual stimulation were also analysed. For each cell, the total number of peaks, maximum peak height, and mean area under the curve (AUC) during the stimulation period was determined, then an average of each value was calculated for each animal. These measures capture key aspects of Ca^{2+} dynamics: the total number of peaks reflects neuronal firing rates, the maximum peak height indicates the peak intensity of neuronal activation, and the AUC captures both the magnitude and

duration of Ca^{2+} transients. These measures have previously been used in the analysis of two-photon imaging data from mouse models of neurodegenerative diseases (Overk et al., 2015; Reznichenko et al., 2012).

To perform peak analysis, the datasets containing the average ΔF at each stimulus timestamp per cell (generated from steps 4a and 4b, Fig. 4.7), were inputted into OriginLab 2023 and semi-automatic peak detection was performed. To visualise Ca^{2+} peaks, a graph was plotted for one random cell, and using the peak integration tool, the parameters for automatic peak detection were defined. This included setting the baseline to 1 (as all data that underwent peak detection was normalised to 1), detecting local maximum changes of 20% of the height of the baseline (i.e., identifying peaks as Ca^{2+} fluctuations with at least 1 peak datapoint at a minimum of 1.2 a.u.), and filtering by positive peaks only (i.e., only those above baseline). The 'find peaks' tool automatically detected the presence of peaks in the sample dataset (Fig. 4.8), which was manually verified before saving the protocol.

The peak integration tool in OriginLab calculated peak area using the trapezoid rule. This method approximates AUC by dividing each peak into small trapezoid segments and calculating the area of each. The total area of each peak was calculated as:

$$AUC = \sum_{i=1}^{n-1} \left[\left(\frac{y_i + y_{i+1}}{2} \right) - 1 \right] * (x_{i+1} - x_i)$$

Where y_i and y_{i+1} are ΔF values at consecutive timepoints x_i and x_{i+1}. The mean of adjacent ΔF values was taken to provide an estimation of the area and the baseline value of 1 is subtracted to ensure only signal above baseline is included in the peak area.

The saved peak analysis protocol was then applied to the batch peak analysis tool in OriginLab, which allowed for the simultaneous detection of peaks for every cell per animal. This was performed for each dataset per animal (the overall mean ΔF at each timestamp, and the average ΔF at each timestamp for each individual orientation of stimulus). 10% of each dataset was manually checked for error prior to recording data. Although rare, the most common error was misidentifying the termination of a peak (i.e., when it had reached baseline or had finished decaying), although any premature termination observed was only in the order of milliseconds. For these datasets, peak identification was manually adjusted to include the entire peak for analysis.

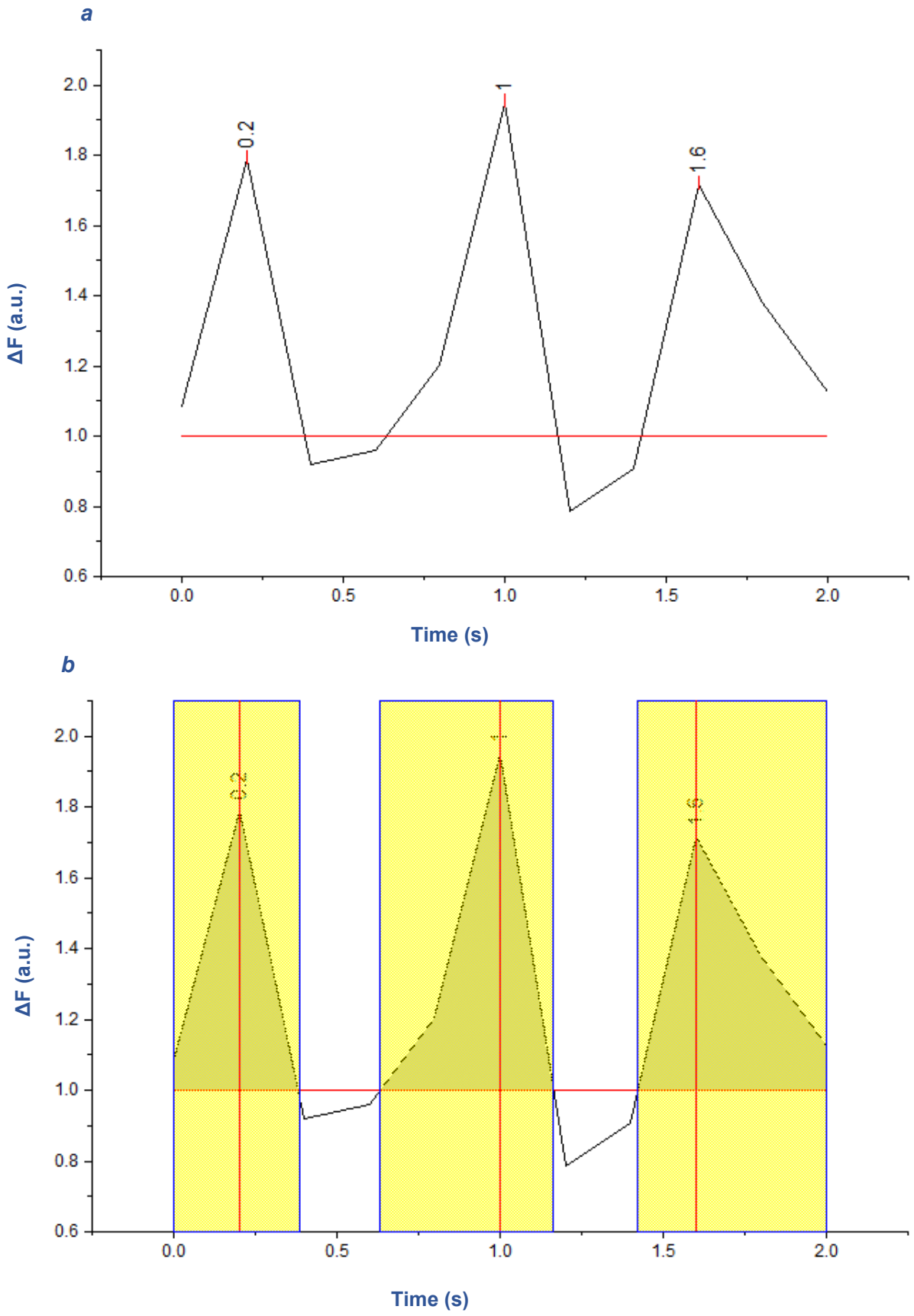

Figure 4.8: Calcium Peak Analysis. Representative images showing calcium peak analysis in OriginLab. ***a)*** Three distinct peaks detected, showing the maximum height of each peak and the baseline (red line) set at 1. ***b)*** The peak areas are automatically calculated, as shown by the grey areas within the yellow peak zones.

4.2.2.4 Statistical Analysis

As described in the General Methods chapter of this thesis, all datasets were checked for the assumptions of parametric testing prior to statistical analysis. This included the Shapiro-Wilk test for normal distribution and the Levene's test for equal variance. Datasets that did not pass these tests ($p < 0.05$) underwent transformation by square root or $\log_{10}$ transformation, depending on the severity of skewness. For datasets that still did not pass parametric assumptions after transformation, alternative non-parametric testing was used. All datasets that underwent two-way mixed ANOVAs were checked for violations of sphericity using Mauchly's test of sphericity. All relevant datasets passed this test ($p > 0.05$).

For analysis of overall stimulus-induced Ca^{2+} responses that are not separated by orientation-specific response, C57BL6/J and *App*^{NLGF} means were compared using unpaired T-tests for parametric data or Mann-Whitney U tests as a non-parametric alternative. For data that was split by the Ca^{2+} response to individual stimulus orientations, i.e., there were within subject repeated measures (orientation), but also between subject measures (orientation and genotype), two-way mixed ANOVAs were performed for parametric data. For non-parametric data, as there is no direct non-parametric alternative to the two-way mixed ANOVA, a Freidman's test to assess the main effect of orientation was performed, followed by separate Mann-Whitney U tests to check for differences in each orientation response between C57BL6/J and *App*^{NLGF} animals. As performing multiple Mann-Whitney U tests can increase type I error rate, the alpha rate was adjusted by Bonferroni correction to help control for this.

4.2.3 Results

4.2.3.1 Overall Calcium Dynamics of the Retrosplenial Cortex at 23 Months of Age

To characterise RSC Ca^{2+} dynamics in 22–23-month-old *App*^{NLGF} and C57BL6/J animals, *in-vivo* two-photon imaging was performed on awake, head fixed mice. For this experiment, 8 C57BL6/J and 9 *App*^{NLGF} animals were used. As described in the Methods section of this chapter, a surgical craniotomy was created and the Ca^{2+}-sensitive dye GCaMP6F was injected into the caudal dysgranular RSC. During imaging, the animal was positioned on a treadmill and exposed to visual stimuli, in the form of circular drifting gratings, on LCD screens positioned to the left and front of the treadmill. As described in the Methods section, each animal was presented with 24 trials of stimuli. The trials consisted of different combinations of 4 different spatial orientations and 2 different spatial positions of the stimulus. Each trial was formed of 2 seconds of stimulus followed by 6 seconds of inter-trial-interval (i.e., the

baseline, or “dark” periods). Each trial was repeated 10 times and an average ΔF for each trial was recorded for each timepoint per cell in the ROI.

4.2.3.1.1 Baseline Calcium Fluorescence

To explore whether there were any differences in resting dysgranular RSC Ca^{2+} levels between C57BL6/J and *App*^{NLGF} animals, the mean fluorescence during the inter-trial-interval period was calculated. This data was normally distributed (Shapiro-Wilk test $p > 0.05$) and exhibited equal variance (Levene’s test $p > 0.05$). An unpaired T-test revealed no significant difference in the average baseline ΔF between C57BL6/J and *App*^{NLGF} animals ($t(15) = 1.946$, $p = 0.0707$, Fig. 4.9).

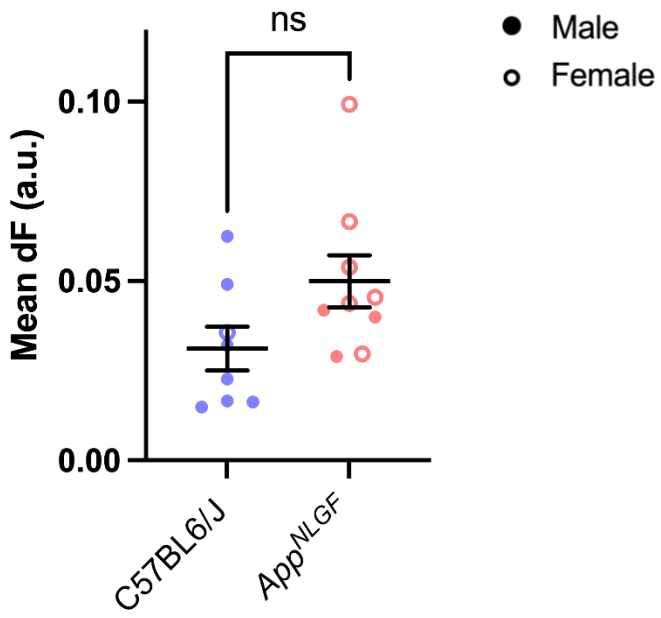

Figure 4.9: Baseline Calcium Activity in the Retrosplenial Cortex. The mean calcium fluorescence (dF) during baseline periods between visual stimuli, in animals aged 22-23 months. Black bars indicate the group mean +/- the standard error of the mean. Results unpaired T-test shown (ns = non-significant). The key indicates animal sex. C57BL6/Js: n = 8. *App*^{NLGFs}: n = 9.

4.2.3.1.2 Stimulus-Induced Calcium Fluorescence

To provide a visual representation of the average Ca^{2+} response of each genotype, the average normalised ΔF (ΔF/F) from all 24 trials at each experimental timepoint was calculated (Fig. 4.10b). Subsequently, for each animal, the total average ΔF/F across all cells was calculated, followed by a total average for each genotype. This data was not normally distributed (Shapiro-Wilk test $p < 0.05$) and exhibited unequal variance (Levene's test $p < 0.05$). As this was not remedied by transformation, a Mann-Whitney U test was performed to compare the mean stimulus Ca^{2+} response between C57BL6/J and *App*^{NLGF} animals. This test revealed that *App*^{NLGFs} exhibited a significantly lower average stimulus-induced Ca^{2+} response compared to C57BL6/J animals ($U = 60$, $z = 2.309$, $p = 0.021$, Fig. 4.10a).

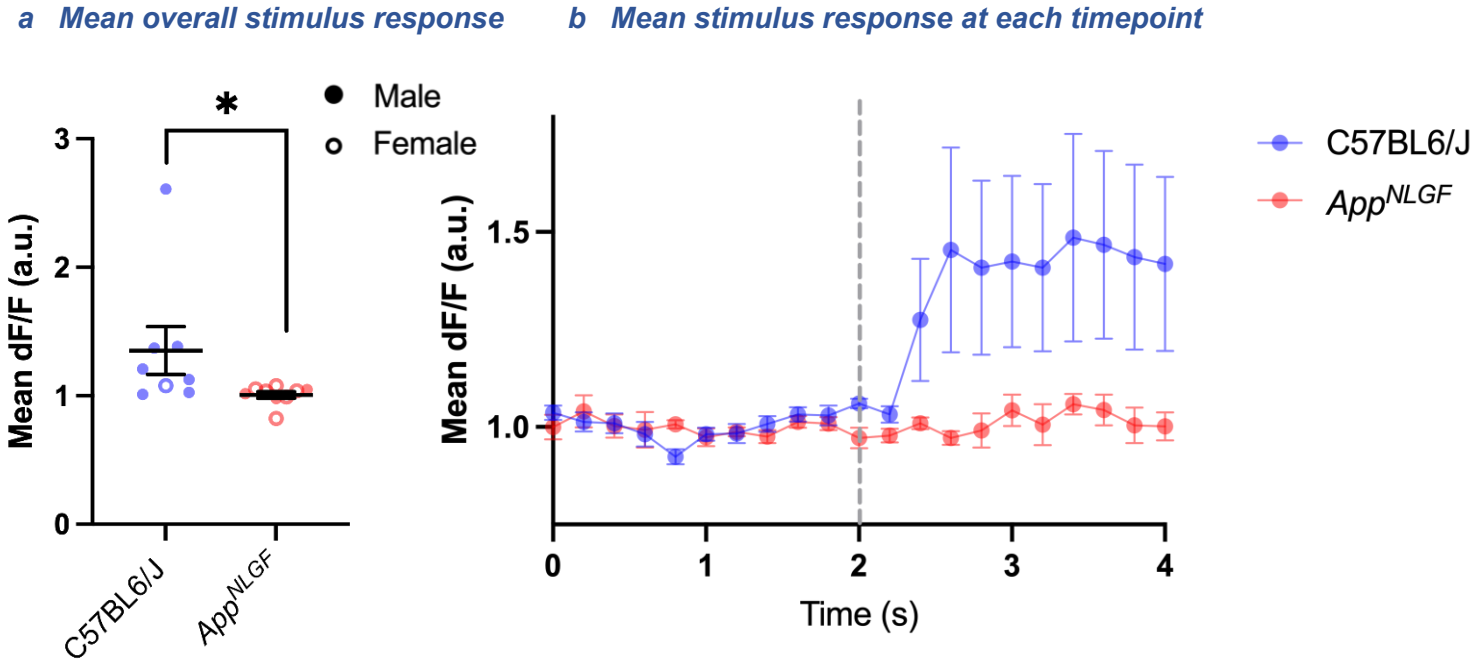

Figure 4.10: Mean Calcium Response to Visual Stimulation. The mean change in calcium fluorescence during visual stimulation, normalised by the mean baseline fluorescence (dF/F), in animals aged 22-23 months. ***a)*** Data points depict the mean dF/F for the stimulus period of each animal, and the black bars indicate the group mean +/- the standard error of the mean. Results from Mann-Whitney U test shown (* = $p < 0.05$). The key indicates animal sex. ***b)*** Data points indicate the mean dF/F at each time point across all animals, with bars representing the SEM. The key indicates animal genotype. C57BL6/Js: n = 8. *App*^{NLGFs}: n = 9.

4.2.3.1.3 Calcium Peak Analysis

To further examine the stimulus-induced Ca^{2+} response of both genotypes, the average ΔF/F at each stimulus timepoint for each cell per animal was inputted into OriginLab 2023, and peak analysis was semi-automatically conducted as described in the Methods section of this chapter. For each cell per animal, total number of peaks, average maximum peak height, and average peak area, were derived from the average ΔF/F data. Subsequently, the average of each measure was calculated across all cells per animal.

The data for the mean number of peaks exhibited normal distribution (Shapiro-Wilk test $p > 0.05$) and equal variance (Levene's test $p > 0.05$). An unpaired T-test revealed that *App*^{NLGFs} exhibited significantly fewer Ca^{2+} peaks on average during presentation of the visual stimuli ($t(15) = 4.432$, $p = 0.0005$, Fig. 4.11a). The data for the mean maximum peak height was not normally distributed (Shapiro-Wilk test $p < 0.05$) and exhibited unequal variance (Levene's test $p < 0.05$). As this was not remedied via transformation, a Mann-Whitney U test was performed to examine the difference between the mean maximum Ca^{2+} peak heights during visual stimulation between C57BL6/J and *App*^{NLGF} animals. *App*^{NLGFs} exhibited significantly lower maximum peak heights compared to C57BL6/Js ($U = 61$, $z = 2.41$, $p = 0.0152$, Fig. 4.11b). The data for the mean Ca^{2+} peak area also did not meet the assumptions of parametric testing, however it successfully underwent $\log_{10}$ transformation prior to analysis. An unpaired T-test revealed that *App*^{NLGFs} exhibited significantly lower average peak areas compared to C57BL6/J counterparts ($t(15) = 2.542$, $p = 0.0225$, Fig. 4.11c).

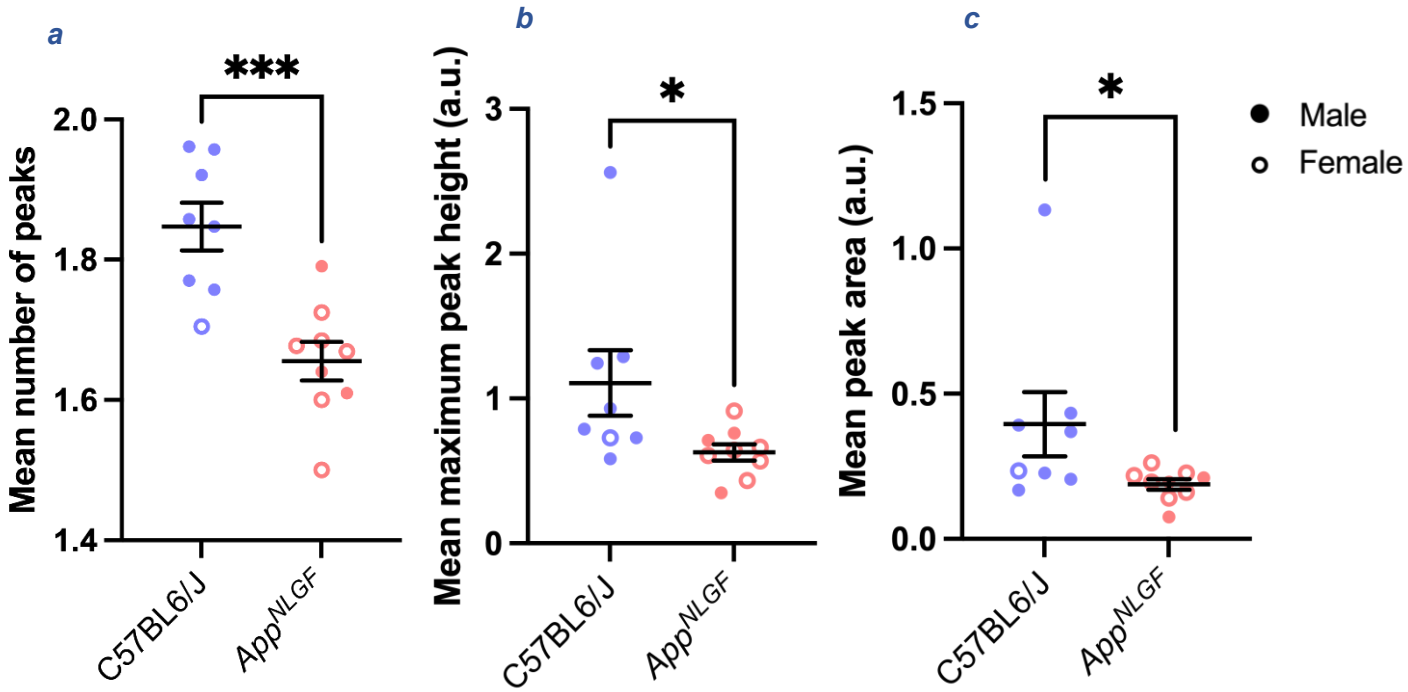

Figure 4.11: Calcium Peak Analysis During Visual Stimulation. a) The mean number of calcium peaks, ***b)*** the mean maximum peak height (arbitrary units), and ***c)*** the mean peak area (arbitrary units) during a protocol of visual stimulation. Data points indicate the mean for each animal across all stimulus trials, with the black bars representing the group mean +/- the standard error of the mean. Results of unpaired T-test or Mann-Whitney U test shown (* = $p < 0.05$, *** = $p < 0.001$). The key indicates animal sex. C57BL6/Js: n = 8. *App*^{NLGFs}: n = 9.

4.2.3.2 *Orientation-Specific Calcium Activity of the Retrosplenial Cortex at 23 Months of Age*

4.2.3.2.1 Stimulus-Induced Calcium Fluorescence

To determine the individual effects of the different orientations of visual stimuli among the 24 trials, the mean ΔF/F response to each specific stimulus orientation was calculated, as described in the Methods section of this chapter. Mean ΔF/F at each stimulus timepoint for C57BL6/J and *App*^{NLGF} animals is depicted in Fig. 4.12.

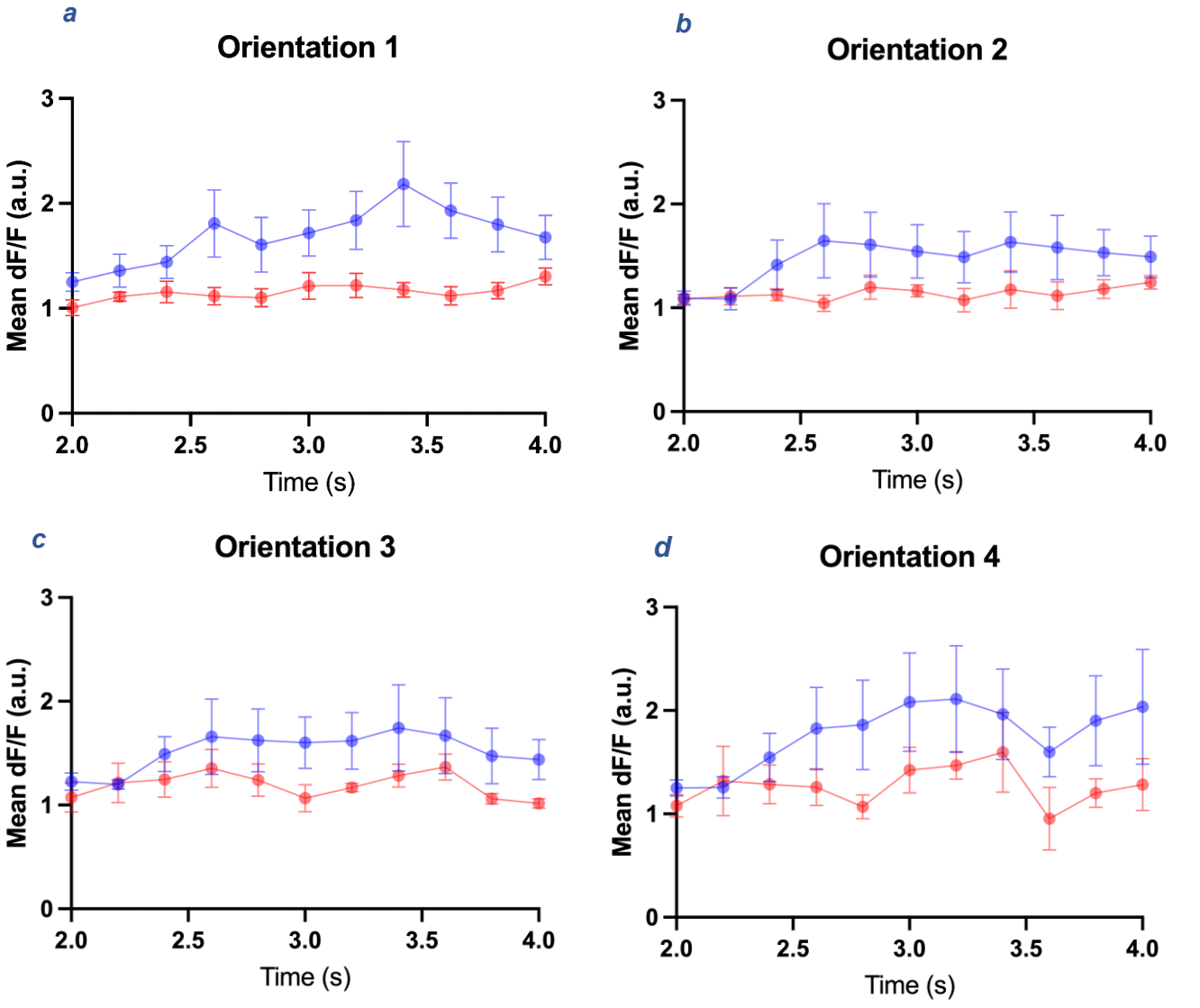

Figure 4.12: Mean Calcium Response to Visual Stimulation at Each Spatial Orientation. The mean change in calcium fluorescence during visual stimulation, normalised by the mean baseline fluorescence (dF/F), in animals aged 22-23 months. Data points indicate the mean dF/F at each time point across all animals, for each relevant stimulus orientation, with bars representing the standard error of the mean. The key indicates animal genotype. C57BL6/Js: n = 8. *App*^{NLGFs}: n = 9.

As with the overall fluorescence data described earlier, the total average ΔF/F during the stimulus period for the trials presenting the relevant orientations was calculated.

The dataset for orientation-specific Ca^{2+} response was not normally distributed (Shapiro-Wilk test $p < 0.05$) and exhibited unequal variance (Levene's test $p < 0.05$). This was not successfully remedied via transformation, so a Friedman test followed by multiple Mann-Whitney U tests were performed as an alternative to the parametric two-way mixed ANOVA. The Friedman test showed no significant differences in the fluorescence response across the different orientations ($\chi^2(3) = 4.412$, $p = 0.220$). As the Friedman ranks the combination of data from C57BL6/J and *App*^{NLGFs}, it could mask any potential differences between genotypes, so interactions of interest were analysed with Mann-Whitney U tests, with the alpha adjusted to 0.0125 by Bonferroni correction. For orientation 1, the Mann-Whitney U test revealed a significant decrease in overall ΔF/F during the stimulus period for *App*^{NLGF} compared to C57BL6/Js ($U = 7$, $z = -2.051$, $p = 0.0037$, Fig. 4.13). For orientations 2, 3, and 4, separate Mann-Whitney U tests showed no significant difference between genotypes (orientation 2: ($U = 21$, $z = -1.144$, $p = 0.1672$), orientation 3: ($U = 19$, $z = -1.245$, $p = 0.1139$), orientation 4: ($U = 14$, $z = -2.072$, $p = 0.0360$), Fig. 4.13).

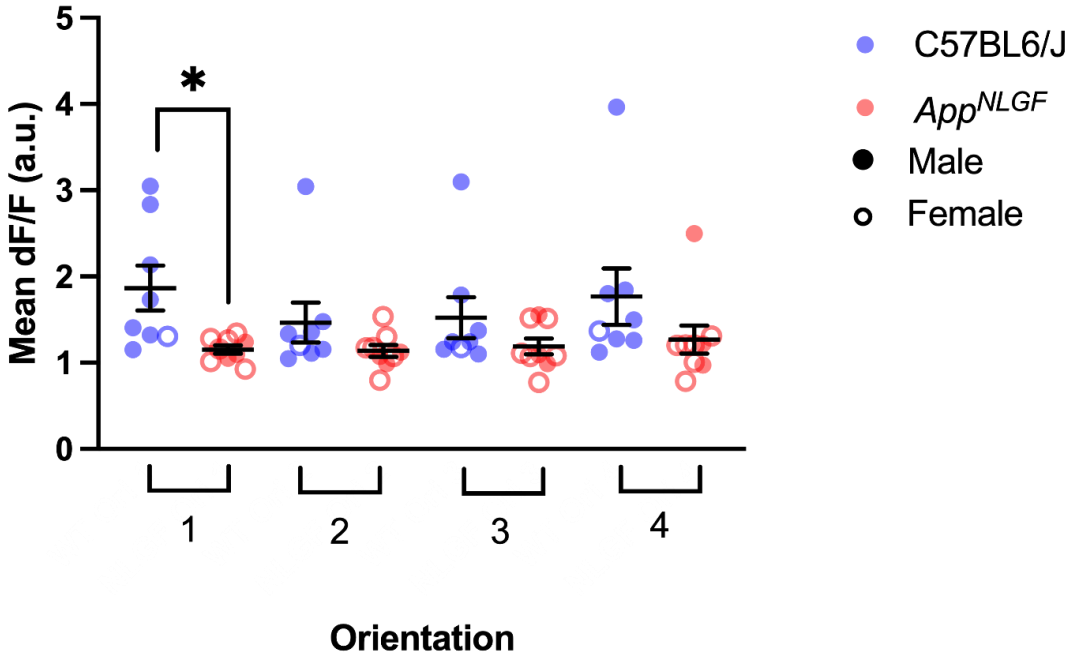

Figure 4.13: Orientation Specific Calcium Response to Visual Stimulation. The mean change in calcium fluorescence during visual stimulation, normalised by the mean baseline fluorescence (dF/F) at each stimulus orientation, in animals aged 22-23 months. Data points indicate the mean dF/F for each animal, with the black bars representing the group mean +/- the standard error of the mean. Significant result of Mann-Whitney U test shown (** = $p < 0.01$). The key indicates animal genotype and sex. C57BL6/Js: n = 8. *App*^{NLGFs}: n = 9.

4.2.3.2.2 Calcium Peak Analysis

As with data averaged across all trials, data separated by orientation was also inputted into OriginLab 2023 for peak analysis.

This data exhibited equal variance (Levene's test $p > 0.05$) but was not normally distributed (Shapiro-Wilk test $p < 0.05$), so a $\log_{10}$ transformation was applied prior to statistical analysis. A two-way mixed ANOVA revealed a significant main effect of genotype on the overall average peak number ($F(1, 15) = 9.952$, $p = 0.007$, $\eta p^2 = 0.399$). The main effect of orientation was not significant ($F(3, 45) = 0.864$, $p = 0.467$, $\eta p^2 = 0.054$), and the interaction between genotype and orientation was also not significant ($F(3, 45) = 1.089$, $p = 0.363$, $\eta p^2 = 0.068$, Fig. 4.14).

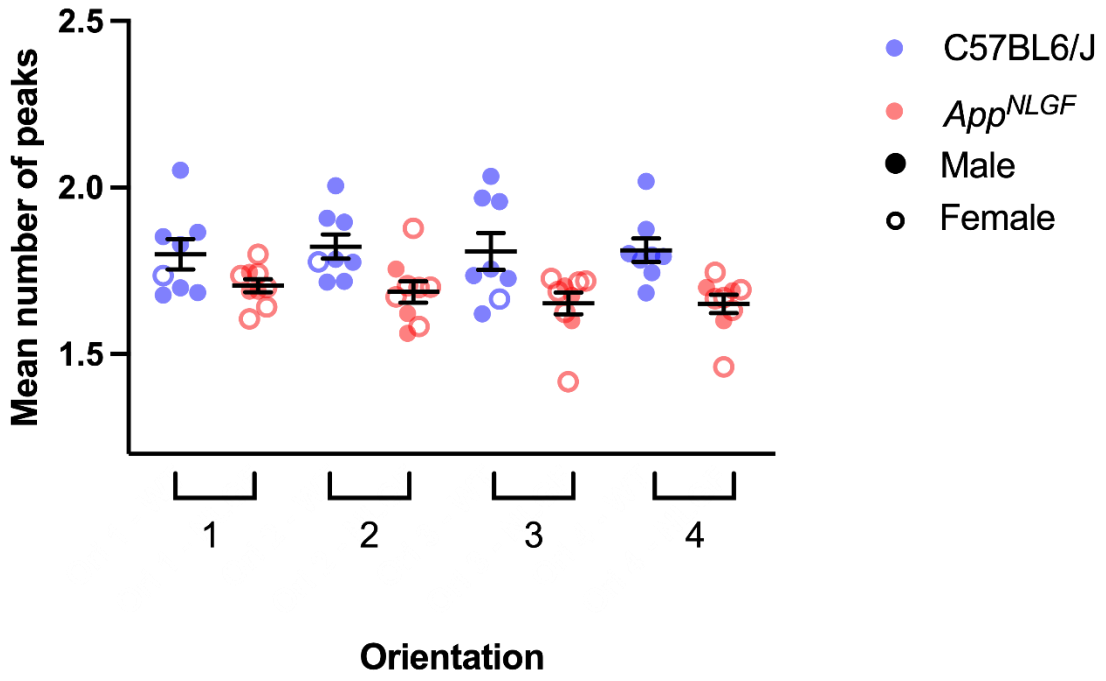

Figure 4.14: Orientation Specific Number of Calcium Peaks. The mean number of calcium peaks during each stimulus orientation, in animals aged 22-23 months. Raw (untransformed) data shown, with data points indicating the mean for each animal and the black bars representing the group mean +/- the standard error of the mean. The key indicates animal genotype and sex. C57BL6/Js: n = 8. *App*^{NLGFs}: n = 9.

The mean maximum peak height was also calculated for each cell per animal, then averaged for each animal. The data for orientation-specific mean maximum Ca^{2+} peak height exhibited equal variance (Levene's test $p > 0.05$) but was not normally

distributed (Shapiro-Wilk test $p < 0.05$). This data therefore underwent $\log_{10}$ transformation prior to statistical analysis. A two-way mixed ANOVA revealed a non-significant main effect of genotype ($F(1,15) = 2.848$, $p = 0.112$, $\eta p^2 = 0.160$). The main effect of orientation was also not significant ($F(3,45) = 3.278$, $p = 0.055$, $\eta p^2 = 0.431$). The genotype*orientation interaction was not significant ($F(3,45) = 0.422$, $p = 0.738$, $\eta p^2 = 0.027$) (Fig. 4.15)

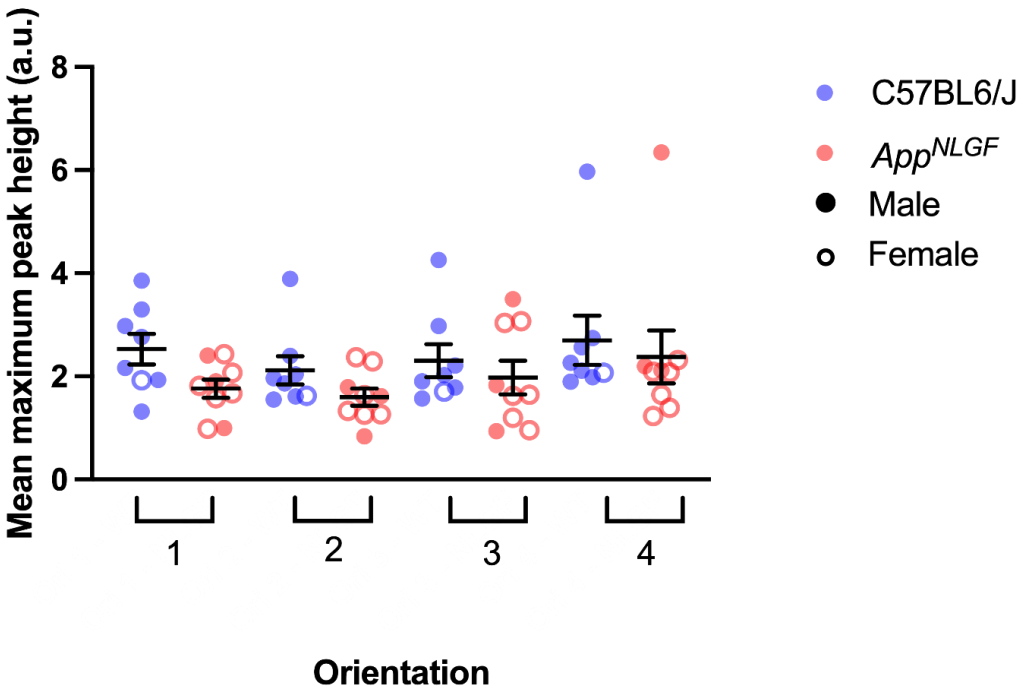

Figure 4.15: Orientation Specific Maximum Calcium Peak Height. The mean maximum calcium peak height during each stimulus orientation, in animals aged 22-23 months. Raw (untransformed) data shown, with data points indicating the mean for each animal and the black bars representing the group mean +/- the standard error of the mean. Key indicates animal genotype and sex. C57BL6/Js: n = 8. *App*^{NLGFs}: n = 9.

The mean peak area was also calculated for each cell per animal, and an average for each animal was determined. The data for orientation-specific Ca^{2+} peak area exhibited equal variance (Levene's test $p > 0.05$) but was not normally distributed (Shapiro-Wilk test $p < 0.05$). The dataset therefore underwent log_{10} transformation. A two-way mixed ANOVA revealed a non-significant main effect of genotype ($F(1,15) = 3.218$, $p = 0.093$, $\eta p^2 = 0.177$). The main effect of orientation was also not significant ($F(3,45) = 1.579$, $p = 0.207$, $\eta p^2 = 0.095$). The genotype*orientation interaction was also non-significant ($F(3,45) = 0.540$, $p = 0.658$, $\eta p^2 = 0.035$, Fig. 4.16).

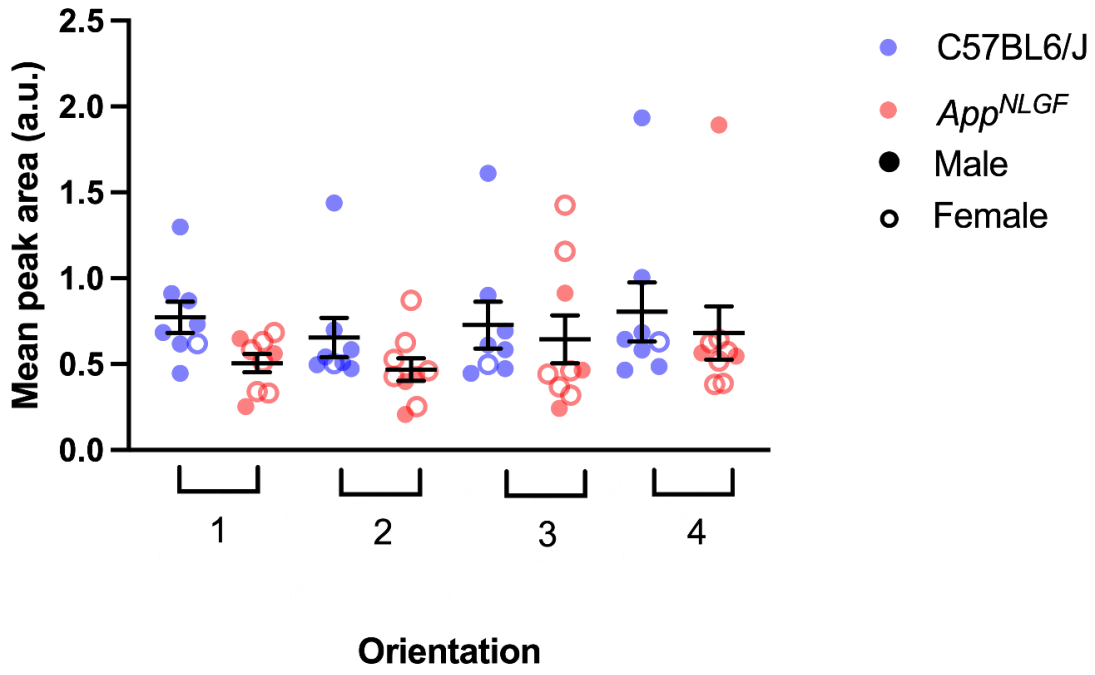

Figure 4.16: Orientation Specific Calcium Peak Area. The mean calcium peak area during each stimulus orientation, in animals aged 22-23 months. Raw (untransformed) data shown, with data points indicating the mean for each animal and the black bars representing the group mean +/- the standard error of the mean. The key indicates animal genotype and sex. C57BL6/Js: n = 8. *App*^{NLGFs}: n = 9.

4.2.4 Discussion

4.2.4.1 Overview

A large body of clinical and experimental evidence highlights the role of the RSC in in spatial cognition and navigation, with strong evidence also indicating early metabolic, structural, and pathological changes of this brain region in AD (Aggleton et al., 2016). However, in AD research, experimental evidence surrounding the RSC is dominated by transgenic models and as such, very little is known about the function of the RSC in newer models such as the *App*^{NLGF}. Furthermore, it is well established that neuronal Aβ deposition results in Ca^{2+} toxicity both *in vitro* and *in vivo* (Cascella & Cecchi, 2021). *App*^{NLGF} mice exhibit RSC amyloid pathology at 12 months of age (Mehla et al., 2022), however, it is unknown to what extent Aβ deposition specifically influences Ca^{2+} activity in the RSC. Therefore, two-photon Ca^{2+} imaging of the RSC was performed on awake, head-fixed *App*^{NLGF} mice at 22-23 months old.

Owing to its strong connectivity to the visual cortex, the dysgranular RSC can be experimentally stimulated using visual stimuli such as drifting gratings (Powell et al., 2020). For this thesis, LCD screens were used to present different trials of visual stimuli to the animal. Each trial consisted of 2 seconds of drifting gratings followed by 6 seconds of black screen, each repeated ten times in a random order. The gratings were presented to the animal at orientations of 0°, 45°, 90°, and 225° (orientations 1, 2, 3, and 4, respectively). A pipeline of analysis was then performed to compare baseline Ca^{2+} levels between C57BL6/J and *App*^{NLGF} animals, as well as overall stimulus and stimulus-specific Ca^{2+} responses.

4.2.4.2 Baseline Calcium Levels

Firstly, to examine the differences in baseline Ca^{2+} levels between *App*^{NLGF} and C57BL6/J animals, a custom-made code was designed to calculate the average ΔF of each cell during the final 2 seconds of black screen, and a mean baseline ΔF was calculated for each animal. *App*^{NLGF} mice at 22-23 months exhibited slightly elevated baseline Ca^{2+} levels compared to age-matched C57BL6/Js, although this difference was not statistically significant. The elevated resting levels of RSC Ca^{2+} in aged *App*^{NLGFs} suggests a possible increase in the concentration of Ca^{2+} ions in the resting state of the neurons, potentially indicating impairments in the function of Ca^{2+} channels, pumps, and buffers that maintain tight homeostatic control of Ca^{2+} concentration (Joshi et al., 2023). Although this result was non-significant, even minor changes in intracellular resting Ca^{2+} levels may result in altered cellular processes such as neurotransmission and cell survival, and if prolonged, may result in neuronal toxicity and cell death (Cascella & Cecchi, 2021). However, the

numerically elevated resting Ca^{2+} levels observed here contrasts with data from Busche et al., (2008), which showed overall reduced baseline Ca^{2+} activity in the cortical neurons of the APP23xPS45 model at 6-10 months old. However, since the APP23xPS45 mouse is a transgenic model that overexpresses both mutant *APP* and *PSEN1*, the observed difference may be attributed to the additional effect of mutant *PSEN1* and/or the molecular artefacts produced from transgenic overexpression of *APP* (Sasaguri et al., 2022). Furthermore, the substantially younger age of the animals in the Busche study compared to the animals in this thesis may account for inherent differences in neuronal activity. There is evidence from whole cell patch clamp recordings that aging alone increases neuronal Ca^{2+} currents in brain slices and isolated neurons (Campbell et al., 1996; Moore et al., 2023; Raza et al., 2007; Thibault & Landfield, 1996). Therefore, the C57BL6/Js at 22-23 months in this study may have exhibited elevated Ca^{2+} levels, thus any mutant *App*-mediated hyperactivity in the App^{NLGFs} may have been difficult to detect. Importantly, one key limitation of this study is that younger cohorts of App^{NLGFs} were not imaged due to long-term technical issues with the two-photon equipment. Future work should therefore perform two-photon Ca^{2+} imaging of the RSC in several younger cohorts of App^{NLGF} mice to determine if any age-related patterns in resting Ca^{2+} activity emerge.

4.2.4.3 Stimulus-Induced Calcium Responses

Next, the stimulus-induced Ca^{2+} responses of 22–23-month-old C57BL6/J and App^{NLGF} animals were examined. To do this, a further custom-made code was designed to average the ΔF during the entire stimulus period for each cell, averaging across all trials, and normalising it by the mean ΔF of the final 2s of baseline. A mean ΔF/F for each animal was then calculated. Statistical analysis revealed that App^{NLGF} animals exhibited significantly lower average Ca^{2+} response to the visual stimuli compared to C57BL6/Js. When visualising the average timeline of response between both genotypes (Fig. 4.10b), App^{NLGFs} were consistently below C57BL6/Js. Normalisation of fluorescence data adjusted the ΔF values to show changes relative to the baseline level (1), therefore any values above 1 indicated a response to the stimuli. As the average response of App^{NLGFs} was only marginally above 1 (1.01 a.u.), significantly lower than the average response of C57BL6/Js (1.35 a.u.), this may indicate a deficit in visual stimulus induced activity in the RSC in App^{NLGFs} at 22-23 months. As discussed in Chapter 3 of this thesis, behavioural data from a different cohort of 22–23-month App^{NLGFs} showed intact novelty detection during the ON task, thus a deficit in the neural systems responsible for vision is not a likely explanation for the lack of response to visual stimuli during the imaging experiment. Therefore, the very minimal Ca^{2+} response observed in App^{NLGFs} could suggest a potential deficit in the strength of the signals received by the RSC or the ability of the RSC to process visual information from the visual cortex. As previously discussed, the RSC is thought to integrate external visual cues with spatial memory to construct a cognitive map of the environment, enabling an internal sense of direction or position that guides behaviour, such as navigating through an environment by

recalling specific landmarks (Alexander et al., 2023). RSC function is typically implicated in T-maze navigation when intra- and extra-maze cues are put in conflict (Nelson et al., 2015; Pothuizen et al., 2008; Vann & Aggleton, 2004; Vann et al., 2003). Therefore, the deficit observed in the standard spontaneous alternation task at 22-23 months (Chapter 3) is unlikely to solely reflect RSC dysfunction. However, the impairments in discriminating the repositioned object in the OL test, a task shown to require RSC function (Ennaceur et al., 1997; Parron & Save, 2004), may reflect disruptions in RSC Ca^{2+} dynamics, as demonstrated in this chapter.

Cells display distinct Ca^{2+} transient frequencies, amplitudes, and durations depending on the underlying cellular event (Berridge et al., 2000). As such, examining the relative changes in Ca^{2+} intensity alone offers a limited view of RSC function in the *App*^{NLGF} model. To gain deeper insight, this thesis employed peak analysis to characterise RSC Ca^{2+} responses to visual stimuli in greater detail. Firstly, to reflect the frequency of Ca^{2+} transients during presentation of the drifting gratings, the average number of peaks was calculated. *App*^{NLGFs} exhibited significantly fewer average number of peaks compared to C57BL6/J animals. Although the difference was not numerically large (C57BL6/J = 1.85, *App*^{NLGF} = 1.66), the reduced number of Ca^{2+} transients during the 2-second stimulus presentation per trial may still have meaningfully affected synaptic function. For example, even subtle reductions in Ca^{2+} peak frequency may decrease neurotransmitter release, disrupt synaptic plasticity, and impair network communication, ultimately compromising memory function. However, it may be argued that within the 2-second stimulus period, there was a limited number of possible Ca^{2+} events that could have occurred, despite any inherent differences in Ca^{2+} activity between genotypes. Therefore, future work could adapt the stimulus protocol to increase the stimulus period from 2 seconds to 10 seconds, for example, to enhance the quality of the observed difference in peak numbers between the genotypes.

The mean number of Ca^{2+} peaks observed during stimulus response does not fully capture the entirety of any potential Ca^{2+} insult to the cell. For example, although *App*^{NLGFs} exhibit significantly fewer peaks than C57BL6/Js, this measure alone does not account for the maximum intensity of Ca^{2+} load the cells experience at any one time following stimulation. Therefore, the average maximum peak height from each cell was determined using OriginLab, and the mean maximum peak height per animal was calculated. At 22–23 months, the average maximum Ca^{2+} response in *App*^{NLGF} mice was significantly lower than in C57BL6/J controls, with peak amplitudes in *App*^{NLGFs} reaching just over half the magnitude observed in controls (C57BL6/J = 1.11 a.u., *App*^{NLGF} = 0.63 a.u.). Taken with the reduced average number of peaks, it may be concluded that *App*^{NLGFs} exhibited significantly fewer visual stimuli-induced Ca^{2+} responses in the RSC compared to C57BL6/Js, and the maximum responses of *App*^{NLGFs} were significantly lower in amplitude compared to C57BL6/Js. This data partially aligns with data from a recent study by Inayat et al.,

(2023). Using two-photon Ca^{2+} imaging of the CA1 in the hybrid A-TG model (*App*^{NLGF} x GCaMP cross) with a running-based stimulus task, this study also observed lower amplitude Ca^{2+} transients compared to C57BL6/J x GCaMP controls (Inayat et al., 2023). However, in contrast to this thesis, more frequent neuronal firing was observed (Inayat et al., 2023). Interestingly, the effect of weaker but more frequent firing was more pronounced when the animals were running on the treadmill, when compared to still periods (Inayat et al., 2023). In line with the Inayat study, Takamura et al., (2021) also observed an increase in the number of transients in the CA1 of a similar KI hybrid model (AD-G-CaMP7 mice), and Busche et al., (2008) also observed a similar increase in the cortex of the APP23xPS45 transgenic model. Interestingly, an *in vivo* two-photon study of the motor cortex of APPswe/PS1dE9 mice revealed significantly lower Ca^{2+} levels while not moving, but significantly increased amplitude and duration of Ca^{2+} transients while running compared to C57BL6/Js, corresponding with decreased sizes of dendritic spines (Bai et al., 2017). The contrast between the results of this thesis and that of the wider literature could be accounted for by a number of different factors that affect neuronal Ca^{2+} dynamics. For example, the above studies use transgenic or *App*^{NLGF} *x GCaMP* hybrid models, and it is unknown what the effect of transgenes is on factors such as the number of Ca^{2+} transients. Furthermore, the above studies focus on the HPC or general cortical regions and do not specifically focus on the RSC, therefore the brain areas examined may exhibit specific patterns of Ca^{2+} transients that are distinct from RSC activity. Additionally, in the above studies, the experimental animals are of a maximum of 13 months, and as with resting Ca^{2+} levels discussed previously, age may also have an inherent effect on Ca^{2+} transient frequency. Nevertheless, as discussed earlier, lengthening the stimulus period may provide a future avenue to more accurately determine peak frequency in *App*^{NLGF} mice. Furthermore, the nature of neuronal Ca^{2+} transients appears to be highly dependent upon the movement of the animal. As this thesis analysed only periods when the animal remained still, future studies could adopt a movement-based paradigm, such as that used by Inayat et al., (2023), to investigate whether any locomotion-specific alterations in RSC Ca^{2+} activity occur in *App*^{NLGFs}*.*

An additional peak characteristic analysed in this thesis was peak area. Peak area refers to the total fluorescent signal encompassed by the Ca^{2+} peak and indicates both the overall intensity and the duration of fluorescence response. *App*^{NLGFs} exhibited significantly lower mean peak areas compared to C57BL6/Js. This suggests that the average Ca^{2+} response in *App*^{NLGFs} was both weaker and of shorter duration, indicating that the total amount of Ca^{2+} exposure in the retrosplenial neurons of *App*^{NLGF} animals was significantly lower than that of C57BL6/Js. Coinciding with the significantly lower overall fluorescent response, the above results from peak analysis suggests that, in the *App*^{NLGF} model, neurons in the RSC were not firing as frequently, robustly, or for as long as C57BL6/J controls, indicating an overall diminished response to visual stimuli. However, the current method of analysis does not clarify whether the observed reduction reflects fewer responsive cells in the RSC or a general decrease in response magnitude across the population.

Takamura et al., (2021) observed a decline in the number of active neurons with age in AD-G-CaMP7 mice, so it may be hypothesised that *App*^{NLGF} animals in this thesis similarly exhibited a reduced number of active neurons which may account for the dampened response to visual stimuli. To test this hypothesis, future analysis could categorise each cell as responsive or non-responsive, and the number of each could be compared. From the responsive cells, further downstream analysis could be performed to quantify the intensity of response. This would determine whether *App*^{NLGFs} exhibit fewer responsive cells, or the same number of responsive cells but overall weaker responses. Furthermore, one key limitation of peak detection using OriginLab is that, due to the local maximum method of detection that uses one point as a reference to detect peaks, peaks that do not have one maximum point (e.g., double pointed peaks or peaks that plateau before decay) may not have been detected in analysis, and therefore not included for each measure of peak characteristic. Therefore, future work could create a more sophisticated peak detection protocol that accounts for variation in peaks, or a smaller subset of neurons could be analysed to allow for manual peak detection based on specific parameters.

Overall, however, the results provide a strong indication of a dampening in stimulus-induced Ca^{2+} response in the *App*^{NLGF} RSC. Along with the slightly increased resting Ca^{2+} levels in the model, this is an interesting and novel finding. It could be suggested that, perhaps due to Aβ-mediated failure of Ca^{2+} clearance mechanisms, elevated resting Ca^{2+} levels result in the dampening of Ca^{2+} response to visual stimuli. For instance, if resting neuronal $[Ca^{2+}]_i$ was elevated, the ability of the neurons to produce a marked Ca^{2+} peak in response to stimuli may have been impaired, affecting the ability of the RSC to process visual information. This may disrupt input to surrounding networks, resulting in less effective transmission of visual information and contributing to navigation and memory deficits observed in this model.

Dampening of Ca^{2+} responses observed in the *App*^{NLGF} model may also indicate Aβ-mediated disruptions of signalling related to LTP. Although the Calcium Hypothesis of AD generally suggests that Aβ induces neuronal Ca^{2+} overload, evidence shows that Aβ can reduce neuronal Ca^{2+} influx by inhibiting VGCCs (Degawa et al., 2021; Joshi et al., 2023; Nimmrich et al., 2008). VGCCs function in low threshold rhythmic Ca^{2+} currents and blocking of these channels inhibits LTP (Izumi et al., 2018; Nevian & Sakmann, 2006). In support of this, a recent study found that oral administration of the drug SAK3 significantly enhanced activity of Cav3.1 and Cav3.3 VGCCs, promoted ACh release in the HPC, and improved cognitive function in 12-month-old *App*^{NLGF} mice (Degawa et al., 2021). Enhancing Ca^{2+} currents in AD models may appear paradoxical given the evidence of Aβ-mediated Ca^{2+} toxicity, however, it is hypothesised that specifically enhancing VGCCs in AD is cognitively beneficial as it enhances cholinergic signalling and normalises Ca^{2+} currents that restores the

function of LTP (Yabuki et al., 2017). Evidence of altered synaptic plasticity in the *App*^{NLGF} model is further supported by findings from Ni et al., (2023), who reported significantly reduced expression of serine racemase in the RSC of 12-month-old *App*^{NLGFs} (Ni et al., 2023). Serine racemase is the enzyme responsible for converting L-serine to D-serine, an endogenous co-agonist of NMDARs, and is predominantly localised in neurons (Balu et al., 2014). Therefore, these findings suggest diminished NMDAR co-activation in the RSC of *App*^{NLGF} mice, which may underlie the blunted stimulus-evoked Ca^{2+} transients reported in this thesis. Notably, this deficit occurred in the absence of overt neuronal loss in the RSC, indicating early synaptic impairments in the absence of neurodegeneration within the RSC (Ni et al., 2023).

Despite the absence of marked neuron loss in the RSC, 12-month-old *App*^{NLGF} mice exhibited significantly reduced neuronal density in the HPC (Ni et al., 2023). Specifically, previous work using primary hippocampal cultures derived from *App*^{NLF} mice has demonstrated that $A\beta_{42}$ accumulation leads to a loss of mushroom spines, structures associated with synaptic strengthening and memory storage (Tackenberg et al., 2009), through a cascade of Ca^{2+}-related dysregulation (Zhang et al., 2015). Spine loss was attributed to $A\beta_{42}$-mediated overactivation of metabotropic glutamate receptor 5 (mGluR5), which subsequently elevated ER Ca^{2+} levels, triggering a compensatory downregulation of store-operated Ca^{2+} entry via stromal interaction molecule 2 (STIM2), ultimately reducing cytosolic Ca^{2+} levels and impairing CaMKII activity (Zhang et al., 2015). These synaptic alterations in the *App*^{NLF} model suggest that Aβ-induced Ca^{2+} dysregulation occurs early and may drive synaptic dysfunction prior to overt neurodegeneration. In the present study, *App*^{NLGF} mice, bearing the additional Arctic mutation that accelerates amyloid aggregation (Nilsberth et al., 2001; Sato et al., 2021), exhibited reduced visually evoked Ca^{2+} activity in RSC neurons. This reduction may reflect a similar compensatory response to Aβ-mediated ER Ca^{2+} overload, indicating impairments across broader networks beyond the HPC, consistent with early circuit-level synaptic dysfunction. Indeed, inactivation of the RSC is known to disrupt the stability and spatial coding of hippocampal place cells (Cooper & Mizumori, 2001), suggesting that RSC dysfunction may contribute to concurrent hippocampal impairments in the *App*^{NLGF} model, as suggested by the subtle spatial memory deficits described in Chapter 3.

Overall, the data from this thesis and wider literature suggest that Ca^{2+} dysregulation in AD is not a simple matter of increased or decreased levels of Ca^{2+}, but a dysfunction of the complex mechanisms that tune the fine intracellular Ca^{2+} homeostasis. Interestingly, evidence suggests an early reduction in neuronal Ca^{2+} levels in Parkinson's disease, a progressive neurological disorder affecting movement control (Betzer & Jensen, 2018). This reduction is driven by the activation of SERCA by α-synuclein aggregates in the brain, resulting in excessive Ca^{2+} sequestering by the ER but reduced cytosolic Ca^{2+} levels, initiating neuronal dysfunction pathways that trigger later increases in $[Ca^{2+}]_i$ (Betzer et al., 2018). This,

combined with the data presented here, indicates a potential common effect of Aβ on neuronal Ca^{2+} levels in AD.

Reflecting the complex and opposing effects of Aβ on neuronal Ca^{2+} dynamics, many studies suggest that rather than a uniform increase or decrease in neuronal Ca^{2+} levels, elevated activity is often specifically localised to areas of plaque deposition. For example, several two-photon studies using transgenic models have demonstrated weaker overall neuronal Ca^{2+} activity, but hyperactive neurons in close proximity to Aβ plaques (Busche et al., 2008; Doostdar et al., 2021; Korzhova et al., 2021; Kuchibhotla et al., 2008; Takamura et al., 2021). These papers suggest that there may be a redistribution of neuronal activity within the brain as a response to Aβ deposition which may disrupt neuronal networks involved in memory. For example, localised hyperactivity may be a direct effect of Aβ via the inhibition of glutamate reuptake, or an indirect effect such as Aβ-induced dysfunction of inhibitory neurons (Takamura et al., 2021; Zott et al., 2019). Interestingly, *App*^{NLGF} mice at 7 months also showed a reduced number of active hippocampal place cells, but hyperactivity of the remaining place cells near plaques (Takamura et al., 2021). The analysis in this thesis did not account for localised Ca^{2+} hyperactivity as plaques were not examined in two-photon imaging. Therefore, future work could use staining techniques such as thioflavin to identify plaques in the RSC, allowing specific examination of the effect of distance from plaques on Ca^{2+} activity *in vivo*. It may be hypothesised that the *App*^{NLGF} model also exhibits hyperactive neurons in the vicinity of Aβ plaques, and hypoactive neurons at more distal sites from plaques. Therefore, the approach of this thesis to examine all cells in the imaging ROI without accounting for Aβ locality may have masked the presence of hyperactive neurons in *App*^{NLGFs}.

It may be argued, however, that the Aβ in its plaque state is not necessary for this localised Ca^{2+} hyperactivity. Studies using transgenic mice have demonstrated that soluble Aβ species also induce similar localised Ca^{2+} increases (Bai et al., 2017; Busche et al., 2012). This suggests that Ca^{2+} hyperactivity is very early functional impairment in transgenic AD models, however this is yet to be studied in 2nd generation models. Contrastingly, however, an earlier paper found Ca^{2+} hyperactivity near plaques in aged Tg2576 and APP/PS1 mice but not in younger animals with no plaque deposition (Kuchibhotla et al., 2008). However, this study did not examine the presence of soluble Aβ so it is unclear whether the younger cohort of animals exhibited such pathology. Nevertheless, collective Ca^{2+} imaging data seems to support a complex role of Aβ in Ca^{2+}-mediated neuronal hyperactivity, albeit some may argue the role of soluble Aβ should be emphasised. The rTg4510 model of NFT pathology, however, exhibit functionally intact visual cortex neurons with no significant difference in resting or stimulus-induced Ca^{2+} activity, arguably adding more weight to the importance of the role of Aβ in Ca^{2+} dysregulation in AD (Kuchibhotla et al., 2014).

4.2.4.3.1 Orientation-Specific Calcium Responses

To further interrogate RSC function in the *App*^{NLGF} model, stimulus-specific Ca^{2+} responses were analysed. Neurons of the visual cortex and RSC preferentially respond to certain angles or orientations of visual stimuli in the environment (Glickfeld et al., 2013; Ortiz-Cruz et al., 2022; Powell et al., 2020; Zhang et al., 2017). Orientation selectivity in the RSC may help encode direction of movement by detecting the specific angles of shapes and contours within the environment, allowing animals to interpret visual features whilst navigating their surroundings (Powell et al., 2020). In the visual cortex, differences in orientation selectivity have been linked to deficits in visual processing in behavioural tasks (Goel et al., 2018). It may be hypothesised that alterations in orientation selectivity of the RSC could indicate deficits in interpreting the visual environment and encoding the direction of movement during navigation. However, there is no information regarding the integrity of orientation selectivity in the RSC of *App*^{NLGF} mice. In this thesis, analysis of the average fluorescence response across all stimulus trials may have masked any differences in orientation-specific responses between C57BL6/Js and *App*^{NLGFs}. Therefore, a further analysis protocol was developed to individually calculate the average responses of each individual orientation of stimuli, using the relevant trials only.

When comparing the average normalised response (ΔF/F) to the four different orientations of stimuli, *App*^{NLGFs} exhibited significantly lower average response to orientation 1 compared to C57BL6/J mice, with no significant differences observed in the response to all other orientations. Analysis of Ca^{2+} peaks revealed that *App*^{NLGF} mice exhibited a reduced number of peaks in response to visual stimuli compared to C57BL6/Js across all orientations. Stimulus orientation itself had no significant effect, suggesting that the number of Ca^{2+} peaks in response to visual stimuli did not significantly differ according to the angle of the stimulus presented to the animal. Furthermore, maximum peak heights were consistent across genotypes and stimulus orientations. This suggests that while peak frequency was affected in *App*^{NLGFs}, strength of Ca^{2+} transients were comparable between genotypes when statistically isolating each orientation. Analysis of the mean peak areas in response to the different orientations also indicated that the orientation of stimulus, or the genotype of the animal, did not significantly alter the mean Ca^{2+} peak area. Overall, the above analysis suggests that *App*^{NLGFs} exhibited reduced neuronal firing in the RSC in response to visual stimuli across all orientations, however, when neurons did respond, the strength and duration was broadly maintained across stimuli of each orientation and position.

The dampened dF/F in response to orientation 1 may suggest that *App*^{NLGFs} exhibited impairment in orientation selectivity to orientation 1. This could indicate that the RSC did not effectively respond to or process information from the surroundings, potentially reflecting deficits in the formation of cognitive maps from visual cues to

guide navigation through the environment. Interestingly, it was previously shown that hyperactive neurons in the sensory cortex of APP23xPS45 mice lost orientation and direction selectivity (Grienberger et al., 2012). In the present study, whilst the RSC response in *App*^{NLGFs} was broadly *hypo*active, the analysis did not distinguish between individual subsets of neurons that may have been hypo- or *hyper*active. Therefore, *App*^{NLGFs} may also exhibit a subset of hyperactive neurons responsible for the diminished response to visual stimuli at orientation 1 in this experiment.

Data from orientation-specific responses appears to somewhat contrast the data observed when averaging the responses across all trials. For example, *App*^{NLGFs} consistently exhibited significantly lower means for ΔF/F, number of peaks, maximum peak amplitude, and peak areas compared to C57BL6/J animals when averaging across all stimulus trials (Fig. 4.10, 4.11). However, when the data was split by stimulus orientation, the difference was a lot more subtle. It may be suggested that whilst there were overall differences in these parameters between C57BL6/Js and *App*^{NLGFs} across all stimulus trials, the difference did not generally apply when responses to individual stimulus orientations are considered. The observed difference in the pooled data cohort may be explained by cumulative effects of combining data across all orientations, increasing the number of datapoints used in analysis, which may make small but consistent differences between genotypes more detectable. This is reflected by Figure 4.12, which shows a trend that *App*^{NLGFs} consistently exhibited lower ΔF/F compared to C57BL6/Js. In other words, splitting the data by orientation reduced the number of trials used in analysis and thus may have reduced statistical power and diluted the effect of genotype. It may also be explained by statistical noise or variability within each orientation dataset, a common limitation of fluorescent Ca^{2+} data, as indicated by large SEM bars (Fig. 4.12). For the overall dataset, some of the noise may be averaged out so a clearer picture of genotype differences could be observed.

Overall, these findings provide an initial insight into Ca^{2+} dynamics in the *App*^{NLGF} model, revealing that, contrary to the original hypothesis, Ca^{2+} responses to visual stimuli were diminished. However, future experiments and analyses could be performed to enhance the robustness of this evidence. One crucial limitation of this study was that Ca^{2+} imaging was restricted to the RSC, and so the data offers only a partial view of Ca^{2+} dynamics in the *App*^{NLGF} brain. Future research could address this by utilising “top hat” cranial window surgery to access deeper regions of the brain, such as the HPC. Another major limitation arose from unexpected failure of the two-photon imaging equipment, which prevented imaging of younger cohorts of animals. Consequently, the effect of progressive Aβ deposition on RSC Ca^{2+} dynamics is still unclear. To address these key limitations without relying on two-photon imaging, experience-induced *c-fos* expression, a neural marker of learning and memory, was subsequently assessed in the HPC and RSC of *App*^{NLGFs} at 14-16 months.

4.3 Experiment 2: *c-fos* Expression in the Retrosplenial Cortex and Hippocampus

4.3.1 Introduction

As discussed earlier, synaptic Ca^{2+} influx triggers a process called LTP, which subsequently drives a series of intracellular signalling cascades resulting in gene expression (Schaefer et al., 2017). An example of the genes that have been implicated in LTP processes are IEGs. IEGs are genetic sequences that are rapidly and transiently expressed following a wide variety of stimuli (Barros et al., 2015). *c-fos, egr-1* and *Arc* are examples of common IEGs involved in processing events of learning and memory (Minatohara et al., 2015).

Arguably the most widely studied IEGs is *c-fos*. Following discovery of the *c-fos* gene as the proto-oncogene involved in osteosarcoma development, c-Fos was found in brain tissue after seizures and exposure to noxious stimuli (Curran et al., 1982; Morgan et al., 1987; Saffen et al., 1988). Once detected in the brain, c-Fos was then implicated in learning and memory (Kaczmarek & Nikołajew, 1990; Maleeva et al., 1989; Tischmeyer et al., 1990). Following synaptic-activity induced Ca^{2+} influx, transcription factors such as cyclic adenosine monophosphate (cAMP) response element-binding protein (CREB) are phosphorylated by activated kinases and bind the promotor region of the *c-fos* gene, initiating transcription to mRNA (Hudson, 2018; Lara Aparicio et al., 2022). *c-fos* mRNA is then translated to a 62kDa protein which forms a heterodimer with c-jun to form the Activator-Protein 1 (AP-1) transcription factor complex (Lara Aparicio et al., 2022). AP-1 binds specific sequences in the promotor region of a variety of target genes, regulating their expression (Chiu et al., 1988; Halazonetis et al., 1988; Kouzarides & Ziff, 1988). Importantly, neuronal c-Fos supports synaptic plasticity and neurodevelopment by regulating genes involved in synaptic stability (Velazquez et al., 2015). *c-fos* expression can be detected in the brain by immunostaining neuronal *c-fos* mRNA or c-Fos protein. High levels of c-Fos are indicative of recent neuronal activity and are associated with plasticity of the neuron (Minatohara et al., 2015). c-Fos is therefore widely considered as a marker for neuronal activity derived from learning and memory (Bullitt, 1990; Goelet et al., 1986; Hall et al., 2001; Vann et al., 2000).

Learning induces *c-fos* expression in subsets of neurons within brain regions, with expression patterns that typically reflect the nature and cognitive demands of the task. For example, c-Fos has been detected in rodent HPC following spatial tasks such as the RAM and the T-maze alternation (He et al., 2002; Nagahara & Handa, 1995). Moreover, *c-fos* expression in the RSC is induced by RAM, MWM, ON, and OL tasks (Czajkowski et al., 2014; de Landeta et al., 2020; Milczarek et al., 2018; Pothuizen et al., 2009; Sheppard et al., 2024). Interestingly, studies have suggested

that beyond its role as a marker of neuronal activity, c-Fos contributes towards memory processes. For example, inhibition of HPC *c-fos* expression via administration of antisense oligonucleotides has been shown to impair spatial memory formation during the RAM task (He et al., 2002). Furthermore, mice generated with CNS specific *c-fos* knockout have shown impairments in the MWM task (Fleischmann et al., 2003; Paylor et al., 1994). The behavioural deficits in these mice correlated with electrophysiological evidence of LTP reduction in CA1 and CA3 synapses (Fleischmann et al., 2003). Restoration of hippocampal LTP by tetanisation was blocked by NMDAR specific inhibitor (Fleischmann et al., 2003), suggesting that c-Fos is required for NMDAR-dependent LTP and hippocampal learning.

Perhaps unexpectedly, several studies have shown *c-fos* overexpression in hippocampal slices from AD patients compared to age-matched cognitively healthy patients (Lu et al., 1998; Marcus et al., 1998; Sajan et al., 2007; Zhang et al., 1992). Reflecting this, recent studies have demonstrated neuronal hyperactivity along with increased *c-fos* expression in the visual cortex of 4-6 month pre-plaque human *APP* transgenic mice following light deprivation (L'Esperance et al., 2024; Niraula et al., 2023). Similarly, the pre-plaque *App*^{NLGF} mouse model exhibits significantly more c-Fos positive cells in the CA1 region of the HPC compared to C57BL6/Js, after a “what-where” memory task in which the mice were tested on their ability to retrieve learned associations in an empty arena (Tan et al., 2023). Enhanced *c-fos* expression in some studies may be indicative of Ca^{2+}-mediated cellular stress responses rather than learning and memory. For example, it may indicate neuronal hyperactivity in AD pathogenesis, a neurotoxic phenomenon that has been evidenced in several human and rodent studies (Busche & Konnerth, 2015). Contrastingly, some studies show reduced hippocampal *c-fos* expression in human AD brains (Palop et al., 2003). Several transgenic models of AD also exhibit reduced hippocampal *c-fos* expression, coinciding with deficits in spatial memory tasks (Chin et al., 2005; España et al., 2010; Palop et al., 2005; Palop et al., 2003). Interestingly, in mouse models, reduced c-Fos levels appear to correlate with the relative levels of $A\beta_{40}$ and $A\beta_{42}$ peptides but not plaque load, suggesting that *c-fos* expression is sensitive to the effects of early stage amyloid accumulation that may reflect neuronal dysfunction prior to overt plaque deposition (Palop et al., 2005; Palop et al., 2003). Reflecting this, Poirier et al., (2011) showed downregulated rostral granular RSC *c-fos* expression in pre-plaque Tg2576 mice at 5 months of age, but upregulated *c-fos* expression in the same model at 23 months following exposure to a novel context. The varying patterns of *c-fos* expression across various models of amyloid pathology likely reflect the different stages of amyloid-driven neuronal dysfunction, with pre-plaque increases in c-Fos likely representing an excitotoxic state while early reduction may reflect suppressed neuronal activity or disrupted network function, and later increases potentially reflecting further excitotoxicity or compensatory mechanisms. To date, however, the function of *c-fos* expression in *App*^{NLGF} mice following plaque deposition is unclear, and it is not yet known whether its expression is specifically altered in the RSC of *App*^{NLGFs}.

4.3.2 Methods

4.3.2.1 Introduction

This Methods section outlines the procedures used to assess *c-fos* expression in the RSC and HPC of mid-aged *App*^{NLGFs} and C57BL6/Js following exposure to novel objects. It includes a description of the behavioural task, an overview of the IHC detection of c-Fos protein, and the processing of brain sections for statistical analysis. For full methodological details, please refer to the General Methods chapter.

4.3.2.2 Subjects

A cohort of 40 14–16-month-old *App*^{NLGF} mice and age-matched C57BL6/J controls were obtained from in-house breeding as described in the General Methods chapter of this thesis. 10 *App*^{NLGF} and 10 C57BL6/J mice experienced the 'object exploration' condition. For control conditions, 10 *App*^{NLGF} and 10 C57BL6/J mice experienced the 'home cage' condition, as described below. Each group consisted of exactly equal numbers of male and female mice.

4.3.2.3 Procedure

The procedure for this experiment was adapted from Baumgartel et al., (2018). A small pilot study was performed based on this protocol to validate RSC and HPC *c-fos* expression in young C57BL6/J animals prior to this experiment (Appendix 4). Testing consisted of three consecutive days: on days 1 and 2, the animals were habituated to the OF arena for 10 and 5 minutes, respectively. On the third day, animals were either kept in their home cage (control condition) or exposed to a 10-minute object exploration session, during which two identical objects were placed approximately 15cm from opposing walls of the arena.

Animals were culled by transcardial perfusion immediately from their home cage (control animals) or 30 minutes following object exploration, as described in the General Methods chapter of this thesis. Habituation and experimentation were counterbalanced so that morning and afternoon sessions contained a mixture of genotypes and conditions.

4.3.2.4 c-Fos Detection

To detect c-Fos protein, brains were coronally sliced using a freezing microtome and IHC was performed, as described in the General Methods chapter. Eight brain slices (both hemispheres) were imaged from each animal using a Leica DMRB brightfield microscope with an Olympus DP73 camera. Images were taken at 25X magnification for navigation of the ROI. Once located, images of the ROI were taken at 100X magnification for analysis. The ROIs, the caudal dysgranular RSC (Fig. 4.17) and the CA1 area of the HPC (Fig. 4.18), were found with reference to the Allen Scalable Brain Atlas (Lein et al., 2007). The RSC was located at the following approximate coordinates: M/L (medial/lateral) = +/- 0.4mm, A/P (anterior/posterior from bregma) = -1.9mm, D/V (dorsal/ventral from skull surface) = 4.7mm. The CA1 was found at M/L = +/-2.1mm, A/P = -2.87mm, D/V = 3.3mm.

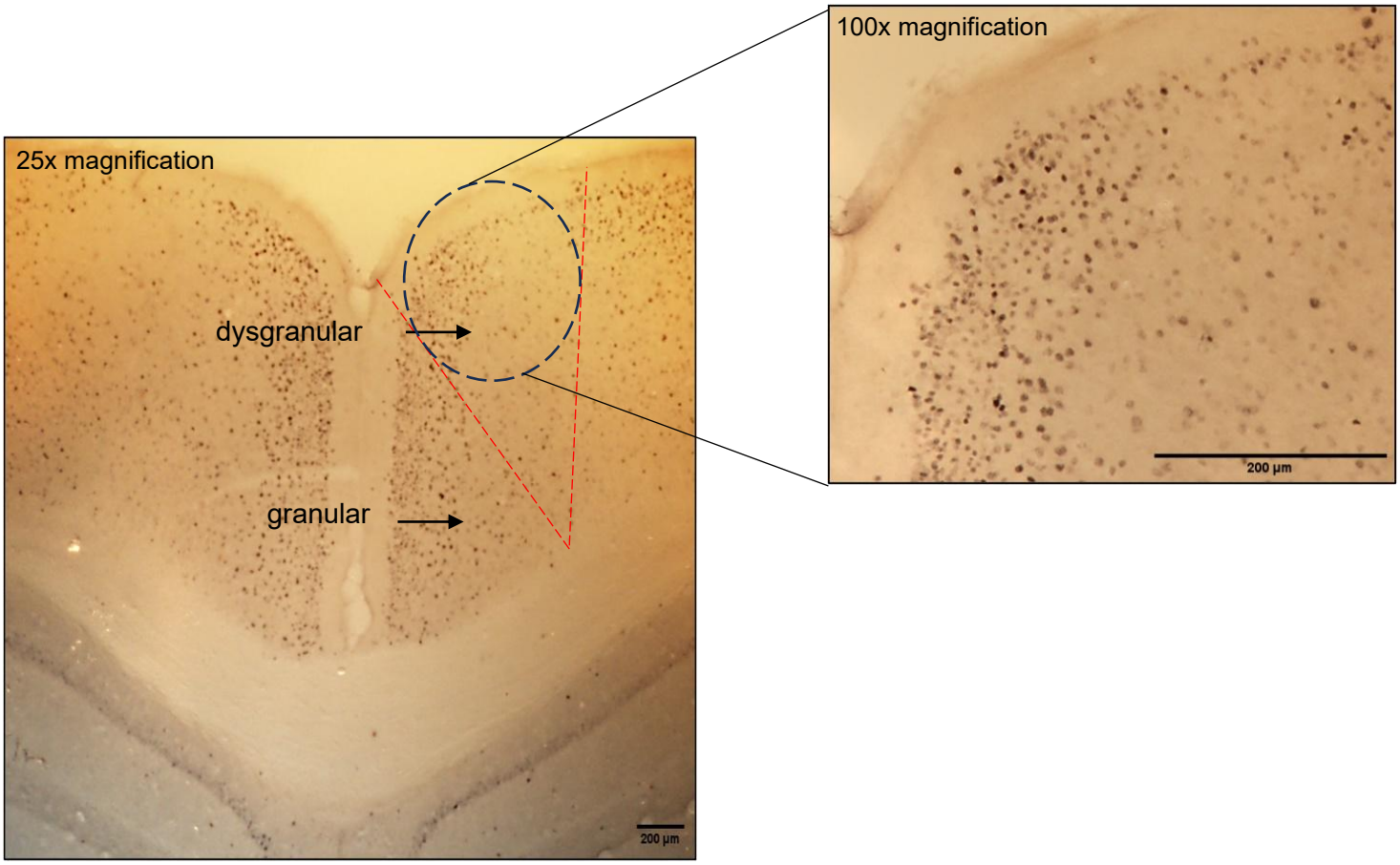

Figure 4.17: Representative Images of c-Fos Staining of the Retrosplenial Cortex. Left: 25x magnification, showing the approximate granular and dysgranular regions of the retrosplenial cortex (separated by red dashed lines). Right: 100x magnification image used for analysis, showing appearance of distinct dark areas stained by anti-cFos. Images taken with Leica DMRB microscope with Olympus DP73 camera. Scale bar = 200µm.

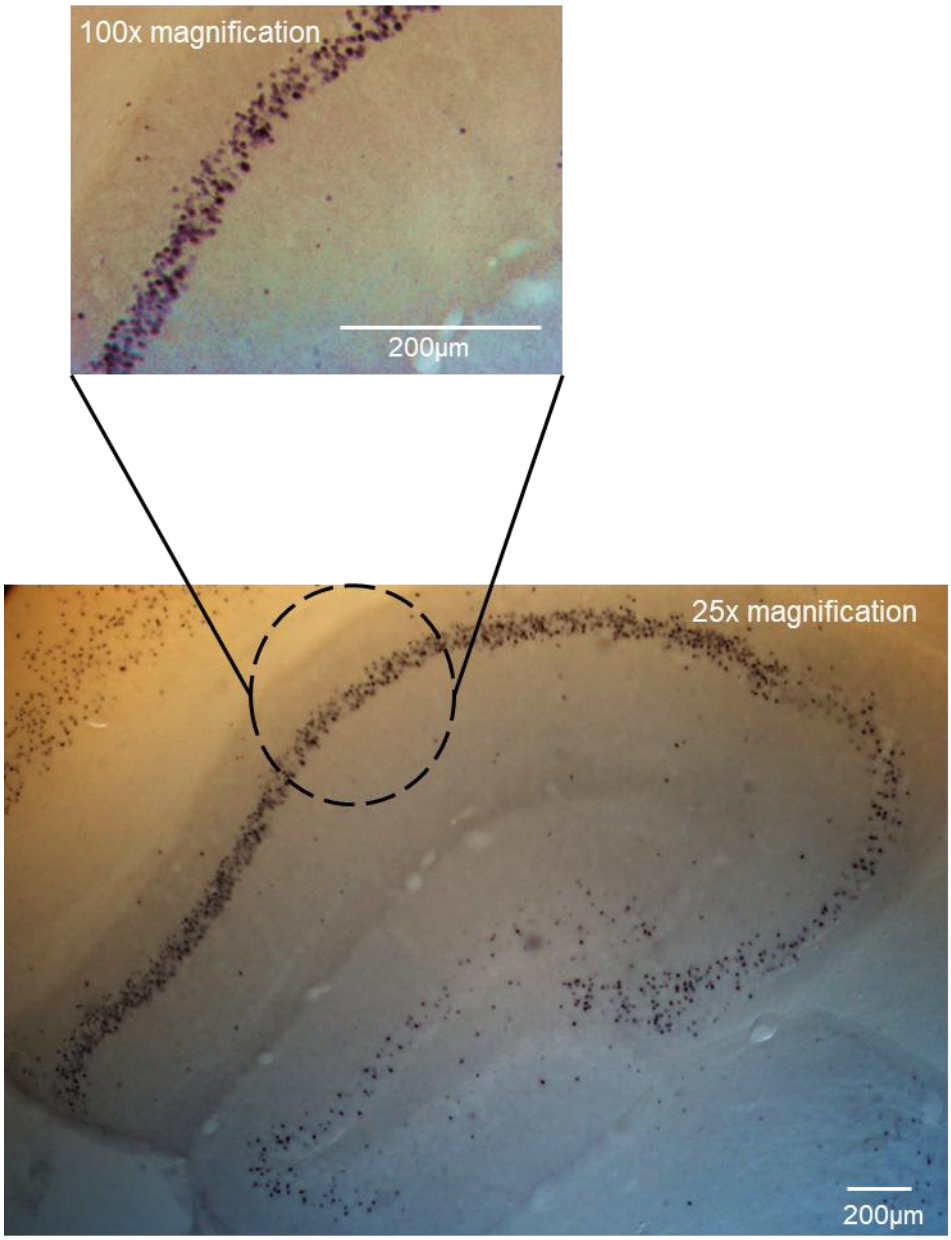

Figure 4.18: Representative Images of c-Fos Staining of the Hippocampus. Bottom: 25x magnification, showing the approximate CA1 region of the hippocampus. Top: 100x magnification image used for analysis, showing distinct c-Fos positive staining. Images taken with Leica DMRB microscope with Olympus DP73 camera. Scale bar = 200µm.

Images were then uploaded to ImageJ (Rasband, 1997-2018). The images were converted to an 8-bit greyscale image, and the contrast was enhanced by 0.5% (Fig. 4.19). The threshold was adjusted to allow all stained areas to appear as white 'dots'; lower and upper threshold values of approximately 100 and 200, respectively, were chosen and adjusted slightly for each image to allow all staining to be distinct (Fig. 4.19). A bounding rectangle of fixed size (300 x 200μM) was positioned over the ROI and the 'analyse particles' function was used to detect the number of c-Fos positive cells (c-Fos count). The 'analyse particles' function identified c-Fos positive cells as white areas with a circularity of 0.3-1% and diameter of 5-10μM (Beretta et al., 2023). The number of c-Fos positive cells was calculated for each hemisphere per slice. A sum of total c-Fos count was calculated for each slice and an average for each animal was calculated. All analysis was performed blind to the genotype and experiment condition.

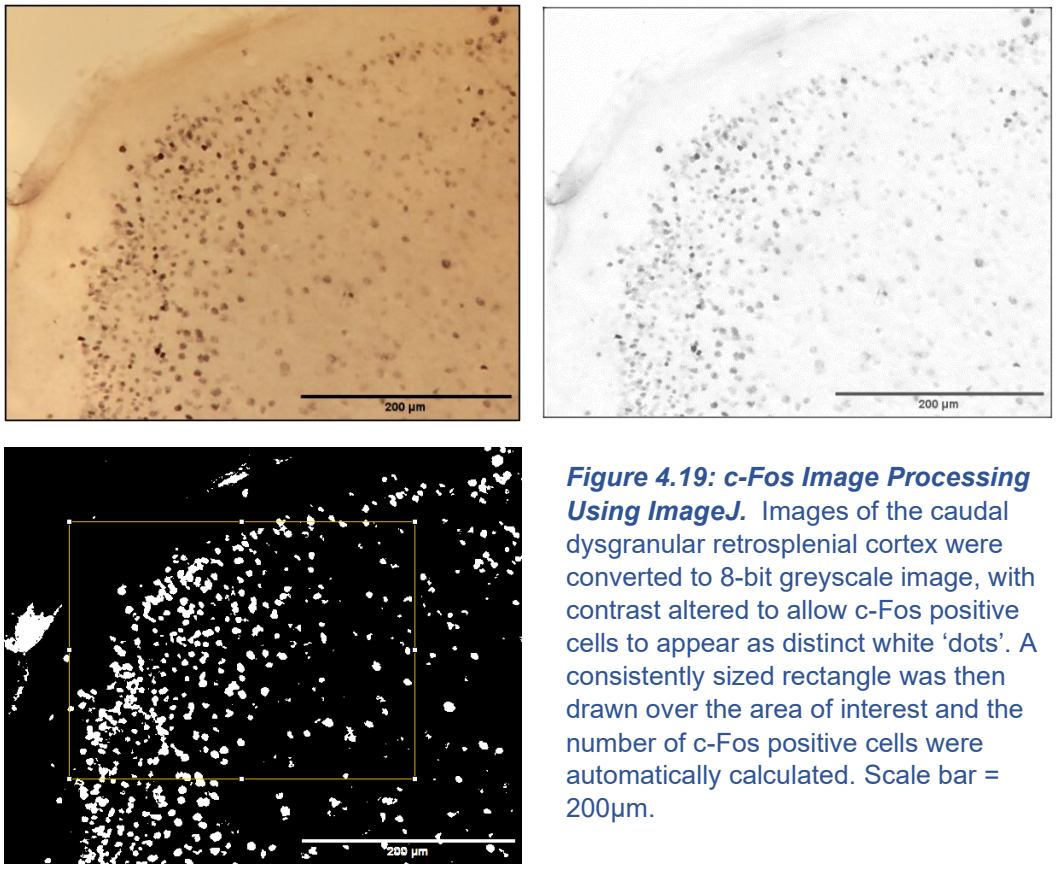

Figure 4.19: c-Fos Image Processing Using ImageJ. Images of the caudal dysgranular retrosplenial cortex were converted to 8-bit greyscale image, with contrast altered to allow c-Fos positive cells to appear as distinct white 'dots'. A consistently sized rectangle was then drawn over the area of interest and the number of c-Fos positive cells were automatically calculated. Scale bar = 200μm.

4.3.2.5 Measuring Exploratory Behaviour

For all animals that underwent the test condition, i.e., investigated two identical objects in an OF arena, exploratory behaviour was measured and compared between genotypes to determine whether any potential differences in RSC or HPC c-Fos could be explained by exploratory differences. As described in the General Methods chapter of this thesis, the time an animal spent actively investigating objects in the arena was manually scored using EthoVision XT13. The total exploration time of both objects was then calculated for each animal. Furthermore, the total distance travelled of each animal in the test condition was automatically calculated by EthoVision XT13.

4.3.2.6 Statistical Analysis

As outlined in the General Methods chapter, all datasets were assessed for normality and homogeneity of variance prior to statistical analysis. Data that met these assumptions were analysed using appropriate parametric tests, such as unpaired t-tests or two-way ANOVA. In cases where assumptions were violated, suitable data transformations were applied, as detailed in the General Methods chapter.

4.3.3 Results

4.3.3.1 c-fos Expression in the Retrosplenial Cortex

As the caudal dysgranular RSC was the focus of Ca^{2+} imaging in the 22–23-month-old cohort, this same region was prioritised for *c-fos* expression analysis following novel object exposure in a mid-aged group, to provide a complementary measure of neuronal activity.

The c-Fos count data for the RSC exhibited equal variance (Levene's test > 0.05) but was not normally distributed (Shapiro-Wilk test < 0.05). The dataset therefore underwent square root transformation prior to analysis. To determine whether object exploration significantly increased *c-fos* expression compared to remaining in the homecage, a two-way ANOVA was performed. The analysis revealed a non-significant main effect of genotype ($F(1, 36) = 0.965$, $p = 0.333$, $\eta p^2 = 0.026$). However, the effect of condition (homecage or object exploration) was significant ($F(1, 36) = 19.849$, $p < 0.001$, $\eta p^2 = 0.355$, Fig. 4.20), with animals in the object exploration group exhibiting a significantly higher number of c-Fos positive cells than the homecage group. This suggests there was a clear impact of experiment condition on *c-fos* expression in the RSC. The interaction between genotype and

condition was not significant ($F(1, 36) = 0.795$, $p = 0.378$, $\eta p^2 = 0.022$), indicating that the effect of condition did not depend on the genotype of the animal.

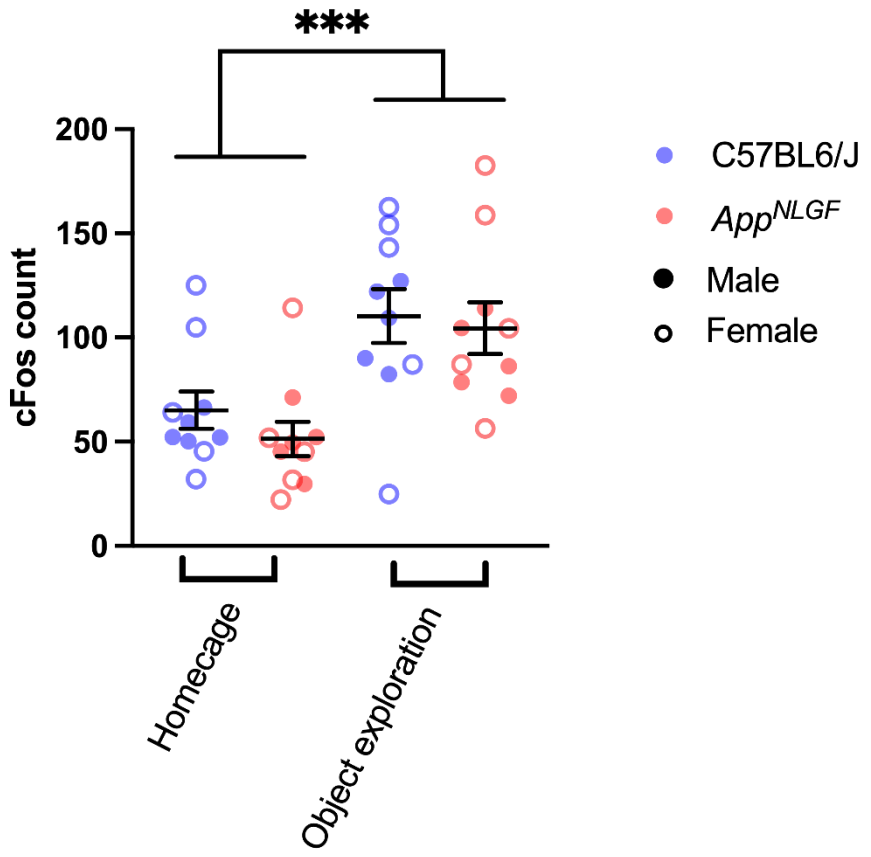

Figure 4.20: Baseline and Experience Induced c-fos Expression in the Caudal Dysgranular Retrosplenial Cortex. The mean number of c-Fos positive cells observed in the homecage control and object exploration groups, in animals aged 14-16 months. Datapoints represent the mean raw (untransformed) data for each animal, and black bars represent group means +/- standard error of the mean. Result of two-way ANOVA shown (*** = $p < 0.001$). The key indicates animal genotype and sex. The homecage and object exploration groups each contained 10 C57BL6/Js and 10 *App*^{NLGF} animals.

4.3.3.2 c-fos Expression in the Hippocampus

The number of c-Fos positive cells in the CA1 region of the HPC was also quantified for both the object exploration and homecage control groups.

This data exhibited equal variance (Levene's test > 0.05) and was normally distributed (Shapiro-Wilk test > 0.05). A two-way ANOVA revealed a significant main effect of genotype ($F(1, 36) = 4.759$, $p = .036$, $\eta p^2 = 0.117$), with *App*^{NLGF} animals showing lower overall levels of c-Fos positive cells. As with the RSC, the main effect of condition was also significant ($F(1, 36) = 26.906$, $p < 0.001$, $\eta p^2 = 0.428$, Fig. 4.21), with the CA1 region of the object exploration groups exhibiting higher *c-fos* expression than that of the homecage controls. The condition*genotype interaction was not significant $F(1, 36) = .026$, $p = 0.872$, $\eta p^2 = 0.001$).

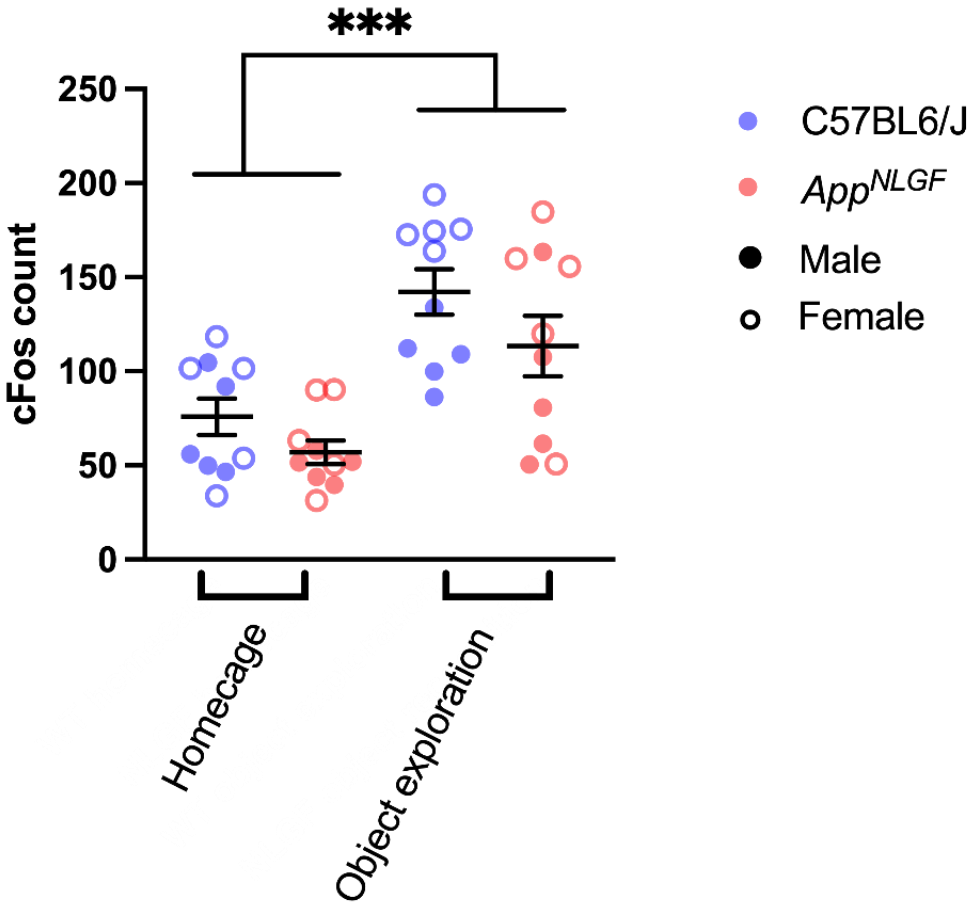

Figure 4.21: Baseline and Experience Induced c-fos Expression in the Hippocampus. The mean number of c-Fos positive cells observed in the homecage control and object exploration groups, in animals aged 14-16 months. Datapoints represent the mean raw (untransformed) data for each animal, and black bars represent group means +/- standard error of the mean. Result of two-way ANOVA shown (*** = $p < 0.001$). The key indicates animal genotype and sex. The homecage and object exploration groups each contained 10 C57BL6/Js and 10 *App*^{NLGF} animals.

4.3.3.3 Object Contact Times

For the object exploration groups, object contact time was manually scored using EthoVision XT13 to determine whether any potential changes in c-Fos levels could be attributed to increased object interaction. This data exhibited equal variance (Levene's test > 0.05) and was normally distributed (Shapiro-Wilk test > 0.05). An unpaired T-test revealed no significant difference in the object contact times between the C57BL6/J and *App*^{NLGF} object exploration groups (t(18) = 1.277, p = 0.218, Fig. 4.22).

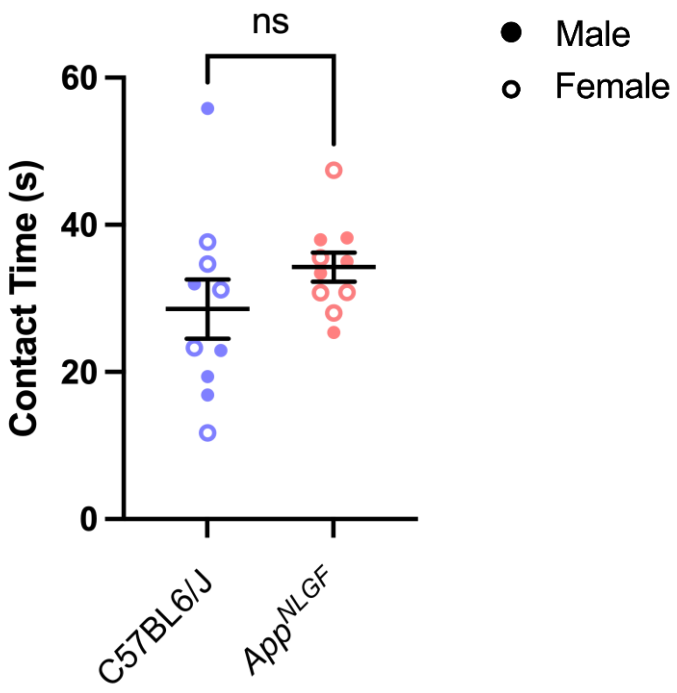

Figure 4.22: Object Contact Times During the Object Exploration Task. The mean object interaction times (in seconds) in animals aged 14-16 months. Black bars representing the mean +/- standard error of the mean. The graph displays the results of unpaired T-test (ns = non-significant). The key indicates animal sex. C57BL6/J n = 10, *App*^{NLGF} n = 10.

4.3.3.4 Distance Travelled

The mean distance travelled travel during the object interaction task was automatically tracked using EthoVision XT13 to determine whether any changes in locomotion could account for changes in *c-fos* expression. The dataset for distance travelled during object exploration both exhibited equal variance (Levene's test > 0.05) and normal distribution (Shapiro-Wilk test > 0.05). Unpaired T-tests revealed no significant differences in the distance travelled between C57BL6/J and *App*^{NLGF} animals (t(18) = 0.869, p = 0.396, Fig. 4.23).

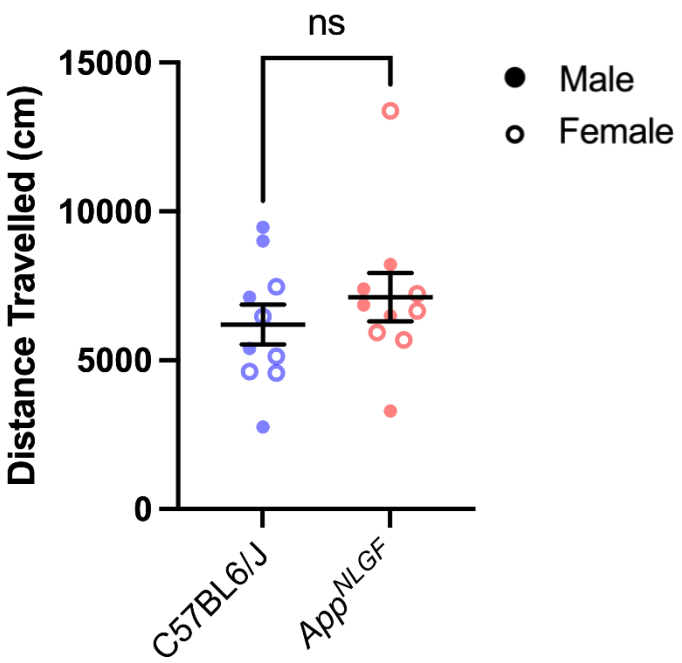

Figure 4.23: Distance Travelled During the Object Exploration Task. The mean distance travelled (in centimetres) in the object exploration task for c-Fos expression analysis. Animals aged 14-16 months. Black bars represent the mean +/- standard error of the mean. Results of unpaired T-tests shown (ns = non-significant). The key indicates animal sex. C57BL6/Js: n = 10. *App*^{NLGFs}: n = 10.

4.3.4 Discussion

To gain additional insight into neuronal activity in the *App*^{NLGF} model, the 14–16-month-old cohort originally intended for Ca^{2+} imaging was instead used to assess experience-induced c-fos expression in the RSC and HPC. This experiment, adapted from Baumgartel et al., (2018), utilised c-Fos protein levels as an established marker of recent neuronal activity linked to learning and memory (Baumgärtel et al., 2018; Lara Aparicio et al., 2022). Notably, *c-fos* expression is frequently altered in post-mortem AD brain tissue and animal models of AD (Chin et al., 2005; España et al., 2010; L'Esperance et al., 2024; Lu et al., 1998; Marcus et al., 1998; Niraula et al., 2023; Palop et al., 2005; Palop et al., 2003; Poirier et al., 2011; Sajan et al., 2007; Tan et al., 2023; Zhang et al., 1992), suggesting that similar disruptions in the *App*^{NLGF} model may reflect Aβ-mediated neuronal dysfunction associated with memory impairment.

To assess experience-driven c-Fos expression, animals explored novel objects for 10 minutes and were culled 30 minutes later, while controls remained in their homecages. c-Fos levels were then quantified via IHC. The brain regions selected for analysis included the caudal dysgranular RSC, the area also selected for Ca^{2+} imaging in the 22–23-month-old group, to facilitate a degree of comparison between the two groups. The c-Fos experiment also provided a valuable opportunity to examine neural activity in the HPC, a deeper brain region that was not accessible with the available two-photon microscopy setup. Therefore, c-Fos analysis also included the CA1 region of the HPC due to its critical role in spatial learning and memory processes and its sensitivity to AD pathology (Jeong & Singer, 2022; Rao et al., 2022; Suthana et al., 2009). Furthermore, its location (ventral and slightly rostral to the caudal dysgranular RSC), allowed it to be easily imaged and compared alongside the RSC, enabling insights into how amyloid deposition may affect the activity of these interconnected regions in the *App*^{NLGF} model. To test the protocol and determine whether simple object exploration conditions induced *c-fos* expression in the RSC and CA1, a pilot study using a small group of 5–6-month-old C57BL6/Js was conducted as described in Appendix 4. The results from the study confirmed that c-Fos protein was present in both brain areas following object exploration, however, there were also relatively high c-Fos levels in the control group. The control group in the pilot experiment was exposed to an empty arena for the same time period as the test group, and also culled 30 minutes following exposure. However, for the mid-aged *App*^{NLGF} experiment, homecage controls were chosen over empty context controls. The advantages and drawbacks of this choice of control will be addressed below.

In the caudal dysgranular RSC, both genotypes exhibited increased c-Fos expression following object exploration compared to the homecage condition. However, c-Fos levels did not differ significantly between C57BL6/J and *App*^{NLGF}

mice across both homecage and object exploration groups, indicating no genotype-specific differences in *c-fos* expression in this region. In the CA1 region of the HPC, object interaction also resulted in significantly higher c-Fos levels compared to the homecage condition for both genotypes. However, *App*^{NLGF} mice exhibited lower overall c-Fos levels across both conditions compared to C57BL6/Js, suggesting a reduced overall activity in this region. For the object interaction groups, no differences in object exploration or distance travelled were observed between C57BL6/Js and *App*^{NLGFs}. This indicates specific changes in *c-fos* expression in the *App*^{NLGF} brain, as c-Fos levels were not confounded by changes in exploratory behaviour. However, from this experiment, it cannot be concluded that the *c-fos* expression in the test groups was specific to object exploration because of the homecage controls used. The homecage control was selected for this experiment because the empty context control group in the pilot experiment showed c-Fos levels that was comparable to the object exploration group, likely due to the novelty of the OF arena or stress of handling, despite prior habituation. It was therefore anticipated that the use of an empty context control group in the main experiment may render it difficult to differentiate between baseline and novelty-induced c-Fos levels. In the absence of active learning or in passive environments, such as during well-trained tasks or while remaining in the home cage, the rodent brain typically exhibits low levels of c-Fos positive neurons (Anokhin et al., 2001). Therefore, the homecage control in this experiment was used in the aim to provide a more static baseline level of neuronal *c-fos* expression as the animals were in a familiar, non-stimulating environment immediately prior to perfusion. As environmental manipulation is sufficient to induce *c-fos* expression (Nikolaev et al., 2002), minimising external stimulation may allow for a more accurate comparison of basal c-Fos levels of the *App*^{NLGF} and C57BL6/J RSC and HPC. However, the major caveat to this is that it is impossible to differentiation *c-fos* expression due to environmental novelty or general exploratory behaviour from expression induced by actual object exploration. This experiment therefore focused on experience-induced *c-fos* expression rather than object-interaction based *c-fos* expression. For future experiments aiming to understand neural activity specific to object interaction, a refined habituation protocol should be developed to minimise excessive *c-fos* expression in an empty context control group. This would allow for specific isolation of the effect of object exploration on *c-fos* expression whilst controlling for movement and environmental stimuli, and may be used alongside a homecage control to reflect basal neuronal activity in the *App*^{NLGF} model.

Overall, the results of this experiment suggest that 14–16-month-old *App*^{NLGF} animals were capable of modulating activity of the RSC and HPC in response to exploratory behaviour or environmental stimuli, as indicated by similar *c-fos* expression patterns in test groups compared to homecage controls. In the RSC, c-Fos expression levels appeared unaffected in the *App*^{NLGF} model, suggesting preserved activity in this region. Similarly, Poirier et al., (2011), reported no significant difference in *c-fos* expression in the caudal granular RSC following exposure to a novel environment in Tg2576 animals at 5, 11, 17 and 23 months,

despite a trend showing increased *c-fos* expression with age. However, a significant reduction in *c-fos* expression was reported in the rostral granular RSC at 5 months, followed by a significant increase at 23 months, with no detectable differences observed at intermediate ages (Poirier et al., 2011).

Interestingly, the study observed that *c-fos* activity decreased in the presence of APP-derived amino acid residues but increased after the accumulation of Aβ plaques (Poirier et al., 2011). Moreover, the inverse pattern of cytochrome oxidase levels to *c-fos* expression was observed; cytochrome oxidase levels decreased in Tg2576s with age, with 5 month animals exhibiting significantly higher levels than age matched controls (Poirier et al., 2011). The authors suggested that this pattern highlights the different effects of early and later emerging amyloid pathology in RSC metabolism. For instance, there may be a gradual shift from initial compensatory mitochondrial activation due to oxidative stress, to plaque-mediated mitochondrial dysfunction in later stages of pathology, with oxidative stress and antioxidant response potentially modulating *c-fos* expression. To investigate whether App^{NLGFs} follow a similar pattern, future research should assess novelty-induced c-Fos levels and corresponding cytochrome oxidase levels in the RSC across different ages, including young, pre-plaque animals and older animals with substantial plaque accumulation. This additional experiment may determine how neuronal activity and metabolism are modulated over time in the App^{NLGF} RSC, and may help clarify whether the function of the RSC is compromised in this model, mirroring deficits observed in progressive stages of AD. Furthermore, future experiments should also investigate *c-fos* expression in the granular RSC and the rostral region of both RSC areas, alongside the caudal dysgranular region analysed in this thesis. This approach could provide a more comprehensive understanding of the RSC function in the App^{NLGF} model and how neurodegenerative changes in the model manifest across the different regions. Reflecting its connectivity with sensory and visual areas, c-Fos alterations of the dysgranular RSC may indicate deficits in visual processing (Aggleton et al., 2021; Powell et al., 2020; van Groen & Wyss, 1992a, 1992b). In contrast, alterations of c-Fos expression in the granular RSC may provide a more direct insight into the function of spatial memory in the App^{NLGF} model due to its strong associations with the HPC (Aggleton et al., 2021; Vann et al., 2009; Wyss & Van Groen, 1992). As Poirier et al., (2011) evidenced substantial differences in *c-fos* expression in the granular RSC, a similar result in the App^{NLGF} model may reflect similar region-specific alterations in neuronal activity.

In this thesis, the unchanged dysgranular RSC *c-fos* expression in 14–16-month-old App^{NLGF} model contrasts with the two-photon imaging data, which showed that 22–23-month-old App^{NLGFs} exhibited significantly lower Ca^{2+} response to visual stimuli compared to C57BL6/J controls. Although the large difference in ages between the two experimental groups may account for inherent progressive synaptic changes in the model, the discrepancy between the results may also reflect differences in how neuronal activity is captured by each measure. For example, two-photon Ca^{2+}

imaging provides a measure of Ca^{2+} pulses in real time, whereas *c-fos* activity is typically modulated over a longer period. Therefore, reduced RSC Ca^{2+} transients in the *App*^{NLGF} model may reflect a decrease in immediate synaptic activity, indicating a weakened response to visual stimuli. However, unchanged RSC *c-fos* expression indicates that general neuronal activity and synaptic plasticity may not be significantly altered in *App*^{NLGFs} at 14-16 months. This may be explained by compensatory Ca^{2+}-independent mechanisms that may maintain network stability of RSC despite the observed deficits in Ca^{2+} activity within a selected region. Contrastingly, however, data from this thesis indicates reduced *c-fos* expression in the CA1 region of 14–16-month-old *App*^{NLGF} HPC, despite no significant differences in object exploration or distance travelled between *App*^{NLGFs} and C57BL6/Js in the test groups. This corroborates with several studies using transgenic mice that evidence *c-fos* hypoactivity in the HPC associated with deficits in spatial memory tasks (Chin et al., 2005; España et al., 2010; Palop et al., 2005; Palop et al., 2003), and some human post-mortem studies (Palop et al., 2003). In this thesis, the decrease in *c-fos* expression in the *App*^{NLGFs} occurred regardless of the specific behavioural context. This pattern suggests a possible baseline deficit in hippocampal activity that may disrupt the encoding and retrieval of spatial information. Such a deficit could underlie the impairments in spatial memory tasks, including the OiP, OL, and spontaneous alternation tasks, as discussed in Chapter 3 of this thesis. Furthermore, the consistent reduction in hippocampal *c-fos* expression may be indicative of impaired LTP, thus impairments in the strengthening of synaptic connections that may be reflective of Aβ mediated changes to the HPC. The observed baseline deficit in CA1 *c-fos* expression suggests that two-photon imaging of the HPC could potentially reveal more pronounced impairments in Ca^{2+} dynamics than what was detected in the RSC in this study. However, reduced overall hippocampal *c-fos* expression in the *App*^{NLGF} model contrasts with several studies evidencing hippocampal *c-fos* hyperactivity human AD brains (Lu et al., 1998; Marcus et al., 1998; Sajan et al., 2007; Zhang et al., 1992). Reconciling this, studies have evidenced a biphasic expression curve of hippocampal *c-fos*; that is, acute neuronal activity in the HPC increases *c-fos* expression, but chronic activation decreases it (Calais et al., 2013; Corbett et al., 2017; Renthal et al., 2008; Tsankova et al., 2004). This may suggest that hippocampal *c-fos* expression is dependent upon variable levels of neuronal hyperactivity observed in different stages of AD.

Importantly, the data in this thesis also contrasts with a recent study reporting significantly increased CA1 *c-fos* expression in the *App*^{NLGF} model following a combined “what-where-when” episodic memory task (Tan et al., 2023). As with the RSC, variations in hippocampal *c-fos* expression may stem from several experimental differences including the disease stage and level of amyloid burden, different stimuli, and experimental methodology. For example, the Tan study used *App*^{NLGF} animals at 3 and 8 months, whereas at 14-16 months, the animals used for the experiment in this thesis may represent a different disease stage and thus different hippocampal *c-fos* responses. Furthermore, many studies, including the experiments by Tan and Poirer include male mice only, whereas the experiment in

this thesis used equal numbers of males and females. Male and female rodents often exhibit different patterns of *c-fos* expression which may influence variability between experiments. For example, sex differences in *c-fos* expression have been observed in the rodent brain in response to environmental stressors such as noise and restraint, notably affecting key regions such as the HPC (Babb et al., 2013; Fernández-Quezada et al., 2022). Additionally, variable environmental stimuli used in different experiments may also explain differential neuronal *c-fos* expression. For example, the combined "what-where-when" task in the Tan study used a square box divided into two compartments, each containing an object or a female conspecific rodent. The experiment in this thesis employed a standard OF arena without compartments or social elements, in contrast to the more complex design in the Tan study. It may be argued that added complexity may have increased stimulation and/or stress and thus enhanced *c-fos* expression compared to simpler experiments. On the contrary, the protocol used in this thesis may not have provided sufficient stimulation to robustly engage the brain regions under investigation, thereby limiting the likelihood of detecting genotype-specific effects. Areas such as the PRh may have shown more pronounced alterations following passive exposure to novel objects, whereas tasks with greater spatial demands such as the T-maze or RAM may have elicited stronger activity in the HPC and RSC, potentially amplifying genotype-related differences in *c-fos* expression that remained subtle under the conditions used here.

An additional key source of variability between rodent c-Fos studies is the timing of perfusion following experimental manipulation. *c-fos* expression is transient and typically follows a bell-shaped curve, commonly peaking at around 20-90 minutes post exposure to stimuli (Lara Aparicio et al., 2022). Therefore, culling the animal at a specific timepoint captures a unique snapshot of *c-fos* expression at one moment, thus affecting comparability of experiments. Additionally, the specificity of the antibody to c-Fos in its mRNA or protein form may also influence results. As mRNA is translated to protein, protein detection may require longer intervals after stimulation to accurately reflect c-Fos levels (Chaudhuri, 1997). The Poirier and Tan papers assessed c-Fos protein levels 90 minutes following stimulus exposure (Poirier et al., 2011; Tan et al., 2023). However, since this thesis measured *c-fos* expression 30 minutes after object exposure, it is possible that the peak expression, where genotype differences may have been most pronounced, was missed. Future studies should examine c-Fos levels at multiple time points, including around 90 minutes post-exposure, to better capture peak expression and reveal potential genotype-dependent differences.

Furthermore, when comparing between transgenic and 2nd generation model studies, it is important to note that inherent variations in neuronal biochemistry make it difficult to dissociate experimental differences from differences that are induced by the effects of the cellular artefacts observed in transgenic models. Indeed, the premise of this thesis is that the *App*^{NLGF} model must be characterised as the inability

of transgenic mice to accurately reflect the AD brain environment has likely contributed to the stalling of progress in AD drug development. The difference in *c-fos* expression and Ca^{2+} activity may stem from underlying differences in brain pathology between the two types of models. Transgenic models, commonly overexpressing mutant *APP* and/or *PSEN* genes, often exhibit enhanced plaque burden and thus the observed *c-fos* hyperactivity may be due to differences in levels of amyloid-induced excitotoxicity, synaptic function, and metabolic and neuroinflammatory responses.

In summary, this thesis reveals novel insights into neuronal activity in the App^{NLGF} model, highlighting subtle yet distinct alterations. While resting Ca^{2+} levels were slightly elevated, App^{NLGFs} at 22-23 months displayed unexpectedly diminished Ca^{2+} responses to visual stimuli, suggesting Aβ-mediated disruptions in RSC function. These findings challenge the notion of global Ca^{2+} overload in AD and point instead to a more nuanced, context-dependent dysregulation. Alternatively, the absence of hallmark AD features in App^{NLGFs} such as neuronal loss and tau pathology may explain the lack of pronounced Ca^{2+} elevation typically associated with AD. Furthermore, although alterations in *c-fos* expression were less pronounced than hypothesised, region-specific differences were evident at 14-16 months. RSC *c-fos* expression appeared largely preserved, despite reduced Ca^{2+} responses observed at an older age, whereas hippocampal c-Fos levels were consistently lower in App^{NLGFs}, potentially reflecting earlier impairments in hippocampal function. These findings suggest that neuronal dysfunction in this model may be regionally selective and potentially shaped by both age and pathology. Future studies incorporating hippocampal Ca^{2+} imaging and age-comparative analyses are warranted to further clarify the progression and regional specificity of neuronal dysfunction in this model.

Chapter 5: General Discussion

5.1 General Overview

Since 1995, numerous 1st generation mouse models of AD have been developed to overexpress mutant *APP* and develop substantial plaque deposition. However, the artefacts produced by aberrantly expressed *APP* result in difficulties interpreting and translating data from these models (Sasaguri et al., 2022). As a result, 2nd generation models were created, including the *App*^{NLGF} model, in which humanised mutant *App* is expressed at endogenous levels (Saito et al., 2014). However, there is a paucity of data regarding the cognitive and synaptic function of this model, therefore it is unclear whether *App*^{NLGFs} accurately represent AD pathology. Finding and characterising an accurate model of AD is essential for several reasons. For example, advancing research into disease mechanisms or identifying new therapeutic targets relies on reliable animal models to capture aspects of the disease, aiding development of disease modifying therapies rather than relying on symptom masking drugs. Furthermore, many AD drugs fail clinical studies, with disease-modifying drugs exhibiting a failure rate of 99.6% between 2002 and 2012 (Cummings et al., 2014). It may be argued that this high attrition rate of AD drugs is likely because preclinical models do not mimic the human disease closely enough. Reliable models of AD could aid the progression of preclinical research into drug safety and efficacy by providing a platform to test potential drugs, reducing drug discovery failures by increasing the likelihood that the outcomes of preclinical studies translate to human patients.

Whilst the *App*^{NLGF} mouse model does not fully reflect the complexity of AD, it may be a valuable platform to study the contribution of Aβ deposition on key pathological features of the disease, without the confounding effect of overexpression related artefacts observed in transgenic models of AD (Sasaguri et al., 2022). In this model, very little is known about the effect of endogenously expressed mutant *App* on systems commonly affected in AD such as memory processes and anxiety-like behaviour. This thesis aimed to contribute to the field of AD research by providing a comprehensive evaluation of the *App*^{NLGF} mouse model of amyloid pathology. This involved a battery of object recognition tests to examine specific memory functions, a T-maze task to assess spatial working memory, and assessment of anxiety-like tendencies using the widely characterised OF and EPM tests.

Valid models of AD can also offer valuable insights into the timeline of disease progression, potentially allowing researchers to identify critical therapeutic windows by observing early behavioural and biochemical changes. These insights may be key to the future development of preventative therapies. However, due to time constraints and practical limitations, animals in AD research are often not aged beyond approximately 12 months. As around 81% of AD patents are 75 or older (Hebert et al., 2013), it could be argued that studying the brain in an aged context is key to producing translatable data in AD research. For example, it may more

accurately mirror the progressive and chronic nature of the disease by accounting for the cumulative effects of aging on the brain that younger animals may not exhibit, such as accumulation of neurotoxic cellular debris with age (Lee & Kim, 2022). This increases the likelihood that pathology in the model aligns with that of elderly AD patients, the primary demographic affected by the disease (Ulaganathan & Pitchaimani, 2023). Therefore, with the aim to capture the trajectory of disease onset and progression, this thesis examined the behavioural phenotype of the *App*^{NLGF} model across multiple age groups, spanning young, mid-aged, and older cohorts.

In addition to cognition, very little is known about the function of neuronal activity in this model, particularly in extrahippocampal regions such as the RSC. PET studies revealed the RSC as one of the first brain areas to show metabolic changes in MCI, the precursor to AD, highlighting its role as an early site of pathology (Desgranges et al., 2002; Nestor et al., 2003). Findings from transgenic mouse models of AD also suggest an important role of the RSC in AD development. However, data on RSC function in 2nd generation mouse models, such as the *App*^{NLGF} mouse, remains sparse. Therefore, the additional aim of this thesis was to assess the integrity of neuronal activity in the *App*^{NLGF} model through Ca^{2+} imaging and *c-fos* expression analysis, and to determine whether potential alterations in such processes occurred in parallel to cognitive alterations.

5.2 Key Findings

Chapter 3 of this thesis evaluated the behavioural phenotype of the *App*^{NLGF} model, broadly focusing on memory processes and anxiety-like behaviour. Behavioural tests were selected to assess key aspects of hippocampal and broader cortical function, given the known vulnerability of these regions in AD (Braak & Braak, 1991; Rao et al., 2022; Terstege et al., 2024). Memory was assessed using a battery of object recognition tasks that exploit rodents' innate preference for novelty and can probe components of episodic-like memory, typically the first memory system to decline in AD (Tromp et al., 2015).

To evaluate the function of the combined “what” and “where” aspects of episodic-like memory in the *App*^{NLGF} model, the OiP task was conducted on 22–23-month animals, a time point at which Aβ deposition was presumed to be maximal. The OiP task engages the HPC and its broader network, including the PRh, mPFC, and RSC, regions implicated in episodic memory and early AD pathology (Barker & Warburton, 2011; Braak & Braak, 1991; Chen et al., 2017; Tulving & Markowitsch, 1998; Vann & Aggleton, 2002). The ON task was conducted alongside the OiP task to assess the individual modality of object recognition independently of spatial memory, primarily relying on intact PRh function (Brown & Aggleton, 2001; Bussey et al., 1999; Evans et al., 2019; Good, Hale, et al., 2007; Hale & Good, 2005; Hsiao et al., 1996; Mumby

& Pinel, 1994). At 22-23 months, both *App*^{NLGFs} and C57BL6/Js exhibited impaired OiP performance, but intact novel object recognition, suggesting age-related deficits in associative memory. Subsequently, the OL task was carried out to assess object-location memory independently of object identity memory, providing a more targeted evaluation of hippocampal and RSC function while minimising the influence of broader networks, which may have shown age-related decline in even the C57BL6/J animals at such an advanced age (Barker & Warburton, 2011; Ennaceur et al., 1997; Parron & Save, 2004). This task was performed on animals at 4-6, 8-10, and 22–23-months to track the emergence and progression of potential spatial memory deficits across different ages. *App*^{NLGFs} exhibited impaired OL discrimination at the two oldest age points, suggesting potential amyloid-related impairments of the HPC and RSC.

In addition to episodic memory, working memory is another critical aspect of memory that progressively deteriorates in AD, further contributing to the hallmark cognitive decline (Stopford et al., 2012). In humans, working memory enables the temporary retention and manipulation of information to guide goal-directed behaviour (Chai et al., 2018). In rodents, spatial working memory can be assessed by the T-maze spontaneous alternation task, which relies on their innate tendency to explore less recently visited areas (Deacon & Rawlins, 2006). As with spatial object recognition tasks, the spontaneous alternation task is especially sensitive to HPC disruptions (Bannerman et al., 1999; Dudchenko et al., 2000). In Chapter 3 of this thesis, the T-maze spontaneous alternation task was carried out in groups of *App*^{NLGFs} and age-matched C57BL6/J controls across several age points. Unexpectedly, deficits in alternation were only observed in *App*^{NLGFs} at 22-23 months. This finding highlights the phenotypic subtlety of the *App*^{NLGF} model, despite reported hippocampal plaque deposition at as young as 4 months (Saito et al., 2014). Given this early pathological burden, greater and more consistent sensitivity to spatial tasks was anticipated. The reported saturation of plaque deposition at around 7 months (Saito et al., 2014), makes the absence of consistent spatial memory deficits across both the OL and spontaneous alternation tasks particularly intriguing, suggesting such impairments may be driven more by downstream synaptic dysfunction rather than amyloid burden alone.

A further aim of Chapter 3 was to assess anxiety-like behaviour in the *App*^{NLGF} mouse model. Traditionally, pre-clinical AD research has focused on cognitive symptoms such as memory loss but has failed to assess NPS symptoms such as anxiety, which also affect the quality of life for AD patients (Pless et al., 2023). Therefore, studying NPS symptoms in addition to memory in mouse models of AD is crucial to understand whether the model reflects key behavioural aspects of the disease. In this thesis, the OF and EPM tasks were carried out to assess anxiety-like behaviour in *App*^{NLGF} animals at a range of different ages. Both tasks rely on rodents' preference for sheltered spaces, such as the periphery of the OF arena or the closed arms of the EPM. However, excessive avoidance of open spaces is said to indicate a state of heightened anxiety that may override their natural tendency to explore novel

environments (Gencturk & Unal, 2024). The performance of *App*^{NLGFs} revealed an interesting behavioural profile: while older *App*^{NLGFs} (22-23 months) showed increased thigmotaxis in the OF arena, they consistently preferred the open arms of the EPM across all ages tested. Although both tests are cited as anxiety-related tests, the findings of this thesis highlight that they likely probe distinct aspects of behaviour: the OF primarily reflects general anxiety and avoidance of exposed spaces, while EPM engages processes related to risk assessment and behavioural inhibition. These findings may suggest that *App*^{NLGFs} exhibit early and persistent impairments in decision-making or inhibitory control, which coexist with heightened anxiety-like behaviour that emerges in later life.

When interpreting the findings from behavioural experiments it is important to note that changes in locomotor activity were observed across tasks, which may or may not have influenced performance outcomes. In some cases, *App*^{NLGFs} showed increased activity relative to C57BL6/Js (e.g., greater distance travelled at 12–14 months in the EPM), while in others they showed reduced activity (e.g., lower distance travelled at 22–23 months in the spontaneous alternation task). Contrastingly, in the OL and OF tests, activity levels decreased with age regardless of genotype, whereas in the ON and OiP tests no group differences in locomotion were evident. Such variability makes it difficult to draw firm conclusions about the role of locomotion as a confounding factor, though it may plausibly contribute to some of the observed behavioural outcomes. For example, greater activity could have enhanced open arm exploration in the EPM, while reduced activity may have contributed to lower alternation rates in the spontaneous alternation task. Taken together, these considerations highlight the complexity of interpreting behavioural data in the *App*^{NLGF} model, where performance outcomes may reflect an interplay between genuine cognitive or affective changes and more general shifts in activity levels.

Overall, the behavioural outcomes described in this thesis are integrated with findings from the literature in Figure 5.1 to provide an overarching view of the *App*^{NLGF} phenotype across cognitive and affective domains. Although early and substantial amyloid deposition is a consistent pathological feature of this model (Latif-Hernandez et al., 2019; Mehla et al., 2019; Saito et al., 2014; Wang et al., 2022), the trajectory of behavioural impairments is less uniform. In the present study, cognitive deficits were relatively subtle and mostly restricted to advanced ages, with performance remaining intact earlier in life. This pattern aligns with reports of preserved function in some studies, but contrasts with others describing earlier and more progressive impairments across tasks. In terms of affective behaviour, this thesis identified a profile of persistent disinhibitory-like behaviour, aligning with other studies as one of the most consistently reported outcomes in the wider literature. However, the late emerging anxiety-like behaviour observed here occurs amidst variable reports, including studies showing similar effects, the opposite pattern of behaviour, or no evidence of anxiety-related changes. As illustrated in Figure 5.1,

these findings suggest that while the *App*^{NLGF} model does capture certain features relevant to AD, it does not necessarily follow a linear trajectory of overt cognitive decline. Instead, it displays a heterogeneous, task-dependent behavioural profile that may only partially reflect the timeline of amyloid deposition.

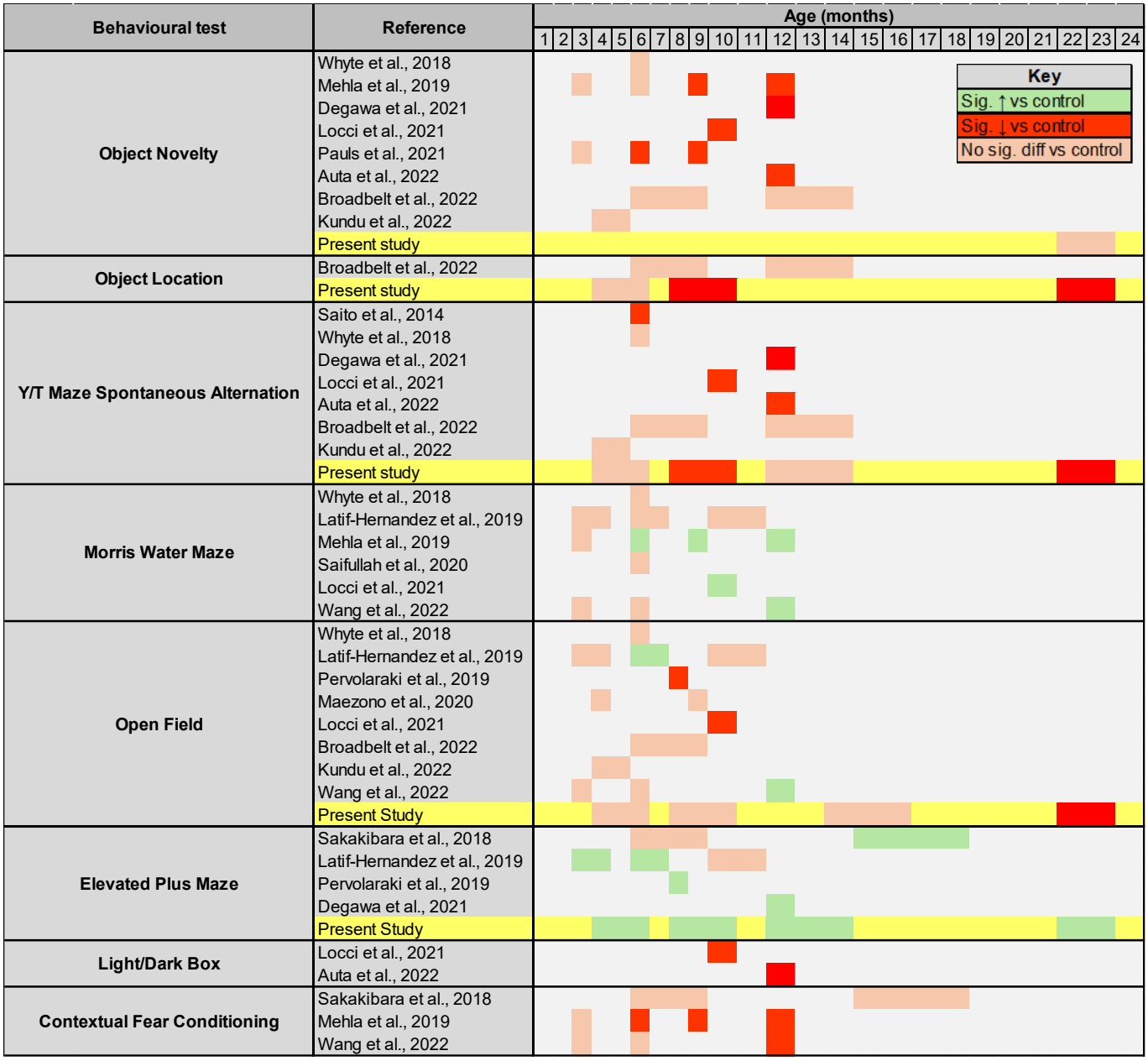

Figure 5.1: Timeline of Cognitive Deficits and Affective Alterations in the App^{NLGF} Mouse Model: Comparison of Present Findings with Published Literature. The behavioural phenotype of the *App*^{NLGF} model in a range of behavioural tests including the Object Novelty (ON), Object Location (OL), Y or T-maze spontaneous alternation, and Morris Water Maze (MWM), Open Field (OF), Elevated Plus Maze (EPM), and Light/Dark Box (LDB). Results from this thesis highlighted in yellow. The colour code indicates a significant increase (green) or decrease (red) from the control line ($p < 0.05$) or no significant difference from the control line (orange) ($p > 0.05$). The control lines used are *App*^{NL} or C57BL6/J. For the ON and OL test, the measure used is discrimination ratio/index or percentage of time interacting with novel object(s). For the spontaneous alternation task, the measure is percentage spontaneous alternation. For MWM, the measure is escape latency. For the OF test, the measure used is time spent in the inner zone or inner zone ratio. For EPM, the measure is time in the open arms or number of open arm crossings. For LDB, the measure is time spent in the light compartment.

In addition to behavioural characterisation, this thesis also aimed to assess synaptic alterations in the *App*^{NLGF} model in key regions supporting spatial and object-based memory. Chapter 4 therefore described two complementary methods to evaluate neuronal activity in the *App*^{NLGF} model. The first subchapter described the use of two-photon Ca^{2+} imaging to evaluate dynamic, real-time Ca^{2+} responses in the RSC of 22–23-month animals. The second subchapter consisted of *c-fos* expression analysis in a mid-aged cohort to assess activity-related gene expression in the RSC and HPC. Assessment of these measures in the *App*^{NLGF} mouse model is particularly pertinent, as alterations in Ca^{2+} signalling and *c-fos* expression are commonly reported in AD and other experimental models of AD, reflecting impaired neuronal activity and synaptic dysfunction (Babaei et al., 2025; Joshi et al., 2023). The analyses revealed that *App*^{NLGFs} exhibited significantly reduced Ca^{2+} responses to visual stimuli compared to C57BL6/J controls, as reflected by lower overall fluorescence changes, fewer and smaller transient events, and reduced total activity over time. Moreover, whilst *c-fos* expression was unaffected in the RSC, it was significantly decreased in the HPC relative to control animals. These findings suggest the *App*^{NLGF} model exhibits regional and context specific deficits in neuronal activity, reflecting alterations in both immediate functional responses and longer-term activity-dependent gene expression that may underlie the subtle cognitive impairments observed.

Overall, this work provides a broad behavioural characterisation of the *App*^{NLGF} model, at a range of ages that has not previously been examined. Given the wealth of evidence from genetically modified and infusion models of amyloid pathology, changes in memory function were unexpectedly mild with late onset in *App*^{NLGF} mice. This suggests that the model may have limited utility for studying the progression of AD pathology or for evaluating early therapeutic interventions. Additionally, while changes in neuronal activity were observed as hypothesised, the unexpected reduction, rather than increase, in stimulus-evoked Ca^{2+} transients challenges the classical Ca^{2+} Hypothesis of AD and underscores the difficulty of attributing the complexity of AD pathogenesis to a single mechanistic theory.

5.3 Limitations and Future Directions

5.3.1 Characterisation of the *App*^{NLGF} Model

There is a plethora of behavioural tasks that may be employed to assess the function of memory in AD models. However, one limitation of this thesis is that certain behavioural characteristics of the *App*^{NLGF} model remain unexplored or require further exploration. For example, the “what” and “where” aspects of episodic-like memory were addressed with the ON, OiP, and OL tasks, however, due to time constraints, only animals at 22-23 months were assessed with the OiP and ON tasks. Future studies should assess OiP performance at younger age groups to

determine whether *App*^{NLGF} animals exhibit impairments in integrating object and location information at earlier age points, before generalised age-related deficits appear in both C57BL6/J and *App*^{NLGF} genotypes. This will build on the findings of this thesis by tracking disease progression and potentially isolating genotype-specific deficits in the *App*^{NLGF} animals. Moreover, as ON, OiP, and OL tasks in this thesis employed only a 10-minute retention delay, future characterisation of the *App*^{NLGF} model could benefit from extending the retention delays to probe the neural circuits involved in long-term object recognition memory. Additionally, the "when" paradigm was not characterised in this study, therefore future work should perform the TO task to assess the ability of *App*^{NLGFs} to discriminate the relative recency of object exposure, which could provide further insights into deficits of the HPC and associated networks (Barker & Warburton, 2011).

Similarly, the extent of spatial working memory deficits in the *App*^{NLGF} model could be further explored using tasks such as the MWM and RAM. These tasks would offer deeper insights into the function of real-time memory updating and spatial navigation in the *App*^{NLGF} model. The additional tasks also provide an opportunity to validate and strengthen the findings of the T-maze task in this thesis, which suggests that *App*^{NLGFs} only exhibit impairments in spatial working memory at a very advanced age. Moreover, there is more consistent evidence of RSC involvement in tasks such as the rotated T-maze alternation and rotated RAM compared to the standard spontaneous alternation task used in this thesis (Nelson et al., 2015; Vann et al., 2009). Therefore, performing these additional tasks to engage the RSC could provide a more sensitive and targeted assessment of RSC function in the *App*^{NLGF} model. This approach may also uncover additional behavioural deficits that align with reduced Ca^{2+} levels observed in the two-photon imaging experiment of this thesis. Given the mild reduction in stimulus-evoked Ca^{2+} activity in the RSC, it could be predicted that tasks that explicitly tax RSC-dependent navigation could reveal subtle behavioural impairments not captured by simpler paradigms.

As with memory characterisation, there are numerous tests that may be carried out to assess the NPS-like phenotype of rodent models of AD. In an effort to provide an insight to the affective state of the *App*^{NLGF} model, this study carried the OF and EPM tasks to assess thigmotaxis and avoidance aspects of anxiety-like behaviour. While, as discussed in Chapter 3, the 3D maze may offer a more nuanced assessment of anxiety with its more ambiguous escape context (Ennaceur & Chazot, 2016), additional behavioural tests are warranted to more comprehensively evaluate anxiety-like behaviour in the *App*^{NLGF} model. For example, the social interaction task could provide additional insights into approach-avoidant behaviour, where reduced interaction with an unfamiliar conspecific typically indicates an anxiogenic response (File, 1985; Lezak et al., 2017). Depression is commonly observed in AD and may play an active role in AD pathogenesis (Huang et al., 2024). Behavioural despair in rodents is often used as a depression-like construct and can be assessed with the tail suspension task and forced swim tests, in which immobility is typically interpreted

as a depression-like state (Gencturk & Unal, 2024). Furthermore, anhedonia may also be assessed in the *App*^{NLGF} model using a sucrose preference test, and may provide an additional behavioural correlation to human depression (Gencturk & Unal, 2024). There is limited data regarding these additional measures of affective behaviour in *App*^{NLGF} mice, however, recent studies have shown that *App*^{NLGFs} exhibit increased immobility in the tail suspension test and reduced social interaction time at 10-12 months (Degawa et al., 2021; Locci et al., 2021), suggesting the presence of depression and anxiety-like behaviours in this model. However, further studies across a broader age span are needed to fully characterise the progression and nature of these behavioural changes in *App*^{NLGF} mice.

A further consideration is the apparent individual variability within the *App*^{NLGF} cohorts, particularly in the behavioural experiments, suggesting that intrinsic traits, such as baseline activity, stress responses, or other physiological characteristics, may modulate the impact of the mutation. For example, these factors could either exacerbate or attenuate cognitive and affective phenotypes in individual animals, potentially contributing to the subtle and heterogenous outcomes observed. Therefore, future large-scale studies combining comprehensive behavioural profiling with molecular markers, including Ca^{2+} signalling, *c-fos* expression, and amyloid pathology, could help disentangle these individual differences and provide a more nuanced understanding of how intrinsic traits shape behavioural outcomes. Multivariate modelling approaches may be particularly useful for uncovering if specific behavioural outcomes, such as diminished T-maze alternation, may align with other behavioural traits, like increased thigmotaxis, or with specific molecular features. This could help reveal why the mutation exerts a stronger impact in some animals than others, and may highlight the complex interplay of factors that shape behavioural outcomes.

In this thesis, neuronal activity in the *App*^{NLGF} mouse was characterised using two-photon Ca^{2+} imaging and *c-fos* expression analysis. To complement the findings of this thesis and to achieve a more comprehensive understanding of the patterns of neuronal activation in the *App*^{NLGF} model, additional experiments are warranted. For example, electrophysiological studies could be utilised to directly capture neuronal action potentials with sub-millisecond temporal resolution, offering critical insights into the precise timing and frequency of neuronal firing. Although cellular activity recorded by two-photon Ca^{2+} imaging generally correlates to results from *in vivo* electrophysiological recording (Grienberger et al., 2022), utilising electrophysiology in addition to two-photon imaging in the *App*^{NLGF} model may reveal patterns such as high frequency bursts of activity that remain undetected in two-photon Ca^{2+} imaging due to the comparatively reduced temporal accuracy. Furthermore, it could be hypothesised that these signals may not always closely align if there are Aβ-mediated changes in Ca^{2+} signalling or handling mechanisms. Therefore, combining the two methods may help differentiate physiological action potentials from abnormal

Ca^{2+} transients that occur independently of neuronal firing, thus providing a deeper insight into potential pathological changes in the *App*^{NLGF} brain.

As discussed earlier in this thesis, Ca^{2+} dynamics in mouse models of amyloid pathology are highly dependent upon the proximity of individual neurons to amyloid plaques. However, the experimental design for this thesis did not account for this, potentially limiting the interpretation of the results. Consequently, future research should assess spatial differences in Ca^{2+} transients by focusing on imaging a smaller subset of neurons and utilising statistical approaches to evaluate the impact of plaque proximity on baseline and stimulus-induced Ca^{2+} dynamics in the RSC. This approach would provide critical insights into how local Aβ accumulation influences neuronal activity and Ca^{2+} signalling in the *App*^{NLGF} model. Moreover, applying this method to other brain regions, such as the HPC, would offer a more comprehensive understanding of how Aβ pathology disrupts Ca^{2+} dynamics across the brain, revealing potential regional-specific dysfunction that may contribute to the broader behavioural changes observed in the *App*^{NLGF} model. Focusing on a smaller region within the selected ROI also has additional advantages, for example, it facilitates easier calculation of the number of responsive and unresponsive neurons, a detail which remains unclear in this thesis. Furthermore, specific neuronal populations can be imaged chronically in animals implanted with a cranial window by utilising co-ordinates and unique patterns of blood vessels to consistently locate the same neurons over multiple imaging sessions. This approach enables longitudinal assessment of Ca^{2+} dynamics in the *App*^{NLGF} model, which may offer insights into the effect of disease progression on Ca^{2+} dynamics. For example, it may reveal patterns of hypoactivity or hyperactivity at different stages of pathology, providing information on the temporal pattern of neuronal Ca^{2+} dysregulation in the *App*^{NLGF} model. Chronic neuronal activity can also be assessed *in vivo* with the implantation of small, portable two-photon microscopes, known as miniscopes (Chen et al., 2022). These devices provide a unique opportunity to monitor neuronal Ca^{2+} firing in freely moving animals, enabling simultaneous imaging and behavioural assessment. For instance, by implanting miniscopes into regions such as the RSC or HPC, future studies using the *App*^{NLGF} model could directly examine how neuronal activity correlates with performance in tasks like the OiP, OL, and SA. This experiment could determine whether impaired task performance directly correlates to dysregulation of Ca^{2+} dynamics, offering a potential insight into the synaptic basis of deficits in spatial memory and processing in this model. Specifically, chronic imaging may enable the identification of place cells in the HPC, for example, allowing for a detailed analysis of the number, activity, spatial tuning, and remapping of place cells, providing further insights into hippocampal dysfunction in this model.

A major limitation of the two-photon imaging experiment in this thesis was that only one age group was imaged, restricting the ability to capture the dynamic effects of progressive Aβ deposition on neuronal function. Future studies should address this by including multiple age groups to better characterise neuronal Ca^{2+} changes

associated with disease progression in the *App*^{NLGF} model. While the longitudinal study proposed above could partially resolve this, practical constraints such as the deterioration of GCaMP signals and cranial window quality over time may necessitate imaging different cohorts of animals at distinct age points, allowing for a wider range of ages and stages of disease to be assessed. Based on the evidence gathered in this thesis, however, it is expected that *App*^{NLGFs} would exhibit normal or only subtly altered stimulus-evoked Ca^{2+} transients at younger age points. However, it would be valuable to investigate whether these changes are region-specific (e.g., if they differ in the HPC compared to the RSC) and whether they reflect a pattern of hypoactivity or hyperactivity with age.

To characterise neuronal activation at an earlier age, and in the absence of a functioning two-photon microscope, *c-fos* expression analysis in mid-aged *App*^{NLGFs} was employed following an object exploration task. Future experiments in the *App*^{NLGF} model could build upon the findings of this thesis by examining *c-fos* expression following more specific behavioural tasks such as the OiP or spontaneous alternation tasks. While this study used an object exploration task to evoke neuronal *c-fos* expression, the use of the homecage controls limited the ability to isolate object exploration-related differences in expression. Inclusion of an empty context control group would enable more precise assessment of whether object exploration fails to engage relevant brain areas in the *App*^{NLGF} mouse, potentially reflecting the molecular underpinnings of behavioural deficits. Additionally, such experiments should include *App*^{NLGFs} and control animals at multiple age points and incorporate Aβ staining. This approach would facilitate analysis of how progressive plaque deposition affects *c-fos* expression and determine whether the biphasic pattern observed in Tg2576 mice is recapitulated in the *App*^{NLGF} model (Poirier et al., 2011). Furthermore, combining *c-fos* analysis with metabolic markers such as cytochrome oxidase could provide insight into how metabolic activity in the *App*^{NLGF} RSC and HPC correlate with amyloid pathology and age-related shifts in neuronal activation.

A general limitation of this thesis is the lack of statistical analyses to assess potential sex differences in behaviour and neuronal activity. Most experimental cohorts throughout this thesis comprised of 10-12 animals in total, with approximately half of each sex. The 22–23-month-old cohort, however, had a less balanced distribution due to limited availability, as these animals were acquired from another researcher. The mismatch complicates interpretation, particularly since the 22–23-month-old *App*^{NLGF} group used for behavioural experiments comprised of predominantly females, whereas the corresponding C57BL6/J control group were mostly males. In humans, AD is more prevalent in women than men (Beam et al., 2018), and female mouse models of AD similarly exhibit earlier or more severe pathology and cognitive impairments than their male counterparts (Kolahchi et al., 2024). Consequently, any differences observed between *App*^{NLGFs} and C57BL6/Js at 22-23 months, or between this cohort and younger age groups, may be amplified by the overrepresentation of

females. Importantly, the sample size for each sex within each group was likely too small to provide sufficient statistical power to detect meaningful sex-specific differences. Although visual inspection of the data did not suggest a consistent pattern of sex-related effects, the limited sample size prevents firm conclusions. To address this in future studies, power analyses should be used to determine the appropriate number of male and female animals required for meaningful comparison. Incorporating sex as a biological variable in this way would help clarify whether *App*^{NLGFs} replicate sex-dependent patterns observed in AD and other mouse models of AD, and thus whether it offers translatability to the human condition. Notably, when examining sex effects across age groups, consideration of the oestrous cycle in females may be useful to account for age-related hormonal fluctuations that could influence behaviour and neuronal function.

A further limitation of the experiments presented in this thesis is the use of C57BL/6J mice as controls rather than the *App*^{NL} model. Although *App*^{NLGF} mice are maintained on a C57BL/6J background, which is a commonly used control for the *App*^{NLGF} model, the *App*^{NL} model may be considered a more appropriate control. Unlike C57BL6/J mice, *App*^{NL} mice carry the same humanised *App* sequence and Swedish mutation as *App*^{NLGFs}, but lacks the additional Arctic and Iberian mutations that drive amyloid pathology (Saito et al., 2014). Importantly, *App*^{NL} mice do not develop plaques, making them a more precise genetic control for isolating the effects of the added mutations present in the *App*^{NLGF} model, whilst controlling for the increased levels of CTF-β fragments induced by the Swedish mutation (Saito et al., 2014). Although CTF-β levels in these APP-KI models remain lower than those seen in transgenic lines (Saito et al., 2014), they may still influence aspects of neuronal function and behaviour. As such, the use of C57BL/6J mice rather than *App*^{NL} controls in this thesis introduces the possibility that some of the observed changes in behaviour and neuronal activity may, in part, reflect the cumulative effects of both Aβ pathology and elevated CTF-β levels. Moreover, the C57BL6/J controls used in this study were non-littermate animals, bred in-house from externally sourced C57BL6/J animals. Although they were housed under identical conditions and handled similarly, they were maintained in separate cages from the *App*^{NLGF} line. While this approach reduced the number of animals required, avoiding the surplus associated with breeding heterozygous pairs to produce littermate controls, it also potentially introduced sources of variance that were not fully controlled for. For example, despite the fact that the *App*^{NLGF} line is maintained on a C57BL6/J background, genetic variability from externally sourced C57BL6/J colonies, epigenetic differences, or variation in maternal environment across litters may have influenced phenotypic outcomes (Holmdahl & Malissen, 2012). Therefore, the use of littermate controls, whether C57BL6/J, *App*^{NL}, or both, would have better accounted for these factors by ensuring a shared genetic and early-life environment.

A major limitation of this thesis is the absence of biochemical analyses of brain tissue from experimental animals, with the exception of the c-Fos cohort, due to time

constraints. Therefore, future work should perform comprehensive analyses of brain tissue from *App*^{NLGFs} at a range of different ages to characterise biochemical changes which may underlie behavioural and synaptic changes. As Saito et al., (2014) evidenced progressive plaque deposition in the *App*^{NLGF} model from as early as 2 months old, it is not unreasonable to assume that the mice in the present study also showed age-related accumulation of Aβ. However, as Aβ deposition was not measured in this study, it is unclear whether any observed changes are truly related to progressive amyloid pathology or confounded by other factors, such as neuroinflammation or synaptic dysfunction. Therefore, future work should employ enzyme-linked immunosorbent assays (ELISA) or IHC techniques on brain tissue from *App*^{NLGF} and C57BL6/J animals across a range of ages to assess levels of soluble amyloid species, plaque burden, microglial activation (indicated by Iba-1), pro-inflammatory cytokines such as TNF-α, IL-1β, and IL-6, and synaptic density markers such as synaptophysin and PSD-95. Furthermore, alterations in levels of Brain-Derived Neurotrophic Factor may offer insights into synaptic plasticity in the *App*^{NLGF} model, with decreased levels indicating a diminished capacity for synaptic remodelling (Gao et al., 2022). Moreover, given the absence of a comprehensive histological assessment of amyloid pathology, a related limitation is the lack of genotyping of the *App*^{NLGF} progeny. Although the breeding stock were homozygous animals sourced from a previously genotyped colony at Cardiff University, genotyping the experimental animals would have provided additional reassurance regarding the genetic identity of the animals, particularly given the subtlety of the observed phenotypes.

In addition to the proposed two-photon imaging of *App*^{NLGFs} across different ages, biochemical analyses of brain tissue from these animals could be conducted to help identify mechanisms underlying potential disruptions in Ca^{2+} homeostasis. For example, the function of Ca^{2+} regulation could be assessed by IHC staining of plasma membrane channels such as VGCCs, SOCCs, and NMDARs and examining expression, distribution, and density of these channels in specific brain regions to reflect potential alterations in neuronal Ca^{2+} entry. Furthermore, patterns of IP_3R and RyR expression may be analysed to determine potential dysregulation of intracellular release mechanisms in the *App*^{NLGF} brain. In addition to patterns of expression, changes in receptor activation could be assessed by quantifying activated downstream proteins through western blotting or ELISA. For example, increased phosphorylated CREB expression may indicate increased activation of Ca^{2+} channels such as IP_3Rs, VGCCs and NMDARs. Combining these markers with staining for plaque pathology may reveal distinct patterns of Ca^{2+} receptor density. For example, increased receptor density near plaques could suggest a mechanism of localised hyperactivity observed in other studies (Doostdar et al., 2021; Inayat et al., 2023; Takamura et al., 2021). To assess potential oxidative stress in *App*^{NLGFs}, oxidative damage can be inferred by measuring the levels of lipid peroxidation, which reflects the extent of membrane damage induced by reactive oxygen species. Together, future biochemical analyses of inflammation, Ca^{2+} dysregulation, synaptic alterations may provide greater insight into the mechanisms underlying the subtle

behavioural changes observed in this thesis, and further clarify the extent to which amyloid pathology contributes to cognitive decline. Nevertheless, even with these key experimental limitations, the overall pattern of behavioural and neuronal activity changes was modest.

5.3.2 Utilisation of the *App^{NLGF}* Model and Future Directions for Modelling Alzheimer's Disease

Despite the additional experiments that are required to further characterise this model, the findings of this thesis suggest that the *App^{NLGFs}* exhibit mostly subtle alterations in memory, affective behaviour, and neuronal activity.

The phenotypic subtlety of the *App^{NLGF}* model likely reflects that it does not fully replicate AD pathology. For example, although *App^{NLGFs}* are reported to exhibit plaque deposition from as early as 2 months old (Saito et al., 2014), the behavioural deficits observed in this thesis primarily emerged in animals at a much more advanced age. This suggests that in the absence of other key pathologies such as tau hyperphosphorylation and overt cell loss, amyloid alone appears insufficient to produce significant functional effects in the *App^{NLGF}* model, except from when advanced age is a contributing and likely dominant factor. Whilst the absence of such changes in *App^{NLGF}* mice arguably makes it a valuable model of preclinical AD, where patients typically exhibit substantial Aβ deposition prior to tau pathology, neuronal loss, and marked memory decline (Cho et al., 2021), the ability to detect behavioural changes in such models is critical for the strategic timing and evaluation of therapeutic intervention. Notably, the findings of this thesis demonstrate that the *App^{NLGF}* model exhibits only subtle behavioural alterations, which presents a key limitation. With minimal and inconsistent functional impairments, it may be difficult to assess the efficacy of therapeutic interventions as there is little measurable deficit to target or rescue. That said, this study identified early and significant behavioural alterations in the EPM test, which could potentially isolate the role of amyloid on behavioural disinhibition. However, it is possible that these findings reflect a task-specific complication of Aβ expression in this model rather than an accurate representation of AD-related behaviours.

In my view, this thesis reiterates that despite amyloid accumulation and deposition being a major aspect of AD pathology, it is not the entire picture of the disease. As such, more sophisticated models are required, and potential modelling avenues will be discussed later. Crucially, however, it must be reiterated that the *App^{NLGF}* model is a model of amyloid pathology, and so it cannot be expected that the *App^{NLGF}* model will accurately and comprehensively reflect each aspect of known behavioural and biochemical alterations in AD. It may therefore be used to isolate and investigate the effects of amyloid pathology independently of the distinct or additive roles of

other AD pathology such as neuron loss and tau pathology. This presents the advantage of studying the specific effects of amyloid-targeting drugs *in vivo*. However, a major caveat to this is the question of how accurately the mutant *App* and subsequent amyloid deposition in *App*^{NLGF} animals reflects amyloid in AD. As discussed in the General Introduction of this thesis, *App*^{NLGFs} exhibit three FAD mutations in the endogenous *App* gene. In humans, just one of these mutations appears sufficient to cause severe disease. However, in this thesis, *App*^{NLGFs} are not severely cognitively impaired, reiterating that Aβ is not sufficient alone to cause severe changes in memory, affective state, or neuronal activity. Importantly, no humans are known to possess all three of these mutations, and so the effect of potential interactions between these mutations in the *App*^{NLGF} model is unknown. Both factors could contribute to the *App*^{NLGF} model exhibiting pathological or neuronal consequences not observed in humans, rendering them a potentially inaccurate model for pre-clinical testing.

Conversely, it may be argued that the presence of three FAD mutations enhances the practicality of these models for laboratory studies, allowing aggressive Aβ accumulation in an achievable time scale. However, whilst FAD and SAD share key pathological features such as plaque deposition, tau hyperphosphorylation, neuroinflammation, and oxidative stress, the upstream mechanisms of these shared pathological hallmarks are different. For example, FAD is driven by mutations predominantly in *APP*, *PSEN1* or *PSEN2* genes that are directly linked to increased synthesis of amyloid peptides (Meraz-Ríos et al., 2014). SAD, however, is a result of a broader interplay between age, genetic, and environmental risk factors, many of which may be unknown (Migliore & Coppedè, 2022). Genome-wide association studies have linked most SAD risk genes to decreased clearance of Aβ as well as overproduction, indicating that the mechanism of plaque deposition in SAD may be more complex than FAD (Bertram et al., 2007; Quan et al., 2023). Consequently, potential disease modifying therapies tested in mouse models with FAD mutations may not translate to SAD in clinical practice as the underlying mechanisms of amyloid pathology differ. In *App*^{NLGFs}, this is particularly the case for drugs that target amyloid metabolism, clearance, or deposition as the Arctic mutation present in the *App* gene results in Aβ that is susceptible to rapid aggregation and resistant to proteolytic degradation (Nilsberth et al., 2001; Sasaguri et al., 2022; Tsubuki et al., 2003). Moreover, immunotherapies may also not be tested in the *App*^{NLGF} model due to its unusually high affinity for anti-Aβ antibodies, even in the presence of denaturing agent guanidine hydrochloride, suggesting that it will not accurately reflect how patients will respond to potential treatments (Saito et al., 2014). To address this issue, a 3rd generation model was developed (*App*^{NLF} x *Psen1*^{P117L} mice) (Sato et al., 2021). These mice do not carry the problematic Arctic mutation, rendering them suitable for screening drugs that aim to enhance Aβ degradation. This is especially relevant since the Aβ-degrading enzyme neprilysin is a key therapeutic target in AD research. Furthermore, the 3rd generation model incorporates a mutant *Psen1* gene, which is more relevant to FAD than the *App*^{NLGF} model as most FAD-causing mutations reside in this gene (Scearce-Levie et

al., 2020). However, despite exhibiting more aggressive Aβ deposition and neuroinflammation than the *App*^{NLGF} model, it is unclear whether this model also exhibits tau deposition and neuronal cell death, so further characterisation of this model is required (Sato et al., 2021).

Given the above considerations, it could be argued that the *App*^{NLGF} and 3rd generation models may have limited relevance to SAD, which accounts for the majority of AD cases (Dorszewska et al., 2016). Ideally, therefore, the focus should be on understanding and modelling the mechanisms of SAD. However, this has remained challenging in AD research due to the heterogeneity of the disease. To address this, Model Organism Development and Evaluation for Late-onset AD (MODEL-AD) research groups are using specialised gene-editing techniques to insert SAD risk genes into rodent hosts, aging the animals and incorporating environmental stressors. For example, the Jackson Laboratory recently developed the LOAD1 and LOAD2 mouse models as part of the MODEL-AD consortium (Kotredes et al., 2021; Kotredes et al., 2024). The LOAD1 model was created by incorporating humanised *APOEε4* and *Trem2*R47*H risk gene sequences into the genome of a C57BL6/J host. These animals exhibited evidence of systemic inflammation and metabolic alterations, however, they did not exhibit amyloid plaques, hyperphosphorylated tau, neuronal loss, or cognitive deficits, even when aged up to 24 months (Kotredes et al., 2021). The LOAD2 model was subsequently created by humanising the Aβ sequence of the *App* gene of LOAD1 mice, and exposing it to a high fat/high sugar diet, key environmental risk factors for SAD (Morris et al., 2003; Oblak et al., 2022). After 16 months of age, LOAD2 mice exhibited elevated insoluble $A\beta_{42}$ species, age-dependent reduction in brain volume, and subtle cognitive deficits (Kotredes et al., 2024). These mice, however, did not exhibit plaque and tau pathologies, and so the authors recommended this model to target other pathologies of SAD independent of amyloid and tau (Kotredes et al., 2024). However, isolating specific pathologies in a model, as seen with the *App*^{NLGF} model, may overlook critical interactions between AD pathologies. Furthermore, relying on separate models for distinct AD pathologies may result in inconsistent findings or overemphasis on certain aspects of the disease, complicating the interpretation of outcomes and compromising translatability to human patients. However, replicating all potential genetic and environmental risk factors for SAD in a single model is likely unfeasible, given the highly individual nature of the disease. As seen with the LOAD1 and LOAD2 models discussed above, attempts to create a typical combination of SAD risk factors in one model risks oversimplifying the contributions of key risk factors to AD pathogenesis. Additionally, critical SAD risk factors may still be unknown, and so may be overlooked when attempting to model SAD.

The above complexities may underscore why accurately modelling AD, and thus developing effective treatments, remains particularly challenging. However, this does not render the *App*^{NLGF} model obsolete; rather, it highlights opportunities for

refinement to better reflect the multifaceted nature of AD and improve the translatability of experimental findings. A notable advancement of the *App*^{NLGF} mouse model is the recent development of the *App*^{NLGF} rat model (Pang et al., 2022). The *App*^{NLGF} rat model was created using Clustered Regularly Interspaced Short Palindromic Repeats (CRISPR)/CRISPR-associated protein 9 (CRISPR/Cas9) gene editing technology to knock-in the humanised *App* gene containing the Swedish, Beyreuther/Iberian, and Arctic FAD mutations into the genome of Sprague-Dawley rats, driven by the rat endogenous promotor. Behavioural testing of 5-month-old *App*^{NLGF} rats revealed an anxiogenic phenotype in the OF test, impaired spatial working memory in the MWM task, and impaired object-location associations in a PAL task (Pang et al., 2022). Biochemical analysis of *App*^{NLGF} rat brain tissue revealed plaque deposition in key brain areas (HPC, cortex, and subcortical regions), but not in the cerebellum, from 1 month of age, in the absence of substantial levels of proteolytic fragments such as CTF-α and CTF-β (Pang et al., 2022). Interestingly, in parallel with AD patients, female *App*^{NLGF} exhibited more rapid amyloid deposition compared to male rats (Pang et al., 2022). Immunostaining revealed that *App*^{NLGF} rats also exhibited age-dependent increase in tau phosphorylation from 6 months of age, with PET scans showing significant tau labelling in the CA1 (Pang et al., 2022). Iba1 and GFAP staining was significantly increased in 6- and 9-month-old rats, suggesting a state of enhanced gliosis in these animals (Pang et al., 2022). Furthermore, biochemical analysis revealed reductions in synaptic markers synaptophysin and PSD-95 in 9-month-old animals, and electron microscopy showed decreased synaptic density in the HPC, EC, and PFC in 12-month-old rats, suggesting synaptic impairments at these ages (Pang et al., 2022). Moreover, NeuN staining demonstrated neuronal loss in the HPC of the 12 and 22-month-old groups, coinciding with an overall reduction in brain volume in these groups (Pang et al., 2022). Apoptotic markers BAX/Bcl-2 and cleaved caspase-3/pro-caspase 3 were significantly elevated in *App*^{NLGF} rat brains at 6-months-old, and necroptosis markers receptor-interacting protein kinase 1 (RIPK1) and mixed lineage kinase domain-like protein (MLKL) were increased in 6- and 12-month-old *App*^{NLGF} rat brains compared to littermate controls, suggesting apoptotic and necroptotic cell death pathways contributing to neuronal loss (Pang et al., 2022). The study also examined *App*^{NLGF} mice and found a similar progressive pattern of Aβ deposition and gliosis (Pang et al., 2022). Interestingly, despite very low tau levels in *App*^{NLGF} mice, this study observed a small but significant increase in tau phosphorylation in 12-month-old *App*^{NLGF} mice compared to C57BL6/J mice (Pang et al., 2022). These mice also exhibited decreased PSD95 levels whereas synaptophysin levels were unchanged compared to controls (Pang et al., 2022). In contrast to the rat model, *App*^{NLGF} mice did not show any signs of apoptosis or necroptosis.

Overall, the *App*^{NLGF} rat model may be a more accurate and nuanced model of AD, reflecting key pathological hallmarks without the confounding effects of overexpression related artefacts typically seen in transgenic models. The *App*^{NLGF} rat model may be a valuable tool to target specific disease mechanisms and observe how modulating one pathway may influence others, informing the prioritisation and

refinement of therapeutic strategies. Furthermore, future multi-target approaches may be more accurately tested in this model due to its ability to exhibit core AD pathologies. In AD research, however, rats are less commonly used than mice as there is a shortage of appropriate genetic manipulation tools. However, rats are behaviourally, physiologically, and genetically more similar to humans than mice (Bryda, 2013; Wildner, 2019). In particular, the alternative splicing of the *Mapt* gene in rats more closely resembles that of humans (Hanes et al., 2009). In adult humans, the ratio of tau isoforms containing three repeat regions (3R) and four repeat regions (4R) is equal, however, in cases of severe AD, production of the 3R isoform is increased (Espinoza et al., 2008; Takuma et al., 2003). Importantly, rats continue to produce the 3R isoform in adulthood but mice do not (Takuma et al., 2003). Furthermore, transgenic rats overexpressing *APP* have been shown to develop substantial tau pathology (Cohen et al., 2013). These results suggest that accumulation of Aβ plaques leads to hyperphosphorylation of tau in the App^{NLGF} rat model but not the mouse model, suggesting that rats may be a more relevant model to study the interplay between amyloid and tau pathologies. This comparison between the rat and mouse App^{NLGF} models highlights an important distinction: whilst both models exhibit progressive amyloid deposition and gliosis, only the rat model develops tau pathology and cell death, suggesting a critical role of tau in neuronal death in AD. It may be argued that amyloid accumulation and neuroinflammation alone are insufficient to cause neuronal loss in AD, but may play a role in inducing tau-mediated neuronal death. Interestingly, however, insertion of a humanised tau gene into the App^{NLGF} mouse genome results in tau hyperphosphorylation but no cell loss (Hashimoto et al., 2019), suggesting there is a complex interaction between the pathologies that should be delineated further. Future work in the App^{NLGF} rat model should examine neuronal activity (including Ca^{2+} regulation) and whether it also exhibits metabolic and vascular abnormalities which may also contribute to the observed neuronal death. However, while rodents share genetic and physiological similarities with humans, their relative simplicity may limit their ability to accurately replicate the complexity of AD. Consequently, the future of AD research may involve the use of more closely related species, such as non-human primates like marmosets. By more closely paralleling the cognitive, physiological, and genetic nature of humans, these models may provide a deeper understanding of AD pathogenesis, enhancing translatability of findings and increasing the likelihood of successful therapeutic interventions. Recently, the world's first non-human primate model of FAD was developed by introducing a deletion in exon 9 of the marmoset *PSEN1* gene. Initial findings indicate increased $Aβ_{42}$:$Aβ_{40}$ production and uncleaved PSEN-1 protein in *in vitro* fibroblast cultures derived from the model, indicating neuronal perturbation associated with AD (Sasaguri et al., 2022). However, this model concept is still in its infancy and requires further characterisation to establish its validity for future studies.

5.4 Thesis Conclusions

This thesis provides a novel characterisation of the cognitive function and neuronal activity of the *App*^{NLGF} mouse model of amyloid pathology. Behavioural testing revealed subtle spatial memory deficits, most pronounced at 23 months, and substantial disinhibitory-like behaviour from 4 months of age. Experience-induced hippocampal *c-fos* expression and cortical Ca^{2+} activity was reduced at 15 and 23 months, respectively, suggesting underlying synaptic dysfunction. Overall, the subtle nature of the *App*^{NLGF} model raises concerns about its validity and future use for AD research. Despite the reported early amyloid deposition and neuroinflammation, this thesis demonstrates only mild behavioural and synaptic effects. A reliable model should exhibit progressive pathology alongside clear, human-relevant behavioural decline, yet the *App*^{NLGF} model shows limited deficits until very advanced ages. Furthermore, and arguably most importantly, the *App*^{NLGF} model lacks key hallmarks such as NFT deposition and overt neuronal loss (Saito et al., 2014). These key points support the view that amyloid alone is not sufficient to drive substantial neurodegeneration. Moreover, the limited use of the model in studying amyloid-based immunotherapies reinforces the need for new models to better capture the multifaceted nature of AD. AD is a complex disorder with diverse environmental and genetic influences, and it is likely that critical aspects of its pathogenesis remain poorly understood. Developing and characterising a more accurate model is essential for understanding underlying mechanisms and identifying new therapeutic targets. This thesis therefore recommends a shift towards identifying new models of AD that more faithfully replicate known aspects of AD pathology.

Chapter 6: References

Aggleton, J. P., Albasser, M. M., Aggleton, D. J., Poirier, G. L., & Pearce, J. M. (2010). Lesions of the rat perirhinal cortex spare the acquisition of a complex configural visual discrimination yet impair object recognition. *Behav Neurosci*, *124*(1), 55-68. https://doi.org/10.1037/a0018320

Aggleton, J. P., Neave, N., Nagle, S., & Sahgal, A. (1995). A comparison of the effects of medial prefrontal, cingulate cortex, and cingulum bundle lesions on tests of spatial memory: evidence of a double dissociation between frontal and cingulum bundle contributions. *J Neurosci*, *15*(11), 7270-7281. https://doi.org/10.1523/JNEUROSCI.15-11-07270.1995

Aggleton, J. P., Pralus, A., Nelson, A. J., & Hornberger, M. (2016). Thalamic pathology and memory loss in early Alzheimer's disease: moving the focus from the medial temporal lobe to Papez circuit. *Brain*, *139*(Pt 7), 1877-1890. https://doi.org/10.1093/brain/aww083

Aggleton, J. P., Wright, N. F., Vann, S. D., & Saunders, R. C. (2012). Medial temporal lobe projections to the retrosplenial cortex of the macaque monkey. *Hippocampus*, *22*(9), 1883-1900. https://doi.org/10.1002/hipo.22024

Aggleton, J. P., Yanakieva, S., Sengpiel, F., & Nelson, A. J. (2021). The separate and combined properties of the granular (area 29) and dysgranular (area 30) retrosplenial cortex. *Neurobiol Learn Mem*, *185*, 107516. https://doi.org/10.1016/j.nlm.2021.107516

Aizenstein, H. J., Nebes, R. D., Saxton, J. A., Price, J. C., Mathis, C. A., Tsopelas, N. D.,…Klunk, W. E. (2008). Frequent amyloid deposition without significant cognitive impairment among the elderly. *Arch Neurol*, *65*(11), 1509-1517. https://doi.org/10.1001/archneur.65.11.1509

Ajoolabady, A., Lindholm, D., Ren, J., & Pratico, D. (2022). ER stress and UPR in Alzheimer's disease: mechanisms, pathogenesis, treatments. *Cell Death Dis*, *13*(8), 706. https://doi.org/10.1038/s41419-022-05153-5

Alberdi, E., Sánchez-Gómez, M. V., Cavaliere, F., Pérez-Samartín, A., Zugaza, J. L., Trullas, R.,…Matute, C. (2010). Amyloid beta oligomers induce Ca2+ dysregulation and neuronal death through activation of ionotropic glutamate receptors. *Cell Calcium*, *47*(3), 264-272. https://doi.org/10.1016/j.ceca.2009.12.010

Albert, M. S., DeKosky, S. T., Dickson, D., Dubois, B., Feldman, H. H., Fox, N. C.,…Phelps, C. H. (2011). The diagnosis of mild cognitive impairment due to Alzheimer's disease: recommendations from the National Institute on Aging-Alzheimer's Association workgroups on diagnostic guidelines for Alzheimer's disease. *Alzheimers Dement*, *7*(3), 270-279. https://doi.org/10.1016/j.jalz.2011.03.008

Alexander, A. S., & Nitz, D. A. (2015). Retrosplenial cortex maps the conjunction of internal and external spaces. *Nat Neurosci*, *18*(8), 1143-1151. https://doi.org/10.1038/nn.4058

Alexander, A. S., Place, R., Starrett, M. J., Chrastil, E. R., & Nitz, D. A. (2023). Rethinking retrosplenial cortex: Perspectives and predictions. *Neuron*, *111*(2), 150-175. https://doi.org/10.1016/j.neuron.2022.11.006

Allwright, M., Mundell, H. D., McCorkindale, A. N., Lindley, R. I., Austin, P. J., Guennewig, B., & Sutherland, G. T. (2023). Ranking the risk factors for Alzheimer's disease; findings from the UK Biobank study. *Aging Brain*, *3*, 100081. https://doi.org/10.1016/j.nbas.2023.100081

Alonso, A. C., Zaidi, T., Grundke-Iqbal, I., & Iqbal, K. (1994). Role of abnormally phosphorylated tau in the breakdown of microtubules in Alzheimer disease.

Proc Natl Acad Sci U S A, *91*(12), 5562-5566. https://doi.org/10.1073/pnas.91.12.5562
Alzheimer, A., Stelzmann, R. A., Schnitzlein, H. N., & Murtagh, F. R. (1995). An English translation of Alzheimer's 1907 paper, "Uber eine eigenartige Erkankung der Hirnrinde". *Clin Anat*, *8*, 429-431.
Anokhin, K. V., Ryabinin, A. E., & Sudakov, K. V. (2001). Expression of the c-fos gene in the mouse brain during the acquisition of defensive behavior habits. *Neurosci Behav Physiol*, *31*(2), 139-143. https://doi.org/10.1023/a:1005299804902
Antunes, M., & Biala, G. (2012). The novel object recognition memory: neurobiology, test procedure, and its modifications. *Cogn Process*, *13*(2), 93-110. https://doi.org/10.1007/s10339-011-0430-z
Arendash, G. W., King, D. L., Gordon, M. N., Morgan, D., Hatcher, J. M., Hope, C. E., & Diamond, D. M. (2001). Progressive, age-related behavioral impairments in transgenic mice carrying both mutant amyloid precursor protein and presenilin-1 transgenes. *Brain Res*, *891*(1-2), 42-53. https://doi.org/10.1016/s0006-8993(00)03186-3
Arias-Cavieres, A., Barrientos, G. C., Sánchez, G., Elgueta, C., Muñoz, P., & Hidalgo, C. (2018). Ryanodine Receptor-Mediated Calcium Release Has a Key Role in Hippocampal LTD Induction. *Front Cell Neurosci*, *12*, 403. https://doi.org/10.3389/fncel.2018.00403
Arispe, N., Diaz, J. C., & Simakova, O. (2007). Abeta ion channels. Prospects for treating Alzheimer's disease with Abeta channel blockers. *Biochim Biophys Acta*, *1768*(8), 1952-1965. https://doi.org/10.1016/j.bbamem.2007.03.014
Arispe, N., Rojas, E., & Pollard, H. B. (1993). Alzheimer disease amyloid beta protein forms calcium channels in bilayer membranes: blockade by tromethamine and aluminum. *Proc Natl Acad Sci U S A*, *90*(2), 567-571. https://doi.org/10.1073/pnas.90.2.567
Assini, F. L., Duzzioni, M., & Takahashi, R. N. (2009). Object location memory in mice: pharmacological validation and further evidence of hippocampal CA1 participation. *Behav Brain Res*, *204*(1), 206-211. https://doi.org/10.1016/j.bbr.2009.06.005
Association, A. P. (2013). *Diagnostic and statistical manual of mental disorders: DSM-V* (5th ed.). American Psychiatric Association. .
Association, A. P. (2022). *Diagnostic and statistical manual of mental disorders: DSM-5-TR /* (5th ed.).
Auger, S. D., Mullally, S. L., & Maguire, E. A. (2012). Retrosplenial cortex codes for permanent landmarks. *PLoS One*, *7*(8), e43620. https://doi.org/10.1371/journal.pone.0043620
Auta, J., Locci, A., Guidotti, A., Davis, J. M., & Dong, H. (2022). Sex-dependent sensitivity to positive allosteric modulation of GABA action in an APP knock-in mouse model of Alzheimer's disease: Potential epigenetic regulation. *Curr Res Neurobiol*, *3*, 100025. https://doi.org/10.1016/j.crneur.2021.100025
Avila, J., & Perry, G. (2021). A Multilevel View of the Development of Alzheimer's Disease. *Neuroscience*, *457*, 283-293. https://doi.org/10.1016/j.neuroscience.2020.11.015
Awad, M., Warren, J. E., Scott, S. K., Turkheimer, F. E., & Wise, R. J. (2007). A common system for the comprehension and production of narrative speech. *J*

Neurosci, *27*(43), 11455-11464. https://doi.org/10.1523/JNEUROSCI.5257-06.2007
Babaei, P., Faraji, N., & Eyvani, K. (2025). c-Fos Expression Differentially Acts in the Healthy Brain Compared with Alzheimer's Disease. *Gene Expression*, *24*(3), 209-218.
Babb, J. A., Masini, C. V., Day, H. E., & Campeau, S. (2013). Stressor-specific effects of sex on HPA axis hormones and activation of stress-related neurocircuitry. *Stress*, *16*(6), 664-677. https://doi.org/10.3109/10253890.2013.840282
Baddeley, A. (2000). The episodic buffer: a new component of working memory? *Trends Cogn Sci*, *4*(11), 417-423. https://doi.org/10.1016/s1364-6613(00)01538-2
Baddeley, A., Logie, R., Bressi, S., Della Sala, S., & Spinnler, H. (1986). Dementia and working memory. *Q J Exp Psychol A*, *38*(4), 603-618. https://doi.org/10.1080/14640748608401616
Baddeley, A. D., Bressi, S., Della Sala, S., Logie, R., & Spinnler, H. (1991). The decline of working memory in Alzheimer's disease. A longitudinal study. *Brain*, *114 (Pt 6)*, 2521-2542. https://doi.org/10.1093/brain/114.6.2521
Baddeley, A. D., & Hitch, G. (1974). Working Memory. *Psychology of Learning and Motivation*, *8*, 47-89.
Bai, F., Watson, D. R., Yu, H., Shi, Y., Yuan, Y., & Zhang, Z. (2009). Abnormal resting-state functional connectivity of posterior cingulate cortex in amnestic type mild cognitive impairment. *Brain Res*, *1302*, 167-174. https://doi.org/10.1016/j.brainres.2009.09.028
Bai, Y., Li, M., Zhou, Y., Ma, L., Qiao, Q., Hu, W.,…Gan, W. B. (2017). Abnormal dendritic calcium activity and synaptic depotentiation occur early in a mouse model of Alzheimer's disease. *Mol Neurodegener*, *12*(1), 86. https://doi.org/10.1186/s13024-017-0228-2
Baillon, S., Gasper, A., Wilson-Morkeh, F., Pritchard, M., Jesu, A., & Velayudhan, L. (2019). Prevalence and Severity of Neuropsychiatric Symptoms in Early- Versus Late-Onset Alzheimer's Disease. *Am J Alzheimers Dis Other Demen*, *34*(7-8), 433-438. https://doi.org/10.1177/1533317519841191
Baker, K. B., & Kim, J. J. (2002). Effects of stress and hippocampal NMDA receptor antagonism on recognition memory in rats. *Learn Mem*, *9*(2), 58-65. https://doi.org/10.1101/lm.46102
Balducci, C., Beeg, M., Stravalaci, M., Bastone, A., Sclip, A., Biasini, E.,…Forloni, G. (2010). Synthetic amyloid-beta oligomers impair long-term memory independently of cellular prion protein. *Proc Natl Acad Sci U S A*, *107*(5), 2295-2300. https://doi.org/10.1073/pnas.0911829107
Balu, D. T., Takagi, S., Puhl, M. D., Benneyworth, M. A., & Coyle, J. T. (2014). D-serine and serine racemase are localized to neurons in the adult mouse and human forebrain. *Cell Mol Neurobiol*, *34*(3), 419-435. https://doi.org/10.1007/s10571-014-0027-z
Bannerman, D. M., Rawlins, J. N., McHugh, S. B., Deacon, R. M., Yee, B. K., Bast, T.,…Feldon, J. (2004). Regional dissociations within the hippocampus--memory and anxiety. *Neurosci Biobehav Rev*, *28*(3), 273-283. https://doi.org/10.1016/j.neubiorev.2004.03.004
Bannerman, D. M., Yee, B. K., Good, M. A., Heupel, M. J., Iversen, S. D., & Rawlins, J. N. (1999). Double dissociation of function within the hippocampus: a comparison of dorsal, ventral, and complete hippocampal cytotoxic lesions.

Behav Neurosci, *113*(6), 1170-1188. https://doi.org/10.1037//0735-7044.113.6.1170
Bano, D., & Ankarcrona, M. (2018). Beyond the critical point: An overview of excitotoxicity, calcium overload and the downstream consequences. *Neurosci Lett*, *663*, 79-85. https://doi.org/10.1016/j.neulet.2017.08.048
Bao, F., Wicklund, L., Lacor, P. N., Klein, W. L., Nordberg, A., & Marutle, A. (2012). Different β-amyloid oligomer assemblies in Alzheimer brains correlate with age of disease onset and impaired cholinergic activity. *Neurobiol Aging*, *33*(4), 825.e821-813. https://doi.org/10.1016/j.neurobiolaging.2011.05.003
Baranello, R. J., Bharani, K. L., Padmaraju, V., Chopra, N., Lahiri, D. K., Greig, N. H.,…Sambamurti, K. (2015). Amyloid-beta protein clearance and degradation (ABCD) pathways and their role in Alzheimer's disease. *Curr Alzheimer Res*, *12*(1), 32-46. https://doi.org/10.2174/1567205012666141218140953
Barbas, H., & Zikopoulos, B. (2007). The prefrontal cortex and flexible behavior. *Neuroscientist*, *13*(5), 532-545. https://doi.org/10.1177/1073858407301369
Barbier, P., Zejneli, O., Martinho, M., Lasorsa, A., Belle, V., Smet-Nocca, C.,…Landrieu, I. (2019). Role of Tau as a Microtubule-Associated Protein: Structural and Functional Aspects. *Front Aging Neurosci*, *11*, 204. https://doi.org/10.3389/fnagi.2019.00204
Barker, G. R., Bird, F., Alexander, V., & Warburton, E. C. (2007). Recognition memory for objects, place, and temporal order: a disconnection analysis of the role of the medial prefrontal cortex and perirhinal cortex. *J Neurosci*, *27*(11), 2948-2957. https://doi.org/10.1523/JNEUROSCI.5289-06.2007
Barker, G. R., & Warburton, E. C. (2008). NMDA receptor plasticity in the perirhinal and prefrontal cortices is crucial for the acquisition of long-term object-in-place associative memory. *J Neurosci*, *28*(11), 2837-2844. https://doi.org/10.1523/JNEUROSCI.4447-07.2008
Barker, G. R., & Warburton, E. C. (2011). When is the hippocampus involved in recognition memory? *J Neurosci*, *31*(29), 10721-10731. https://doi.org/10.1523/JNEUROSCI.6413-10.2011
Barker, G. R., & Warburton, E. C. (2015). Object-in-place associative recognition memory depends on glutamate receptor neurotransmission within two defined hippocampal-cortical circuits: a critical role for AMPA and NMDA receptors in the hippocampus, perirhinal, and prefrontal cortices. *Cereb Cortex*, *25*(2), 472-481. https://doi.org/10.1093/cercor/bht245
Barker, G. R., Warburton, E. C., Koder, T., Dolman, N. P., More, J. C., Aggleton, J. P.,…Brown, M. W. (2006). The different effects on recognition memory of perirhinal kainate and NMDA glutamate receptor antagonism: implications for underlying plasticity mechanisms. *J Neurosci*, *26*(13), 3561-3566. https://doi.org/10.1523/JNEUROSCI.3154-05.2006
Barros, V. N., Mundim, M., Galindo, L. T., Bittencourt, S., Porcionatto, M., & Mello, L. E. (2015). The pattern of c-Fos expression and its refractory period in the brain of rats and monkeys. *Front Cell Neurosci*, *9*, 72. https://doi.org/10.3389/fncel.2015.00072
Barry, A. E., Klyubin, I., Mc Donald, J. M., Mably, A. J., Farrell, M. A., Scott, M.,…Rowan, M. J. (2011). Alzheimer's disease brain-derived amyloid-β-mediated inhibition of LTP in vivo is prevented by immunotargeting cellular prion protein. *J Neurosci*, *31*(20), 7259-7263. https://doi.org/10.1523/JNEUROSCI.6500-10.2011

Barthélemy, N. R., Salvadó, G., Schindler, S. E., He, Y., Janelidze, S., Collij, L. E.,…Hansson, O. (2024). Highly accurate blood test for Alzheimer's disease is similar or superior to clinical cerebrospinal fluid tests. *Nat Med*, *30*(4), 1085-1095. https://doi.org/10.1038/s41591-024-02869-z

Basso, E., Fante, L., Fowlkes, J., Petronilli, V., Forte, M. A., & Bernardi, P. (2005). Properties of the permeability transition pore in mitochondria devoid of Cyclophilin D. *J Biol Chem*, *280*(19), 18558-18561. https://doi.org/10.1074/jbc.C500089200

Bastin, C., & Delhaye, E. (2023). Targeting the function of the transentorhinal cortex to identify early cognitive markers of Alzheimer's disease. *Cogn Affect Behav Neurosci*, *23*(4), 986-996. https://doi.org/10.3758/s13415-023-01093-5

Bats, S., Thoumas, J. L., Lordi, B., Tonon, M. C., Lalonde, R., & Caston, J. (2001). The effects of a mild stressor on spontaneous alternation in mice. *Behav Brain Res*, *118*(1), 11-15. https://doi.org/10.1016/s0166-4328(00)00285-0

Baumgart, M., Snyder, H. M., Carrillo, M. C., Fazio, S., Kim, H., & Johns, H. (2015). Summary of the evidence on modifiable risk factors for cognitive decline and dementia: A population-based perspective. *Alzheimers Dement*, *11*(6), 718-726. https://doi.org/10.1016/j.jalz.2015.05.016

Baumgärtel, K., Green, A., Hornberger, D., Lapira, J., Rex, C., Wheeler, D. G., & Peters, M. (2018). PDE4D regulates Spine Plasticity and Memory in the Retrosplenial Cortex. *Sci Rep*, *8*(1), 3895. https://doi.org/10.1038/s41598-018-22193-0

Beam, C. R., Kaneshiro, C., Jang, J. Y., Reynolds, C. A., Pedersen, N. L., & Gatz, M. (2018). Differences Between Women and Men in Incidence Rates of Dementia and Alzheimer's Disease. *J Alzheimers Dis*, *64*(4), 1077-1083. https://doi.org/10.3233/JAD-180141

Beauquis, J., Vinuesa, A., Pomilio, C., Pavía, P., Galván, V., & Saravia, F. (2014). Neuronal and glial alterations, increased anxiety, and cognitive impairment before hippocampal amyloid deposition in PDAPP mice, model of Alzheimer's disease. *Hippocampus*, *24*(3), 257-269. https://doi.org/10.1002/hipo.22219

Becker, J. T. (1988). Working memory and secondary memory deficits in Alzheimer's disease. *J Clin Exp Neuropsychol*, *10*(6), 739-753. https://doi.org/10.1080/01688638808402811

Bekris, L. M., Yu, C. E., Bird, T. D., & Tsuang, D. W. (2010). Genetics of Alzheimer disease. *J Geriatr Psychiatry Neurol*, *23*(4), 213-227. https://doi.org/10.1177/0891988710383571

Belfiore, R., Rodin, A., Ferreira, E., Velazquez, R., Branca, C., Caccamo, A., & Oddo, S. (2019). Temporal and regional progression of Alzheimer's disease-like pathology in 3xTg-AD mice. *Aging Cell*, *18*(1), e12873. https://doi.org/10.1111/acel.12873

Belzung, C., & Philippot, P. (2007). Anxiety from a phylogenetic perspective: is there a qualitative difference between human and animal anxiety? *Neural Plast*, *2007*, 59676. https://doi.org/10.1155/2007/59676

Benitez, D. P., Jiang, S., Wood, J., Wang, R., Hall, C. M., Peerboom, C.,…Cummings, D. M. (2021). Knock-in models related to Alzheimer's disease: synaptic transmission, plaques and the role of microglia. *Mol Neurodegener*, *16*(1), 47. https://doi.org/10.1186/s13024-021-00457-0

Benzing, W. C., Wujek, J. R., Ward, E. K., Shaffer, D., Ashe, K. H., Younkin, S. G., & Brunden, K. R. (1999). Evidence for glial-mediated inflammation in aged

APP(SW) transgenic mice. *Neurobiol Aging*, *20*(6), 581-589. https://doi.org/10.1016/s0197-4580(99)00065-2
Beretta, C. A., Liu, S., Stegemann, A., Gan, Z., Wang, L., Tan, L. L., & Kuner, R. (2023). Quanty-cFOS, a Novel ImageJ/Fiji Algorithm for Automated Counting of Immunoreactive Cells in Tissue Sections. *Cells*, *12*(5). https://doi.org/10.3390/cells12050704
Berg-Johnsen, J., & Langmoen, I. A. (1992). The effect of isoflurane on excitatory synaptic transmission in the rat hippocampus. *Acta Anaesthesiol Scand*, *36*(4), 350-355. https://doi.org/10.1111/j.1399-6576.1992.tb03480.x
Berlingeri, M., Bottini, G., Basilico, S., Silani, G., Zanardi, G., Sberna, M.,…Paulesu, E. (2008). Anatomy of the episodic buffer: a voxel-based morphometry study in patients with dementia. *Behav Neurol*, *19*(1-2), 29-34. https://doi.org/10.1155/2008/828937
Bermudez-Contreras, E., Clark, B. J., & Wilber, A. (2020). The Neuroscience of Spatial Navigation and the Relationship to Artificial Intelligence. *Front Comput Neurosci*, *14*, 63. https://doi.org/10.3389/fncom.2020.00063
Berridge, M. J. (2010). Calcium hypothesis of Alzheimer's disease. *Pflugers Arch*, *459*(3), 441-449. https://doi.org/10.1007/s00424-009-0736-1
Berridge, M. J., Lipp, P., & Bootman, M. D. (2000). The versatility and universality of calcium signalling. *Nat Rev Mol Cell Biol*, *1*(1), 11-21. https://doi.org/10.1038/35036035
Berron, D., Vogel, J. W., Insel, P. S., Pereira, J. B., Xie, L., Wisse, L. E. M.,…Hansson, O. (2021). Early stages of tau pathology and its associations with functional connectivity, atrophy and memory. *Brain*, *144*(9), 2771-2783. https://doi.org/10.1093/brain/awab114
Bertagna, N. B., Dos Santos, P. G. C., Queiroz, R. M., Fernandes, G. J. D., Cruz, F. C., & Miguel, T. T. (2021). Involvement of the ventral, but not dorsal, hippocampus in anxiety-like behaviors in mice exposed to the elevated plus maze: participation of CRF1 receptor and PKA pathway. *Pharmacol Rep*, *73*(1), 57-72. https://doi.org/10.1007/s43440-020-00182-3
Bertoglio, L. J., & Carobrez, A. P. (2002). Anxiolytic effects of ethanol and phenobarbital are abolished in test-experienced rats submitted to the elevated plus maze. *Pharmacol Biochem Behav*, *73*(4), 963-969. https://doi.org/10.1016/s0091-3057(02)00958-9
Bertoglio, L. J., & Carobrez, A. P. (2003). Anxiolytic-like effects of NMDA/glycine-B receptor ligands are abolished during the elevated plus-maze trial 2 in rats. *Psychopharmacology (Berl)*, *170*(4), 335-342. https://doi.org/10.1007/s00213-003-1558-z
Bertram, L., McQueen, M. B., Mullin, K., Blacker, D., & Tanzi, R. E. (2007). Systematic meta-analyses of Alzheimer disease genetic association studies: the AlzGene database. *Nat Genet*, *39*(1), 17-23. https://doi.org/10.1038/ng1934
Betzer, C., & Jensen, P. H. (2018). Reduced Cytosolic Calcium as an Early Decisive Cellular State in Parkinson's Disease and Synucleinopathies. *Front Neurosci*, *12*, 819. https://doi.org/10.3389/fnins.2018.00819
Betzer, C., Lassen, L. B., Olsen, A., Kofoed, R. H., Reimer, L., Gregersen, E.,…Jensen, P. H. (2018). Alpha-synuclein aggregates activate calcium pump SERCA leading to calcium dysregulation. *EMBO Rep*, *19*(5). https://doi.org/10.15252/embr.201744617

Bezprozvanny, I. (2009). Calcium signaling and neurodegenerative diseases. *Trends Mol Med*, *15*(3), 89-100. https://doi.org/10.1016/j.molmed.2009.01.001
Bezprozvanny, I., & Mattson, M. P. (2008). Neuronal calcium mishandling and the pathogenesis of Alzheimer's disease. *Trends Neurosci*, *31*(9), 454-463. https://doi.org/10.1016/j.tins.2008.06.005
Billings, L. M., Oddo, S., Green, K. N., McGaugh, J. L., & LaFerla, F. M. (2005). Intraneuronal Abeta causes the onset of early Alzheimer's disease-related cognitive deficits in transgenic mice. *Neuron*, *45*(5), 675-688. https://doi.org/10.1016/j.neuron.2005.01.040
Bittner, T., Burgold, S., Dorostkar, M. M., Fuhrmann, M., Wegenast-Braun, B. M., Schmidt, B.,…Herms, J. (2012). Amyloid plaque formation precedes dendritic spine loss. *Acta Neuropathol*, *124*(6), 797-807. https://doi.org/10.1007/s00401-012-1047-8
Blanchard, D. C., Griebel, G., Pobbe, R., & Blanchard, R. J. (2011). Risk assessment as an evolved threat detection and analysis process. *Neurosci Biobehav Rev*, *35*(4), 991-998. https://doi.org/10.1016/j.neubiorev.2010.10.016
Bliss, T. V., & Collingridge, G. L. (1993). A synaptic model of memory: long-term potentiation in the hippocampus. *Nature*, *361*(6407), 31-39. https://doi.org/10.1038/361031a0
Bliss, T. V., Collingridge, G. L., & Morris, R. G. (2014). Synaptic plasticity in health and disease: introduction and overview. *Philos Trans R Soc Lond B Biol Sci*, *369*(1633), 20130129. https://doi.org/10.1098/rstb.2013.0129
Bloom, G. S. (2014). Amyloid-β and tau: the trigger and bullet in Alzheimer disease pathogenesis. *JAMA Neurol*, *71*(4), 505-508. https://doi.org/10.1001/jamaneurol.2013.5847
Bode, D. C., Baker, M. D., & Viles, J. H. (2017). Ion Channel Formation by Amyloid-β42 Oligomers but Not Amyloid-β40 in Cellular Membranes. *J Biol Chem*, *292*(4), 1404-1413. https://doi.org/10.1074/jbc.M116.762526
Bomasang-Layno, E., & Bronsther, R. (2021). Diagnosis and Treatment of Alzheimer's Disease:: An Update. *Dela J Public Health*, *7*(4), 74-85. https://doi.org/10.32481/djph.2021.09.009
Borchelt, D. R., Ratovitski, T., van Lare, J., Lee, M. K., Gonzales, V., Jenkins, N. A.,…Sisodia, S. S. (1997). Accelerated amyloid deposition in the brains of transgenic mice coexpressing mutant presenilin 1 and amyloid precursor proteins. *Neuron*, *19*(4), 939-945. https://doi.org/10.1016/s0896-6273(00)80974-5
Bourin, M., & Hascoët, M. (2003). The mouse light/dark box test. *Eur J Pharmacol*, *463*(1-3), 55-65. https://doi.org/10.1016/s0014-2999(03)01274-3
Bouwman, F. H., Frisoni, G. B., Johnson, S. C., Chen, X., Engelborghs, S., Ikeuchi, T.,…Teunissen, C. (2022). Clinical application of CSF biomarkers for Alzheimer's disease: From rationale to ratios. *Alzheimers Dement (Amst)*, *14*(1), e12314. https://doi.org/10.1002/dad2.12314
Bouyeure, A., & Noulhiane, M. (2020). Memory: Normative development of memory systems. *Handb Clin Neurol*, *173*, 201-213. https://doi.org/10.1016/B978-0-444-64150-2.00018-6
Braak, H., & Braak, E. (1991). Neuropathological stageing of Alzheimer-related changes. *Acta Neuropathol*, *82*(4), 239-259. https://doi.org/10.1007/BF00308809

Braak, H., & Braak, E. (1997). Frequency of stages of Alzheimer-related lesions in different age categories. *Neurobiol Aging*, *18*(4), 351-357. https://doi.org/10.1016/s0197-4580(97)00056-0
Braak, H., Braak, E., Grundke-Iqbal, I., & Iqbal, K. (1986). Occurrence of neuropil threads in the senile human brain and in Alzheimer's disease: a third location of paired helical filaments outside of neurofibrillary tangles and neuritic plaques. *Neurosci Lett*, *65*(3), 351-355. https://doi.org/10.1016/0304-3940(86)90288-0
Braak, H., Thal, D. R., Ghebremedhin, E., & Del Tredici, K. (2011). Stages of the pathologic process in Alzheimer disease: age categories from 1 to 100 years. *J Neuropathol Exp Neurol*, *70*(11), 960-969. https://doi.org/10.1097/NEN.0b013e318232a379
Brini, M., Calì, T., Ottolini, D., & Carafoli, E. (2014). Neuronal calcium signaling: function and dysfunction. *Cell Mol Life Sci*, *71*(15), 2787-2814. https://doi.org/10.1007/s00018-013-1550-7
Broadbelt, T., Mutlu-Smith, M., Carnicero-Senabre, D., Saido, T. C., Saito, T., & Wang, S. H. (2022). Impairment in novelty-promoted memory via behavioral tagging and capture before apparent memory loss in a knock-in model of Alzheimer's disease. *Sci Rep*, *12*(1), 22298. https://doi.org/10.1038/s41598-022-26113-1
Brodmann, K. (1909). Vergleichende Lokalisationslehre der Grosshirnrinde in ihren Prinzipien dargestellt auf Grund des Zellenbaues. In: Barth.
Brown, M. W., & Aggleton, J. P. (2001). Recognition memory: what are the roles of the perirhinal cortex and hippocampus? *Nat Rev Neurosci*, *2*(1), 51-61. https://doi.org/10.1038/35049064
Bryda, E. C. (2013). The Mighty Mouse: the impact of rodents on advances in biomedical research. *Mo Med*, *110*(3), 207-211.
Buckner, R. L., Snyder, A. Z., Shannon, B. J., LaRossa, G., Sachs, R., Fotenos, A. F.,…Mintun, M. A. (2005). Molecular, structural, and functional characterization of Alzheimer's disease: evidence for a relationship between default activity, amyloid, and memory. *J Neurosci*, *25*(34), 7709-7717. https://doi.org/10.1523/JNEUROSCI.2177-05.2005
Bullitt, E. (1990). Expression of c-fos-like protein as a marker for neuronal activity following noxious stimulation in the rat. *J Comp Neurol*, *296*(4), 517-530. https://doi.org/10.1002/cne.902960402
Busche, M. A., Chen, X., Henning, H. A., Reichwald, J., Staufenbiel, M., Sakmann, B., & Konnerth, A. (2012). Critical role of soluble amyloid-β for early hippocampal hyperactivity in a mouse model of Alzheimer's disease. *Proc Natl Acad Sci U S A*, *109*(22), 8740-8745. https://doi.org/10.1073/pnas.1206171109
Busche, M. A., Eichhoff, G., Adelsberger, H., Abramowski, D., Wiederhold, K. H., Haass, C.,…Garaschuk, O. (2008). Clusters of hyperactive neurons near amyloid plaques in a mouse model of Alzheimer's disease. *Science*, *321*(5896), 1686-1689. https://doi.org/10.1126/science.1162844
Busche, M. A., & Konnerth, A. (2015). Neuronal hyperactivity--A key defect in Alzheimer's disease? *Bioessays*, *37*(6), 624-632. https://doi.org/10.1002/bies.201500004
Buss, R. R., Gould, T. W., Ma, J., Vinsant, S., Prevette, D., Winseck, A.,…Oppenheim, R. W. (2006). Neuromuscular development in the absence of programmed cell death: phenotypic alteration of motoneurons and muscle.

J Neurosci, *26*(52), 13413-13427. https://doi.org/10.1523/JNEUROSCI.3528-06.2006
Bussey, T. J., Muir, J. L., & Aggleton, J. P. (1999). Functionally dissociating aspects of event memory: the effects of combined perirhinal and postrhinal cortex lesions on object and place memory in the rat. *J Neurosci*, *19*(1), 495-502.
Butler, W. N., Smith, K. S., van der Meer, M. A. A., & Taube, J. S. (2017). The Head-Direction Signal Plays a Functional Role as a Neural Compass during Navigation. *Curr Biol*, *27*(9), 1259-1267. https://doi.org/10.1016/j.cub.2017.03.033
Cai, C., Lin, P., Cheung, K. H., Li, N., Levchook, C., Pan, Z.,…Ma, J. (2006). The presenilin-2 loop peptide perturbs intracellular Ca2+ homeostasis and accelerates apoptosis. *J Biol Chem*, *281*(24), 16649-16655. https://doi.org/10.1074/jbc.M512026200
Calais, J. B., Valvassori, S. S., Resende, W. R., Feier, G., Athié, M. C., Ribeiro, S.,…Ojopi, E. B. (2013). Long-term decrease in immediate early gene expression after electroconvulsive seizures. *J Neural Transm (Vienna)*, *120*(2), 259-266. https://doi.org/10.1007/s00702-012-0861-4
Calvo-Rodriguez, M., Hernando-Perez, E., Nuñez, L., & Villalobos, C. (2019). Amyloid β Oligomers Increase ER-Mitochondria Ca2+ Cross Talk in Young Hippocampal Neurons and Exacerbate Aging-Induced Intracellular Ca2+ Remodelling. *Front Cell Neurosci*, *13*, 22. https://doi.org/10.3389/fncel.2019.00022
Campbell, L. W., Hao, S. Y., Thibault, O., Blalock, E. M., & Landfield, P. W. (1996). Aging changes in voltage-gated calcium currents in hippocampal CA1 neurons. *J Neurosci*, *16*(19), 6286-6295. https://doi.org/10.1523/JNEUROSCI.16-19-06286.1996
Cao, W., Lin, S., Xia, Q. Q., Du, Y. L., Yang, Q., Zhang, M. Y.,…Luo, J. H. (2018). Gamma Oscillation Dysfunction in mPFC Leads to Social Deficits in Neuroligin 3 R451C Knockin Mice. *Neuron*, *97*(6), 1253-1260.e1257. https://doi.org/10.1016/j.neuron.2018.02.001
Carobrez, A. P., & Bertoglio, L. J. (2005). Ethological and temporal analyses of anxiety-like behavior: the elevated plus-maze model 20 years on. *Neurosci Biobehav Rev*, *29*(8), 1193-1205. https://doi.org/10.1016/j.neubiorev.2005.04.017
Carola, V., D'Olimpio, F., Brunamonti, E., Mangia, F., & Renzi, P. (2002). Evaluation of the elevated plus-maze and open-field tests for the assessment of anxiety-related behaviour in inbred mice. *Behav Brain Res*, *134*(1-2), 49-57. https://doi.org/10.1016/s0166-4328(01)00452-1
Caruso, D., Barron, A. M., Brown, M. A., Abbiati, F., Carrero, P., Pike, C. J.,…Melcangi, R. C. (2013). Age-related changes in neuroactive steroid levels in 3xTg-AD mice. *Neurobiol Aging*, *34*(4), 1080-1089. https://doi.org/10.1016/j.neurobiolaging.2012.10.007
Cascella, R., & Cecchi, C. (2021). Calcium Dyshomeostasis in Alzheimer's Disease Pathogenesis. *Int J Mol Sci*, *22*(9). https://doi.org/10.3390/ijms22094914
Castro, D. M., Dillon, C., Machnicki, G., & Allegri, R. F. (2010). The economic cost of Alzheimer's disease: Family or public health burden? *Dement Neuropsychol*, *4*(4), 262-267. https://doi.org/10.1590/S1980-57642010DN40400003
Chai, W. J., Abd Hamid, A. I., & Abdullah, J. M. (2018). Working Memory From the Psychological and Neurosciences Perspectives: A Review. *Front Psychol*, *9*, 401. https://doi.org/10.3389/fpsyg.2018.00401

Chan, M., Austen, J. M., Eacott, M. J., Easton, A., & Sanderson, D. J. (2019). The NMDA receptor antagonist MK-801 fails to impair long-term recognition memory in mice when the state-dependency of memory is controlled. *Neurobiol Learn Mem*, *161*, 57-62. https://doi.org/10.1016/j.nlm.2019.03.006
Chan, S. L., Mayne, M., Holden, C. P., Geiger, J. D., & Mattson, M. P. (2000). Presenilin-1 mutations increase levels of ryanodine receptors and calcium release in PC12 cells and cortical neurons. *J Biol Chem*, *275*(24), 18195-18200. https://doi.org/10.1074/jbc.M000040200
Chapleau, M., Iaccarino, L., Soleimani-Meigooni, D., & Rabinovici, G. D. (2022). The Role of Amyloid PET in Imaging Neurodegenerative Disorders: A Review. *J Nucl Med*, *63*(Suppl 1), 13S-19S. https://doi.org/10.2967/jnumed.121.263195
Chaudhuri, A. (1997). Neural activity mapping with inducible transcription factors. *Neuroreport*, *8*(16), v-ix.
Cheignon, C., Tomas, M., Bonnefont-Rousselot, D., Faller, P., Hureau, C., & Collin, F. (2018). Oxidative stress and the amyloid beta peptide in Alzheimer's disease. *Redox Biol*, *14*, 450-464. https://doi.org/10.1016/j.redox.2017.10.014
Chen, G., Chen, K. S., Knox, J., Inglis, J., Bernard, A., Martin, S. J.,…Morris, R. G. (2000). A learning deficit related to age and beta-amyloid plaques in a mouse model of Alzheimer's disease. *Nature*, *408*(6815), 975-979. https://doi.org/10.1038/35050103
Chen, G. F., Xu, T. H., Yan, Y., Zhou, Y. R., Jiang, Y., Melcher, K., & Xu, H. E. (2017). Amyloid beta: structure, biology and structure-based therapeutic development. *Acta Pharmacol Sin*, *38*(9), 1205-1235. https://doi.org/10.1038/aps.2017.28
Chen, K., Tian, Z., & Kong, L. (2022). Advances of optical miniscopes for. *Front Neurosci*, *16*, 994079. https://doi.org/10.3389/fnins.2022.994079
Chen, L. L., Lin, L. H., Barnes, C. A., & McNaughton, B. L. (1994). Head-direction cells in the rat posterior cortex. II. Contributions of visual and ideothetic information to the directional firing. *Exp Brain Res*, *101*(1), 24-34. https://doi.org/10.1007/BF00243213
Chen, L. L., Lin, L. H., Green, E. J., Barnes, C. A., & McNaughton, B. L. (1994). Head-direction cells in the rat posterior cortex. I. Anatomical distribution and behavioral modulation. *Exp Brain Res*, *101*(1), 8-23. https://doi.org/10.1007/BF00243212
Chen, W., Gamache, E., Rosenman, D. J., Xie, J., Lopez, M. M., Li, Y. M., & Wang, C. (2014). Familial Alzheimer's mutations within APPTM increase Aβ42 production by enhancing accessibility of ε-cleavage site. *Nat Commun*, *5*, 3037. https://doi.org/10.1038/ncomms4037
Chen, Y., Dang, M., & Zhang, Z. (2021a). Brain mechanisms underlying neuropsychiatric symptoms in Alzheimer's disease: a systematic review of symptom-general and -specific lesion patterns. *Mol Neurodegener*, *16*(1), 38. https://doi.org/10.1186/s13024-021-00456-1
Chen, Y., Wang, J., Cui, C., Su, Y., Jing, D., Wu, L.,…Liang, Z. (2021b). Evaluating the association between brain atrophy, hypometabolism, and cognitive decline in Alzheimer's disease: a PET/MRI study. *Aging (Albany NY)*, *13*(5), 7228-7246. https://doi.org/10.18632/aging.202580
Chen, Y., & Yu, Y. (2023). Tau and neuroinflammation in Alzheimer's disease: interplay mechanisms and clinical translation. *J Neuroinflammation*, *20*(1), 165. https://doi.org/10.1186/s12974-023-02853-3

Cheng, I. H., Scearce-Levie, K., Legleiter, J., Palop, J. J., Gerstein, H., Bien-Ly, N.,…Mucke, L. (2007). Accelerating amyloid-beta fibrillization reduces oligomer levels and functional deficits in Alzheimer disease mouse models. *J Biol Chem*, *282*(33), 23818-23828. https://doi.org/10.1074/jbc.M701078200
Cheung, K. H., Mei, L., Mak, D. O., Hayashi, I., Iwatsubo, T., Kang, D. E., & Foskett, J. K. (2010). Gain-of-function enhancement of IP3 receptor modal gating by familial Alzheimer's disease-linked presenilin mutants in human cells and mouse neurons. *Sci Signal*, *3*(114), ra22. https://doi.org/10.1126/scisignal.2000818
Chidambaram, S. B., Rathipriya, A. G., Bolla, S. R., Bhat, A., Ray, B., Mahalakshmi, A. M.,…Sakharkar, M. K. (2019). Dendritic spines: Revisiting the physiological role. *Prog Neuropsychopharmacol Biol Psychiatry*, *92*, 161-193. https://doi.org/10.1016/j.pnpbp.2019.01.005
Chin, J., Palop, J. J., Puoliväli, J., Massaro, C., Bien-Ly, N., Gerstein, H.,…Mucke, L. (2005). Fyn kinase induces synaptic and cognitive impairments in a transgenic mouse model of Alzheimer's disease. *J Neurosci*, *25*(42), 9694-9703. https://doi.org/10.1523/JNEUROSCI.2980-05.2005
Chiu, R., Boyle, W. J., Meek, J., Smeal, T., Hunter, T., & Karin, M. (1988). The c-Fos protein interacts with c-Jun/AP-1 to stimulate transcription of AP-1 responsive genes. *Cell*, *54*(4), 541-552. https://doi.org/10.1016/0092-8674(88)90076-1
Cho, J., & Sharp, P. E. (2001). Head direction, place, and movement correlates for cells in the rat retrosplenial cortex. *Behav Neurosci*, *115*(1), 3-25. https://doi.org/10.1037/0735-7044.115.1.3
Cho, S. H., Woo, S., Kim, C., Kim, H. J., Jang, H., Kim, B. C.,…Seo, S. W. (2021). Disease progression modelling from preclinical Alzheimer's disease (AD) to AD dementia. *Sci Rep*, *11*(1), 4168. https://doi.org/10.1038/s41598-021-83585-3
Choo, I. H., Lee, D. Y., Oh, J. S., Lee, J. S., Lee, D. S., Song, I. C.,…Woo, J. I. (2010). Posterior cingulate cortex atrophy and regional cingulum disruption in mild cognitive impairment and Alzheimer's disease. *Neurobiol Aging*, *31*(5), 772-779. https://doi.org/10.1016/j.neurobiolaging.2008.06.015
Chouliaras, L., & O'Brien, J. T. (2023). The use of neuroimaging techniques in the early and differential diagnosis of dementia. *Mol Psychiatry*, *28*(10), 4084-4097. https://doi.org/10.1038/s41380-023-02215-8
Chrastil, E. R. (2018). Heterogeneity in human retrosplenial cortex: A review of function and connectivity. *Behav Neurosci*, *132*(5), 317-338. https://doi.org/10.1037/bne0000261
Chung, J. A., & Cummings, J. L. (2000). Neurobehavioral and neuropsychiatric symptoms in Alzheimer's disease: characteristics and treatment. *Neurol Clin*, *18*(4), 829-846. https://doi.org/10.1016/s0733-8619(05)70228-0
Chételat, G., Landeau, B., Eustache, F., Mézenge, F., Viader, F., de la Sayette, V.,…Baron, J. C. (2005). Using voxel-based morphometry to map the structural changes associated with rapid conversion in MCI: a longitudinal MRI study. *Neuroimage*, *27*(4), 934-946. https://doi.org/10.1016/j.neuroimage.2005.05.015
Citri, A., & Malenka, R. C. (2008). Synaptic plasticity: multiple forms, functions, and mechanisms. *Neuropsychopharmacology*, *33*(1), 18-41. https://doi.org/10.1038/sj.npp.1301559
Citron, M., Oltersdorf, T., Haass, C., McConlogue, L., Hung, A. Y., Seubert, P.,…Selkoe, D. J. (1992). Mutation of the beta-amyloid precursor protein in

familial Alzheimer's disease increases beta-protein production. *Nature*, *360*(6405), 672-674. https://doi.org/10.1038/360672a0
Clement, A., Wiborg, O., & Asuni, A. A. (2020). Steps Towards Developing Effective Treatments for Neuropsychiatric Disturbances in Alzheimer's Disease: Insights From Preclinical Models, Clinical Data, and Future Directions. *Front Aging Neurosci*, *12*, 56. https://doi.org/10.3389/fnagi.2020.00056
Cohen, R. M., Rezai-Zadeh, K., Weitz, T. M., Rentsendorj, A., Gate, D., Spivak, I.,…Town, T. (2013). A transgenic Alzheimer rat with plaques, tau pathology, behavioral impairment, oligomeric aβ, and frank neuronal loss. *J Neurosci*, *33*(15), 6245-6256. https://doi.org/10.1523/JNEUROSCI.3672-12.2013
Cohen, S. J., & Stackman, R. W. (2015). Assessing rodent hippocampal involvement in the novel object recognition task. A review. *Behav Brain Res*, *285*, 105-117. https://doi.org/10.1016/j.bbr.2014.08.002
Cohen-Mansfield, J. (2001). Nonpharmacologic interventions for inappropriate behaviors in dementia: a review, summary, and critique. *Am J Geriatr Psychiatry*, *9*(4), 361-381.
Cole, J. C., & Rodgers, R. J. (1994). Ethological evaluation of the effects of acute and chronic buspirone treatment in the murine elevated plus-maze test: comparison with haloperidol. *Psychopharmacology (Berl)*, *114*(2), 288-296. https://doi.org/10.1007/BF02244851
Collett, T. S., & Graham, P. (2004). Animal navigation: path integration, visual landmarks and cognitive maps. *Curr Biol*, *14*(12), R475-477. https://doi.org/10.1016/j.cub.2004.06.013
Cooper, B. G., Manka, T. F., & Mizumori, S. J. (2001). Finding your way in the dark: the retrosplenial cortex contributes to spatial memory and navigation without visual cues. *Behav Neurosci*, *115*(5), 1012-1028. https://doi.org/10.1037//0735-7044.115.5.1012
Cooper, B. G., & Mizumori, S. J. (1999). Retrosplenial cortex inactivation selectively impairs navigation in darkness. *Neuroreport*, *10*(3), 625-630. https://doi.org/10.1097/00001756-199902250-00033
Cooper, B. G., & Mizumori, S. J. (2001). Temporary inactivation of the retrosplenial cortex causes a transient reorganization of spatial coding in the hippocampus. *J Neurosci*, *21*(11), 3986-4001. https://doi.org/10.1523/JNEUROSCI.21-11-03986.2001
Corbett, B. F., You, J. C., Zhang, X., Pyfer, M. S., Tosi, U., Iascone, D. M.,…Chin, J. (2017). ΔFosB Regulates Gene Expression and Cognitive Dysfunction in a Mouse Model of Alzheimer's Disease. *Cell Rep*, *20*(2), 344-355. https://doi.org/10.1016/j.celrep.2017.06.040
Corder, E. H., Saunders, A. M., Strittmatter, W. J., Schmechel, D. E., Gaskell, P. C., Small, G. W.,…Pericak-Vance, M. A. (1993). Gene dose of apolipoprotein E type 4 allele and the risk of Alzheimer's disease in late onset families. *Science*, *261*(5123), 921-923. https://doi.org/10.1126/science.8346443
Corsi, A., Bombieri, C., Valenti, M. T., & Romanelli, M. G. (2022). Tau Isoforms: Gaining Insight into *MAPT* Alternative Splicing. *Int J Mol Sci*, *23*(23). https://doi.org/10.3390/ijms232315383
Coutureau, E., & Di Scala, G. (2009). Entorhinal cortex and cognition. *Prog Neuropsychopharmacol Biol Psychiatry*, *33*(5), 753-761. https://doi.org/10.1016/j.pnpbp.2009.03.038

Craddock, R., Vasalauskaite, A., Ranson, A., & Sengpiel, F. (2023). Experience dependent plasticity of higher visual cortical areas in the mouse. *Cereb Cortex*, *33*(15), 9303-9312. https://doi.org/10.1093/cercor/bhad203
Cras, P., Kawai, M., Lowery, D., Gonzalez-DeWhitt, P., Greenberg, B., & Perry, G. (1991). Senile plaque neurites in Alzheimer disease accumulate amyloid precursor protein. *Proc Natl Acad Sci U S A*, *88*(17), 7552-7556. https://doi.org/10.1073/pnas.88.17.7552
Crawley, J., & Goodwin, F. K. (1980). Preliminary report of a simple animal behavior model for the anxiolytic effects of benzodiazepines. *Pharmacol Biochem Behav*, *13*(2), 167-170. https://doi.org/10.1016/0091-3057(80)90067-2
Crawley, J. N. (1981). Neuropharmacologic specificity of a simple animal model for the behavioral actions of benzodiazepines. *Pharmacol Biochem Behav*, *15*(5), 695-699. https://doi.org/10.1016/0091-3057(81)90007-1
Cruz-Morales, S. E., Santos, N. R., & Brandão, M. L. (2002). One-trial tolerance to midazolam is due to enhancement of fear and reduction of anxiolytic-sensitive behaviors in the elevated plus-maze retest in the rat. *Pharmacol Biochem Behav*, *72*(4), 973-978. https://doi.org/10.1016/s0091-3057(02)00813-4
Cummings, J. L., Morstorf, T., & Zhong, K. (2014). Alzheimer's disease drug-development pipeline: few candidates, frequent failures. *Alzheimers Res Ther*, *6*(4), 37. https://doi.org/10.1186/alzrt269
Curran, T., Peters, G., Van Beveren, C., Teich, N. M., & Verma, I. M. (1982). FBJ murine osteosarcoma virus: identification and molecular cloning of biologically active proviral DNA. *J Virol*, *44*(2), 674-682. https://doi.org/10.1128/JVI.44.2.674-682.1982
Czajkowski, R., Jayaprakash, B., Wiltgen, B., Rogerson, T., Guzman-Karlsson, M. C., Barth, A. L.,…Silva, A. J. (2014). Encoding and storage of spatial information in the retrosplenial cortex. *Proc Natl Acad Sci U S A*, *111*(23), 8661-8666. https://doi.org/10.1073/pnas.1313222111
d'Isa, R., Comi, G., & Leocani, L. (2021). Apparatus design and behavioural testing protocol for the evaluation of spatial working memory in mice through the spontaneous alternation T-maze. *Sci Rep*, *11*(1), 21177. https://doi.org/10.1038/s41598-021-00402-7
Dale, E., Pehrson, A. L., Jeyarajah, T., Li, Y., Leiser, S. C., Smagin, G.,…Sanchez, C. (2016). Effects of serotonin in the hippocampus: how SSRIs and multimodal antidepressants might regulate pyramidal cell function. *CNS Spectr*, *21*(2), 143-161. https://doi.org/10.1017/S1092852915000425
Dalley, J. W., & Roiser, J. P. (2012). Dopamine, serotonin and impulsivity. *Neuroscience*, *215*, 42-58. https://doi.org/10.1016/j.neuroscience.2012.03.065
Davis, M., Rainnie, D., & Cassell, M. (1994). Neurotransmission in the rat amygdala related to fear and anxiety. *Trends Neurosci*, *17*(5), 208-214. https://doi.org/10.1016/0166-2236(94)90106-6
Dawson, G. R., Crawford, S. P., Stanhope, K. J., Iversen, S. D., & Tricklebank, M. D. (1994). One-trial tolerance to the effects of chlordiazepoxide on the elevated plus maze may be due to locomotor habituation, not repeated drug exposure. *Psychopharmacology (Berl)*, *113*(3-4), 570-572. https://doi.org/10.1007/BF02245242
Dawson, G. R., Seabrook, G. R., Zheng, H., Smith, D. W., Graham, S., O'Dowd, G.,…Sirinathsinghji, D. J. (1999). Age-related cognitive deficits, impaired long-term potentiation and reduction in synaptic marker density in mice lacking the

beta-amyloid precursor protein. *Neuroscience*, *90*(1), 1-13. https://doi.org/10.1016/s0306-4522(98)00410-2
Dawson, G. R., & Tricklebank, M. D. (1995). Use of the elevated plus maze in the search for novel anxiolytic agents. *Trends Pharmacol Sci*, *16*(2), 33-36. https://doi.org/10.1016/s0165-6147(00)88973-7
De Felice, F. G., Velasco, P. T., Lambert, M. P., Viola, K., Fernandez, S. J., Ferreira, S. T., & Klein, W. L. (2007). Abeta oligomers induce neuronal oxidative stress through an N-methyl-D-aspartate receptor-dependent mechanism that is blocked by the Alzheimer drug memantine. *J Biol Chem*, *282*(15), 11590-11601. https://doi.org/10.1074/jbc.M607483200
De Jonghe, C., Esselens, C., Kumar-Singh, S., Craessaerts, K., Serneels, S., Checler, F.,…De Strooper, B. (2001). Pathogenic APP mutations near the gamma-secretase cleavage site differentially affect Abeta secretion and APP C-terminal fragment stability. *Hum Mol Genet*, *10*(16), 1665-1671. https://doi.org/10.1093/hmg/10.16.1665
de Landeta, A. B., Pereyra, M., Medina, J. H., & Katche, C. (2020). Anterior retrosplenial cortex is required for long-term object recognition memory. *Sci Rep*, *10*(1), 4002. https://doi.org/10.1038/s41598-020-60937-z
de Landeta, A. B., Pereyra, M., Miranda, M., Bekinschtein, P., Medina, J. H., & Katche, C. (2021). Functional connectivity of anterior retrosplenial cortex in object recognition memory. *Neurobiol Learn Mem*, *186*, 107544. https://doi.org/10.1016/j.nlm.2021.107544
Deacon, R. M., Cholerton, L. L., Talbot, K., Nair-Roberts, R. G., Sanderson, D. J., Romberg, C.,…Rawlins, J. N. (2008). Age-dependent and -independent behavioral deficits in Tg2576 mice. *Behav Brain Res*, *189*(1), 126-138. https://doi.org/10.1016/j.bbr.2007.12.024
Deacon, R. M., & Rawlins, J. N. (2006). T-maze alternation in the rodent. *Nat Protoc*, *1*(1), 7-12. https://doi.org/10.1038/nprot.2006.2
Dean, R. L., Scozzafava, J., Goas, J. A., Regan, B., Beer, B., & Bartus, R. T. (1981). Age-related differences in behavior across the life span of the C57BL/6J mouse. *Exp Aging Res*, *7*(4), 427-451. https://doi.org/10.1080/03610738108259823
Degawa, T., Kawahata, I., Izumi, H., Shinoda, Y., & Fukunaga, K. (2021). T-type Ca2+ channel enhancer SAK3 administration improves the BPSD-like behaviours in AppNL-G-F/NL-G-F knock-in mice. *J Pharmacol Sci*, *146*(1), 1-9. https://doi.org/10.1016/j.jphs.2021.02.006
Del Prete, D., Checler, F., & Chami, M. (2014). Ryanodine receptors: physiological function and deregulation in Alzheimer disease. *Mol Neurodegener*, *9*, 21. https://doi.org/10.1186/1750-1326-9-21
Demuro, A., Mina, E., Kayed, R., Milton, S. C., Parker, I., & Glabe, C. G. (2005). Calcium dysregulation and membrane disruption as a ubiquitous neurotoxic mechanism of soluble amyloid oligomers. *J Biol Chem*, *280*(17), 17294-17300. https://doi.org/10.1074/jbc.M500997200
Desgranges, B., Baron, J. C., Lalevée, C., Giffard, B., Viader, F., de La Sayette, V., & Eustache, F. (2002). The neural substrates of episodic memory impairment in Alzheimer's disease as revealed by FDG-PET: relationship to degree of deterioration. *Brain*, *125*(Pt 5), 1116-1124. https://doi.org/10.1093/brain/awf097
Dhana, K., Franco, O. H., Ritz, E. M., Ford, C. N., Desai, P., Krueger, K. R.,…Rajan, K. B. (2022). Healthy lifestyle and life expectancy with and without Alzheimer's

dementia: population based cohort study. *BMJ*, *377*, e068390. https://doi.org/10.1136/bmj-2021-068390
Dias, R., Robbins, T. W., & Roberts, A. C. (1996). Dissociation in prefrontal cortex of affective and attentional shifts. *Nature*, *380*(6569), 69-72. https://doi.org/10.1038/380069a0
Dillon, G. M., Qu, X., Marcus, J. N., & Dodart, J. C. (2008). Excitotoxic lesions restricted to the dorsal CA1 field of the hippocampus impair spatial memory and extinction learning in C57BL/6 mice. *Neurobiol Learn Mem*, *90*(2), 426-433. https://doi.org/10.1016/j.nlm.2008.05.008
Diniz, B. S., Butters, M. A., Albert, S. M., Dew, M. A., & Reynolds, C. F. (2013). Late-life depression and risk of vascular dementia and Alzheimer's disease: systematic review and meta-analysis of community-based cohort studies. *Br J Psychiatry*, *202*(5), 329-335. https://doi.org/10.1192/bjp.bp.112.118307
Dodart, J. C., Meziane, H., Mathis, C., Bales, K. R., Paul, S. M., & Ungerer, A. (1999). Behavioral disturbances in transgenic mice overexpressing the V717F beta-amyloid precursor protein. *Behav Neurosci*, *113*(5), 982-990. https://doi.org/10.1037//0735-7044.113.5.982
Donovan, N. J., Locascio, J. J., Marshall, G. A., Gatchel, J., Hanseeuw, B. J., Rentz, D. M.,…Study, H. A. B. (2018). Longitudinal Association of Amyloid Beta and Anxious-Depressive Symptoms in Cognitively Normal Older Adults. *Am J Psychiatry*, *175*(6), 530-537. https://doi.org/10.1176/appi.ajp.2017.17040442
Doostdar, N., Airey, J., Radulescu, C. I., Melgosa-Ecenarro, L., Zabouri, N., Pavlidi, P.,…Barnes, S. J. (2021). Multi-scale network imaging in a mouse model of amyloidosis. *Cell Calcium*, *95*, 102365. https://doi.org/10.1016/j.ceca.2021.102365
Dorszewska, J., Prendecki, M., Oczkowska, A., Dezor, M., & Kozubski, W. (2016). Molecular Basis of Familial and Sporadic Alzheimer's Disease. *Curr Alzheimer Res*, *13*(9), 952-963. https://doi.org/10.2174/1567205013666160314150501
Drzezga, A., Becker, J. A., Van Dijk, K. R., Sreenivasan, A., Talukdar, T., Sullivan, C.,…Sperling, R. A. (2011). Neuronal dysfunction and disconnection of cortical hubs in non-demented subjects with elevated amyloid burden. *Brain*, *134*(Pt 6), 1635-1646. https://doi.org/10.1093/brain/awr066
Dubois, B., Feldman, H. H., Jacova, C., Cummings, J. L., Dekosky, S. T., Barberger-Gateau, P.,…Scheltens, P. (2010). Revising the definition of Alzheimer's disease: a new lexicon. *Lancet Neurol*, *9*(11), 1118-1127. https://doi.org/10.1016/S1474-4422(10)70223-4
Dubois, B., Feldman, H. H., Jacova, C., Dekosky, S. T., Barberger-Gateau, P., Cummings, J.,…Scheltens, P. (2007). Research criteria for the diagnosis of Alzheimer's disease: revising the NINCDS-ADRDA criteria. *Lancet Neurol*, *6*(8), 734-746. https://doi.org/10.1016/S1474-4422(07)70178-3
Dubois, B., Feldman, H. H., Jacova, C., Hampel, H., Molinuevo, J. L., Blennow, K.,…Cummings, J. L. (2014). Advancing research diagnostic criteria for Alzheimer's disease: the IWG-2 criteria. *Lancet Neurol*, *13*(6), 614-629. https://doi.org/10.1016/S1474-4422(14)70090-0
Dubois, B., Hampel, H., Feldman, H. H., Scheltens, P., Aisen, P., Andrieu, S.,…Washington DC, U. S. A. (2016). Preclinical Alzheimer's disease: Definition, natural history, and diagnostic criteria. *Alzheimers Dement*, *12*(3), 292-323. https://doi.org/10.1016/j.jalz.2016.02.002
Dudchenko, P. A. (2001). How do animals actually solve the T maze? *Behav Neurosci*, *115*(4), 850-860.

Dudchenko, P. A., Wood, E. R., & Eichenbaum, H. (2000). Neurotoxic hippocampal lesions have no effect on odor span and little effect on odor recognition memory but produce significant impairments on spatial span, recognition, and alternation. *J Neurosci*, *20*(8), 2964-2977.
Dudchenko, P. A., Wood, E. R., & Smith, A. (2019). A new perspective on the head direction cell system and spatial behavior. *Neurosci Biobehav Rev*, *105*, 24-33. https://doi.org/10.1016/j.neubiorev.2019.06.036
Duff, K., Eckman, C., Zehr, C., Yu, X., Prada, C. M., Perez-tur, J.,…Younkin, S. (1996). Increased amyloid-beta42(43) in brains of mice expressing mutant presenilin 1. *Nature*, *383*(6602), 710-713. https://doi.org/10.1038/383710a0
Dunnett, S. B., Nathwani, F., & Brasted, P. J. (1999). Medial prefrontal and neostriatal lesions disrupt performance in an operant delayed alternation task in rats. *Behav Brain Res*, *106*(1-2), 13-28. https://doi.org/10.1016/s0166-4328(99)00076-5
Economidou, D., Theobald, D. E., Robbins, T. W., Everitt, B. J., & Dalley, J. W. (2012). Norepinephrine and dopamine modulate impulsivity on the five-choice serial reaction time task through opponent actions in the shell and core sub-regions of the nucleus accumbens. *Neuropsychopharmacology*, *37*(9), 2057-2066. https://doi.org/10.1038/npp.2012.53
Edwards, E. R., Spira, A. P., Barnes, D. E., & Yaffe, K. (2009). Neuropsychiatric symptoms in mild cognitive impairment: differences by subtype and progression to dementia. *Int J Geriatr Psychiatry*, *24*(7), 716-722. https://doi.org/10.1002/gps.2187
Edwards, S., Trepel, D., Ritchie, C., Hviid Hahn-Pedersen, J., Robinson, D. E., Sum Chan, M.,…Evans, M. (2024). Real world outcomes, healthcare utilisation and costs of Alzheimer's disease in England. *Aging and Health Research*, *4*(1), 100180.
Eimer, W. A., & Vassar, R. (2013). Neuron loss in the 5XFAD mouse model of Alzheimer's disease correlates with intraneuronal Aβ42 accumulation and Caspase-3 activation. *Mol Neurodegener*, *8*, 2. https://doi.org/10.1186/1750-1326-8-2
El Haj, M., & Kapogiannis, D. (2016). Time distortions in Alzheimer's disease: a systematic review and theoretical integration. *NPJ Aging Mech Dis*, *2*, 16016. https://doi.org/10.1038/npjamd.2016.16
El Haj, M., Roche, J., Jardri, R., Kapogiannis, D., Gallouj, K., & Antoine, P. (2017). Clinical and neurocognitive aspects of hallucinations in Alzheimer's disease. *Neurosci Biobehav Rev*, *83*, 713-720. https://doi.org/10.1016/j.neubiorev.2017.02.021
Elduayen, C., & Save, E. (2014). The retrosplenial cortex is necessary for path integration in the dark. *Behav Brain Res*, *272*, 303-307. https://doi.org/10.1016/j.bbr.2014.07.009
Ennaceur, A., & Chazot, P. L. (2016). Preclinical animal anxiety research - flaws and prejudices. *Pharmacol Res Perspect*, *4*(2), e00223. https://doi.org/10.1002/prp2.223
Ennaceur, A., & Delacour, J. (1988). A new one-trial test for neurobiological studies of memory in rats. 1: Behavioral data. *Behav Brain Res*, *31*(1), 47-59. https://doi.org/10.1016/0166-4328(88)90157-x
Ennaceur, A., Neave, N., & Aggleton, J. P. (1996). Neurotoxic lesions of the perirhinal cortex do not mimic the behavioural effects of fornix transection in

the rat. *Behav Brain Res*, *80*(1-2), 9-25. https://doi.org/10.1016/0166-4328(96)00006-x
Ennaceur, A., Neave, N., & Aggleton, J. P. (1997). Spontaneous object recognition and object location memory in rats: the effects of lesions in the cingulate cortices, the medial prefrontal cortex, the cingulum bundle and the fornix. *Exp Brain Res*, *113*(3), 509-519. https://doi.org/10.1007/pl00005603
Epstein, R. A. (2008). Parahippocampal and retrosplenial contributions to human spatial navigation. *Trends Cogn Sci*, *12*(10), 388-396. https://doi.org/10.1016/j.tics.2008.07.004
Epstein, R. A., Higgins, J. S., Jablonski, K., & Feiler, A. M. (2007). Visual scene processing in familiar and unfamiliar environments. *J Neurophysiol*, *97*(5), 3670-3683. https://doi.org/10.1152/jn.00003.2007
Esparza, T. J., Zhao, H., Cirrito, J. R., Cairns, N. J., Bateman, R. J., Holtzman, D. M., & Brody, D. L. (2013). Amyloid-β oligomerization in Alzheimer dementia versus high-pathology controls. *Ann Neurol*, *73*(1), 104-119. https://doi.org/10.1002/ana.23748
España, J., Valero, J., Miñano-Molina, A. J., Masgrau, R., Martín, E., Guardia-Laguarta, C.,…Saura, C. A. (2010). beta-Amyloid disrupts activity-dependent gene transcription required for memory through the CREB coactivator CRTC1. *J Neurosci*, *30*(28), 9402-9410. https://doi.org/10.1523/JNEUROSCI.2154-10.2010
Espinoza, M., de Silva, R., Dickson, D. W., & Davies, P. (2008). Differential incorporation of tau isoforms in Alzheimer's disease. *J Alzheimers Dis*, *14*(1), 1-16. https://doi.org/10.3233/jad-2008-14101
Etcheberrigaray, R., Hirashima, N., Nee, L., Prince, J., Govoni, S., Racchi, M.,…Alkon, D. L. (1998). Calcium responses in fibroblasts from asymptomatic members of Alzheimer's disease families. *Neurobiol Dis*, *5*(1), 37-45. https://doi.org/10.1006/nbdi.1998.0176
Etienne, A. S., & Jeffery, K. J. (2004). Path integration in mammals. *Hippocampus*, *14*(2), 180-192. https://doi.org/10.1002/hipo.10173
Evangelisti, E., Cascella, R., Becatti, M., Marrazza, G., Dobson, C. M., Chiti, F.,…Cecchi, C. (2016). Binding affinity of amyloid oligomers to cellular membranes is a generic indicator of cellular dysfunction in protein misfolding diseases. *Sci Rep*, *6*, 32721. https://doi.org/10.1038/srep32721
Evans, C. E., Miners, J. S., Piva, G., Willis, C. L., Heard, D. M., Kidd, E. J.,…Kehoe, P. G. (2020). ACE2 activation protects against cognitive decline and reduces amyloid pathology in the Tg2576 mouse model of Alzheimer's disease. *Acta Neuropathol*, *139*(3), 485-502. https://doi.org/10.1007/s00401-019-02098-6
Evans, C. E., Thomas, R. S., Freeman, T. J., Hvoslef-Eide, M., Good, M. A., & Kidd, E. J. (2019). Selective reduction of APP-BACE1 activity improves memory via NMDA-NR2B receptor-mediated mechanisms in aged PDAPP mice. *Neurobiol Aging*, *75*, 136-149. https://doi.org/10.1016/j.neurobiolaging.2018.11.011
Fang, C., Hernandez, P., Liow, K., Damiano, E., Zetterberg, H., Blennow, K.,…Maccecchini, M. (2023). Buntanetap, a Novel Translational Inhibitor of Multiple Neurotoxic Proteins, Proves to Be Safe and Promising in Both Alzheimer's and Parkinson's Patients. *J Prev Alzheimers Dis*, *10*(1), 25-33. https://doi.org/10.14283/jpad.2022.84
Farina, F. R., Pavithra, P., An, H., Marquez, M., O'Loughlin, P., Regan, J.,…Griffith, J. W. (2023). Validation of the Fear and Avoidance of Memory Loss scale in

community-based older adults. *Alzheimers Dement (Amst)*, *15*(2), e12432. https://doi.org/10.1002/dad2.12432
Farrer, L. A., Cupples, L. A., Haines, J. L., Hyman, B., Kukull, W. A., Mayeux, R.,…van Duijn, C. M. (1997). Effects of age, sex, and ethnicity on the association between apolipoprotein E genotype and Alzheimer disease. A meta-analysis. APOE and Alzheimer Disease Meta Analysis Consortium. *JAMA*, *278*(16), 1349-1356.
Fernandes, C., & File, S. E. (1996). The influence of open arm ledges and maze experience in the elevated plus-maze. *Pharmacol Biochem Behav*, *54*(1), 31-40. https://doi.org/10.1016/0091-3057(95)02171-x
Fernández Espejo, E. (1997). Structure of the mouse behaviour on the elevated plus-maze test of anxiety. *Behav Brain Res*, *86*(1), 105-112. https://doi.org/10.1016/s0166-4328(96)02245-0
Fernández-Quezada, David, Luquín, S., Ruvalcaba-Delgadillo, Yaveth, García-Estrada,…Fernando. (2022). Sex Differences in the Expression of c-fos in a Rat Brain after Exposure to Environmental Noise. *Sustainability*, *14*(5), 2798.
Ferreira, I. L., Bajouco, L. M., Mota, S. I., Auberson, Y. P., Oliveira, C. R., & Rego, A. C. (2012). Amyloid beta peptide 1-42 disturbs intracellular calcium homeostasis through activation of GluN2B-containing N-methyl-d-aspartate receptors in cortical cultures. *Cell Calcium*, *51*(2), 95-106. https://doi.org/10.1016/j.ceca.2011.11.008
Ferreira, S. T., & Klein, W. L. (2011). The Aβ oligomer hypothesis for synapse failure and memory loss in Alzheimer's disease. *Neurobiol Learn Mem*, *96*(4), 529-543. https://doi.org/10.1016/j.nlm.2011.08.003
Ferreira, S. T., Lourenco, M. V., Oliveira, M. M., & De Felice, F. G. (2015). Soluble amyloid-β oligomers as synaptotoxins leading to cognitive impairment in Alzheimer's disease. *Front Cell Neurosci*, *9*, 191. https://doi.org/10.3389/fncel.2015.00191
Ferreiro, E., Oliveira, C. R., & Pereira, C. (2004). Involvement of endoplasmic reticulum Ca2+ release through ryanodine and inositol 1,4,5-triphosphate receptors in the neurotoxic effects induced by the amyloid-beta peptide. *J Neurosci Res*, *76*(6), 872-880. https://doi.org/10.1002/jnr.20135
Ferretti, L., McCurry, S. M., Logsdon, R., Gibbons, L., & Teri, L. (2001). Anxiety and Alzheimer's disease. *J Geriatr Psychiatry Neurol*, *14*(1), 52-58. https://doi.org/10.1177/089198870101400111
Ferris, C. S., Inman, C. S., & Hamann, S. (2024). FMRI correlates of autobiographical memory: Comparing silent retrieval with narrated retrieval. *Neuropsychologia*, *196*, 108842. https://doi.org/10.1016/j.neuropsychologia.2024.108842
File, S. E. (1985). Animal models for predicting clinical efficacy of anxiolytic drugs: social behaviour. *Neuropsychobiology*, *13*(1-2), 55-62. https://doi.org/10.1159/000118163
File, S. E. (1993). The interplay of learning and anxiety in the elevated plus-maze. *Behav Brain Res*, *58*(1-2), 199-202. https://doi.org/10.1016/0166-4328(93)90103-w
File, S. E., & Wardill, A. G. (1975). Validity of head-dipping as a measure of exploration in a modified hole-board. *Psychopharmacologia*, *44*(1), 53-59. https://doi.org/10.1007/BF00421184
File, S. E., & Zangrossi, H. (1993). "One-trial tolerance" to the anxiolytic actions of benzodiazepines in the elevated plus-maze, or the development of a phobic

state? *Psychopharmacology (Berl)*, *110*(1-2), 240-244. https://doi.org/10.1007/BF02246980
File, S. E., Zangrossi, H., Viana, M., & Graeff, F. G. (1993). Trial 2 in the elevated plus-maze: a different form of fear? *Psychopharmacology (Berl)*, *111*(4), 491-494. https://doi.org/10.1007/BF02253541
Fleischmann, A., Hvalby, O., Jensen, V., Strekalova, T., Zacher, C., Layer, L. E.,…Gass, P. (2003). Impaired long-term memory and NR2A-type NMDA receptor-dependent synaptic plasticity in mice lacking c-Fos in the CNS. *J Neurosci*, *23*(27), 9116-9122. https://doi.org/10.1523/JNEUROSCI.23-27-09116.2003
Flores-Cordero, J. A., Pérez-Pérez, A., Jiménez-Cortegana, C., Alba, G., Flores-Barragán, A., & Sánchez-Margalet, V. (2022). Obesity as a Risk Factor for Dementia and Alzheimer's Disease: The Role of Leptin. *Int J Mol Sci*, *23*(9). https://doi.org/10.3390/ijms23095202
Folstein, M. F., Folstein, S. E., & McHugh, P. R. (1975). "Mini-mental state". A practical method for grading the cognitive state of patients for the clinician. *J Psychiatr Res*, *12*(3), 189-198. https://doi.org/10.1016/0022-3956(75)90026-6
Forloni, G., & Balducci, C. (2018). Alzheimer's Disease, Oligomers, and Inflammation. *J Alzheimers Dis*, *62*(3), 1261-1276. https://doi.org/10.3233/JAD-170819
Fortin, N. J., Agster, K. L., & Eichenbaum, H. B. (2002). Critical role of the hippocampus in memory for sequences of events. *Nat Neurosci*, *5*(5), 458-462. https://doi.org/10.1038/nn834
Fowles, D. C. (2024). Arousal, Gray's theory of anxiety, and the etiology of psychopathy. *Biol Psychol*, *188*, 108772. https://doi.org/10.1016/j.biopsycho.2024.108772
Fratiglioni, L., Ahlbom, A., Viitanen, M., & Winblad, B. (1993). Risk factors for late-onset Alzheimer's disease: a population-based, case-control study. *Ann Neurol*, *33*(3), 258-266. https://doi.org/10.1002/ana.410330306
Frautschy, S. A., Yang, F., Irrizarry, M., Hyman, B., Saido, T. C., Hsiao, K., & Cole, G. M. (1998). Microglial response to amyloid plaques in APPsw transgenic mice. *Am J Pathol*, *152*(1), 307-317.
Frey, U., & Morris, R. G. (1997). Synaptic tagging and long-term potentiation. *Nature*, *385*(6616), 533-536. https://doi.org/10.1038/385533a0
Frick, A., Besson, G., Salmon, E., & Delhaye, E. (2023). Perirhinal cortex is associated with fine-grained discrimination of conceptually confusable objects in Alzheimer's disease. *Neurobiol Aging*, *130*, 1-11. https://doi.org/10.1016/j.neurobiolaging.2023.06.003
Frisoni, G. B., Lorenzi, M., Caroli, A., Kemppainen, N., Någren, K., & Rinne, J. O. (2009). In vivo mapping of amyloid toxicity in Alzheimer disease. *Neurology*, *72*(17), 1504-1511. https://doi.org/10.1212/WNL.0b013e3181a2e896
Funahashi, S. (2013). Space representation in the prefrontal cortex. *Prog Neurobiol*, *103*, 131-155. https://doi.org/10.1016/j.pneurobio.2012.04.002
Funahashi, S. (2017). Working Memory in the Prefrontal Cortex. *Brain Sci*, *7*(5). https://doi.org/10.3390/brainsci7050049
Futter, J. E., & Aggleton, J. P. (2006). How rats perform spatial working memory tasks: limitations in the use of egocentric and idiothetic working memory. *Q J Exp Psychol (Hove)*, *59*(1), 77-99. https://doi.org/10.1080/02724990544000068

Fyhn, M., Hafting, T., Treves, A., Moser, M. B., & Moser, E. I. (2007). Hippocampal remapping and grid realignment in entorhinal cortex. *Nature*, *446*(7132), 190-194. https://doi.org/10.1038/nature05601

Förster, S., Grimmer, T., Miederer, I., Henriksen, G., Yousefi, B. H., Graner, P.,…Drzezga, A. (2012). Regional expansion of hypometabolism in Alzheimer's disease follows amyloid deposition with temporal delay. *Biol Psychiatry*, *71*(9), 792-797. https://doi.org/10.1016/j.biopsych.2011.04.023

Gallagher, D., Coen, R., Kilroy, D., Belinski, K., Bruce, I., Coakley, D.,…Lawlor, B. A. (2011). Anxiety and behavioural disturbance as markers of prodromal Alzheimer's disease in patients with mild cognitive impairment. *Int J Geriatr Psychiatry*, *26*(2), 166-172. https://doi.org/10.1002/gps.2509

Galloway, D. A., Phillips, A. E. M., Owen, D. R. J., & Moore, C. S. (2019). Phagocytosis in the Brain: Homeostasis and Disease. *Front Immunol*, *10*, 790. https://doi.org/10.3389/fimmu.2019.00790

Gamache, J., Benzow, K., Forster, C., Kemper, L., Hlynialuk, C., Furrow, E.,…Koob, M. D. (2019). Factors other than hTau overexpression that contribute to tauopathy-like phenotype in rTg4510 mice. *Nat Commun*, *10*(1), 2479. https://doi.org/10.1038/s41467-019-10428-1

Games, D., Adams, D., Alessandrini, R., Barbour, R., Berthelette, P., Blackwell, C.,…Gillespie, F. (1995). Alzheimer-type neuropathology in transgenic mice overexpressing V717F beta-amyloid precursor protein. *Nature*, *373*(6514), 523-527. https://doi.org/10.1038/373523a0

Gao, L., Zhang, Y., Sterling, K., & Song, W. (2022). Brain-derived neurotrophic factor in Alzheimer's disease and its pharmaceutical potential. *Transl Neurodegener*, *11*(1), 4. https://doi.org/10.1186/s40035-022-00279-0

Garcia-Alloza, M., Robbins, E. M., Zhang-Nunes, S. X., Purcell, S. M., Betensky, R. A., Raju, S.,…Frosch, M. P. (2006). Characterization of amyloid deposition in the APPswe/PS1dE9 mouse model of Alzheimer disease. *Neurobiol Dis*, *24*(3), 516-524. https://doi.org/10.1016/j.nbd.2006.08.017

Garcia-Casas, P., Rossini, M., Filadi, R., & Pizzo, P. (2023). Mitochondrial Ca2+ signaling and Alzheimer's disease. *Cell Calcium*, *113*, 102757. https://doi.org/10.1016/j.ceca.2023.102757

Garwood, C. J., Pooler, A. M., Atherton, J., Hanger, D. P., & Noble, W. (2011). Astrocytes are important mediators of Aβ-induced neurotoxicity and tau phosphorylation in primary culture. *Cell Death Dis*, *2*(6), e167. https://doi.org/10.1038/cddis.2011.50

Gauthier, S., Reisberg, B., Zaudig, M., Petersen, R., Ritchie, K., Broich, K.,…Winblad, B. (2006). Mild cognitive impairment. *The Lancet*, *367*(9518), 1262-1270.

Geda, Y. E., Roberts, R. O., Knopman, D. S., Petersen, R. C., Christianson, T. J., Pankratz, V. S.,…Rocca, W. A. (2008). Prevalence of neuropsychiatric symptoms in mild cognitive impairment and normal cognitive aging: population-based study. *Arch Gen Psychiatry*, *65*(10), 1193-1198. https://doi.org/10.1001/archpsyc.65.10.1193

Gee, K. R., Brown, K. A., Chen, W. N., Bishop-Stewart, J., Gray, D., & Johnson, I. (2000). Chemical and physiological characterization of fluo-4 Ca(2+)-indicator dyes. *Cell Calcium*, *27*(2), 97-106. https://doi.org/10.1054/ceca.1999.0095

Gencturk, S., & Unal, G. (2024). Rodent tests of depression and anxiety: Construct validity and translational relevance. *Cogn Affect Behav Neurosci*, *24*(2), 191-224. https://doi.org/10.3758/s13415-024-01171-2

Gengler, S., Hamilton, A., & Hölscher, C. (2010). Synaptic plasticity in the hippocampus of a APP/PS1 mouse model of Alzheimer's disease is impaired in old but not young mice. *PLoS One*, *5*(3), e9764. https://doi.org/10.1371/journal.pone.0009764

Ghosal, K., Vogt, D. L., Liang, M., Shen, Y., Lamb, B. T., & Pimplikar, S. W. (2009). Alzheimer's disease-like pathological features in transgenic mice expressing the APP intracellular domain. *Proc Natl Acad Sci U S A*, *106*(43), 18367-18372. https://doi.org/10.1073/pnas.0907652106

Giannakopoulos, P., Herrmann, F. R., Bussière, T., Bouras, C., Kövari, E., Perl, D. P.,…Hof, P. R. (2003). Tangle and neuron numbers, but not amyloid load, predict cognitive status in Alzheimer's disease. *Neurology*, *60*(9), 1495-1500. https://doi.org/10.1212/01.wnl.0000063311.58879.01

Gil-Bea, F. J., Aisa, B., Schliebs, R., & Ramírez, M. J. (2007). Increase of locomotor activity underlying the behavioral disinhibition in tg2576 mice. *Behav Neurosci*, *121*(2), 340-344. https://doi.org/10.1037/0735-7044.121.2.340

Gili, T., Cercignani, M., Serra, L., Perri, R., Giove, F., Maraviglia, B.,…Bozzali, M. (2011). Regional brain atrophy and functional disconnection across Alzheimer's disease evolution. *J Neurol Neurosurg Psychiatry*, *82*(1), 58-66. https://doi.org/10.1136/jnnp.2009.199935

Gincel, D., Zaid, H., & Shoshan-Barmatz, V. (2001). Calcium binding and translocation by the voltage-dependent anion channel: a possible regulatory mechanism in mitochondrial function. *Biochem J*, *358*(Pt 1), 147-155. https://doi.org/10.1042/0264-6021:3580147

Glenner, G. G., & Wong, C. W. (1984). Alzheimer's disease: initial report of the purification and characterization of a novel cerebrovascular amyloid protein. *Biochem Biophys Res Commun*, *120*(3), 885-890. https://doi.org/10.1016/s0006-291x(84)80190-4

Glickfeld, L. L., Histed, M. H., & Maunsell, J. H. (2013). Mouse primary visual cortex is used to detect both orientation and contrast changes. *J Neurosci*, *33*(50), 19416-19422. https://doi.org/10.1523/JNEUROSCI.3560-13.2013

Goate, A., Chartier-Harlin, M. C., Mullan, M., Brown, J., Crawford, F., Fidani, L.,…James, L. (1991). Segregation of a missense mutation in the amyloid precursor protein gene with familial Alzheimer's disease. *Nature*, *349*(6311), 704-706. https://doi.org/10.1038/349704a0

Goedert, M. (2009). Oskar Fischer and the study of dementia. *Brain*, *132*(Pt 4), 1102-1111. https://doi.org/10.1093/brain/awn256

Goel, A., Cantu, D. A., Guilfoyle, J., Chaudhari, G. R., Newadkar, A., Todisco, B.,…Portera-Cailliau, C. (2018). Impaired perceptual learning in a mouse model of Fragile X syndrome is mediated by parvalbumin neuron dysfunction and is reversible. *Nat Neurosci*, *21*(10), 1404-1411. https://doi.org/10.1038/s41593-018-0231-0

Goel, P., Chakrabarti, S., Goel, K., Bhutani, K., Chopra, T., & Bali, S. (2022). Neuronal cell death mechanisms in Alzheimer's disease: An insight. *Front Mol Neurosci*, *15*, 937133. https://doi.org/10.3389/fnmol.2022.937133

Goelet, P., Castellucci, V. F., Schacher, S., & Kandel, E. R. (1986). The long and the short of long-term memory--a molecular framework. *Nature*, *322*(6078), 419-422. https://doi.org/10.1038/322419a0

Good, M. A., & Bannerman, D. M. (2025). Hippocampal Synaptic Plasticity: Integrating Memory and Anxiety Impairments in the Early Stages of

Alzheimer's Disease. *Curr Top Behav Neurosci*, *69*, 27-48. https://doi.org/10.1007/7854_2024_565
Good, M. A., Barnes, P., Staal, V., McGregor, A., & Honey, R. C. (2007). Context- but not familiarity-dependent forms of object recognition are impaired following excitotoxic hippocampal lesions in rats. *Behav Neurosci*, *121*(1), 218-223. https://doi.org/10.1037/0735-7044.121.1.218
Good, M. A., & Hale, G. (2007). The "Swedish" mutation of the amyloid precursor protein (APPswe) dissociates components of object-location memory in aged Tg2576 mice. *Behav Neurosci*, *121*(6), 1180-1191. https://doi.org/10.1037/0735-7044.121.6.1180
Good, M. A., Hale, G., & Staal, V. (2007). Impaired "episodic-like" object memory in adult APPswe transgenic mice. *Behav Neurosci*, *121*(2), 443-448. https://doi.org/10.1037/0735-7044.121.2.443
Goodwin, G. J., Moeller, S., Nguyen, A., Cummings, J. L., & John, S. E. (2023). Network Analysis of Neuropsychiatric Symptoms in Alzheimer's Disease. *Res Sq*. https://doi.org/10.21203/rs.3.rs-2852697/v1
Gray, J. (1982). Précis of The neuropsychology of anxiety: An enquiry into the functions of the septo-hippocampal system. *The Behavioral and Brain Sciences*, *5*(3), 469-484.
Green, K. N., Demuro, A., Akbari, Y., Hitt, B. D., Smith, I. F., Parker, I., & LaFerla, F. M. (2008). SERCA pump activity is physiologically regulated by presenilin and regulates amyloid beta production. *J Cell Biol*, *181*(7), 1107-1116. https://doi.org/10.1083/jcb.200706171
Green, R. C., Cupples, L. A., Go, R., Benke, K. S., Edeki, T., Griffith, P. A.,…Group, M. S. (2002). Risk of dementia among white and African American relatives of patients with Alzheimer disease. *JAMA*, *287*(3), 329-336. https://doi.org/10.1001/jama.287.3.329
Griebel, G., & Holmes, A. (2013). 50 years of hurdles and hope in anxiolytic drug discovery. *Nat Rev Drug Discov*, *12*(9), 667-687. https://doi.org/10.1038/nrd4075
Grienberger, C., Giovannucci, A., Zeiger, W., & Portera-Cailliau, C. (2022). Two-photon calcium imaging of neuronal activity. *Nat Rev Methods Primers*, *2*(1). https://doi.org/10.1038/s43586-022-00147-1
Grienberger, C., Rochefort, N. L., Adelsberger, H., Henning, H. A., Hill, D. N., Reichwald, J.,…Konnerth, A. (2012). Staged decline of neuronal function in vivo in an animal model of Alzheimer's disease. *Nat Commun*, *3*, 774. https://doi.org/10.1038/ncomms1783
Griessner, J., Pasieka, M., Böhm, V., Grössl, F., Kaczanowska, J., Pliota, P.,…Haubensak, W. (2021). Central amygdala circuit dynamics underlying the benzodiazepine anxiolytic effect. *Mol Psychiatry*, *26*(2), 534-544. https://doi.org/10.1038/s41380-018-0310-3
Griffiths, B. J., & Jensen, O. (2023). Gamma oscillations and episodic memory. *Trends Neurosci*, *46*(10), 832-846. https://doi.org/10.1016/j.tins.2023.07.003
Griffiths, J., & Grant, S. G. N. (2023). Synapse pathology in Alzheimer's disease. *Semin Cell Dev Biol*, *139*, 13-23. https://doi.org/10.1016/j.semcdb.2022.05.028
Gros, A., Lim, A. W. H., Hohendorf, V., White, N., Eckert, M., McHugh, T. J., & Wang, S. H. (2022). Behavioral and Cellular Tagging in Young and in Early Cognitive Aging. *Front Aging Neurosci*, *14*, 809879. https://doi.org/10.3389/fnagi.2022.809879

Gros, A., & Wang, S. H. (2018). Behavioral tagging and capture: long-term memory decline in middle-aged rats. *Neurobiol Aging*, *67*, 31-41. https://doi.org/10.1016/j.neurobiolaging.2018.02.023
Grundke-Iqbal, I., Iqbal, K., Tung, Y. C., Quinlan, M., Wisniewski, H. M., & Binder, L. I. (1986). Abnormal phosphorylation of the microtubule-associated protein tau (tau) in Alzheimer cytoskeletal pathology. *Proc Natl Acad Sci U S A*, *83*(13), 4913-4917. https://doi.org/10.1073/pnas.83.13.4913
Guerreiro, R., & Bras, J. (2015). The age factor in Alzheimer's disease. *Genome Med*, *7*, 106. https://doi.org/10.1186/s13073-015-0232-5
Guerreiro, R., Wojtas, A., Bras, J., Carrasquillo, M., Rogaeva, E., Majounie, E.,…Group, A. G. A. (2013). TREM2 variants in Alzheimer's disease. *N Engl J Med*, *368*(2), 117-127. https://doi.org/10.1056/NEJMoa1211851
Gulisano, W., Melone, M., Li Puma, D. D., Tropea, M. R., Palmeri, A., Arancio, O.,…Puzzo, D. (2018). The effect of amyloid-β peptide on synaptic plasticity and memory is influenced by different isoforms, concentrations, and aggregation status. *Neurobiol Aging*, *71*, 51-60. https://doi.org/10.1016/j.neurobiolaging.2018.06.025
Hajnóczky, G., Csordás, G., Das, S., Garcia-Perez, C., Saotome, M., Sinha Roy, S., & Yi, M. (2006). Mitochondrial calcium signalling and cell death: approaches for assessing the role of mitochondrial Ca2+ uptake in apoptosis. *Cell Calcium*, *40*(5-6), 553-560. https://doi.org/10.1016/j.ceca.2006.08.016
Halazonetis, T. D., Georgopoulos, K., Greenberg, M. E., & Leder, P. (1988). c-Jun dimerizes with itself and with c-Fos, forming complexes of different DNA binding affinities. *Cell*, *55*(5), 917-924. https://doi.org/10.1016/0092-8674(88)90147-x
Hale, G., & Good, M. (2005). Impaired visuospatial recognition memory but normal object novelty detection and relative familiarity judgments in adult mice expressing the APPswe Alzheimer's disease mutation. *Behav Neurosci*, *119*(4), 884-891. https://doi.org/10.1037/0735-7044.119.4.884
Hall, J., Thomas, K. L., & Everitt, B. J. (2001). Fear memory retrieval induces CREB phosphorylation and Fos expression within the amygdala. *Eur J Neurosci*, *13*(7), 1453-1458. https://doi.org/10.1046/j.0953-816x.2001.01531.x
Hampel, H., Hardy, J., Blennow, K., Chen, C., Perry, G., Kim, S. H.,…Vergallo, A. (2021). The Amyloid-β Pathway in Alzheimer's Disease. *Mol Psychiatry*, *26*(10), 5481-5503. https://doi.org/10.1038/s41380-021-01249-0
Handley, S. L., & Mithani, S. (1984). Effects of alpha-adrenoceptor agonists and antagonists in a maze-exploration model of 'fear'-motivated behaviour. *Naunyn Schmiedebergs Arch Pharmacol*, *327*(1), 1-5. https://doi.org/10.1007/BF00504983
Hanes, J., Zilka, N., Bartkova, M., Caletkova, M., Dobrota, D., & Novak, M. (2009). Rat tau proteome consists of six tau isoforms: implication for animal models of human tauopathies. *J Neurochem*, *108*(5), 1167-1176. https://doi.org/10.1111/j.1471-4159.2009.05869.x
Hanley, J. G. (2008). AMPA receptor trafficking pathways and links to dendritic spine morphogenesis. *Cell Adh Migr*, *2*(4), 276-282. https://doi.org/10.4161/cam.2.4.6510
Hansen, K. B., Yi, F., Perszyk, R. E., Furukawa, H., Wollmuth, L. P., Gibb, A. J., & Traynelis, S. F. (2018). Structure, function, and allosteric modulation of NMDA receptors. *J Gen Physiol*, *150*(8), 1081-1105. https://doi.org/10.1085/jgp.201812032

Hardingham, G. E., & Bading, H. (2010). Synaptic versus extrasynaptic NMDA receptor signalling: implications for neurodegenerative disorders. *Nat Rev Neurosci*, *11*(10), 682-696. https://doi.org/10.1038/nrn2911
Hardy, J. A., & Higgins, G. A. (1992). Alzheimer's disease: the amyloid cascade hypothesis. *Science*, *256*(5054), 184-185. https://doi.org/10.1126/science.1566067
Harkany, T., Abrahám, I., Timmerman, W., Laskay, G., Tóth, B., Sasvári, M.,…Luiten, P. G. (2000). beta-amyloid neurotoxicity is mediated by a glutamate-triggered excitotoxic cascade in rat nucleus basalis. *Eur J Neurosci*, *12*(8), 2735-2745. https://doi.org/10.1046/j.1460-9568.2000.00164.x
Hartman, R. E., Izumi, Y., Bales, K. R., Paul, S. M., Wozniak, D. F., & Holtzman, D. M. (2005). Treatment with an amyloid-beta antibody ameliorates plaque load, learning deficits, and hippocampal long-term potentiation in a mouse model of Alzheimer's disease. *J Neurosci*, *25*(26), 6213-6220. https://doi.org/10.1523/JNEUROSCI.0664-05.2005
Hashimoto, H., Monserratt, L., Nguyen, P., Feil, D., Harwood, D., Mandelkern, M. A., & Sultzer, D. L. (2006). Anxiety and regional cortical glucose metabolism in patients with Alzheimer's disease. *J Neuropsychiatry Clin Neurosci*, *18*(4), 521-528. https://doi.org/10.1176/jnp.2006.18.4.521
Hashimoto, S., Ishii, A., Kamano, N., Watamura, N., Saito, T., Ohshima, T.,…Saido, T. C. (2018). Endoplasmic reticulum stress responses in mouse models of Alzheimer's disease: Overexpression paradigm. *J Biol Chem*, *293*(9), 3118-3125. https://doi.org/10.1074/jbc.M117.811315
Hashimoto, S., Matsuba, Y., Kamano, N., Mihira, N., Sahara, N., Takano, J.,…Saito, T. (2019). Tau binding protein CAPON induces tau aggregation and neurodegeneration. *Nat Commun*, *10*(1), 2394. https://doi.org/10.1038/s41467-019-10278-x
Hashimoto, T., Fujii, D., Naka, Y., Kashiwagi-Hakozaki, M., Matsuo, Y., Matsuura, Y.,…Iwatsubo, T. (2020). Collagenous Alzheimer amyloid plaque component impacts on the compaction of amyloid-β plaques. *Acta Neuropathol Commun*, *8*(1), 212. https://doi.org/10.1186/s40478-020-01075-5
Hatami, A., Monjazeb, S., Milton, S., & Glabe, C. G. (2017). Familial Alzheimer's Disease Mutations within the Amyloid Precursor Protein Alter the Aggregation and Conformation of the Amyloid-β Peptide. *J Biol Chem*, *292*(8), 3172-3185. https://doi.org/10.1074/jbc.M116.755264
Hayashi, T., Oguro, M., & Sato, N. (2020). Involvement of the retrosplenial cortex in the processing of the temporal aspect of episodic-like memory in rats. *Neurosci Res*, *154*, 52-55. https://doi.org/10.1016/j.neures.2019.05.005
He, J., Yamada, K., & Nabeshima, T. (2002). A role of Fos expression in the CA3 region of the hippocampus in spatial memory formation in rats. *Neuropsychopharmacology*, *26*(2), 259-268. https://doi.org/10.1016/S0893-133X(01)00332-3
Hebert, L. E., Weuve, J., Scherr, P. A., & Evans, D. A. (2013). Alzheimer disease in the United States (2010-2050) estimated using the 2010 census. *Neurology*, *80*(19), 1778-1783. https://doi.org/10.1212/WNL.0b013e31828726f5
Henderson, J. M., Larson, C. L., & Zhu, D. C. (2008). Full scenes produce more activation than close-up scenes and scene-diagnostic objects in parahippocampal and retrosplenial cortex: an fMRI study. *Brain Cogn*, *66*(1), 40-49. https://doi.org/10.1016/j.bandc.2007.05.001

Henley, J. M., & Wilkinson, K. A. (2013). AMPA receptor trafficking and the mechanisms underlying synaptic plasticity and cognitive aging. *Dialogues Clin Neurosci*, *15*(1), 11-27. https://doi.org/10.31887/DCNS.2013.15.1/jhenley
Hernández, F., Cuadros, R., Ollá, I., García, C., Ferrer, I., Perry, G., & Avila, J. (2019). Differences in structure and function between human and murine tau. *Biochim Biophys Acta Mol Basis Dis*, *1865*(8), 2024-2030. https://doi.org/10.1016/j.bbadis.2018.08.010
Herrup, K. (2015). The case for rejecting the amyloid cascade hypothesis. *Nat Neurosci*, *18*(6), 794-799. https://doi.org/10.1038/nn.4017
Hidalgo, C., & Arias-Cavieres, A. (2016). Calcium, Reactive Oxygen Species, and Synaptic Plasticity. *Physiology (Bethesda)*, *31*(3), 201-215. https://doi.org/10.1152/physiol.00038.2015
Hillhouse, T. M., & Porter, J. H. (2015). A brief history of the development of antidepressant drugs: from monoamines to glutamate. *Exp Clin Psychopharmacol*, *23*(1), 1-21. https://doi.org/10.1037/a0038550
Hohoff, C. (2009). Anxiety in mice and men: a comparison. *J Neural Transm (Vienna)*, *116*(6), 679-687. https://doi.org/10.1007/s00702-009-0215-z
Holcomb, L. A., Gordon, M. N., Jantzen, P., Hsiao, K., Duff, K., & Morgan, D. (1999). Behavioral changes in transgenic mice expressing both amyloid precursor protein and presenilin-1 mutations: lack of association with amyloid deposits. *Behav Genet*, *29*(3), 177-185. https://doi.org/10.1023/a:1021691918517
Holmdahl, R., & Malissen, B. (2012). The need for littermate controls. *Eur J Immunol*, *42*(1), 45-47. https://doi.org/10.1002/eji.201142048
Hong, W., Liu, W., Desousa, A. O., Young-Pearse, T., & Walsh, D. M. (2023). Methods for the isolation and analysis of Aβ from postmortem brain. *Front Neurosci*, *17*, 1108715. https://doi.org/10.3389/fnins.2023.1108715
Honig, L. S., Sabbagh, M. N., van Dyck, C. H., Sperling, R. A., Hersch, S., Matta, A.,…Kramer, L. (2024). Updated safety results from phase 3 lecanemab study in early Alzheimer's disease. *Alzheimers Res Ther*, *16*(1), 105. https://doi.org/10.1186/s13195-024-01441-8
Hoshino, K., Uga, D. A., & de Paula, H. M. (2004). The compulsive-like aspect of the head dipping emission in rats with chronic electrolytic lesion in the area of the median raphe nucleus. *Braz J Med Biol Res*, *37*(2), 245-250. https://doi.org/10.1590/s0100-879x2004000200012
Howerton, A. R., Roland, A. V., & Bale, T. L. (2014). Dorsal raphe neuroinflammation promotes dramatic behavioral stress dysregulation. *J Neurosci*, *34*(21), 7113-7123. https://doi.org/10.1523/JNEUROSCI.0118-14.2014
Hsiao, K., Chapman, P., Nilsen, S., Eckman, C., Harigaya, Y., Younkin, S.,…Cole, G. (1996). Correlative memory deficits, Abeta elevation, and amyloid plaques in transgenic mice. *Science*, *274*(5284), 99-102. https://doi.org/10.1126/science.274.5284.99
Huang, Y. Y., Gan, Y. H., Yang, L., Cheng, W., & Yu, J. T. (2024). Depression in Alzheimer's Disease: Epidemiology, Mechanisms, and Treatment. *Biol Psychiatry*, *95*(11), 992-1005. https://doi.org/10.1016/j.biopsych.2023.10.008
Huang, Z., Jordan, J. D., & Zhang, Q. (2024). Myelin Pathology in Alzheimer's Disease: Potential Therapeutic Opportunities. *Aging Dis*, *15*(2), 698-713. https://doi.org/10.14336/AD.2023.0628
Hudson, A. E. (2018). Genetic Reporters of Neuronal Activity: c-Fos and G-CaMP6. *Methods Enzymol*, *603*, 197-220. https://doi.org/10.1016/bs.mie.2018.01.023

Hughes, R. N. (2004). The value of spontaneous alternation behavior (SAB) as a test of retention in pharmacological investigations of memory. *Neurosci Biobehav Rev*, *28*(5), 497-505. https://doi.org/10.1016/j.neubiorev.2004.06.006
Hunsaker, M. R., Mooy, G. G., Swift, J. S., & Kesner, R. P. (2007). Dissociations of the medial and lateral perforant path projections into dorsal DG, CA3, and CA1 for spatial and nonspatial (visual object) information processing. *Behav Neurosci*, *121*(4), 742-750. https://doi.org/10.1037/0735-7044.121.4.742
Hunsberger, H. C., Pinky, P. D., Smith, W., Suppiramaniam, V., & Reed, M. N. (2019). The role of APOE4 in Alzheimer's disease: strategies for future therapeutic interventions. *Neuronal Signal*, *3*(2), NS20180203. https://doi.org/10.1042/NS20180203
Hunt, D. L., & Castillo, P. E. (2012). Synaptic plasticity of NMDA receptors: mechanisms and functional implications. *Curr Opin Neurobiol*, *22*(3), 496-508. https://doi.org/10.1016/j.conb.2012.01.007
Inayat, S., McAllister, B. B., Chang, H., Lacoursiere, S. G., Whishaw, I. Q., Sutherland, R. J., & Mohajerani, M. H. (2023). Weak-hyperactive hippocampal CA1 neurons in the prodromal stage of Alzheimer's disease in hybrid App. *Neurobiol Aging*, *130*, 154-171. https://doi.org/10.1016/j.neurobiolaging.2023.06.002
Insel, T. R., Ninan, P. T., Aloi, J., Jimerson, D. C., Skolnick, P., & Paul, S. M. (1984). A benzodiazepine receptor-mediated model of anxiety. Studies in nonhuman primates and clinical implications. *Arch Gen Psychiatry*, *41*(8), 741-750. https://doi.org/10.1001/archpsyc.1984.01790190015002
Irizarry, M. C., McNamara, M., Fedorchak, K., Hsiao, K., & Hyman, B. T. (1997). APPSw transgenic mice develop age-related A beta deposits and neuropil abnormalities, but no neuronal loss in CA1. *J Neuropathol Exp Neurol*, *56*(9), 965-973. https://doi.org/10.1097/00005072-199709000-00002
Itkin, A., Dupres, V., Dufrêne, Y. F., Bechinger, B., Ruysschaert, J. M., & Raussens, V. (2011). Calcium ions promote formation of amyloid β-peptide (1-40) oligomers causally implicated in neuronal toxicity of Alzheimer's disease. *PLoS One*, *6*(3), e18250. https://doi.org/10.1371/journal.pone.0018250
Izumi, H., Shinoda, Y., Saito, T., Saido, T. C., Sato, K., Yabuki, Y.,…Fukunaga, K. (2018). The Disease-modifying Drug Candidate, SAK3 Improves Cognitive Impairment and Inhibits Amyloid beta Deposition in App Knock-in Mice. *Neuroscience*, *377*, 87-97. https://doi.org/10.1016/j.neuroscience.2018.02.031
Jack, C. R., Bennett, D. A., Blennow, K., Carrillo, M. C., Dunn, B., Haeberlein, S. B.,…Contributors. (2018). NIA-AA Research Framework: Toward a biological definition of Alzheimer's disease. *Alzheimers Dement*, *14*(4), 535-562. https://doi.org/10.1016/j.jalz.2018.02.018
Jack, C. R., Knopman, D. S., Jagust, W. J., Petersen, R. C., Weiner, M. W., Aisen, P. S.,…Trojanowski, J. Q. (2013). Tracking pathophysiological processes in Alzheimer's disease: an updated hypothetical model of dynamic biomarkers. *Lancet Neurol*, *12*(2), 207-216. https://doi.org/10.1016/S1474-4422(12)70291-0
Jacob, P. Y., Casali, G., Spieser, L., Page, H., Overington, D., & Jeffery, K. (2017). An independent, landmark-dominated head-direction signal in dysgranular retrosplenial cortex. *Nat Neurosci*, *20*(2), 173-175. https://doi.org/10.1038/nn.4465
Jacobsen, J. S., Wu, C. C., Redwine, J. M., Comery, T. A., Arias, R., Bowlby, M.,…Bloom, F. E. (2006). Early-onset behavioral and synaptic deficits in a

mouse model of Alzheimer's disease. *Proc Natl Acad Sci U S A*, *103*(13), 5161-5166. https://doi.org/10.1073/pnas.0600948103
Jaffard, R., Dubois, M., & Galey, D. (1981). Memory of a choice direction in a T maze as measured by spontaneous alternation in mice: Effects of intertrial interval and reward. *Behavioural Processes*, *6*(1), 11-21.
Jahn, H. (2013). Memory loss in Alzheimer's disease. *Dialogues Clin Neurosci*, *15*(4), 445-454. https://doi.org/10.31887/DCNS.2013.15.4/hjahn
Javonillo, D. I., Tran, K. M., Phan, J., Hingco, E., Kramár, E. A., da Cunha, C.,…LaFerla, F. M. (2021). Systematic Phenotyping and Characterization of the 3xTg-AD Mouse Model of Alzheimer's Disease. *Front Neurosci*, *15*, 785276. https://doi.org/10.3389/fnins.2021.785276
Jaworski, T., Dewachter, I., Lechat, B., Croes, S., Termont, A., Demedts, D.,…Van Leuven, F. (2009). AAV-tau mediates pyramidal neurodegeneration by cell-cycle re-entry without neurofibrillary tangle formation in wild-type mice. *PLoS One*, *4*(10), e7280. https://doi.org/10.1371/journal.pone.0007280
Jeong, N., & Singer, A. C. (2022). Learning from inhibition: Functional roles of hippocampal CA1 inhibition in spatial learning and memory. *Curr Opin Neurobiol*, *76*, 102604. https://doi.org/10.1016/j.conb.2022.102604
Ji, Y., Wang, X., Kalicki, C., Menta, B. W., Baumgardner, M., Koppel, S. J.,…Swerdlow, R. H. (2019). Effects of Microglial Cytokines on Alzheimer's Disease-Related Phenomena. *J Alzheimers Dis*, *67*(3), 1021-1034. https://doi.org/10.3233/JAD-180820
Jin, M., Shepardson, N., Yang, T., Chen, G., Walsh, D., & Selkoe, D. J. (2011). Soluble amyloid beta-protein dimers isolated from Alzheimer cortex directly induce Tau hyperphosphorylation and neuritic degeneration. *Proc Natl Acad Sci U S A*, *108*(14), 5819-5824. https://doi.org/10.1073/pnas.1017033108
Jobson, D. D., Hase, Y., Clarkson, A. N., & Kalaria, R. N. (2021). The role of the medial prefrontal cortex in cognition, ageing and dementia. *Brain Commun*, *3*(3), fcab125. https://doi.org/10.1093/braincomms/fcab125
Johansson, M., Stomrud, E., Lindberg, O., Westman, E., Johansson, P. M., van Westen, D.,…Hansson, O. (2020). Apathy and anxiety are early markers of Alzheimer's disease. *Neurobiol Aging*, *85*, 74-82. https://doi.org/10.1016/j.neurobiolaging.2019.10.008
Jonsson, T., Stefansson, H., Steinberg, S., Jonsdottir, I., Jonsson, P. V., Snaedal, J.,…Stefansson, K. (2013). Variant of TREM2 associated with the risk of Alzheimer's disease. *N Engl J Med*, *368*(2), 107-116. https://doi.org/10.1056/NEJMoa1211103
Joshi, M., Joshi, S., Khambete, M., & Degani, M. (2023). Role of calcium dysregulation in Alzheimer's disease and its therapeutic implications. *Chem Biol Drug Des*, *101*(2), 453-468. https://doi.org/10.1111/cbdd.14175
Joyashiki, E., Matsuya, Y., & Tohda, C. (2011). Sominone improves memory impairments and increases axonal density in Alzheimer's disease model mice, 5XFAD. *Int J Neurosci*, *121*(4), 181-190. https://doi.org/10.3109/00207454.2010.541571
Jun, H., Bramian, A., Soma, S., Saito, T., Saido, T. C., & Igarashi, K. M. (2020). Disrupted Place Cell Remapping and Impaired Grid Cells in a Knockin Model of Alzheimer's Disease. *Neuron*, *107*(6), 1095-1112.e1096. https://doi.org/10.1016/j.neuron.2020.06.023
Justice, N. J. (2018). The relationship between stress and Alzheimer's disease. *Neurobiol Stress*, *8*, 127-133. https://doi.org/10.1016/j.ynstr.2018.04.002

Kaczmarek, L., & Nikołajew, E. (1990). c-fos protooncogene expression and neuronal plasticity. *Acta Neurobiol Exp (Wars)*, *50*(4-5), 173-179.
Kalia, M. (2003). Dysphagia and aspiration pneumonia in patients with Alzheimer's disease. *Metabolism*, *52*(10 Suppl 2), 36-38. https://doi.org/10.1016/s0026-0495(03)00300-7
Kamatham, P. T., Shukla, R., Khatri, D. K., & Vora, L. K. (2024). Pathogenesis, diagnostics, and therapeutics for Alzheimer's disease: Breaking the memory barrier. *Ageing Res Rev*, *101*, 102481. https://doi.org/10.1016/j.arr.2024.102481
Kametani, F., & Haga, S. (2015). Accumulation of carboxy-terminal fragments of APP increases phosphodiesterase 8B. *Neurobiol Aging*, *36*(2), 634-637. https://doi.org/10.1016/j.neurobiolaging.2014.09.029
Kang, J., Lemaire, H. G., Unterbeck, A., Salbaum, J. M., Masters, C. L., Grzeschik, K. H.,…Müller-Hill, B. (1987). The precursor of Alzheimer's disease amyloid A4 protein resembles a cell-surface receptor. *Nature*, *325*(6106), 733-736. https://doi.org/10.1038/325733a0
Kaufer, D. I., Cummings, J. L., Christine, D., Bray, T., Castellon, S., Masterman, D.,…DeKosky, S. T. (1998). Assessing the impact of neuropsychiatric symptoms in Alzheimer's disease: the Neuropsychiatric Inventory Caregiver Distress Scale. *J Am Geriatr Soc*, *46*(2), 210-215. https://doi.org/10.1111/j.1532-5415.1998.tb02542.x
Kaur, G., Pawlik, M., Gandy, S. E., Ehrlich, M. E., Smiley, J. F., & Levy, E. (2017). Lysosomal dysfunction in the brain of a mouse model with intraneuronal accumulation of carboxyl terminal fragments of the amyloid precursor protein. *Mol Psychiatry*, *22*(7), 981-989. https://doi.org/10.1038/mp.2016.189
Kawarabayashi, T., Younkin, L. H., Saido, T. C., Shoji, M., Ashe, K. H., & Younkin, S. G. (2001). Age-dependent changes in brain, CSF, and plasma amyloid (beta) protein in the Tg2576 transgenic mouse model of Alzheimer's disease. *J Neurosci*, *21*(2), 372-381.
Keene, C. S., & Bucci, D. J. (2009). Damage to the retrosplenial cortex produces specific impairments in spatial working memory. *Neurobiol Learn Mem*, *91*(4), 408-414. https://doi.org/10.1016/j.nlm.2008.10.009
Kenwood, M. M., Kalin, N. H., & Barbas, H. (2022). The prefrontal cortex, pathological anxiety, and anxiety disorders. *Neuropsychopharmacology*, *47*(1), 260-275. https://doi.org/10.1038/s41386-021-01109-z
Kepp, K. P., Robakis, N. K., Høilund-Carlsen, P. F., Sensi, S. L., & Vissel, B. (2023). The amyloid cascade hypothesis: an updated critical review. *Brain*, *146*(10), 3969-3990. https://doi.org/10.1093/brain/awad159
Keshavarzi, S., Bracey, E. F., Faville, R. A., Campagner, D., Tyson, A. L., Lenzi, S. C.,…Margrie, T. W. (2022). Multisensory coding of angular head velocity in the retrosplenial cortex. *Neuron*, *110*(3), 532-543.e539. https://doi.org/10.1016/j.neuron.2021.10.031
Kessels, H. W., Nguyen, L. N., Nabavi, S., & Malinow, R. (2010). The prion protein as a receptor for amyloid-beta. *Nature*, *466*(7308), E3-4; discussion E4-5. https://doi.org/10.1038/nature09217
Khachaturian, Z. S. (1987). Hypothesis on the regulation of cytosol calcium concentration and the aging brain. *Neurobiol Aging*, *8*(4), 345-346. https://doi.org/10.1016/0197-4580(87)90073-x

Khachaturian, Z. S. (1989). Calcium, membranes, aging, and Alzheimer's disease. Introduction and overview. *Ann N Y Acad Sci*, *568*, 1-4. https://doi.org/10.1111/j.1749-6632.1989.tb12485.x
Killin, L. O., Starr, J. M., Shiue, I. J., & Russ, T. C. (2016). Environmental risk factors for dementia: a systematic review. *BMC Geriatr*, *16*(1), 175. https://doi.org/10.1186/s12877-016-0342-y
Kim, D. H., Kim, H. A., Han, Y. S., Jeon, W. K., & Han, J. S. (2020). Recognition memory impairments and amyloid-beta deposition of the retrosplenial cortex at the early stage of 5XFAD mice. *Physiol Behav*, *222*, 112891. https://doi.org/10.1016/j.physbeh.2020.112891
Kim, H. S., Kim, E. M., Lee, J. P., Park, C. H., Kim, S., Seo, J. H.,…Suh, Y. H. (2003). C-terminal fragments of amyloid precursor protein exert neurotoxicity by inducing glycogen synthase kinase-3beta expression. *FASEB J*, *17*(13), 1951-1953. https://doi.org/10.1096/fj.03-0106fje
Kim, J., Kang, H., Lee, Y. B., Lee, B., & Lee, D. (2023). A quantitative analysis of spontaneous alternation behaviors on a Y-maze reveals adverse effects of acute social isolation on spatial working memory. *Sci Rep*, *13*(1), 14722. https://doi.org/10.1038/s41598-023-41996-4
Kinney, J. W., Bemiller, S. M., Murtishaw, A. S., Leisgang, A. M., Salazar, A. M., & Lamb, B. T. (2018). Inflammation as a central mechanism in Alzheimer's disease. *Alzheimers Dement (N Y)*, *4*, 575-590. https://doi.org/10.1016/j.trci.2018.06.014
Kirichok, Y., Krapivinsky, G., & Clapham, D. E. (2004). The mitochondrial calcium uniporter is a highly selective ion channel. *Nature*, *427*(6972), 360-364. https://doi.org/10.1038/nature02246
Kirova, A. M., Bays, R. B., & Lagalwar, S. (2015). Working memory and executive function decline across normal aging, mild cognitive impairment, and Alzheimer's disease. *Biomed Res Int*, *2015*, 748212. https://doi.org/10.1155/2015/748212
Kitazawa, M., Oddo, S., Yamasaki, T. R., Green, K. N., & LaFerla, F. M. (2005). Lipopolysaccharide-induced inflammation exacerbates tau pathology by a cyclin-dependent kinase 5-mediated pathway in a transgenic model of Alzheimer's disease. *J Neurosci*, *25*(39), 8843-8853. https://doi.org/10.1523/JNEUROSCI.2868-05.2005
Kitazawa, M., Yamasaki, T. R., & LaFerla, F. M. (2004). Microglia as a potential bridge between the amyloid beta-peptide and tau. *Ann N Y Acad Sci*, *1035*, 85-103. https://doi.org/10.1196/annals.1332.006
Kjelstrup, K. G., Tuvnes, F. A., Steffenach, H. A., Murison, R., Moser, E. I., & Moser, M. B. (2002). Reduced fear expression after lesions of the ventral hippocampus. *Proc Natl Acad Sci U S A*, *99*(16), 10825-10830. https://doi.org/10.1073/pnas.152112399
Klimova, B., Maresova, P., Valis, M., Hort, J., & Kuca, K. (2015). Alzheimer's disease and language impairments: social intervention and medical treatment. *Clin Interv Aging*, *10*, 1401-1407. https://doi.org/10.2147/CIA.S89714
Klunk, W., Mathis, CA, Price, JC, DeKosky, ST, Lopresti, BJ, Tsopelas, ND, Saxton, JA, Nebes, RD. (2009). Amyloid Imaging with PET in Alzheimer's Disease, Mild Cognitive Impairment, and Clinically Unimpaired Subjects. *PET in the Evaluation of Alzheimer's Disease and Related Disorders*, pp 119–147.
Klunk, W. E., Engler, H., Nordberg, A., Wang, Y., Blomqvist, G., Holt, D. P.,…Långström, B. (2004). Imaging brain amyloid in Alzheimer's disease with

Pittsburgh Compound-B. *Ann Neurol*, *55*(3), 306-319. https://doi.org/10.1002/ana.20009
Koenig, A. M., Arnold, S. E., & Streim, J. E. (2016). Agitation and Irritability in Alzheimer's Disease: Evidenced-Based Treatments and the Black-Box Warning. *Curr Psychiatry Rep*, *18*(1), 3. https://doi.org/10.1007/s11920-015-0640-7
Koffie, R. M., Hyman, B. T., & Spires-Jones, T. L. (2011). Alzheimer's disease: synapses gone cold. *Mol Neurodegener*, *6*(1), 63. https://doi.org/10.1186/1750-1326-6-63
Kolahchi, Z., Henkel, N., Eladawi, M. A., Villarreal, E. C., Kandimalla, P., Lundh, A.,…Cuevas, E. (2024). Sex and Gender Differences in Alzheimer's Disease: Genetic, Hormonal, and Inflammation Impacts. *Int J Mol Sci*, *25*(15). https://doi.org/10.3390/ijms25158485
Korzhova, V., Marinković, P., Njavro, J. R., Goltstein, P. M., Sun, F., Tahirovic, S.,…Liebscher, S. (2021). Long-term dynamics of aberrant neuronal activity in awake Alzheimer's disease transgenic mice. *Commun Biol*, *4*(1), 1368. https://doi.org/10.1038/s42003-021-02884-7
Kotredes, K. P., Oblak, A., Pandey, R. S., Lin, P. B., Garceau, D., Williams, H.,…Howell, G. R. (2021). Uncovering Disease Mechanisms in a Novel Mouse Model Expressing Humanized APOEε4 and Trem2*R47H. *Front Aging Neurosci*, *13*, 735524. https://doi.org/10.3389/fnagi.2021.735524
Kotredes, K. P., Pandey, R. S., Persohn, S., Elderidge, K., Burton, C. P., Miner, E. W.,…Oblak, A. L. (2024). Characterizing molecular and synaptic signatures in mouse models of late-onset Alzheimer's disease independent of amyloid and tau pathology. *Alzheimers Dement*, *20*(6), 4126-4146. https://doi.org/10.1002/alz.13828
Kouzarides, T., & Ziff, E. (1988). The role of the leucine zipper in the fos-jun interaction. *Nature*, *336*(6200), 646-651. https://doi.org/10.1038/336646a0
Kozhevnikov, M., & Puri, J. (2023). Different Types of Survey-Based Environmental Representations: Egocentric vs. Allocentric Cognitive Maps. *Brain Sci*, *13*(5). https://doi.org/10.3390/brainsci13050834
Krabbe, G., Halle, A., Matyash, V., Rinnenthal, J. L., Eom, G. D., Bernhardt, U.,…Heppner, F. L. (2013). Functional impairment of microglia coincides with Beta-amyloid deposition in mice with Alzheimer-like pathology. *PLoS One*, *8*(4), e60921. https://doi.org/10.1371/journal.pone.0060921
Kuchibhotla, K. V., Goldman, S. T., Lattarulo, C. R., Wu, H. Y., Hyman, B. T., & Bacskai, B. J. (2008). Abeta plaques lead to aberrant regulation of calcium homeostasis in vivo resulting in structural and functional disruption of neuronal networks. *Neuron*, *59*(2), 214-225. https://doi.org/10.1016/j.neuron.2008.06.008
Kuchibhotla, K. V., Wegmann, S., Kopeikina, K. J., Hawkes, J., Rudinskiy, N., Andermann, M. L.,…Hyman, B. T. (2014). Neurofibrillary tangle-bearing neurons are functionally integrated in cortical circuits in vivo. *Proc Natl Acad Sci U S A*, *111*(1), 510-514. https://doi.org/10.1073/pnas.1318807111
Kundu, P., Stagaman, K., Kasschau, K., Holden, S., Shulzhenko, N., Sharpton, T. J., & Raber, J. (2022). Fecal Implants From AppNL-G-F and AppNL-G-F/E4 Donor Mice Sufficient to Induce Behavioural Phenotypes in Germ-Free Mice. *Front Behav Neurosci*, *16*, 791128. https://doi.org/10.3389/fnbeh.2022.791128

Kwak, Y. T., Yang, Y., & Koo, M. S. (2017). Anxiety in Dementia. *Dement Neurocogn Disord*, *16*(2), 33-39. https://doi.org/10.12779/dnd.2017.16.2.33
Kwapis, J. L., Jarome, T. J., Lee, J. L., Gilmartin, M. R., & Helmstetter, F. J. (2014). Extinguishing trace fear engages the retrosplenial cortex rather than the amygdala. *Neurobiol Learn Mem*, *113*, 41-54. https://doi.org/10.1016/j.nlm.2013.09.007
Kwapis, J. L., Jarome, T. J., Lee, J. L., & Helmstetter, F. J. (2015). The retrosplenial cortex is involved in the formation of memory for context and trace fear conditioning. *Neurobiol Learn Mem*, *123*, 110-116. https://doi.org/10.1016/j.nlm.2015.06.007
Kwart, D., Gregg, A., Scheckel, C., Murphy, E. A., Paquet, D., Duffield, M.,…Tessier-Lavigne, M. (2019). A Large Panel of Isogenic APP and PSEN1 Mutant Human iPSC Neurons Reveals Shared Endosomal Abnormalities Mediated by APP β-CTFs, Not Aβ. *Neuron*, *104*(2), 256-270.e255. https://doi.org/10.1016/j.neuron.2019.07.010
L'Esperance, O. J., McGhee, J., Davidson, G., Niraula, S., Smith, A. S., Sosunov, A. A.,…Subramanian, J. (2024). Functional Connectivity Favors Aberrant Visual Network c-Fos Expression Accompanied by Cortical Synapse Loss in a Mouse Model of Alzheimer's Disease. *J Alzheimers Dis*, *101*(1), 111-131. https://doi.org/10.3233/JAD-240776
La-Vu, M., Tobias, B. C., Schuette, P. J., & Adhikari, A. (2020). To Approach or Avoid: An Introductory Overview of the Study of Anxiety Using Rodent Assays. *Front Behav Neurosci*, *14*, 145. https://doi.org/10.3389/fnbeh.2020.00145
Laczó, J., Parizkova, M., & Moffat, S. D. (2018). Spatial navigation, aging and Alzheimer's disease. *Aging (Albany NY)*, *10*(11), 3050-3051. https://doi.org/10.18632/aging.101634
Laird, F. M., Cai, H., Savonenko, A. V., Farah, M. H., He, K., Melnikova, T.,…Wong, P. C. (2005). BACE1, a major determinant of selective vulnerability of the brain to amyloid-beta amyloidogenesis, is essential for cognitive, emotional, and synaptic functions. *J Neurosci*, *25*(50), 11693-11709. https://doi.org/10.1523/JNEUROSCI.2766-05.2005
Lalonde, R. (2002). The neurobiological basis of spontaneous alternation. *Neurosci Biobehav Rev*, *26*(1), 91-104. https://doi.org/10.1016/s0149-7634(01)00041-0
Lalonde, R., Lewis, T. L., Strazielle, C., Kim, H., & Fukuchi, K. (2003). Transgenic mice expressing the betaAPP695SWE mutation: effects on exploratory activity, anxiety, and motor coordination. *Brain Res*, *977*(1), 38-45. https://doi.org/10.1016/s0006-8993(03)02694-5
Lambert, M. P., Barlow, A. K., Chromy, B. A., Edwards, C., Freed, R., Liosatos, M.,…Klein, W. L. (1998). Diffusible, nonfibrillar ligands derived from Abeta1-42 are potent central nervous system neurotoxins. *Proc Natl Acad Sci U S A*, *95*(11), 6448-6453. https://doi.org/10.1073/pnas.95.11.6448
Lanctôt, K. L., Amatniek, J., Ancoli-Israel, S., Arnold, S. E., Ballard, C., Cohen-Mansfield, J.,…Boot, B. (2017). Neuropsychiatric signs and symptoms of Alzheimer's disease: New treatment paradigms. *Alzheimers Dement (N Y)*, *3*(3), 440-449. https://doi.org/10.1016/j.trci.2017.07.001
Landfield, P. W. (1987). 'Increased calcium-current' hypothesis of brain aging. *Neurobiol Aging*, *8*(4), 346-347. https://doi.org/10.1016/0197-4580(87)90074-1

Landfield, P. W., & Pitler, T. A. (1984). Prolonged Ca2+-dependent afterhyperpolarizations in hippocampal neurons of aged rats. *Science*, *226*(4678), 1089-1092. https://doi.org/10.1126/science.6494926
Lang, P. J., Davis, M., & Ohman, A. (2000). Fear and anxiety: animal models and human cognitive psychophysiology. *J Affect Disord*, *61*(3), 137-159. https://doi.org/10.1016/s0165-0327(00)00343-8
Lanz, T. A., Carter, D. B., & Merchant, K. M. (2003). Dendritic spine loss in the hippocampus of young PDAPP and Tg2576 mice and its prevention by the ApoE2 genotype. *Neurobiol Dis*, *13*(3), 246-253. https://doi.org/10.1016/s0969-9961(03)00079-2
Lara Aparicio, S. Y., Laureani Fierro, Á., Aranda Abreu, G. E., Toledo Cárdenas, R., García Hernández, L. I., Coria Ávila, G. A.,…Pérez Estudillo, C. A. (2022). Current Opinion on the Use of c-Fos in Neuroscience. *NeuroSci*, *3*(4), 687-702. https://doi.org/10.3390/neurosci3040050
Latif-Hernandez, A., Sabanov, V., Ahmed, T., Craessaerts, K., Saito, T., Saido, T., & Balschun, D. (2020). The two faces of synaptic failure in AppNL-G-F knock-in mice. *Alzheimers Res Ther*, *12*(1), 100. https://doi.org/10.1186/s13195-020-00667-6
Latif-Hernandez, A., Shah, D., Craessaerts, K., Saido, T., Saito, T., De Strooper, B.,…D'Hooge, R. (2019). Subtle behavioral changes and increased prefrontal-hippocampal network synchronicity in APPNL-G-F mice before prominent plaque deposition. *Behav Brain Res*, *364*, 431-441. https://doi.org/10.1016/j.bbr.2017.11.017
Lauritzen, I., Pardossi-Piquard, R., Bauer, C., Brigham, E., Abraham, J. D., Ranaldi, S.,…Checler, F. (2012). The β-secretase-derived C-terminal fragment of βAPP, C99, but not Aβ, is a key contributor to early intraneuronal lesions in triple-transgenic mouse hippocampus. *J Neurosci*, *32*(46), 16243-11655a. https://doi.org/10.1523/JNEUROSCI.2775-12.2012
Laurén, J., Gimbel, D. A., Nygaard, H. B., Gilbert, J. W., & Strittmatter, S. M. (2009). Cellular prion protein mediates impairment of synaptic plasticity by amyloid-beta oligomers. *Nature*, *457*(7233), 1128-1132. https://doi.org/10.1038/nature07761
Lautenschlager, N. T., Cupples, L. A., Rao, V. S., Auerbach, S. A., Becker, R., Burke, J.,…Farrer, L. A. (1996). Risk of dementia among relatives of Alzheimer's disease patients in the MIRAGE study: What is in store for the oldest old? *Neurology*, *46*(3), 641-650. https://doi.org/10.1212/wnl.46.3.641
Lee, H. K. (2006). Synaptic plasticity and phosphorylation. *Pharmacol Ther*, *112*(3), 810-832. https://doi.org/10.1016/j.pharmthera.2006.06.003
Lee, J., & Kim, H. J. (2022). Normal Aging Induces Changes in the Brain and Neurodegeneration Progress: Review of the Structural, Biochemical, Metabolic, Cellular, and Molecular Changes. *Front Aging Neurosci*, *14*, 931536. https://doi.org/10.3389/fnagi.2022.931536
Lee, J., Retamal, C., Cuitiño, L., Caruano-Yzermans, A., Shin, J. E., van Kerkhof, P.,…Bu, G. (2008). Adaptor protein sorting nexin 17 regulates amyloid precursor protein trafficking and processing in the early endosomes. *J Biol Chem*, *283*(17), 11501-11508. https://doi.org/10.1074/jbc.M800642200
Lee, M. S., Kwon, Y. T., Li, M., Peng, J., Friedlander, R. M., & Tsai, L. H. (2000). Neurotoxicity induces cleavage of p35 to p25 by calpain. *Nature*, *405*(6784), 360-364. https://doi.org/10.1038/35012636

Lein, E. S., Hawrylycz, M. J., Ao, N., Ayres, M., Bensinger, A., Bernard, A.,…Jones, A. R. (2007). Genome-wide atlas of gene expression in the adult mouse brain. *Nature*, *445*(7124), 168-176. https://doi.org/10.1038/nature05453
Leissring, M. A., Murphy, M. P., Mead, T. R., Akbari, Y., Sugarman, M. C., Jannatipour, M.,…LaFerla, F. M. (2002). A physiologic signaling role for the gamma -secretase-derived intracellular fragment of APP. *Proc Natl Acad Sci U S A*, *99*(7), 4697-4702. https://doi.org/10.1073/pnas.072033799
Leoutsakos, J. M., Forrester, S. N., Lyketsos, C. G., & Smith, G. S. (2015). Latent Classes of Neuropsychiatric Symptoms in NACC Controls and Conversion to Mild Cognitive Impairment or Dementia. *J Alzheimers Dis*, *48*(2), 483-493. https://doi.org/10.3233/JAD-150421
Leroy, K., Ando, K., Laporte, V., Dedecker, R., Suain, V., Authelet, M.,…Brion, J. P. (2012). Lack of tau proteins rescues neuronal cell death and decreases amyloidogenic processing of APP in APP/PS1 mice. *Am J Pathol*, *181*(6), 1928-1940. https://doi.org/10.1016/j.ajpath.2012.08.012
Lesné, S., Ali, C., Gabriel, C., Croci, N., MacKenzie, E. T., Glabe, C. G.,…Buisson, A. (2005). NMDA receptor activation inhibits alpha-secretase and promotes neuronal amyloid-beta production. *J Neurosci*, *25*(41), 9367-9377. https://doi.org/10.1523/JNEUROSCI.0849-05.2005
Lester, A. W., Moffat, S. D., Wiener, J. M., Barnes, C. A., & Wolbers, T. (2017). The Aging Navigational System. *Neuron*, *95*(5), 1019-1035. https://doi.org/10.1016/j.neuron.2017.06.037
Leverenz, J. B., & Raskind, M. A. (1998). Early amyloid deposition in the medial temporal lobe of young Down syndrome patients: a regional quantitative analysis. *Exp Neurol*, *150*(2), 296-304. https://doi.org/10.1006/exnr.1997.6777
Levy-Lahad, E., Wasco, W., Poorkaj, P., Romano, D. M., Oshima, J., Pettingell, W. H.,…Wang, K. (1995). Candidate gene for the chromosome 1 familial Alzheimer's disease locus. *Science*, *269*(5226), 973-977. https://doi.org/10.1126/science.7638622
Lezak, K. R., Missig, G., & Carlezon, W. A. (2017). Behavioral methods to study anxiety in rodents. *Dialogues Clin Neurosci*, *19*(2), 181-191. https://doi.org/10.31887/DCNS.2017.19.2/wcarlezon
Li, B., Chohan, M. O., Grundke-Iqbal, I., & Iqbal, K. (2007). Disruption of microtubule network by Alzheimer abnormally hyperphosphorylated tau. *Acta Neuropathol*, *113*(5), 501-511. https://doi.org/10.1007/s00401-007-0207-8
Li, N., Liu, K., Qiu, Y., Ren, Z., Dai, R., Deng, Y., & Qing, H. (2016). Effect of Presenilin Mutations on APP Cleavage; Insights into the Pathogenesis of FAD. *Front Aging Neurosci*, *8*, 51. https://doi.org/10.3389/fnagi.2016.00051
Li, S., Hong, S., Shepardson, N. E., Walsh, D. M., Shankar, G. M., & Selkoe, D. (2009). Soluble oligomers of amyloid Beta protein facilitate hippocampal long-term depression by disrupting neuronal glutamate uptake. *Neuron*, *62*(6), 788-801. https://doi.org/10.1016/j.neuron.2009.05.012
Li, S., Jin, M., Koeglsperger, T., Shepardson, N. E., Shankar, G. M., & Selkoe, D. J. (2011). Soluble Aβ oligomers inhibit long-term potentiation through a mechanism involving excessive activation of extrasynaptic NR2B-containing NMDA receptors. *J Neurosci*, *31*(18), 6627-6638. https://doi.org/10.1523/JNEUROSCI.0203-11.2011
Li, S., Jin, M., Liu, L., Dang, Y., Ostaszewski, B. L., & Selkoe, D. J. (2018). Decoding the synaptic dysfunction of bioactive human AD brain soluble Aβ to inspire

novel therapeutic avenues for Alzheimer's disease. *Acta Neuropathol Commun*, *6*(1), 121. https://doi.org/10.1186/s40478-018-0626-x
Li, S., & Selkoe, D. J. (2020). A mechanistic hypothesis for the impairment of synaptic plasticity by soluble Aβ oligomers from Alzheimer's brain. *J Neurochem*, *154*(6), 583-597. https://doi.org/10.1111/jnc.15007
Li, X., Feng, X., Sun, X., Hou, N., Han, F., & Liu, Y. (2022). Global, regional, and national burden of Alzheimer's disease and other dementias, 1990-2019. *Front Aging Neurosci*, *14*, 937486. https://doi.org/10.3389/fnagi.2022.937486
Li, X. X., & Li, Z. (2018). The impact of anxiety on the progression of mild cognitive impairment to dementia in Chinese and English data bases: a systematic review and meta-analysis. *Int J Geriatr Psychiatry*, *33*(1), 131-140. https://doi.org/10.1002/gps.4694
Li, Y., Schoufour, J., Wang, D. D., Dhana, K., Pan, A., Liu, X.,…Hu, F. B. (2020). Healthy lifestyle and life expectancy free of cancer, cardiovascular disease, and type 2 diabetes: prospective cohort study. *BMJ*, *368*, l6669. https://doi.org/10.1136/bmj.l6669
Liao, Y. F., Wang, B. J., Cheng, H. T., Kuo, L. H., & Wolfe, M. S. (2004). Tumor necrosis factor-alpha, interleukin-1beta, and interferon-gamma stimulate gamma-secretase-mediated cleavage of amyloid precursor protein through a JNK-dependent MAPK pathway. *J Biol Chem*, *279*(47), 49523-49532. https://doi.org/10.1074/jbc.M402034200
Lichtenthaler, S. F., Wang, R., Grimm, H., Uljon, S. N., Masters, C. L., & Beyreuther, K. (1999). Mechanism of the cleavage specificity of Alzheimer's disease gamma-secretase identified by phenylalanine-scanning mutagenesis of the transmembrane domain of the amyloid precursor protein. *Proc Natl Acad Sci U S A*, *96*(6), 3053-3058. https://doi.org/10.1073/pnas.96.6.3053
Liebscher, S., Page, R. M., Käfer, K., Winkler, E., Quinn, K., Goldbach, E.,…Hübener, M. (2014). Chronic γ-secretase inhibition reduces amyloid plaque-associated instability of pre- and postsynaptic structures. *Mol Psychiatry*, *19*(8), 937-946. https://doi.org/10.1038/mp.2013.122
Lim, S., & Goldman, M. S. (2013). Balanced cortical microcircuitry for maintaining information in working memory. *Nat Neurosci*, *16*(9), 1306-1314. https://doi.org/10.1038/nn.3492
Lindeza, P., Rodrigues, M., Costa, J., Guerreiro, M., & Rosa, M. M. (2020). Impact of dementia on informal care: a systematic review of family caregivers' perceptions. *BMJ Support Palliat Care*. https://doi.org/10.1136/bmjspcare-2020-002242
Ling, Y., Morgan, K., & Kalsheker, N. (2023). Amyloid precursor protein (APP) and the biology of proteolytic processing: relevance to Alzheimer's disease. *The International Journal of Biochemistry and Cell Biology*, *35*(11), 1505-1535.
Lisman, J., Schulman, H., & Cline, H. (2002). The molecular basis of CaMKII function in synaptic and behavioural memory. *Nat Rev Neurosci*, *3*(3), 175-190. https://doi.org/10.1038/nrn753
Lisman, J., Yasuda, R., & Raghavachari, S. (2012). Mechanisms of CaMKII action in long-term potentiation. *Nat Rev Neurosci*, *13*(3), 169-182. https://doi.org/10.1038/nrn3192
Lister, R. G. (1987). The use of a plus-maze to measure anxiety in the mouse. *Psychopharmacology (Berl)*, *92*(2), 180-185. https://doi.org/10.1007/BF00177912

Lister, R. G. (1990). Ethologically-based animal models of anxiety disorders. *Pharmacol Ther*, *46*(3), 321-340. https://doi.org/10.1016/0163-7258(90)90021-s
Liu, J., Chang, L., Song, Y., Li, H., & Wu, Y. (2019). The Role of NMDA Receptors in Alzheimer's Disease. *Front Neurosci*, *13*, 43. https://doi.org/10.3389/fnins.2019.00043
Locci, A., Orellana, H., Rodriguez, G., Gottliebson, M., McClarty, B., Dominguez, S.,…Dong, H. (2021). Comparison of memory, affective behavior, and neuropathology in APP. *Behav Brain Res*, *404*, 113192. https://doi.org/10.1016/j.bbr.2021.113192
Loeffler, D. A. (2023). Antibody-Mediated Clearance of Brain Amyloid-β: Mechanisms of Action, Effects of Natural and Monoclonal Anti-Aβ Antibodies, and Downstream Effects. *J Alzheimers Dis Rep*, *7*(1), 873-899. https://doi.org/10.3233/ADR-230025
Logsdon, A. F., Lucke-Wold, B. P., Turner, R. C., Li, X., Adkins, C. E., Mohammad, A. S.,…Lockman, P. R. (2017). A mouse Model of Focal Vascular Injury Induces Astrocyte Reactivity, Tau Oligomers, and Aberrant Behavior. *Arch Neurosci*, *4*(2). https://doi.org/10.5812/archneurosci.44254
Lopez-Lee, C., Torres, E. R. S., Carling, G., & Gan, L. (2024). Mechanisms of sex differences in Alzheimer's disease. *Neuron*, *112*(8), 1208-1221. https://doi.org/10.1016/j.neuron.2024.01.024
Lourenco, M. V., Clarke, J. R., Frozza, R. L., Bomfim, T. R., Forny-Germano, L., Batista, A. F.,…De Felice, F. G. (2013). TNF-α mediates PKR-dependent memory impairment and brain IRS-1 inhibition induced by Alzheimer's β-amyloid oligomers in mice and monkeys. *Cell Metab*, *18*(6), 831-843. https://doi.org/10.1016/j.cmet.2013.11.002
Lozano, Y. R., Page, H., Jacob, P. Y., Lomi, E., Street, J., & Jeffery, K. (2017). Retrosplenial and postsubicular head direction cells compared during visual landmark discrimination. *Brain Neurosci Adv*, *1*, 2398212817721859. https://doi.org/10.1177/2398212817721859
Lu, J. X., Qiang, W., Yau, W. M., Schwieters, C. D., Meredith, S. C., & Tycko, R. (2013). Molecular structure of β-amyloid fibrils in Alzheimer's disease brain tissue. *Cell*, *154*(6), 1257-1268. https://doi.org/10.1016/j.cell.2013.08.035
Lu, W., Mi, R., Tang, H., Liu, S., Fan, M., & Wang, L. (1998). Over-expression of c-fos mRNA in the hippocampal neurons in Alzheimer's disease. *Chin Med J (Engl)*, *111*(1), 35-37.
Lukoyanov, N. V., & Lukoyanova, E. A. (2006). Retrosplenial cortex lesions impair acquisition of active avoidance while sparing fear-based emotional memory. *Behav Brain Res*, *173*(2), 229-236. https://doi.org/10.1016/j.bbr.2006.06.026
Lyketsos, C. G., Carrillo, M. C., Ryan, J. M., Khachaturian, A. S., Trzepacz, P., Amatniek, J.,…Miller, D. S. (2011). Neuropsychiatric symptoms in Alzheimer's disease. *Alzheimers Dement*, *7*(5), 532-539. https://doi.org/10.1016/j.jalz.2011.05.2410
Lyketsos, C. G., Lopez, O., Jones, B., Fitzpatrick, A. L., Breitner, J., & DeKosky, S. (2002). Prevalence of neuropsychiatric symptoms in dementia and mild cognitive impairment: results from the cardiovascular health study. *JAMA*, *288*(12), 1475-1483. https://doi.org/10.1001/jama.288.12.1475
Lüscher, C., & Malenka, R. C. (2012). NMDA receptor-dependent long-term potentiation and long-term depression (LTP/LTD). *Cold Spring Harb Perspect Biol*, *4*(6). https://doi.org/10.1101/cshperspect.a005710

Ma, Q. L., Yang, F., Rosario, E. R., Ubeda, O. J., Beech, W., Gant, D. J.,…Cole, G. M. (2009). Beta-amyloid oligomers induce phosphorylation of tau and inactivation of insulin receptor substrate via c-Jun N-terminal kinase signaling: suppression by omega-3 fatty acids and curcumin. *J Neurosci*, *29*(28), 9078-9089. https://doi.org/10.1523/JNEUROSCI.1071-09.2009

Ma, X., Zheng, C., Chen, Y., Pereira, F., & Li, Z. (2023). Working memory and reward increase the accuracy of animal location encoding in the medial prefrontal cortex. *Cereb Cortex*, *33*(5), 2245-2259. https://doi.org/10.1093/cercor/bhac205

Maezono, S. E. B., Kanuka, M., Tatsuzawa, C., Morita, M., Kawano, T., Kashiwagi, M.,…Hayashi, Y. (2020). Progressive Changes in Sleep and Its Relations to Amyloid-β Distribution and Learning in Single. *eNeuro*, *7*(2). https://doi.org/10.1523/ENEURO.0093-20.2020

Maguire, E. A. (2001a). Neuroimaging studies of autobiographical event memory. *Philos Trans R Soc Lond B Biol Sci*, *356*(1413), 1441-1451. https://doi.org/10.1098/rstb.2001.0944

Maguire, E. A. (2001b). The retrosplenial contribution to human navigation: a review of lesion and neuroimaging findings. *Scand J Psychol*, *42*(3), 225-238. https://doi.org/10.1111/1467-9450.00233

Mah, L., Binns, M. A., Steffens, D. C., & Initiative, A. s. D. N. (2015). Anxiety symptoms in amnestic mild cognitive impairment are associated with medial temporal atrophy and predict conversion to Alzheimer disease. *Am J Geriatr Psychiatry*, *23*(5), 466-476. https://doi.org/10.1016/j.jagp.2014.10.005

Maleeva, N. E., Ivolgina, G. L., Anokhin, K. V., & Limborskaia, S. A. (1989). Analysis of the expression of the c-fos proto-oncogene in the rat cerebral cortex during learning. *Genetika*, *25*(6), 1119-1121.

Malenka, R. C. (1994). Synaptic plasticity in the hippocampus: LTP and LTD. *Cell*, *78*(4), 535-538. https://doi.org/10.1016/0092-8674(94)90517-7

Manabe, T., Teramoto, S., Tamiya, N., Okochi, J., & Hizawa, N. (2015). Risk Factors for Aspiration Pneumonia in Older Adults. *PLoS One*, *10*(10), e0140060. https://doi.org/10.1371/journal.pone.0140060

Mannix, R., Berglass, J., Berkner, J., Moleus, P., Qiu, J., Andrews, N.,…Meehan, W. P. (2014). Chronic gliosis and behavioral deficits in mice following repetitive mild traumatic brain injury. *J Neurosurg*, *121*(6), 1342-1350. https://doi.org/10.3171/2014.7.JNS14272

Manocha, G. D., Floden, A. M., Miller, N. M., Smith, A. J., Nagamoto-Combs, K., Saito, T.,…Combs, C. K. (2019). Temporal progression of Alzheimer's disease in brains and intestines of transgenic mice. *Neurobiol Aging*, *81*, 166-176. https://doi.org/10.1016/j.neurobiolaging.2019.05.025

Manzini, C. S. S., & do Vale, F. A. C. (2020). Emotional disorders evidenced by family caregivers of older people with Alzheimer's disease. *Dement Neuropsychol*, *14*(1), 56-61. https://doi.org/10.1590/1980-57642020dn14-010009

Marcus, D. L., Strafaci, J. A., Miller, D. C., Masia, S., Thomas, C. G., Rosman, J.,…Freedman, M. L. (1998). Quantitative neuronal c-Fos and c-Jun expression in Alzheimer’s disease. *Neurobiology of Aging*, *19*(5), 393-400.

Mark, R. E., & Brehmer, Y. (2022). Preclinical Alzheimer's dementia: a useful concept or another dead end? *Eur J Ageing*, *19*(4), 997-1004. https://doi.org/10.1007/s10433-022-00735-w

Mark, R. J., Pang, Z., Geddes, J. W., Uchida, K., & Mattson, M. P. (1997). Amyloid beta-peptide impairs glucose transport in hippocampal and cortical neurons: involvement of membrane lipid peroxidation. *J Neurosci*, *17*(3), 1046-1054. https://doi.org/10.1523/JNEUROSCI.17-03-01046.1997

Martins, M. J., Fischmeister, F. P., Puig-Waldmüller, E., Oh, J., Geissler, A., Robinson, S.,…Beisteiner, R. (2014). Fractal image perception provides novel insights into hierarchical cognition. *Neuroimage*, *96*, 300-308. https://doi.org/10.1016/j.neuroimage.2014.03.064

Masliah, E., Mallory, M., Ge, N., & Saitoh, T. (1992). Amyloid precursor protein is localized in growing neurites of neonatal rat brain. *Brain Res*, *593*(2), 323-328. https://doi.org/10.1016/0006-8993(92)91329-d

Masliah, E., Sisk, A., Mallory, M., & Games, D. (2001). Neurofibrillary pathology in transgenic mice overexpressing V717F beta-amyloid precursor protein. *J Neuropathol Exp Neurol*, *60*(4), 357-368. https://doi.org/10.1093/jnen/60.4.357

Masuda, A., Kobayashi, Y., Kogo, N., Saito, T., Saido, T. C., & Itohara, S. (2016). Cognitive deficits in single App knock-in mouse models. *Neurobiol Learn Mem*, *135*, 73-82. https://doi.org/10.1016/j.nlm.2016.07.001

Matsuzaki, M., Honkura, N., Ellis-Davies, G. C., & Kasai, H. (2004). Structural basis of long-term potentiation in single dendritic spines. *Nature*, *429*(6993), 761-766. https://doi.org/10.1038/nature02617

Mattson, M. P. (2010). ER calcium and Alzheimer's disease: in a state of flux. *Sci Signal*, *3*(114), pe10. https://doi.org/10.1126/scisignal.3114pe10

Mattson, M. P., Cheng, B., Davis, D., Bryant, K., Lieberburg, I., & Rydel, R. E. (1992). beta-Amyloid peptides destabilize calcium homeostasis and render human cortical neurons vulnerable to excitotoxicity. *J Neurosci*, *12*(2), 376-389. https://doi.org/10.1523/JNEUROSCI.12-02-00376.1992

Maurer, K., Volk, S., & Gerbaldo, H. (1997). Auguste D and Alzheimer's disease. *Lancet*, *349*(9064), 1546-1549. https://doi.org/10.1016/S0140-6736(96)10203-8

Mawuenyega, K. G., Sigurdson, W., Ovod, V., Munsell, L., Kasten, T., Morris, J. C.,…Bateman, R. J. (2010). Decreased clearance of CNS beta-amyloid in Alzheimer's disease. *Science*, *330*(6012), 1774. https://doi.org/10.1126/science.1197623

McCarron, M., McCallion, P., Reilly, E., & Mulryan, N. (2014). A prospective 14-year longitudinal follow-up of dementia in persons with Down syndrome. *J Intellect Disabil Res*, *58*(1), 61-70. https://doi.org/10.1111/jir.12074

McDonald, C. R., Gharapetian, L., McEvoy, L. K., Fennema-Notestine, C., Hagler, D. J., Holland, D.,…Initiative, A. s. D. N. (2012). Relationship between regional atrophy rates and cognitive decline in mild cognitive impairment. *Neurobiol Aging*, *33*(2), 242-253. https://doi.org/10.1016/j.neurobiolaging.2010.03.015

McElroy, D. L., Sabir, H., Glass, A. E., Greba, Q., & Howland, J. G. (2024). The anterior retrosplenial cortex is required for short-term object in place recognition memory retrieval: Role of ionotropic glutamate receptors in male and female Long-Evans rats. *Eur J Neurosci*, *59*(9), 2260-2275. https://doi.org/10.1111/ejn.16284

McHugh, S. B., Deacon, R. M., Rawlins, J. N., & Bannerman, D. M. (2004). Amygdala and ventral hippocampus contribute differentially to mechanisms of fear and anxiety. *Behav Neurosci*, *118*(1), 63-78. https://doi.org/10.1037/0735-7044.118.1.63

McKhann, G. M., Knopman, D. S., Chertkow, H., Hyman, B. T., Jack, C. R., Kawas, C. H.,…Phelps, C. H. (2011). The diagnosis of dementia due to Alzheimer's disease: recommendations from the National Institute on Aging-Alzheimer's Association workgroups on diagnostic guidelines for Alzheimer's disease. *Alzheimers Dement*, *7*(3), 263-269. https://doi.org/10.1016/j.jalz.2011.03.005
McTeague, L. M., & Lang, P. J. (2012). The anxiety spectrum and the reflex physiology of defense: from circumscribed fear to broad distress. *Depress Anxiety*, *29*(4), 264-281. https://doi.org/10.1002/da.21891
Mehla, J., Deibel, S. H., Karem, H., Hossain, S., Lacoursiere, S. G., Sutherland, R. J.,…McDonald, R. J. (2022). Dramatic impacts on brain pathology, anxiety, and cognitive function in the knock-in APP. *Alzheimers Res Ther*, *14*(1), 143. https://doi.org/10.1186/s13195-022-01085-6
Mehla, J., Lacoursiere, S. G., Lapointe, V., McNaughton, B. L., Sutherland, R. J., McDonald, R. J., & Mohajerani, M. H. (2019). Age-dependent behavioral and biochemical characterization of single APP knock-in mouse (APP. *Neurobiol Aging*, *75*, 25-37. https://doi.org/10.1016/j.neurobiolaging.2018.10.026
Mendez, M. F. (2021). The Relationship Between Anxiety and Alzheimer's Disease. *J Alzheimers Dis Rep*, *5*(1), 171-177. https://doi.org/10.3233/ADR-210294
Meraz-Ríos, M. A., Franco-Bocanegra, D., Toral Rios, D., & Campos-Peña, V. (2014). Early onset Alzheimer's disease and oxidative stress. *Oxid Med Cell Longev*, *2014*, 375968. https://doi.org/10.1155/2014/375968
Michelucci, A., Heurtaux, T., Grandbarbe, L., Morga, E., & Heuschling, P. (2009). Characterization of the microglial phenotype under specific pro-inflammatory and anti-inflammatory conditions: Effects of oligomeric and fibrillar amyloid-beta. *J Neuroimmunol*, *210*(1-2), 3-12. https://doi.org/10.1016/j.jneuroim.2009.02.003
Miedel, C. J., Patton, J. M., Miedel, A. N., Miedel, E. S., & Levenson, J. M. (2017). Assessment of Spontaneous Alternation, Novel Object Recognition and Limb Clasping in Transgenic Mouse Models of Amyloid-β and Tau Neuropathology. *J Vis Exp*(123). https://doi.org/10.3791/55523
Mielke, M. M. (2018). Sex and Gender Differences in Alzheimer's Disease Dementia. *Psychiatr Times*, *35*(11), 14-17.
Migliaccio, R., Tanguy, D., Bouzigues, A., Sezer, I., Dubois, B., Le Ber, I.,…Levy, R. (2020). Cognitive and behavioural inhibition deficits in neurodegenerative dementias. *Cortex*, *131*, 265-283. https://doi.org/10.1016/j.cortex.2020.08.001
Migliore, L., & Coppedè, F. (2022). Gene-environment interactions in Alzheimer disease: the emerging role of epigenetics. *Nat Rev Neurol*, *18*(11), 643-660. https://doi.org/10.1038/s41582-022-00714-w
Milczarek, M. M., & Vann, S. D. (2020). The retrosplenial cortex and long-term spatial memory: from the cell to the network. *Curr Opin Behav Sci*, *32*, 50-56. https://doi.org/10.1016/j.cobeha.2020.01.014
Milczarek, M. M., Vann, S. D., & Sengpiel, F. (2018). Spatial Memory Engram in the Mouse Retrosplenial Cortex. *Curr Biol*, *28*(12), 1975-1980.e1976. https://doi.org/10.1016/j.cub.2018.05.002
Miller, A. M., Vedder, L. C., Law, L. M., & Smith, D. M. (2014). Cues, context, and long-term memory: the role of the retrosplenial cortex in spatial cognition. *Front Hum Neurosci*, *8*, 586. https://doi.org/10.3389/fnhum.2014.00586
Minatohara, K., Akiyoshi, M., & Okuno, H. (2015). Role of Immediate-Early Genes in Synaptic Plasticity and Neuronal Ensembles Underlying the Memory Trace. *Front Mol Neurosci*, *8*, 78. https://doi.org/10.3389/fnmol.2015.00078

Minoshima, S., Giordani, B., Berent, S., Frey, K. A., Foster, N. L., & Kuhl, D. E. (1997). Metabolic reduction in the posterior cingulate cortex in very early Alzheimer's disease. *Ann Neurol*, *42*(1), 85-94. https://doi.org/10.1002/ana.410420114
Mintun, M. A., Lo, A. C., Duggan Evans, C., Wessels, A. M., Ardayfio, P. A., Andersen, S. W.,…Skovronsky, D. M. (2021). Donanemab in Early Alzheimer's Disease. *N Engl J Med*, *384*(18), 1691-1704. https://doi.org/10.1056/NEJMoa2100708
Mitchell, A. S., Czajkowski, R., Zhang, N., Jeffery, K., & Nelson, A. J. D. (2018). Retrosplenial cortex and its role in spatial cognition. *Brain Neurosci Adv*, *2*, 2398212818757098. https://doi.org/10.1177/2398212818757098
Mitchell, J. B., & Laiacona, J. (1998). The medial frontal cortex and temporal memory: tests using spontaneous exploratory behaviour in the rat. *Behav Brain Res*, *97*(1-2), 107-113. https://doi.org/10.1016/s0166-4328(98)00032-1
Mokhtar, S. H., Bakhuraysah, M. M., Cram, D. S., & Petratos, S. (2013). The Beta-amyloid protein of Alzheimer's disease: communication breakdown by modifying the neuronal cytoskeleton. *Int J Alzheimers Dis*, *2013*, 910502. https://doi.org/10.1155/2013/910502
Mokrisova, I., Laczo, J., Andel, R., Gazova, I., Vyhnalek, M., Nedelska, Z.,…Hort, J. (2016). Real-space path integration is impaired in Alzheimer's disease and mild cognitive impairment. *Behav Brain Res*, *307*, 150-158. https://doi.org/10.1016/j.bbr.2016.03.052
Moncada, D., Ballarini, F., & Viola, H. (2015). Behavioral Tagging: A Translation of the Synaptic Tagging and Capture Hypothesis. *Neural Plast*, *2015*, 650780. https://doi.org/10.1155/2015/650780
Moncada, D., & Viola, H. (2007). Induction of long-term memory by exposure to novelty requires protein synthesis: evidence for a behavioral tagging. *J Neurosci*, *27*(28), 7476-7481. https://doi.org/10.1523/JNEUROSCI.1083-07.2007
Moore, S. J., Cazares, V. A., Temme, S. J., & Murphy, G. G. (2023). Age-related deficits in neuronal physiology and cognitive function are recapitulated in young mice overexpressing the L-type calcium channel, Cav1.3. *Aging Cell*, *22*(3), e13781. https://doi.org/10.1111/acel.13781
Morgan, J. I., Cohen, D. R., Hempstead, J. L., & Curran, T. (1987). Mapping patterns of c-fos expression in the central nervous system after seizure. *Science*, *237*(4811), 192-197. https://doi.org/10.1126/science.3037702
Moriguchi, S., Kita, S., Fukaya, M., Osanai, M., Inagaki, R., Sasaki, Y.,…Fukunaga, K. (2018). Reduced expression of Na+/Ca2+ exchangers is associated with cognitive deficits seen in Alzheimer's disease model mice. *Neuropharmacology*, *131*, 291-303. https://doi.org/10.1016/j.neuropharm.2017.12.037
Morley, J. E., Farr, S. A., Nguyen, A. D., & Xu, F. (2019). Editorial: What is the Physiological Function of Amyloid-Beta Protein? *J Nutr Health Aging*, *23*(3), 225-226. https://doi.org/10.1007/s12603-019-1162-5
Mormino, E. C., Kluth, J. T., Madison, C. M., Rabinovici, G. D., Baker, S. L., Miller, B. L.,…Initiative, A. s. D. N. (2009). Episodic memory loss is related to hippocampal-mediated beta-amyloid deposition in elderly subjects. *Brain*, *132*(Pt 5), 1310-1323. https://doi.org/10.1093/brain/awn320
Morris, M. C., Evans, D. A., Bienias, J. L., Tangney, C. C., Bennett, D. A., Aggarwal, N.,…Wilson, R. S. (2003). Dietary fats and the risk of incident Alzheimer

disease. *Arch Neurol*, *60*(2), 194-200. https://doi.org/10.1001/archneur.60.2.194
Morris, R. (1984). Developments of a water-maze procedure for studying spatial learning in the rat. *J Neurosci Methods*, *11*(1), 47-60. https://doi.org/10.1016/0165-0270(84)90007-4
Mosconi, L., Sorbi, S., de Leon, M. J., Li, Y., Nacmias, B., Myoung, P. S.,…Pupi, A. (2006). Hypometabolism exceeds atrophy in presymptomatic early-onset familial Alzheimer's disease. *J Nucl Med*, *47*(11), 1778-1786.
Moser, M. B., Rowland, D. C., & Moser, E. I. (2015). Place cells, grid cells, and memory. *Cold Spring Harb Perspect Biol*, *7*(2), a021808. https://doi.org/10.1101/cshperspect.a021808
Mostafa, R., Michalikova, S., & Ennaceur, A. (2002). A 3D spatial navigation task for assessing memory in rodents. *Neuroscience Research Communications*, *31*(1), 19-28.
Mouzon, B. C., Bachmeier, C., Ojo, J. O., Acker, C. M., Ferguson, S., Paris, D.,…Crawford, F. (2018). Lifelong behavioral and neuropathological consequences of repetitive mild traumatic brain injury. *Ann Clin Transl Neurol*, *5*(1), 64-80. https://doi.org/10.1002/acn3.510
Mroczko, B., Groblewska, M., & Litman-Zawadzka, A. (2019). The Role of Protein Misfolding and Tau Oligomers (TauOs) in Alzheimer's Disease (AD). *Int J Mol Sci*, *20*(19). https://doi.org/10.3390/ijms20194661
Mullan, M., Crawford, F., Axelman, K., Houlden, H., Lilius, L., Winblad, B., & Lannfelt, L. (1992). A pathogenic mutation for probable Alzheimer's disease in the APP gene at the N-terminus of beta-amyloid. *Nat Genet*, *1*(5), 345-347. https://doi.org/10.1038/ng0892-345
Muller, R. U., & Kubie, J. L. (1987). The effects of changes in the environment on the spatial firing of hippocampal complex-spike cells. *J Neurosci*, *7*(7), 1951-1968. https://doi.org/10.1523/JNEUROSCI.07-07-01951.1987
Mumby, D. G., Gaskin, S., Glenn, M. J., Schramek, T. E., & Lehmann, H. (2002). Hippocampal damage and exploratory preferences in rats: memory for objects, places, and contexts. *Learn Mem*, *9*(2), 49-57. https://doi.org/10.1101/lm.41302
Mumby, D. G., & Pinel, J. P. (1994). Rhinal cortex lesions and object recognition in rats. *Behav Neurosci*, *108*(1), 11-18. https://doi.org/10.1037//0735-7044.108.1.11
Murakami, T., Yoshida, T., Matsui, T., & Ohki, K. (2015). Wide-field Ca(2+) imaging reveals visually evoked activity in the retrosplenial area. *Front Mol Neurosci*, *8*, 20. https://doi.org/10.3389/fnmol.2015.00020
Nagahara, A. H., & Handa, R. J. (1995). Fetal alcohol exposure alters the induction of immediate early gene mRNA in the rat prefrontal cortex after an alternation task. *Alcohol Clin Exp Res*, *19*(6), 1389-1397. https://doi.org/10.1111/j.1530-0277.1995.tb00997.x
Nakai, J., Ohkura, M., & Imoto, K. (2001). A high signal-to-noise Ca(2+) probe composed of a single green fluorescent protein. *Nat Biotechnol*, *19*(2), 137-141. https://doi.org/10.1038/84397
Nasr, S., Echavarria, C. E., & Tootell, R. B. (2014). Thinking outside the box: rectilinear shapes selectively activate scene-selective cortex. *J Neurosci*, *34*(20), 6721-6735. https://doi.org/10.1523/JNEUROSCI.4802-13.2014
Neave, N., Lloyd, S., Sahgal, A., & Aggleton, J. P. (1994). Lack of effect of lesions in the anterior cingulate cortex and retrosplenial cortex on certain tests of spatial

memory in the rat. *Behav Brain Res*, *65*(1), 89-101. https://doi.org/10.1016/0166-4328(94)90077-9
Nelson, A. J., Powell, A. L., Holmes, J. D., Vann, S. D., & Aggleton, J. P. (2015). What does spatial alternation tell us about retrosplenial cortex function? *Front Behav Neurosci*, *9*, 126. https://doi.org/10.3389/fnbeh.2015.00126
Nelson, P. T., Head, E., Schmitt, F. A., Davis, P. R., Neltner, J. H., Jicha, G. A.,…Scheff, S. W. (2011). Alzheimer's disease is not "brain aging": neuropathological, genetic, and epidemiological human studies. *Acta Neuropathol*, *121*(5), 571-587. https://doi.org/10.1007/s00401-011-0826-y
Nestor, P. J., Fryer, T. D., Ikeda, M., & Hodges, J. R. (2003). Retrosplenial cortex (BA 29/30) hypometabolism in mild cognitive impairment (prodromal Alzheimer's disease). *Eur J Neurosci*, *18*(9), 2663-2667. https://doi.org/10.1046/j.1460-9568.2003.02999.x
Neuner, S. M., Tcw, J., & Goate, A. M. (2020). Genetic architecture of Alzheimer's disease. *Neurobiol Dis*, *143*, 104976. https://doi.org/10.1016/j.nbd.2020.104976
Nevian, T., & Sakmann, B. (2006). Spine Ca2+ signaling in spike-timing-dependent plasticity. *J Neurosci*, *26*(43), 11001-11013. https://doi.org/10.1523/JNEUROSCI.1749-06.2006
Ng, L. L., Chow, J., & Lau, K. F. (2024). The AICD interactome: implications in neurodevelopment and neurodegeneration. *Biochem Soc Trans*, *52*(6), 2539-2556. https://doi.org/10.1042/BST20241510
Ni, X., Inoue, R., Wu, Y., Yoshida, T., Yaku, K., Nakagawa, T.,…Mori, H. (2023). Regional contributions of D-serine to Alzheimer's disease pathology in male AppNL-G-F/NL-G-F mice. *Front Aging Neurosci*, *15*, 1211067. https://doi.org/10.3389/fnagi.2023.1211067
Nicotera, P., Leist, M., & Ferrando-May, E. (1998). Intracellular ATP, a switch in the decision between apoptosis and necrosis. *Toxicol Lett*, *102-103*, 139-142. https://doi.org/10.1016/s0378-4274(98)00298-7
Nikolaev, E., Kaczmarek, L., Zhu, S. W., Winblad, B., & Mohammed, A. H. (2002). Environmental manipulation differentially alters c-Fos expression in amygdaloid nuclei following aversive conditioning. *Brain Res*, *957*(1), 91-98. https://doi.org/10.1016/s0006-8993(02)03606-5
Nilsberth, C., Westlind-Danielsson, A., Eckman, C. B., Condron, M. M., Axelman, K., Forsell, C.,…Lannfelt, L. (2001). The 'Arctic' APP mutation (E693G) causes Alzheimer's disease by enhanced Abeta protofibril formation. *Nat Neurosci*, *4*(9), 887-893. https://doi.org/10.1038/nn0901-887
Nimmrich, V., Grimm, C., Draguhn, A., Barghorn, S., Lehmann, A., Schoemaker, H.,…Bruehl, C. (2008). Amyloid beta oligomers (A beta(1-42) globulomer) suppress spontaneous synaptic activity by inhibition of P/Q-type calcium currents. *J Neurosci*, *28*(4), 788-797. https://doi.org/10.1523/JNEUROSCI.4771-07.2008
Niraula, S., Doderer, J. J., Indulkar, S., Berry, K. P., Hauser, W. L., L'Esperance, O. J.,…Subramanian, J. (2023). Excitation-inhibition imbalance disrupts visual familiarity in amyloid and non-pathology conditions. *Cell Rep*, *42*(1), 111946. https://doi.org/10.1016/j.celrep.2022.111946
Norman, G., & Eacott, M. J. (2004). Impaired object recognition with increasing levels of feature ambiguity in rats with perirhinal cortex lesions. *Behav Brain Res*, *148*(1-2), 79-91. https://doi.org/10.1016/s0166-4328(03)00176-1

O'Keefe, J. (1976). Place units in the hippocampus of the freely moving rat. *Exp Neurol*, *51*(1), 78-109. https://doi.org/10.1016/0014-4886(76)90055-8
Oakley, H., Cole, S. L., Logan, S., Maus, E., Shao, P., Craft, J.,…Vassar, R. (2006). Intraneuronal beta-amyloid aggregates, neurodegeneration, and neuron loss in transgenic mice with five familial Alzheimer's disease mutations: potential factors in amyloid plaque formation. *J Neurosci*, *26*(40), 10129-10140. https://doi.org/10.1523/JNEUROSCI.1202-06.2006
Oblak, A. L., Kotredes, K. P., Pandey, R. S., Reagan, A. M., Ingraham, C., Perkins, B.,…Howell, G. R. (2022). Interacts With High Fat/High Sugar Diet to Accelerate Alzheimer's Disease-Relevant Phenotypes in Mice. *Front Aging Neurosci*, *14*, 886575. https://doi.org/10.3389/fnagi.2022.886575
Oddo, S., Caccamo, A., Shepherd, J. D., Murphy, M. P., Golde , T. E., Kayed , R.,…LaFerla, F. M. (2003). Triple-Transgenic Model of Alzheimer's Disease with Plaques and Tangles : Intracellular Aβ and Synaptic Dysfunction. *Neuron*, *39*(3), 409-421.
Ognibene, E., Middei, S., Daniele, S., Adriani, W., Ghirardi, O., Caprioli, A., & Laviola, G. (2005). Aspects of spatial memory and behavioral disinhibition in Tg2576 transgenic mice as a model of Alzheimer's disease. *Behav Brain Res*, *156*(2), 225-232. https://doi.org/10.1016/j.bbr.2004.05.028
Ohkawara, T., Nagase, H., Koh, C. S., & Nakayama, K. (2011). The amyloid precursor protein intracellular domain alters gene expression and induces neuron-specific apoptosis. *Gene*, *475*(1), 1-9. https://doi.org/10.1016/j.gene.2010.11.014
Olton, D. S., Collison, C., & Werz, M. A. (1978). Spatial memory and radial arm maze performance of rats. *Learning and Motivation*, *8*(3), 289-314.
Ono, K. (2018). Alzheimer's disease as oligomeropathy. *Neurochem Int*, *119*, 57-70. https://doi.org/10.1016/j.neuint.2017.08.010
Ono, K., Condron, M. M., & Teplow, D. B. (2009). Structure-neurotoxicity relationships of amyloid beta-protein oligomers. *Proc Natl Acad Sci U S A*, *106*(35), 14745-14750. https://doi.org/10.1073/pnas.0905127106
Ortiz-Cruz, C. A., Marquez, E. J., Linares-García, C. I., Perera-Murcia, G. R., & Ramiro-Cortés, Y. (2022). Haploinsufficiency of Shank3 increases the orientation selectivity of V1 neurons. *Sci Rep*, *12*(1), 22230. https://doi.org/10.1038/s41598-022-26402-9
Osman, A., Kamkar, N., Speechley, M., Ali, S., & Montero-Odasso, M. (2022). Fall risk-increasing drugs and gait performance in community-dwelling older adults: A systematic review. *Ageing Res Rev*, *77*, 101599. https://doi.org/10.1016/j.arr.2022.101599
Oster-Granite, M. L., McPhie, D. L., Greenan, J., & Neve, R. L. (1996). Age-dependent neuronal and synaptic degeneration in mice transgenic for the C terminus of the amyloid precursor protein. *J Neurosci*, *16*(21), 6732-6741. https://doi.org/10.1523/JNEUROSCI.16-21-06732.1996
Ou, Y. N., Xu, W., Li, J. Q., Guo, Y., Cui, M., Chen, K. L.,…Initiative, A. s. D. N. (2019). FDG-PET as an independent biomarker for Alzheimer's biological diagnosis: a longitudinal study. *Alzheimers Res Ther*, *11*(1), 57. https://doi.org/10.1186/s13195-019-0512-1
Overk, C. R., Rockenstein, E., Florio, J., Cheng, Q., & Masliah, E. (2015). Differential calcium alterations in animal models of neurodegenerative disease: Reversal by FK506. *Neuroscience*, *310*, 549-560. https://doi.org/10.1016/j.neuroscience.2015.08.068

Pacher, P., & Hajnóczky, G. (2001). Propagation of the apoptotic signal by mitochondrial waves. *EMBO J*, *20*(15), 4107-4121. https://doi.org/10.1093/emboj/20.15.4107
Pachitariu, M., Stringer, C., Dipoppa, M., Schröder, S., Rossi, L., Dalgleish, H., & Carandini, M. (2017). Suite2p: beyond 10,000 neurons with standard two-photon microscopy. In: BioRxiv.
Palop, J. J., Chin, J., Bien-Ly, N., Massaro, C., Yeung, B. Z., Yu, G. Q., & Mucke, L. (2005). Vulnerability of dentate granule cells to disruption of arc expression in human amyloid precursor protein transgenic mice. *J Neurosci*, *25*(42), 9686-9693. https://doi.org/10.1523/JNEUROSCI.2829-05.2005
Palop, J. J., Jones, B., Kekonius, L., Chin, J., Yu, G. Q., Raber, J.,…Mucke, L. (2003). Neuronal depletion of calcium-dependent proteins in the dentate gyrus is tightly linked to Alzheimer's disease-related cognitive deficits. *Proc Natl Acad Sci U S A*, *100*(16), 9572-9577. https://doi.org/10.1073/pnas.1133381100
Pan, T. T., Liu, C., Li, D. M., Zhang, T. H., Zhang, W., Zhao, S. L.,…Liu, H. (2022). Retrosplenial Cortex Effects Contextual Fear Formation Relying on Dysgranular Constituent in Rats. *Front Neurosci*, *16*, 886858. https://doi.org/10.3389/fnins.2022.886858
Pang, K., Jiang, R., Zhang, W., Yang, Z., Li, L. L., Shimozawa, M.,…Lu, B. (2022). An App knock-in rat model for Alzheimer's disease exhibiting Aβ and tau pathologies, neuronal death and cognitive impairments. *Cell Res*, *32*(2), 157-175. https://doi.org/10.1038/s41422-021-00582-x
Parameshwaran, K., Dhanasekaran, M., & Suppiramaniam, V. (2008). Amyloid beta peptides and glutamatergic synaptic dysregulation. *Exp Neurol*, *210*(1), 7-13. https://doi.org/10.1016/j.expneurol.2007.10.008
Pardossi-Piquard, R., Petit, A., Kawarai, T., Sunyach, C., Alves da Costa, C., Vincent, B.,…Checler, F. (2005). Presenilin-dependent transcriptional control of the Abeta-degrading enzyme neprilysin by intracellular domains of betaAPP and APLP. *Neuron*, *46*(4), 541-554. https://doi.org/10.1016/j.neuron.2005.04.008
Park, M. (2018). AMPA Receptor Trafficking for Postsynaptic Potentiation. *Front Cell Neurosci*, *12*, 361. https://doi.org/10.3389/fncel.2018.00361
Park, P., Volianskis, A., Sanderson, T. M., Bortolotto, Z. A., Jane, D. E., Zhuo, M.,…Collingridge, G. L. (2014). NMDA receptor-dependent long-term potentiation comprises a family of temporally overlapping forms of synaptic plasticity that are induced by different patterns of stimulation. *Philos Trans R Soc Lond B Biol Sci*, *369*(1633), 20130131. https://doi.org/10.1098/rstb.2013.0131
Parra Bravo, C., Naguib, S. A., & Gan, L. (2024). Cellular and pathological functions of tau. *Nat Rev Mol Cell Biol*, *25*(11), 845-864. https://doi.org/10.1038/s41580-024-00753-9
Parron, C., & Save, E. (2004). Comparison of the effects of entorhinal and retrosplenial cortical lesions on habituation, reaction to spatial and non-spatial changes during object exploration in the rat. *Neurobiol Learn Mem*, *82*(1), 1-11. https://doi.org/10.1016/j.nlm.2004.03.004
Paula-Lima, A. C., Adasme, T., SanMartín, C., Sebollela, A., Hetz, C., Carrasco, M. A.,…Hidalgo, C. (2011). Amyloid β-peptide oligomers stimulate RyR-mediated Ca2+ release inducing mitochondrial fragmentation in hippocampal neurons and prevent RyR-mediated dendritic spine remodeling produced by BDNF.

Antioxid Redox Signal, *14*(7), 1209-1223. https://doi.org/10.1089/ars.2010.3287
Pauls, E., Bayod, S., Mateo, L., Alcalde, V., Juan-Blanco, T., Sánchez-Soto, M.,…Aloy, P. (2021). Identification and drug-induced reversion of molecular signatures of Alzheimer's disease onset and progression in App. *Genome Med*, *13*(1), 168. https://doi.org/10.1186/s13073-021-00983-y
Paylor, R., Johnson, R. S., Papaioannou, V., Spiegelman, B. M., & Wehner, J. M. (1994). Behavioral assessment of c-fos mutant mice. *Brain Res*, *651*(1-2), 275-282. https://doi.org/10.1016/0006-8993(94)90707-2
Pchitskaya, E., Popugaeva, E., & Bezprozvanny, I. (2018). Calcium signaling and molecular mechanisms underlying neurodegenerative diseases. *Cell Calcium*, *70*, 87-94. https://doi.org/10.1016/j.ceca.2017.06.008
Pellow, S., Chopin, P., File, S. E., & Briley, M. (1985). Validation of open:closed arm entries in an elevated plus-maze as a measure of anxiety in the rat. *J Neurosci Methods*, *14*(3), 149-167. https://doi.org/10.1016/0165-0270(85)90031-7
Pengas, G., Hodges, J. R., Watson, P., & Nestor, P. J. (2010). Focal posterior cingulate atrophy in incipient Alzheimer's disease. *Neurobiol Aging*, *31*(1), 25-33. https://doi.org/10.1016/j.neurobiolaging.2008.03.014
Penley, S. C., Gaudet, C. M., & Threlkeld, S. W. (2013). Use of an eight-arm radial water maze to assess working and reference memory following neonatal brain injury. *J Vis Exp*(82), 50940. https://doi.org/10.3791/50940
Pentkowski, N. S., Rogge-Obando, K. K., Donaldson, T. N., Bouquin, S. J., & Clark, B. J. (2021). Anxiety and Alzheimer's disease: Behavioral analysis and neural basis in rodent models of Alzheimer's-related neuropathology. *Neurosci Biobehav Rev*, *127*, 647-658. https://doi.org/10.1016/j.neubiorev.2021.05.005
Perl, D. P. (2010). Neuropathology of Alzheimer's disease. *Mt Sinai J Med*, *77*(1), 32-42. https://doi.org/10.1002/msj.20157
Perry, R. J., & Hodges, J. R. (1999). Attention and executive deficits in Alzheimer's disease. A critical review. *Brain*, *122 (Pt 3)*, 383-404. https://doi.org/10.1093/brain/122.3.383
Pervolaraki, E., Hall, S. P., Foresteire, D., Saito, T., Saido, T. C., Whittington, M. A.,…Dachtler, J. (2019). Insoluble Aβ overexpression in an. *Dis Model Mech*, *12*(9). https://doi.org/10.1242/dmm.040550
Peters, M. E., Schwartz, S., Han, D., Rabins, P. V., Steinberg, M., Tschanz, J. T., & Lyketsos, C. G. (2015). Neuropsychiatric symptoms as predictors of progression to severe Alzheimer's dementia and death: the Cache County Dementia Progression Study. *Am J Psychiatry*, *172*(5), 460-465. https://doi.org/10.1176/appi.ajp.2014.14040480
Petkus, A. J., Reynolds, C. A., Wetherell, J. L., Kremen, W. S., Pedersen, N. L., & Gatz, M. (2016). Anxiety is associated with increased risk of dementia in older Swedish twins. *Alzheimers Dement*, *12*(4), 399-406. https://doi.org/10.1016/j.jalz.2015.09.008
Pierrot, N., Ghisdal, P., Caumont, A. S., & Octave, J. N. (2004). Intraneuronal amyloid-beta1-42 production triggered by sustained increase of cytosolic calcium concentration induces neuronal death. *J Neurochem*, *88*(5), 1140-1150. https://doi.org/10.1046/j.1471-4159.2003.02227.x
Pierrot, N., Santos, S. F., Feyt, C., Morel, M., Brion, J. P., & Octave, J. N. (2006). Calcium-mediated transient phosphorylation of tau and amyloid precursor

protein followed by intraneuronal amyloid-beta accumulation. *J Biol Chem*, *281*(52), 39907-39914. https://doi.org/10.1074/jbc.M606015200
Pietrzak, R. H., Lim, Y. Y., Neumeister, A., Ames, D., Ellis, K. A., Harrington, K.,…Australian Imaging, B. o., and Lifestyle Research Group. (2015). Amyloid-β, anxiety, and cognitive decline in preclinical Alzheimer disease: a multicenter, prospective cohort study. *JAMA Psychiatry*, *72*(3), 284-291. https://doi.org/10.1001/jamapsychiatry.2014.2476
Pietrzak, R. H., Scott, J. C., Neumeister, A., Lim, Y. Y., Ames, D., Ellis, K. A.,…Australian Imaging, B. o. a. L. A. R. G. (2014). Anxiety symptoms, cerebral amyloid burden and memory decline in healthy older adults without dementia: 3-year prospective cohort study. *Br J Psychiatry*, *204*, 400-401. https://doi.org/10.1192/bjp.bp.113.134239
Pikor, D., Hurła, M., Słowikowski, B., Szymanowicz, O., Poszwa, J., Banaszek, N.,…Dorszewska, J. (2024). Calcium Ions in the Physiology and Pathology of the Central Nervous System. *Int J Mol Sci*, *25*(23). https://doi.org/10.3390/ijms252313133
Plant, L. D., Boyle, J. P., Smith, I. F., Peers, C., & Pearson, H. A. (2003). The production of amyloid beta peptide is a critical requirement for the viability of central neurons. *J Neurosci*, *23*(13), 5531-5535. https://doi.org/10.1523/JNEUROSCI.23-13-05531.2003
Pless, A., Ware, D., Saggu, S., Rehman, H., Morgan, J., & Wang, Q. (2023). Understanding neuropsychiatric symptoms in Alzheimer's disease: challenges and advances in diagnosis and treatment. *Front Neurosci*, *17*, 1263771. https://doi.org/10.3389/fnins.2023.1263771
Plosker, G. L. (2015). Memantine extended release (28 mg once daily): a review of its use in Alzheimer's disease. *Drugs*, *75*(8), 887-897. https://doi.org/10.1007/s40265-015-0400-3
Poirier, G. L., Amin, E., Good, M. A., & Aggleton, J. P. (2011). Early-onset dysfunction of retrosplenial cortex precedes overt amyloid plaque formation in Tg2576 mice. *Neuroscience*, *174*, 71-83. https://doi.org/10.1016/j.neuroscience.2010.11.025
Porsteinsson, A. P., Isaacson, R. S., Knox, S., Sabbagh, M. N., & Rubino, I. (2021). Diagnosis of Early Alzheimer's Disease: Clinical Practice in 2021. *J Prev Alzheimers Dis*, *8*(3), 371-386. https://doi.org/10.14283/jpad.2021.23
Pothuizen, H. H., Aggleton, J. P., & Vann, S. D. (2008). Do rats with retrosplenial cortex lesions lack direction? *Eur J Neurosci*, *28*(12), 2486-2498. https://doi.org/10.1111/j.1460-9568.2008.06550.x
Pothuizen, H. H., Davies, M., Aggleton, J. P., & Vann, S. D. (2010). Effects of selective granular retrosplenial cortex lesions on spatial working memory in rats. *Behav Brain Res*, *208*(2), 566-575. https://doi.org/10.1016/j.bbr.2010.01.001
Pothuizen, H. H., Davies, M., Albasser, M. M., Aggleton, J. P., & Vann, S. D. (2009). Granular and dysgranular retrosplenial cortices provide qualitatively different contributions to spatial working memory: evidence from immediate-early gene imaging in rats. *Eur J Neurosci*, *30*(5), 877-888. https://doi.org/10.1111/j.1460-9568.2009.06881.x
Poulin, S. P., Dautoff, R., Morris, J. C., Barrett, L. F., Dickerson, B. C., & Initiative, A. s. D. N. (2011). Amygdala atrophy is prominent in early Alzheimer's disease and relates to symptom severity. *Psychiatry Res*, *194*(1), 7-13. https://doi.org/10.1016/j.pscychresns.2011.06.014

Powell, A., Connelly, W. M., Vasalauskaite, A., Nelson, A. J. D., Vann, S. D., Aggleton, J. P.,…Ranson, A. (2020). Stable Encoding of Visual Cues in the Mouse Retrosplenial Cortex. *Cereb Cortex*, *30*(8), 4424-4437. https://doi.org/10.1093/cercor/bhaa030
Powell, A. L., Vann, S. D., Olarte-Sánchez, C. M., Kinnavane, L., Davies, M., Amin, E.,…Nelson, A. J. D. (2017). The retrosplenial cortex and object recency memory in the rat. *Eur J Neurosci*, *45*(11), 1451-1464. https://doi.org/10.1111/ejn.13577
Pozueta, J., Lefort, R., & Shelanski, M. L. (2013). Synaptic changes in Alzheimer's disease and its models. *Neuroscience*, *251*, 51-65. https://doi.org/10.1016/j.neuroscience.2012.05.050
Price, J. L., Davis, P. B., Morris, J. C., & White, D. L. (1991). The distribution of tangles, plaques and related immunohistochemical markers in healthy aging and Alzheimer's disease. *Neurobiol Aging*, *12*(4), 295-312. https://doi.org/10.1016/0197-4580(91)90006-6
Prut, L., & Belzung, C. (2003). The open field as a paradigm to measure the effects of drugs on anxiety-like behaviors: a review. *European Journal of Pharmacology*, *463*(1-3), 3-33.
Purro, S. A., Nicoll, A. J., & Collinge, J. (2018). Prion Protein as a Toxic Acceptor of Amyloid-β Oligomers. *Biol Psychiatry*, *83*(4), 358-368. https://doi.org/10.1016/j.biopsych.2017.11.020
Puzzo, D., Privitera, L., Leznik, E., Fà, M., Staniszewski, A., Palmeri, A., & Arancio, O. (2008). Picomolar amyloid-beta positively modulates synaptic plasticity and memory in hippocampus. *J Neurosci*, *28*(53), 14537-14545. https://doi.org/10.1523/JNEUROSCI.2692-08.2008
Pádua, M. S., Guil-Guerrero, J. L., & Lopes, P. A. (2024). Behaviour Hallmarks in Alzheimer's Disease 5xFAD Mouse Model. *Int J Mol Sci*, *25*(12). https://doi.org/10.3390/ijms25126766
Quan, M., Cao, S., Wang, Q., Wang, S., & Jia, J. (2023). Genetic Phenotypes of Alzheimer's Disease: Mechanisms and Potential Therapy. *Phenomics*, *3*(4), 333-349. https://doi.org/10.1007/s43657-023-00098-x
Querfurth, H. W., & Selkoe, D. J. (1994). Calcium ionophore increases amyloid beta peptide production by cultured cells. *Biochemistry*, *33*(15), 4550-4561. https://doi.org/10.1021/bi00181a016
Quiroz, Y. T., Schultz, A. P., Chen, K., Protas, H. D., Brickhouse, M., Fleisher, A. S.,…Reiman, E. M. (2015). Brain Imaging and Blood Biomarker Abnormalities in Children With Autosomal Dominant Alzheimer Disease: A Cross-Sectional Study. *JAMA Neurol*, *72*(8), 912-919. https://doi.org/10.1001/jamaneurol.2015.1099
Rabin, L. A., Smart, C. M., & Amariglio, R. E. (2017). Subjective Cognitive Decline in Preclinical Alzheimer's Disease. *Annu Rev Clin Psychol*, *13*, 369-396. https://doi.org/10.1146/annurev-clinpsy-032816-045136
Radde, R., Bolmont, T., Kaeser, S. A., Coomaraswamy, J., Lindau, D., Stoltze, L.,…Jucker, M. (2006). Abeta42-driven cerebral amyloidosis in transgenic mice reveals early and robust pathology. *EMBO Rep*, *7*(9), 940-946. https://doi.org/10.1038/sj.embor.7400784
Rahman, A., Jackson, H., Hristov, H., Isaacson, R. S., Saif, N., Shetty, T.,…Mosconi, L. (2019). Sex and Gender Driven Modifiers of Alzheimer's: The Role for Estrogenic Control Across Age, Race, Medical, and Lifestyle Risks. *Front Aging Neurosci*, *11*, 315. https://doi.org/10.3389/fnagi.2019.00315

Rajan, K. B., Weuve, J., Barnes, L. L., McAninch, E. A., Wilson, R. S., & Evans, D. A. (2021). Population estimate of people with clinical Alzheimer's disease and mild cognitive impairment in the United States (2020-2060). *Alzheimers Dement*, *17*(12), 1966-1975. https://doi.org/10.1002/alz.12362
Ramakers, I. H., Verhey, F. R., Scheltens, P., Hampel, H., Soininen, H., Aalten, P.,…Investigators, A. s. D. N. I. a. D. (2013). Anxiety is related to Alzheimer cerebrospinal fluid markers in subjects with mild cognitive impairment. *Psychol Med*, *43*(5), 911-920. https://doi.org/10.1017/S0033291712001870
Ramiro-Cortés, Y., Hobbiss, A. F., & Israely, I. (2014). Synaptic competition in structural plasticity and cognitive function. *Philos Trans R Soc Lond B Biol Sci*, *369*(1633), 20130157. https://doi.org/10.1098/rstb.2013.0157
Rao, Y. L., Ganaraja, B., Murlimanju, B. V., Joy, T., Krishnamurthy, A., & Agrawal, A. (2022). Hippocampus and its involvement in Alzheimer's disease: a review. *3 Biotech*, *12*(2), 55. https://doi.org/10.1007/s13205-022-03123-4
Rapoport, M., Dawson, H. N., Binder, L. I., Vitek, M. P., & Ferreira, A. (2002). Tau is essential to beta -amyloid-induced neurotoxicity. *Proc Natl Acad Sci U S A*, *99*(9), 6364-6369. https://doi.org/10.1073/pnas.092136199
Rasband, W. S. (1997-2018). Image J. In. Maryland, USA: U. S. National Institutes of Health, Bethesda.
Ray, B., Maloney, B., Sambamurti, K., Karnati, H. K., Nelson, P. T., Greig, N. H., & Lahiri, D. K. (2020). Rivastigmine modifies the α-secretase pathway and potentially early Alzheimer's disease. *Transl Psychiatry*, *10*(1), 47. https://doi.org/10.1038/s41398-020-0709-x
Raza, M., Deshpande, L. S., Blair, R. E., Carter, D. S., Sombati, S., & DeLorenzo, R. J. (2007). Aging is associated with elevated intracellular calcium levels and altered calcium homeostatic mechanisms in hippocampal neurons. *Neurosci Lett*, *418*(1), 77-81. https://doi.org/10.1016/j.neulet.2007.03.005
Rebeck, G. W., Reiter, J. S., Strickland, D. K., & Hyman, B. T. (1993). Apolipoprotein E in sporadic Alzheimer's disease: allelic variation and receptor interactions. *Neuron*, *11*(4), 575-580. https://doi.org/10.1016/0896-6273(93)90070-8
Reddy, P. H. (2013). Amyloid beta-induced glycogen synthase kinase 3β phosphorylated VDAC1 in Alzheimer's disease: implications for synaptic dysfunction and neuronal damage. *Biochim Biophys Acta*, *1832*(12), 1913-1921. https://doi.org/10.1016/j.bbadis.2013.06.012
Reed, M. N., Hofmeister, J. J., Jungbauer, L., Welzel, A. T., Yu, C., Sherman, M. A.,…Cleary, J. P. (2011). Cognitive effects of cell-derived and synthetically derived Aβ oligomers. *Neurobiol Aging*, *32*(10), 1784-1794. https://doi.org/10.1016/j.neurobiolaging.2009.11.007
Reilly, J. F., Games, D., Rydel, R. E., Freedman, S., Schenk, D., Young, W. G.,…Bloom, F. E. (2003). Amyloid deposition in the hippocampus and entorhinal cortex: quantitative analysis of a transgenic mouse model. *Proc Natl Acad Sci U S A*, *100*(8), 4837-4842. https://doi.org/10.1073/pnas.0330745100
Renthal, W., Carle, T. L., Maze, I., Covington, H. E., Truong, H. T., Alibhai, I.,…Nestler, E. J. (2008). Delta FosB mediates epigenetic desensitization of the c-fos gene after chronic amphetamine exposure. *J Neurosci*, *28*(29), 7344-7349. https://doi.org/10.1523/JNEUROSCI.1043-08.2008
Reznichenko, L., Cheng, Q., Nizar, K., Gratiy, S. L., Saisan, P. A., Rockenstein, E. M.,…Masliah, E. (2012). In vivo alterations in calcium buffering capacity in

transgenic mouse model of synucleinopathy. *J Neurosci*, *32*(29), 9992-9998. https://doi.org/10.1523/JNEUROSCI.1270-12.2012
Ribé, E. M., Pérez, M., Puig, B., Gich, I., Lim, F., Cuadrado, M.,…Gómez-Isla, T. (2005). Accelerated amyloid deposition, neurofibrillary degeneration and neuronal loss in double mutant APP/tau transgenic mice. *Neurobiol Dis*, *20*(3), 814-822. https://doi.org/10.1016/j.nbd.2005.05.027
Ricciarelli, R., & Fedele, E. (2017). The Amyloid Cascade Hypothesis in Alzheimer's Disease: It's Time to Change Our Mind. *Curr Neuropharmacol*, *15*(6), 926-935. https://doi.org/10.2174/1570159X15666170116143743
Roberson, E. D., Scearce-Levie, K., Palop, J. J., Yan, F., Cheng, I. H., Wu, T.,…Mucke, L. (2007). Reducing endogenous tau ameliorates amyloid beta-induced deficits in an Alzheimer's disease mouse model. *Science*, *316*(5825), 750-754. https://doi.org/10.1126/science.1141736
Roberts, R. O., Aakre, J. A., Kremers, W. K., Vassilaki, M., Knopman, D. S., Mielke, M. M.,…Petersen, R. C. (2018). Prevalence and Outcomes of Amyloid Positivity Among Persons Without Dementia in a Longitudinal, Population-Based Setting. *JAMA Neurol*, *75*(8), 970-979. https://doi.org/10.1001/jamaneurol.2018.0629
Robinson, O. J., Vytal, K., Cornwell, B. R., & Grillon, C. (2013). The impact of anxiety upon cognition: perspectives from human threat of shock studies. *Front Hum Neurosci*, *7*, 203. https://doi.org/10.3389/fnhum.2013.00203
Rocca, P., Leotta, D., Liffredo, C., Mingrone, C., Sigaudo, M., Capellero, B.,…Bogetto, F. (2010). Neuropsychiatric symptoms underlying caregiver stress and insight in Alzheimer's disease. *Dement Geriatr Cogn Disord*, *30*(1), 57-63. https://doi.org/10.1159/000315513
Rochat, L., Billieux, J., Juillerat Van der Linden, A. C., Annoni, J. M., Zekry, D., Gold, G., & Van der Linden, M. (2013). A multidimensional approach to impulsivity changes in mild Alzheimer's disease and control participants: cognitive correlates. *Cortex*, *49*(1), 90-100. https://doi.org/10.1016/j.cortex.2011.08.004
Rodgers, R., Haller, J., Holmes, A., Halasz, J., Walton, T.J., Brain, P.F. (1999). Corticosterone response to the plus-maze : High correlation with risk assessment in rats and mice. *Physiology & Behaviour*, *68*(1-2), 47-53.
Rodgers, R., Perrault, G., & Sanger, D. (1997). Risk Assessment Behaviour: Evaluation of Utility in the Study of 5-HT-Related Drugs in the Rat Elevated Plus-Maze Test. *Pharmacology Biochemistry and Behaviour*, *57*(4), 817-827.
Rodgers, R., Perrault, G., Sanger, D., & Griebel, G. (1997). Risk Assessment Behaviour: Evaluation of Utility in the Study of 5-HT-Related Drugs in the Rat Elevated Plus-Maze Test. *Pharmacology Biochemistry and Behaviour*, *57*(4), 817-827.
Rodgers, R. J., & Cole, J. C. (1993). Anxiety enhancement in the murine elevated plus maze by immediate prior exposure to social stressors. *Physiol Behav*, *53*(2), 383-388. https://doi.org/10.1016/0031-9384(93)90222-2
Rodgers, R. J., Nikulina, E. M., & Cole, J. C. (1994). Dopamine D1 and D2 receptor ligands modulate the behaviour of mice in the elevated plus-maze. *Pharmacol Biochem Behav*, *49*(4), 985-995. https://doi.org/10.1016/0091-3057(94)90253-4
Rodríguez-Giraldo, M., González-Reyes, R. E., Ramírez-Guerrero, S., Bonilla-Trilleras, C. E., Guardo-Maya, S., & Nava-Mesa, M. O. (2022). Astrocytes as a Therapeutic Target in Alzheimer's Disease-Comprehensive Review and

Recent Developments. *Int J Mol Sci*, *23*(21). https://doi.org/10.3390/ijms232113630
Rogaev, E. I., Sherrington, R., Rogaeva, E. A., Levesque, G., Ikeda, M., Liang, Y.,…Tsuda, T. (1995). Familial Alzheimer's disease in kindreds with missense mutations in a gene on chromosome 1 related to the Alzheimer's disease type 3 gene. *Nature*, *376*(6543), 775-778. https://doi.org/10.1038/376775a0
Rosende-Roca, M., Abdelnour, C., Esteban, E., Tartari, J. P., Alarcon, E., Martínez-Atienza, J.,…Boada, M. (2021). The role of sex and gender in the selection of Alzheimer patients for clinical trial pre-screening. *Alzheimers Res Ther*, *13*(1), 95. https://doi.org/10.1186/s13195-021-00833-4
Rupp, N. J., Wegenast-Braun, B. M., Radde, R., Calhoun, M. E., & Jucker, M. (2011). Early onset amyloid lesions lead to severe neuritic abnormalities and local, but not global neuron loss in APPPS1 transgenic mice. *Neurobiol Aging*, *32*(12), 2324.e2321-2326. https://doi.org/10.1016/j.neurobiolaging.2010.08.014
Ryan, N. S., Rossor, M. N., & Fox, N. C. (2015). Alzheimer's disease in the 100 years since Alzheimer's death. *Brain*, *138*(Pt 12), 3816-3821. https://doi.org/10.1093/brain/awv316
Sabbagh, M. N., Hendrix, S., & Harrison, J. E. (2019). FDA position statement "Early Alzheimer's disease: Developing drugs for treatment, Guidance for Industry". *Alzheimers Dement (N Y)*, *5*, 13-19. https://doi.org/10.1016/j.trci.2018.11.004
Saffen, D. W., Cole, A. J., Worley, P. F., Christy, B. A., Ryder, K., & Baraban, J. M. (1988). Convulsant-induced increase in transcription factor messenger RNAs in rat brain. *Proc Natl Acad Sci U S A*, *85*(20), 7795-7799. https://doi.org/10.1073/pnas.85.20.7795
Saifullah, M. A. B., Komine, O., Dong, Y., Fukumoto, K., Sobue, A., Endo, F.,…Mizoguchi, H. (2020). Touchscreen-based location discrimination and paired associate learning tasks detect cognitive impairment at an early stage in an App knock-in mouse model of Alzheimer's disease. *Mol Brain*, *13*(1), 147. https://doi.org/10.1186/s13041-020-00690-6
Saito, T., Matsuba, Y., Mihira, N., Takano, J., Nilsson, P., Itohara, S.,…Saido, T. C. (2014). Single App knock-in mouse models of Alzheimer's disease. *Nat Neurosci*, *17*(5), 661-663. https://doi.org/10.1038/nn.3697
Sajan, F. D., Martiniuk, F., Marcus, D. L., Frey, W. H., Hite, R., Bordayo, E. Z., & Freedman, M. L. (2007). Apoptotic gene expression in Alzheimer's disease hippocampal tissue. *Am J Alzheimers Dis Other Demen*, *22*(4), 319-328. https://doi.org/10.1177/1533317507302447
Sakakibara, Y., Sekiya, M., Saito, T., Saido, T. C., & Iijima, K. M. (2018). Cognitive and emotional alterations in App knock-in mouse models of Aβ amyloidosis. *BMC Neurosci*, *19*(1), 46. https://doi.org/10.1186/s12868-018-0446-8
Salloway, S., Chalkias, S., Barkhof, F., Burkett, P., Barakos, J., Purcell, D.,…Smirnakis, K. (2022). Amyloid-Related Imaging Abnormalities in 2 Phase 3 Studies Evaluating Aducanumab in Patients With Early Alzheimer Disease. *JAMA Neurol*, *79*(1), 13-21. https://doi.org/10.1001/jamaneurol.2021.4161
Sanders, H., Rennó-Costa, C., Idiart, M., & Lisman, J. (2015). Grid Cells and Place Cells: An Integrated View of their Navigational and Memory Function. *Trends Neurosci*, *38*(12), 763-775. https://doi.org/10.1016/j.tins.2015.10.004
Santulli, G., Nakashima, R., Yuan, Q., & Marks, A. R. (2017). Intracellular calcium release channels: an update. *J Physiol*, *595*(10), 3041-3051. https://doi.org/10.1113/JP272781

Sanz-Blasco, S., Valero, R. A., Rodríguez-Crespo, I., Villalobos, C., & Núñez, L. (2008). Mitochondrial Ca2+ overload underlies Abeta oligomers neurotoxicity providing an unexpected mechanism of neuroprotection by NSAIDs. *PLoS One*, *3*(7), e2718. https://doi.org/10.1371/journal.pone.0002718

Sarazin, M., Chauviré, V., Gerardin, E., Colliot, O., Kinkingnéhun, S., de Souza, L. C.,…Dubois, B. (2010). The amnestic syndrome of hippocampal type in Alzheimer's disease: an MRI study. *J Alzheimers Dis*, *22*(1), 285-294. https://doi.org/10.3233/JAD-2010-091150

Sasaguri, H., Hashimoto, S., Watamura, N., Sato, K., Takamura, R., Nagata, K.,…Saido, T. C. (2022). Recent Advances in the Modeling of Alzheimer's Disease. *Front Neurosci*, *16*, 807473. https://doi.org/10.3389/fnins.2022.807473

Sasaguri, H., Nilsson, P., Hashimoto, S., Nagata, K., Saito, T., De Strooper, B.,…Saido, T. C. (2017). APP mouse models for Alzheimer's disease preclinical studies. *EMBO J*, *36*(17), 2473-2487. https://doi.org/10.15252/embj.201797397

Sasaguri, H., Sato, K., Kumita, W., Inoue, T., Kurotaki, Y., Nagata, K.,…Sasaki, E. (2022). Generation of non-human primate models of Alzheimer's disease. *Alzheimer's Association*, *17*(S3), e052561.

Sato, K., Watamura, N., Fujioka, R., Mihira, N., Sekiguchi, M., Nagata, K.,…Sasaguri, H. (2021). A third-generation mouse model of Alzheimer's disease shows early and increased cored plaque pathology composed of wild-type human amyloid β peptide. *J Biol Chem*, *297*(3), 101004. https://doi.org/10.1016/j.jbc.2021.101004

Sawaguchi, T., & Iba, M. (2001). Prefrontal cortical representation of visuospatial working memory in monkeys examined by local inactivation with muscimol. *J Neurophysiol*, *86*(4), 2041-2053. https://doi.org/10.1152/jn.2001.86.4.2041

Scahill, R. I., Schott, J. M., Stevens, J. M., Rossor, M. N., & Fox, N. C. (2002). Mapping the evolution of regional atrophy in Alzheimer's disease: unbiased analysis of fluid-registered serial MRI. *Proc Natl Acad Sci U S A*, *99*(7), 4703-4707. https://doi.org/10.1073/pnas.052587399

Scearce-Levie, K., Sanchez, P. E., & Lewcock, J. W. (2020). Leveraging preclinical models for the development of Alzheimer disease therapeutics. *Nat Rev Drug Discov*, *19*(7), 447-462. https://doi.org/10.1038/s41573-020-0065-9

Schaefer, N., Rotermund, C., Blumrich, E. M., Lourenco, M. V., Joshi, P., Hegemann, R. U.,…Turner, A. J. (2017). The malleable brain: plasticity of neural circuits and behavior - a review from students to students. *J Neurochem*, *142*(6), 790-811. https://doi.org/10.1111/jnc.14107

Scheuner, D., Eckman, C., Jensen, M., Song, X., Citron, M., Suzuki, N.,…Younkin, S. (1996). Secreted amyloid beta-protein similar to that in the senile plaques of Alzheimer's disease is increased in vivo by the presenilin 1 and 2 and APP mutations linked to familial Alzheimer's disease. *Nat Med*, *2*(8), 864-870. https://doi.org/10.1038/nm0896-864

Schwaller, B. (2010). Cytosolic Ca2+ buffers. *Cold Spring Harb Perspect Biol*, *2*(11), a004051. https://doi.org/10.1101/cshperspect.a004051

Schönheit, B., Zarski, R., & Ohm, T. G. (2004). Spatial and temporal relationships between plaques and tangles in Alzheimer-pathology. *Neurobiol Aging*, *25*(6), 697-711. https://doi.org/10.1016/j.neurobiolaging.2003.09.009

Scuteri, D., Corasaniti, M. T., Tonin, P., Nicotera, P., & Bagetta, G. (2021). New trends in pharmacological control of neuropsychiatric symptoms of dementia. *Curr Opin Pharmacol*, *61*, 69-76. https://doi.org/10.1016/j.coph.2021.09.002

Seabrook, G. R., Smith, D. W., Bowery, B. J., Easter, A., Reynolds, T., Fitzjohn, S. M.,…Hill, R. G. (1999). Mechanisms contributing to the deficits in hippocampal synaptic plasticity in mice lacking amyloid precursor protein. *Neuropharmacology*, *38*(3), 349-359. https://doi.org/10.1016/s0028-3908(98)00204-4

Seibenhener, M. L., & Wooten, M. C. (2015). Use of the Open Field Maze to measure locomotor and anxiety-like behavior in mice. *J Vis Exp*(96), e52434. https://doi.org/10.3791/52434

Selkoe, D. J. (2002). Alzheimer's disease is a synaptic failure. *Science*, *298*(5594), 789-791. https://doi.org/10.1126/science.1074069

Sengupta, A., Kabat, J., Novak, M., Wu, Q., Grundke-Iqbal, I., & Iqbal, K. (1998). Phosphorylation of tau at both Thr 231 and Ser 262 is required for maximal inhibition of its binding to microtubules. *Arch Biochem Biophys*, *357*(2), 299-309. https://doi.org/10.1006/abbi.1998.0813

Setem, J., Pinheiro, A., Motta, V., Morato, S., & Cruz, A. (1999). Ethopharmacological Analysis of 5-HT Ligands on the Rat Elevated Plus-Maze. *Pharmacology Biochemistry and Behaviour*, *62*(3), 515-521.

Shah, D., Gsell, W., Wahis, J., Luckett, E. S., Jamoulle, T., Vermaercke, B.,…De Strooper, B. (2022). Astrocyte calcium dysfunction causes early network hyperactivity in Alzheimer's disease. *Cell Rep*, *40*(8), 111280. https://doi.org/10.1016/j.celrep.2022.111280

Shankar, G. M., Bloodgood, B. L., Townsend, M., Walsh, D. M., Selkoe, D. J., & Sabatini, B. L. (2007). Natural oligomers of the Alzheimer amyloid-beta protein induce reversible synapse loss by modulating an NMDA-type glutamate receptor-dependent signaling pathway. *J Neurosci*, *27*(11), 2866-2875. https://doi.org/10.1523/JNEUROSCI.4970-06.2007

Shankar, G. M., Li, S., Mehta, T. H., Garcia-Munoz, A., Shepardson, N. E., Smith, I.,…Selkoe, D. J. (2008). Amyloid-beta protein dimers isolated directly from Alzheimer's brains impair synaptic plasticity and memory. *Nat Med*, *14*(8), 837-842. https://doi.org/10.1038/nm1782

Sharma, V., Cohen, N., Sood, R., Ounallah-Saad, H., Gal-Ben-Ari, S., & Rosenblum, K. (2018). Trace Fear Conditioning: Procedure for Assessing Complex Hippocampal Function in Mice. *Bio Protoc*, *8*(16), e2475. https://doi.org/10.21769/BioProtoc.2475

Sheppard, P. A. S., Oomen, C. A., Bussey, T. J., & Saksida, L. M. (2024). The Granular Retrosplenial Cortex Is Necessary in Male Rats for Object-Location Associative Learning and Memory, But Not Spatial Working Memory or Visual Discrimination and Reversal, in the Touchscreen Operant Chamber. *eNeuro*, *11*(6). https://doi.org/10.1523/ENEURO.0120-24.2024

Sherrington, R., Rogaev, E. I., Liang, Y., Rogaeva, E. A., Levesque, G., Ikeda, M.,…St George-Hyslop, P. H. (1995). Cloning of a gene bearing missense mutations in early-onset familial Alzheimer's disease. *Nature*, *375*(6534), 754-760. https://doi.org/10.1038/375754a0

Shin, L. M., & Liberzon, I. (2010). The neurocircuitry of fear, stress, and anxiety disorders. *Neuropsychopharmacology*, *35*(1), 169-191. https://doi.org/10.1038/npp.2009.83

Shinoda, Y., Tanaka, T., Tominaga-Yoshino, K., & Ogura, A. (2010). Persistent synapse loss induced by repetitive LTD in developing rat hippocampal neurons. *PLoS One*, *5*(4), e10390. https://doi.org/10.1371/journal.pone.0010390
Shirwany, N. A., Payette, D., Xie, J., & Guo, Q. (2007). The amyloid beta ion channel hypothesis of Alzheimer's disease. *Neuropsychiatr Dis Treat*, *3*(5), 597-612.
Shoji, H., Takao, K., Hattori, S., & Miyakawa, T. (2016). Age-related changes in behavior in C57BL/6J mice from young adulthood to middle age. *Mol Brain*, *9*, 11. https://doi.org/10.1186/s13041-016-0191-9
Singh, B., Day, C. M., Abdella, S., & Garg, S. (2024). Alzheimer's disease current therapies, novel drug delivery systems and future directions for better disease management. *J Control Release*, *367*, 402-424. https://doi.org/10.1016/j.jconrel.2024.01.047
Smith, I. F., Hitt, B., Green, K. N., Oddo, S., & LaFerla, F. M. (2005). Enhanced caffeine-induced Ca2+ release in the 3xTg-AD mouse model of Alzheimer's disease. *J Neurochem*, *94*(6), 1711-1718. https://doi.org/10.1111/j.1471-4159.2005.03332.x
Snyder, S. W., Ladror, U. S., Wade, W. S., Wang, G. T., Barrett, L. W., Matayoshi, E. D.,…Holzman, T. F. (1994). Amyloid-beta aggregation: selective inhibition of aggregation in mixtures of amyloid with different chain lengths. *Biophys J*, *67*(3), 1216-1228. https://doi.org/10.1016/S0006-3495(94)80591-0
Solstad, T., Boccara, C. N., Kropff, E., Moser, M. B., & Moser, E. I. (2008). Representation of geometric borders in the entorhinal cortex. *Science*, *322*(5909), 1865-1868. https://doi.org/10.1126/science.1166466
Soucek, T., Cumming, R., Dargusch, R., Maher, P., & Schubert, D. (2003). The regulation of glucose metabolism by HIF-1 mediates a neuroprotective response to amyloid beta peptide. *Neuron*, *39*(1), 43-56. https://doi.org/10.1016/s0896-6273(03)00367-2
Sperling, R. A., Aisen, P. S., Beckett, L. A., Bennett, D. A., Craft, S., Fagan, A. M.,…Phelps, C. H. (2011). Toward defining the preclinical stages of Alzheimer's disease: recommendations from the National Institute on Aging-Alzheimer's Association workgroups on diagnostic guidelines for Alzheimer's disease. *Alzheimers Dement*, *7*(3), 280-292. https://doi.org/10.1016/j.jalz.2011.03.003
Spuch, C., Ortolano, S., & Navarro, C. (2012). New insights in the amyloid-Beta interaction with mitochondria. *J Aging Res*, *2012*, 324968. https://doi.org/10.1155/2012/324968
Spät, A., Szanda, G., Csordás, G., & Hajnóczky, G. (2008). High- and low-calcium-dependent mechanisms of mitochondrial calcium signalling. *Cell Calcium*, *44*(1), 51-63. https://doi.org/10.1016/j.ceca.2007.11.015
Squire, L. R. (1987). The organization and neural substrates of human memory. *Int J Neurol*, *21-22*, 218-222.
Stacho, M., & Manahan-Vaughan, D. (2022). Mechanistic flexibility of the retrosplenial cortex enables its contribution to spatial cognition. *Trends Neurosci*, *45*(4), 284-296. https://doi.org/10.1016/j.tins.2022.01.007
Steinberg, M., Shao, H., Zandi, P., Lyketsos, C. G., Welsh-Bohmer, K. A., Norton, M. C.,…Investigators, C. C. (2008). Point and 5-year period prevalence of neuropsychiatric symptoms in dementia: the Cache County Study. *Int J Geriatr Psychiatry*, *23*(2), 170-177. https://doi.org/10.1002/gps.1858

Stopford, C. L., Thompson, J. C., Neary, D., Richardson, A. M., & Snowden, J. S. (2012). Working memory, attention, and executive function in Alzheimer's disease and frontotemporal dementia. *Cortex*, *48*(4), 429-446. https://doi.org/10.1016/j.cortex.2010.12.002

Stouffer, K. M., Grande, X., Düzel, E., Johansson, M., Creese, B., Witter, M. P.,…Berron, D. (2024). Amidst an amygdala renaissance in Alzheimer's disease. *Brain*, *147*(3), 816-829. https://doi.org/10.1093/brain/awad411

Strom, A., Iaccarino, L., Edwards, L., Lesman-Segev, O. H., Soleimani-Meigooni, D. N., Pham, J.,…Initiative, A. s. D. N. (2022). Cortical hypometabolism reflects local atrophy and tau pathology in symptomatic Alzheimer's disease. *Brain*, *145*(2), 713-728. https://doi.org/10.1093/brain/awab294

Stutzmann, G. E., Smith, I., Caccamo, A., Oddo, S., Laferla, F. M., & Parker, I. (2006). Enhanced ryanodine receptor recruitment contributes to Ca2+ disruptions in young, adult, and aged Alzheimer's disease mice. *J Neurosci*, *26*(19), 5180-5189. https://doi.org/10.1523/JNEUROSCI.0739-06.2006

Sugar, J., Witter, M. P., van Strien, N. M., & Cappaert, N. L. (2011). The retrosplenial cortex: intrinsic connectivity and connections with the (para)hippocampal region in the rat. An interactive connectome. *Front Neuroinform*, *5*, 7. https://doi.org/10.3389/fninf.2011.00007

Supnet, C., Grant, J., Kong, H., Westaway, D., & Mayne, M. (2006). Amyloid-beta-(1-42) increases ryanodine receptor-3 expression and function in neurons of TgCRND8 mice. *J Biol Chem*, *281*(50), 38440-38447. https://doi.org/10.1074/jbc.M606736200

Suthana, N. A., Ekstrom, A. D., Moshirvaziri, S., Knowlton, B., & Bookheimer, S. Y. (2009). Human hippocampal CA1 involvement during allocentric encoding of spatial information. *J Neurosci*, *29*(34), 10512-10519. https://doi.org/10.1523/JNEUROSCI.0621-09.2009

Suzuki, N., Cheung, T. T., Cai, X. D., Odaka, A., Otvos, L., Eckman, C.,…Younkin, S. G. (1994). An increased percentage of long amyloid beta protein secreted by familial amyloid beta protein precursor (beta APP717) mutants. *Science*, *264*(5163), 1336-1340. https://doi.org/10.1126/science.8191290

Svoboda, E., McKinnon, M. C., & Levine, B. (2006). The functional neuroanatomy of autobiographical memory: a meta-analysis. *Neuropsychologia*, *44*(12), 2189-2208. https://doi.org/10.1016/j.neuropsychologia.2006.05.023

Tackenberg, C., Ghori, A., & Brandt, R. (2009). Thin, stubby or mushroom: spine pathology in Alzheimer's disease. *Curr Alzheimer Res*, *6*(3), 261-268. https://doi.org/10.2174/156720509788486554

Taguchi, H., Planque, S., Nishiyama, Y., Symersky, J., Boivin, S., Szabo, P.,…Paul, S. (2008). Autoantibody-catalyzed hydrolysis of amyloid beta peptide. *J Biol Chem*, *283*(8), 4714-4722. https://doi.org/10.1074/jbc.M707983200

Tahami Monfared, A. A., Byrnes, M. J., White, L. A., & Zhang, Q. (2022). The Humanistic and Economic Burden of Alzheimer's Disease. *Neurol Ther*, *11*(2), 525-551. https://doi.org/10.1007/s40120-022-00335-x

Tait, S. W., & Green, D. R. (2013). Mitochondrial regulation of cell death. *Cold Spring Harb Perspect Biol*, *5*(9). https://doi.org/10.1101/cshperspect.a008706

Takahashi, N., Kawamura, M., Shiota, J., Kasahata, N., & Hirayama, K. (1997). Pure topographic disorientation due to right retrosplenial lesion. *Neurology*, *49*(2), 464-469. https://doi.org/10.1212/wnl.49.2.464

Takamura, R., Mizuta, K., Sekine, Y., Islam, T., Saito, T., Sato, M.,…Hayashi, Y. (2021). Modality-Specific Impairment of Hippocampal CA1 Neurons of

Alzheimer's Disease Model Mice. *J Neurosci*, *41*(24), 5315-5329. https://doi.org/10.1523/JNEUROSCI.0208-21.2021
Takuma, H., Arawaka, S., & Mori, H. (2003). Isoforms changes of tau protein during development in various species. *Brain Res Dev Brain Res*, *142*(2), 121-127. https://doi.org/10.1016/s0165-3806(03)00056-7
Tampi, R. R., Tampi, D. J., Balachandran, S., & Srinivasan, S. (2016). Antipsychotic use in dementia: a systematic review of benefits and risks from meta-analyses. *Ther Adv Chronic Dis*, *7*(5), 229-245. https://doi.org/10.1177/2040622316658463
Tan, R. H., Wong, S., Hodges, J. R., Halliday, G. M., & Hornberger, M. (2013). Retrosplenial cortex (BA 29) volumes in behavioral variant frontotemporal dementia and Alzheimer's disease. *Dement Geriatr Cogn Disord*, *35*(3-4), 177-182. https://doi.org/10.1159/000346392
Tan, S., Tong, W. H., & Vyas, A. (2023). Impaired episodic-like memory in a mouse model of Alzheimer's disease is associated with hyperactivity in prefrontal-hippocampal regions. *Dis Model Mech*, *16*(3). https://doi.org/10.1242/dmm.049945
Tang, J., Huang, H., Muirhead, R. C. J., Zhou, Y., Li, J., DeFelice, J.,…Matthews, P. M. (2024). Associations of amyloid-β oligomers and plaques with neuropathology in the. *Brain Commun*, *6*(4), fcae218. https://doi.org/10.1093/braincomms/fcae218
Tanzi, R. E. (2005). The synaptic Abeta hypothesis of Alzheimer disease. *Nat Neurosci*, *8*(8), 977-979. https://doi.org/10.1038/nn0805-977
Tanzi, R. E., Gusella, J. F., Watkins, P. C., Bruns, G. A., St George-Hyslop, P., Van Keuren, M. L.,…Neve, R. L. (1987). Amyloid beta protein gene: cDNA, mRNA distribution, and genetic linkage near the Alzheimer locus. *Science*, *235*(4791), 880-884. https://doi.org/10.1126/science.2949367
Tassone, V. K., Gholamali Nezhad, F., Demchenko, I., Rueda, A., & Bhat, V. (2024). Amygdala biomarkers of treatment response in major depressive disorder: An fMRI systematic review of SSRI antidepressants. *Psychiatry Res Neuroimaging*, *338*, 111777. https://doi.org/10.1016/j.pscychresns.2023.111777
Taube, J. S. (2007). The head direction signal: origins and sensory-motor integration. *Annu Rev Neurosci*, *30*, 181-207. https://doi.org/10.1146/annurev.neuro.29.051605.112854
Teri, L., Ferretti, L. E., Gibbons, L. E., Logsdon, R. G., McCurry, S. M., Kukull, W. A.,…Larson, E. B. (1999). Anxiety of Alzheimer's disease: prevalence, and comorbidity. *J Gerontol A Biol Sci Med Sci*, *54*(7), M348-352. https://doi.org/10.1093/gerona/54.7.m348
Terstege, D. J., Galea, L. A. M., Epp, J. R., & Initiative, A. s. D. N. (2024). Retrosplenial hypometabolism precedes the conversion from mild cognitive impairment to Alzheimer's disease. *Alzheimers Dement*, *20*(12), 8979-8986. https://doi.org/10.1002/alz.14258
Texidó, L., Martín-Satué, M., Alberdi, E., Solsona, C., & Matute, C. (2011). Amyloid β peptide oligomers directly activate NMDA receptors. *Cell Calcium*, *49*(3), 184-190. https://doi.org/10.1016/j.ceca.2011.02.001
Thal, D. R., Rüb, U., Orantes, M., & Braak, H. (2002). Phases of A beta-deposition in the human brain and its relevance for the development of AD. *Neurology*, *58*(12), 1791-1800. https://doi.org/10.1212/wnl.58.12.1791

Thibault, O., & Landfield, P. W. (1996). Increase in single L-type calcium channels in hippocampal neurons during aging. *Science*, *272*(5264), 1017-1020. https://doi.org/10.1126/science.272.5264.1017
Tinsley, C. J., Fontaine-Palmer, N. S., Vincent, M., Endean, E. P., Aggleton, J. P., Brown, M. W., & Warburton, E. C. (2011). Differing time dependencies of object recognition memory impairments produced by nicotinic and muscarinic cholinergic antagonism in perirhinal cortex. *Learn Mem*, *18*(7), 484-492. https://doi.org/10.1101/lm.2274911
Tischmeyer, W., Kaczmarek, L., Strauss, M., Jork, R., & Matthies, H. (1990). Accumulation of c-fos mRNA in rat hippocampus during acquisition of a brightness discrimination. *Behav Neural Biol*, *54*(2), 165-171. https://doi.org/10.1016/0163-1047(90)91366-j
Todd, T. P., & Bucci, D. J. (2015). Retrosplenial Cortex and Long-Term Memory: Molecules to Behavior. *Neural Plast*, *2015*, 414173. https://doi.org/10.1155/2015/414173
Toescu, E. C., & Verkhratsky, A. (2007). The importance of being subtle: small changes in calcium homeostasis control cognitive decline in normal aging. *Aging Cell*, *6*(3), 267-273. https://doi.org/10.1111/j.1474-9726.2007.00296.x
Tolar, M., Hey, J., Power, A., & Abushakra, S. (2021). Neurotoxic Soluble Amyloid Oligomers Drive Alzheimer's Pathogenesis and Represent a Clinically Validated Target for Slowing Disease Progression. *Int J Mol Sci*, *22*(12). https://doi.org/10.3390/ijms22126355
Tong, B. C., Wu, A. J., Li, M., & Cheung, K. H. (2018). Calcium signaling in Alzheimer's disease & therapies. *Biochim Biophys Acta Mol Cell Res*, *1865*(11 Pt B), 1745-1760. https://doi.org/10.1016/j.bbamcr.2018.07.018
Tovote, P., Fadok, J. P., & Lüthi, A. (2015). Neuronal circuits for fear and anxiety. *Nat Rev Neurosci*, *16*(6), 317-331. https://doi.org/10.1038/nrn3945
Townsend, M., Shankar, G. M., Mehta, T., Walsh, D. M., & Selkoe, D. J. (2006). Effects of secreted oligomers of amyloid beta-protein on hippocampal synaptic plasticity: a potent role for trimers. *J Physiol*, *572*(Pt 2), 477-492. https://doi.org/10.1113/jphysiol.2005.103754
Trask, S., & Fournier, D. I. (2022). Examining a role for the retrosplenial cortex in age-related memory impairment. *Neurobiol Learn Mem*, *189*, 107601. https://doi.org/10.1016/j.nlm.2022.107601
Treit, D., Menard, J., & Royan, C. (1993). Anxiogenic stimuli in the elevated plus-maze. *Pharmacol Biochem Behav*, *44*(2), 463-469. https://doi.org/10.1016/0091-3057(93)90492-c
Tromp, D., Dufour, A., Lithfous, S., Pebayle, T., & Després, O. (2015). Episodic memory in normal aging and Alzheimer disease: Insights from imaging and behavioral studies. *Ageing Res Rev*, *24*(Pt B), 232-262. https://doi.org/10.1016/j.arr.2015.08.006
Tsankova, N. M., Kumar, A., & Nestler, E. J. (2004). Histone modifications at gene promoter regions in rat hippocampus after acute and chronic electroconvulsive seizures. *J Neurosci*, *24*(24), 5603-5610. https://doi.org/10.1523/JNEUROSCI.0589-04.2004
Tsao, A., Moser, M. B., & Moser, E. I. (2013). Traces of experience in the lateral entorhinal cortex. *Curr Biol*, *23*(5), 399-405. https://doi.org/10.1016/j.cub.2013.01.036
Tsubuki, S., Takaki, Y., & Saido, T. C. (2003). Dutch, Flemish, Italian, and Arctic mutations of APP and resistance of Abeta to physiologically relevant

proteolytic degradation. *Lancet*, *361*(9373), 1957-1958. https://doi.org/10.1016/s0140-6736(03)13555-6
Tsui, K. C., Roy, J., Chau, S. C., Wong, K. H., Shi, L., Poon, C. H.,…Lim, L. W. (2022). Distribution and inter-regional relationship of amyloid-beta plaque deposition in a 5xFAD mouse model of Alzheimer's disease. *Front Aging Neurosci*, *14*, 964336. https://doi.org/10.3389/fnagi.2022.964336
Tu, H., Nelson, O., Bezprozvanny, A., Wang, Z., Lee, S. F., Hao, Y. H.,…Bezprozvanny, I. (2006). Presenilins form ER Ca2+ leak channels, a function disrupted by familial Alzheimer's disease-linked mutations. *Cell*, *126*(5), 981-993. https://doi.org/10.1016/j.cell.2006.06.059
Tucker, L. B., & McCabe, J. T. (2021). Measuring Anxiety-Like Behaviors in Rodent Models of Traumatic Brain Injury. *Front Behav Neurosci*, *15*, 682935. https://doi.org/10.3389/fnbeh.2021.682935
Tulving, E., & Markowitsch, H. J. (1998). Episodic and declarative memory: role of the hippocampus. *Hippocampus*, *8*(3), 198-204. https://doi.org/10.1002/(SICI)1098-1063(1998)8:3
Twick, M., & Levy, D. A. (2021). Fractionating the episodic buffer. *Brain Cogn*, *154*, 105800. https://doi.org/10.1016/j.bandc.2021.105800
Ueda, K., Shinohara, S., Yagami, T., Asakura, K., & Kawasaki, K. (1997). Amyloid beta protein potentiates Ca2+ influx through L-type voltage-sensitive Ca2+ channels: a possible involvement of free radicals. *J Neurochem*, *68*(1), 265-271. https://doi.org/10.1046/j.1471-4159.1997.68010265.x
Ulaganathan, S., & Pitchaimani, A. (2023). Spontaneous and familial models of Alzheimer's disease: Challenges and advances in preclinical research. *Life Sci*, *328*, 121918. https://doi.org/10.1016/j.lfs.2023.121918
Um, J. W., Nygaard, H. B., Heiss, J. K., Kostylev, M. A., Stagi, M., Vortmeyer, A.,…Strittmatter, S. M. (2012). Alzheimer amyloid-β oligomer bound to postsynaptic prion protein activates Fyn to impair neurons. *Nat Neurosci*, *15*(9), 1227-1235. https://doi.org/10.1038/nn.3178
Vakalopoulos, C. (2017). Alzheimer's Disease: The Alternative Serotonergic Hypothesis of Cognitive Decline. *J Alzheimers Dis*, *60*(3), 859-866. https://doi.org/10.3233/JAD-170364
van der Kant, R., & Goldstein, L. S. (2015). Cellular functions of the amyloid precursor protein from development to dementia. *Dev Cell*, *32*(4), 502-515. https://doi.org/10.1016/j.devcel.2015.01.022
van Groen, T., & Wyss, J. M. (1990). Connections of the retrosplenial granular a cortex in the rat. *J Comp Neurol*, *300*(4), 593-606. https://doi.org/10.1002/cne.903000412
van Groen, T., & Wyss, J. M. (1992a). Connections of the retrosplenial dysgranular cortex in the rat. *J Comp Neurol*, *315*(2), 200-216. https://doi.org/10.1002/cne.903150207
van Groen, T., & Wyss, J. M. (1992b). Projections from the laterodorsal nucleus of the thalamus to the limbic and visual cortices in the rat. *J Comp Neurol*, *324*(3), 427-448. https://doi.org/10.1002/cne.903240310
Van Groen, T., & Wyss, J. M. (2003). Connections of the retrosplenial granular b cortex in the rat. *J Comp Neurol*, *463*(3), 249-263. https://doi.org/10.1002/cne.10757
Vann, S. D., & Aggleton, J. P. (2002). Extensive cytotoxic lesions of the rat retrosplenial cortex reveal consistent deficits on tasks that tax allocentric spatial memory. *Behav Neurosci*, *116*(1), 85-94.

Vann, S. D., & Aggleton, J. P. (2004). Testing the importance of the retrosplenial guidance system: effects of different sized retrosplenial cortex lesions on heading direction and spatial working memory. *Behav Brain Res*, *155*(1), 97-108. https://doi.org/10.1016/j.bbr.2004.04.005
Vann, S. D., & Aggleton, J. P. (2005). Selective dysgranular retrosplenial cortex lesions in rats disrupt allocentric performance of the radial-arm maze task. *Behav Neurosci*, *119*(6), 1682-1686. https://doi.org/10.1037/0735-7044.119.6.1682
Vann, S. D., Aggleton, J. P., & Maguire, E. A. (2009). What does the retrosplenial cortex do? *Nat Rev Neurosci*, *10*(11), 792-802. https://doi.org/10.1038/nrn2733
Vann, S. D., Brown, M. W., Erichsen, J. T., & Aggleton, J. P. (2000). Fos imaging reveals differential patterns of hippocampal and parahippocampal subfield activation in rats in response to different spatial memory tests. *J Neurosci*, *20*(7), 2711-2718. https://doi.org/10.1523/JNEUROSCI.20-07-02711.2000
Vann, S. D., Kristina Wilton, L. A., Muir, J. L., & Aggleton, J. P. (2003). Testing the importance of the caudal retrosplenial cortex for spatial memory in rats. *Behav Brain Res*, *140*(1-2), 107-118. https://doi.org/10.1016/s0166-4328(02)00274-7
Vaz, M., Silva, V., Monteiro, C., & Silvestre, S. (2022). Role of Aducanumab in the Treatment of Alzheimer's Disease: Challenges and Opportunities. *Clin Interv Aging*, *17*, 797-810. https://doi.org/10.2147/CIA.S325026
Velazquez, F. N., Prucca, C. G., Etienne, O., D'Astolfo, D. S., Silvestre, D. C., Boussin, F. D., & Caputto, B. L. (2015). Brain development is impaired in c-fos -/- mice. *Oncotarget*, *6*(19), 16883-16901. https://doi.org/10.18632/oncotarget.4527
Verkhratsky, A., & Nedergaard, M. (2018). Physiology of Astroglia. *Physiol Rev*, *98*(1), 239-389. https://doi.org/10.1152/physrev.00042.2016
Vermunt, L., Sikkes, S. A. M., van den Hout, A., Handels, R., Bos, I., van der Flier, W. M.,…groups, I. D. s. (2019). Duration of preclinical, prodromal, and dementia stages of Alzheimer's disease in relation to age, sex, and APOE genotype. *Alzheimers Dement*, *15*(7), 888-898. https://doi.org/10.1016/j.jalz.2019.04.001
Villemagne, V. L., Burnham, S., Bourgeat, P., Brown, B., Ellis, K. A., Salvado, O.,…Group, A. I. B. a. L. A. R. (2013). Amyloid β deposition, neurodegeneration, and cognitive decline in sporadic Alzheimer's disease: a prospective cohort study. *Lancet Neurol*, *12*(4), 357-367. https://doi.org/10.1016/S1474-4422(13)70044-9
Villemagne, V. L., Pike, K. E., Chételat, G., Ellis, K. A., Mulligan, R. S., Bourgeat, P.,…Rowe, C. C. (2011). Longitudinal assessment of Aβ and cognition in aging and Alzheimer disease. *Ann Neurol*, *69*(1), 181-192. https://doi.org/10.1002/ana.22248
Viola, K. L., & Klein, W. L. (2015). Amyloid β oligomers in Alzheimer's disease pathogenesis, treatment, and diagnosis. *Acta Neuropathol*, *129*(2), 183-206. https://doi.org/10.1007/s00401-015-1386-3
Viswanathan, A., & Greenberg, S. M. (2011). Cerebral amyloid angiopathy in the elderly. *Ann Neurol*, *70*(6), 871-880. https://doi.org/10.1002/ana.22516
Vitek, G. E., Decourt, B., & Sabbagh, M. N. (2023). Lecanemab (BAN2401): an anti-beta-amyloid monoclonal antibody for the treatment of Alzheimer disease. *Expert Opin Investig Drugs*, *32*(2), 89-94. https://doi.org/10.1080/13543784.2023.2178414

Vlček, K., & Laczó, J. (2014). Neural correlates of spatial navigation changes in mild cognitive impairment and Alzheimer's disease. *Front Behav Neurosci*, *8*, 89. https://doi.org/10.3389/fnbeh.2014.00089
Vogel-Ciernia, A., & Wood, M. A. (2014). Examining object location and object recognition memory in mice. *Curr Protoc Neurosci*, *69*, 8.31.31-17. https://doi.org/10.1002/0471142301.ns0831s69
Vogt, B. A., & Miller, M. W. (1983). Cortical connections between rat cingulate cortex and visual, motor, and postsubicular cortices. *J Comp Neurol*, *216*(2), 192-210. https://doi.org/10.1002/cne.902160207
Vogt, B. A., & Peters, A. (1981). Form and distribution of neurons in rat cingulate cortex: areas 32, 24, and 29. *J Comp Neurol*, *195*(4), 603-625. https://doi.org/10.1002/cne.901950406
Walf, A. A., & Frye, C. A. (2007). The use of the elevated plus maze as an assay of anxiety-related behavior in rodents. *Nat Protoc*, *2*(2), 322-328. https://doi.org/10.1038/nprot.2007.44
Walker, D. L., & Gold, P. E. (1992). Impairment of spontaneous alternation performance by an NMDA antagonist: attenuation with non-NMDA treatments. *Behav Neural Biol*, *58*(1), 69-71. https://doi.org/10.1016/0163-1047(92)90952-z
Wall, P. M., & Messier, C. (2000). Ethological confirmatory factor analysis of anxiety-like behaviour in the murine elevated plus-maze. *Behav Brain Res*, *114*(1-2), 199-212. https://doi.org/10.1016/s0166-4328(00)00229-1
Walsh, C., Ridler, T., Margetts-Smith, G., Garcia Garrido, M., Witton, J., Randall, A. D., & Brown, J. T. (2022). β Bursting in the Retrosplenial Cortex Is a Neurophysiological Correlate of Environmental Novelty Which Is Disrupted in a Mouse Model of Alzheimer's Disease. *J Neurosci*, *42*(37), 7094-7109. https://doi.org/10.1523/JNEUROSCI.0890-21.2022
Walsh, D. M., Klyubin, I., Fadeeva, J. V., Cullen, W. K., Anwyl, R., Wolfe, M. S.,…Selkoe, D. J. (2002). Naturally secreted oligomers of amyloid beta protein potently inhibit hippocampal long-term potentiation in vivo. *Nature*, *416*(6880), 535-539. https://doi.org/10.1038/416535a
Walsh, D. M., Lomakin, A., Benedek, G. B., Condron, M. M., & Teplow, D. B. (1997). Amyloid beta-protein fibrillogenesis. Detection of a protofibrillar intermediate. *J Biol Chem*, *272*(35), 22364-22372. https://doi.org/10.1074/jbc.272.35.22364
Wang, C., Chen, X., & Knierim, J. J. (2020). Egocentric and allocentric representations of space in the rodent brain. *Curr Opin Neurobiol*, *60*, 12-20. https://doi.org/10.1016/j.conb.2019.11.005
Wang, H., Song, L., Laird, F., Wong, P. C., & Lee, H. K. (2008). BACE1 knock-outs display deficits in activity-dependent potentiation of synaptic transmission at mossy fiber to CA3 synapses in the hippocampus. *J Neurosci*, *28*(35), 8677-8681. https://doi.org/10.1523/JNEUROSCI.2440-08.2008
Wang, J., Dickson, D. W., Trojanowski, J. Q., & Lee, V. M. (1999). The levels of soluble versus insoluble brain Abeta distinguish Alzheimer's disease from normal and pathologic aging. *Exp Neurol*, *158*(2), 328-337. https://doi.org/10.1006/exnr.1999.7085
Wang, L., Yin, Y. L., Liu, X. Z., Shen, P., Zheng, Y. G., Lan, X. R.,…Wang, J. Z. (2020). Current understanding of metal ions in the pathogenesis of Alzheimer's disease. *Transl Neurodegener*, *9*, 10. https://doi.org/10.1186/s40035-020-00189-z

Wang, M., Zhang, H., Liang, J., Huang, J., Wu, T., & Chen, N. (2025). Calcium signaling hypothesis: A non-negligible pathogenesis in Alzheimer's disease. *J Adv Res*. https://doi.org/10.1016/j.jare.2025.01.007
Wang, S., Ichinomiya, T., Savchenko, P., Devulapalli, S., Wang, D., Beltz, G.,…Head, B. P. (2022). Age-Dependent Behavioral and Metabolic Assessment of. *Front Mol Neurosci*, *15*, 909989. https://doi.org/10.3389/fnmol.2022.909989
Wang, S., Yabuki, Y., Matsuo, K., Xu, J., Izumi, H., Sakimura, K.,…Fukunaga, K. (2018). T-type calcium channel enhancer SAK3 promotes dopamine and serotonin releases in the hippocampus in naive and amyloid precursor protein knock-in mice. *PLoS One*, *13*(12), e0206986. https://doi.org/10.1371/journal.pone.0206986
Wang, W. Y., Tan, M. S., Yu, J. T., & Tan, L. (2015). Role of pro-inflammatory cytokines released from microglia in Alzheimer's disease. *Ann Transl Med*, *3*(10), 136. https://doi.org/10.3978/j.issn.2305-5839.2015.03.49
Wang, X. J. (1999). Synaptic basis of cortical persistent activity: the importance of NMDA receptors to working memory. *J Neurosci*, *19*(21), 9587-9603. https://doi.org/10.1523/JNEUROSCI.19-21-09587.1999
Wang, Y., Shi, Y., & Wei, H. (2017). Calcium Dysregulation in Alzheimer's Disease: A Target for New Drug Development. *J Alzheimers Dis Parkinsonism*, *7*(5). https://doi.org/10.4172/2161-0460.1000374
Warburton, E. C., Barker, G. R., & Brown, M. W. (2013). Investigations into the involvement of NMDA mechanisms in recognition memory. *Neuropharmacology*, *74*, 41-47. https://doi.org/10.1016/j.neuropharm.2013.04.013
Warburton, E. C., & Brown, M. W. (2015). Neural circuitry for rat recognition memory. *Behav Brain Res*, *285*, 131-139. https://doi.org/10.1016/j.bbr.2014.09.050
Webster, S. J., Bachstetter, A. D., Nelson, P. T., Schmitt, F. A., & Van Eldik, L. J. (2014). Using mice to model Alzheimer's dementia: an overview of the clinical disease and the preclinical behavioral changes in 10 mouse models. *Front Genet*, *5*, 88. https://doi.org/10.3389/fgene.2014.00088
Webster, S. J., Bachstetter, A. D., & Van Eldik, L. J. (2013). Comprehensive behavioral characterization of an APP/PS-1 double knock-in mouse model of Alzheimer's disease. *Alzheimers Res Ther*, *5*(3), 28. https://doi.org/10.1186/alzrt182
Wei, Z., Lin, B. J., Chen, T. W., Daie, K., Svoboda, K., & Druckmann, S. (2020). A comparison of neuronal population dynamics measured with calcium imaging and electrophysiology. *PLoS Comput Biol*, *16*(9), e1008198. https://doi.org/10.1371/journal.pcbi.1008198
Weiss, S., & Derdikman, D. (2018). Role of the head-direction signal in spatial tasks: when and how does it guide behavior? *J Neurophysiol*, *120*(1), 78-87. https://doi.org/10.1152/jn.00560.2017
Werheid, K., & Clare, L. (2007). Are faces special in Alzheimer's disease? Cognitive conceptualisation, neural correlates, and diagnostic relevance of impaired memory for faces and names. *Cortex*, *43*(7), 898-906. https://doi.org/10.1016/s0010-9452(08)70689-0
White, H. E., Goswami, A., & Tucker, A. S. (2021). The Intertwined Evolution and Development of Sutures and Cranial Morphology. *Front Cell Dev Biol*, *9*, 653579. https://doi.org/10.3389/fcell.2021.653579

Whitwell, J. L. (2010). Progression of atrophy in Alzheimer's disease and related disorders. *Neurotox Res*, *18*(3-4), 339-346. https://doi.org/10.1007/s12640-010-9175-1
Whyte, L. S., Hemsley, K. M., Lau, A. A., Hassiotis, S., Saito, T., Saido, T. C.,…Sargeant, T. J. (2018). Reduction in open field activity in the absence of memory deficits in the App. *Behav Brain Res*, *336*, 177-181. https://doi.org/10.1016/j.bbr.2017.09.006
Wiegert, J. S., & Oertner, T. G. (2013). Long-term depression triggers the selective elimination of weakly integrated synapses. *Proc Natl Acad Sci U S A*, *110*(47), E4510-4519. https://doi.org/10.1073/pnas.1315926110
Wildner, G. (2019). Are rats more human than mice? *Immunobiology*, *224*(1), 172-176. https://doi.org/10.1016/j.imbio.2018.09.002
Wilson, D. I., Watanabe, S., Milner, H., & Ainge, J. A. (2013). Lateral entorhinal cortex is necessary for associative but not nonassociative recognition memory. *Hippocampus*, *23*(12), 1280-1290. https://doi.org/10.1002/hipo.22165
Wilt, B. A., Burns, L. D., Wei Ho, E. T., Ghosh, K. K., Mukamel, E. A., & Schnitzer, M. J. (2009). Advances in light microscopy for neuroscience. *Annu Rev Neurosci*, *32*, 435-506. https://doi.org/10.1146/annurev.neuro.051508.135540
Wimmer, M. E., Hernandez, P. J., Blackwell, J., & Abel, T. (2012). Aging impairs hippocampus-dependent long-term memory for object location in mice. *Neurobiol Aging*, *33*(9), 2220-2224. https://doi.org/10.1016/j.neurobiolaging.2011.07.007
Winters, B. D., & Bussey, T. J. (2005). Glutamate receptors in perirhinal cortex mediate encoding, retrieval, and consolidation of object recognition memory. *J Neurosci*, *25*(17), 4243-4251. https://doi.org/10.1523/JNEUROSCI.0480-05.2005
Wirths, O., & Zampar, S. (2020). Neuron Loss in Alzheimer's Disease: Translation in Transgenic Mouse Models. *Int J Mol Sci*, *21*(21). https://doi.org/10.3390/ijms21218144
Wiseman, F. K., Al-Janabi, T., Hardy, J., Karmiloff-Smith, A., Nizetic, D., Tybulewicz, V. L.,…Strydom, A. (2015). A genetic cause of Alzheimer disease: mechanistic insights from Down syndrome. *Nat Rev Neurosci*, *16*(9), 564-574. https://doi.org/10.1038/nrn3983
Wolbers, T., Klatzky, R. L., Loomis, J. M., Wutte, M. G., & Giudice, N. A. (2011). Modality-independent coding of spatial layout in the human brain. *Curr Biol*, *21*(11), 984-989. https://doi.org/10.1016/j.cub.2011.04.038
Wolf, A., Bauer, B., Abner, E. L., Ashkenazy-Frolinger, T., & Hartz, A. M. (2016). A Comprehensive Behavioral Test Battery to Assess Learning and Memory in 129S6/Tg2576 Mice. *PLoS One*, *11*(1), e0147733. https://doi.org/10.1371/journal.pone.0147733
Wright, A. L., Zinn, R., Hohensinn, B., Konen, L. M., Beynon, S. B., Tan, R. P.,…Vissel, B. (2013). Neuroinflammation and neuronal loss precede Aβ plaque deposition in the hAPP-J20 mouse model of Alzheimer's disease. *PLoS One*, *8*(4), e59586. https://doi.org/10.1371/journal.pone.0059586
Wu, D., Chen, Q., Chen, X., Han, F., Chen, Z., & Wang, Y. (2023). The blood-brain barrier: structure, regulation, and drug delivery. *Signal Transduct Target Ther*, *8*(1), 217. https://doi.org/10.1038/s41392-023-01481-w

Wu, J., Anwyl, R., & Rowan, M. J. (1995). beta-Amyloid-(1-40) increases long-term potentiation in rat hippocampus in vitro. *Eur J Pharmacol*, *284*(3), R1-3. https://doi.org/10.1016/0014-2999(95)00539-w
Wyss, J. M., & Van Groen, T. (1992). Connections between the retrosplenial cortex and the hippocampal formation in the rat: a review. *Hippocampus*, *2*(1), 1-11. https://doi.org/10.1002/hipo.450020102
Xiao, N. A., Zhang, J., Zhou, M., Wei, Z., Wu, X. L., Dai, X. M.,…Chen, X. C. (2015). Reduction of Glucose Metabolism in Olfactory Bulb is an Earlier Alzheimer's Disease-related Biomarker in 5XFAD Mice. *Chin Med J (Engl)*, *128*(16), 2220-2227. https://doi.org/10.4103/0366-6999.162507
Yabuki, Y., Matsuo, K., Izumi, H., Haga, H., Yoshida, T., Wakamori, M.,…Fukunaga, K. (2017). Pharmacological properties of SAK3, a novel T-type voltage-gated Ca. *Neuropharmacology*, *117*, 1-13. https://doi.org/10.1016/j.neuropharm.2017.01.011
Yadollahikhales, G., & Rojas, J. C. (2023). Anti-Amyloid Immunotherapies for Alzheimer's Disease: A 2023 Clinical Update. *Neurotherapeutics*, *20*(4), 914-931. https://doi.org/10.1007/s13311-023-01405-0
Yamada, K., Arai, M., Suenaga, T., & Ichitani, Y. (2017). Involvement of hippocampal NMDA receptors in encoding and consolidation, but not retrieval, processes of spontaneous object location memory in rats. *Behav Brain Res*, *331*, 14-19. https://doi.org/10.1016/j.bbr.2017.05.006
Yamamoto, T., & Hirano, A. (1985). Nucleus raphe dorsalis in Alzheimer's disease: neurofibrillary tangles and loss of large neurons. *Ann Neurol*, *17*(6), 573-577. https://doi.org/10.1002/ana.410170608
Yang, S. N., Tang, Y. G., & Zucker, R. S. (1999). Selective induction of LTP and LTD by postsynaptic [Ca2+]i elevation. *J Neurophysiol*, *81*(2), 781-787. https://doi.org/10.1152/jn.1999.81.2.781
Yang, S. T., Shi, Y., Wang, Q., Peng, J. Y., & Li, B. M. (2014). Neuronal representation of working memory in the medial prefrontal cortex of rats. *Mol Brain*, *7*, 61. https://doi.org/10.1186/s13041-014-0061-2
Yang, Z., Zou, Y., & Wang, L. (2023). Neurotransmitters in Prevention and Treatment of Alzheimer's Disease. *Int J Mol Sci*, *24*(4). https://doi.org/10.3390/ijms24043841
Yankner, B. A., Duffy, L. K., & Kirschner, D. A. (1990). Neurotrophic and neurotoxic effects of amyloid beta protein: reversal by tachykinin neuropeptides. *Science*, *250*(4978), 279-282. https://doi.org/10.1126/science.2218531
Ye, B. S., Kim, H. J., Kim, Y. J., Jung, N. Y., Lee, J. S., Lee, J.,…Seo, S. W. (2018). Longitudinal outcomes of amyloid positive versus negative amnestic mild cognitive impairments: a three-year longitudinal study. *Sci Rep*, *8*(1), 5557. https://doi.org/10.1038/s41598-018-23676-w
Yiannopoulou, K. G., & Papageorgiou, S. G. (2020). Current and Future Treatments in Alzheimer Disease: An Update. *J Cent Nerv Syst Dis*, *12*, 1179573520907397. https://doi.org/10.1177/1179573520907397
Yoshiike, Y., Kayed, R., Milton, S. C., Takashima, A., & Glabe, C. G. (2007). Pore-forming proteins share structural and functional homology with amyloid oligomers. *Neuromolecular Med*, *9*(3), 270-275. https://doi.org/10.1007/s12017-007-0003-6
Yu, D., Li, T., Ding, Q., Wu, Y., Fu, Z., Zhan, X.,…Jia, Y. (2024). Maintenance of delay-period activity in working memory task is modulated by local network

structure. *PLoS Comput Biol*, *20*(9), e1012415. https://doi.org/10.1371/journal.pcbi.1012415
Yu, Z., & Luo, F. (2024). The Role of Reactive Oxygen Species in Alzheimer's Disease: From Mechanism to Biomaterials Therapy. *Adv Healthc Mater*, e2304373. https://doi.org/10.1002/adhm.202304373
Zhang, D., Yu, B., Liu, J., Jiang, W., Xie, T., Zhang, R.,…Yao, H. (2017). Altered visual cortical processing in a mouse model of MECP2 duplication syndrome. *Sci Rep*, *7*(1), 6468. https://doi.org/10.1038/s41598-017-06916-3
Zhang, H., Chen, L., Johnston, K. G., Crapser, J., Green, K. N., Ha, N. M.,…Xu, X. (2023a). Degenerate mapping of environmental location presages deficits in object-location encoding and memory in the 5xFAD mouse model for Alzheimer's disease. *Neurobiol Dis*, *176*, 105939. https://doi.org/10.1016/j.nbd.2022.105939
Zhang, H., Wu, L., Pchitskaya, E., Zakharova, O., Saito, T., Saido, T., & Bezprozvanny, I. (2015). Neuronal Store-Operated Calcium Entry and Mushroom Spine Loss in Amyloid Precursor Protein Knock-In Mouse Model of Alzheimer's Disease. *J Neurosci*, *35*(39), 13275-13286. https://doi.org/10.1523/JNEUROSCI.1034-15.2015
Zhang, H. Y., Wang, S. J., Liu, B., Ma, Z. L., Yang, M., Zhang, Z. J., & Teng, G. J. (2010). Resting brain connectivity: changes during the progress of Alzheimer disease. *Radiology*, *256*(2), 598-606. https://doi.org/10.1148/radiol.10091701
Zhang, P., Hirsch, E. C., Damier, P., Duyckaerts, C., & Javoy-Agid, F. (1992). c-fos protein-like immunoreactivity: distribution in the human brain and over-expression in the hippocampus of patients with Alzheimer's disease. *Neuroscience*, *46*(1), 9-21. https://doi.org/10.1016/0306-4522(92)90004-I
Zhang, Y., Chen, H., Li, R., Sterling, K., & Song, W. (2023b). Amyloid β-based therapy for Alzheimer's disease: challenges, successes and future. *Signal Transduct Target Ther*, *8*(1), 248. https://doi.org/10.1038/s41392-023-01484-7
Zhang, Y., Li, P., Feng, J., & Wu, M. (2016). Dysfunction of NMDA receptors in Alzheimer's disease. *Neurol Sci*, *37*(7), 1039-1047. https://doi.org/10.1007/s10072-016-2546-5
Zhang, Y., Rózsa, M., Liang, Y., Bushey, D., Wei, Z., Zheng, J.,…Looger, L. L. (2023c). Fast and sensitive GCaMP calcium indicators for imaging neural populations. *Nature*, *615*(7954), 884-891. https://doi.org/10.1038/s41586-023-05828-9
Zhang, Y., Zhao, Y., Zhang, L., Yu, W., Wang, Y., & Chang, W. (2019). Cellular Prion Protein as a Receptor of Toxic Amyloid-β42 Oligomers Is Important for Alzheimer's Disease. *Front Cell Neurosci*, *13*, 339. https://doi.org/10.3389/fncel.2019.00339
Zhang, Y. W., Thompson, R., Zhang, H., & Xu, H. (2011). APP processing in Alzheimer's disease. *Mol Brain*, *4*, 3. https://doi.org/10.1186/1756-6606-4-3
Zhao, J., O'Connor, T., & Vassar, R. (2011). The contribution of activated astrocytes to Aβ production: implications for Alzheimer's disease pathogenesis. *J Neuroinflammation*, *8*, 150. https://doi.org/10.1186/1742-2094-8-150
Zhong, M. Z., Peng, T., Duarte, M. L., Wang, M., & Cai, D. (2024). Updates on mouse models of Alzheimer's disease. *Mol Neurodegener*, *19*(1), 23. https://doi.org/10.1186/s13024-024-00712-0
Zhou, Y., KLi, WTakahashi, E. (2015). Cav2.2-mediated NMDA receptor signaling in short-term memory. *Integrative Molecular Medicine*, *2*(2), 131-134.

Zhu, X. C., Yu, J. T., Jiang, T., Wang, P., Cao, L., & Tan, L. (2015). CR1 in Alzheimer's disease. *Mol Neurobiol*, *51*(2), 753-765. https://doi.org/10.1007/s12035-014-8723-8

Zoeteweij, J. P., van de Water, B., de Bont, H. J., Mulder, G. J., & Nagelkerke, J. F. (1992). Involvement of intracellular Ca2+ and K+ in dissipation of the mitochondrial membrane potential and cell death induced by extracellular ATP in hepatocytes. *Biochem J*, *288 (Pt 1)*, 207-213. https://doi.org/10.1042/bj2880207

Zott, B., Simon, M. M., Hong, W., Unger, F., Chen-Engerer, H. J., Frosch, M. P.,…Konnerth, A. (2019). A vicious cycle of β amyloid-dependent neuronal hyperactivation. *Science*, *365*(6453), 559-565. https://doi.org/10.1126/science.aay0198

Zvolensky, M. J., Lejuez, C. W., & Eifert, G. H. (2000). Prediction and control: operational definitions for the experimental analysis of anxiety. *Behav Res Ther*, *38*(7), 653-663. https://doi.org/10.1016/s0005-7967(99)00090-x

Ávila-Villanueva, M., Marcos Dolado, A., Gómez-Ramírez, J., & Fernández-Blázquez, M. (2022). Brain Structural and Functional Changes in Cognitive Impairment Due to Alzheimer's Disease. *Front Psychol*, *13*, 886619. https://doi.org/10.3389/fpsyg.2022.886619

Chapter 7: Appendices

7.1 Appendix 1: Mean Baseline ΔF

This VBA macro, developed using the XLTools function in Microsoft Excel, was designed to calculate the mean raw ΔF during the 2-second dark screen period immediately preceding the onset of the visual stimulus in Ca^{2+} imaging experiments. The macro loops through the files containing data for each cell in the ROI for each animal and calculates an overall mean baseline ΔF for each animal.

```
Sub LoopThroughFiles()
    Dim xFd As FileDialog
    Dim xFdItem As Variant
    Dim xFileName As String
    Set xFd =
Application.FileDialog(msoFileDialogFolderPicker)
    If xFd.Show = -1 Then
        xFdItem = xFd.SelectedItems(1) &
Application.PathSeparator
        xFileName = Dir(xFdItem & "*.xls*")
        Do While xFileName <> ""
            With Workbooks.Open(xFdItem & xFileName)


                ' raw_averages Macro
    Range("O28").Select
    ActiveCell.Formula = _
"=AVERAGE(O2:O25)"
Range("P28").Select
    ActiveCell.Formula = _
"=AVERAGE(P2:P25)"
Range("Q28").Select
    ActiveCell.Formula = _
"=AVERAGE(Q2:Q25)"
    Range("R28").Select
    ActiveCell.Formula = _
```

```
"=AVERAGE(R2:R25)"
    Range("S28").Select
    ActiveCell.Formula = _
"=AVERAGE(S2:S25)"
Range("T28").Select
    ActiveCell.Formula = _
"=AVERAGE(T2:T25)"
Range("U28").Select
    ActiveCell.Formula = _
"=AVERAGE(U2:U25)"
Range("V28").Select
ActiveCell.Formula = _
"=AVERAGE(V2:V25)"
Range("W28").Select
ActiveCell.Formula = _
"=AVERAGE(W2:W25)"
    Range("X28").Select
    ActiveCell.Formula = _
"=AVERAGE(X2:X25)"
    Range("Y28").Select
ActiveCell.Formula = _
"=AVERAGE(Y2:Y25)"
Range("Z28").Select
    ActiveCell.Formula = _
"=AVERAGE(Z2:Z25)"
Range("AA28").Select
    ActiveCell.Formula = _
"=AVERAGE(AA2:AA25)"
Range("AB28").Select
    ActiveCell.Formula = _
"=AVERAGE(AB2:AB25)"
```

```
    Range("AC28").Select
    ActiveCell.Formula = _
"=AVERAGE(AC2:AC25)”
Range("AD28").Select
    ActiveCell.Formula = _
"=AVERAGE(AD2:AD25)”
Range("AE28").Select
    ActiveCell.Formula = _
"=AVERAGE(AE2:AE25)”
Range("AF28").Select
ActiveCell.Formula = _
"=AVERAGE(AF2:AF25)”
Range("AG28").Select
ActiveCell.Formula = _
"=AVERAGE(AG2:AG25)”

Range("AH28").Select
ActiveCell.Formula = _
"=AVERAGE(AH2:AH25)”
Range("AI28").Select
ActiveCell.Formula = _
"=AVERAGE(AI2:AI25)”
Range(“O28:AI28”).Select
    Selection.Copy
    Windows("raw averages.xlsx").Activate
Sheets("Sheet1").Select
    ActiveCell.Offset(1, 0).Select
    Selection.PasteSpecial Paste:=xlPasteValues,
Operation:=xlNone, SkipBlanks _
        :=False, Transpose:=False
    For Each wb In Application.Workbooks
```

```
     Select Case wb.Name
             Case ThisWorkbook.Name
                 ' do nothing
Case Else
wb.Close SaveChanges:=True
     End Select
Next wb

End With
            xFileName = Dir
        Loop
    End If
End Sub
```

7.2 Appendix 2: Mean Stimulus Response (ΔF/F)

This VBA macro was designed to calculate the mean ΔF during initial 2-seconds of visual stimuli during Ca^{2+} imaging, normalising it by the average of the 2-seconds of baseline ΔF immediately prior to stimulus onset. The macro loops through the files containing data for each cell in the ROI for each animal and calculates an overall mean normalised stimulus response for each animal.

```
Sub LoopThroughFiles()
    Dim xFd As FileDialog
    Dim xFdItem As Variant
    Dim xFileName As String
    Set xFd =
Application.FileDialog(msoFileDialogFolderPicker)
    If xFd.Show = -1 Then
        xFdItem = xFd.SelectedItems(1) &
Application.PathSeparator
        xFileName = Dir(xFdItem & "*.xls*")
        Do While xFileName <> ""
            With Workbooks.Open(xFdItem & xFileName)

                ' overall_averages Macro
    Range("O27").Select
    ActiveCell.Formula = _
"=AVERAGE(O2:O25)/AVERAGE($O$2:$X$25)"
Range("P27").Select
    ActiveCell.Formula = _
"=AVERAGE(P2:P25)/AVERAGE($O$2:$X$25)"
Range("Q27").Select
    ActiveCell.Formula = _
"=AVERAGE(Q2:Q25)/AVERAGE($O$2:$X$25)"
    Range("R27").Select
    ActiveCell.Formula = _
```

```
"=AVERAGE(R2:R25)/AVERAGE($O$2:$X$25)"
    Range("S27").Select
    ActiveCell.Formula = _
"=AVERAGE(S2:S25)/AVERAGE($O$2:$X$25)"
Range("T27").Select
    ActiveCell.Formula = _
"=AVERAGE(T2:T25)/AVERAGE($O$2:$X$25)"
Range("U27").Select
    ActiveCell.Formula = _
"=AVERAGE(U2:U25)/AVERAGE($O$2:$X$25)"
Range("V27").Select
ActiveCell.Formula = _
"=AVERAGE(V2:V25)/AVERAGE($O$2:$X$25)"
Range("W27").Select
ActiveCell.Formula = _
"=AVERAGE(W2:W25)/AVERAGE($O$2:$X$25)"
    Range("X27").Select
    ActiveCell.Formula = _
"=AVERAGE(X2:X25)/AVERAGE($O$2:$X$25)"
    Range("Y27").Select
ActiveCell.Formula = _
"=AVERAGE(Y2:Y25)/AVERAGE($O$2:$X$25)"
Range("Z27").Select
    ActiveCell.Formula = _
"=AVERAGE(Z2:Z25)/AVERAGE($O$2:$X$25)"
Range("AA27").Select
    ActiveCell.Formula = _
"=AVERAGE(AA2:AA25)/AVERAGE($O$2:$X$25)"
Range("AB27").Select
    ActiveCell.Formula = _
"=AVERAGE(AB2:AB25)/AVERAGE($O$2:$X$25)"
```

```
    Range("AC27").Select
    ActiveCell.Formula = _
"=AVERAGE(AC2:AC25)/AVERAGE($O$2:$X$25)”
Range("AD27").Select
    ActiveCell.Formula = _
"=AVERAGE(AD2:AD25)/AVERAGE($O$2:$X$25)”
Range("AE27").Select
    ActiveCell.Formula = _
"=AVERAGE(AE2:AE25)/AVERAGE($O$2:$X$25)”
Range("AF27").Select
ActiveCell.Formula = _
"=AVERAGE(AF2:AF25)/AVERAGE($O$2:$X$25)”
Range("AG27").Select
ActiveCell.Formula = _
"=AVERAGE(AG2:AG25)/AVERAGE($O$2:$X$25)”

Range("AH27").Select
ActiveCell.Formula = _
"=AVERAGE(AH2:AH25)/AVERAGE($O$2:$X$25)”
Range("AI27").Select
ActiveCell.Formula = _
"=AVERAGE(AI2:AI25)/AVERAGE($O$2:$X$25)”
Range(“O27:AI27”).Select
    Selection.Copy
    Windows("overall averages.xlsx").Activate
Sheets("Sheet1").Select
    ActiveCell.Offset(1, 0).Select
    Selection.PasteSpecial Paste:=xlPasteValues,
Operation:=xlNone, SkipBlanks _
        :=False, Transpose:=False
    For Each wb In Application.Workbooks
```

```
     Select Case wb.Name
             Case ThisWorkbook.Name
                 ' do nothing
Case Else
wb.Close SaveChanges:=True
     End Select
Next wb

End With
            xFileName = Dir
        Loop
    End If
End Sub
```

7.3 Appendix 3: Orientation-Specific Stimulus Response (ΔF/F)

This VBA macro was designed to calculate a mean ΔF/F for the response to stimuli presented at four different spatial orientations, by separately calculating the mean ΔF in response to each orientation and normalising it by the 2-seconds of baseline immediately prior to the relevant stimulus trials. Again, this loop macro calculates an overall mean ΔF/F for each animal at each stimulus orientation by automatically looping through all datasets representing all cells in the ROI for each animal.

```
Sub LoopThroughFiles()
    Dim xFd As FileDialog
    Dim xFdItem As Variant
    Dim xFileName As String
    Set xFd =
Application.FileDialog(msoFileDialogFolderPicker)
    If xFd.Show = -1 Then
        xFdItem = xFd.SelectedItems(1) &
Application.PathSeparator
        xFileName = Dir(xFdItem & "*.xls*")
        Do While xFileName <> ""
            With Workbooks.Open(xFdItem & xFileName)


                ' 4 ori Macro
    Range("y34").Select
    ActiveCell.Formula = _
"=AVERAGE(y2,y6,y10,y14,y18,y22)/average(o2:x2,o6:x6,o10:x10,o
14:x14,o18:x18,o22:x22)"
    Range("z34").Select
ActiveCell.Formula = _
"=AVERAGE(z2,z6,z10,z14,z18,z22)/average(o2:x2,o6:x6,o10:x10,o
14:x14,o18:x18,o22:x22)"
Range("aa34").Select
    ActiveCell.Formula = _
```

```
"=AVERAGE(aa2,aa6,aa10,aa14,aa18,aa22)/average(o2:x2,o6:x6,o10
:x10,o14:x14,o18:x18,o22:x22)"

Range("ab34").Select

    ActiveCell.Formula = _

"=AVERAGE(ab2,ab6,ab10,ab14,ab18,ab22)/average(o2:x2,o6:x6,o10
:x10,o14:x14,o18:x18,o22:x22)"

Range("ac34").Select

    ActiveCell.Formula = _

"=AVERAGE(ac2,ac6,ac10,ac14,ac18,ac22)/average(o2:x2,o6:x6,o10
:x10,o14:x14,o18:x18,o22:x22)"

    Range("ad34").Select

    ActiveCell.Formula = _

"=AVERAGE(ad2,ad6,ad10,ad14,ad18,ad22)/average(o2:x2,o6:x6,o10
:x10,o14:x14,o18:x18,o22:x22)"

    Range("ae34").Select

    ActiveCell.Formula = _

"=AVERAGE(ae2,ae6,ae10,ae14,ae18,ae22)/average(o2:x2,o6:x6,o10
:x10,o14:x14,o18:x18,o22:x22)"

Range("af34").Select

    ActiveCell.Formula = _

"=AVERAGE(af2,af6,af10,af14,af18,af22)/average(o2:x2,o6:x6,o10
:x10,o14:x14,o18:x18,o22:x22)"

Range("ag34").Select

    ActiveCell.Formula = _

"=AVERAGE(ag2,ag6,ag10,ag14,ag18,ag22)/average(o2:x2,o6:x6,o10
:x10,o14:x14,o18:x18,o22:x22)"

Range("ah34").Select

ActiveCell.Formula = _

"=AVERAGE(ah2,ah6,ah10,ah14,ah18,ah22)/average(o2:x2,o6:x6,o10
:x10,o14:x14,o18:x18,o22:x22)"

Range("ai34").Select

ActiveCell.Formula = _

"=AVERAGE(ai2,ai6,ai10,ai14,ai18,ai22)/average(o2:x2,o6:x6,o10
:x10,o14:x14,o18:x18,o22:x22)"
```

```
    Range("y35").Select
    ActiveCell.Formula = _
"=AVERAGE(y3,y7,y11,y15,y19,y23)/average(o3:x3,o7:x7,o11:x11,o
15:x15,o19:x19,o23:x23)"
    Range("z35").Select
ActiveCell.Formula = _
"=AVERAGE(z3,z7,z11,z15,z19,z23)/average(o3:x3,o7:x7,o11:x11,o
15:x15,o19:x19,o23:x23)"
Range("aa35").Select
    ActiveCell.Formula = _
"=AVERAGE(aa3,aa7,aa11,aa15,aa19,aa23)/average(o3:x3,o7:x7,o11
:x11,o15:x15,o19:x19,o23:x23)"
Range("ab35").Select
    ActiveCell.Formula = _
"=AVERAGE(ab3,ab7,ab11,ab15,ab19,ab23)/average(o3:x3,o7:x7,o11
:x11,o15:x15,o19:x19,o23:x23)"
Range("ac35").Select
    ActiveCell.Formula = _
"=AVERAGE(ac3,ac7,ac11,ac15,ac19,ac23)/average(o3:x3,o7:x7,o11
:x11,o15:x15,o19:x19,o23:x23)"
    Range("ad35").Select
    ActiveCell.Formula = _
"=AVERAGE(ad3,ad7,ad11,ad15,ad19,ad23)/average(o3:x3,o7:x7,o11
:x11,o15:x15,o19:x19,o23:x23)"
    Range("ae35").Select
    ActiveCell.Formula = _
"=AVERAGE(ae3,ae7,ae11,ae15,ae19,ae23)/average(o3:x3,o7:x7,o11
:x11,o15:x15,o19:x19,o23:x23)"
Range("af35").Select
    ActiveCell.Formula = _
"=AVERAGE(af3,af7,af11,af15,af19,af23)/average(o3:x3,o7:x7,o11
:x11,o15:x15,o19:x19,o23:x23)"
Range("ag35").Select
```

```
    ActiveCell.Formula = _
"=AVERAGE(ag3,ag7,ag11,ag15,ag19,ag23)/average(o3:x3,o7:x7,o11
:x11,o15:x15,o19:x19,o23:x23)"
Range("ah35").Select
ActiveCell.Formula = _
"=AVERAGE(ah3,ah7,ah11,ah15,ah19,ah23)/average(o3:x3,o7:x7,o11
:x11,o15:x15,o19:x19,o23:x23)"
Range("ai35").Select
ActiveCell.Formula = _
"=AVERAGE(ai3,ai7,ai11,ai15,ai19,ai23)/average(o3:x3,o7:x7,o11
:x11,o15:x15,o19:x19,o23:x23)"


    Range("y36").Select
    ActiveCell.Formula = _
"=AVERAGE(y4,y8,y12,y16,y20,y24)/average(o4:x4,o8:x8,o12:x12,o
16:x16,o20:x20,o24:x24)"
    Range("z36").Select
ActiveCell.Formula = _
"=AVERAGE(z4,z8,z12,z16,z20,z24)/average(o4:x4,o8:x8,o12:x12,o
16:x16,o20:x20,o24:x24)"
Range("aa36").Select
    ActiveCell.Formula = _
"=AVERAGE(aa4,aa8,aa12,aa16,aa20,aa24)/average(o4:x4,o8:x8,o12
:x12,o16:x16,o20:x20,o24:x24)"
Range("ab36").Select
    ActiveCell.Formula = _
"=AVERAGE(ab4,ab8,ab12,ab16,ab20,ab24)/average(o4:x4,o8:x8,o12
:x12,o16:x16,o20:x20,o24:x24)"
Range("ac36").Select
    ActiveCell.Formula = _
"=AVERAGE(ac4,ac8,ac12,ac16,ac20,ac24)/average(o4:x4,o8:x8,o12
:x12,o16:x16,o20:x20,o24:x24)"
    Range("ad36").Select
    ActiveCell.Formula = _
```

```
"=AVERAGE(ad4,ad8,ad12,ad16,ad20,ad24)/average(o4:x4,o8:x8,o12
:x12,o16:x16,o20:x20,o24:x24)"

    Range("ae36").Select

    ActiveCell.Formula = _

"=AVERAGE(ae4,ae8,ae12,ae16,ae20,ae24)/average(o4:x4,o8:x8,o12
:x12,o16:x16,o20:x20,o24:x24)"

Range("af36").Select

    ActiveCell.Formula = _

"=AVERAGE(af4,af8,af12,af16,af20,af24)/average(o4:x4,o8:x8,o12
:x12,o16:x16,o20:x20,o24:x24)"

Range("ag36").Select

    ActiveCell.Formula = _

"=AVERAGE(ag4,ag8,ag12,ag16,ag20,ag24)/average(o4:x4,o8:x8,o12
:x12,o16:x16,o20:x20,o24:x24)"

Range("ah36").Select

ActiveCell.Formula = _

"=AVERAGE(ah4,ah8,ah12,ah16,ah20,ah24)/average(o4:x4,o8:x8,o12
:x2,o16:x16,o20:x20,o24:x24)"

Range("ai36").Select

ActiveCell.Formula = _

"=AVERAGE(ai4,ai8,ai12,ai16,ai20,ai24)/average(o4:x4,o8:x8,o12
:x2,o16:x16,o20:x20,o24:x24)"


      Range("y37").Select

  ActiveCell.Formula = _

"=AVERAGE(y5,y9,y13,y17,y21,y25)/average(o5:x5,o9:x9,o13:x13,o
17:x17,o21:x21,o25:x25)"

    Range("z37").Select

ActiveCell.Formula = _

"=AVERAGE(z5,z9,z13,z17,z21,z25)/average(o5:x5,o9:x9,o13:x13,o
17:x17,o21:x21,o25:x25)"

Range("aa37").Select

    ActiveCell.Formula = _
```

```
"=AVERAGE(aa5,aa9,aa13,aa17,aa21,aa25)/average(o5:x5,o9:x9,o13
:x13,o17:x17,o21:x21,o25:x25)"

Range("ab37").Select

    ActiveCell.Formula = _

"=AVERAGE(ab5,ab9,ab13,ab17,ab21,ab25)/average(o5:x5,o9:x9,o13
:x13,o17:x17,o21:x21,o25:x25)"

Range("ac37").Select

    ActiveCell.Formula = _

"=AVERAGE(ac5,ac9,ac13,ac17,ac21,ac25)/average(o5:x5,o7:x7,o13
:x13,o17:x17,o21:x21,o25:x25)"

    Range("ad37").Select

    ActiveCell.Formula = _

"=AVERAGE(ad5,ad9,ad13,ad17,ad21,ad25)/average(o5:x5,o9:x9,o13
:x13,o17:x17,o21:x21,o25:x25)"

    Range("ae37").Select

    ActiveCell.Formula = _

"=AVERAGE(ae5,ae9,ae13,ae17,ae21,ae25)/average(o5:x5,o9:x9,o13
:x13,o19:x19,o21:x21,o25:x25)"

Range("af37").Select

    ActiveCell.Formula = _

"=AVERAGE(af5,af9,af13,af17,af21,af25)/average(o5:x5,o9:x9,o13
:x13,o17:x17,o21:x21,o25:x25)"

Range("ag37").Select

    ActiveCell.Formula = _

"=AVERAGE(ag5,ag9,ag13,ag17,ag21,ag25)/average(o5:x5,o9:x9,o13
:x13,o17:x17,o19:x19,o25:x25)"

Range("ah37").Select

ActiveCell.Formula = _

"=AVERAGE(ah5,ah9,ah13,ah17,ah21,ah25)/average(o5:x5,o9:x9,o13
:x13,o17:x17,o21:x21,o25:x25)"

Range("ai37").Select

ActiveCell.Formula = _

"=AVERAGE(ai5,ai9,ai13,ai17,ai21,ai25)/average(o5:x5,o9:x9,o13
:x13,o17:x17,o21:x21,o25:x25)"
```

```
Range("Y34:Ai34").Select
    Selection.Copy
    Windows("4 ori data.xlsx").Activate
Sheets("ori1").Select
    ActiveCell.Offset(1, 0).Select
    Selection.PasteSpecial Paste:=xlPasteValues,
Operation:=xlNone, SkipBlanks _
        :=False, Transpose:=False
    For Each wb In Application.Workbooks
     Select Case wb.Name
             Case ThisWorkbook.Name
                 ' do nothing
             Case Else
     End Select
Next wb
Workbooks(xFileName).Activate
Range("Y35:Ai35").Select
    Selection.Copy

    Windows("4 ori data.xlsx").Activate
Sheets("ori2").Select
    ActiveCell.Offset(1, 0).Select
    Selection.PasteSpecial Paste:=xlPasteValues,
Operation:=xlNone, SkipBlanks _
        :=False, Transpose:=False
    For Each wb In Application.Workbooks
     Select Case wb.Name
             Case ThisWorkbook.Name
                 ' do nothing
             Case Else
     End Select
```

```
Next wb


Workbooks(xFileName).Activate
Range("Y36:Ai36").Select
    Selection.Copy
    Windows("4 ori data.xlsx").Activate
Sheets("ori3").Select
    ActiveCell.Offset(1, 0).Select
    Selection.PasteSpecial Paste:=xlPasteValues,
Operation:=xlNone, SkipBlanks _
        :=False, Transpose:=False
    For Each wb In Application.Workbooks
     Select Case wb.Name
             Case ThisWorkbook.Name
                 ' do nothing
             Case Else
     End Select
Next wb


Workbooks(xFileName).Activate
Range("Y37:Ai37").Select
    Selection.Copy
    Windows("4 ori data.xlsx").Activate
Sheets("ori4").Select
    ActiveCell.Offset(1, 0).Select
    Selection.PasteSpecial Paste:=xlPasteValues,
Operation:=xlNone, SkipBlanks _
        :=False, Transpose:=False
    For Each wb In Application.Workbooks
     Select Case wb.Name
             Case ThisWorkbook.Name
```

```
                ' do nothing
            Case Else
                wb.Close SaveChanges:=True
     End Select
Next wb
End With
            xFileName = Dir
        Loop
    End If
End Sub
```

7.4 Appendix 4: Pilot c-Fos study

7.4.1 Overview

This section outlines the pilot study conducted to assess whether object exploration induced *c-fos* expression, an indirect measure of neuronal activity (Lara Aparicio et al., 2022), in the RSC and HPC of young C57BL6/J mice. An additional aim of this pilot experiment was to refine the IHC c-Fos staining protocol, image processing, and quantification analysis before a larger experiment was conducted.

7.4.2 Procedure

For this pilot experiment, a group of 7 male C57BL6/J mice (5-6 months old) were sourced from excess stocks from Cardiff University. The animals were housed as described in the General Methods section of this thesis.

The testing procedure was adapted from Baumgartel et al., (2018) and spanned three consecutive days. For the first two days, each animal was habituated to a square OF arena for 5 minutes each day. On the third day, the animal underwent the test procedure; either 15 minutes in the empty OF arena or 15 minutes in the arena with two identical objects, positioned diagonally opposite. Four animals experienced the 'object exploration' condition and three experienced the 'empty context' control condition. After the test procedure, each animal was placed in its home cage for 30 minutes, then was culled by transcardial perfusion. Coronal brain sections were then processed for IHC analysis of *c-fos* expression in the caudal dysgranular RSC and the CA1 of the HPC, as described in the General Methods chapter of this thesis.

7.4.3 Results

7.4.3.1 c-fos Expression in the Retrosplenial Cortex and Hippocampus

Unpaired T-tests revealed no significant difference in *c-fos* expression between the empty context and object exploration groups in either the RSC ($t(5) = 0.627$, $p = 0.559$, Fig. 7.1a), or HPC: ($t(5) = 1.890$, $p = 0.117$, Fig. 7.1b).

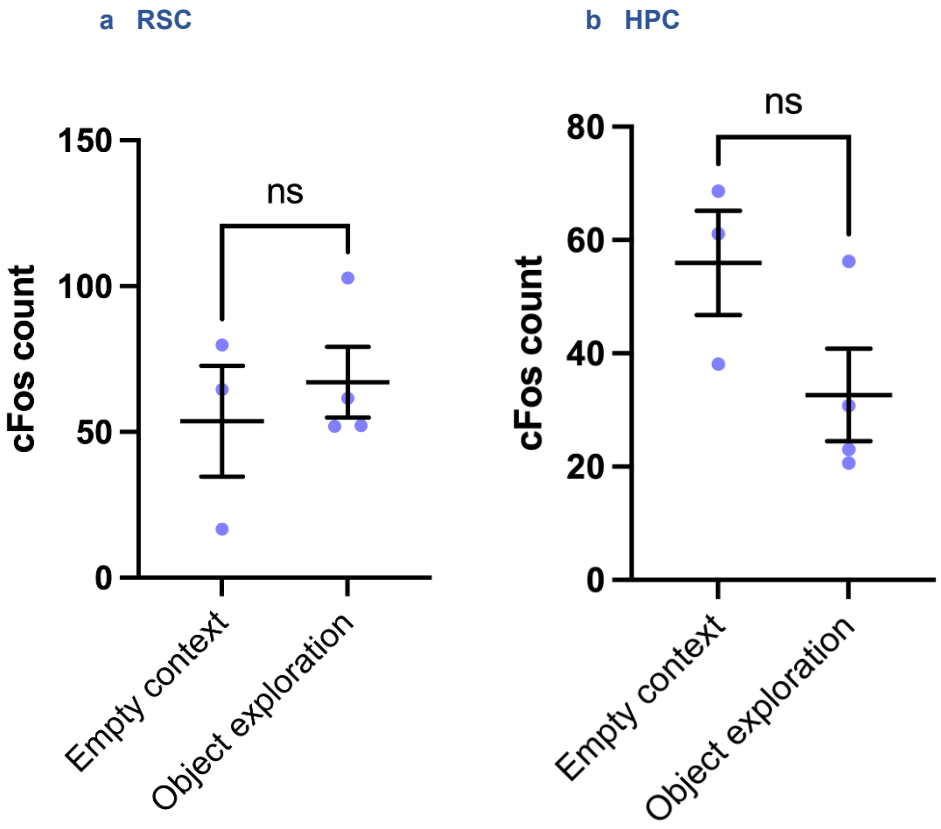

Figure 7.1: Pilot Analysis of c-fos Expression Following Object Exploration. No significant difference in c-Fos positive cells between the empty context and object exploration groups in the ***a)*** Retrosplenial Cortex (RSC) and ***b)*** Hippocampus (HPC). Results from unpaired T-tests shown (ns = non-significant).

7.4.3.2 Object Contact Times and Distance Travelled

The object exploration time and distance travelled of the animals during the test trial was assessed to determine whether any changes may account for any alterations in c-Fos expression, albeit this was a non-significant result. An unpaired T-test revealed no significant difference in distance moved ($t(5) = 0.828$, $p = 0.445$, Fig. 7.2b) during the test.

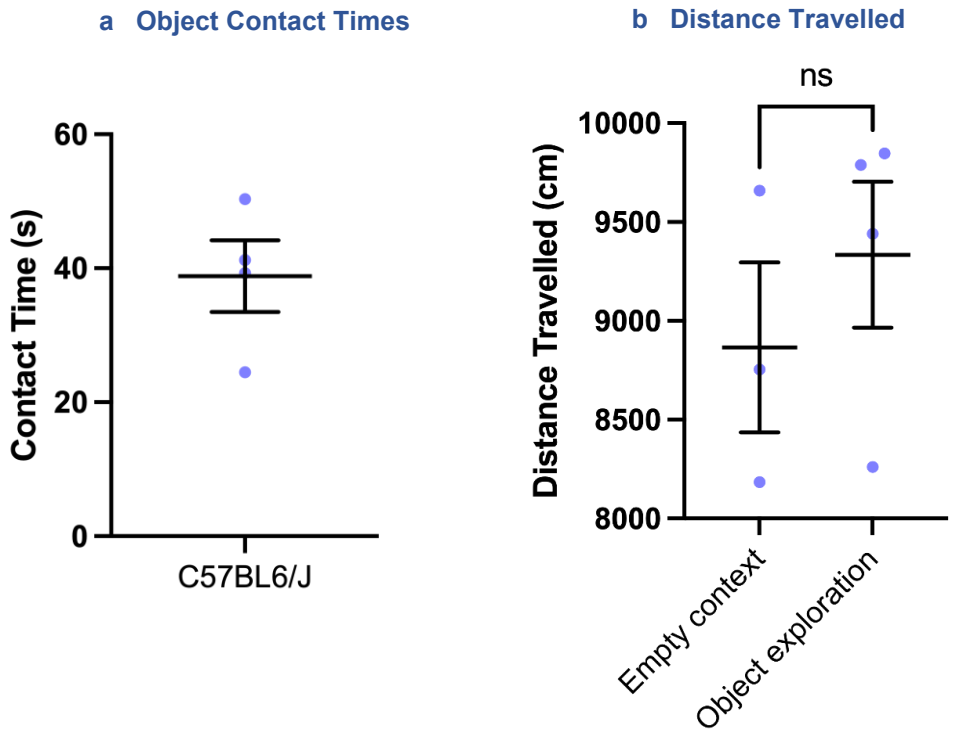

Figure 7.2: Object Contact Times and Distance Travelled During Object Exploration. a) Total object interaction time of animals in the object exploration group. ***b)*** No significant differences were detected in the distance travelled between the object exploration and empty context groups. Results of unpaired T-tests shown (ns= non-significant).

7.4.4 Conclusions

This pilot study successfully detected c-Fos positive cells in the RSC and HPC following exposure to an OF arena with and without novel objects. Unexpectedly, c-Fos levels in the empty context group were similar to that in the object exploration group. Although there was a trend indicating higher RSC c-Fos levels in the object exploration group, this difference did not reach statistical significance. In contrast, in the HPC, the object exploration group showed a lower mean c-Fos count, although this trend also did not reach significance. There were no significant differences in the distance travelled between the empty context and object exploration groups. The lack of a significant difference in *c-fos* expression is likely due to high basal levels in the empty context group induced by handling, environmental changes, or exploratory activity (Lara Aparicio et al., 2022). This effect, compounded by the small sample size, limited the ability to detect novelty-induced response in the object exploration group. To address this, the main c-Fos experiment of this thesis (Chapter 4, Experiment 2) incorporated a homecage control rather than an empty context control, minimising basal expression in the control group. This approach, while shifting the focus from examining the specific effect of novel objects on RSC and HPC c-Fos levels, provided a more stable baseline for comparing basal c-Fos levels

and examining experience-induced difference between C57BL6/J and *App*^{NLGF} animals in the main experiment.